Year : 2013

THE LATE BERRIASIAN- EARLY VALANGINIAN INTERVAL: EVIDENCES OF MAJOR ENVIRONMENTAL CHANGES BEFORE THE VALANGINIAN EPISODE

Morales Chloé

UNIL | Université de Lausanne
Faculté des géosciences et de l'environnement
Institut des Sciences de la Terre

THE LATE BERRIASIAN- EARLY VALANGINIAN INTERVAL :

EVIDENCES OF MAJOR ENVIRONMENTAL CHANGES BEFORE THE VALANGINIAN EPISODE

Thèse de doctorat

présentée à la faculté des géosciences et de l'environnement
de l'Université de Lausanne

pour l'obtention du grade de

Docteur ès Sciences

par

Chloé Morales

diplômée en géologie de l'Université de Bourgogne, Dijon, France

Jury:
Prof. Eric Verrecchia, Université de Lausanne (Président du jury)
Prof. Karl B. Föllmi, Université de Lausanne (Directeur de thèse)
Dr. Thierry Adatte, Université de Lausanne (Expert interne)
Prof. Jörg Mutterlose, Ruhr-Universität, Bochum (Expert externe)
Prof. Jean-François Deconinck, Université de Bourgogne, Dijon (Expert externe)
Dr Annie Arnaud-Vanneau, Université Joseph Fourrier, Grenoble (Expert externe)

LAUSANNE, 2013

UNIL | Université de Lausanne
FACULTE DES GEOSCIENCES ET DE L'ENVIRONNEMENT
INSTITUT DES SCIENCES DE LA TERRE

THE LATE BERRIASIAN- EARLY VALANGINIAN INTERVAL :

EVIDENCES OF MAJOR ENVIRONMENTAL CHANGES BEFORE THE VALANGINIAN EPISODE

Chloé Morales

diplômée en géologie de l'Université de Bourgogne, Dijon, France

LAUSANNE, 2013

UNIL | Université de Lausanne
Décanat Géosciences et de l'Environnement
bâtiment Géopolis
CH-1015 Lausanne

IMPRIMATUR

Vu le rapport présenté par le jury d'examen, composé de

Président de la séance publique :	M. le Professeur Eric Verrecchia
Président du colloque :	M. le Professeur Eric Verrecchia
Directeur de thèse :	M. le Professeur Karl Föllmi
Expert externe :	M. le Professeur Jörg Mutterlose
Experte externe :	Mme le Docteur Annie Arnaud-Vanneau
Expert externe :	M. le Professeur Jean-François Deconinck
Expert interne :	M. le Docteur Thierry Adatte

Le Doyen de la Faculté des géosciences et de l'environnement autorise l'impression de la thèse de

Madame Chloé MORALES

Titulaire d'un
Master en Géobiosphère
Université de Bourgogne, Dijon/France

intitulée

THE LATE BERRIASIAN-EARLY VALANGINIAN INTERVAL : EVIDENCE OF MAJOR ENVIRONMENTAL CHANGE BEFORE THE VALANGINIAN EPISODE

Lausanne, le 17 mai 2013

Pour le doyen de la Faculté des géosciences et de l'environnement

Professeur Eric Verrecchia, vice-doyen

TABLE OF CONTENTS

1. INTRODUCTION ***p.17***

1.1. THE EARLY CRETACEOUS WORLD: AN OVERVIEW **p.19**
1.2. A TIME OF REPEATED PALAEOENVIRONMENTAL CHANGE **p.21**
1.3. THE VALANGINIAN EPISODE **p.23**
1.4. WHICH INCEPTION FOR THE PERTURBATION **p.24**
1.5. GOALS OF THE THESIS AND PROCEDURE **p.26**
References **p.27**

2. BERRIASIAN AND EARLY VALANGINIAN ENVIRONMENTAL CHANGE ALONG A TRANSECT FROM THE JURA PLATFORM TO THE VOCONTIAN BASIN ***p.33***

ABSTRACT **p.35**
2.1. INTRODUCTION **p.36**
2.2. GEOLOGICAL SETTING **p.38**
2.2.1. The Jura platform *p.38*
2.2.2.The Vocontian Basin *p.42*
2.3. MATERIAL AND METHODS **p.42**
2.3.1. Biostratigraphy *p.42*
2.3.2. Microfacies and sequence stratigraphy *p.43*
2.3.3. Carbon and oxygen stable-isotope analyses *p.44*
2.3.4. Phosphorus content *p.44*
2.3.5. Whole-rock and clay mineralogy *p.46*
2.3.6. Palynology *p.46*
2.4. RESULTS **p.46**
2.4.1. Biostratigraphy *p.46*
2.4.2. Carbon and oxygen stable-isotope analyses *p.48*
2.4.3. Phosphorus contents *p.49*
2.4.4. Mineralogy *p.51*
2.4.5. Evolution of microfacies *p.52*
2.4.6. Terrestrial palynology *p.55*
2.5. INTERPRETATIONS **p.55**
2.5.1. Sequence stratigraphy *p.55*
2.5.2. Diagenesis *p.58*

2.5.3. Age control and correlation of the sections *p.59*
2.5.4. Carbonate platform architecture and morphology *p.59*
2.6. DISCUSSION **p.64**
2.6.1. Modifications in the carbon cycle *p.64*
2.6.2. Palaeoclimatic and palaeoenvironmental change *p.65*
2.6.2.1. Climatic change **p.65**
2.6.2.2. Detrital fluxes and nutrient levels **p.68**
2.7. CONCLUSIONS **p.69**
References **p.70**

3. EVOLUTION OF THE HELVETIC PLATFORM THROUGH THE BERRIASIAN-VALANGINIAN BOUNDARY ***p.79***

3.1. INTRODUCTION **p.81**
3.2. GEOLOGICAL SETTING **p.82**
3.3. MATERIAL AND METHODS **p.84**
3.3.1. Biostratigraphy *p.84*
3.3.2. Microfacies and sequence stratigraphy *p.88*
3.3.3. Stable-isotope analyses *p.88*
3.3.4. Phosphorus content *p.88*
3.3.5. Whole-rock and clay mineralogy *p.88*
3.4. RESULTS **p.89**
3.4.1. Sedimentology and microfacies *p.89*
- Säntis section p.89
- Dräckloch section p.92
- Vitznau section p.96
3.4.2. Stable carbon-isotope analyses *p.100*
3.4.3. Phosphorus content *p.100*
3.4.4. Bulk-rock mineralogy *p.101*
3.5. INTERPRETATION **p.102**
3.5.1. Sequence stratigraphy *p.102*
- Säntis section p.103
- Dräckloch section p.104
- Vitznau section p.105
3.5.2. Diagenesis *p.106*
3.5.3. Age control and correlation of the sections *p.106*
3.6. DISCUSSION **p.110**
3.6.1. Palaeogeography, sea-level change and tectonics *p.110*
3.6.2. Palaeoenvironmental and palaeoclimatic changes *p.115*
3.7. CONCLUSIONS **p.116**
References **p.116**

4. PALAEOENVIRONMENTAL CHANGE THROUGH THE ONSET OF THE VALANGINIAN CARBON-ISOTOPE EXCURSION: EVIDENCE FROM THE MID-POLISH TROUGH. p.121

ABSTRACT p.123
4.1. INTRODUCTION p.124
4.2. GEOLOGICAL SETTING p.126
4.3. MATERIAL AND METHODS p.127
4.3.1. Preparation of microfauna and palynofacies p.127
4.3.2. Stable-isotope analyses p.128
4.3.3. Whole-rock and clay p.128
4.3.4. Major and trace elements p.130
4.3.5. Rock-Eval analyses p.130
4.4. RESULTS p.131
4.4.1. Sedimentology and stratigraphy p.131
4.4.2. Stable isotopes p.132
4.1.1. Whole-rock carbonate and selected fossil groups p.132
4.1.2. $\delta^{13}C_{org}$ values of total organic carbon p.133
4.4.3. Mineralogy p.134
4.4.3.1. Whole-rock mineralogy p.134
4.4.3.2. Clay mineralogy p.134
4.4.4. Major and trace elements p.134
4.4.5. Total organic carbon contents, Rock-Eval data, and palynofacies results p.136
4.5. DISCUSSION p.138
4.5.1. Evaluation of the diagenetic overprint p.138
4.5.1.1. Whole rock isotopic data p.138
4.5.1.2. Ostracods, foraminifera and bivalve fragments p.139
4.5.1.3. Mineralogical and Rock-Eval data p.139
4.5.2. Chemostratigraphic significance p.139
5.3. Palaeoclimatic and palaeoenvironmental changes p.141
5.3.1. Temperature *vs* salinity changes p.141
5.3.2. Chronology and implication of changes in mineralogy and major and trace element composition p.142
5.3.4. Organic-matter preservation and characterisation p.146
4.5.4. Changes in atmospheric CO_2 and the carbon cycle p.147
4.6. CONCLUSIONS p.150
References p.151

5. TWO PULSES IN ATMOSPHERIC CO_2 LEADING TO THE VALANGINIAN PERTURBATION IN THE GLOBAL CARBON p.159

5.1. INTRODUCTION p.161
5.2. GEOLOGICAL SETTING p.162
5.3. MATERIEL AND METHOD p.163
5.3.1. Organic carbon isotope analyses p.165
5.3.2. Rock-Eval Analyses p.165
5.4. RESULTS p.165
5.5. DISCUSSION p.166
5.5.1. Evaluation of the diagenetic impact p.166
5.5.2. The perturbation of the carbon cycle: a link with atmospheric pCO_2 changes p.169
5.5.3. Which effect on palaeoenvironments? p.172
5.6. CONCLUSION p.176
References p.177

6. CONCLUSIONS p.183

6.1. SYNTHESIS p. 185
6.1.1 An improved stratigraphic scheme p.185
6.1.2. Evidence for tectonic instability and activity p.185
6.1.3. Sea-level variations p.186
6.1.4. Climate change p.186
6.1.5. Changes in nutrient availability and ecological changes p.186
6.1.6. Platform morphology p.188
6.1.7. Atmospheric pCO_2 as a possible trigger p.188
6.2. GENERAL CONCLUSIONS AND OUTLOOK p.188
References p.189

REMERCIEMENTS

Bien que le manuscrit de thèse soit indexé au nom d'un seul auteur, ce travail n'aurait pas été possible sans le soutien d'une grande équipe qui inclut le chef, les collègues, les amis et la famille ; la délimitation des catégories précédemment citées n'étant pas toujours bien établie. Bien que ces quatre années de thèse aient demandé beaucoup de travail et d'investissement personnel, elles ont également été riches de rencontres professionnelles et amicales, de rires et d'émotions. La géologie nous apprend à reconsidérer la notion de temps, et si ces quelques années peuvent paraître courtes, elles représentent une période clé à l'échelle d'une vie. Pour cela je souhaite remercier l'ensemble des personnes qui m'ont aidé et soutenu depuis mon arrivée à Lausanne.

Mes premières pensées vont naturellement vers mon chef, Karl, qui m'avait pourtant avertit un jour qu'il n'aime pas que je l'appelle « chef»… Il est à l'origine de ce projet, dont le sujet m'a tout de suite passionnée, et je lui suis profondément reconnaissante de m'avoir engagée. Merci Karl d'avoir su susciter tout plein de questions, et donc la recherche de réponses ; bref d'avoir éveillé ma curiosité scientifique et de m'avoir transmis ta passion pour le Crétacé ! Merci également de m'avoir donné l'opportunité de me présenter à la communauté scientifique lors de nombreux congrès ; et merci enfin, et c'est très important pour moi, de m'avoir donné confiance dans tous les moments difficiles traversés.

Je tiens également à remercier Thierry Adatte, qui s'est beaucoup impliqué dans l'élaboration de ce travail. J'ai beaucoup appris à tes cotés, ton avis critique et les perpétuelles remises en question des résultats et leurs interprétations m'ont beaucoup aidé. J'ai énormément apprécié discuter avec toi, et pas seulement pour ton sens de l'humour !
Je suis également reconnaissante envers les personnes qui m'ont apporté leur aide dans les laboratoires : Tiffany Monnier, Jean-Claude Lavanchy, Pierre Vonlanthen, Claudia Baumgartner, mais aussi Célia et Alicia.

I also would like to thank the members of the jury : Annie Arnaud-Vanneau, Jean-François Deconinck and Jörg Mutterlose for their interest and the stimulating discussions we had before and during the defense.
Je remercie en particulier Annie pour les longues heures passées devant le microscope à mes cotés, pour m'apprendre les secrets des foraminifères et me transmettre ses connaissances (ou partie du moins) en stratigraphie séquentielle. Merci également à Jean-François pour son esprit critique et nos discussions argileuses, qui déjà me passionnaient à Dijon.

J'ajouterai deux mentions spéciales : la première est pour Jorge Spangenberg qui a fait son possible pour passer des séries d'échantillons dans des temps plus ou moins raisonnables. Ca a été un plaisir de travailler avec toi (malgré que tu râles un peu de temps en temps... tu retrouves toujours le sourire !). La seconde est pour Laurent Nicod, qui a grogné aussi un peu lorsque je lui ai apporté mes séries de talons … J'ai découvert par la suite qu'à travers ce mode de communication il cachait en fait une grande sensibilité ! Laurent, merci tu participes grandement à la vie de l'institut…

L’uni de Lausanne a également la chance d’avoir deux secrétaires de choc, Krystel et Anne-Marie, souriantes et à l’écoute en toutes circonstances, et prêtes à venir en en aide en toutes circonstances (même malade avec un bidou de 8 mois), merci à elles !!!

J’ai eu la chance de trouver une deuxième famille à l’unil. Parmi eux, ca a été un plaisir de partager mon bureau avec de formidables collocs. Hassan, since the begining both of us knew that everything would be ok, indeed every thing is ok now and that is thanks to you. Thank you for understanding and supporting me... Brahim, mon Bibi, dire que je me souviens de toi, tu étais… ben tout comme maintenant : sympa, gentil et marrant… Non mon Bibi, tu n’as pas changé !! Ma toute dernière colloc, Lulu, qui n’est pas la dernière à se marrer… et qui nous fournit soirée après soirée des dossiers pour la fin de sa thèse ! Au 4ème étage, Vivie (la femme de ma vie ^^), merci pour ton soutien et nos interminables discussions, quelle que soit l’heure du jour ou de la nuit ! Un grand merci à ce vieux brigand de Remy ; Francesca et ces délicieux risottos, Arthur, qui commence les blackouts avant les soirées… ca promet… et Tonio et Romain pour compléter la fine équipe ! M’oubliez pas pour le Jaggers quand j’serai docteur…

Mais également Johnny, la reine des frites, Alex sans qui les congrès et les social dinners n’auraient définitivement pas été les mêmes, Alicia du pays des merveilles spécialiste des franges années septante.

Je n’oublie bien sur pas les anciens : Stéphane, Mélo merci pour ces bons moments dès mon arrivée, il n’y a plus de bleue qui tienne maintenant ! Mais aussi Sandrine, Laure, Caroline R., Claire, Guillaume.

Il y aussi tous les bon moments partagés autour d’un café ou d’une bière au Zélig, merci à Quentin, Erika, Philippe, Pierre, Maria, Andrès, Loraine, Lorène, David F., David L., Gladys, Robert, Nicklaus, Laetitia, Goran, Anders, Anne-Cécile, Nathalie, Eric … et m’excuse pour ceux que j’aurais oublié !

Au delà des frontières de la Suisse, merci aux géologues dijonnais en particuliers les anciens du master, Paco, et un clin d’œil tout particulièrement pour Naouel (a bientôt à Montpellier !).

Je remercie également Cyril de m’avoir aidée à franchir les montagnes du Jura pour venir en Suisse.

Un indispensable soutien m’a également été apporté presque chaque mardi par Clémence, qui est bilingue français-romand maintenant, et qui a assuré pendant les hauts, les bas, les milieux… enfin qui assure tout court quoi.

Evidemment je remercie du fond du cœur ma famille et les forfaits téléphone all-inclusive qui ont permis de conserver un contact illimité dans le temps ! Ju, P’pa, M’man, M’mie, ben je vous aime quoi !

ABSTRACT

The Valanginian is a period of major palaeoenvironmental changes, which led to a global perturbation of the carbon cycle. This perturbation is widely expressed in the inorganic stable isotope record by a positive shift of 1.7‰, documented in deep and shallow–marine environments. The onset of the $\delta^{13}C_{carb}$ excursion is dated as latest early Valanginian (late *B. campylotoxus* ammonite zone). Several palaeoenvironmental changes are however described from the time period preceding the positive carbon-isotope excursion and going as far back as the Berriasian. This project aims at pinpointing and reconstructing the timing of these changes in order to better understand their role as potentially controlling factors and the dynamics leading to and governing the perturbation.

In order to achieve this, a detailed stratigraphic analysis of a series of key sections in the Jura Mountains, the Helvetic Alps, and the Vocontian, Lombardian and Polish Basins was performed. An important aspect was to improve age control on these sections and for this, biostraphically meaningful groups including benthic foraminifera, calpionellids and nannofossils, sequence stratigraphy (in the shallow-water sections) and carbon-isotope stratigraphy was used.

Bathymetric transects were established across the Jura and the Helvetic carbonate platforms. In the Helvetic area, block tectonic activity was found to have played a preponderant role during the late Berriasian, leading to an emersion in the uplifted part of a tilted block, a deepening along the sinking part of the block, and the deposit of a falling stage systems tract in the platform slope area.

Fieldwork, facies and microfacies analyses permitted to constrain long-term sea-level variations: a transgressive trend is observed through the early-late Berriasian boundary, followed by a generally regressive trend in the late Berriasian, and an alternation of transgressive/regressive trends in the latest Berriasian and the early Valanginian. Particularly important is a major transgression during the latest Berriasian, which was accompagnied by hardground formation, phosphogenesis and deposition of pelagic carbonate on top of the emerged and then drowned photozoan platform and the shift from photozoan to heterozoan carbonate production in the Helvetic realm. The main condensation phase of the Weissert episode probably occurred within a transgressive interval.

A stepwise increase in humidity is recorded in the NW Tethyan area since the early Berriasian, reaching a maximum in the latest Berriasian and the early Valanginian. A decrease in humid conditions occurred in the middle part of the early Valanginian, followed by a renewed increase in the late early Valanginian, which corresponds to the onset of the $\delta^{13}C_{carb}$ positive shift. This is first accompanied by a local increase in nutrients (early late Berriasian), then by the disappearance of lagoonal environments (latest Berriasian-early Valanginian) and consequently by a widespread increase in nutrients, which was also facilitated by the change to a swell-dominated platform ramp, increasing the bypass of continental fluxes (detrital output, pollen, dissolved inorganic and organic carbon). In parallel, a turn from photozoan to heterozoan carbonate production is observed in shallow-water environments, with a slight time lag between the Jura and the Helvetic platforms. The environmental conditions of the settlement of these heterozoan carbonates are still perplexing because they correspond to high nutrient levels but less humid conditions on the continent.

An increase in pCO_2, highlighted by the difference between $\delta^{13}C_{carb}$ and $\delta^{13}C_{org}$ trends, is viewed as a general trigger of these palaeoenvironmental changes. Two pulses are potentially defined: the first corresponds to the change toward heterozoan carbonate production and the second to the general drowning of carbonate platform during the Weissert episode.

RESUME

Le Valanginien est une période caractérisée par des changements paléo-environnementaux majeurs qui ont conduit à une perturbation globale du cycle du carbone. Cette perturbation est exprimée dans les archives sédimentaires par une excursion positive des isotopes du carbone de 1.7‰, enregistrée dans les environnements de bassin et de plate-forme. Le début de l'excursion positive en $\delta^{13}C_{carb}$ date de la fin du Valanginien inférieur (fin de la zone à ammonite *B. campylotoxus*). De nombreux changements paléo-environnementaux sont cependant décrits dès le Berriasien. Le but de ce projet est de mettre en évidence ces changements et de préciser leur chronologie dans le but de mieux comprendre les facteurs de contrôle et la dynamique générale de la perturbation.

Ainsi, une série de coupes clés ont été analysées dans les régions du Jura français et suisse, dans les Alpes helvétiques, ainsi que dans les bassins vocontien, lombard et polonais. Un important travail de datation a été effectué en utilisant la biostratigraphie (foraminifères benthiques, calpionelles et nannofossiles, en fonction de la profondeur de dépôt des coupes étudiées), la chimiostratigraphie, et la stratigraphie séquentielle.
Ensuite, des transects ont pu être établis le long des plates-formes carbonatées du Jura et helvétique. Dans la région helvétique, l'existence d'une tectonique de bloc a joué un rôle prépondérant durant le Berriasien supérieur : l'enregistrement sédimentaire montre une émersion sur la crête du bloc, un approfondissement à l'arrière du bloc, et un « falling stage system tract » au pied du bloc basculé.
Les analyses de terrain, ainsi que les faciès et microfaciès ont permis de contraindre les variations du niveau marin pour la période étudiée : une transgression est enregistrée autour de la limite Berriasien inférieur-Berriasien supérieur, suivie d'une régression au Berriasien supérieur et d'alternances transgression/régression au Berriasien terminal - Valanginien inférieur. La phase majeure de condensation de l'évènement valanginien de Weissert se produit probablement dans un intervalle transgressif.

Une augmentation de l'humidité par étapes est enregistrée dans la région nord-ouest téthysienne depuis le Berriasien inférieur ; celle-ci atteint son maximum au Berriasien terminal - Valanginien inférieur. Une diminution de l'humidité se produit ensuite dans la partie médiane du Valanginien inférieur, suivie par le renouvellement des conditions humides à la fin du Valanginien inférieur (ces dernières correspondant à l'initiation de l'excursion positive en $\delta^{13}C_{carb}$). Ces variations du cycle hydrologique sont accompagnées d'augmentations du taux de nutriments dans les eaux océaniques, de manière locale dans un premier temps (au début du Berriasien supérieur), puis de manière plus étendue avec la disparition des barrières et des environnements de lagon (au Berriasien terminal- Valanginien inférieur). En effet, les marges continentales adoptant des morphologies de rampes dominées par la houle, les flux continentaux (apports détritiques, pollens, carbone organique et inorganique dissout) sont plus facilement transportés en direction de l'océan. En parallèle, un changement de production carbonatée de photozoaire à hétérozoaire est observé dans les environnements marins peu profonds, avec un léger décalage dans le temps entre les plates-formes du Jura et helvétique. Les conditions environnementales avec lesquelles ces carbonates hétérozoaires s'installent restent énigmatiques car les eaux océaniques sont riches en nutriments alors que les continents subissent une baisse de l'humidité durant cette période.

Une augmentation en paliers de la pCO_2, soulignée par la différence entre les valeurs en $\delta^{13}C_{carb}$ et $\delta^{13}C_{org}$, est considérée comme étant le déclencheur des changements paléo-environnementaux majeurs qui ont mené à l'évènement valanginien de Weissert. Deux augmentations peuvent potentiellement être mises en évidence : la première correspond au changement de production carbonatée vers des association hétérozoaires, et la seconde concorde avec l'ennoiement général des plates-formes carbonatées.

CHAPTER 1:

INTRODUCTION

1. INTRODUCTION

1.1. THE EARLY CRETACEOUS WORLD: AN OVERVIEW

The Cretaceous is famous for the biological mass extinction that lead (amongst others) to the disappearance of dinosaurs at the end of the period, 65.5 ma ago (Ogg *et al.*, 2008). If the giant reptiles have fascinated young and less young children for decades, less is known by the public about Earth and life in general during this period. This work focuses on the Berriasian and Valanginian – the first two stages of the Cretaceous; as such, an overview of the Early Cretaceous extending from 145.5 to 99.6 ma (Ogg *et al.*, 2008) is presented here.

The evolution of the general palaeogeographic and palaeotectonic framework of the Early Cretaceous is determined by the break-up of the supercontinent Pangaea, which was initiated in the Early Permian. The Gondwana and Laurasia continents continue their separation with the opening of the mid-Atlantic, which started in the Early Jurassic (Stämpfli and Borel, 2002) in addition to the on-going opening of the Tethys. Furthermore the Early Cretaceous is characterised by the initiation of the rifting of the South-Atlantic involving the separation of Gondwana into the South American and African continents (Fig. 1.1).

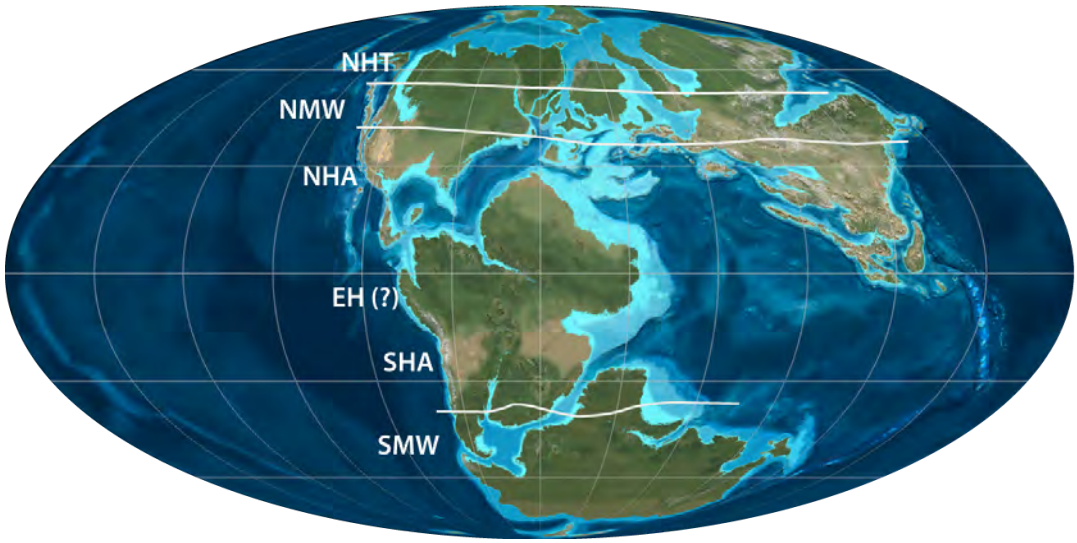

Fig. 1.1: Palaeogeographic map of the Early Cretaceous (Aptian, after Blakey, 2005: *http://jan.ucc.nau.edu/~rcb7/index.html*) and position of the climatic belts (after Chumakov, 1995 and Scotese, 2002: *http://www.scotese.com/*).
Keys: NHT, Northern High-latitude Temperate Humid belt; NMW, Northern Mid-latitude Temperate Humid belt; NHA, Northern Hot Arid belt; EH, Equatorial Humid belt; SHA, Southern Hot Arid belt; SMW, Southern Mid-latitude Temperate Humid belt

The Cretaceous was one of the warmest periods of the Phanerozoic (Frakes, 1979). It has long been postulated that ice caps were absent at the poles. Thus, the temperature gradient from the poles to the equator was lower than the actual.

The climate belts have been reconstructed as follows (Fig. 1.1): a high latitude temperate humid belt with moderately warm conditions extended from the poles to approximately 50°; a mid-latitude warm humid belt with subtropical conditions had an extension from 50° to 30°N, and a hot arid belt from 30° to the equator (Chumakov *et al.*, 1995, Scotese, 2002 and Vakrameev, 2010; in Kujau, 2012). The occurrence of a laterally persistent humid equatorial belt during the Early Cretaceous is not established. Rainy conditions near the palaeoequator are supported by the occurrence of coal deposits in northern Peru, Colombia and in the Middle East (McCabe and Totman Parrish, 1992 and references therein ; Scotese, 2002), and arid conditions are rather reported in areas corresponding to the center of the Gondwana continent (Brazil, central Africa after Chumakov *et al.*, 1995 and Scotese, 2002). Furthermore, the absence of polar ice caps is questioned since ice-rafted deposits and glendonites were discovered for restricted time slices (Valanginian, Aptian), and used as an indicator of cooling phases (Price, 1999).

On the continents, the fauna was largely dominated by reptiles, which were highly diversified and colonised various environments. Birds became numerous and started their diversification. To the contrary, mammals were not abundant and represented by relatively few families. The Early Cretaceous is also a period of diversification for some insects groups (Ross *et al.*, 2000; Mostovski *et al.*, 2003), in particular for orthopters (e.g. grashopper, cricket and locust), hemipters (e.g. bugs), odonatopters (e.g. dragonflies and damselflies), neuropters (e.g. lacewings) and some coleopters (Ross et al., 2000; Krell, 2000). Among others, the appearance of isopters (termites, able to digest lignin) occurred during the earliest Cretaceous (Berriasian; Mayhew, 2002). The Early Cretaceous also witnessed the origin and the progressive diversification of angiosperms (Hickey and Doyle, 1977; but compare also Martin *et al.*, 1989). They particularly developed during the late Early Cretaceous, and progressively occupied ecological niches, which were previously inhabited by gymnosperms and pteridophytes (Lidgard and Crane, 1990).

The marine realm was characterised by a sea level, which was in average 100m higher than today, implying the inundation of continental shelves and the extension of epicontinental shallow-water areas (Haq et *al.*, 1987). The high sea level and the globally warm climate favoured the development of carbonate platforms during the Cretaceous. Reef biota are commonly found in Cretaceous deposits, with the abundance and diversification of photozoan organisms (e.g. light-dependant organisms living in warm and nutrient-depleted waters) such as scleractinian corals, large benthic foraminiferas, rudists and dasycladaceans (Hallock and Schlager, 1986; Masse, 1992; Höfling and Scott, 2002; Philip, 2003).

1.2. A TIME OF REPEATED PALAEOENVIRONMENTAL CHANGE

During the Early Cretaceous, carbonate platforms underwent a succession of modifications in their mode of production (Fig. 1.2).

Repeated changes from photozoan to heterozoan (e.g. suspension-feeding organisms such as crinoids, bryozoans, brachiopods and serpulids; absence of corals; James, 1997; Philip, 2003) are observed. Phases of heterozoan carbonate production were interrupted by phases of condensation during which a few tens of centimetres of phosphate and glauconite-rich sedimentary layers were formed during long periods of up to few million years.

These platform drowning phases are often associated with positive excursions in the $\delta^{13}C$ record and phases of widespread anoxia in the deeper oceans (Fig. 1.2). These episodes of major palaeoenvironmental change are called oceanic anoxic events (OAEs; Schlanger and Jenkyns, 1976; Arthur and Schlanger, 1979, Jenkyns, 1980). They are mostly attributed to major volcanic phases leading to the formation of large igneous provinces (LIP) and/or important phases in oceanic crust production (Larson, 1991; Courtillot and Renne, 2003; Weissert *et al.*, 1998).

The release of volcanogenic CO_2 in the atmosphere is assumed to be a major trigger of OAEs. Subsequent intensified greenhouse conditions were supposed to cause enhanced nutrient fluxes to the ocean, which result in the fertilization of ocean waters, the enhanced preservation of organic matter (Larson, 1991; Larson and Erba, 1999; Rullkötter, 2000; Mort, 2006) and the decrease or the disappearance of calcifying organisms associated with nutrient-depleted waters in both pelagic (nannoconid crises, Erba, 2004) and neritic environments (Masse and Philip, 1981; Föllmi *et al.*, 1994, 2007; Weissert *et al.*, 1998,) as detailed in Fig. 1.3. With this scheme, the isotopic signature of OAEs is mainly explained by the increased preservation of marine organic-matter in the deep basins.

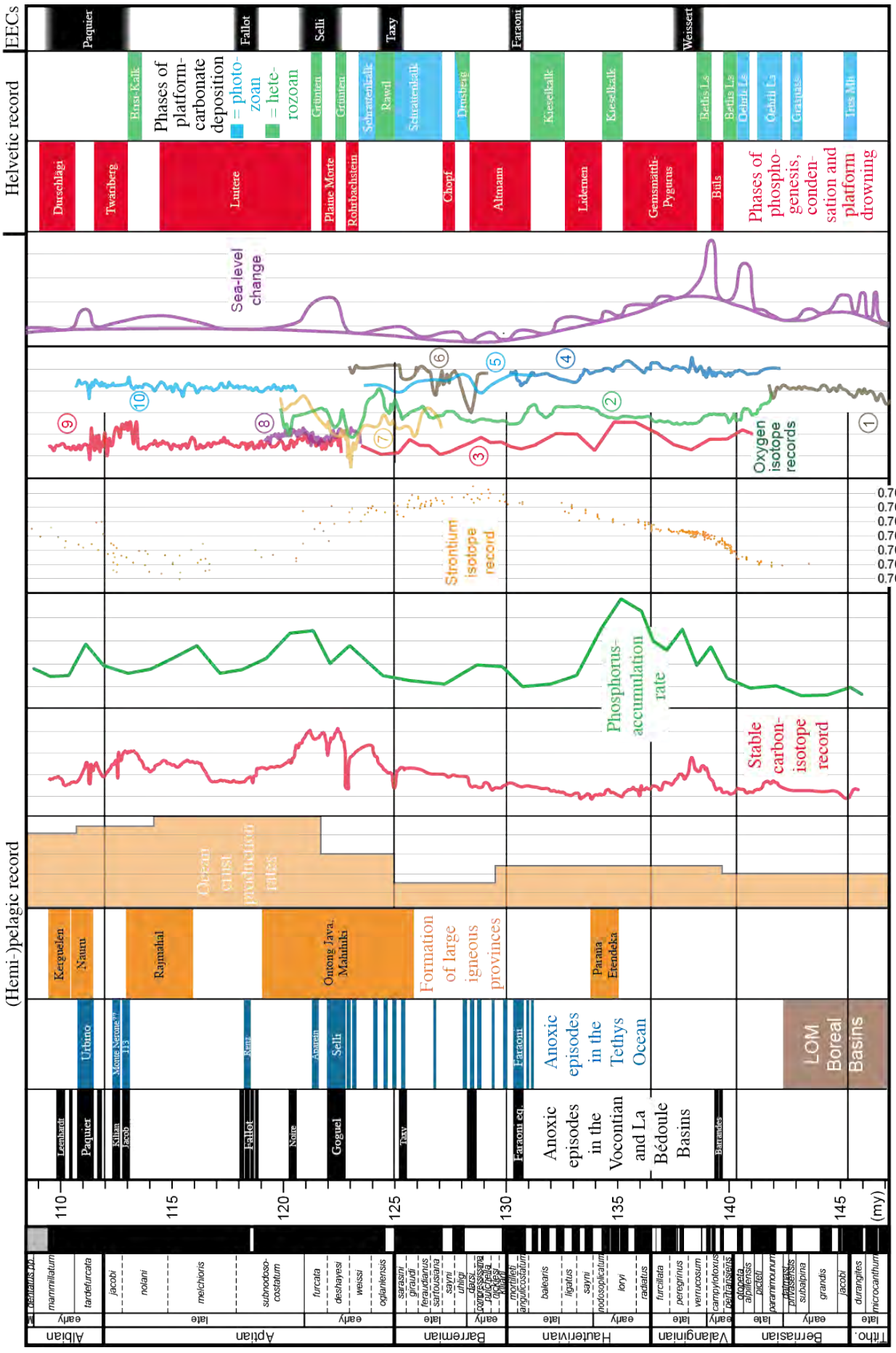

Fig. 1.2: Synthesis diagram showing general paleoceanographic and paleoenvironmental trends correlated with temporal trends in Helvetic platform growth (Föllmi *et al.*, 2007).

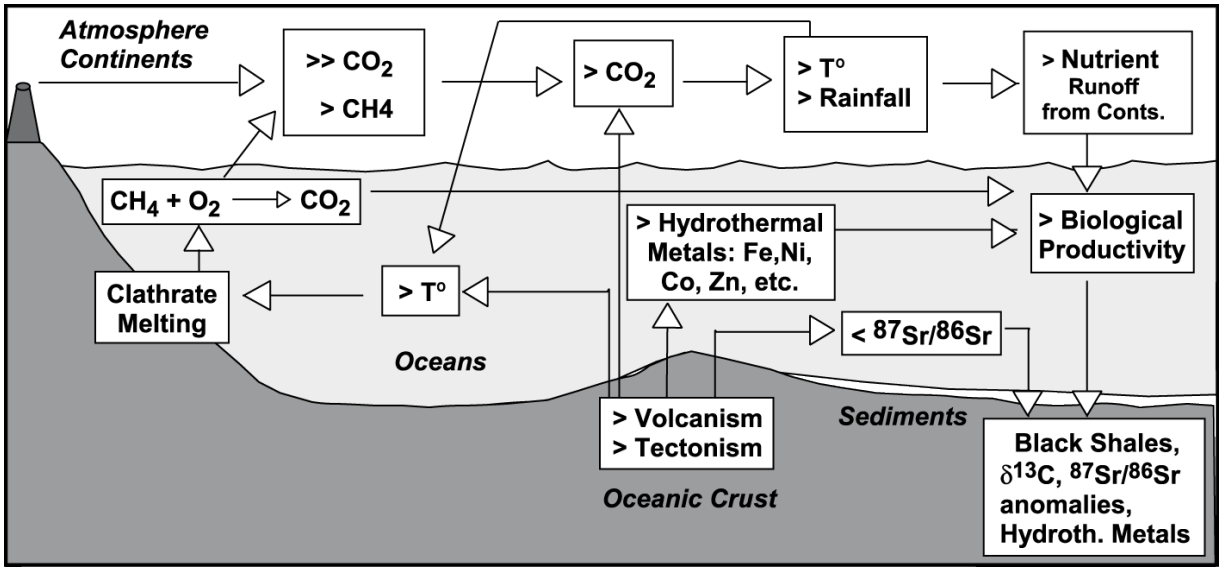

Fig. 1.3: Processes which relate igneous events to biological and geological responses recorded in marine sediments (Erba, 2004).

1.3. THE VALANGINIAN EPISODE

The Valanginian records the oldest perturbation in the global carbon cycle of the Cretaceous (the "Weissert Event"; Erba *et al.*, 2004), which is associated with a decline in nannoconids (Erba *et al.*, 2004; Bornemann and Mutterlose, 2008; Barbu and Melinte-Dobrinescu, 2008; Barbarin *et al.*, 2012) and a platform drowning phase (Masse and Philip, 1981; Funk *et al.*, 1993; Föllmi, 1996; Weissert *et al.*, 1998, Wortmann and Weissert, 2000; Föllmi *et al.*, 1994, 2006, 2007). The carbon perturbation results in a $\delta^{13}C$ positive shift of about 1.7 ‰ recorded in shallow and deep-water carbonates, and of 3 to 4 ‰ in terrestrial plants (Gröcke *et al.*, 2005; Nunn *et al.*, 2010). The initiation of the $\delta^{13}C_{carb}$ positive shift occurred in the late *Busnardoides campylotoxus* ammonite zone (latest early Valanginian) and the maximum of the perturbation is reached in the *Saynoceras verrucosum* ammonite zone (earliest late Valanginian) (Hennig *et al.*, 1999; Duchamp-Alphonse *et al.*, 2007; Föllmi *et al.*, 2007). This episode was originally associated with a OAE and thought to represent the first Cretaceous OAE; recent studies have, however, demonstrated that organic-matter deposits for the Valanginian are mixed terrestrial and marine and that widespread anoxia lack for this interval (Westermann *et al.*, 2010; Kujau *et al.*, 2012).

In parallel, enhanced humidity is recorded in the NW Tethyan area during the onset of the $\delta^{13}C$ positive shift (Duchamp-Alphonse *et al.*, 2007; Fesneau, 2008; Westermann, 2010; Föllmi, 2012), which is considered as an important driver of the perturbation.

Consequently, Westermann *et al.* (2010) postulate that the storage of terrestrial organic matter on the continent in combination with the drowning of carbonate platforms may explain the Valanginian $\delta^{13}C$ positive shift. Indeed, enhanced coal and charcoal deposition occurred during the Early Cretaceous (Budyko et al., 1987; Haszeldine, 1989), favoured by the general context of the break-up of Pangaea and the formation of continental graben (Stämpfli and Borel, 2002; Föllmi, 2012). Coal depositions are known from USA, Russia, China, India, Indonesia, Australia and Canada (Ziegler et al., 1987; McCabe and Totman Parrish, 1992) for a period starting in the Berriasian up to the Hauterivian. A precise age control is difficult for continental deposits, thus the role of these deposits as a trigger for the Valanginian carbon isotope excursion remains hypothetical.

Further debated points concerning the Valanginian interval are the presence of polar ice and sea-level change. The presence of rafted deposits and glendonites is highlighted by Price (1999) and paralleled with phases of rapid and abrupt sea-level changes, and more arid climate conditions. McArthur *et al.* (2003) indicate cooler conditions in the late Valanginian using $\delta^{18}O$ and Mg/Ca measurements as temperature proxies.

These interpretations are presently debated because 1) rafted deposits are not necessary carried by icebergs but also by trees; 2) glendonites form under cold but not necessarily under freezing conditions and can additionally be related to anoxia, high alkalinity, and high P concentrations; 3) the cooling phase may not have been sufficient to have induced the formation of polar ice caps and the interpretation of the temperature proxies may have been biased by ad-hoc assumptions with regards to salinity; 4) recent TEX86 measurements across latitudes indicate warm to very warm sea surface water temperatures during the Valanginian (Litter et al., 2011); 5) Sea-level change during this period is debated (Haq *et al.*, 1987; Hardenbol *et al.*, 1998; Schlager, 1981). This latter point is relatively problematic because different authors consider the latest early and early late Valanginian characterized by a transgression (Weissert *et al.*, 1998) or as regressive (Jacquin *et al.*, 1998; Price, 1999; Gréselle and Pittet, 2010). The question of polar ice for the Valanginian is, however, not addressed in this contribution because this problem rather concerns the late Valanginian interval and the consequences of the Weissert episode (Weissert and Erba, 2004).

As a general trigger for the Valanginian episode, enhanced pCO_2 linked to the eruption of the Paraña-Etendeka continental LIP (hotspot linked with the opening of the South Atlantic ocean) is commonly evoked (Lini *et al.*, 1992; Erba *et al.*, 2004; Weissert and Erba, 2004), but the most recent age dates indicate a Hauterivian age (Thiede and Vasconcelos, 2010; Ogg *et al.*, 2008), which postdates the Weissert episode.

1.4. WHICH INCEPTION FOR THE PERTURBATION?

Important palaeoenvironmental changes precede the Valanginian Weissert episode, for which eventual causal links have not been clearly established so far (Fig. 1.4). For example, in the Vocontian Basin organic-matter rich layers are observed in sediments predating the $\delta^{13}C$ positive shift: the "Barrandes layers" dated from the *B. campylotoxus* ammonite zone testify of local and short-term anoxic conditions during the early Valanginian (Reboulet *et al.*, 2003; Westermann *et al.*, 2010). More recently, Kujau (2012) postulated a two-step increase in pCO_2 in the early Valanginian mainly on the basis of $\delta^{13}C_{org}$ trends (compared to $\delta^{13}C_{carb}$ trends) and the evolution of palynomorphs in the Vocontian Basin.

The Helvetic shelf, which records the main drowning phase in the late Valanginian-earliest Hauterivian with the condensed phosphate-rich Gemsmättli beds (*S. verrucosum* to *C. Loryi*), witnessed a precursor drowning episode in the early Valanginian documented by the Büls Beds (Kuhn, 1996; Föllmi *et al.*, 2007) dated as the late *T. pertransiens* to early *B. campylotoxus* ammonite zones (Kuhn, 1996).

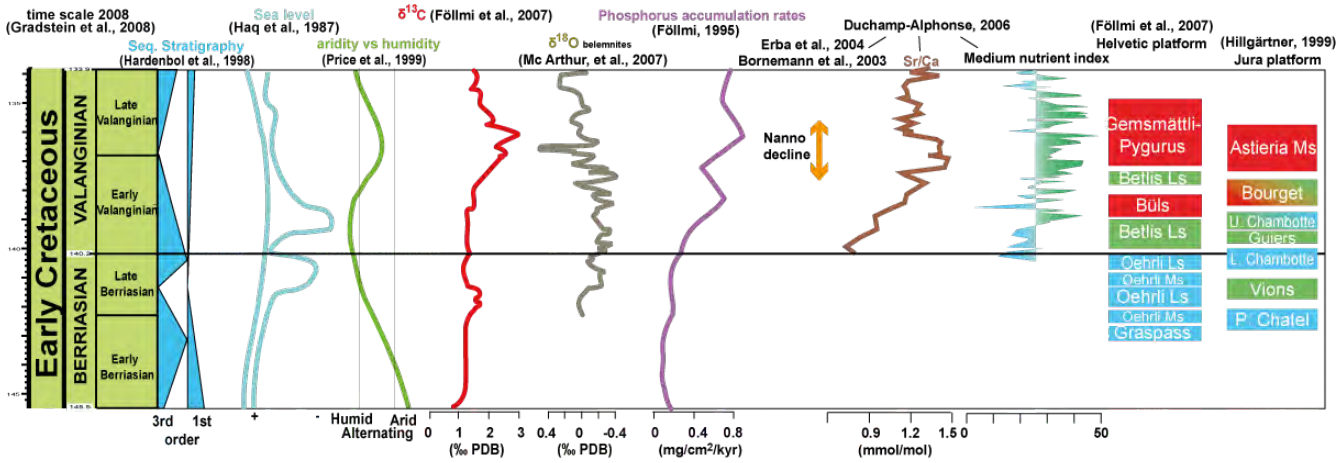

Fig. 1.4: Synthesis of palaeoenvironmental changes recorded through the Berriasian-Valanginian interval.

Moreover, the Helvetic platform records a change in floro-faunal assemblages from photozoan to heterozoan close to the Berriasian-Valanginian boundary. In the Jura, the heterozoan formations of the Calcaires Roux and Bourget Formations were partially deposited during the carbon isotope excursion (Hennig, 2003); however, questions remain open with regards to their age and sequence stratigraphic significance. With that, the correlation between the Jura and Helvetic platforms is not well assessed and the timing of the change toward heterozoan factories and the drowning phases is poorly constrained.

Condensation phases are also reported further to the north in Poland, where phosphatic levels of Valanginian age are observed (Kutek *et al.*, 1989). Again, the timing of phosphogenesis is not well established and as such the correlation with the Tethyan Realm and the Weissert episode remains unclear.

Studies carried out in the Atlantic and the Tethys demonstrated by various proxies (phosphorus accumulation rates, Sr/Ca ratio, nannofossils) that the fertilization of tropical waters already started near the Berriasian-Valanginian boundary (Duchamp-Alphonse *et al.*, 2007; Föllmi *et al.*, 2007; Bornemann and Mutterlose, 2008). This raises the question of the onset of the perturbation.

The Berriasian is also a period of palaeoclimatic and palaeoenvironmental changes. Various authors indicate a progressively enhanced humidity starting already in the early Berriasian (Persoz and Remane, 1976; Adatte, 1988; Hallam *et al.*, 1991; Deconinck, 1993; Price, 1999; Schnyder *et al.*, 2005, 2006; Lindström and Erlström, 2011). Sea-level changes of large amplitude are recorded (Haq *et al.*, 1987; Blanc, 1996; Jacquin *et al.*, 1998; Gréselle, 2007). The Jura platform witnessed a period of mesotrophic conditions with the deposition of the Vions Formation and Unité Supérieure Gréseuse in the early late Berriasian (Blanc, 1996; Hillgärtner, 1999), which might be viewed as one of the premises of the Weissert episode.

1.5. GOALS OF THE THESIS AND PROCEDURE

The goal of this contribution is to reconstruct the palaeoclimatic and palaeoenvironmental conditions, which were present before the Valanginian $\delta^{13}C_{carb}$ shift in order to evaluate its importance as a potential trigger of the Weissert episode.

Basinal sections provide a relatively complete record, and their hemipelagic to pelagic sediments allow for series of geochemical and investigations. Because carbonate platforms are at the interface between the marine and the continental realms, they are very sensitive to environmental changes and constitute a key record for the understanding of the Berriasian-Valanginian period. Platform sediments are, however, more sensitive to diagenetic effects, and the application and interpretation of geochemical data is more challenging.

A focus on the NW margin of the Tethys is presented because of the relatively good biostratigraphic control available in this area. The Vocontian Basin provides hemipelagic sections well contrained by ammonites, nannofossils, and calpionellids. The Jura platform is relatively well dated (benthic foraminifera, green algae, ostracods, and sparse calpionellids and ammonites). A first important goal of this thesis is thus to establish a platform-basin transect from the Jura platform to the Vocontian Basin.

This is possible by the application of biostratigraphic, sequence-stratigraphic and chemostratigraphic tools, which permit to constrain sea-level changes, continental detrital fluxes, nutrient increases, ecological changes and changes in the platform architecture.

A second goal of this contribution is to apply a similar approach to a selection of sections of the Helvetic platform, which represents the more distal part of the northern Tethyan platform and its transition into the outer shelf. Particular attention was paid to the establishment of an age model and a correlation with the Jura record. This also allows the identification of autocyclic and allocyclic sedimentary changes.

A third goal of this thesis was an investigation of the uppermost Berriasian and Valanginian deposits of the Polish Basin and the associated record of the palaeoenvironmental changes. The correlation of the Polish data with the Jura and Helvetic platform and the Vocontian Trough permits to highlight more general palaeoenvironmental changes.

The fourth and final goal of this thesis is the evaluation of pCO_2 as a potential trigger for the palaeoenvironmental and palaeoclimatic changes highlighted in the preceding chapters. A focus on the carbon cycle perturbation is carried out in the hypostratotypic section of Angles (Vocontian Basin), with a comparison of the organic and inorganic carbon isotope records.

References

Adatte, T. (1988) *Etude sédimentologique, minéralogique, micropaléontologique et stratigraphique du Berriasien - Valanginien du Jura central.*, Neuchatel, Neuchatel, 481 pp.

Arthur, M.A. and Schlanger, S.O. (1979) Cretaceous "Oceanic Anoxic Events" as Causal Factors in Development of Reef-Reservoired Giant Oil Fields. *The American Association of Petroleum Geologists Bulletin*, **63,** 870-885.

Barbarin, N., Bonin, A., Mattioli, E., Pucéat, E., Cappetta, H., Gréselle, B., Pittet, B., Vennin, E. and Joachimski, M. (2012) Evidence for a complex Valanginian nannoconid decline in the Vocontian basin (South East France). *Marine Micropaleontology*, **84,** 37-53.

Barbu, V. and Melinte-Dobrinescu, M.C. (2008) Latest Jurassic to earliest Cretaceous paleoenvironmental changes in the Southern Carpathians, Romania: regional record of the late Valanginian nutrification event. *Cretaceous Research*, **29,** 790-802.

Blanc, E. (1996) *Transect plate-forme - bassin dans les séries carbonatées du Berriasien supérieur et du Valanginien inférieur (domaines Jurassiens et nord-Vocontien). Chronostratigraphie et transferts de sédiments.*, Joseph Fournier, Grenoble, 312

pp.

Bornemann, A. and Mutterlose, J. (2008) Calcareous nannofossil and d13C records from the Early Cretaceous of the Western Atlantic ocean: evidence of enhanced fertilization accross the Berriasian-Valanginian transition. *palaios*, **23,** 821-832.

Budyko, M.I., Ronov, A.B. and Yanshin, A.L. (1987) *History of the Earth's Atmosphere*. Springer-Verlag, 139 pp.

Courtillot, V.E. and Renne, P.R. (2003) On the ages of flood basalt events. *Comptes Rendus Geosciences*, **335,** 113-140.

Chumakov, N.M. (1995) The problem of warm biosphere. *Stratigraphy and Geological Correlation*, **3,** 205-215.

Deconinck, J.-F. (1993) Clay Mineralogy of the Late Tithonian-Berriasian deep-sea carbonates of the Vocontian trough (SE France): Relationships with sequence stratigraphy. *Bull. Centres Rech. Explor.-Prod. Elf Aquitaine*, **17,** 222-234.

Duchamp-Alphonse, S., Gardin, S., Fiet, N., Bartolini, A., Blamart, D. and Pagel, M. (2007) Fertilization of the northwestern Tethys (Vocontian basin, SE France) during the Valanginian carbon isotope perturbation: Evidence from calcareous nannofossils and trace element data. *Palaeogeography, Palaeoclimatology, Palaeoecology*, **243,** 132-151.

Haszeldine, R.S. (1989) Coal reviewed: depositional controls, modern analogues and ancient climates. In: *Deltas: Sites and Traps for Fossil Fuels* (Eds M.K.G. Whaetely and K.T. Pickering), **41**, pp. 289-308. Geological Society, London, Special Publications.

Erba, E. (2004) Calcareous nannofossils and Mesozoic oceanic anoxic events. *Marine Micropaleontology*, **52,** 85-106.

Erba, E., Bartolini, A. and Larson, R.L. (2004) Valanginian Weissert oceanic anoxic event. *Geology*, **32,** 149-152.

Fesneau, C. (2008) *Enregistrement des changements climatiques dans le domaine Téthysien au Valanginien*, Université de Bourgogne, Dijon, 340 pp.

Föllmi, K.B. (1996) The phosphorus cycle, phosphogenesis and marine phosphate-rich deposits. *Earth-Science Reviews*, **40,** 55-124.

Föllmi, K.B., Godet, A., Bodin, S. and Linder, P. (2006) Interactions between environmental change and shallow water carbonate buildup along the northern Tethyan margin and their impact on the Early Cretaceous carbon isotope record. *Paleoceanography*, **21,** PA4211.

Föllmi, K.B., Bodin, S., Godet, A., Linder, P. and van de Schootbrugge, B. (2007) Unlocking paleo-environmental information from Early Cretaceous shelf sediments in the Helvetic Alps: stratigraphy is the key! *Swiss journal of geosciences*, **100,** 349-369.

Föllmi, K.B. (2012) Early Cretaceous life, climate and anoxia. *Cretaceous Research*, **35,** 230-257.

Frakes, L.A. (1979) *Climates Throughout Geologic Time*. Elsevier, 322 pp.

Funk, H., Föllmi, K.B. and Mohr, H.M. (1993) Evolution of the Tithonian-Aptian Carbonate Platform along the Northern Tehyan Margin, Eastern Helvetic Alps. In: *Cretaceous Carbonate Platforms* (Eds J.A.T. Simo, R.W. Scott and J.-P. Masse),

pp. 387-408. American Association of Petroleum Geologists, Tulsa.

Gréselle, B. and Pittet, B. (2010) Sea-level reconstructions from the Peri-Vocontian Zone (South-east France) point to Valanginian glacio-eustasy. *sedimentology*, **57,** 1640-1684.

Gröcke, D.R., Price, G.D., Robinson, S.A., Baraboshkin, E.Y., Mutterlose, J. and Ruffell, A.H. (2005) The Upper Valanginian (Early Cretaceous) positive carbon-isotope event recorded in terrestrial plants. *Earth and Planetary Science Letters*, **240,** 495-509.

Hallam, A., Grose, J.A. and Ruffell, A.H. (1991) Palaeoclimatic significance of changes in clay mineralogy across the Jurassic-Cretaceous boundary in England and France. *Palaeogeography, Palaeoclimatology, Palaeoecology*, **81,** 173-187.

Haq, B.U., Hardenbol, J. and Vail, P.R. (1987) Chronology of Fluctuating Sea Levels Since the Triassic. *Science*, **235,** 1156-1167.

Hardenbol, J., Thierry, J., Farley, M.B., Jacquin, T., De Graciansky, P.-C. and Vail, P.R. (1998) Mesozoic and cenozoic sequence statigraphy of european basins. Mesozoic and Cenozoic sequence chronostratigraphic framework of european basins. . *SEPM (Society for Sedimentary Geology)*, **Special Publication 60**.

Hay, W.W. and Floegel, S. New thoughts about the Cretaceous climate and oceans. *Earth-Science Reviews*, **115,** 262-272.

Hallock, P. and Schlager, W. (1986) Nutrient excess and the demise of coral reefs and carbonate platforms. *palaios*, **1,** 389-398.

Hennig, S. (2003) *Geochemical and sedimentological evidence for environmental changes in the Valanginian (early Cretaceous) ofthe Tethys region*, ETH Zurich, 189 pp.

Hennig, S., Weissert, H. and Bulot, L.G. (1999) C-isotope stratigraphy, a calibration tool between ammonite- and magnetostratigraphy. *Geologica Carpathica*, **50,** 91-96.

Hickey, L.J. and Doyle, J.A. (1977) Early Cretaceous fossil evidence for angiosperm evolution. *The Botanical Review*, **43,** 3-104.

Hillgärtner, H. (1999) *The evolution of the French Jura platform during the Late Berriasian to Early Valanginian: controlling factors and timing*, Université de Fribourg, Fribourg, 203 pp.

Höfling, R. and Scott, R.W. (2002) Early and Mid-Cretaceous Buildups. *SEPM (Society for Sedimentary Geology)*, **Spec. pub. 72,** 521-548.

Jacquin, T., Rusciadelli, G., Amédro, F., De Graciansky, P.-C. and Magniez-Jannin, F. (1998) The North Atlantic cycle: an overview of 2nd-order transgressive/regressive facies cycle in the Lower Cretaceous of Western Europe. *SEPM (Society for Sedimentary Geology) Special Publication*, **60,** 397-409.

James, N.P. (1997) *The cool-water carbonate depositional realm*. SEPM, special publication. 440 pp.

Jenkyns, H.C. (1980) Cretaceous anoxic events: from continents to oceans. *Journal of the Geological Society*, **137,** 171-188.

Krell, F.-T. (2000) The fossil record of Mesozoic and Tertiary Scarabaeoidea (Coleoptera: Polyphaga). *Invertebrate Taxonomy*, **14,** 871-905.

Kuhn, O. (1996) *Der Einfluss von Verwitterung auf die Paläozeanographie zu Beginn des Kreide-Treibhausklimas (Valanginian und Hauterivian) in der West-Tethys*, Eidgenössische Technische Hochschule Zürich, 380 pp.

Kujau, A. (2012) *Climatic and environmental dynamics during the Valanginian carbon isotope event - Evidence from geochemistry and palynology*, Ruhr Universität, Bochum, 175 pp.

Kujau, A., Heimhofer, U., Ostertag-Henning, C., Gréselle, B. and Mutterlose, J. (2012) No evidence for anoxia during the Valanginian carbon isotope event - an organic-geochemical study from the Vocontian Basin, SE France. *Global and Planetary Change*, **doi: 10.1016/j.gloplacha.2012.04.007**.

Kutek, J., Marcinowski, R. and Wiedmann, J. (1989) The Wąwał Section, Central Poland - An important Link between Boreal and Tethyan Valanginian In: *Cretaceous of the Western Tethys.* (Ed J. Wiedmann), pp. 717-754. Proceedings of the 3rd International Cretaceous Symposium, Tübingen.

Larson, R.L. (1991) Latest pulse of Earth: Evidence for a mid-Cretaceous superplume. *Geology*, **19,** 547-550.

Larson, R.L. and Erba, E. (1999) Onset of the mid-Cretaceous greenhouse in the Barremian-Aptian: Igneous events and the biological, sedimentary, and geochemical responses during the Early Cretaceous (Valanginian-Hauterivian): Evidence from oxygen and carbon stable isotope. *Paleoceanography*, **14,** 663-678.

Lidgard , S. and Crane, P.R. (1990) Angiosperm diversification and Cretaceous floristic trends: A comparison of palynofloras and leaf macrofloras. *Paleobiology*, **16,** 77-93.

Lindström, S. and Erlström, M. (2011) The Jurassic-Cretaceous transition of the Fårarp-1 core, southern Sweden: Sedimentological and phytological indications of climate change. *Palaeogeography, Palaeoclimatology, Palaeoecology*, **308,** 445-475.

Lini, A., Weissert, H. and Erba, E. (1992) The Valanginian carbon isotope event: a first episode of greenhouse conditions during the Cretaceous. *Terra Nova*, **4,** 374-384.

Littler, K., Robinson, S.A., Bown, P.R., Nederbragt, J. and Pancost, R.D. (2011) High sea-surface temperatures during the Early Cretaceous Epoch. *Nature geosciences*, **4,** 169-172.

Masse, J.P. (1992) The Lower Cretaceous Mesogean benthic ecosystems: palaeoecologic aspects and palaeobiogeographic implications. *Palaeogeography, Palaeoclimatology, Palaeoecology*, **91,** 331-345.

Masse, J.P. and Philip, J. (1981) Cretaceous coral-rudistid buildups of France. *SEPM Special publication*, **30,** 399-426.

Mayhew, P.J. (2002) Shifts in hexapod diversification and what Haldane could have said. *Proceedings of the Royal Society of London*, **269,** 969-974.

Mc Arthur J.M., Janssen N.M.M., Reboulet S., Leng, M.J., M.F., T. and B, V.D.S. (2007) Palaeotemperatures, polar ice-volume, and isotope stratigraphy (Mg/Ca, δ18O, δ13C, 87Sr/86Sr): The Early Cretaceous (Berriasian, Valanginian, Hauterivian). *Palaeogeography, Palaeoclimatology,Palaeoecology*, **248,** 341-430.

McCabe, P.J. and Totman Parrish, J. (1992) Tectonic and climatic controls on the

distribution and quality of Cretaceous coals. In: *Controls on the Distribution and Quality of Cretaceous Coals* (Eds P.J. McCabe and J. Totman Parrish), **267**, pp. 1-16. The Geological Society of America, Special Publication.

Mort, H.P. (2006) *Biogeochemical Changes during the Cenomanian-Turonian Oceanic Anoxic Event (OAE 2)*, Université de Neuchâtel, Neuchâtel, 205 pp.

Mostovski, M.B., Jarzembowski, E.A., Coram, R.A. and Ansorge, J. (2000) Curious snipe-flies (Diptera: Rhagionidae) from the Purbeck of Dorset, the Wealden of the Weald and the Lower Cretaceous of Spain and Transbaikalia. *Proceedings of the Geologists Association*, **111,** 153-160.

Mostovski, M.B., Jarzembowski, E.A. and Coram, R.A. (2003) Horseflies and athericids (Diptera: Tabanidae, Athericidae) from the Lower Cretaceous of England and Transbaikalia. *Paleontological Journal*, **37,** 162-169.

Nunn, E.V., Price, G.D., Gröcke, D.R., Baraboshkin, E.Y., Leng, M.J. and Hart, M.B. (2010) The Valanginian positive carbon isotope event in Arctic Russia: Evidence from terrestrial and marine isotope records and implications for global carbon cycling. *Cretaceous Research*, **31,** 577-592.

Ogg, J.G., Ogg, G. and Gradstein F.M. (2008) The Concise Geologic Time scale, pp. 177. Cambridge University press.

Persoz, F. and Remane, J. (1976) Minéralogie et géochiie des formations à la limite Jurassique-Crétacé dans le Jura et le Bassin Vocontien. *Eclogae Geologicae Helveticae*, **69,** 1-38.

Philip, J. (2003) Peri-Tethyan neritic carbonate areas: distribution through time and driving factors. *Palaeogeography, Palaeoclimatology, Palaeoecology*, **196,** 19-37.

Price, G.D. (1999) The evidence and implications of polar ice during the Mesozoic. *Earth-Science Reviews*, **48,** 183-210.

Reboulet, S., Mattioli, E., Pittet, B., Baudin, F., Olivero, D. and Proux, O. (2003) Ammonoid and nannoplankton abundance in Valanginian (early Cretaceous) limestone-marl successions from the southeast France Basin: carbonate dilution or productivity? *Palaeogeography, Palaeoclimatology, Palaeoecology*, **201,** 113-139.

Rullkötter, R. (2000) Organic matter: The driving force for early diagenesis. In: *Marine Geochemistry* (Eds H.D. Schulz and M. Zabel), pp. 129-172. Springer.

Schlager, W. (1981) The paradox of drowned reefs and carbonate platforms. *Geological Society of America Bulletin*, **92,** 197-211.

Schlanger, S.O. and Jenkyns, H.C. (1976) Cretaceous oceanic anoxic events: causes and consequences. . *Geologie en Mijnbouw*, **55,** 179-184.

Schnyder, J., Gorin, G., Soussi, M., Baudin, F. and Deconinck, J.-F. (2005) Enregistrement de la variation climatique au passage Jurassique/Crétacé sur la marge sud de la Téthys : minéralogie des argiles et palynofaciès de la coupe du Jebel Meloussi (Tunisie centrale, formation Sidi Kralif). *Bulletin de la société géologique de France*, **176,** 171-182.

Schnyder, J., Ruffell, A., Deconinck, J.-F. and Baudin, F. (2006) Conjunctive use of spectral gamma-ray logs and clay mineralogy in defining late Jurassic-early Cretaceous palaeoclimate change (Dorset, U.K.). *Palaeogeography, Palaeoclimatology, Palaeoecology*, **229,** 303-320.

Stampfli, G.M. and Borel, G.D. (2002) A plate tectonic model for the Paleozoic and Mesozoic constrained by dynamic plate boundaries and restored synthetic oceanic isochrons. *Earth and Planetary Science Letters*, **196,** 17-33.

Scotese, C.R. (2002) Paleomap Project. *http://www.scotese.com/*

Skelton, P. (2003) *The Cretaceous World*. The Open University, Milton Keynes, UK.

Thiede, D.S. and Vasconcelos, P.M. (2010) Paraná flood basalts: Rapid extrusion hypothesis confirmed by new 40Ar/39Ar results. *Geology*, **38,** 747-750.

Vakhrameev, V.A. (2010) *Jurassic and Cretaceous Floras and Climates of the Earth*. Cambridge University Press.

Weissert, H. and Erba, E. (2004) Volcanism, CO2 and palaeoclimate: a Late Jurassic–Early Cretaceous carbon and oxygen isotope record. *Journal of the Geological Society, London*, **161,** 1-8.

Weissert, H., Lini, A., Föllmi, K.B. and Kuhn, O. (1998) Correlation of Early Cretaceous carbon isotope stratigraphy and platform drowning events: a possible link? *Palaeogeography, Palaeoclimatology, Palaeoecology*, **137,** 189-203.

Westermann, S. (2010) *Trace-element and phosphorus contents in sediments associated with Cretaceous anoxic events*, Université de Lausanne, 223 pp.

Westermann, S., Föllmi, K.B., Adatte, T., Matera, V., Schnyder, J., Fleitmann, D., Fiet, N., Ploch, I. and Duchamp-Alphonse, S. (2010) The Valanginian $\delta^{13}C$ excursion may not be an expression of a global oceanic anoxic event. *Earth and Planetary Science Letters*, **290,** 118-131.

Wortmann, U.G. and Weissert, H. (2000) Tying platform drowning to perturbations of the global carbon cycle with a $\delta^{13}C_{org}$ -curve from the Valanginian of DSDP Site 416. *Terra Nova*, **12,** 289-294.

Ziegler, P.A., Raymond, A.L., Gierlowski, T.C., Horell, M.A., Rowley, D.B. and Lottes, A.L. (1987) Coal, climate and terrestrial productivity: the present and early Cretaceous compared. In: *Coal and coal-bearing strata: Recent advances* (Ed A.C. Scott), **32**, pp. 25-49. Geological Society, London, Special Publications.

CHAPTER 2:

BERRIASIAN AND EARLY VALANGINIAN ENVIRONMENTAL CHANGE ALONG A TRANSECT FROM THE JURA PLATFORM TO THE VOCONTIAN BASIN

2. BERRIASIAN AND EARLY VALANGINIAN ENVIRONMENTAL CHANGE ALONG A TRANSECT FROM THE JURA PLATFORM TO THE VOCONTIAN BASIN

published in Sedimentology (Special issue: Alpine sedimentology, vol.60 (1)

CHLOE MORALES*, SILVIA GARDIN**, JOHANN SCHNYDER**, JORGE SPANGENBERG*, ANNIE ARNAUD-VANNEAU***, HUBERT ARNAUD***, THIERRY ADATTE* and KARL B. FÖLLMI*

**Institute of Earth Sciences, Université de Lausanne, Géopolis, 1015 Lausanne, Switzerland (E-mail: chloe.morales@unil.ch)*

***University Pierre and Marie Curie, ISTeP, UMR7193, Case 117, 4, place Jussieu, 75252 Paris Cedex 05*

****Association Dolomieu, 18 boulevard Maréchal Leclerc, 38000 Grenoble, France*

ABSTRACT

Valanginian sedimentary archives display a positive anomaly in the carbon-isotope record which is associated with a crisis in neritic and pelagic carbonate production. This study aims to reconstruct the evolution of palaeoenvironments in the Jura area and the Vocontian Basin during late Berriasian and early Valanginian times, in order to better understand the controlling factors leading to the Valanginian episode of major environmental change. Three sections along a transect through the Jura platform (Switzerland and France) and the Vocontian Basin (France) have been studied. Stratigraphic correlations have been established by combining biostratigraphy (benthic foraminifera, ammonites and calpionellids), with geochemistry ($\delta^{13}C$ trends) and sequence stratigraphy. A change from a rimmed ramp to a swell-dominated ramp morphology is observed through the Berriasian–Valanginian boundary. The disappearance of the barrier appears to have been controlled by large sea-level variations in combination with the arrival of significantly more humid climate conditions. This barrier played a major role in the distribution of geochemical, mineralogical and palynological fluxes toward the basin: during the Berriasian, continental fluxes (detrital particles, nutrients, pollen and spores) were buffered by the platform morphology, whereas in the early Valanginian they were more readily transported toward the basin. The initiation of a major transgression onto lateritic soils, leading to their intense reworking, instigated a fertilisation of ocean waters during the earliest Valanginian and with that a change toward heterozoan carbonate production and subsequently to the demise of the already weakened carbonate platform.

Keywords: Climate change, Berriasian, Valanginian, Carbonate platform, Jura Mountains, Vocontian Basin

2.1. INTRODUCTION

The Valanginian stage is known for major perturbations in neritic and pelagic carbonate production (Masse and Philip, 1981; Weissert *et al.*, 1998; Föllmi *et al.*, 2007). Palaeoenvironmental change preceding and leading to these perturbations appears to have occurred during the earliest Valanginian and eventually during the latest Berriasian (Kuhn, 1996; Föllmi, 2012).

Along the northern Tethyan margin, an important phase of platform growth started in the early Berriasian, thereby replacing the lagoonal and brackish environments which characterise the so-called 'Purbeck beds'. This phase ended in the early late Valanginian with a crisis in carbonate production (Masse and Philip, 1981; Föllmi *et al.*, 1994, 2007; Föllmi, 2012; Weissert *et al.*, 1998). The platform drowning phase goes along with a global perturbation of the carbon cycle manifested by the aforementioned positive $\delta^{13}C$ shift of about 1.5 to 2‰ recorded both in platform and basinal environments (Lini, 1992; Hennig, 2003), a decline in calcareous nannofossil abundance in pelagic settings (Erba, 2004), and the widespread occurrence of condensed layers and hiati in platform and shelf environments in general (Masse and Phillip, 1981; Funk *et al.*, 1993; Föllmi *et al.*, 1994, 2007; Weissert *et al*., 1998). The latter are interpreted as platform-drowning unconformities, which include the time span between the *Saynoceras verrucosum* and *Crioceratites loryi* ammonite zones (early late Valanginian to middle early Hauterivian) in the Jura, the Helvetic and the Provence platforms (Kuhn, 1996; Hennig, 2003; Föllmi *et al.*, 2007). In some cases, an earlier platform drowning phase is observed, such as in the Helvetic domain (late *Tirnovella pertransiens* and early *Busnardoites campylotoxus* zones: middle early Valanginian; Wyssling, 1986; Kuhn, 1996; Föllmi *et al.*, 2007) and, in other cases, a persistence in platform growth is documented, such as on the Provence platform (in Olioulles; Bonin, 2011). This time of major palaeoenvironmental change has been called Weissert episode (Erba *et al.*, 2004; Föllmi, 2012).

Between its installation in the early Berriasian and its demise in the early late Valanginian, the Tethyan carbonate platform witnessed several modifications linked to changes in sea-level, climate and nutrient stocks. For instance, ecological modifications leading to a change from photozoan to heterozoan carbonate production are observed at the Berriasian–Valanginian boundary in the Helvetic Province. In the Jura, these changes are different: Blanc (1996) and Hillgärtner (1999) observed repeated changes from oligotrophic to mesotrophic conditions in the late Berriasian, and the persistence of oligotrophic environments in the early Valanginian.

Moreover, major changes in climate conditions and associated humidity have been inferred for the western European area from the early Berriasian onwards (Adatte, 1988; Hallam *et al*., 1991; Deconinck, 1993; Price, 1999; Schnyder *et al.*, 2005, 2006; Lindström and Erlström, 2011). Independently, various proxies indicate that the Tethyan basins underwent a phase of enhanced fertilization after the earliest Valanginian (Föllmi,

1995; Duchamp Alphonse *et al.*, 2007) and were the subject of presumed cooling after the late early Valanginian (McArthur *et al.*, 2003).

The timing of these environmental changes within the platform is not always well established; this is due, in particular, to the difficulty of obtaining detailed age control in shallow-water sections. Moreover, sequence-stratigraphic and sea-level interpretations differ for the considered period (Arnaud *et al.*, 1981; Blanc, 1996; Pasquier and Strasser, 1997; Hennig *et al.*, 1999; Hillgärtner and Strasser, 2003; Gréselle and Pittet, 2010). Useful and correlatable platform $\delta^{13}C$ records from this period are relatively sparse, which is partly related to diagenetic distortion of the isotope signal (Pasquier and Strasser, 1997; Hennig, 2003; Gréselle, 2007). Consequently, correlations with basinal settings remain problematic, and knowledge of the factors and mechanisms of palaeoenvironmental change preceding and possibly triggering the Weissert episode (Erba *et al.*, 2004) is correspondingly limited.

This study aims to: (i) establish a stratigraphical framework for shallow-water sections of the Jura platform by combining the already existing benthic foraminiferal stratigraphy with a revised calpionellid stratigraphy and the $\delta^{13}C$ record for the late Berriasian/early Valanginian interval; (ii) construct a new sequence stratigraphic model to better understand sea-level variations; (iii) correlate shallow-water and hemipelagic sections on the basis of the above-mentioned data; and (iv) implement the existing palaeoenvironmental datasets in order to compare platform and basin records and better understand the climate and environmental history of the Jura area during the late Berriasian/early Valanginian interval.

For this purpose, the key sections of Juracime (western Switzerland), La Chambotte (eastern France) and Montclus (south-eastern France) have been chosen to establish a proximal/distal transect. The selection of the sections depended on the representativeness of the Jura record for proximal areas (Juracime) or their relative completeness for outer platform areas and the adjacent basin (La Chambotte and Montclus). Furthermore, the selected sections are known for their weak diagenetic overprint (Darsac, 1983; Adatte, 1988).

With the elaboration of this transect, and with the use of isotope ($\delta^{13}C$), mineralogical (whole-rock and clay fraction), geochemical (phosphorus contents) and palynological analyses, a correlation between the Jura platform and the Vocontian basin is proposed, and the implications of our data for the reconstruction of sea-level variations, climate change, ecological modifications and platform morphology during the late Berriasian and early Valanginian are discussed.

2.2. GEOLOGICAL SETTING

2.2.1. The Jura platform

The sections of Juracime and La Chambotte are composed of platform carbonate and belong to the Neuchâtel and southern Jura, respectively (Fig. 2.1). The Juracime section is situated close to the village of Cornaux (canton of Neuchâtel, western Switzerland), in a quarry (operated by Juracime SA) within the anticline of Serroue (47° 2' 16.4976" N, 7° 0' 20.6778" E).

In the Juracime section, Berriasian and lowermost Valanginian sediments crop out with a total thickness of 30 m, which is representative of very near-shore settings. The Berriasian transgression onto Purbeck beds is documented by the succession of marine shallow-water carbonates composed by the formations of the 'Unité Inférieure Oolitique', the 'Unité Moyenne Calcaire Massive' and the 'Unité Supérieure Gréseuse' [Charollais and Steinhauser (1971) outcrop images are shown in Fig. 2.2A].

The 'Unité Inférieure Oolitique' mainly consists of oolitic facies typical of highly hydrodynamic conditions; the 'Unité Moyenne Calcaire Massive' is characterised by mudstone including bird's eyes and epikarst, which indicates a lagoonal environment with episodic emersions; and the overlying 'Unité Supérieure Gréseuse' is composed of bioclastic packstone with higher quartz contents (Charollais and Steinhauser, 1971; Adatte, 1988; Blanc, 1996). At the top of the "Unité Supérieure Gréseuse", a succession of (at least) three erosional surfaces is observed (Fig. 2.2B and C): two of them are karstified, and the highest one is strongly erosive and marks the base of the deposits of the Calcaire Roux Formation. Moreover, the absence of marker foraminifera in this interval (between 26 m and 27 m) just below the base of the Calcaire Roux Formation prevents biostratigraphic age control for this interval. The uppermost erosional surface, at the base of the Calcaire Roux Formation, is furthermore reported from many sections in the Jura (Steinhauser, 1969; Steinhauser and Charollais, 1971).

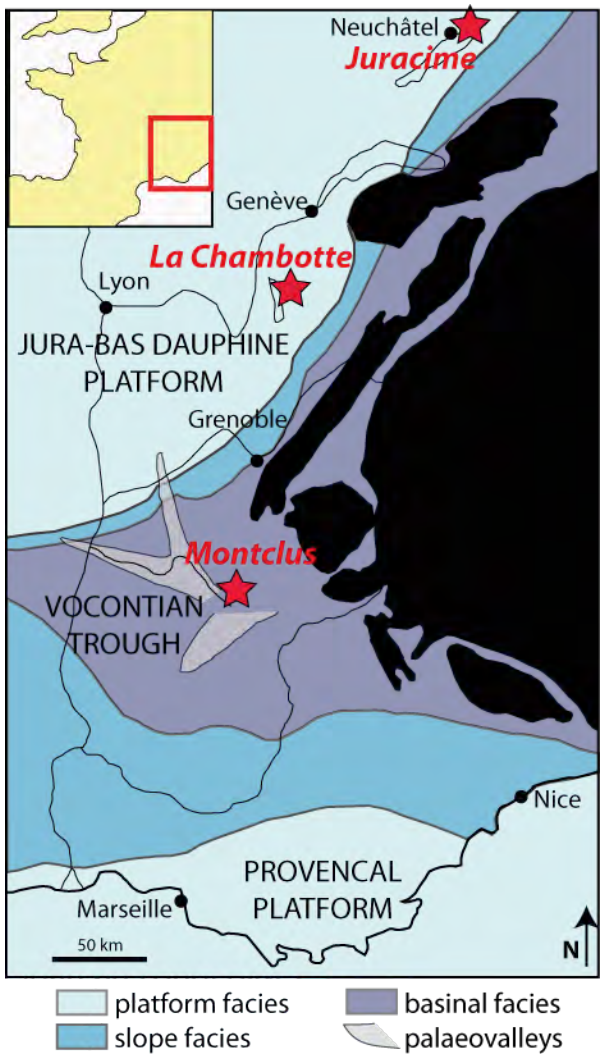

Fig. 2.1: Location of the studied sections: Juracime (Neuchâtel, Switzerland), La Chambotte and Montclus (SE France).

The age control of the Juracime section relies on benthic foraminifera (Blanc, 1996), which indicate an early Berriasian age for the ‘Unité Inférieure Oolitique’ and ‘Unité Moyenne Calcaire Massive’, and a late Berriasian age for the ‘Unité Supérieure Gréseuse’.

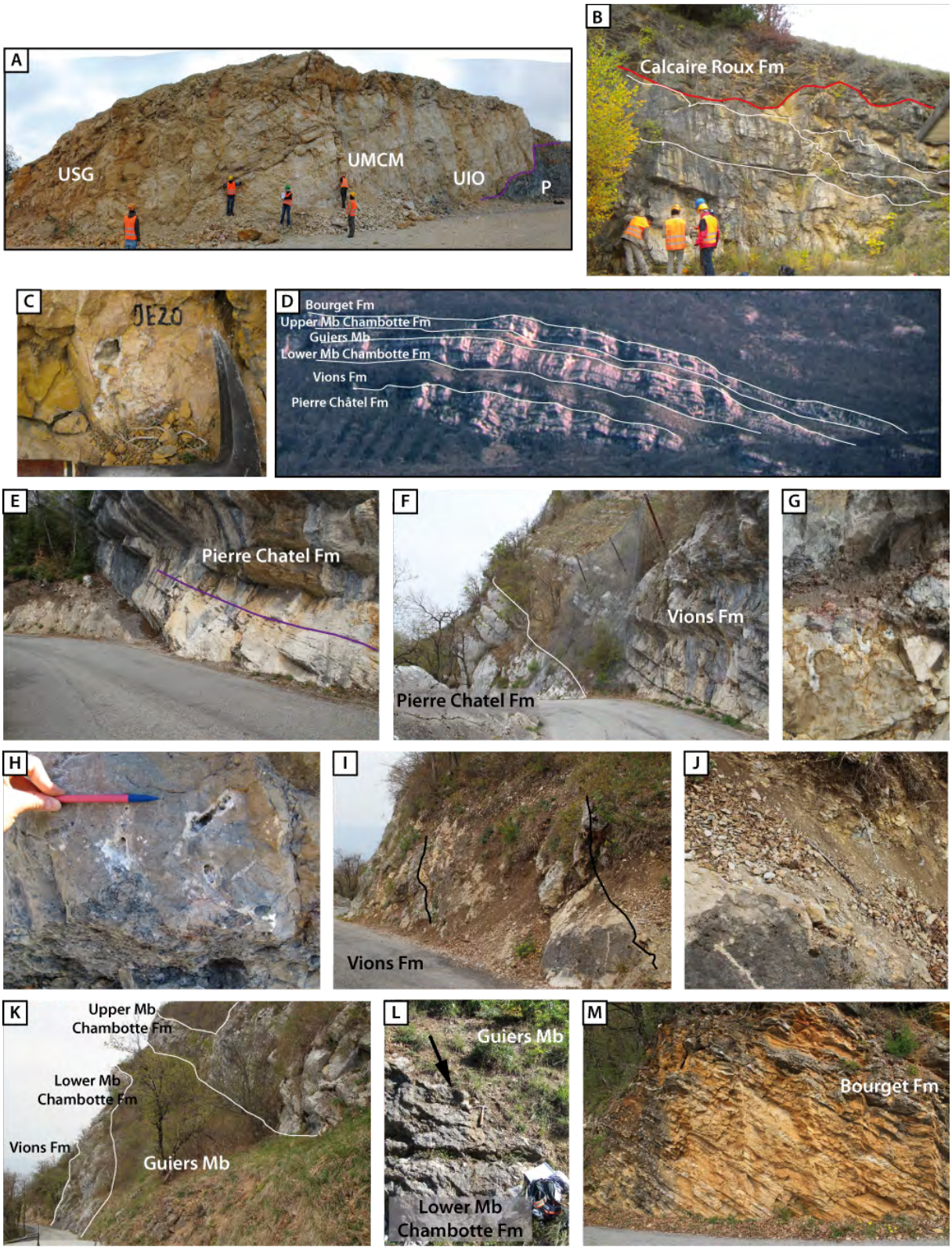

Fig. 2.2: Stratigraphical and sedimentological observations in the Juracime quarry (A) to (C) and La Chambotte section (D) to (M).
(A) Berriasian marine carbonate deposits [Unité Inférieure Oolitique (UIO), Unité Moyenne Calcaire Massive (UMCM) and Unité Supérieure Gréseuse (USG) Formations] lying on top of the Purbeckian (P). Persons for scale are *ca* 1.8 m tall. (B) Erosional surface within the Calcaire Roux Formation on top of the highly karstified Unité Supérieure Gréseuse Formation (emersive surfaces in white). (C) Detail of a root trace in the Unité Supérieure Gréseuse Formation; for scale, the total length of the hammer is 29 cm. (D) General view of the La Chambotte section; the outcropping serie is about 130 m high. (E) The prominent and thickly bedded succession of the Pierre Châtel Formation. Purple line: sequence boundary a; for scale, the recessive marly interval is 45 cm thick. (F) Marked difference of competence between the Pierre Châtel and the Vions Formations. (G) Palaeosol within the Vions Formation corresponding to SBb. (H) Root traces, Vions Formation (length of the pen: 15 cm). (I) Emersive surfaces at the top of the Vions Formation (left surface: SBc, corresponding to *d1* of Darsac, 1983; right surface: SBd). Distance between SBc and SBd: 6 m. (J) Detail of the highest epikarst of the Vions Formation (field of view measurement: 60 cm). (K) Difference of competence between the Vions Formation, the Lower and Upper Members of the Chambotte Formation (of 26 and 16.5 m thick, respectively), and the Guiers Member (15 m thick). (L) Epikarst at the top of the lower Member of the Chambotte Formation (for scale, the hammer is 29 cm long). (M) Hydrodynamic iron and silica-rich facies of the Bourget Formation: submarine dune structure with centimetric white chert layers.

Adatte (1988) found a reworked *Pfenderina neocomiensis* in the Calcaire Roux Formation suggesting that it post-dates the Berriasian. A late Valanginian age is suggested by Steinhauser and Charollais (1971) who proposed a correlation with the Bourget Formation in the meridional Jura (assessed by Blanc, 1996, by sequence stratigraphy) whereas Donze and Thieuloy (1975) proposed an early Valanginian age based on ostracod biostratigraphy.

The La Chambotte section is located above the Bourget Lake (eastern France), and crops out within the western flank of the Gros Foug anticline (45° 47' 12.7896", N 5° 51' 55.0296" E; Fig. 2.1). It has been well-studied (Steinhauser, 1969; Darsac, 1983; Arnaud Vanneau and Arnaud, 1991; Charollais *et al.*, 1992; Blanc, 1996; Hillgärtner, 1999; Gréselle, 2007) because it is one of the most complete sections of the Jura area (Blanc, 1996) and influenced by only minor burial diagenesis as shown by clay-mineralogical analyses (Darsac, 1983). The section is dated by benthic foraminifera, green algae, charophytes and calpionellids (Darsac, 1983; Charollais *et al.*, 1992; Blanc, 1996), the latter allowing a rather good correlation with more distal domains.

The sedimentary succession of about 130 m begins with the Pierre Châtel Formation, which follows on top of dolomitised sediments (Fig. 2.2E). The sediments overlying the Pierre Châtel Formation constitute the Vions Formation and are characterised by the superposition of lagoonal and open-marine facies enriched in siliciclastics and frequently interrupted by palaeosols and epikarst (Blanc, 1996; Hillgärtner, 1999; Fig. 2.2F, G, H and I). Calpionellids (*Calpionellopsis* sp.) of late Berriasian age have been found in this formation (Darsac, 1983; Blanc, 1996).

The overlying Lower Member of the Chambotte Formation is very similar to the Pierre-Châtel Formation with deposits of inner to open lagoonal facies depleted in quartz. The overlying Guiers Member reflects both a renewed increase in detrital fluxes and a deepening with the deposition of open-shelf sediments (Fig. 2.2). A calpionellid of latest Berriasian to earliest Valanginian age (*Lorenziella hungarica*, calpionellid zone D3/E.) has been found in this formation (Blanc, 1996). The Upper Member of the Chambotte Formation constitutes the uppermost oligotrophic sediments in the measured section with shelf to open lagoonal deposits. Biostratigraphically relevant calpionellids were not found in the Guiers Member and the overlying Upper Member of the Chambotte Formation in the section, but Deville (1990) found a specimen of *Calpionellites darderi* associated with the marker foraminifera *Montsalevia salevensis* indicating an early Valanginian age for equivalent layers in the Salève section located about 50 km NNE to La Chambotte. The early Valanginian age of the Guiers Member and Upper Member of the Chambotte Formation has been corroborated by the work of Darsac (1983) who described three ammonites within sequence C in the Revard section, below the first appearance of the marker foraminifer *Montsalevia salevensis*: *Tirnovella* cf. *alpillensis*, (late Berriasian calpionellid zone D3 after Blanc *et al.*, 1992, and Bulot and Thieuloy, 1994), *Thurmanniceras thurmanni* (late Berriasian, lowermost *Thurmanniceras otopeta* zone after Blanc and Bulot, 1992) and *Neocomites neocomiensis* (first appearance in the later part of the *T. pertransiens* zone after Bulot and Thieuloy, 1994). Similar age indications have been obtained from the Fontanil sector (12 km north towards Grenoble): in the slope section of Valetière, ammonite specimens of *Thurmanniceras pertransiens*, characteristic of the early Valanginian, have been found in a marly interval (Arnaud *et al.*, 1981), which is laterally correlated to levels containing the relevant foraminifera *Montsalevia elevate,* but which is below levels in which the first occurrence of *Monsalevia salevensis* was observed (Chapelière section; Blanc, 1996). This observation signifies that *Montsalevia salevensis* first appeared in the *T. pertransiens* ammonite zone and supports an early Valanginian age for the Guiers Member and the Upper Chambotte Formation in the La Chambotte section.

A surface has been observed on top of the Upper Member of the Chambotte Formation that has been interpreted as a hardground (Charollais *et al.*, 1992; Hillgärtner, 1999) or as a palaeosol (Gréselle, 2007); and marks the abrupt passage to the Bourget Formation. The latter is characterised by thinly layered oolitic sands rich in echinodermal debris and silica nodules (Fig. 2.2). The Bourget Formation and its lithological equivalent in the Neuchâtel Jura, the Calcaire Roux Formation, are dated by ammonites (Busnardo *et al.*, 1979) yielding an age ranging from the *T. pertransiens* to *S. verrucosum* zones.

Hennig (2003) demonstrated that the onset of the $\delta^{13}C$ positive shift, which characterises the Weissert episode, is recorded at the top of the Calcaire Roux Formation. This formation is located below the condensed layers of Astieria Marls and constitutes the last record of a carbonate platform dating from before and during the onset of the Weissert episode.

The correlation between the Neuchâtel and the southern Jura domains is principally based on benthic foraminiferal biostratigraphy. More particularly, the first occurrence (FO) and last occurrence (LO) of *Pseudotextulariella courtionnensis*, *Pavlovecina allobrogensis*, *Montsalevia elevata, Montsalevia salevensis* and *Pfenderina neocomiensis* allow for a relatively good correlation between the shallow-water sections (Darsac, 1983; Boisseau, 1987; Blanc, 1996; Figs 1 and 2).

2.2.2.The Vocontian Basin

The section of Montclus is located in the southern Alps (SE France), on the departmental road between the villages of Serres and Montclus (44° 25' 0.9222" N ; 5° 41' 25.4754" E). In Berriasian and Valanginian times, the area was an intracratonic basin fringed to the north, west and south-west by the carbonate platforms of the Jura, Ardèche and Provence, respectively (Fig. 2.1). The section of Montclus has been chosen because it displays a relatively complete record (absence of major slumps) representative of a basinal setting, and previous studies highlight the absence of major diagenetic impact, at leat in marly interbeds (Deconinck and Chamley, 1983; Deconinck *et al.*, 1985 Deconinck, 1987a;). It consists of a hemipelagic marl-limestone alternation, which is well-dated by ammonites (Le Hégarat, 1971) and calpionellids (Pasquier, 1995; Hillgärtner, 1999). Limestone lithologies dominate the base of the section (Berriasian), marly intervals become progressively important in the lowermost Valanginian and dominant at the top of the section (upper part of the lower Valanginian). A slumped interval is observed in sediments corresponding to calpionellid zone D1.

2.3. MATERIAL AND METHODS

2.3.1. Biostratigraphy

The sections of Juracime and La Chambotte were re-examined for their benthic foraminiferal and calpionellid biostratigraphies (using thin sections). The biostratigraphic framework of the basinal section of Montclus was complemented by an analysis of calcareous nannofossils: 120 samples from the marly intervals were selected and processed following standard methodology for preparation of calcareous nannofossils (the pipette straw slide method) Each slide was investigated thoroughly (300 fields of view at 1500X) to search and count nannofossil markers and key species. Calcareous nannofossil taxonomy relies mainly on Applegate & Bergen (1988), Bralower *et al.* (1989) and Bown (1998). The calcareous nannofossil scheme adopted is that established by Bralower *et al.* (1989, 1995) for the Jurassic–Cretaceous transition and that of Sissingh (1977) refined by Applegate & Bergen (1988) for the Early Cretaceous.

2.3.2. Microfacies and sequence stratigraphy

A total of 172 thin sections were used. Since the microfacies of the Juracime and La Chambotte sections have already been studied in detail (Darsac, 1983; Blanc, 1996; Hillgärtner, 1999; Gréselle, 2007), a synthesis of those studies was performed and the evolution of microfacies retraced following the classification of Arnaud-Vanneau (2005), which is detailed in Fig. 2.3. This classification was especially established for Lower Cretaceous platform carbonates and allows the identification of palaeoenvironments principally as a function of ecological associations, which themselves depend on water depth and light, nutrient availability, oxygen and salinity, temperature, nature of the substrate, sedimentation rate and hydrodynamic conditions. Twelve microfacies zones have thereby been identified, from F0 corresponding to pelagic or hemipelagic environments, to F11 which is attributed to tidal and supratidal environments. In the present study, the identified microfacies zones range from F2 to F11; for example, from the platform slope underneath the storm-weather wave base to emersive environments.

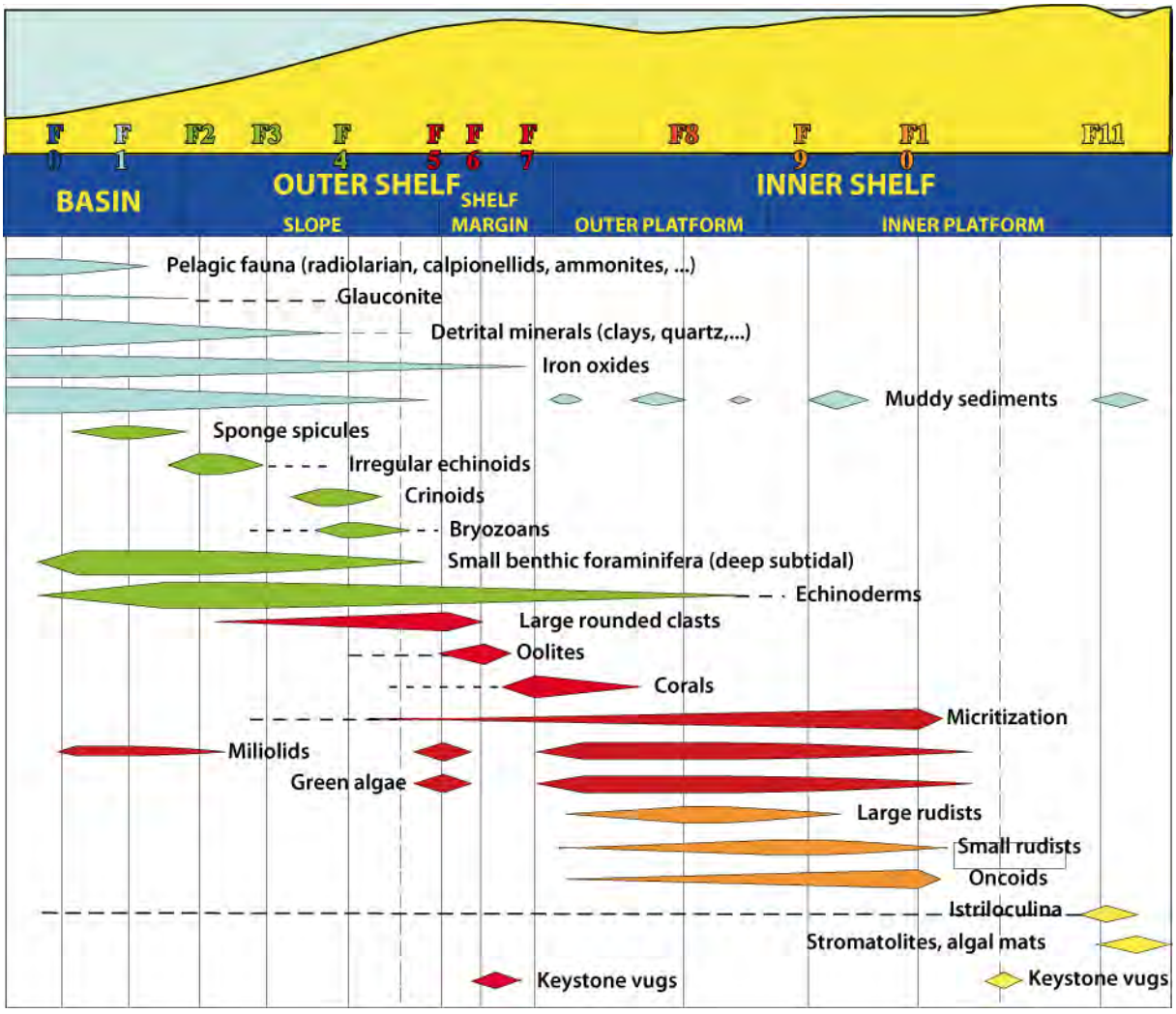

Fig. 2.3: Ideal distribution of faunas on a shelf-basin transect and resulting distribution of microfacies. Classification after Arnaud-Vanneau *et al.*, 2005. F0: Biomicrite with radiolaria and calpionellids. F1: Wackestone with sponge spicules. F2: Wackestone with spatangidae. F3: Grainstone/packstone with rounded echinoderm debris and small foraminifera. F4: Grainstone/packstone with crinoids and bryozoans. F5: Grainstone with large rounded debris. F6: Grainstone with oolites. F7: Grainstone/packstone with corals; Boundstone. F8: Wackestone/packstone with large foraminifera, sometimes accompanied by large rudists. F9: Packstone/grainstone with Miliolidae and rudists. F10: Packstone/grainstone with oncolites and *Bacinella*. F11: Mudstone with bird's eyes; emersion facies.

2.3.3. Carbon and oxygen stable-isotope analyses

Carbon and oxygen-isotope analyses were performed on whole-rock samples following the procedures described by Spangenberg and Macko (1998), Spangenberg *et al.* (1999) and Spangenberg and Herlec (2006). Visible calcite veins were removed during sample preparation in order to limit the diagenetic signature. Samples were run on a Thermo Fisher Scientific (formerly ThermoQuest/ Finnigan, Bremen, Germany) GasBench II preparation device interfaced with a Thermo Fisher Scientific Delta Plus XL continuous flow isotope ratio mass spectrometer (IRMS). Carbon dioxide was extracted at 70°C. Ratios of carbon and oxygen isotopes are reported in the delta (δ) notation as the per mil (‰) deviation relative to the Vienna–Pee Dee belemnite standard (VPDB). Replicate analyses have demonstrated an analytical reproducibility of the international calcite standard NBS-19 and of the laboratory standards Carrara Marble of better than ±0.05‰ for $\delta^{13}C$ and ±0.1‰ for $\delta^{18}O$. A total of 208 samples were analysed for their stable isotope content (29 from La Juracime, 83 from La Chambotte and 96 from Montclus).

2.3.4. Phosphorus content

Total phosphorus (P) content was measured on 239 whole-rock samples (90 from La Chambotte section and 149 from Montclus) following the procedure described in Bodin *et al.* (2006). The concentration of P was obtained in ppm by calibration with known standard solutions using a UV/Vis photospectrometer (Perkin Elmer UV/Vis Photospectrometer Lambda 10, Perkin Elmer, Waltham, MA, USA; λ = 865 nm) with a mean precision of 5%. Phosphorus accumulation rates (PAR) were then calculated for the basinal section of Montclus [with PAR = [P] (mg/g) x sedimentation rate (cm/kyr) x rock density] and are expressed in $mg/cm^2/kyr$. As rock density depends upon its mineralogy, rock densities equal to 2.5 g/cm^3 and 2.3 g/cm^3 have been used for limestone and marlstone, respectively (Attewell and Farmer, 1976). Sedimentation rates were evaluated by identification of Milankovitch cycles: marl/limestone couplets (assumed to correspond to precession cycles of 20 ka) were counted and sedimentation rates were estimated for each eccentricity cycle (of 100 ka).

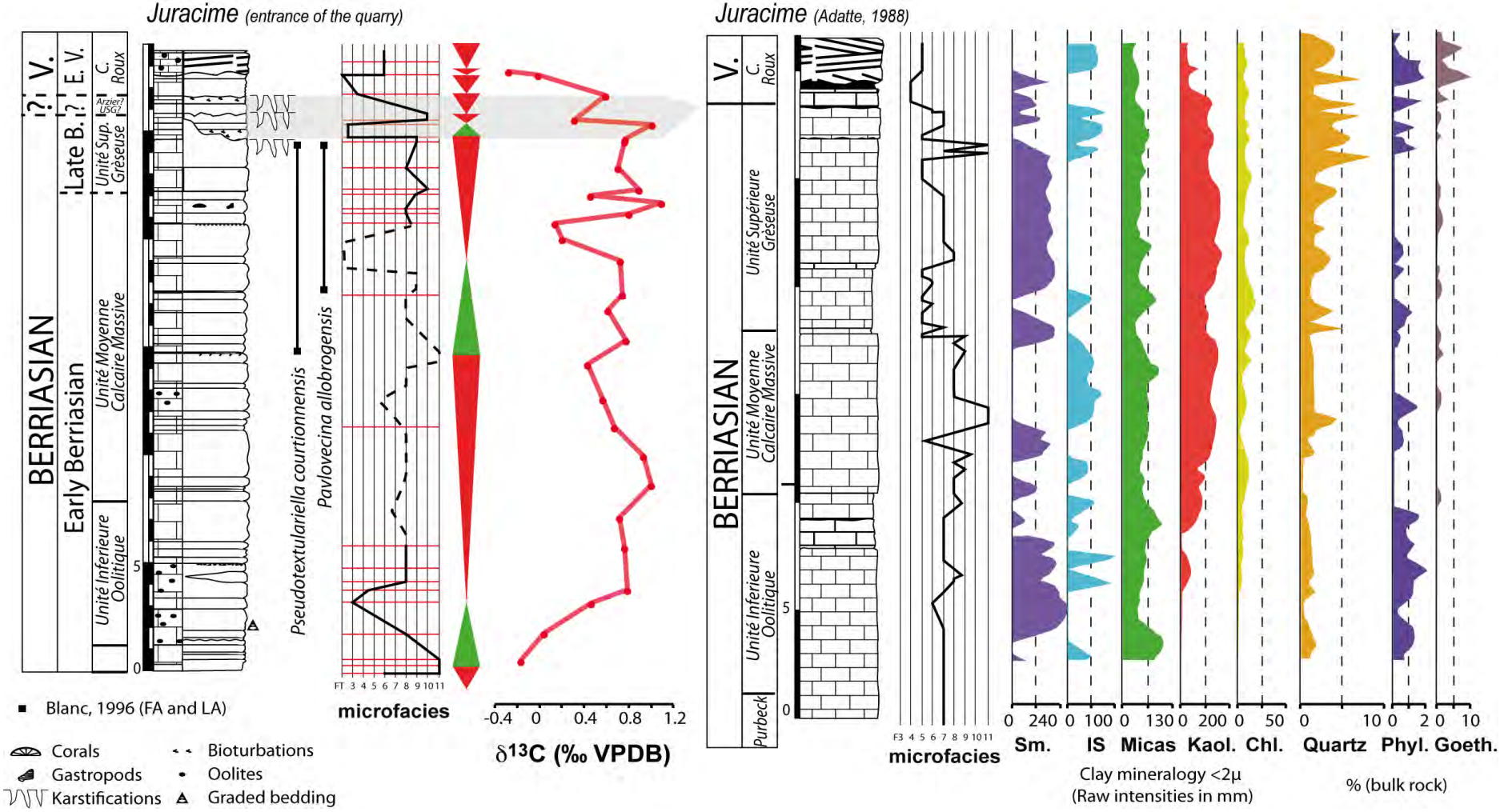

Fig. 2.4: Evolution of microfacies, $\delta^{13}C$ values and mineralogical content of the Juracime section. Mineralogical and a part of microfacies analyses are redrawn from Adatte (1988; the dotted line is extrapolated from these results), marker species reported from Blanc (1996). The interval in grey highlights the sedimentary record observed at the entrance of the quarry, which is not preserved further to the south where Adatte (1988) and Blanc (1996) sampled the section.

2.3.5. Whole-rock and clay mineralogy

The analysis of the whole-rock and clay mineralogy was carried out by X-ray diffraction. Measurements were performed on a Thermo Scientific ARL X'TRA IP2500 diffractometer (Thermo Fisher Scientific, Ecublens, Switzerland) with a semi-quantification method using external standards and following the procedures by Kübler (1983, 1987) and Adatte *et al.* (1996). Clay minerals were analysed for the <2 µm fraction, on which the peak intensities of identified minerals were measured in cps and the proportion of clay minerals was estimated in relative per cent. The precision is 5 to 10% for phyllosilicates and 5% for grain minerals. A total of 222 samples were run for bulk-rock analyses (138 from Montclus and 84 from La Chambotte) and 79 samples were analysed for their clay mineralogical content (Montclus section).

2.3.6. Palynology

Eight samples from the basinal section of Montclus were studied for their palynological content. Marly samples were selected; however only five of them contained sufficient amounts of miospores. Cleaned and crushed samples were treated with HCl and HF following the standard palynological preparation techniques of Traverse (2007). The residue was sieved over an 11 µm mesh sieve, and a short oxidation with HNO_3 was performed on all residues. On each sample, counting of 300 sporomorphes was performed from strew mounts in order to study their content in spores and pollen.

2.4. RESULTS

2.4.1. Biostratigraphy

The determination of benthic foraminifera in La Juracime and La Chambotte sections confirms the previous taxon range zones identified by Darsac (1983) and followed by Blanc (1996) for the marker species *Pseudotextulariella courtionnensis*, *Pavlovecina allobrogensis*, *Montsalevia elevata*, *Pfenderina neocomiensis* and *Montsalevia salevensis* (Figs 2.4 and 2.5). Certain biostratigraphic improvements are noted here: a specimen of *Montsalevia elevata* was found below the *d1* of Darsac (1983); and a *Calpionellopsis simplex* was found in the Lower Member of the Chambotte Formation which ranges in calpionellid zone D.

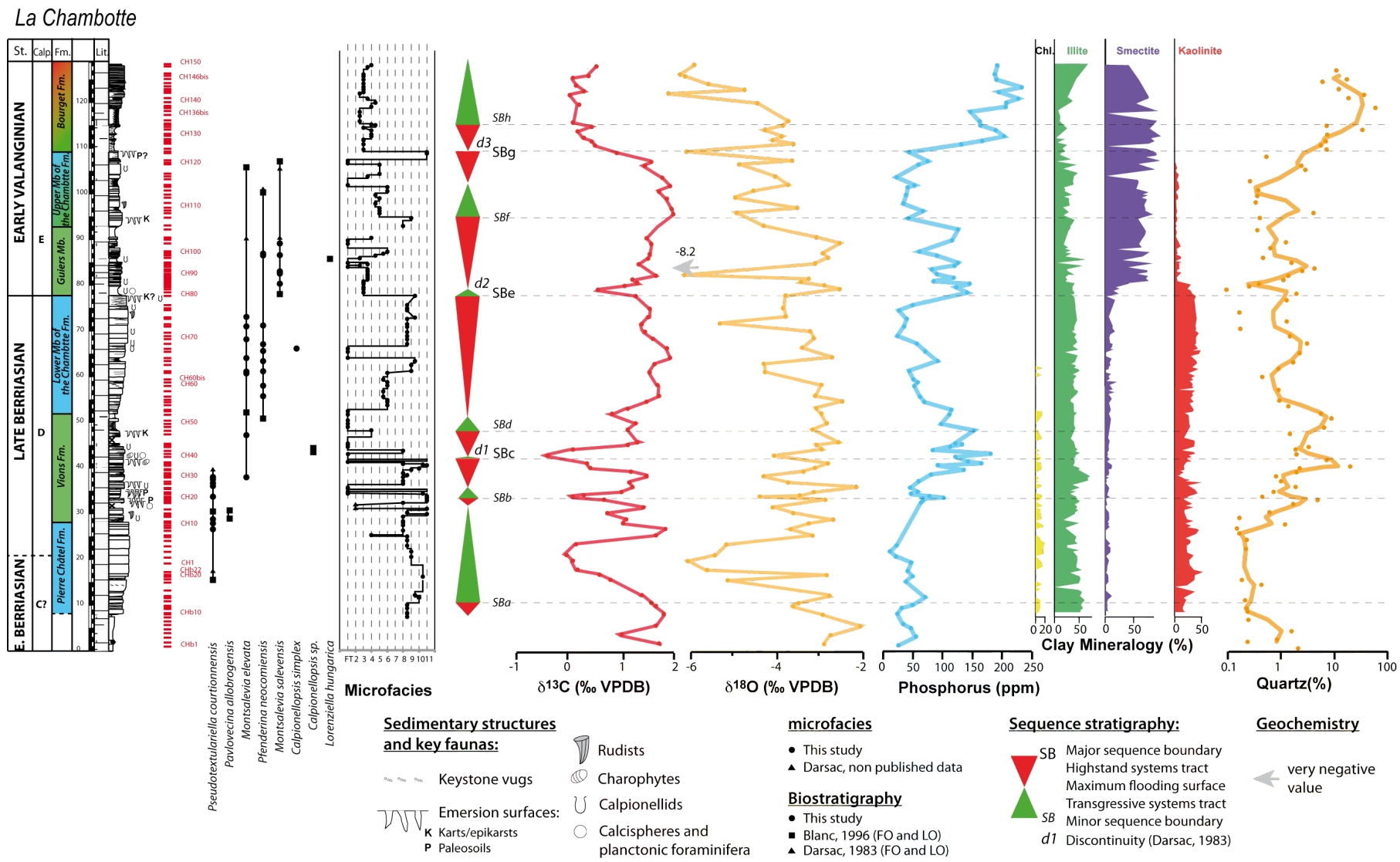

Fig. 2.5: Sedimentological and microfacies analyses, evolution of stable isotope, phosphorus, clay minerals and quartz contents in La Chambotte section.
Sedimentological analyses compiled after Darsac (1983), Blanc (1996), Hillgärtner (1999) and this work.
Marker species compiled after Darsac (1983), Blanc (1996) and this work.

At Montclus, the biostratigraphy has been improved by the analysis of marker nannofossils species (Fig. 2.6). *Nannoconus wintereri*, *Nannoconus steinmanni minor* and nannofossils species (Fig. 2.6). *Nannoconus wintereri*, *Nannoconus steinmanni minor* and *Nannoconus kamptneri minor* occur at the base of the section, indicating the lowermost Berriasian NJK-D zone (Bralower *et al.*, 1989; Bralower *et al.*, 1995). The FO of *N. steinmanni steinmanni*, marker of the NK-1 zone (Bralower *et al.*, 1989; Bralower *et al.*, 1995) was observed at 12 m. The NK-2A zone starts at 24.3 m with the FO of *Retecapsa angustiforata* and the NK-2B at 36.2 m with the FO of *Percivalia fenestrata* (Bralower *et al.*, 1989 pareil). The LO of *Rhagodiscus nebulosus* around 54.2 m provides further evidence of a late Berriasian age (Duchamp-Alphonse et al 2008). The early Valanginian zone NK-3A is determined by the FO of *Calcicalathina oblongata* at 72.2 m (Bralower *et al.*, 1989; Bralower *et al.*, 1995), while the base of CC3-B is marked by the FO of *Eiffellithus windii* around 95.8 m (Applegate and Bergen, 1988). The FO of *Rhagodiscus dekaeneli* observed around 91.3 m and rare occurrences of *Pickelhaube umbellata* from 99.2 m help to better constrain the early Valanginian (Duchamp-Alphonse et al 2007).

2.4.2. Carbon and oxygen stable-isotope analyses

The three sections exhibit relatively similar long-term trends in $\delta^{13}C$ values: an increase during the early Berriasian, relatively stable values in the late Berriasian, and a decrease in the early Valanginian. Nevertheless, important differences were observed on shorter time scales. The Juracime section (Fig. 2.4) shows a progressive increase in $\delta^{13}C$ values of 1.2‰ during the early Berriasian ('Unité Inférieure Oolitique'). In the late early Berriasian ('Unité Moyenne Calcaire Massive') a more or less progressive decrease in $\delta^{13}C$ values of 0.8‰ is followed by an abrupt increase of 1‰ at the top of the "Unité Moyenne Calcaire Massive". Stable values of about 0.8‰ were observed in the 'Unité Supérieure Gréseuse' and finally a decrease to -0.3‰ occurred at the top of the section.

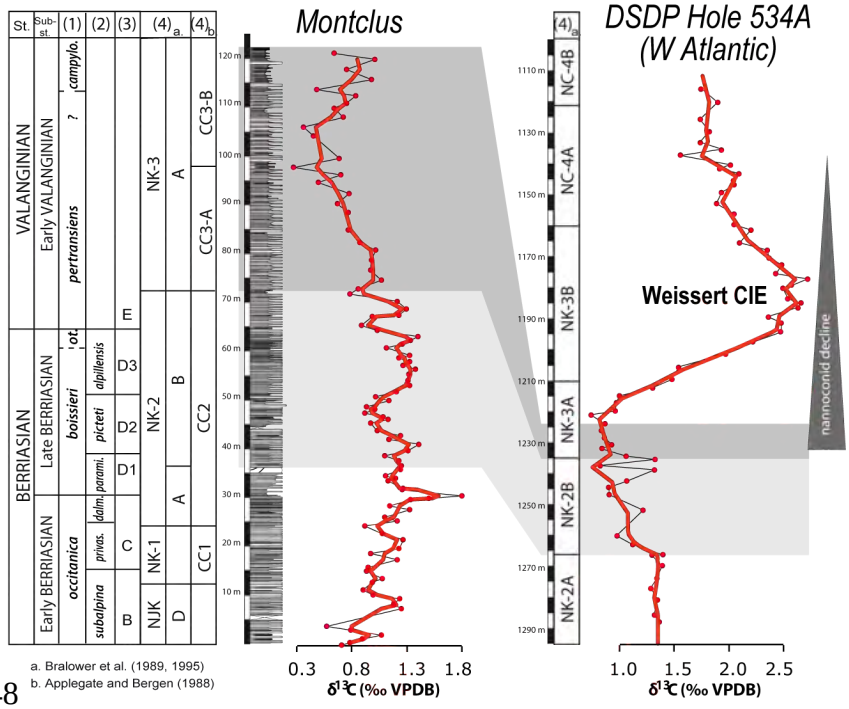

Fig. 2.6: Biostratigraphy and chemostratigraphy of the section of Montclus; comparison with the west Atlantic record (DSDP Hole 534A; Mutterlose & Bornemann, 2008). The correlation used is based on calcareous nannofossils: light grey: NK2-B; dark grey: NK3-A (correlable part). The Weissert CIE is not recorded in Montclus.

The La Chambotte section exhibits strong $\delta^{13}C$ variations (Fig. 2.5): a drop of 1.8‰ was observed in the Pierre Châtel Formation, followed by a succession of shifts of an amplitude of approximately 1.8‰ in the Vions Formation. Then, relatively stable values of about 1.7‰ occur in the Lower Member of the Chambotte Formation, the Guiers Member and the Upper Member of the Chambotte Formation, with the exception of a slight negative shift at the limit between the Lower Member of the Chambotte Formation and the Guiers Member. Finally, a negative shift of 1.5‰ in $\delta^{13}C$ values was observed at the limit between the Upper Member of the Chambotte and the Bourget Formations, followed by relatively stable and lighter $\delta^{13}C$ values of 0.3 ± 0.2‰.

The section of Montclus (Figs 2.6 and 2.7) showed a progressive increase in $\delta^{13}C$ values of about 0.8‰ during the early Berriasian (calpionellid zones B and C), followed by a decrease of 0.6‰ in the late Berriasian (calpionellid sub-zones D1 and D2). The latest Berriasian is characterised by a renewed increase in $\delta^{13}C$ values of 0.3‰ (calpionellid sub-zone D3), and the early Valanginian showed a progressive decrease of 0.9‰ followed by a slight increase of 0.4‰ at the top of the section. A correlation coefficient between $\delta^{13}C$ and $\delta^{18}O$ values was calculated for each section and the values are 0 for Juracime, and 0.1 for La Chambotte and Montclus.

2.4.3. Phosphorus contents

Total P (P_{tot}) was measured in absolute content (ppm) and then converted into accumulation rates (PAR) for the basinal section of Montclus (Fig. 2.7). This conversion was not implemented for platform sections, given the occurrence of numerous hiatuses, the duration of which cannot be estimated with sufficient accuracy.

At La Chambotte (Fig. 2.5), three intervals of enhanced P_{tot} contents were observed: the first occurs in the Vions Formation, the second in the Guiers Member, and the third in the Bourget Formation. At Montclus, the P_{tot} contents show comparable trends in its various expressions: absolute contents (ppm) and accumulation rates (PAR) based on calpionellid stratigraphy and cyclostratigraphy. Only the PAR based on the cyclostratigraphy is shown in Fig. 2.7. In the early Berriasian (until the *Dalmasiceras dalmasi* ammonite sub-zone), low values were observed in limestone lithologies and slightly higher values were measured in marly lithologies. Then, in the latest early Berriasian and the late Berriasian (from the *D. dalmasi* to the *T. otopeta* ammonite zones) relatively low values occurred in both lithologies. An increase in P_{tot} values in both lithologies was again present in the early Valanginian.

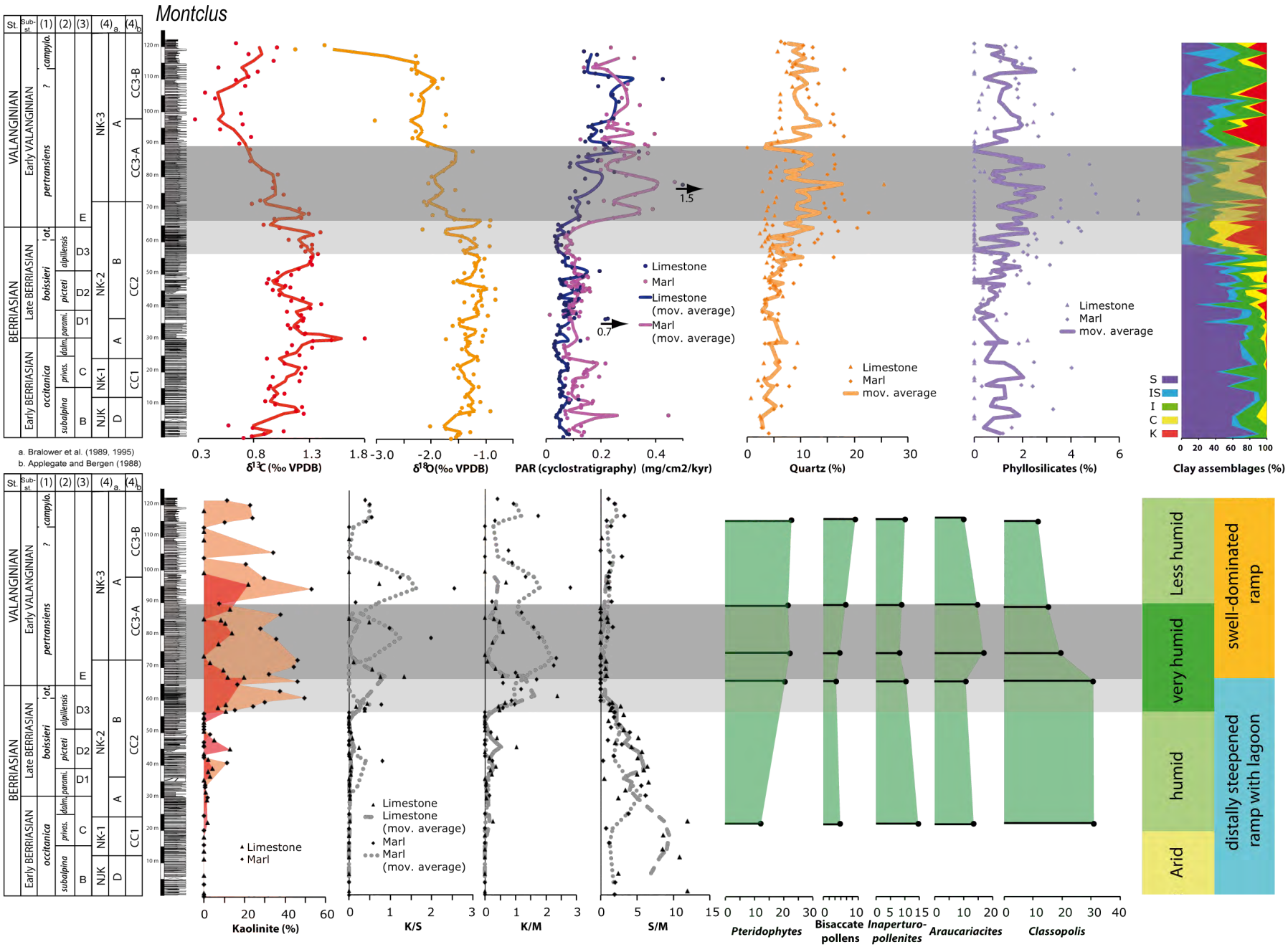
Montclus
St
Sub-st
(1)
(2)
(3)
(4)a.
(4)b
VALANGINIAN
BERRIASIAN
Early VALANGINIAN
Late BERRIASIAN
Early BERRIASIAN
pertransiens
campylo.
boissieri
picteti
alpillensis
parami.
dalm.
privas.
occitanica
subalpina
NJK
NK-1
NK-2
NK-3
CC1
CC2
CC3-A
CC3-B
a. Bralower et al. (1989, 1995)
b. Applegate and Bergen (1988)
δ13C (‰ VPDB)
δ18O(‰ VPDB)
PAR (cyclostratigraphy) (mg/cm2/kyr)
Quartz (%)
Phyllosilicates (%)
Clay assemblages (%)
Limestone
Marl
Limestone (mov. average)
Marl (mov. average)
mov. average
S
IS
I
C
K
Kaolinite (%)
K/S
K/M
S/M
Pteridophytes
Bisaccate pollens
Inaperturo-pollenites
Araucariacites
Classopolis
Less humid
very humid
humid
Arid
swell-dominated ramp
distally steepened ramp with lagoon

Fig. 2.7: Results of geochemical, mineralogical and palynological analyses performed on the section of Montclus. Biostratigraphy is indicated by ammonite zones and subzones (1) and (2), capionellids (3), and nannofossils [(4a) following Bralower *et al.*, 1989 and Bralower *et al.*, 1995; (4b) following Applegate and Bergen, 1988]. The quartz and phyllosilicate contents are expressed in relative percentage of the total mineralogical composition. Similarly, palynological results are expressed in relative percentage of the total composition in pollen and spores. K/S, K/M and S/M are peak ratios of selected clay species: kaolinite, smectite and micas

2.4.4. Mineralogy

The evolution of whole-rock and clay-mineralogy assemblages of the section of Montclus is compared with the results obtained by Darsac (1983) and Adatte (1988) for the sections of La Chambotte and Juracime, respectively. Note that Adatte (1988) sampled the section of Juracime in the same quarry but a few tens of metres to the south, where the thickness between the main emersive surfaces of the Unité Supérieure Gréseuse and the Calcaire Roux Formation is reduced (Fig. 2.4). In the Juracime section, kaolinite and chlorite (expressed in raw intensities) appear in the 'Unité Inférieure Oolitique' (Fig. 2.4). The proportion of these minerals increases at the base of the 'Unité Moyenne Calcaire Massive' and they reach relatively high contents up to the top of the 'Unité Supérieure Gréseuse', where the kaolinite content sharply diminishes. The quartz content is relatively low at the base of the section (about 20%), and higher contents were observed in the 'Unité Supérieure Gréseuse' and Calcaire Roux Formation (average values of 40%).

In the La Chambotte section, two major changes in clay assemblages were observed (Fig. 2.5). The first occurs at the limit between the Lower Member of the Chambotte Formation and the Guiers Member, where the assemblages show an abrupt change from 30% toward 5% for kaolinite and 10% toward 60% for smectite. The second takes place at the limit between the Upper Member of the Chambotte Formation and the Bourget Formation, where kaolinite disappears definitively from the clay assemblages.

In Montclus (Fig. 2.7), the lower Berriasian deposits are dominated by smectite, which represents about 70% of the clay minerals (the rest being mostly represented by mica). Kaolinite appears in low relative quantities in the uppermost lower Berriasian (*Berriasella privasensis* subzone, calpionellid zone C), slightly increases in the lower upper Berriasian (*Malbosiceras paramimounum* and *B. picteti* subzones, calpionellid zones D1 and D2) and decreases again (*Berriasella. picteti* and *Tirnovella alpillensis* subzones, calpionellid zone D2 and D3). In the uppermost Berriasian (at the boundary of the *S. boissieri* and *T. otopeta* zones, late calpionellid zone D3) and the lowermost Valanginian, the proportion of kaolinite abruptly increases up to 50%, at the expense of smectite for which relative contents drop to values between 0% and 25%. The kaolinite content remains relatively constant during the lower Valanginian (15 to 20% on average) whereas the smectite content increases in the upper part of the lower Valanginian,

reaching 40% in the upper part of the section. Moreover, the differentiation between marly and calcareous lithologies shows that marl is highly enriched in kaolinite compared with limestone (two to three times on average), the maximum of enrichment, however, coincides in both lithologies. The chlorite content roughly follows the kaolinite trend, except for the upper part of the lower Valanginian where it decreases. The clay minerals of Montclus are characterised by low contents in illite–smectite mixed-layers, which rarely exceed 10%. In parallel, quartz and phyllosilicates roughly covary: they increase in the uppermost Berriasian (*T. alpillensis* subzone, calpionellid zone D3), culminate through the Berriasian–Valanginian boundary and decrease slightly in the upper part of the lower Valanginian.

2.4.5. Evolution of microfacies

In the Juracime section (Fig. 2.4), the base of the 'Unité Inférieure Oolitique' (early Berriasian) is characterised by a progressive deepening of facies from the lagoonal and emersive environments belonging to the Purbeck beds (F11) to outer shelf settings with abundant echinodermal debris, peloids and glauconite (F3).

The microfacies near the top of the 'Unité Inférieure Oolitique' and most of the overlying 'Unité Moyenne Calcaire Massive' indicate outer lagoonal environments (F8, after Adatte, 1988) with the occurrence of foraminifer-rich and micritic sediments deposited under relatively weak hydrodynamic conditions.

A deepening toward outer shelf facies is observed within the 'Unité Moyenne Calcaire Massive', as well as through the transition to the overlying 'Unité Supérieure Gréseuse' (Adatte, 1988).

The lagoonal facies returns in the basal part of the 'Unité Supérieure Gréseuse'. Subsequently, micritic, inner lagoonal facies with green algae and miliolids (F9 and F10) alternate with quartz-rich facies containing a mix of outer-shelf faunas with ostracods and sponge spicules, and inner lagoonal faunas with thin miliolids. This type of facies does not characterise a specific palaeoenvironment but rather a mix of different settings, and is classified as transgressive facies (FT) as shown in Fig. 2.8. Finally, the Calcaire Roux Formation is characterised by ferruginous facies rich in oolites and crinoids (F6).

In the La Chambotte section, the Pierre Châtel Formation shows a facies evolving from outer (F8/9) to inner lagoonal environments (F10/11), and then back to outer lagoonal environments with sparse rudists and *Bacinella* (F8). A maximum depth is observed at 32 m, with deep quiet outer-shelf deposits (F1/F2). The whole formation is characterised by the proliferation of foraminifera, already noted by Blanc (1996) and Hillgärtner (1999). The top of the formation is a karstified surface which marks the passage to the Vions Formation (Fig. 2.2).

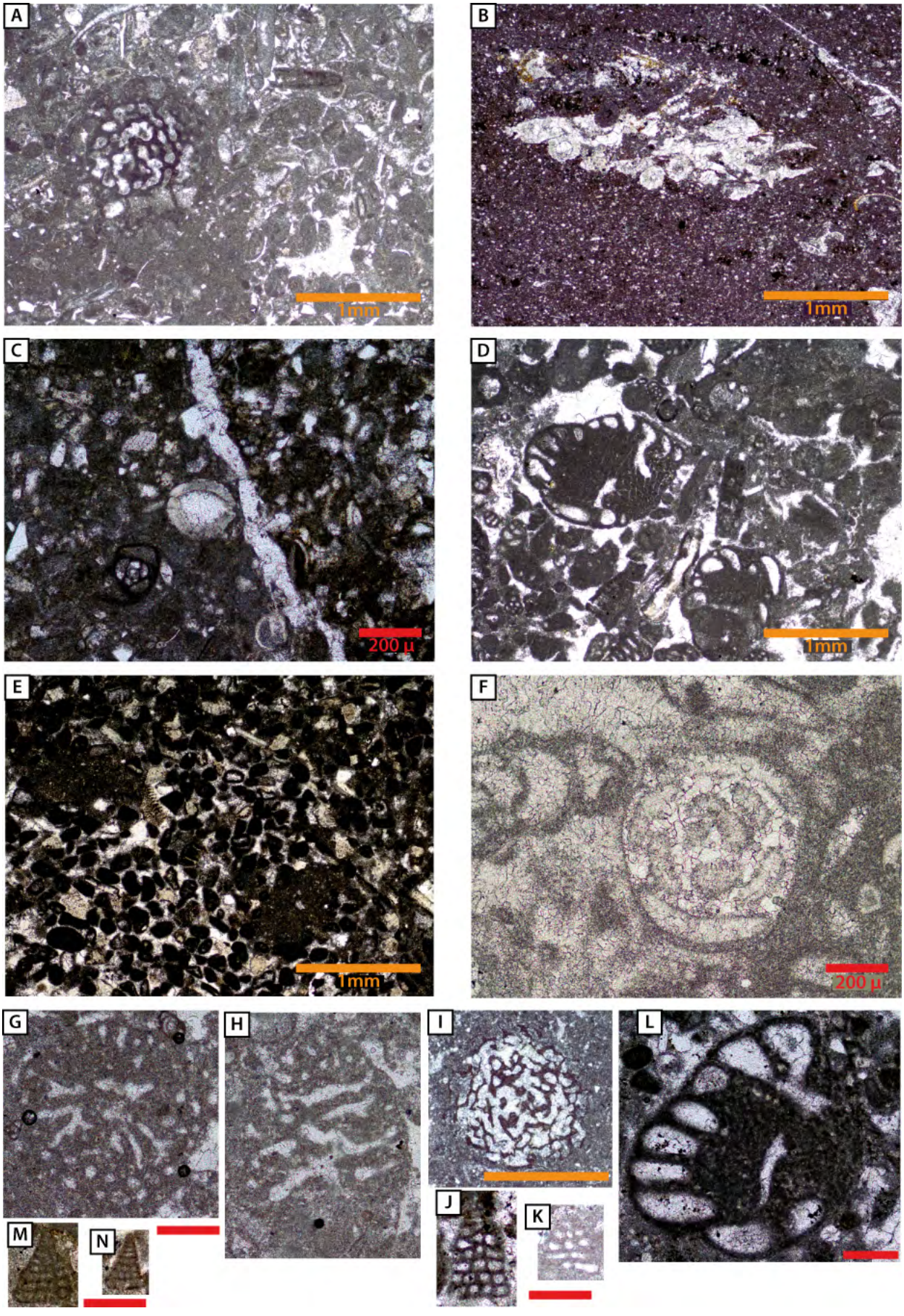
A
1mm
B
1mm
C
200 µ
D
1mm
E
1mm
F
200 µ
G
H
I
L
M
N
J
K

Fig. 2.8: Details of thin sections in La Chambotte. (A) Reworked *Pavlovecina allobrogensis* (thin section B68 of Darsac corresponding to transgressive facies of sequence b), x10. (B) brackish level with charophyte fauna (thin section B70 of Darsac, 1983; corresponding to SBc), x4. (C) Reworked charophyte in the overlying transgressive layer (sample CH39), x10. (D) Diversified and foraminifer-rich lagoonal facies of the lower Member of the Chambotte Formation with *Pfenderina neocomiensis* (CH69), x4. (E) Outer shelf facies (F3) of the Guiers Member including reworked mud pebbles (CH85), x4. (F) Intraclast dissolution of a miliolid illustrating the emersion phase associated with SBe (CH106), x10. (G) and (H) Marker foraminifera *Pseudotextulariella courtionnensis* (CH11), x10. (I) Marker foraminifera *Pavlovecina allobrogensis* (sample B39 of Darsac, 1983; corresponding to CH14 in this study), x4. (J) and (K) Marker foraminifera *Montsalevia elevata* (CH46 and CH29, respectively), x10. (L) Marker foraminifera *Pfenderina neocomiensis* (CH57), x10. (M) and (N) Marker foraminifera *Montsalevia salevensis* (CH85), x10.

The Vions Formation itself is characterised by a succession of palaeosols that are partly well-expressed by root traces and red-stained surfaces (Fig. 2.2G and H), which initially intercalate with inner lagoonal deposits and higher up with transgressive facies (FT) composed of rounded material of mixed inner (large benthic foraminifera and green algae) and outer-shelf provenance (echinodermal debris, circalittoral foraminifera and calpionellids).

In particular, at 42 m, a surface impregnated with iron oxides is observed (Fig. 2.2I). This emersive surface separates a charophyte-rich level (Fig. 2.7B and C), which typically indicates brackish environments (F11) from a succession of transgressive levels, which contain planktonic foraminifera, calpionellids and calcispheres, together with reworked charophytes and pebbles (FT; Figs 2 and 7). The formation ends with a karstified level that overlies a polygenic conglomerate. The Vions Formation shows a general proliferation of large, quartz-agglutinating foraminifera (*Pseudocyclammina* and *Everticyclammina*).

The overlying Lower Member of the Chambotte Formation consists of deposits including outer to inner lagoonal facies with a rich and diversified fauna principally composed of large benthic foraminifera and green algae. Two shallowing-upward successions are observed, starting with a microfacies characterized by large, reworked benthic foraminifera typical of lagoonal environments (FT) mixed with an outer-shelf fauna (echinoderms, calpionellids and calcispheres), and ending with a micritic facies containing calcareous sponges, rudists and *Bacinella* (F9/10). The lower Member of the Chambotte Formation ends with an irregular surface marking an abrupt change in carbonate fabric.

The overlying Guiers Member marks the deepening of the depositional environment with outer-shelf facies exhibiting a fauna essentially composed of circalittoral foraminifera, echinoderms and bryozoans (F2/3 to F5, exceptionally F6) and including *Bacinella*. The sediments contain an important detrital component. Calpionellids have been identified but they are too poorly preserved to assess an age with certainty.

The upper Member of the Chambotte Formation shows facies evolving between outer shelf and oolitic shoal (F3/4 to F6) and ends with a beach facies (F11). It constitutes the last prominent calcareous interval with a relatively rich and diversified fauna of benthic foraminifera and sparse rudists. This diversity is, however, less important than in the Pierre-Châtel and the Lower Chambotte Formations. Hillgärtner (1999) identified a hardground and Gréselle and Pittet (2010) a palaeosol with root traces at the top of this member.

The Bourget Formation forms the top part of the studied section and reveals an important change in carbonate production: crinoids and bryozoans are predominant in the ecological assemblages, whereas foraminifera are very rare and poorly diversified. Chert dominates the lower, more recessive part of the formation and remains important in the calcareous part near the top of the formation (Fig. 2.2M). The microfacies corresponds to the outer shelf covering a range from deep subtidal environments (F2/3) to shallow subtidal environments (F4/5) with submarine dune structures.

2.4.6. Terrestrial palynology

The palynological assemblages were examined in the basinal section of Montclus. *Classopollis*, *Calliallasporites*, *Araucariacites* and *Inaperturopollenites* dominate the non-saccate pollen assemblages (Fig. 2.7). Few *Perinopollenites*, *Cycadopites*, *Eucommiidites* and *Cerebropollenites* are, however, preserved. Bisaccates are mostly undifferentiated. Spores are represented mainly by *Cyathidites*, *Leiotriletes*, *Gleicheniidites* and undifferentiated deltoids, which all belong to *Pteridophytes*. An important change in the composition of pollen is observed in the earliest Valanginian: bisaccate pollen, *Araucariacites* and *Pteridophytes* become more important, whereas *Classopollis* becomes less abundant. In the late early Valanginian, an increase in bisaccate pollen occurs, to the detriment of *Araucariacites* and *Classopollis.*

2.5. INTERPRETATIONS

2.5.1. Sequence stratigraphy

The Juracime section includes a well-developed sedimentary series of early Berriasian age (‘Unité Inférieure Oolitique’ and ‘Unité Moyenne Calcaire Massive’), whereas the sediments of late Berriasian age represent less than 5m. The 4 m below the erosional truncation at the base of the Calcaire Roux Formation show the juxtaposition

and telescoping of several sequence boundaries (Fig. 2.2B). Unfortunately, it was not possible to date this interval because no biostratigraphically relevant fauna was found. This interval may either date from the late Berriasian (and belong to the 'Unité Supérieure Gréseuse') or from the early Valanginian (and would then belong to the Marnes d'Arzier Formation).

The more complete succession of La Chambotte provided a more detailed insight into the sequence stratigraphy for the considered period (Fig. 2.5). The major discontinuities observed by Darsac (1983; *d1* to *d3* in Fig. 2.5) were taken into account in the present analyses. Indeed, they were defined as maximum-flooding surfaces (mfs) separating different foraminiferal assemblages, and they provide biostratigraphic control.

The first 7 m of the section was not considered because the strong recrystallization related to dolomite formation does not allow for any sequential interpretation. The base of the first sequence (sequence a) is defined by a truncated surface (sequence boundary a: SBa) on top of cross-bedded sediments and marks a change in the geometry of deposition (Fig. 2.2E). The maximum-flooding surface of this sequence is placed in a level containing sponges spicules and calcispheres (microfacies F1/2). Dissolution features and vadose silts are observed all along this sequence and probably are linked to a subsequent sequence boundary within the Vions Formation (SBb).

A second sequence boundary was identified within the base of the Vions Formation (SBb). This formation exhibits a succession of levels containing root traces. The second lowest level shows multiphase infillings in the root traces, in contrast to the other levels. This means that this level formed during longer-lasting emersion. Therefore, it was designated as SBb. The maximum flooding surface of sequence b was placed in the reworked deposits containing calpionellids. Sequence boundary c was placed higher up within the Vions Formation, because of the presence of a level rich in charophytes which is covered by beds containing reworked charophytes, together with calpionellids and planktonic foraminifera, which incorporate both the transgressive surface and the maximum flooding surface. Sequence boundary d is the last emersive level of the Vions Formation, and is characterized by epikarstic structures. The maximum flooding surface of sequence d was placed in the marliest interval situated at the base of sequence d, which fits well with the general shallowing-upward trend of the sequence.

Sequence boundary e was placed at the top of the Lower Member of the Chambotte Formation, where an abrupt change from inner lagoonal (microfacies F9/10) to deep outer-shelf (F3) deposits was observed. About 30 cm below this surface, the presence of an epikarst was described by Blanc (1996), which may be related to an emersion. Sequence boundary f corresponds to an epikarst identified by microfacies*:* the dissolution of magnesium calcite (for example in miliolid tests; Fig. 2.8) and calcite palissadic and asymmetrical cements were recognised. The maximum flooding surface of sequence f was placed in the marliest interval. Sequence f is characterised by the general opening of depositional environments.

Sequence boundary g was placed at the top of the Upper Member of the Chambotte Formation (Figs 2L and 5). The occurrence of a shift in $\delta^{13}C$ and phosphorus values, the drop in kaolinite contents and the abrupt difference in carbonate fabric (with a change to silica-rich, heterozoan facies with echinoderms and bryozoans) all indicate the presence of a major hiatus. Root traces were not observed during this study, but the occurrence of beach facies within the top part of this formation is consistent with subaerial exposure at this level and supports the presence of a sequence boundary (SBf), thereby following Blanc (1996) and Gréselle and Pittet (2010). The uppermost sequence boundary (SBh) is an erosive surface at the base of the more calcareous part of the Bourget Formation, which can be interpreted as resulting from channel infilling or as the base of a submarine dune.

Sequence h is very characteristic in the Jura area, with the deposition of the silica-rich, thinly bedded, cross-laminated deposits of the Bourget Formation, which correspond to the Calcaire Roux Formation in the northern Jura. The upper part of the Bourget Formation is interpreted as a transgressive systems tract (TST), with a maximum flooding surface in the marls on top of this formation, which corresponds to the Asteria Marls (hidden by vegetation and not shown in Fig. 2.5). However, it is possible that sequence boundaries are present within the condensed Asteria Marls (as discussed in the *Geological setting* section). The sequence stratigraphy of this interval is still ambiguous and has not been studied in this contribution.

Unconformities and associated hiatuses are an important component in both sections of the Jura, and in particular the Juracime section shows a highly incomplete record for the late Berriasian–early Valanginian time interval. For the La Chambotte section, the three major discontinuities observed by Darsac (1983) and described as corresponding to maximum flooding intervals and separating four foraminiferal assemblages, are interpreted here as corresponding to sequence boundaries, which are located just below their corresponding maximum flooding surface. The observed changes in foraminiferal assemblages are abrupt and therefore indicate gaps in the sedimentological record: *d1*, *d2* and *d3* (Darsac, 1983) are associated with sequence boundaries SBc, SBe and SBg. Sequence boundary c limits a level rich in charophytes, typically found in brackish environments, to a level containing numerous reworked calpionellids and echinoderms. Calcispheres are present in the overlying interval including the maximum flooding surface. Consequently, the variations in sea level were rapid and of considerable amplitude. Similarly, notable sea-level variations are witnessed by SBe, which separates inner lagoonal from offshore facies. The hiatus associated with SBg is evidenced by the geochemical and mineralogical records. Consequently, SBc SBe and SBg are of major importance because of the duration of their emersion and because they mark important sea-level variations.

2.5.2. Diagenesis

In Montclus (Figs 6 and 7), the determination coefficient calculated for all $\delta^{13}C$ and $\delta^{18}O$ values was very low ($r^2 = 0.1$); the range of values was between -0.5‰ and -2.5‰ for the oxygen isotopes and between 0.3‰ and 1.8‰ for the carbon isotopes. Consequently, both $\delta^{13}C$ and $\delta^{18}O$ values are interpreted here to not have undergone significant diagenetic overprint (Choquette and James, 1987). A similar decrease in $\delta^{18}O$ values starting in the earliest Valanginian was measured on belemnites and whole rock of the Vergol section, which is also located in the Vocontian basin (McArthur *et al.*, 2007), indicating that $\delta^{18}O$ values may have palaeoenvironmental significance. The diagenetic overprint incurred by the clay minerals has already been well-constrained and assessed as relatively minor (Deconinck *et al.*, 1985; Deconinck, 1987a). Indeed, the negative correlation between smectite and kaolinite contents, and the lack of correlation between smectite and illite suggests that sedimentary processes mostly controlled the distribution of clay minerals rather than neoformations during burial diagenesis. This suggestion is also supported by the relatively high kaolinite (up to 50%) and smectite contents (up to 84%) in the clay assemblages.

In the Juracime section, samples have $\delta^{18}O$ values between -3‰ and -7‰ (with a mean of -4.1‰), which indicates a diagenetic overprint (Choquette and James, 1987). Similarly, in La Chambotte (Fig. 2.5), $\delta^{18}O$ values vary between -2‰ and -6‰, signifying alteration during diagenesis. Consequently, the $\delta^{18}O$ trends of these sections will not be considered here.

The low determination coefficient between the carbon and oxygen isotope data ($r^2 = 0$ and 0.1, respectively), as well as the ranges of $\delta^{13}C$ values (between -0.2‰ and 1‰ in the Juracime section and between 0‰ and 2‰ in the La Chambotte section) suggest a weak diagenetic impact on the carbon-isotope records; this is in accordance with the composition and preservation of clay minerals, which also indicate minimal overprint (see below). The Vions Formation exhibits abrupt negative shifts in $\delta^{13}C$ values, which are probably related to the succession of discontinuities partly linked with palaeosols that are common in this formation.

The relatively high content of kaolinite and smectite in La Chambotte section indicate a low diagenetic overprint. For instance, the kaolinite content increases to 40% in the Lower Member of the Chambotte Formation, and the smectite content reaches 70% of the clay assemblages, where the illite crystallinity has the lowest values. Consequently, there is no evidence of an efficient diagenetic overprint in La Chambotte (Kübler, 1987; Kübler and Jaboyedoff, 2000). It is more difficult to estimate the impact of diagenesis on clay minerals in the Juracime section because their content is expressed in raw intensities (data from Adatte, 1988). However kaolinite and smectite dominate the clay assemblages, which indicates that the sedimentary record is well-preserved and that the impact of burial diagenesis has been minimal.

2.5.3. Age control and correlation of the sections

In the earliest Cretaceous, calpionellid biostratigraphy is well-established and permits a link between biostratigraphies based on benthic foraminifera and ammonites (Remane, 1963, 1985, 1998; Deville, 1990; Blanc *et al.*, 1992; Pasquier, 1995; Blanc, 1996; Hillgärtner, 1999). Unfortunately, the occurrence of calpionellids remains rather scarce in shallow-water sediments. Additionally, the $\delta^{13}C$ record helps to improve the correlation between the sections and age control (Figs 2.9 and 2.10). The $\delta^{13}C$ values show relatively similar long-term trends, which appear to be correlated from the Jura Platform to the Vocontian Basin: an increase is observed in the early Berriasian, relatively high $\delta^{13}C$ values persist in the late Berriasian and lighter values are typical in the early Valanginian (Fig. 2.10).

In Montclus, the biostratigraphy based on calcareous nannofossils allows comparison of the results obtained for this section with other basinal sections, for instance with the $\delta^{13}C$ record of sediments in the west Atlantic domain (Bornemann and Mutterlose, 2008; Fig. 2.6). The $\delta^{13}C$ records appear to be poorly correlated for the late Berriasian but both domains exhibit low $\delta^{13}C$ values in the early Valanginian before the positive carbon-isotope excursion (CIE). This suggests that the $\delta^{13}C$ record shows regional variability during the late Berriasian, in contrast to the early Valanginian.

At Montclus, the increase in $\delta^{13}C$ values at the top of the section (Fig. 2.6) cannot be attributed to the onset of the positive CIE of the latest early and early late Valanginian because the Barrandes layers have been observed a few metres above the top of the measured section in a slumped interval. These layers are dated as *B. campylotoxus* ammonite zone (Reboulet and Atrops, 1999) and occur below the onset of the $\delta^{13}C$ shift (Westermann *et al.*, 2010). This implies that the latest early to early late Valanginian CIE is not recorded in the measured platform sections, indicating that the Calcaire Roux and the Bourget Formation are older than the CIE in the two studied sections and can be attributed to the *T. pertransiens* or early *B. campylotoxus* zones (early Valanginian; Fig. 2.9).

2.5.4. Carbonate platform architecture and morphology

Microfacies observations across the Jura platform and panoramas compiled by various authors (Darsac, 1983; Boisseau, 1987; Adatte, 1988; Hillgärtner, 1999; Gréselle, 2007; Gréselle and Pittet, 2011) allow the reconstruction of its morphology (Fig. 2.11).

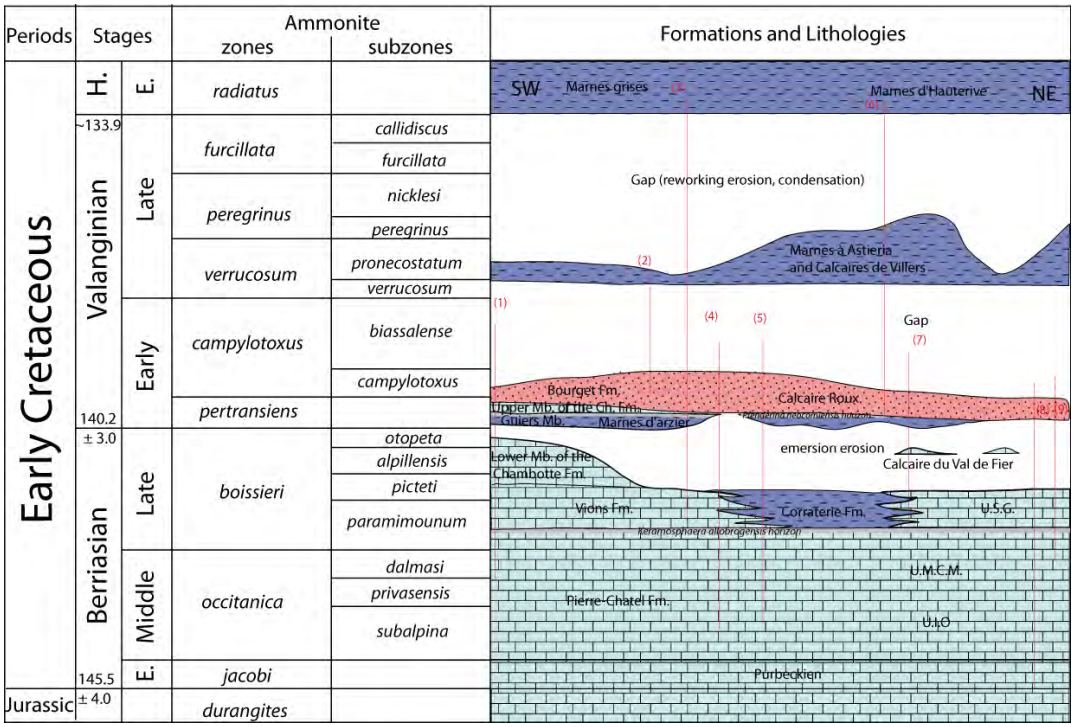

Fig. 2.9: Schematic representation of the Berriasian–Valanginian succession across a SW/NE axis in the French and Swiss Jura. Numeric ages (Myrs) after the International Commission on Stratigraphy (2008), ammonite zonation after Reboulet *et al.* (2006), formations and lithologies after Steinhauser and Charollais (1971), Adatte (1988), Blanc (1996), Hillgärtner (1999), Hennig (2003) and this contribution. Synthesis of the following sections: (1) Chambotte (Blanc, 1996); (2) Lamoura (Hennig, 2003); (3) Le Boulu (Hennig, 2003); (4) Marchairuz (Adatte, 1988, Blanc, 1996); (5) Maréchet (Blanc, 1996); (6) Colas (Hennig, 2003); (7) Champagne-Bonvillars (Blanc, 1996); (8) Juracime carrier (Steinhauser and Charollais, 1971 ; Adatte, 1988); and (9) Landeron (Adatte, 1988).

The shape of clinoforms (Steinhauser and Charollais, 1971; Blanc, 1996; Hillgärtner, 1999), the weak slope angle (estimated at 2° in the south-east direction at the West Chartreuse cliff after Blanc, 1996) and the large extension of shallow-water carbonates all indicate a progressive deepening of environments. However, the presence of resedimented, metre-sized, coral blocks in sediments close to the Jurassic–Cretaceous boundary in the Dauphinois area supports the presence of a distal escarpment (Remane, 1963; Arnaud-Vanneau *et al.*, 1992). Consequently, the platform probably possessed a distally steepened ramp morphology during the Berriasian.

Clinoform shapes have been recognised in the Pierre Châtel and Vions Formations and Lower and Upper Members of the Chambotte Formation (Gréselle, 2007). The lagoons are well-defined (Darsac, 1983; Blanc, 1996; Hillgärtner, 1999) and locally, the development of patch reefs is observed (Steinhauser and Charollais, 1971; Gréselle, 2007).

The Guiers Member represents the first interval without marked lateral variations in thickness (Gréselle, 2007) and indicates the first phase in the evolution of the platform without barrier and inner settings, which is probably due to relative sea-level rise.

The Upper Member of the Chambotte Formation shows the return of clinoform geometries (Gréselle, 2007), but patch reefs are less numerous than in the lower part of the formation (Blanc, 1996; Gréselle, 2007) and lagoonal settings have not been identified. The absence of a lagoonal environment is expressed in the La Chambotte section by the absence of inner lagoonal deposits and the abundance of echinoderms in beach facies (F11). This absence is also supported by wave-ripple and oblique-bedding structures facies in the Jura area that indicate an almost permanent record of wave activity (Gréselle, 2007).

The episode of transgression recorded by the Guiers Member may be considered as the initiation of important morphological changes observed later in the early Valanginian. Indeed, the sediments of the Bourget and Calcaire Roux Formations do not document the presence of a protected lagoon (Arnaud-Vanneau and Arnaud, 1991; Blanc, 1996; Gréselle, 2007), but do show a change toward heterozoan carbonate production (Fig. 2.11). Proximal, nearshore representatives of these formations include pisolith and limonite resulting from the reworking of continental ferruginous soils, and are observed on top of a truncated surface marking a period of emersion and/or hardground formation (including a hiatus which is also documented by the relatively abrupt negative $\delta^{13}C$ shift). Close to the shore, the facies is rich in oolites, indicating a high-energy environment, and then changes to a facies dominated by bryozoans and echinoderms. The platform is interpreted as having a swell-dominated ramp morphology (Read, 1985). These deposits are the last record of a carbonate platform in the Jura before the Valanginian drowning phase, which is documented by the condensed layers of the Couches de Villers and the Asteria Marls (Hennig, 2003).

The Juracime and La Chambotte sections include very different records of the late Berriasian and earliest Valanginian, which show that the northern part of the Jura platform has passed through numerous and prolonged intervals of emersion resulting in a highly incomplete succession, whereas the more distal, meridional part of the Jura platform has preserved a more complete succession. Interestingly, the two sections show relatively similar facies and indicate similar internal, predominantly lagoonal palaeoenvironments during the late early and late Berriasian. Consequently, the differential record between the northern and southern Jura is attributed to inherited morphology and/or differential subsidence (Steinhauser and Charollais, 1971; Blanc, 1996; Hillgärtner, 1999).

Indeed, the morphology of the platform, a distally steepened ramp, implies a progressive increase in depth in a south-east direction; additionally, the sequence and parasequence boundaries observed in the Vions Formation and the ‘Unité Supérieure Gréseuse’ may be of tectonic origin given the abrupt relative sea-level variations that they

exhibit (Figs 4, 5 and 10). A major fault line which was supposed to be active in the late Valanginian (Charollais *et al.*, 1983) or through the Berriasian and Valanginian (Hillgärtner, 1999) is situated along the Vuache range, and may have induced enhanced subsidence in the meridional Jura. However, this fault is relatively minor and its impact on the carbonate deposits was probably not too important. Other major fault zones may therefore have played a role in the distribution of sediments, such as the Vue des Alpes-la Ferrière, or Eclepens-Pontarlier faults. As a consequence, regional tectonic activity may also have interfered with the distribution of the sequences determined in La Chambotte.

Based on the Jura sections, long-term sea-level change is interpreted as follows: a first transgression is observed in the late early Berriasian ('Unité Inférieure Oolitique' and Pierre-Châtel Formations) and the early late Berriasian (Vions Formation and 'Unité Supérieure Gréseuse'), followed by sea-level fall during the late Berriasian (top part of the 'Unité Supérieure Gréseuse' and Vions Formation). A second important transgression is evident in the uppermost Vions Formation and Lower Member of the Chambotte Formation in La Chambotte. This transgression is poorly recorded in the Juracime section given the uncertainty in dating for this time interval and the minimal thickness of the sediments, which possibly belong to this interval, and so its amplitude was probably less important. A second sea-level fall occurred in the latest Berriasian recorded at the top of the Lower Member of the Chambotte Formation, which is followed by a rather abrupt and high-amplitude transgression observed in the Juracime section and deduced from the evolution in microfacies in La Chambotte. The latter transgressive deposits correspond to the Guiers Member and its equivalent in the northern Jura, the Marls of Arziers (Fig. 2.10).

Within the Vocontian basin, numerous slumps dated from near the Berriasian–Valanginian boundary witness the destabilisation of sediments on the slope (Detraz *et al.*, 1987; Detraz and Steinhauser, 1988; Joseph *et al.*, 1988; Bulot *et al.*, 1994; Bulot, 1995; Blanc, 1996). Moreover, the active feeding of submarine canyons during the late Berriasian calpionellid zones D2 and D3 also shows the importance of sea-level fall and/or tectonic activity (Le Doeuff, 1977; Beaudoin *et al.*, 1987; Joseph *et al.*, 1988; Fig. 2.10) and corroborates the sequence stratigraphy scheme proposed herein.

In Montclus, the transgressive intervals correspond to increases in kaolinite content (Fig. 2.10): a first increase of minor amplitude is observed during calpionellid zone D2 and a second, large-amplitude increase is observed during the younger part of calpionellid zone D3. Interestingly, on the platform, the two corresponding transgressive intervals show a decrease in kaolinite content. As a consequence, these transgressive phases, which are associated with sediments enriched in quartz, phyllosilicates and pyrite, may have induced reworking in the surrounding submerged areas.

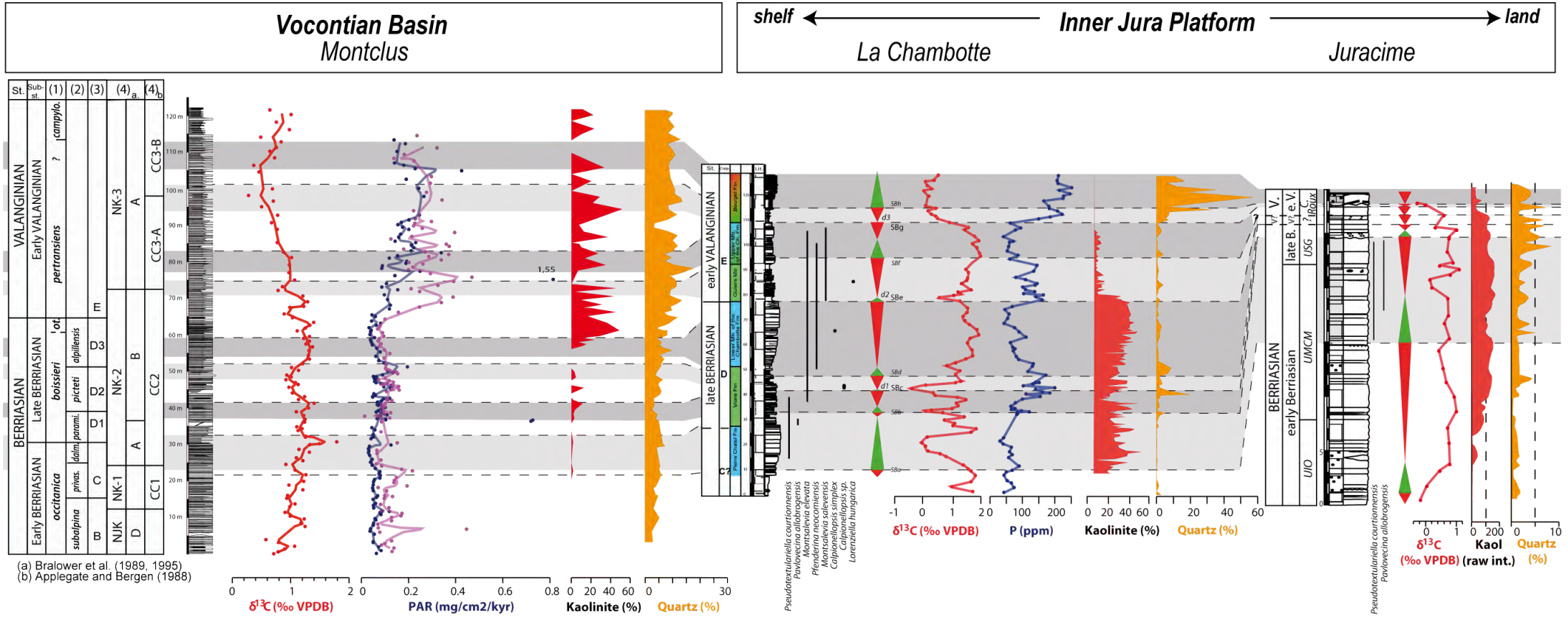

Fig. 2.10: Correlation of the sections of Montclus, La Chambotte and Juracime according to the biostratigraphy and $\delta^{13}C$ trends. Grey rectangles represent correlated intervals and dashed lines represent sequence boundaries.

A long period of emersion is recorded on the platform during the early Valanginian, which is followed by a generalised and large-amplitude transgression during the late early Valanginian with the deposition of the Calcaire Roux. Maximum flooding is probably documented within the Asteria Marls and corresponds to the widespread drowning of carbonate platforms during the latest early and late Valanginian.

The pronounced sea-level variations occurring in the late Berriasian and early Valanginian, have been attributed to the presence of polar ice caps (Price, 1999; Jacquin *et al.*, 1998; Gréselle and Pittet, 2010). An alternative hypothesis implies an increase in oceanic crust production during the early Valanginian, especially at the Pacific and Gondwana margins (Larson, 1991) related to generally enhanced tectonic activity for the Berriasian (Stampfli and Borel, 2002; Stampfli and Hochard, 2009; McArthur *et al.*, 2007) which was also noted in the western Tethyan area (Joseph *et al.*, 1988, Joseph *et al.*, 1989; Homberg *et al.*, in press). A further possibility to explain sea-level change during this period is the formation of large and extensive continental basins related to the continuing break up of Pangaea, and corresponding changes in the water level within those basins (Föllmi, 2012).

2.6. DISCUSSION

2.6.1. Modifications in the carbon cycle

The long-term changes in carbon-isotope composition can be correlated from the Jura to the Vocontian basin, and may reflect modifications in the carbon cycle at least at the regional scale. On the platform, the decrease in $\delta^{13}C$ values during the early Valanginian corresponds to a change in carbonate production from photozoan to heterozoan associations. These palaeoenvironmental changes may have been triggered by enhanced continental fluxes to the ocean involving higher input of both dissolved organic and inorganic carbon (DOC and DIC), as well as nutrients (e.g. Föllmi *et al.*, 2006).

The shift toward heterozoan carbonate production implies the dominance of calcitic producers to the detriment of aragonitic producers, which may also have triggered a decrease in $\delta^{13}C$ values. The $\delta^{13}C$ signature of the Vocontian Basin was influenced by the fluxes of platform-derived particulate carbonate and organic carbon (Reboulet *et al.*, 2003; Föllmi *et al.*, 2006). In the case of the presence of a rimmed platform morphology and photozoan carbonate production, the $\delta^{13}C$ signature of the basin tends to be heavier because of aragonite exportation and the weak influence of terrestrial DOC and DIC.

Reciprocally, without a rimmed platform morphology and heterozoan carbonate production, the $\delta^{13}C$ signature tends to be lighter because continental DIC and DOC fluxes are more important, and exported platform carbonate lacks an aragonite component (Swart & Eberli, 2005; Föllmi *et al.*, 2006). The differential evolution of the $\delta^{13}C$ records during the late Berriasian between the west Atlantic (Bornemann and Mutterlose, 2008) and the northern Tethyan margin may be related to the fact that the northern Tethyan records have been obtained on top of or close to the northern Tethyan carbonate platform, where aragonite production and exportation may have influenced the $\delta^{13}C$ records.

Interestingly, the decrease in $\delta^{13}C$ values in the earliest Valanginian is more important in the platform sections (of 1‰ and 1.3‰ in the Juracime and Chambotte sections, respectively) than in the basinal section of Montclus (0.7‰). This is probably due to a segregation effect with regard to the continental fluxes including light dissolved organic carbon between the platform and the outer shelf (Föllmi *et al.*, 2006; Godet *et al.*, 2008; Stein *et al.*, 2012).

2.6.2. Palaeoclimatic and palaeoenvironmental change

2.6.2.1. Climatic change

The platform sections exhibit similar trends in clay mineralogy, which appear to be inverse to those in the clay record of the basinal section of Montclus (Fig. 2.10). Variations in kaolinite content constitute a key for the understanding the palaeoenvironmental and palaeoclimatic changes affecting the NW Tethyan margin. In the platform sections, the high kaolinite content recorded in the late early and early late Berriasian is interpreted as evidence of a humid and hydrolysing climate on the continent (Adatte, 1988; Chamley, 1989).

The K/Ar age analyses performed on mica in Berriasian successions of the Jura platform indicate a Hercynian age and probably an origin from the Rhenian Massif (Adatte, 1988). The time of kaolinite formation is still debated, ranging from few thousands years up to few millions years (Thiry *et al.*, 1999). The Purbeckian and Upper Portlandian Formations on the Jura platform are devoid of kaolinite (Adatte, 1988), thus the kaolinite provenance may be interpreted as resulting from the weathering of older sedimentary deposits (e.g. paleozoic deposits, Scotese, 2002).

The presence of kaolinite has, however, been recorded in Berriasian sediments of NW Europe (Sladen, 1983; Abbink *et al.*, 2001; Schnyder *et al.*, 2006; Lindström and Erlström, *in press*) and in Tunisia (Schnyder *et al.*, 2005). Because kaolinite-rich deposits are found in an extended geographic area, independently of basins configurations, it is assumed here that the presence of kaolinite observed in the studied sections did not result from the weathering of older sedimentary successions.

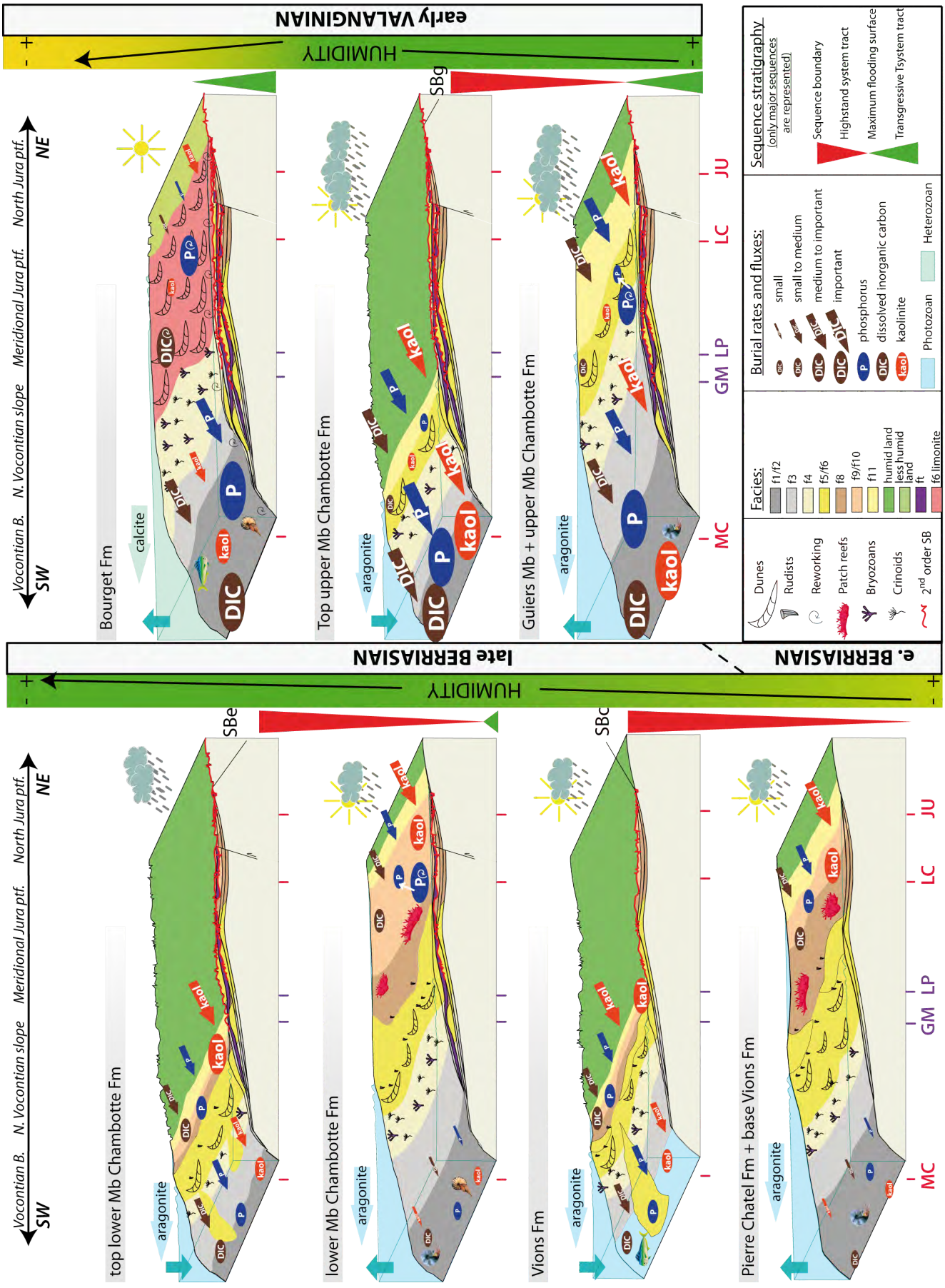

Fig. 2.11: Evolution of the Jura platform through the Berriasian–Valanginian boundary. MC, LC and JU (red colour) represent the sections of Montclus, La Chambotte and Juracime, respectively. GM and LP (purple colour) are the sections of Guiers Mort and La Pointière (Blanc, 1996), and belong to the outer ramp.

The high kaolinite contents on the late Berriasian platform are, however, in contrast to low kaolinite contents in the Vocontian Basin. This discrepancy illustrates well the segregation of kaolinite particles within the inner shelf where the platform has a rimmed morphology (Darsac, 1983; Adatte, 1983, 1988; Deconinck *et al.*, 1985; Godet *et al.*, 2008). In the NW European domain, Hallam *et al.* (1991), Abbink *et al.* (2001) and Schnyder *et al.* (2005) also identified the prevalence of a humid climate during the late Berriasian. The beginning of this increased humidity is recorded from the early Berriasian onwards in England (Deconinck, 1987b; Hallam *et al.*, 1991; Schnyder *et al.*, 2009), the Jura (Adatte, 1988; Fig. 2.4) and the Vocontian basin (late calpionellid zone B in Berrias after Deconinck, 1993; or early calpionellid zone C in Montclus, Fig. 2.7). The humid phase has been postulated to have started at the Jurassic–Cretaceous boundary (Abbink *et al.*, 2001, Lindström and Erlström, 2011), underlining the occurrence of a long-term climatic change.

Previous studies have demonstrated that the phase of important kaolinite depletion during the latest Berriasian (*d2* of Darsac, 1983) is synchronous on the Jura platform (Adatte, 1988). However, this change cannot be attributed to climate change because high kaolinite contents are observed in the basin (Fig. 2.10). In the Vocontian Basin, the clay mineralogy of marl-limestone alternances is majoritary climatically driven (Milankovitch cycles, Deconinck, 1987). Moreover, carbonate mud of platformal origin represents the major part of the calcareous fraction during the Valanginian (Reboulet *et al.*, 2003). Consequentely, a change in sedimentary source seems unlikely. This implies that kaolinite bypassed the platform and was deposited in the basin.

The facies associated with the Guiers Member and the Upper Member of the Chambotte Formation indicate the disappearance of a barrier and better access to marine environments. The rapid high-amplitude transgression on top of a partly emerged ramp with flat relief during the later part of calpionellid zone D3 prevented the deposition of kaolinite on the Jura platform and led to the direct exportation of detrital material into the basin. The high kaolinite contents observed in the TST occurring near the Berriasian–Valanginian boundary on the platform (La Chambotte section) are interpreted to have resulted from reworking of submerged deposits during the transgression, as indicated by mud pebbles observed in thin sections. Finally, later during the early Valanginian, a decrease in kaolinite was observed on the platform and in the basin, which is interpreted as a climate change toward less humid, and less hydrolysing conditions (Figs 2.9 and 2.10).

Surprisingly, the palynological record does not show a phase of enhanced humidity since the early Berriasian (Fig. 2.7). *Classopollis* is usually interpreted to reflect hot and arid conditions and *Araucariacites* indicates hot and slightly more humid conditions (Batten, 1984). Because of their relative compactness and density, the common presence of bisaccate pollen is mostly used as an indicator for temperate and humid conditions, and *Inaperturopollenites* and *Pteridophytes* for humid conditions; indeed, their morphology and weight prevented them from floating over long distances

(Keller *et al.*, 2011). In Montclus, the relative composition of pollen and spores appears to be strongly dependent on platform morphology (Fig. 2.7). The relative content in bisaccate pollen, *Inaperturopollenites* and *Pteridophytes*, is very low during the Berriasian whereas *Classopollis* is common. These trends are completely reversed in the early Valanginian. As with clay minerals the barrier probably induced a segregation of the pollen and spore particles, the lighter and rounder particles (for example, *Classopollis*) being transported toward the basin whereas the others were predominantly trapped in the lagoon (Traverse, 2007). The combined increase in bisaccate pollen and decrease in *Araucariacites* and *Classopollis* is interpreted to result from climate change toward less humid and more temperate conditions during the early Valanginian (Figs 2.9 and 2.10).

2.6.2.2. Detrital fluxes and nutrient levels

During the late Berriasian, a temporary increase in quartz and phosphorus values was observed in the two platform sections (in the Vions Formation and the 'Unité Supérieure Gréseuse'; Figs. 2.4, 2.5 and 2.9). This increase is correlated with a smaller increase in phosphorus accumulation rates observed in the Montclus section, whereas the quartz content remains low during this time period. The quartz is of detrital origin as seen in thin sections (Darsac, 1983; Blanc, 1996; Hillgärtner, 1999; this study); hence, the rimmed morphology of the platform may have buffered the variations in detrital fluxes (Fig. 2.11). This phase of enhanced continental input is dated as calpionellid zone D (later part of D2 by correlation with the basin; Fig. 2.10) and correlated with a succession of transgressive surfaces at the bottom of sequences and parasequences, which document the reworking of continental deposits. The relative sea-level variations involved are sometimes of very high amplitude, as seen from the microfacies analyses. The later part of calpionellid zone D2 also corresponds to the active infilling of submarine canyons and formation of slumps in the basin (Le Doeuff, 1977; Beaudoin *et al.*, 1987; Joseph *et al.*, 1988; Joseph *et al.*, 1989).

Consequently, as stated before, a tectonic implication (tilting of blocks) is probable, which may have lead to enhanced erosion of continental deposits and their transport onto the Jura platform. Nevertheless, a stepwise increase in humidity since the early Berriasian with a peak in calpionellid zone D2 is probably also involved.

A second increase in phosphorus values occurs in the earliest Valanginian and is observed in both platform and basinal environments (Figs 5 and 9). It corresponds to an important sea-level rise, the disappearance of the platform barrier and a tropical climate with a probable peak in humidity.

Detrital quartz was not very abundant on the platform as revealed by whole-rock mineralogy and thin sections. In the basin, high quartz contents were observed (Figs 6 and 9). As these elevated quartz contents are correlated with high phyllosilicate and kaolinite contents, the quartz has, at least in part, a detrital origin which may be related to

the disappearance of the rimmed platform. The increase in phosphorus contents both in marl and limestone lithologies indicates that marine productivity started to increase at that time, which is also documented by the Sr/Ca record and the nannofossils in the hypostratotypic section of Angles (Duchamp-Alphonse, 2006; Duchamp-Alphonse *et al.*, 2007). Therefore, it cannot be excluded that a part of the increase in quartz content is of biogenic origin and related to the presence of radiolarians (since sponge spicules have only sparsely been observed in thin sections).

A third period of increase in phosphorus values was observed on the platform during the early Valanginian, and corresponds to the heterozoan facies of the Calcaire Roux and Bourget Formations and high PAR values in the basin (in particular in limestone lithologies). The quartz measured corresponds mostly to silica of biogenic origin, as observed in thin sections. Consequently, the high phosphorus values are mostly related to high nutrient levels. In addition to the Tethys ocean, this enhanced fertilisation of ocean waters has been recognised in the Atlantic (Bornemann and Mutterlose, 2008) and reaches its maximum during the initiation of the positive $\delta^{13}C$ shift which characterises the Valanginian Weissert episode (Föllmi *et al.*, 2007; Duchamp-Alphonse *et al.*, 2007). This episode is usually proposed as a possible trigger for the drowning of carbonate platforms (Lini *et al.*, 1992; Föllmi *et al.*, 1994; Weissert *et al.*, 1998; Föllmi *et al.*, 2007). The climatic change toward less humid and hydrolysing conditions during the early Valanginian negative carbon-isotope shift is not compatible with a scenario in which primary productivity continues to increase.

The occurrence of a high-amplitude transgression (sequences g and h) leading to widespread inundation of lateritic soils may have induced significant reworking of sediments, which fertilised ocean waters during the middle part of the early Valanginian. During the late early Valanginian, an intensification of winds and marine currents may have led to the upwelling of cold and nutrient-rich waters facilitated by the change in platform morphology and the long-term transgression, assuring the connection between the Boreal and Tethyan Ocean; this is also supported by the increase in $\delta^{18}O$ values observed for this episode (McArthur *et al.*, 2007).

These observations confirm that the Valanginian is a period of major perturbations in carbonate production and that the important excursion in the stable carbon-isotope record was preceded by major environmental change which may have started in the Berriasian with a shift towards more humid climate conditions. This phase is documented by significant sea-level change, a shift between photozoan and heterozoan carbonate production and a general increase in detrital and phosphorus fluxes.

2.7. CONCLUSIONS

In this contribution, two proximal sections of the Jura platform (Juracime and La Chambotte) and a basinal section of the Vocontian Trough (Montclus) were studied in order to unravel palaeoclimatic and palaeoenvironmental conditions during the late Berriasian and early Valanginian. Benthic foraminifera, calpionellids, ammonites, sequence stratigraphies and $\delta^{13}C$ trends have been used to obtain age control in order to correlate the sections along a platform to basin transect. A more accurate early Valanginian age (late *T. pertransiens*/*B. campylotoxus* zones) is proposed for the Bourget and Calcaire Roux Formations which do not record the positive carbon-isotope excursion (CIE) of the Weissert episode in the studied area. The combination of stratigraphical, sedimentological, geochemical and mineralogical approaches along the transect enables the differentiation of the controlling factors in the sedimentation processes. Major sea-level changes have been identified which led to the formation of important hiatuses on the platform and affected the mineralogical record. Sedimentation processes appear to have been driven strongly by the morphology of the platform, which played a major role in the distribution of clay minerals, detrital quartz grains, and pollen and spores, and influenced the $\delta^{13}C$ record. Changes in kaolinite content, therefore, cannot be used as a stratigraphic tool to correlate between the platform and basin because its variations are inverted; however, it remains a useful proxy for tracing palaeoclimatic conditions. The observation of enhanced humidity in the western European domain, which started in the early Berriasian and reached a maximum in the earliest Valanginian, is consistent with previous studies. This paroxysmal phase of humidity combined with significant sea-level variations (abrupt transgression onto a partly emerged ramp) probably led to the disappearance of the barrier near the Berriasian–Valanginian boundary. In parallel, with the disappearance of the barrier and the presence of a humid climate, enhanced nutrient stocks probably induced the fertilisation of basinal waters. Later in the early Valanginian (late *T. pertransiens* zone), the climate became less humid. However, the carbonate producers changed toward heterozoan faunal associations and nutrient contents and marine productivity continued to increase up to the maximum of the CIE of the Weissert episode. The occurrence of a major transgression onto lateritic soils followed by the installation of upwelling along the northern Tethyan margin has been assumed as a possible trigger. Major modifications in climate associated with important sea-level change near the Berriasian–Valanginian boundary led to the restructuring of the northern Tethyan margin and a profound change in sedimentation patterns. Because they play an important role in the nutrient supply of the ocean waters, these factors are considered here as a primer of the Weissert episode.

Acknowledgments

The authors would like to thank Liliane Dufresne for assistance in laboratory work. We are also grateful to Lucie Bonvallet, Maximilien Bôle and Melody Stein for their help in the field, and to Alexis Godet for stimulating discussions. We gratefully acknowledge the constructive and very helpful reviews by Adrian Immenhauser, Jörg Mutterlose and guest editor Helmut Weissert. Financial support from the Swiss National Science Foundation (project 200020_126455) is appreciatively acknowledged.

References

Abbink, O., Targarona, J., Brinkhuis, H. and **Visscher, H.** (2001) Late Jurassic to earliest Cretaceous palaeoclimatic evolution of the southern North Sea. *Global Planet. Change*, **30,** 231-256.

Adatte, T. (1988) *Etude sédimentologique, minéralogique, micropaléontologique et stratigraphique du Berriasien - Valanginien du Jura central.* Université de Neuchâtel, 481 pp.

Adatte, T., Stinnesbeck, W. and **Keller, G.** (1996) Lithostratigraphic and mineralogic correlations of near K/T boundary sediments in northeastern Mexico: Implications for origin and nature of deposition. In: *The Cretaceous-Tertiary Event and Other Catastrophes in Earth History*. (Ed G. Ryder, Fastovsky, D. and Gartner, S.,), **307**, pp. 211-226. Geol. Soc. Am. Spec. Pap., Boulder, Colorado.

Applegate, J.L. and **Bergen, J.A.** (1988) Cretaceous calcareous nannofossil biostratigraphy of sediments recovered from the Galicia Margin of Leg 103. *Proc. Oc. Drill. Progr., Sci. Res.*, **103**.

Arnaud, H., Gidon, M. and **Thieuloy, J.-P.** (1981) Les calcaires du Fontanil des environs de Grenoble: leur place dans la stratigraphie du Néocomien entre le Jura et le domaine vocontien. *Eclog. geol. Helv.*, **74,** 109-137.

Arnaud-Vanneau, A. and **Arnaud, H.** (1991) Sédimentation et variations relatives du niveau de la mer sur les plates-formes carbonatées du Berriasien-Valanginien inférieur et du Barrémien dans les massifs subalpins septentrionnaux et le Jura (Sud-Est de la France). *Bull. Soc. Géol. Fr.*, **162,** 535-545.

Arnaud-Vanneau, A. and **Arnaud, H.** (2005) Carbonate facies and microfacies of the Lower Cretaceous carbonate platforms. In: *The Hauterivian-Lower Aptian sequence stratigraphy from Jura Platform to Vocontian Basin: A multidisciplinary approach* (Ed T. Adatte, Arnaud-Vanneau, A., Arnaud, H., Blanc-Aletru, M.-C., Bodin, S., Carrio-Schaffhauser, E., Föllmi, K. B., Godet, A., Raddadi, M. C. and Vermeulen, J.), **7**, pp. 39-68. Géologie Alpine, Série Spéciale «Colloques et Excursions»

Attewel, P.B. and **Farmer, I.W.** (1976) *Principles of engineering geology*. Chapman and Hall.

Batten, D.J. (1984) Palynology, climate and the development of Late Cretaceous floral

provinces in the Northern Hemisphere; a review. In: *Fossils and Climate* (Ed P. Brenchley), pp. 127-164. Wiley, Chichester and New York.

Beaudoin, B., Joseph, P. and **Cojan, I.** (1987) Resédimentation au Jurassique terminal - Berriasien: Mécanismes et paléomorpologies. *Géol. Alp., mém. H.S.*, **13,** 187-196.

Blanc, E. (1996) *Transect plate-forme - bassin dans les séries carbonatées du Berriasien supérieur et du Valanginien inférieur (domaines Jurassiens et nord-Vocontien). Chronostratigraphie et transferts de sédiments.*, Joseph Fournier, Grenoble, 312 pp.

Blanc, E., Arnaud-Vanneau, A., Arnaud, H., Bulot, L.G., Gidon, M., Thieuloy, J.-P. and **Remane, J.** (1992) Les couches du passage Berriasien-Valanginien dans le sectieur du Fontanil (Isère, France). *Géol. Alp.*, **68,** 3-12.

Bodin, S., Godet, A., Vermeulen, J., Linder, P. and **Föllmi, K.B. (2006)** Biostratigraphy, sedimentology and sequence stratigraphy of the latest Hauterivian – Early Barremian drowning episode of the Northern Tethyan margin (Altmann Member, Helvetic nappes, Switzerland). *Eclog. geol. Helv.*, **99**, 157-174.

Boisseau, T. (1987) *La plate-forme jurassienne et sa bordure subalpine au Berriasien - Valanginian (Chartreuse-Vercors). Analyse et corrélations avec les séries de bassin*. Université scientifique Technologique et Médicale de Grenoble, Grenoble, 413 pp.

Bonin, A. (2011) *Relation entre les variations climatiques, les perturbations du cycle du Carbone et les crises de la production carbonatée: Application au Crétacé inférieur*. Université de Bourgogne, Dijon, 251 pp.

Bornemann, A. and **Mutterlose, J.** (2008) Calcareous nannofossil and $\delta^{13}C$ records from the Early Cretaceous of the Western Atlantic ocean: evidence of enhanced fertilization accross the Berriasian-Valanginian transition. *Palaios*, **23,** 821-832.

Bown, P.R., Rutledge, D.C., Crux, J.A. and Gallagher, L.T. (1998) *Calcareous Nannofossil Biostratigraphy* (Ed. P.R. Bown), pp. 86-102. Chapman and Hall, Cambridge.

Bralower, T.J., Monechi, S. and **Thierstein, H.R.** (1989) Calcareous Nannofossil Zonation of the Jurassic-Cretaceous boundary Interval and Correlation with the Geomagnetic Polarity Timescale. *Mar. Micropal.*, **14,** 153-235.

Bralower, T.J., Leckie, R.M., Sliter, W.V. and **Thierstein, H.R.** (1995) An integrated Cretaceous microfossil biostratigraphy. *SEPM Spec. Publ.*, **54,** 65-79.

Bulot, L.G. (1995) *Les formations à ammonites du Crétacé inférieur dans le Sud-Est de la France (Berriasien à Hauterivien) : biostratigraphie, paléontologie et cycles sédimentaires*. Muséum National d'Histoire Naturelle, Paris, 397 pp.

Bulot, L.G. and **Thieuloy, J.-P.** (1994) Les biohorizons du Valanginien du Sud-Est de la France : un outil fondamental pour les corrélations au sein de la Téthys occidentale. *Géol. Alp., Mém. H.S.*, **20,** 15-42.

Chamley, H. (1989) *Clay Sedimentology*. Springer-Verlag, Berlin.

Charollais, J., Clavel, B., Amato, E., Busnardo, R., Steinhauser, N., Macsotay, O. and **Donze, P. (1983)** Etude préliminaire de la faille du Vuache (Jura méridional). *Bull. Soc. Vaud. Sc. nat.*, **76,** 217-256.

Charollais, J., Clavel, B., Busnardo, R. and **Schroeder, R.** (1992) *Excursion du Groupe Français du Crétacé, Haute-Savoie: 25-27 mai 1992*. Département de géologie et de paléontologie de l'Université de Genève, Genève.

Choquette, P.W. and **James, N.P.** (1987) Diagenesis in Limestones - 3. The Deep Burial Environment. *Geosci. Canada*, **14,** 3-35.

Darsac, C. (1983) *La plate-forme berriaso-valanginienne du Jura méridional aux massifs subalpins (Ain, Savoie)*. Université de Grenoble 1, Grenoble, 319 pp.

Deconinck, J.-F. and **Chamley, H.** (1983) Héritage et diagénèse des minéraux argileux dans les alternances marno-calcaires du Crétacé Inférieur du domaine subalpin. *CR Acad. Sc. - Series II*, **297,** 589-594.

Deconinck, J.-F. (1987a) Identification de l'origine détritique ou diagénétique des assemblages argileux : le cas des alternances marne-calcaire du Crétacé inférieur subalpin. *Bull. Soc. Géol. Fr.*, **8,** 139-145.

Deconinck, J.-F. (1987b) Minéraux argileux des faciès purbeckiens : Jura suisse et français, Dorset (Angleterre), et Boulonnais (France). *Ann. Soc. Géol. Nord*, **106,** 285-297.

Deconinck, J.-F., Beaudoin, B., Chamley, H., Joseph, P. and **Raoult, J.F.** (1985) Contrôles tectonique, eustatique et climatique de la sédimentation argileuse du domaine subalpin français au Malm-Crétacé. *Rev. Géol. Dyn. Géogr. Phys*, **26,** 311-320.

Deville, Q. (1990) Chronostratigraphie et lithostratigraphie synthétique du Jurassique supérieur et du Crétacé inférieur de la partie méridionale du Grand-Salève (Haute-Savoie, France). *Archives des Sciences*, **43,** 215-235.

Delaygue, G., Bard, E., Rollion, C., Jouzel, J., Stièvenard, M., Duplessy, J.-C. and **Ganssen, G.** (2001) Oxygen isotope/salinity relationship in the northern Indian Ocean. *J. Geophys. Res.*, **106,** 4565-4574.

Detraz, H. and **Steinhauser, N.** (1988) Le bassin delphino-helvétique savoyard et sa marge jurassienne sous contrôle tectonique entre le Kimméridgien et le Valanginien. *Eclog. geol. Helv.*, **81,** 125-154.

Detraz, H., Charollais, J. and **Remane, J.** (1987) Le Jurassique supérieur - Valanginian des chaînes subalpines septentrionales (massif des bornes et de Platé, Haute-Savoie; Alpes occidentales): Analyse des resédimentations, architecture du bassin et influences des bordures. *Eclog. geol. Helv.*, **80,** 69-108.

Duchamp-Alphonse, S. (2006) *Changements paléoenvironnementaux et production carbonatée hémipélagique de la marge Nord-Ouest Téthysienne durant le Valanginien. Approches minéralogique, micropaléontologique et géochimique.* Université Orsay, Paris-sud, 303 pp.

Duchamp-Alphonse, S., Gardin, S., Fiet, N., Bartolini, A., Blamart, D. and **Pagel, M.** (2007) Fertilization of the northwestern Tethys (Vocontian basin, SE France) during the Valanginian carbon isotope perturbation: Evidence from calcareous nannofossils and trace element data. *Palaeogeogr., Palaeoclim., Palaeoecol.*, **243,** 132-151.

Emmanuel, L. and **Renard, M.** (1993) Carbonate geochemistry (Mn, $\delta^{13}C$, $\delta^{18}O$) of the late Tithonian – Berriasian pelagic limestones of the Vocontian trough (SE

France). *Bull. Centre Rech., Explor. Prod. Elf-Aquitaine*, **17,** 205-221.

Erba, E. (2004) Calcareous nannofossils and Mesozoic oceanic anoxic events. *Mar. Micropal.*, **52,** 85-106.

Erba, E., Bartolini, A. and **Larson, R.L.** (2004) Valanginian Weissert oceanic anoxic event. *Geology*, **32**, 149–152.

Föllmi, K.B. (1995) 160 m.y. record of marine sedimentary phosphorus burial: Coupling of climate and continental weathering under greenhouse and icehouse conditions. *Geology*, **23,** 859-862.

Föllmi, K.B., Weissert, H., Bisping, M. and **Funk, H.** (1994) Phosphogenesis, carbon-isotope stratigraphy, and carbonate-platform evolution along the Lower Cretaceous northern Tethyan margin. *Geol. Soc. Am. Bull.*, **106,** 729-746.

Föllmi, K.B., Godet, A., Bodin, S. and **Linder, P.** (2006) Interactions between environmental change and shallow water carbonate buildup along the northern Tethyan margin and their impact on the Early Cretaceous carbon isotope record. *Paleoceanography*, **21,** PA4211.

Föllmi, K.B., Bodin, S., Godet, A., Linder, P. and **van de Schootbrugge, B.** (2007) Unlocking paleo-environmental information from Early Cretaceous shelf sediments in the Helvetic Alps: stratigraphy is the key! *Swiss J. Geosci.*, **100,** 349-369.

Föllmi, K.B. (2012) Early Cretaceous life, climate and anoxia. *Cretaceous Res.*, **35,** 230-257.

Funk, H., Föllmi, K.B. and **Mohr, H.M.** (1993) Evolution of the Tithonian-Aptian Carbonate Platform along the Northern Tethyan Margin, Eastern Helvetic Alps. In: *Cretaceous Carbonate Platforms* (Eds. J.A.T. Simo, R.W. Scott and J.-P. Masse), pp. 387-408. AEPG.

Godet, A., Bodin, S., Adatte, T. and **Föllmi, K.B.** (2008) Platform-induced clay-mineral fractionation along a northern Tethyan basin-platform transect: implications for the interpretation of Early Cretaceous climate change (Late Hauterivian-Early Aptian). *Cretaceous Res.*, **29,** 830-847.

Gréselle, B. (2007) *Impact des variations paléoclimatiques sur la sédimentation carbonatée au Valanginien*, Lyon1 Claude-Bernard, Lyon.

Gréselle, B. and **Pittet, B.** (2010) Sea-level reconstructions from the Peri-Vocontian Zone (south-east France) point to Valanginian glacio-eustasy. *Sedimentology*, **57,** 1640-1684.

Hallam, A., Grose, J.A. and **Ruffell, A.H.** (1991) Palaeoclimatic significance of changes in clay mineralogy across the Jurassic-Cretaceous boundary in England and France. *Palaeogeogr., Palaeoclimat., Palaeoecol.*, **81,** 173-187.

Hennig, S., Weissert, H. and **Bulot, L.G.** (1999) C-isotope stratigraphy, a calibration tool between ammonite- and magnetostratigraphy. *Geol. Carpath.*, **50,** 91-96.

Hennig, S. (2003) *Geochemical and sedimentological evidence for environmental changes in the Valanginian (early Cretaceous) of the Tethys region*. ETH Zurich, 189 pp.

Hillgärtner, H. (1999) *The evolution of the French Jura platform during the Late Berriasian to Early Valanginian: controlling factors and timing*. Université de

Fribourg, Fribourg, 203

Hillgartner, H. and **Strasser, A.** (2003) Quantification of high-frequency sea-level fluctuations in shallow-water carbonates: an example from the Berriasian-Valanginian (French Jura). *Palaeogeogr., Palaeoclimat., Palaeoecol.,* **200,** 43-63.

Homberg, C., Schnyder, J. and **Benzaggagh, M.** Late Jurassic-Early Cretaceous faulting in the Southeastern French Basin: does it reflect a tectonic reorganization? *Bull. Soc. Géol. Fr.*, in press.

Jacquin, T., Rusciadelli, G., Amedro, F., De Graciansky, P.-C. and **Magniez-Jannin, F.** (1998) The North Atlantic cycle: an overview of 2nd-order transgressive/regressive facies cycle in the Lower Cretaceous of Western Europe. *SEPM Spec. Publ.*, **60,** 397-409.

Joseph, P., Beaudoin, B., Sempéré, T. and **Maillart, J.** (1988) Vallées sous-marines et systèmes d'épandages carbonatés du Berriasien vocontien (Alpes méridionales françaises). *Bull. Soc. Géol. Fr.*, **8,** 363-374.

Joseph, P., Beaudoin, B., Fries, G. and **Parize, O.** (1989) Les vallées sous-marines enregistrent au Crétacé inférieur le fonctionnement en blocs basculés du domaine vocontien. *CR Acad. Sci. - Series II,* **309,** 1031-1038.

Keller, C.E., Hochuli, P.A., Weissert, H., Bernasconi, S.M., Giorgioni, M. and **Garcia, T.I.** (2011) A volcanically induced climate warming and floral change preceded the onset of OAE1a (Early Cretaceous). *Palaeogeogr., Palaeoclimat., Palaeoecol.*, **305,** 43-49.

Kübler, B. (1983) Dosage quantitatif des minéraux majeurs des roches sédimentaires par diffraction X. *Cahiers de l'Institut de Géologie, Université de Neuchâtel, Suisse,* **AX1.1 and 1.2** 1-13.

Kübler, B. (1987) Cristallinité de l'illite: méthodes normalisées de préparation, méthode normalisée de mesure, méthode automatique normalisée de mesure. *Cahiers de l'Institut de Géologie, Université de Neuchâtel, Suisse,* **ADX 2.**

Kübler, B. and Jaboyedoff, M. (2000) Illite crystallinity *Comptes Rend. Acad. Sci. - Series IIA - Earth Planet. Sci.*, **331,** 75-89.

Kuhn, O. (1996) *Der Einfluss von Verwitterung auf die Paläozeanographie zu Beginn des Kreide-Treibhausklimas (Valanginian und Hauterivian) in der West-Tethys.* Eidgenössische Technische Hochschule Zürich, 380 pp.

Larson, R.L. (1991) Latest pulse of Earth: Evidence for a mid-Cretaceous superplume. *Geology*, **19,** 547-550.

Le Doeuff, D. (1977) *Rythmes et contournements synsédimentaires en série carbonatée alternante. Reconstitution paléomorphologique au Crétacé inférieur dans les chaînes subalpines méridionales*. Université Pierre et Marie Curie, Orsay, 240 pp.

Le Hégarat, G. (1971) *Le Berriasien du Sud-Est de la France,* Université Claude Bernard, Lyon, 567 pp.

Lini, A., Weissert, H. and **Erba, E.** (1992) The Valanginian carbon isotope event: a first episode of greenhouse conditions during the Cretaceous. *Terra Nova*, **4,** 374-384.

Masse, J.P. and **Philip, J.** (1981) Cretaceous coral-rudistid buildups of France. *SEPM Spec. Publ.*, **30,** 399-426.

Mc Arthur J.M., Jansenn N.M.M., Reboulet S., Leng, M.J., Thirlwall M.F. and **Van De Schootbrugge B:** (2007) Palaeotemperatures, polar ice-volume, and isotope stratigraphy (Mg/Ca, δ18O, δ13C, 87Sr/86Sr): The Early Cretaceous (Berriasian, Valanginian, Hauterivian). *Palaeogeogr., Palaeoclimat., Palaeoecol.*, **248,** 341-430.

Miller, K.G., Kominz, M.A., Browning, J.V., Wright, J.D., Moutain, G.S., Katz, M.E., Sugarman, P.J., Cramer, B.S., Christie-Blick, N. and **Pekar, S.F.** (2005) The Phanerozoic record of global sea-level change. *Science*, **310,** 1293-1298.

Pasquier, J.-B. (1995) *Sédimentologie, stratigraphe séquentielle et cyclostratigraphie de la marge Nord-Téthysienne au Berriasien en Suisse occidentale*. Université de Fribourg, Fribourg, 274 pp.

Pasquier, J.-B. and **Strasser, A.** (1997) Platform-to-basin correlation by high-resolution sequence stratigraphy and cyclostratigraphy (Berriasian, Switzerland and France). *Sedimentology*, **44,** 1071-1092.

Price, G.D. (1999) The evidence and implications of polar ice during the Mesozoic. *Earth-Sci. Rev.*, **48,** 183-210.

Reboulet, S. and Atrops, F. (1999) Comments and proposals about the Valanginian-Lower Hauterivian ammonite zonation of south-eastern France. *Eclog. Geol. Helvet.*, **92,** 183-197.

Reboulet, S., Mattioli, E., Pittet, B., Baudin, F., Olivero, D. and **Proux, O.** (2003) Ammonoid and nannoplankton abundance in Valanginian (Early Cretaceous) limestone-marl successions from the southeast France basin: carbonate dilution or productivity? *Palaeogeogr., Palaeoclimat., Palaeoecol.*, **201**, 113-139.

Reboulet, S., Hoedemaeker, P.J., Aguirre-Urreta, M.B., Alsen, P., Atrops, F., Baraboshkin, E.Y., Company, M., Delanoy, G., Dutour, Y., Klein, J., Latil, J.-L., Lukeneder, A., Mitta, V., Mourgues, F.A., Ploch, I., Raisossadat, N., Ropolo, P., Sandoval, J., Tavera, J.M., Vasicek, Z., Vermeulen, J., Arnaud, H., Granier, B. and **Premoli-Silva, I.** (2006) Report on the 2nd international meeting of the IUGS lower Cretaceous ammonite working group, the "Kilian Group" (Neuchâtel, Switzerland, 8 September 2005). *Cretaceous Res.*, **27,** 712-715.

Remane, J. (1963) Les calpionelles dans les couches du passage Jurassique-Crétacé de la fosse vocontienne. *Trav. Lab. Géol. Fac. Sci. Grenoble,* 25-82.

Remane, J. (1985) Calpionellids. In: *Plankton Stratigraphy* (Eds. H.M. Bolli, J.B. Saunders and K. Perch-Nielsen), **1**, pp. 555-572. Cambridge University Press, Cambridge.

Remane, J. (1998) Les calpionelles; possibilities biostratigraphiques et limitations paleobiogeographiques. *Bull. Soc. Géol. Fr.*, **169,** 829-839.

Schnyder, J., Gorin, G., Soussi, M., Baudin, F. and **Deconinck, J.-F.** (2005) Enregistrement de la variation climatique au passage Jurassique/Crétacé sur la marge sud de la Téthys : minéralogie des argiles et palynofaciès de la coupe du Jebel Meloussi (Tunisie centrale, formation Sidi Kralif). *Bull. Soc. Géol. Fr.*, **176,** 171-182.

Schnyder, J., Ruffell, A., Deconinck, J.-F. and **Baudin, F.** (2006) Conjunctive use of spectral gamma-ray logs and clay mineralogy in defining late Jurassic-early Cretaceous palaeoclimate change (Dorset, U.K.). *Palaeogeogr., Palaeoclimat., Palaeoecol.*, **229,** 303-320.

Schnyder, J., Baudin , F. and **Deconinck, J.-F.** (2009) Occurrence of organic-matter-rich beds in Early Cretaceous coastal evaporitic setting (Dorset, UK): a link to long-term palaeoclimate changes? *Cretaceous Res.*, **30**, 356-366.

Scotese, C.R. (2002) Paleomap Project.

Sissingh, W. (1977). Biostratigraphy of Cretaceous calcareous nannoplankton. *Geol. Mijnbouw*, **56,** 37-65.

Spangenberg, J.E. and **Macko, S.A.** (1998) Organic geochemistry of the San Vicente zinc-lead district, eastern Pucarà Basin, Peru. *Chem. Geol.*, **146,** 1-23.

Spangenberg, J.E., Fontboté, L. and **Macko, S.A.** (1999) An evaluation of the inorganic and organic geochemistry of the San Vicente Mississippi Valley-type zinc-lead district, central Peru: implications for ore fluid composition, mixing processes and sulfate reduction. *Econ. Geol.*, **94,** 1067-1092

Spangenberg, J.E. and **Herlec, U.** (2006) Hydrocarbon biomarkers in the Topla-Mezica zinc–lead deposits, Northern Karavanke/Drau range, Slovenia: paleoenvironment at the site of ore formation. *Econ. Geol.*, **101,** 997-1021.

Stampfli, G.M. and **Borel, G.D.** (2002) A plate tectonic model for the Paleozoic and Mesozoic constrained by dynamic plate boundaries and restored synthetic oceanic isochrons. *Earth Planet. Sci. Lett.*, **196,** 17-33.

Stampfli, G. and **Hochard, C.** (2009) Plate tectonics of the Alpine realm. *Geol. Soc., Lond., Spec. Pub.*, **327,** 89-111.

Stein, M., Westermann, S., Adatte, T., Matera, V., Fleitmann, D., Spangenberg, J. and **Föllmi, K.B.** (2012) Late Barremian–Early Aptian paleoenvironmental change: the Cassis-La Bédoule section (SE France). *Cretaceous Res.*, **37**, 209-222.

Steinhauser, N. (1969) *Recherches stratigraphiques dans le Crétacé inferieur de la Savoie occidentale (France)*. Université de Genève, Genève.

Steinhauser, N. and **Charollais, J.** (1971) Observations nouvelles et réflexions sur la stratigraphie du "Valanginien" de la région Neuchateloise et ses rapports avec le Jura méridional. *Géobios*, **4,** 7-59.

Swart, P.K. and **Eberli, G.E.** (2005) The nature of the $\delta^{13}C$ of periplatform sediments: Implications for stratigraphy and the global carbon cycle. *Sedim. Geol.*, **175**, 115-129.

Thirty, M., Simon-Coinçon, R. and Schmitt, J.M. (1999) Paléoaltérations kaolinitiques : signification climatique et signature dans la colonne sédimentaire. *Comptes Rendus de l'Académie des Sciences, Paris, Sciences de la Terre et des Planètes*, **329,** 853-863.

Traverse (2007) *Paleopalynology*. Springer, Dordrecht, 813 pp.

Tripati, A.K., Backman, J., Elderfield, H. and **Ferretti, P.** (2005) Eocene bipolar glaciation associated with global carbon cycle changes. *Nature*, **436,** 341-346.

Weissert, H., Lini, A., Föllmi, K.B. and **Kuhn, O.** (1998) Correlation of Early Cretaceous carbon isotope stratigraphy and platform drowning events: a possible

link? *Palaeogeogr., Palaeoclimat., Palaeoecol.*, **137,** 189-203.
Wyssling, G.W. (1986) Der frühkretazische helvetische Schelf im Vorarlberg und Allgäu. *J. Geol. Bundesanstalt,* **129,** 161-265.

CHAPTER 3:

EVOLUTION OF THE HELVETIC PLATFORM THROUGH THE BERRIASIAN-VALANGINIAN BOUNDARY

3. EVOLUTION OF THE HELVETIC PLATFORM THROUGH THE BERRIASIAN-VALANGINIAN BOUNDARY

CHLOE MORALES*, JORGE SPANGENBERG*, ANNIE ARNAUD-VANNEAU**, THIERRY ADATTE*, AND KARL B. FÖLLMI*

*Institute of Earth Sciences, University of Lausanne, Switzerland (chloe.morales@unil.ch)
** Association Dolomieu, 6 Chemin des Grenouilles, 38700 La Tronche, France

3.1. INTRODUCTION

The late Berriasian - early Valanginian interval is a crucial period to understand as it witnessed significant palaeoenvironmental and palaeoclimatic change prior to the positive carbon-isotope excursion (CIE) of the latest early to late Valanginian Weissert episode. In the western European domain, a phase of enhanced humidity is recorded since the late Berriasian, which probably reached a maximum in the earliest Valanginian (Hallam, 1991; Schnyder *et al.*, 2005; Morales *et al.*, 2013). This was followed by an increase in marine nutrient levels, which is recorded since the earliest Valanginian in western Tethyan basins (Föllmi, 1995; Duchamp Alphonse *et al.*, 2007) and platforms (Föllmi *et al.*, 2007; Morales *et al.*, 2013), which continued in the late Valanginian and was likely implied in the drowning of carbonate platforms during this period. Additionally, large sea-level variations occurred during this period, which are not well constrained and still under debate (Haq *et al.*, 1987; Schlager, 1981; Hardenbol *et al.*, 1998; Gréselle and Pittet, 2010). Increased tectonic activity in the western Tethys inducing regional differences in subsidence rates and sediment reworking also played a role in the palaeoenvironmental modifications during this period (Beaudoin *et al.*, 1987; Joseph *et al.*, 1988, 1989). Furthermore, a change in the morphology of the northern Tethyan carbonate platform from a distally steepened ramp to a swell-dominated ramp and the disappearance of a barrier through the Berriasian-Valanginian boundary documented in the Jura domain may have influenced the distribution of continental fluxes on the northern Tethyan shelf and adjacent basin (Morales et al., 2013).

The Helvetic thrust-and-fold belt in the northern Alps hosts distal parts of the same northern Tethyan carbonate platform and its transition to the outer shelf. Near the Berriasian-Valanginian boundary, a change from photozoan toward heterozoan carbonate production was documented (Ischi, 1978; Wyssling, 1986; Burger, 1985; Mohr, 1992; Föllmi *et al.*, 1994, 2007). In the following, the development of the heterozoan Helvetic platform was interrupted by the succession of two incipient drowning phases leading to the deposition of two condensed phosphatic and glauconitic-rich layers. The first, of

relatively short duration dates from the early Valanginian (late *T. pertransiens* - early *B. campylotoxus* ammonite zone) and is documented by the Büls Bed (Kuhn, 1996). The second, which corresponds to the crisis in carbonate production of the Weissert episode, is of longer duration (*T. verrucosum* to *C. loryi* ammonite zones) and is documented by the Gemsmättli Bed (Haldimann, 1977; Wyssling, 1986; Kuhn, 1996).

The aim of this work is to better understand and constrain the palaeoenvironmental and palaeoclimatic changes occurring before the Valanginian carbonate crisis in order to evaluate their roles as controlling factors leading to the Weissert episode. Subsequently, three sections have been selected along a proximal-distal transect through the northern Tethyan shelf: the sections of the Säntis, Dräckloch, and Vitznau belong to the inner shelf, the barrier and the outer shelf, respectively. The chronostratigraphic framework of the Helvetic platform is constrained by the study of benthic foraminifera and calpionellids, in combination with $\delta^{13}C$ whole-rock analyses. A sequence-stratigraphic frame based on microfacies analyses is proposed here and correlated with that of the Jura Mountains. The results of mineralogical and phosphorus analyses are also included here and are used to examine changes in ecology, nutrients and climate.

3.2. GEOLOGICAL SETTING

The three sections are located in the central and eastern part of Switzerland (Fig. 3.1). During the Alpine orogeny, the area was thrusted, overthrusted and folded in a northward direction, forming the Helvetic fold-and-thrust belt. During the Early Cretaceous, the northern Tethyan carbonate platform developed along the Rhenish shield in a southward direction (Fig. 3.1).

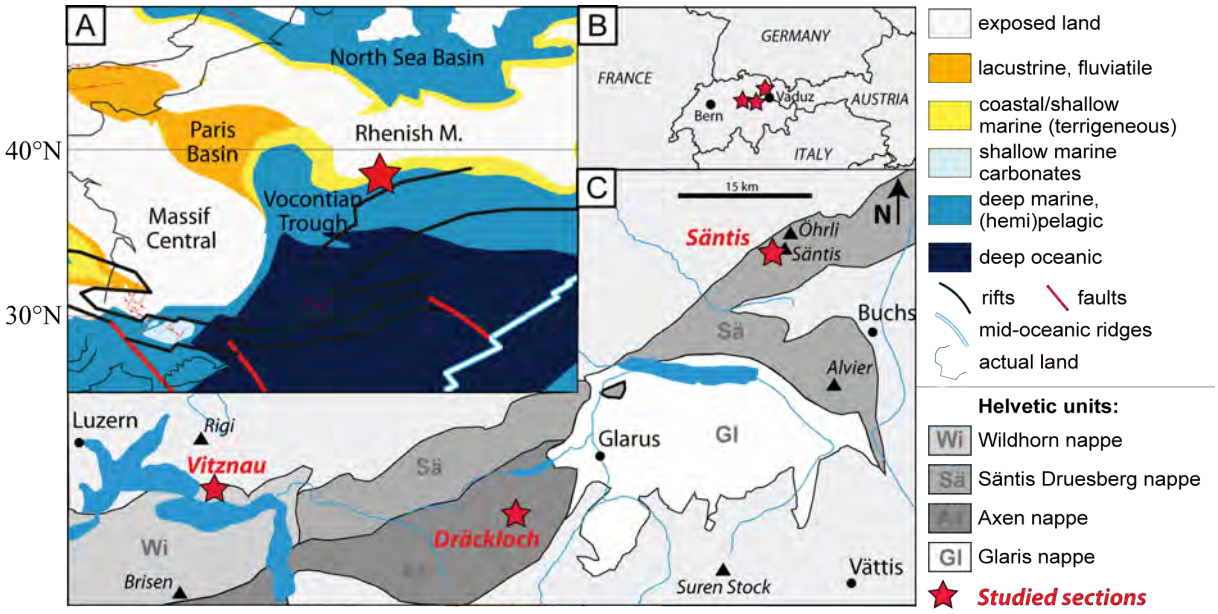

Fig. 3.1: Location of the sections. A) Palaeogeographic map; B) Map of Switzerland; C) Tectonic map.

The succession of Berriasian and Valanginian platform deposits is exposed in Fig. 3.2. It starts with the Zementstein Formation (Fm), characterised by dark monotonous marly deposits dated from the *B. jacobi* and *S. occitanica* zones (early Berriasian) by ammonites and calpionellids (Mohr, 1992). It is overlain by the Öhrli Fm, which documents the development of the photozoan carbonate platform with the deposition of bioclastic and oolitic sands, containing a rich and diversified fauna of benthic foraminifera, corals, green algae and echinoderms (Burger, 1985, 1986).

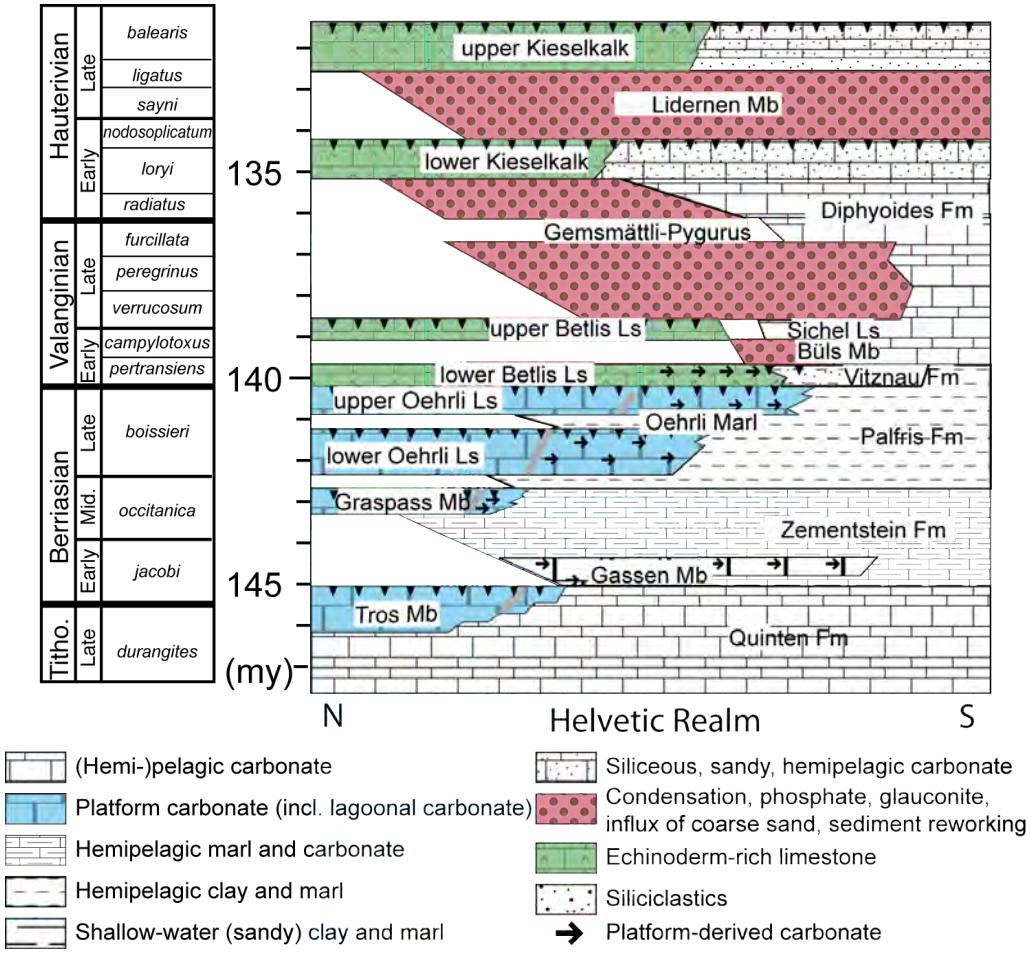

Fig. 3.2: Stratigraphy of the Helvetic Alps for the late Tithonian – Hauterivian interval (modified from Föllmi *et al.*, 2007).

The Öhrli Fm includes two marly and calcareous intervals - the Lower Öhrli Marl Member (LOM), Lower Öhrli Limestone Member (LOL mb), Upper Öhrli Marl Mb (UOM) and Upper Öhrli Limestone Mb (UOL). The age of the Öhrli Fm is poorly constrained. A maximal age is indicated by calpionellids and ammonites, which have been found at the base of the Öhrli Fm and indicate an early Berriasian age (*S. occitanica* zone) (Mohr, 1992). The Öhrli Fm is distally replaced by the monotonous hemipelagic marly succession of the Palfris Fm (Burger, 1985, 1986; Wyssling, 1986).

Both formations are overlain by the marly and sandy Vitznau Fm, which includes turbidites and was dated as early Valanginian by palynomorphs (Pantic and Burger, 1981). The overlaying Betlis Limestone Fm is rich in echinoderms and bryozoans and marks the development of the heterozoan platform. Wyssling (1986) relates the occurrence of an ammonite *Thurmanniceras thurmanni* s.l. originally described by Hauswirth (1912) in the Betlis Limestone Fm, which would attribute a *T. pertransiens* age for the Betlis Limestone Fm (or a part of it). Distal occurrences of the Betlis limestone Fm include the Büls Bed, which has been dated as late *T. pertransiens* - early *B. campylotoxus* (Kuhn, 1996). The overlying Gemsmättli Bed provides a minimal age corresponding to the *T. verrucosum* zone (Wyssling, 1986; Kuhn, 1996; Föllmi et al., 2007).

The Säntis section is located at the feet of the Säntis Mountain close to Schwägalp (canton Appenzell Ausserrhoden), 60km east of Zurich and 20 km northwest of Vaduz. It belongs to the Säntis-Drusberg nappe. The succession studied is approximately 105 m thick and includes the Upper Öhrli Limestone Mb, Vitznau Fm, Betlis Limestone Fm and Gemsmättli Bed (Fig. 3.3).

The Dräckloch section is situated 5 km south of the village of Richisau, 50 km southeast of Zürich and 50 km west of Vaduz on the border between the cantons of Glarus and Schwyz. The outcrop is part of the Gassenstock Mountain (Bös Fulen summit) and part of the Axen nappe. The measured section is 400 m thick and starts with the Öhrli Fm (LOL, UOM, and UOM), and goes on with the Vitznau Fm and the Betlis Limestone Fm (Fig. 3.4). The Betlis Limestone Fm is overlain by the sandy, coarse-grained sediments of the Pygurus Member, which is considered a lateral equivalent of the Gemsmättli Bed.

The Vitznau section is situated on the northern side of the lake of Lucerne, close to the village of Vitznau (Canton of Lucerne), 40 km south of Zürich. Tectonically it belongs to the “Randkette” attached to the Wildhorn nappe. The measured series is approximately 60 m thick and includes the UOM, the UOL, the Vitznau Fm and Betlis Limestone Fm (Fig. 3.5).

3.3. MATERIAL AND METHODS

3.3.1. Biostratigraphy

Benthic foraminiferal assemblages and calpionellids were examined (using thin sections) in order to improve the biostratigraphical framework. In addition, an ammonite was described from the Vitznau section.

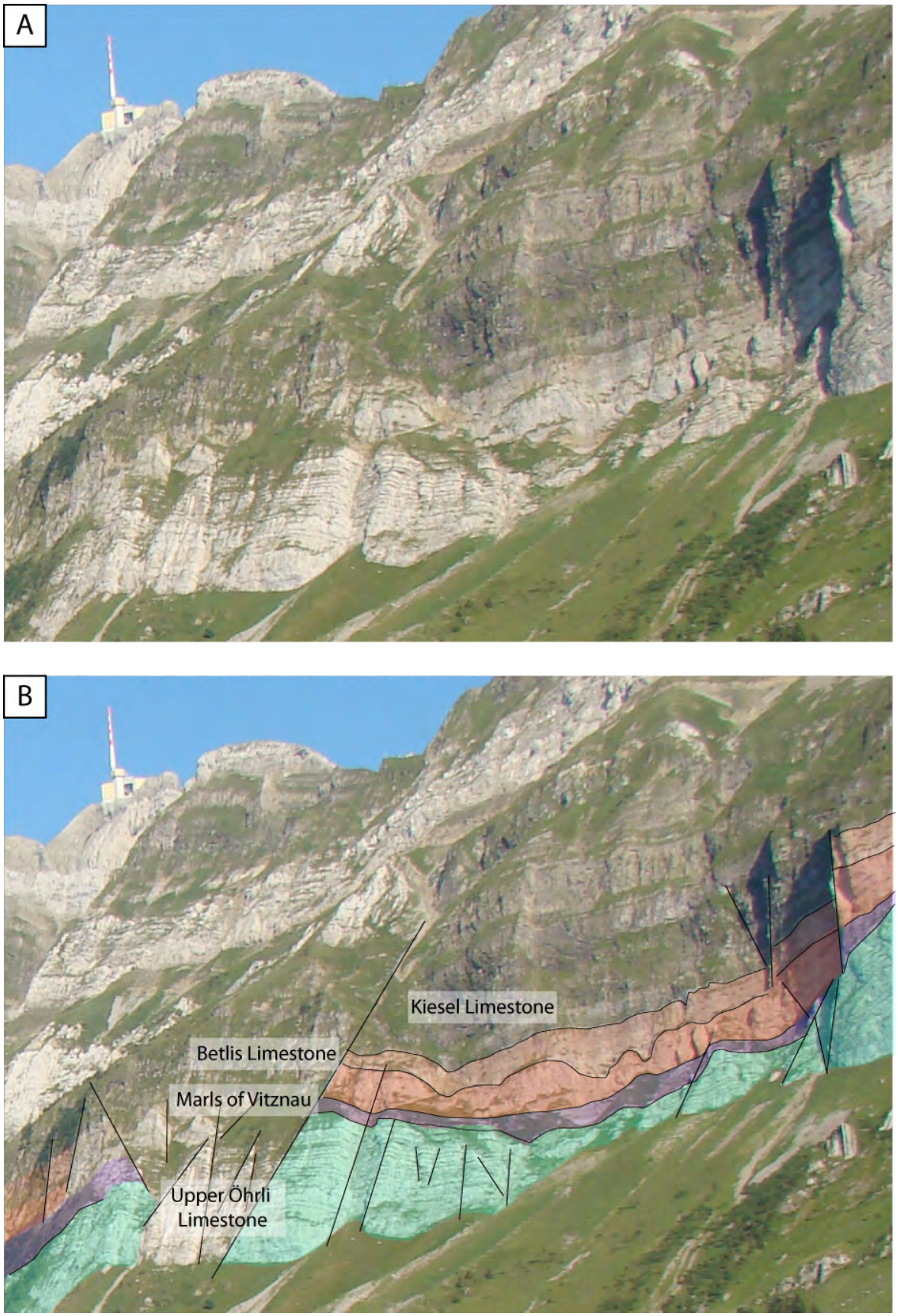

Fig. 3.3: Panorama of the northwestern slope of the Säntis Mountain. A) Image of the section; B) Stratigraphy

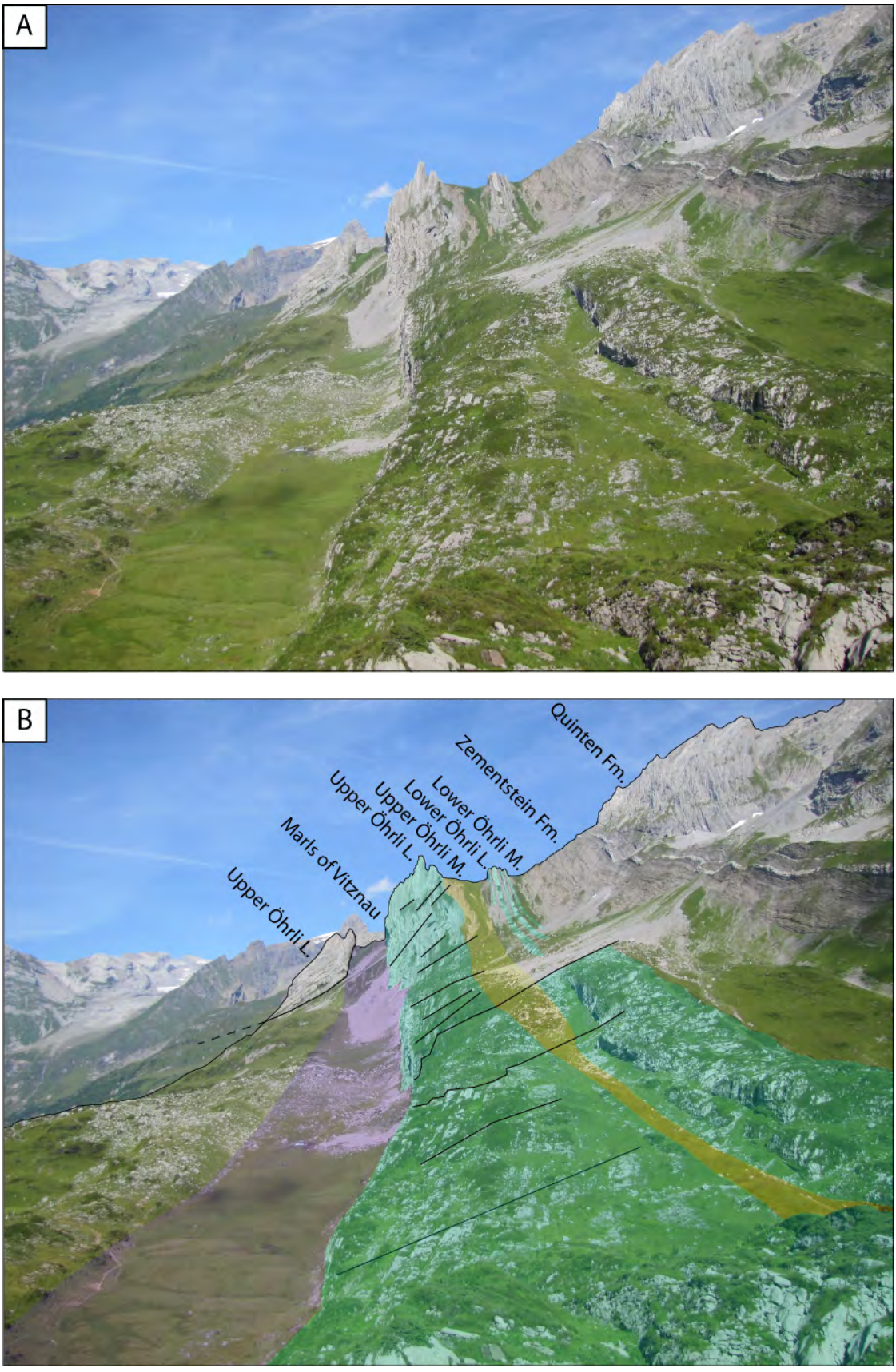

Fig. 3.4: Panorama of the Dräckloch area. A) Image of the section; B) Stratigraphy.

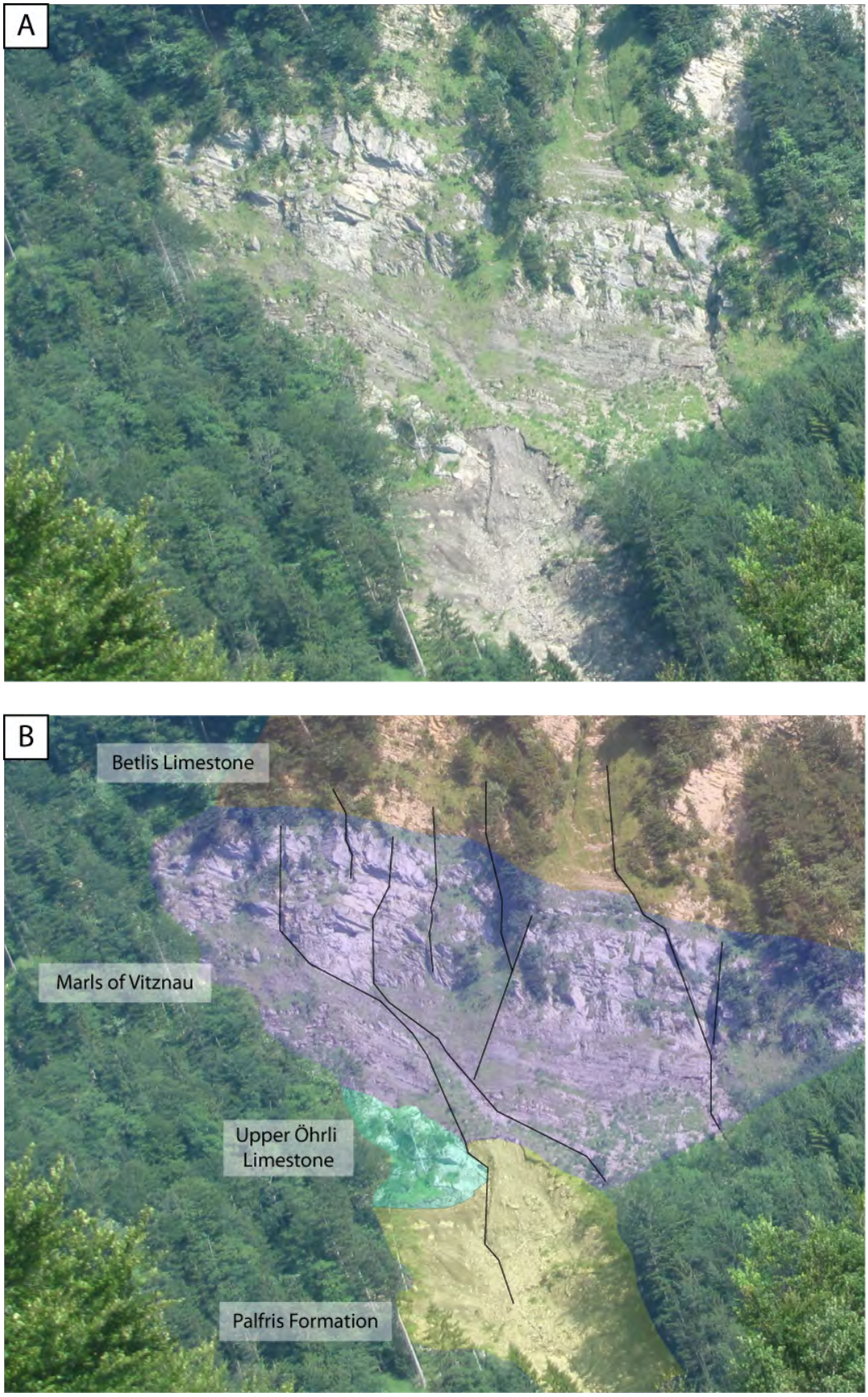

Fig. 3.5: Panorama of the Vitznau section. A) Image of the section; B) Stratigraphy

3.3.2. Microfacies and sequence stratigraphy

In total, 334 thin sections were used (152 for the Säntis section, 134 for the Dräckloch section and 48 for the Vitznau section). The microfacies was described and classified following Arnaud-Vanneau and Arnaud (2005), in which palaeoenvironments are identified principally as a function of ecological associations found in Lower Cretaceous carbonates (Fig. 2.3). These floro-faunal associations depend on water depth and light, nutrient availability, oxygen and salinity, temperature, nature of the substrate, sedimentation rate and hydrodynamic conditions. Twelve microfacies zones are thereby individualised, from F0 corresponding to pelagic or hemipelagic environments, to F11 attributed to tidal and supratidal environments.

3.3.3. Stable-isotope analyses

Carbon and oxygen-isotope contents were analysed on whole rock following the procedures described by Spangenberg and Macko (1998), Spangenberg *et al.* (1999), and Spangenberg and Herlec (2006). Samples were measured on a Thermo Fisher Scientific (formerly ThermoQuest/ Finnigan, Bremen, Germany) GasBench II preparation device interfaced with a Thermo Fisher Scientific Delta Plus XL continuous flow isotope ratio mass spectrometer (IRMS). CO_2 was extracted at 70°C. Ratios of carbon and oxygen isotopes are reported in the delta (δ) notation as the per mil (‰) deviation relative to the Vienna–Pee Dee belemnite standard (VPDB). The replicate analyses demonstrated an analytical reproducibility of the international calcite standard NBS-19 and of the laboratory standards Carrara Marble of better than ±0.05‰ for $\delta^{13}C$ and ±0.1‰ for $\delta^{18}O$. A total of 266 samples were analysed for their stable isotope content (69 from Säntis, 145 from Dräckloch and 52 from Vitznau).

3.3.4. Phosphorus content

Total phosphorus (P) contents were measured on 320 whole-rock samples (129 from the Säntis section, 143 from the Dräckloch section and 48 from the Vitznau section) following the procedure described in Bodin et al. (2006). The concentration of P is obtained in ppm by calibration with known standard solutions using a UV/Vis photospectrometer (Perking Elmer UV/Vis Photospectrometer Lambda 10, λ = 865 nm) with a mean precision of 5%.

3.3.5. Whole-rock and clay mineralogy

The whole-rock mineralogical analyses were carried out by X-ray diffraction. Measurements were performed on a Thermo scientific ARL X'TRA IP2500 diffractometer with a semi-quantification method using external standards and following

the procedures of Kübler (1983, 1987) and Adatte *et al.* (1996). The precision is 5-10% for phyllosilicates and 5% for grain minerals. 113 samples were run for the section of Säntis, 147 for the section of Dräckloch, and 47 for the section of Vitznau. Test measurements were performed to identify clay minerals (on the <2µm fraction) on which the peak intensities of identified minerals were measured in cps and the proportion of clay minerals was estimated in relative per cent.

3.4. RESULTS

3.4.1. Sedimentology and microfacies

- Säntis section

The lower part of the section, belonging to the upper part of the Öhrli Fm, is characterised by shallow-water platform microfacies evolving between the inner and the outer platform and characterised by an abundant fauna of large benthic foraminifera with few green algae, rudists, gastropods, calcareous sponges, corals, bivalves, and echinoderms. In contrast, the upper part of the section, which belongs to the Vitznau Fm and the Betlis Limestone Fm is characterised by deeper outer-platform microfacies with abundant echinoderms, bivalves, bryozoans (Vitznau Fm) and ostracods.

Three epikarstic levels are observed within the Upper Öhrli Limestone Mb. The first epikarst is located at 20 m and is indicated by dissolution features infilled by mud (Fig. 3.6), which affect the underlying sediment up to a depth of 2 m. Below this epikarst, the foraminifera *Pseudotextulariella courtionensis* is observed (Figs. 3.6 and 3.7). Emersive features are also observed at 26 m with infillings of cavities, which may correspond to dissolution features linked with an epikarst, or to mud cracks (Figs. 3.6 and 3.8A). The upper part of the Öhrli Fm (from 26 to 53 m) is dominated by muddy lagoonal facies in which *Montsalevia elevata* and *Pfenderina neocomiensis* were identified.

The marker calpionellid *Calpionellopsis simplex* was also identified (Fig. 3.9). The Öhrli Fm ends with an epikarst including dissolution vugs and infillings occurring on top of inner lagoonal facies characterised by enhanced microbial activity (intense micritisation of clasts), and the abundance of gastropods and miliolids with thin tests. The epikarst horizon separates the Upper Öhrli Fm from the overlaying Vitznau Fm, is a complex surface showing macroscopic perforations infilled by marly sediments of the Vitznau Fm (Fig. 3.6). These perforations are also noted in the immediately overlaying layer, which indicates the superposition of two hardgrounds at the base of the Vitznau Fm in this section.

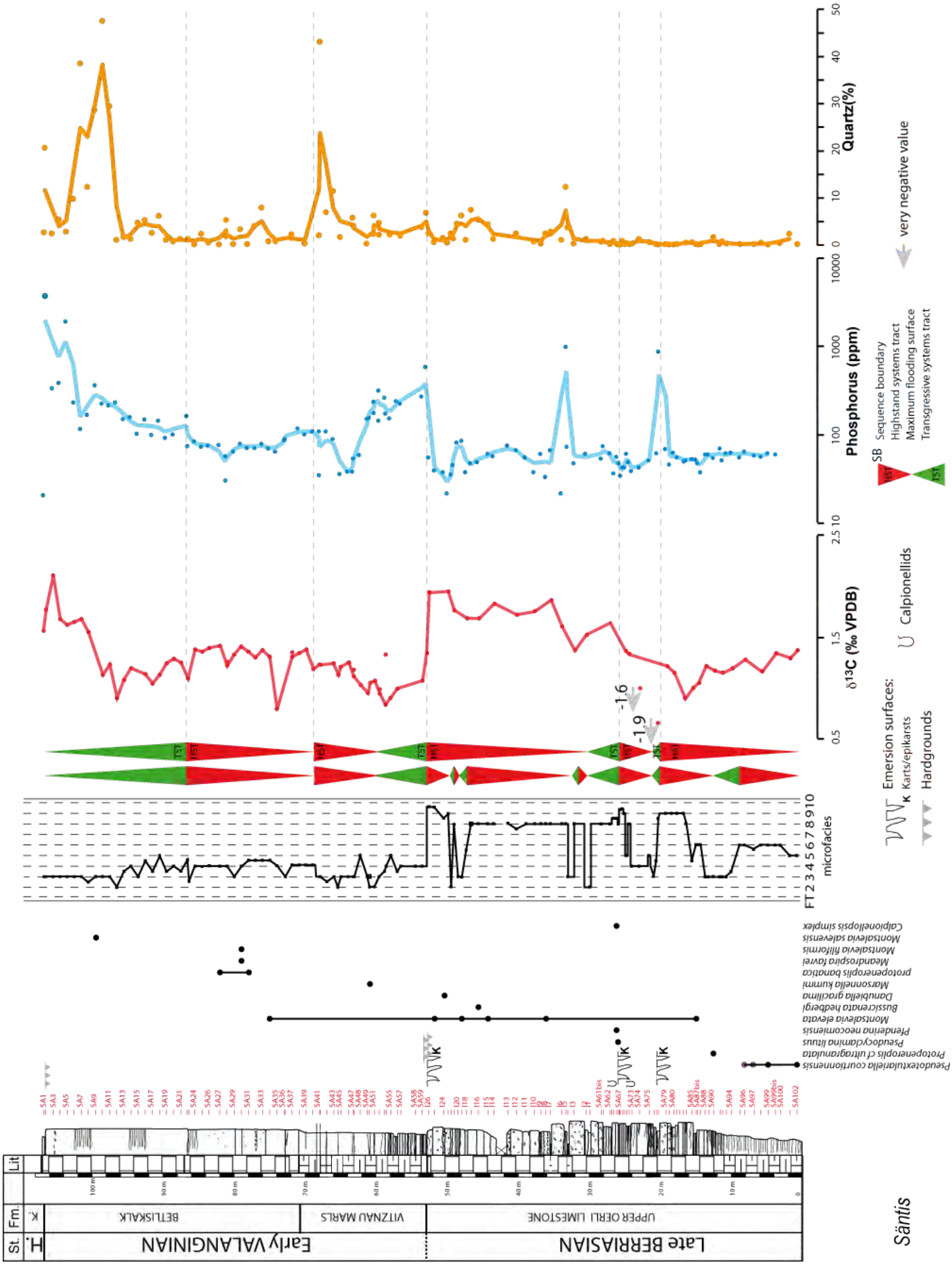

Fig. 3.6: Sedimentological, geochemical and mineralogical analyses performed on the Säntis section. Microfacies classification after Arnaud-Vanneau and Arnaud (2005).

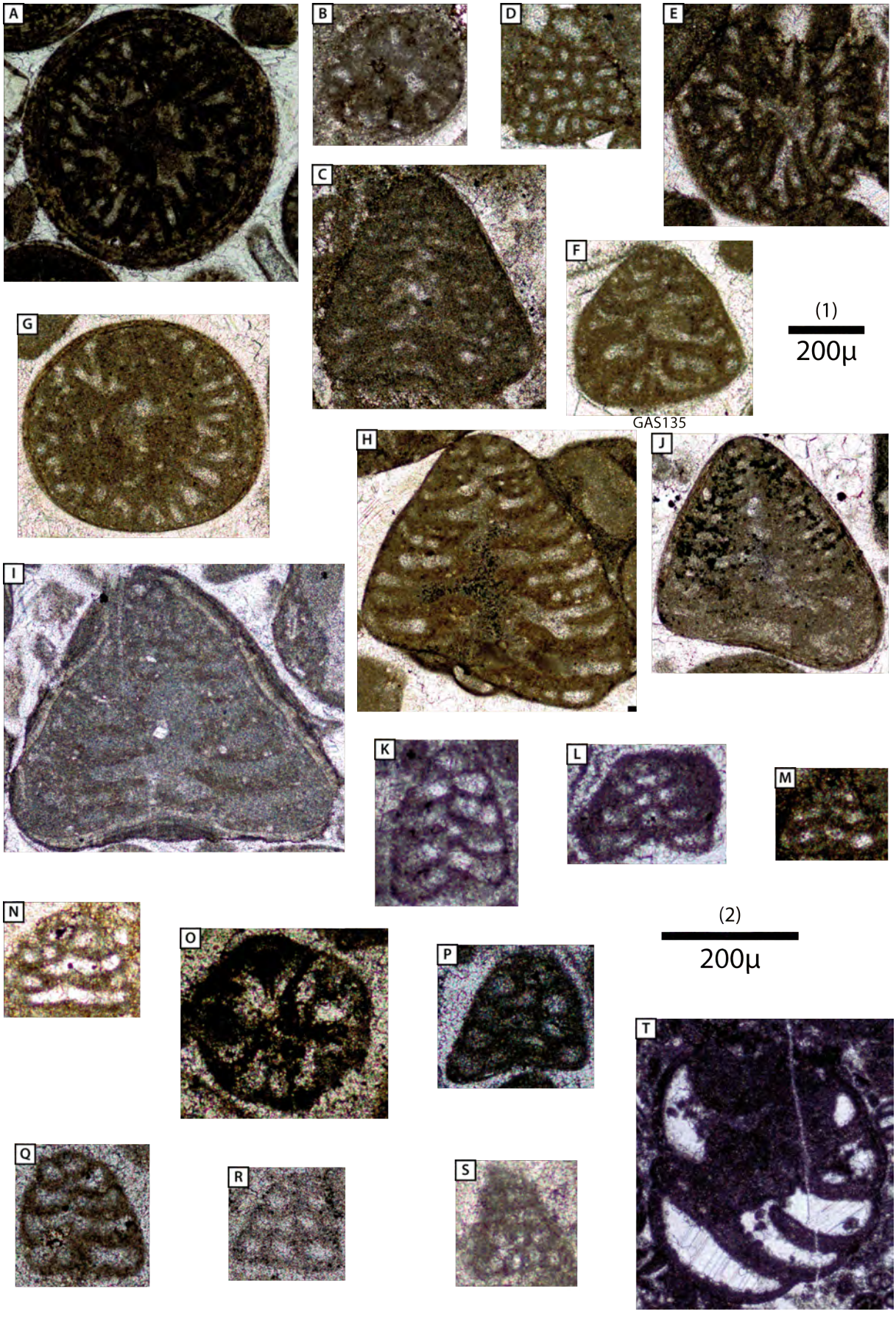
A
B
D
E
C
F
(1)
200µ
GAS135
G
H
J
I
K
L
M
N
O
P
(2)
200µ
T
Q
R
S

Fig. 3.7: Marker benthic foraminifera identified in the studied sections. Scale 1 is used for *Pseudotextulariella courtionensis* (images A to J), scale 2 for *Montsalevia elevata* (K to R), *Montsalevia salevensis* (S), and *Pfenderina neocomiensis* (T). A) Säntis, UOL (SA99); B) Dräckloch, UOM (GAS70); C) Dräckloch, UOL (GAS109); D and E) Dräckloch, UOL (GAS111); F) Dräckloch, UOL (GAS135); G) Dräckloch, UOL (GAS139); H) Dräckloch, UOL (GAS143); I) Dräckloch, UOL (GAS155); J) Vitznau, UOL (Vz40); K) Säntis, UOL (I15); L) Säntis, UOL (SA87); M) Dräckloch, UOL (GAS109); N) Dräckloch, UOL (GAS125); O) Dräckloch, UOL (GAS127); P) Dräckloch, UOL (GAS153); Q) Vitznau, UOL (Vz40); R) Vitznau, UOL (Vz43); S) Säntis, Betlis Limestone Fm (SA9); and T) Säntis, UOL (SA66) (GASV8), Dräckloch.

The base of the Vitznau Fm (53 to 57 m) is characterised by outer-platform microfacies rich in crinoids and bryozoans with an important degree of sedimentary reworking (F4/FT). Sparse reworked corals and calcareous sponges were observed (at 58m, Fig. 3.6). This microfacies is replaced at 57 m by peloidal, crinoid-rich microfacies showing a relatively scarce and poorly diversified fauna of bivalves, bryozoans and circalittoral foraminifera. Very similar microfacies continues up to the top of the section (e.g. to the top of the Vitznau Fm and the Betlis Limestone Fm) with few changes in the relative proportion of bioclasts.

At the base of the Betlis Limestone Fm (from 69 to 72 m), in addition to the biogenic debris mentioned above, oncoids and reworked (sometimes pyritised) bioclasts were observed (F4/FT). Numerous chert nodules occur between 67 and 86.5 m. An erosive surface was identified at 86.5 m, and a level rich in oncoids is present between 94 and 96 m. In the upper part of the Betlis Limestone (from 96 to 107 m), an important increase in detrital quartz was observed. The quartz grains are a few mm large, very blunt and broken. The top of the Betlis Limestone is characterised by a hardground whose perforations are infilled by phosphatic and glauconitic sediment of the overlaying Gemsmättli Beds (Fig. 3.8B and C).

- Dräckloch section

The Dräckloch section is characterised by outer-platform to outer-shelf microfacies (Fig. 3.10). The measured section starts with the relatively deep microfacies types F2/F3, which are rich in quartz, circalittoral foraminifera, sponge spicules, echinoderms, and contain sparse larger agglutinated foraminifera. In the LOL (22-55 m), it evolves toward microfacies type F5, which is mainly constituted of large benthic foraminifera, echinoderms and small oolites, and includes numerous large rounded clasts. The few samples collected from the marly upper part of the LOL and the marl of the UOM (55-130 m) show a microfacies dominated by type F2 and F2/3, with peloids, circalittoral foraminifera and sponge spicules, and with an important detrital component (quartz and clays). Few calpionellids were found and they are generally poorly preserved. A specimen of the marker benthic foraminifera *Pseudotextulariella courtionensis* was found in a more calcareous bank of the UOM (Fig. 3.7).

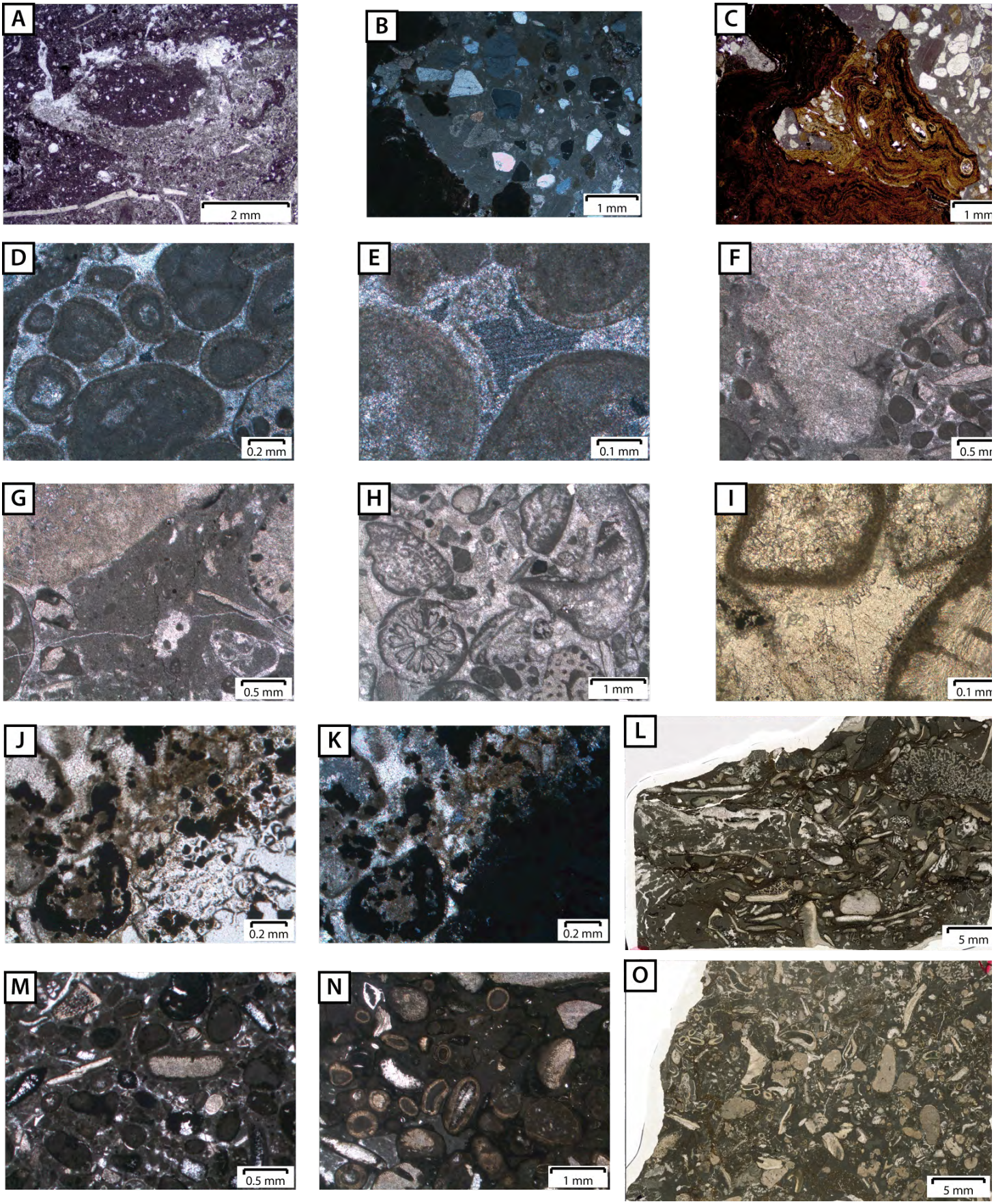
A
2 mm
B
1 mm
C
1 mm
D
0.2 mm
E
0.1 mm
F
0.5 mm
G
0.5 mm
H
1 mm
I
0.1 mm
J
0.2 mm
K
0.2 mm
L
5 mm
M
0.5 mm
N
1 mm
O
5 mm

Fig. 3.8: A) Epikarst with early infillings, UOL (SA79), Säntis; B and C) Phosphatic crust and quartz grains, uppermost Betlis Limestone perforated and filled by sediments of the overlying Gemsmättli Bed (SA2), Säntis; D) Oolitic grainstone, UOL (GAS157), Dräckloch; E) Fringing cements, UOL (GAS157), Dräckloch; F) Dissolution vug with early infillings, UOL (GAS160), Dräckloch; G) Early cements around grains, and late mud infilling UOL (GAS157), Dräckloch; H) Bioclastic grainstone with ahermatypic coral and Neotrocholinas, uppermost UOL (GAS165), Dräckloch; I) Fringing cements, uppermost UOL (Dv8bis), Dräckloch; J and K) Perforation filled by a ferruginous mud, then phosphate, and finally by pyrite (natural and polarised light, respectively), uppermost UOL (Dv8bis), Dräckloch; L) Reworked sediment with a dolomitised sponge, damaged corals, bryozoans, pebbles with serpulids, ostracods and *Lenticulina* in a muddy matrix, lowermost Vitznau Fm (Dv11), Dräckloch; M) Reworked sediment with pyritised platform clasts in a mud matrix, uppermost UOL (Vz45), Vitznau; N) Level of strong sediment reworking with extraclasts of oolitic and crinoidal sediments in a mud matrix, uppermost UOL (Vz48), Vitznau; O) Reworked level containing bryozoans, crinoids, coral debris, serpulids and ostracods, lowermost Vitznau Fm (Vz49), Vitznau.

The microfacies of the overlaying UOL (130-260 m) shows an increasing proportion of large bioclasts originating from shallower-water environments: between 130-174 m, a progressively increasing proportion of large benthic foraminifera, echinoderms, green algae, bivalves, bryozoans (in lower quantities), together with oolites is observed and microfacies types evolve from F2/3 to F6/7 (Fig. 3.8D). At 174 m, a rapid change to microfacies F3 is noted and a similar shallowing-upward trend follows up to 246 m. In these two platform successions (130-260 m), the marker foraminifera *Pseudotextulariella courtionensis* was identified, and between 145 and 240 m *Montsalevia elevata* is present (Fig. 3.7).

Indices of emersion were observed between 236 and 246 m, such as fringing cements and dissolution vugs with early infillings (Fig. 3.8 E, F, G). From 246 m to 260 m, a change in microfacies occurs: the bioclastic assemblages are still constituted by shallow-water organisms but corals and calcareous sponges debris become dominant and benthic foraminifera nearly disappear with the exception of neotrocholinas (Fig. 3.8H). Indications for sedimentary reworking are provided by numerous extraclasts, sponge and herma- and ahermatypic coral debris (Figs. 3.8H and 3.11B). Oolites, rudists, bryozoans, echinoderms and green algae are also present. Several specimens of the marker benthic foraminifera *Conicospirillina basiliensis* and one specimen of *Pseudotextulariella courtionensis* were observed (Fig. 3.7).

Given difficulties in access in the field and the presence of a fault zone, a part of the interval (between 246 and 260 m) was unfortunately not sampled and its thickness was difficult to evaluate (indicated by a fault in Figs. 3.4 and 3.10). The top of the UOL is a hardground (Fig. 11A), whose perforations are filled in by a complex succession of sediments, which are partly phosphatized and which include mud with small peloids, and pyrite (Fig. 3.8J and K). The uppermost bank of the UOL shows evidence of sediment reworking with the occurrence of mud pebbles and extraclasts (sometimes consisting of dolomite). Interestingly circumgranular cements were observed (Fig. 3.8I).

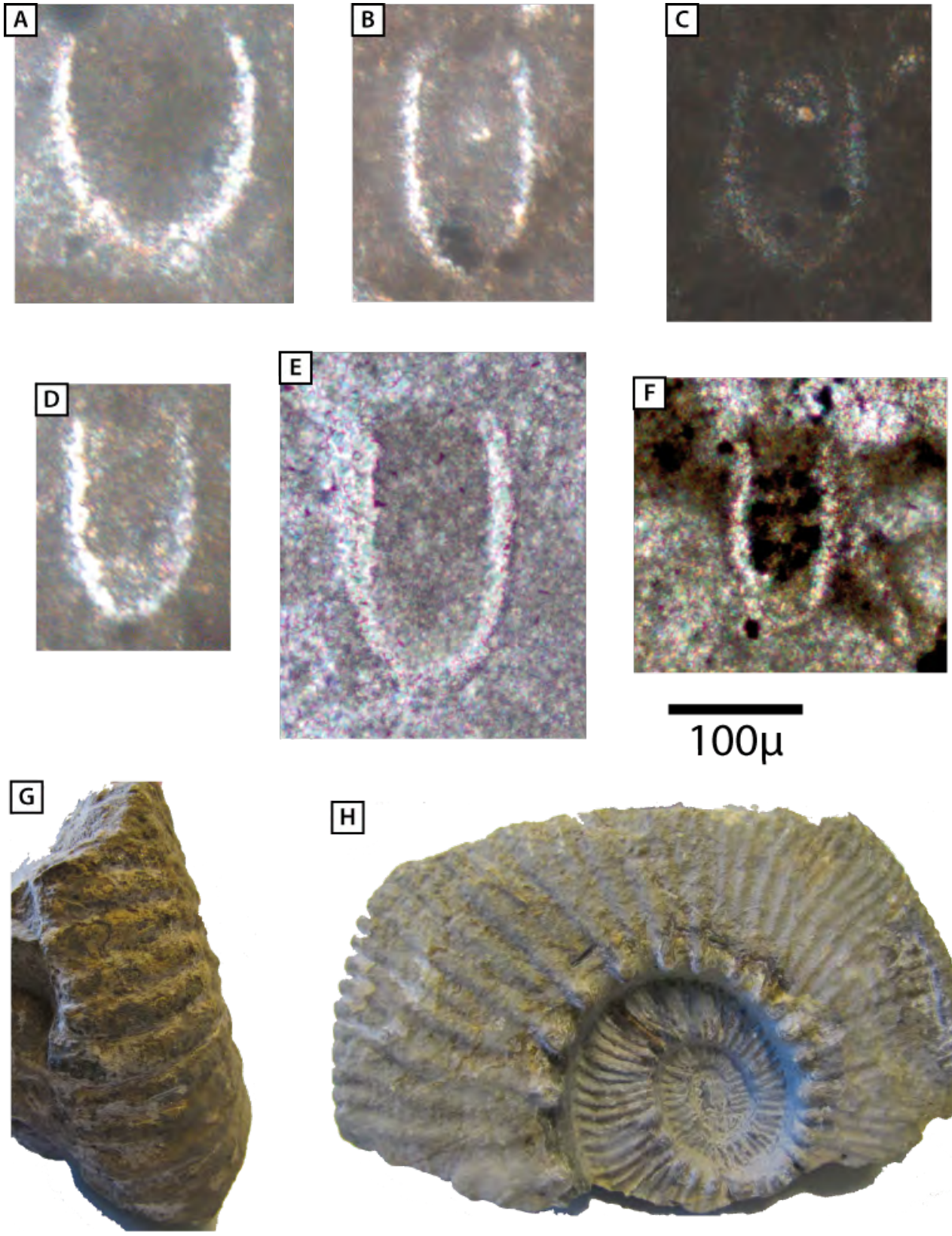

Fig. 3.9: Marker calpionellids and ammonite. A) *Remaniella filipescui*, calp. zones B to D3, UOL (Vz45), Vitznau; B) *Calpionellopsis oblonga*, calp. zones D2 to D3, UOL (Vz45), Vitznau; C) *Calpionellopsis oblonga*, calp. zones D2 to D3, UOL (Vz45), Vitznau; D) *Calpionellopsis simplex*, calp. zones D2 to D3, UOL (Vz45), Vitznau; E) *Calpionellopsis simplex*, calp. zones D2 to D3, UOL (SA66), Säntis; F) possible *Tintinnopsella longa*, calp. zones D1 to E2, Vitznau Fm; G) *Thurmanniceras thurmanni* s.str., ventral view; H) *Thurmanniceras thurmanni* s.str., ombilical view

The overlaying Vitznau Fm starts with a level containing abundant bryozoans, corals, oysters and serpulids floating in a clayey matrix, which appear strongly reworked (Figs. 8L and 11C). A second hardground with perforations filled with pyrite is observed at the top of this bank. The first part of the Vitznau Fm (246-300 m) shows hemipelagic limestone-marl alternations containing abundant oysters in life position or weakly transported, some brachiopods, circalittoral foraminifera and sponge spicules (microfacies F2/F3). The upper part of the Vitznau Fm (300-315 m) becomes richer in clay and oysters are less abundant. Small detrital quartz is abundant in the entire Vitznau Fm. A calpionellid probably belonging to the species *Tintinnopsella longa* was observed (Fig. 3.9F).

The Betlis Limestone Fm begins (at 315 m) with a layer containing oolites, abundant crinoids, sparse bryozoans, small benthic foraminifera, sponges and gastropods, together with reworked mud pebbles of the Vitznau Fm. From 315 to 370 m, a peloidal microfacies with crinoids is present, with an increasing proportion of bryozoan and bivalve fragments, and small-sized detrital quartz grains: the microfacies progressively evolves from F2/F3 to F4. Numerous chert layers and chert nodules are present in the interval between 315 to 357 m (Fig. 3.11D). At 370 m, a level is observed, which contains many crinoids, some bivalves, small benthic foraminifera and *Lenticulina*, ostracods and abundant quartz grains. The bioclasts in this layer appear to have been reworked.

The upper part of the Betlis Limestone Fm has a faunal assemblage similar to the lower part, but bryozoans are not observed and ostracods become more important. An enrichment in clays and quartz is observed, in particular in the top part of the Betlis Limestone corresponding to the Pygurus Mb, where mm-sized, rounded and fractured quartz grains become predominant. The quartz particles are surrounded by a calcitic fringing boarder. Sometimes, a ferruginous border is observed between the quartz grain and the fringing boarder. The uppermost part of this interval is highly bioturbated and is also characterised by the abundance of ostracod shells.

- Vitznau section

The measured section (Fig. 3.12) starts with the upper part of the Palfris Fm, which exhibits a muddy microfacies containing sparse bioclasts such as echinoderms and few reworked circalittoral foraminifera comprising *lenticulinas*. The clayey sediments are bioturbated and include some quartz and pyrite (F1/F2). Toward the top of the Palfris Fm, the microfacies becomes progressively more calcareous, with the apparition of small limestone pebbles of millimetre size, peloids and sparse bryozoans (F3).

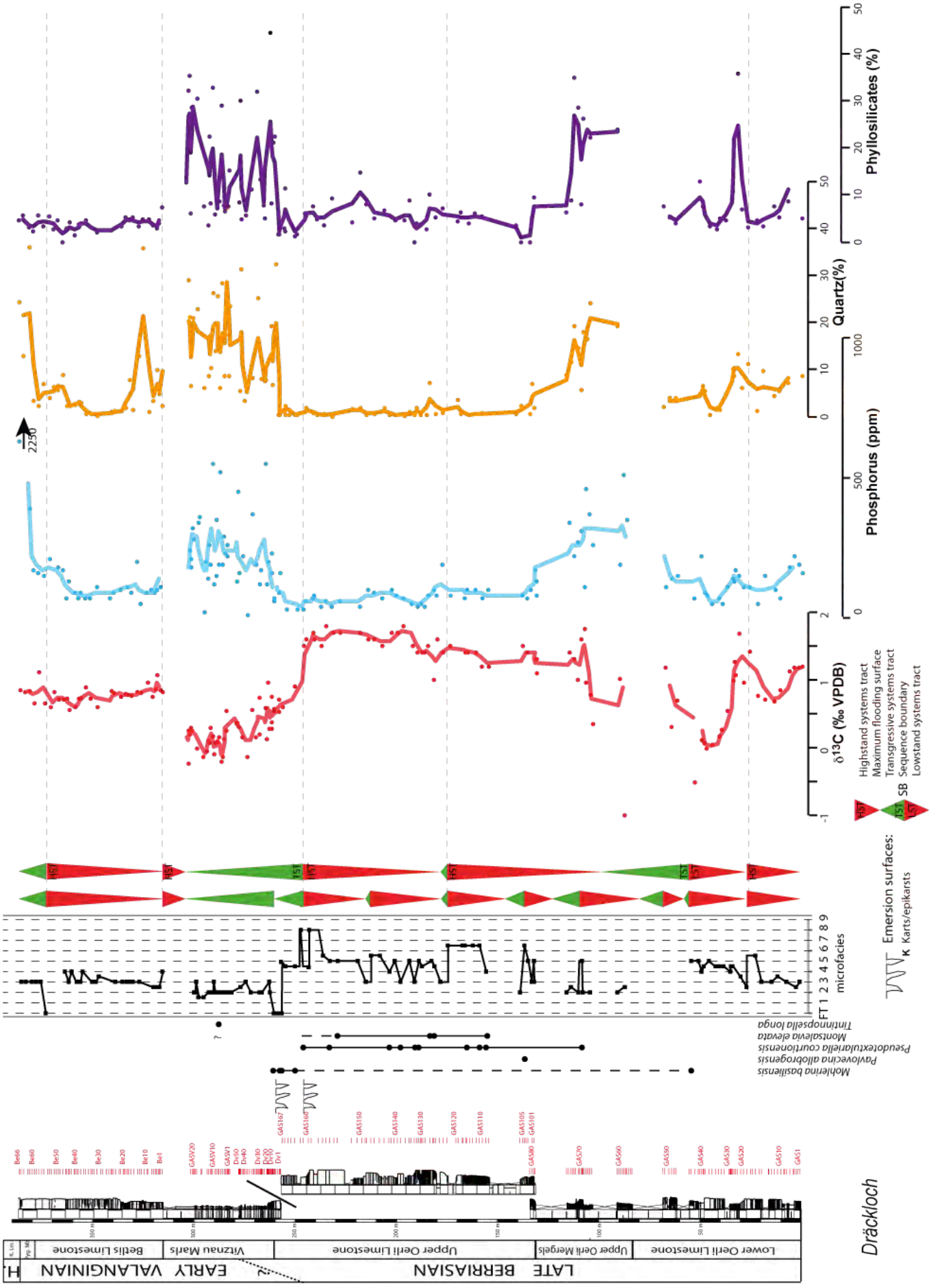

Fig. 3.10: Sedimentological, geochemical and mineralogical analyses performed on the Dräckloch section. Microfacies classification after Arnaud-Vanneau and Arnaud (2005).

The overlying calcareous part is attributed to the UOL (12.5 to 25 m). In the lower part of the UOL (12.5 to 23.4 m), grainstone microfacies with peloids, echinoderms, bryozoans and circumlittoral foraminifera (F3) punctually change to coarser grainstone with mud pebbles, echinoderms, and sparse oolites, large benthic foraminifera, corals and sponges (F5). In this segment, the marker foraminifera *Pseudotextulariella courtionensis* and *Montsalevia elevata* were identified (Fig. 3.7).

The last 1.6 m of the Öhrli Fm show a complex succession of erosive surfaces and hardgrounds. A first irregular erosive surface occurs at 23.4 m and is associated with lag limestone pebbles (Fig. 3.11E). The overlaying calcareous layer is perforated and the borings are infilled by the overlying marly layer (Fig. 3.11F). This thin marly layer is rich in reworked pyritised clasts (Fig. 3.8M). The clasts are mainly composed of bivalve fragments and gastropods, benthic foraminifera including sparse *Neotrocholina*, calpionellids and some calcispheres. The bivalves and gastropod shells are often recrystallised. Specimens of *Calpionellopsis oblonga, Remaniella filipescui* and *Calpionellopsis simplex* were identified (Fig. 3.9). The next two layers have an erosive base (Fig. 3.11G and H) and show a microfacies constituted by peloids, echinoderms, and small benthic foraminifera (F3) with sparse reworked platform debris including benthic foraminifera, oolites and extraclasts (most of them contain oolites). In the uppermost part of the UOL, microfacies is mainly composed of the same type platform debris additionally comprising calcareous sponges, corals, and gastropods; and a hardground is observed on top of the UOL whose perforations are often filled with pyrite (F6/FT, Fig. 3.8N).

A further hardground is observed at the top of the first marl-limestone alternance of the Vitznau Fm. The accompanying microfacies shows intense reworking with ostracods, microbial mats, bryozoans, broken serpulids, micritised crinoids and corals, together with mud pebbles rich in quartz (FT). Platform debris (bryozoans, crinoids, benthic foraminifera, microbial mat remains) together with bivalves and ostracods, are observed up to 26.3 m (FT, Fig. 3.8O). Then from 26.3 to 56.8m, the microfacies consists of monotonous wackestone rich in quartz with ostracods, sponge spicules and serpulids (F1/F2). Numerous oysters were observed, in life position or weakely transported in marly layers, and highly transported and accumulated into calcareous layers.

At 56.8m, an erosive bank containing a bivalve accumulation is observed (Fig. 3.11I). Then a recessive marly interval of 1 m is observed. Finally, the Betlis Limestone Fm shows peloidal echinodermal facies observed in the field (F3) but no thin sections were realised, because of the difficult access in steep terrain and the presence of vegetation hiding the transition between the Vitznau and Betlis Fms.

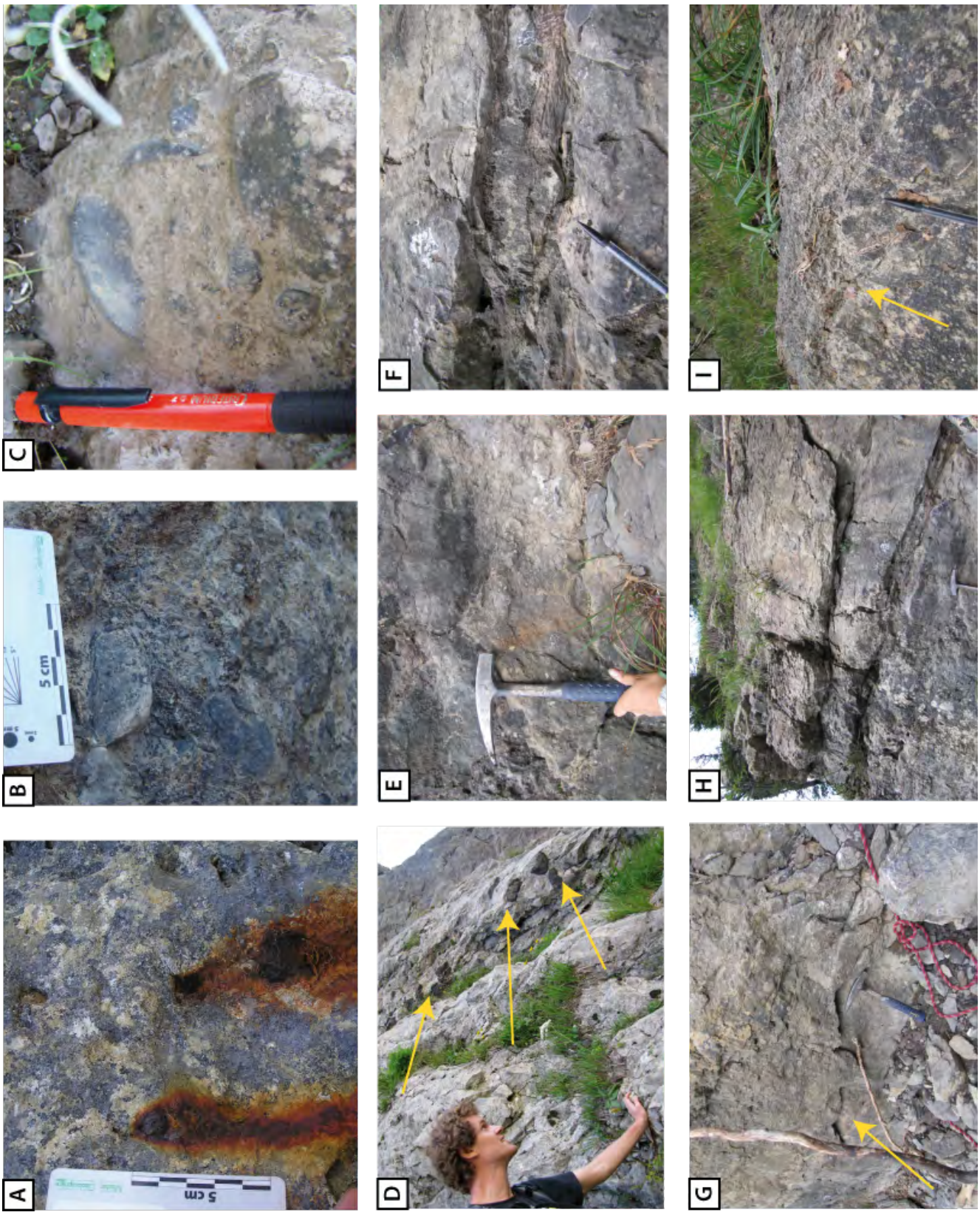

Fig. 3.11: Field observations. A) Perforations with pyrite infillings, top of the UOL (Dv8bis), Dräckloch; B) Level with important sediment reworking, rich in bioclasts of heterogeneous size, top of the UOL (Dv8bis), Dräckloch; C) Level with important sediment reworking rich in oysters and brachiopods, first bank of the Vitznau Fm (Dv11), Dräckloch; D) Chert nodules, Betlis Limestone Fm (Be15), Dräckloch; E) Erosive surface with lag pebbles, UOL (between Vz44and Vz45), Vitznau; F) Recessive level infilling a perforated level, UOL (Vz45), Vitznau; G) Erosive surface, UOL (between Vz46 and Vz46bis), Vitznau. H) View of the top of the UOL, Vitznau; I) Erosive level rich in bivalve shells, upper part of the Vitznau Fm (Vb11), Vitznau.

3.4.2. Stable carbon-isotope analyses

The $\delta^{18}O$ values oscillate between -5 and -2 ‰ in the Säntis section, and -6 and -2 ‰ in the Dräckloch and Vitznau section. The $\delta^{13}C$ long-term trends appear to be relatively similar between the three sections: relatively heavy but noisy values (1 to 1.5‰ in average) are observed in the Öhrli Fm (LOL, UOM and UOL) and its distal equivalent the Palfris Fm. To the contrary, relatively light $\delta^{13}C$ values (0.3 to 0.8 ‰) are recorded in the Vitznau Fm and the Betlis Limestone Fm. The decrease in $\delta^{13}C$ values (0.7‰) is abrupt and occurs at the limit between the UOL and the Vitznau Fm in the Säntis and Vitznau sections, and within the upper part of the UOL in the Dräckloch section. The Säntis section is the only one, which records a $\delta^{13}C$ positive shift of 1.2 ‰ at the top of the Betlis Limestone Fm.

3.4.3. Phosphorus content

In the Säntis section, relatively low P values were measured in the UOL (60 ppm in average), with the exception of two levels presenting values close to 1000 ppm. P values abruptly increase to 580 ppm at the base of the Vitznau Fm. The values stay relatively high in the lower part of the Vitznau Fm (51.5 to 63m) and decrease to 70 ppm in average in the upper part of the Vitznau Fm and the lower part of the Betlis Limestone Fm (between 63 and 86.5 m). The upper part of the Betlis Limestone Fm (86.5 to 106.5 m) shows a progressive increase in P values up to 3700 ppm at its top.

In the Dräckloch section, relatively low P values of 100 ppm in average were observed in the LOL. The values increase to 250 ppm in average in the UOM, and then decrease again to 80 ppm in average in the UOL. P values increase again in the Vitznau Fm with average values of 250 ppm. The Betlis Limestone Fm shows a return to lower values (90 ppm), except for its top (360 to 385 m) where the values first increase to 150 ppm, and then rise to 2250 ppm in the last bank.

In the Vitznau section, P values oscillate around 200 ppm in the Palfris Fm, then decrease to 70 ppm in the UOL, increase to 300 ppm in average for most of the Vitznau Fm (up to 55.5 m) and slightly decrease to 200 ppm in the uppermost Vitznau Fm and the Betlis Limestone Fm.

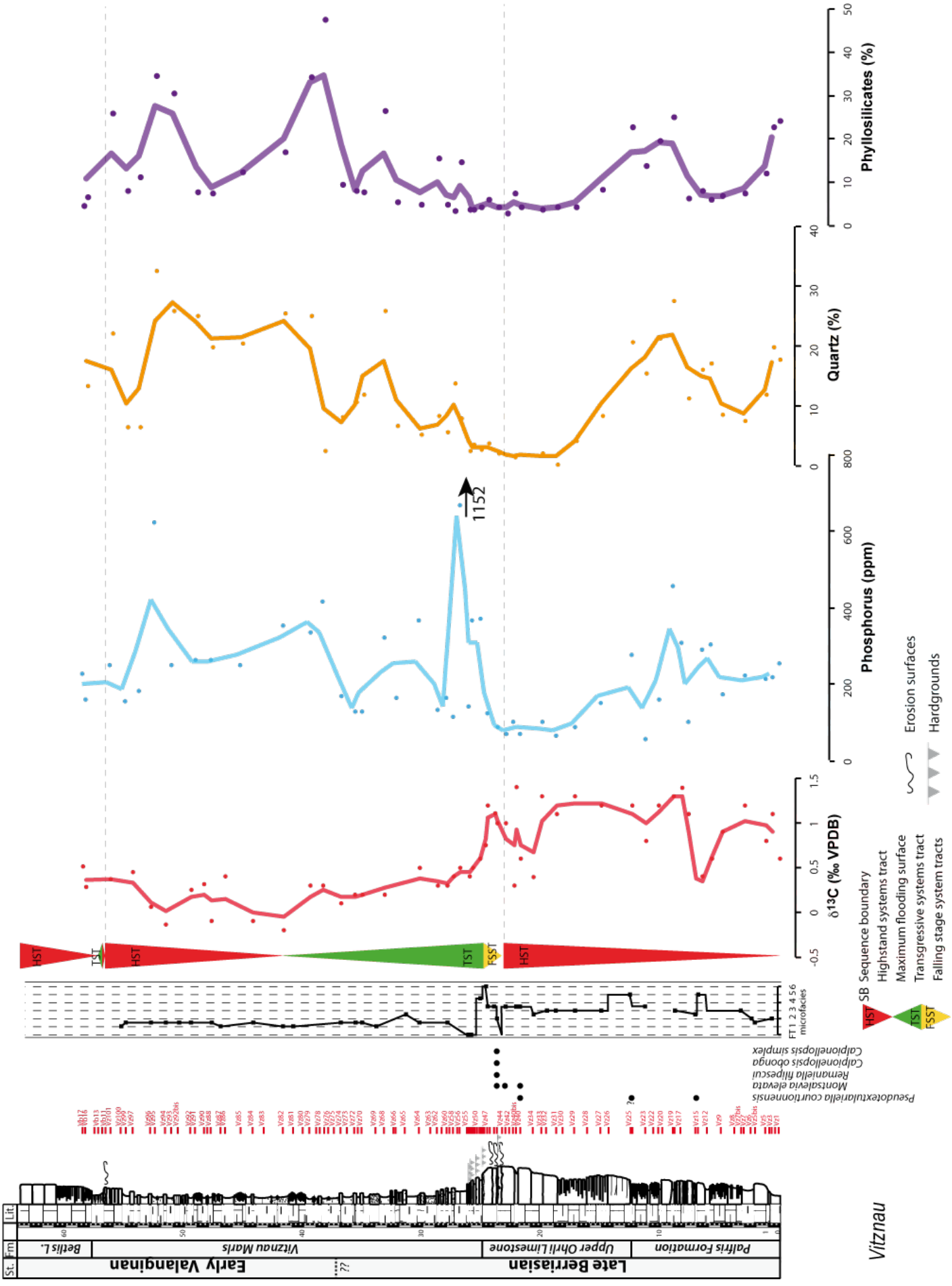

Fig. 3.12: Sedimentological, geochemical and mineralogical analyses performed on the Vitznau section. Microfacies classification after Arnaud-Vanneau and Arnaud (2005).

3.4.4. Bulk-rock mineralogy

In the Säntis section, no clear change in the phyllosilicate relative content was observed: its percentage remains stable around 4%. Quartz is nearly absent at the base of the section (up to 32 m), its contents increase to an average of 3±2% in the upper part of the UOL, the Vitznau Fm, and the lower part of the Betlis Limestone Fm (e.g. from 32 to 96 m). A punctual increase to 44% was noted at 68 m. Near the top of the section corresponding to the upper part of the Betlis Limestone Fm (96 to 106.5 m), the quartz content sharply increases up to 48%.

In Dräckloch, both phyllosilicate and quartz contents increase in the LOL and UOM (from 5 to 35% and from 10 to 25% respectively); they decrease in the UOL (to 5% in average and nearly 0, respectively), and increase again in the Vitznau Fm (calcareous layers have an average phyllosilicate and quartz content of 8% and 9%, respectively, and marly layers have an average phyllosilicate and quartz content of 30% for both). In the Betlis Limestone Fm, the phyllosilicate content drops to 4%, but a different behaviour for the quartz content is observed: relatively high values occur at the base of the formation (36% at 326 m), then the values drop to 1% from 332 to 354m, and finally the quartz content rises to 36% in the uppermost Betlis Limestone Fm (354 to 386 m).

In Vitznau, the quartz and phyllosilicate contents follow the same trends: they increase in the Palfris Fm (up to 20% and 25%, respectively), decrease in the UOL (to 2 and 5%) and increase again in the Vitznau Fm (up to 32 and 47 %, respectively). A decrease (to 17 an 12%, respectively) is noted for the Betlis Limestone Fm.

3.5. INTERPRETATION

3.5.1. Sequence stratigraphy

In this paragraph, only sequences are described because they are defined on the basis of key surfaces and long-term facies and microfacies trends. Parasequences have been interpolated, mostly on the basis of (micro)facies and lithological observations, and indicated in the figures. However, given the relatively coarse sampling resolution, the determination of parasequences should only be considered as an approximation, and will not be discussed in this chapter.

- Säntis section

The first 20 m of the measured section are characterised by photozoan shallow-water limestone deposited at either side of the shoal. At 20 m, dissolution features and early infillings highlight the occurrence of a first epikarst level within inner lagoonal deposits (F9), and therefore of the first sequence boundary of the section. In the following, the facies shows a rather abrupt deepening to relatively deep platform facies (F3), which is followed by a shallowing-upward trend to inner lagoonal environments (F9/10). At 26 m, in most proximal facies, emersive features are noted, which may be linked to an epikarst or mud cracks, and a second sequence boundary is placed at this level. The upper part of the UOL is dominated by outer lagoonal facies (F8) but show abrupt changes to outer platform facies. The uppermost part of the sequence exhibit sediments deposited in confined lagoonal environments and the sequence ends with an epikarst.

This epikarst (at 53 m) marks the third sequence boundary of the Säntis section. This surface is of crucial importance because it is also marked by perforations infilled by the overlaying sediments of the Vitznau Fm, indicating the presence of a hardground. A second and similar hardground is observed in the immediately overlaying layer. In the lowermost part of the Vitznau Fm, facies drastically change to heterozoan associations and are characterised by an important reworking of bryozoans and crinoids, and the abundance of quartz. Within this reworked interval, a level (at 58 m), even shows the reworking and mix of corals and calcareous sponges together with the heterozoan fauna. This interval is witness of an important transgression (transgressive systems tract, TST); and the absence of a transition from photozoan to heterozoan carbonate production highlights the occurrence of a sequence boundary of major importance (at 53 m). The maximum flooding surface is then placed where the deepest microfacies was observed (F2, outer shelf) underneath the storm-weather wave base, rich in sponge spicules and detrital minerals), immediately following the TST. The sequence is characterised by quiet deep-water facies deposited below the photic zone.

The fourth sequence boundary is placed at the base of the Betlis Limestone Fm, where the microfacies indicates increased sediment reworking probably because of stronger hydrodynamic conditions (F4/FT). The maximum flooding surface (mfs) coincides probably with the sequence boundary, as no significant change in facies is observed within this sequence (monotonous outer shelf, below the photic zone but under current agitation: F4).

A fifth sequence boundary is placed where an erosive surface associated with reworked oncoids was observed. The mfs is then placed within the hardground observed at the top of the Betlis Limestone Fm. Within the perforations, sediments of the condensed phosphatic and glauconitic Gemsmättli Bed are preserved. Therefore, sequence boundaries are probably stacked within this level.

- Dräckloch section

Facies of the LOL Mb are characterised by two shallowing-upward trends (up to 25 m and from 25 to 55 m) from deep quiet environments of outer-shelf to shallower subtidal environments (e.g. F2/3 to F5). Since the Dräckloch section is an is an outer-shelf to outer-platform section, sequence boundaries are not necessarily defined by emersive surfaces, and lowstand systems tracts (LST) should be preserved. Thus a first sequence boundary is placed at 25 m. The overlying shallowing-upward interval is associated with a LST. In the following, in the upper part of the LOL and the lower part of the UOM, a deepening upward trend is observed (to F2: outer-shelf environment below storm-weather wave base), which constitutes the TST. The mfs is placed in the more recessive layers, and is probably located in an interval covered by vegetation. The highstand systems tract (HST) is well developed and documents the progressive installation of the platform with facies showing a growing influence of the oolitic and bioclastic shoal. Bioclasts are predominantly constituted by benthic foraminifera, bivalves, and echinoderms, and in low proportions of green algae, corals and bryozoans.

This shallowing-upward trend ends at 175 m with barrier facies (F5/F8) and a return to less hydrodynamic and more external conditions (F3) is noted. Consequently, a second sequence boundary is placed at this level. Similarly, in the following, a second phase of platform installation is observed from 175 to 246 m, and inner-platform (external lagoon) facies with emersion features occurs at the top of this sequence.

From 246 to 260 m, carbonates are still largely dominated by shallow-water organisms, but an abrupt change in the carbonate fabric is observed with a clear dominance of corals and calcareous sponges, and the nearly disappearance of benthic foraminifera (except for *Neotrocholinas* which are found in abundance, two specimens of *Conicospirillina basiliensis* and one specimen of *Pseudotextulariella courtionensis*). However, *Pseudotextulariella courtionensis* is reworked because it is infilled by a micritic mud that shows precipitations of dolomite, the cortication of the foraminifera is broken and taken up into a clast (Fig. 3.7). The specimens of *Conicospirillina basiliensis* are oolitised, thus they may also be reworked. Moreover, at 246 m, the $\delta^{13}C$ record shows an abrupt shift to lighter values, indicating the presence of an important hiatus: a third sequence boundary is therefore placed at this level. Because of the presence of a fault zone near the top of the UOL, the sequence stratigraphic configuration of this part could not be evaluated in detail. Nevertheless, the floro-faunal microfacial association appears to be relatively similar below and on top of this faulted zone, and we assume therefore a certain continuity in facies.

The uppermost banks of the UOL show a grainstone to floatstone microfacies containing numerous debris of corals, bivalves, rudists and bryozoans, and dolomitic extraclasts indicative of confined and very shallow environments close to emersion mixed with mud pebbles of outer-shelf origin. This facies witnesses important sediment reworking, and this interval is interpreted as a TST.

The top of the UOL is probably emersive (or close to the emersion) because circumgranular cements have been observed, and may represent the top of a parasequence within the early TST. The phosphatic and pyritic infillings of the hardground on top of the UOL witness the following major transgression. The major impact of the transgression is also witnessed by the first bank of the Vitznau Fm, which is strongly reworked, and also exhibits a hardground at its top. The mfs of this sequence is placed within the more recessive part of the Vitznau Fm, which is covered by vegetation.

A fourth sequence boundary is placed at the base of the Betlis Limestone Fm (315 m), below a reworked level containing abundant crinoids and bryozoans together with mud pebbles of the Vitznau Fm (F4/FT). The mfs of this sequence is probably combined with the sequence boundary because no deepening trend was observed in this sequence.
A fifth sequence boundary is noted at 370 with, again, a level of important reworking containing abundant crinoids, some bivalves, benthic foraminifera, ostracods, and abundant quartz.

This sequence is characterised by important detrital input, a depletion in the bryozoan fauna and a concentration in ostracod shells. The uppermost part of this interval, which corresponds to the Pygurus Mb, is highly bioturbated and shows an important concentration of large rounded quartz grains. The onset of the condensation phase is probably recorded her, but a glauconitic or phosphatic crust was not observed (as for the Gemsmättli Bed). The mfs of this sequence is probably located just below the Hauterivian Kieselkalk Fm (the boundary between the Betlis and the Kieselkalk Fm is faulted).

- Vitznau section

In the first part of the Vitznau section (from 0 to 23.4 m), sediments become progressively more calcareous. Outer-shelf facies is increasingly interrupted by bioclastic layers containing shallow-water organisms such as large benthic foraminifera (in particular *Pseudotextulariella courtionensis* and *Montsalevia elevata*), echinoderms, corals and sponges) mixed with oolites, which are interpreted as turbidites. The enhanced influence of the carbonate platform is interpreted as the record of a HST.

At 23.5 m, an important erosive surface associated with lag pebbles marks the sequence boundary. From 23.5 to 26.3 m, a succession of erosive surfaces is noted. The top of this interval shows the reworking of partly lithified sediments rich in oolites and bioclasts. Given the relatively distal position of the Vitznau section, this interval is interpreted as a falling-stage system tract. On top of the falling stage system tract (26.3 m), two hardgrounds are observed. The interspersed sediments consist of reworked bryozoans and corals with outer-shelf sediments rich in sponge spicules and ostracods. This is interpreted as the initiation of an important transgression. The mfs of this sequence is placed in the more recessive layers of the Vitznau Fm, which also correspond to a more distal, hemipelagic facies F1).

A second sequence boundary is placed at 56.8m, where an erosive bank containing an important accumulation of bivalve shells (coquina) is observed. This level is interpreted as the expression of the LST. A mfs is then placed within the overlaying marly interval. Only the lower part of the Betlis Limestone Fm is accessible in Vitznau; it is interpreted as the base of a HST.

3.5.2. Diagenesis

All sections are affected by important diagenesis. This is highlighted by the light $\delta^{18}O$ values recorded in the three sections (comprised between-6 and -2‰). Clay mineral analyses were carried out and all sections show the absence or weak presence of kaolinite and smectite whereas equivalent deposits in the Jura contain up to 50% of these minerals (Morales et *al.*, 2013). The three sections, however, include high contents of illite, interstratified illite-smectite, and chlorite. An important proportion of the latter minerals is likely newly formed during the last mesogenetic stadium, during which smectite and kaolinite progressively disappear with burial (Kübler and Jaboyedoff, 2000).

General trends in the $\delta^{13}C$ records appear, however, to be conserved: the trends are similar from one section to another, and correlate relatively well with those of equivalent sections in the Jura Mountains and the Vocontian Basin (La Chambotte, Juracime, Montclus; Morales *et al.*, 2013). Absolute values are not affected much by burial diagenesis: $\delta^{13}C$ values have a range from 0 to 1.5 ‰, which is relatively similar to the record of the Jura sections (0 to 2 ‰), which did not undergo an important diagenetic impact (Morales *et al.*, 2013). Consequently, if the clay mineralogy cannot be used as a proxy for palaeoenvironmental change, general trends in the $\delta^{13}C$ records are rather well conserved and exploitable.

3.5.3. Age control and correlation of the sections

Calpionellids were identified in the different sections. Only a few of them provide an age control because of their rather weak preservation, or the poor proportion in marker species. In the Vitznau section, a Berriasian age is given for the upper part of the UOL by the presence of *Remaniella filipescui* (Fig. 3.9), which extends from calpionellid zones B to D3 (Blanc, 1996) The presence of *Calpionellopsis* in the upper part of the UOL in the sections of Säntis and Vitznau (Fig. 3.9), precise an age of calpionelid zone D2/D3 (Darsac, 1983; Blanc, 1996; Morales *et al.*, 2013). In the section of Dräckloch, a specimen of *Tintinnopsella*, that might belong to *Tintinnopsella longa* (Fig. 3.9) has been found in the Vitznau Marls and might indicate an age ranging from the late Berriasian to the early Valanginian.

The marker foraminifera identified by Blanc (1996) in the Jura Mountains are used as a correlation tool between the sections (Fig. 3.13). Their stratigraphic distributions appear to be consistent with other studies in various areas (Pyreneans after Peybernès, 1976; Provence after Virgone, 1996). We particularly paid attention to the distribution of *Pseudotextulariella courtionensis* since this foraminifer is observed in all three Helvetic sections. This species has a relatively wide geographic distribution since it was observed in Spain (Masse *et al.*, 1999), the French Alps (Arnaud-Vanneau and Darsac, 1984), the French and Swiss Jura (Darsac, 1983; Clavel *et al.*, 1986; Boisseau, 1987; Pasquier, 1995; Blanc, 1996), the Pyrenees (Peybernès, 1976), Provence (Virgone, 1996), and in the Helvetic Alps (Pasquier, 1995). Its biostratigraphic range of early late Berriasian (*S. boissieri* ammonite zone, *M. paramimounum* ammonite subzone that correspond to calpionellid zone D1) that probably extends in the late early Berriasian (calpionellid zone C) was established in the Jura area (Darsac, 1983; Clavel *et al.*, 1986; Boisseau, 1987; Blanc, 1996), and a compatible age range is noted in the Pyrenees and Provence (Peybernes, 1976 and Virgone, 1996).

Pseudotextulariella courtionensis may be associated with another agglutinated foraminifer - *Pavlovecina allobrogensis*, which has a shorter biostratigraphic range. *Pavlovecina allobrogensis* is found in a 1-2 m thick marker horizon in the Jura Mountains (Darsac, 1983; Boisseau, 1987; Blanc, 1996), and indicates an early late Berriasian age (early *S. boissieri* ammonite zone, *M. paramimounum* ammonite subzone; early calpionellid zone D1; Clavel *et al.*, 1986; Blanc, 1996).

The first appearance of *Montsalevia elevata* and *Pfenderina neocomiensis* and the last appearance of *Pseudotextulariella courtionensis* mark the later part of the late Berriasian (Darsac, 1983; Boisseau, 1987; Blanc, 1996). The early Valanginian is characterised by the first appearance of *Montsalevia salevensis* (Darsac, 1983; Boisseau, 1987; Blanc, 1996). Additionally, an ammonite was found in the scree, down of the section of Vitznau (Fig. 3.9). The specimen is a *Thurmanniceras thurmanni* s.str. and indicates the early *T. otopeta* ammonite zone corresponding to the latest Berriasian (Blanc *et al.*, 1992).

Furthermore, the general trends in the $\delta^{13}C$ records are used to correlate the sections within this Helvetic transect, and more particularly the negative shift occurring close to the Berriasian-Valanginian boundary, which is also established from the Vocontian Basin (Morales *et al.*, 2013), and which is mainly attributed to a change in carbonate production from photozoan to heterozoan carbonate production on the platform (Föllmi *et al.*, 2006; Morales *et al.*, 2013). Nevertheless, these changes may be diachronic between the Helvetic and the Jura domains. Consequently, $\delta^{13}C$ trends can be used for correlation within the Helvetic domain, but its validity as a correlating tool with the Jura is not assessed.

The sedimentary succession of the Säntis can be well correlated with that of the southern Jura Mountains. Consequently, sequence boundaries have been named following those defined for the La Chambotte section (Morales *et al.*, 2013). A specimen of *Calpionellopsis simplex* was found in sequence d (upper part of UOL; Fig. 3.13), which indicates a late Berriasian age and is consistent with studies in the Jura Mountains (Darsac, 1983; Blanc, 1996). An interesting point is that *Montsalevia salevensis*, which marks the Valanginian, is found high up in the measured section - in the Betlis Limestone Fm, where it occurs together with *Meandrospira favrei*, *Montsalevia filiformis*, and *Protopeneroplis banatica*. The latter ranges from the late Berriasian to earliest Valanginian (early *T. pertransiens* ammonite zone after Blanc, 1996), which may indicate an earliest Valanginian age for the first sequence of the Betlis Limestone Fm (SBh).

When compared to the $\delta^{13}C$ record of the Vocontian Trough (Fig. 3.14), the rapid decrease in $\delta^{13}C$ values at the boundary between the UOL and the Vitznau Fm indicates the presence of an important hiatus. The presence of *Protopeneroplis banatica* in the Betlis Limestone Fm argues for an age close to the Berriasian-Valanginian boundary for the Vitznau Fm. As such, they may represent a lateral equivalent to the Guiers Mb of the southern Jura Mountains. The Guiers Mb witnessed an important transgressive phase (Steinhauser and Charollais, 1971; Blanc, 1996; Morales *et al.*, 2013), which is coherent with the transgressive interval recorded in the Vitznau Marls. However, in the Jura Mountains the re-appearance of a photozoan carbonate platform facies is observed with the Upper Mb of the Chambotte Fm (sequence f) in the early Valanginian, which is not seen in the Säntis section. This may be related to an enhanced subsidence phase recorded in the Helvetic platform compared to other NW Tethyan areas (Stampfli *et al.*, 2002). This would imply an earliest Valanginian age for the Vitznau Fm in the Säntis section.

The Dräckloch section, which should be more complete given its more distal position compared to the Säntis and the La Chambotte sections, is more complex with regards to its age interpretation.

The joint presence of *Pseudotextulariella courtionensis* and *Pavlovecina allobrogensis* at the base of the UOL is also known from sequence a (equivalent of the Pierre Chatel Fm and lower part of the Vions Fm; Morales *et al.*, 2013). The $\delta^{13}C$ trends are also in favour of this hypothesis (Fig. 3.14). The overlaying sequence contains *Pseudotextulariella courtionensis* together with *Montsalevia elevata*, which is also observed in sequence b of the La Chambotte section (equivalent of the middle part of the Vions Fm). The presence of *Pseudotextulariella courtionensis* and *Montsalevia elevata* in a 90-m interval is surprising if compared to the few metre thick interval in the La Chambotte section (Darsac, 1983; Boisseau, 1987; Blanc, 1996).

This may be explained by the observation that the sequence in which they were found is well developed at Dräckloch indicating the presence of sufficient accommodation space in this outer-platform – outer-shelf section, whereas this sequence

is reduced in the inner-platform section of La Chambotte. This correlation would imply that the higher Berriasian sequences are missing in Dräckloch. Indeed, *Pseudotextulariella courtionensis* is present up to the first emersive layer; and *Pfenderina neocominesis* or *Choffatella pyrenaica* (Peybernès, 1976; Darsac, 1983; Blanc, 1996), which are relatively common species in these higher sequences, were not observed.

As such, an important hiatus maybe present within the upper part of the UOL encompassing sequences c and d (equivalent to the top part of the Vions Mb and the Lower Mb of the Chambotte Fm). A comparison of the $\delta^{13}C$ records of the Säntis and Dräckloch sections would not contradict this interpretation (Fig. 3.13). The uppermost part of the UOL cannot be dated by biostratigraphy because the foraminiferal fauna is relatively poor, and no calpionellid or ammonites were found. As for the Säntis section, the sudden change to more negative values in the $\delta^{13}C$ curve indicates a major hiatus between the top of the UOL and the Vitznau Fm.

A calpionellid, which may belong to *Tintinnopsella longa*, was found in the overlaying Vitznau Fm, which ranges from the latest early Berriasian to the early Valanginian (Blanc, 1996).

For the Vitznau and the Betlis Limestone Fms, an identical sequential succession is proposed as for the Säntis section, and therefore a comparable age model. In contrast to the Säntis section, the $\delta^{13}C$ positive shift of the Weissert episode is not recorded in the Dräckloch section. This may be related to the possibility that condensation starts earlier in this part of the shelf and that only the lower member of the Betlis Limestone Fm is preserved (Kuhn, 1996).

The Vitznau section shows the joint presence of *Pseudotextulariella courtionensis* and *Montsalevia elevata* in the lowermost sequence; consequently its HST should belong to sequence b of the La Chambotte section. The overlaying deposits, which are strongly reworked and interpreted as a falling stage systems tract, have delivered the calpionellids *Calpionellopsis simplex, Calpionellopsis oblonga* and *Remaniella filipescui* (Fig. 3.9), together with a specimen of *Montsalevia elevata* (Fig. 3.7), which indicate a late Berriasian age (late calpionellid zone D1, and D2 after Remane, 1985; Blanc, 1996; Remane *et al.*, 1998). Moreover, *Pseudotextulariella courtionensis*, which is abundant in the underlying sequence (one specimen has been observed in each bioclast-rich layer), is absent in this interval, which is yet rich in platform debris. Its high proportion in oolites and heavy $\delta^{13}C$ signature also link this interval to the late Berriasian sequences of the Dräckloch and Säntis sections, rather than to the earliest Valanginian reworked deposits of the Dräckloch section, which are devoid of oolites and exhibit a lighter $\delta^{13}C$ signature. These deposits are therefore interpreted as the falling stage systems tract of sequence c and d or e.

These sequence boundaries are combined in the Dräckloch section, and an important hiatus is associated with the sequence boundary e in the Säntis section. Consequently, the falling stage system tract might belong or to sequence e, either to the combination of sequences c, d and e.

The Vitznau and Betlis Limestone Fms are correlated to the other sections by sequence stratigraphy. The ammonite *Thurmanniceras thurmanni* s.str. (Fig. 3.9) was found in the scree of the section and indicates the early part of the *T. otopeta* zone (latest Berriasian). Stable isotope and phosphorus analyses performed on the host rock of the ammonite indicate that its origin is from the Vitznau Fm ($\delta^{13}C$: 0.20 ‰; $\delta^{18}O$: -2.70 ‰ and P: 137 ppm). Moreover, ahermatypic corals were found in the host rock of the ammonite, and this type of coral was observed in the early TST of sequence e, in the lower part of the Vitznau Fm. If the determination and the position of the ammonite are correct (*Thurmanniceras thurmanni* s.l. has an extended range to the *T. pertransiens* ammonite zone after Wippich, 2003 and Bujtor, in press), the lower part of the Vitznau Fm at Vitznau would have a latest Berriasian age. The diachronism of the $\delta^{13}C$ negative shift between the Jura and the Helvetic domains is confirmed. Finally, the Betlis Limestone is correlated by sequence stratigraphy to the Dräckloch and Säntis sections.

3.6. DISCUSSION

3.6.1. Palaeogeography, sea-level change and tectonics

The studied sections document the installation and growth of the Helvetic carbonate platform since the early late Berriasian. The elaboration of the transect highlights the occurrence of a more complete sedimentological record in the inner shelf section of Säntis compared to the outer shelf section of Dräckloch, which appears to lack the late Berriasian sequences c and d. This hiatus recorded in the Dräckloch section is linked with an emersion, its duration corresponds to an important part of the *S. boissieri* ammonite zone, e.g. of the late Berriasian. A relatively similar succession is observed in the section of Lämmerenplatten (Pasquier, 1995), which is constituted of similar environments (close to or at the oolitic shoal) but the temporal frame is poorly calibrated. During the Early Cretaceous, the Helvetic region was structured by major fault zones (Funk, 1985; Detraz *et al.*, 1987) and an important subsidence phase is recorded from the Oxfordian to the Hauterivian (Funk, 1985; Stämpfli *et al.*, 2002; Bonin *et al.*, 2012). Thus this differential record is probably linked to a phase of intensified tectonic activity during the late Berriasian - early Valanginian, which probably testifies of the last extensive movements affecting the North Tethyan margin. The general high subsidence rates documented in the Helvetic plateau are usually linked to the general opening of the Alpine Tethys (Stampfli *et al.*, 2002).

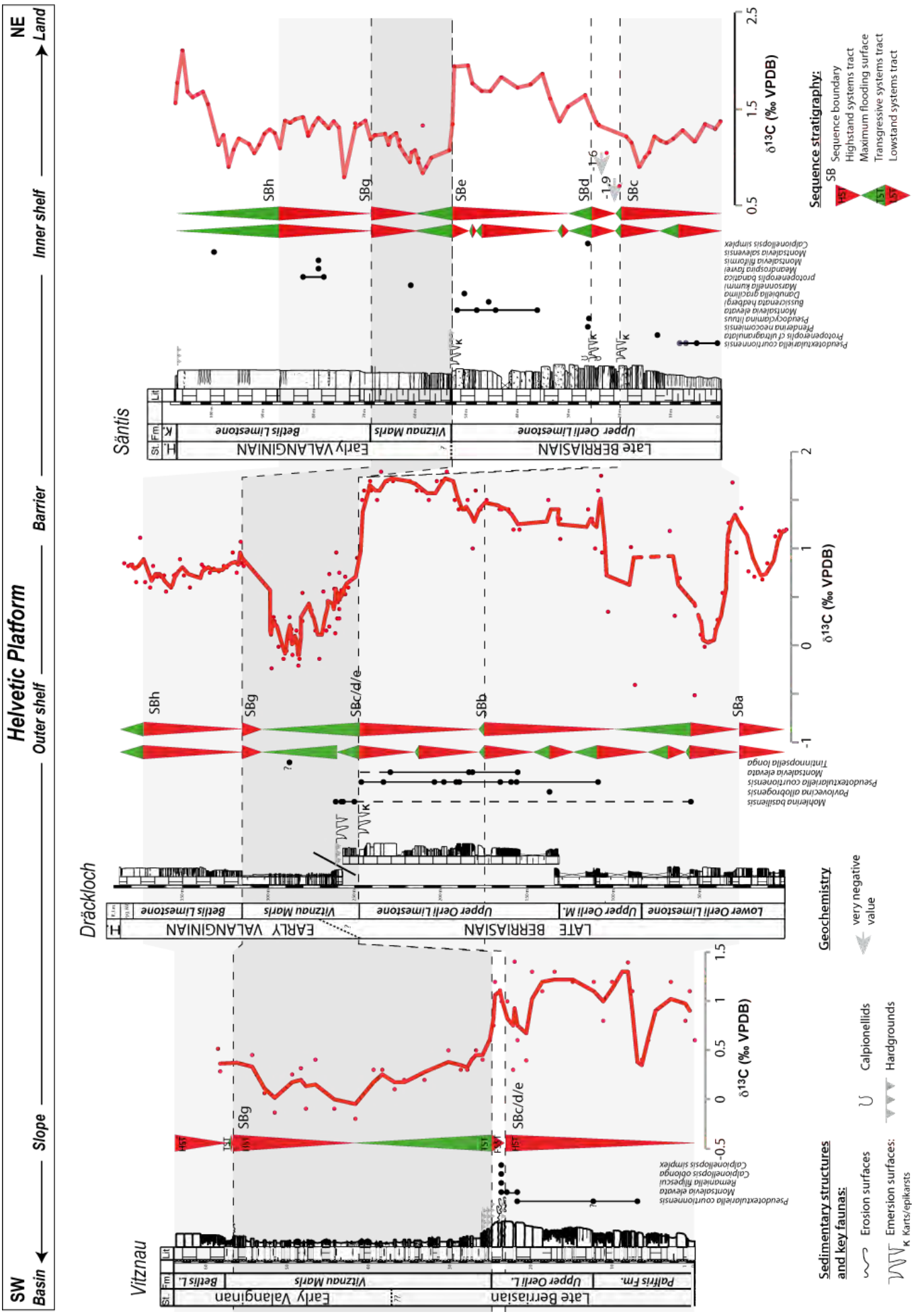

Fig. 3.13: Correlation of the sections across a NE/SW proximal-distal transect.

The Dräckloch section, which is close to the platform barrier, is probably located near the top of a tilted block (range), whereas the Säntis, which is more lagoonal, may be located within the shallow-water basin formed back of the top (Fig. 3.15). The topographic effect of tilting blocks may also be evident in the Säntis section, where parasequences involving high amplitude relative sea-level variations were observed in the sedimentary succession and microfacies of the UOL. The slope section of Vitznau records a falling stage system tract, which is probably linked with the topographic effects of block tilting.

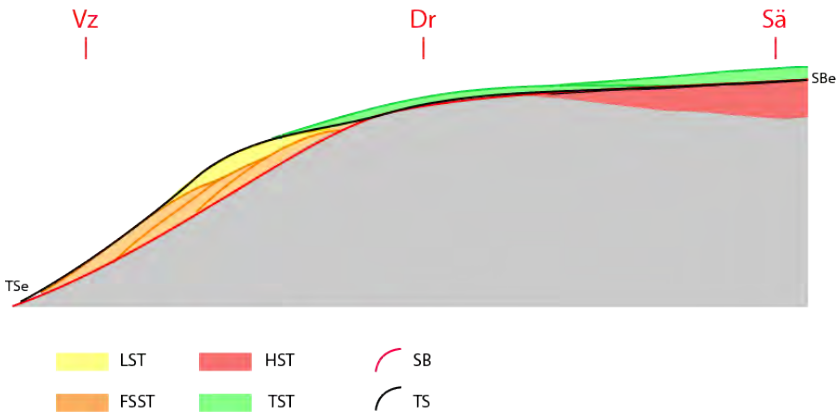

Fig. 3.15: Schematic representation of the depositional sequences during the latest Berriasian and the earliest Valanginian (Vz, Vitznau; Dr, Dräckloch; Sä, Säntis).

In the Jura Mountains, sequences c and d are preserved in the southern, more distal part by a few tens of metres of sediments (35 m the la Chambotte section; upper part of the Vions Fm and lower Mb of the Chambotte Fm; Morales *et al.*, 2013). In the northern Jura, the two sequences are missing or strongly reduced to less than 2 m, such as in the Juracime section. The implication of tectonic activity as a trigger for differential space accommodation between the northern and southern Jura is also discussed in Morales *et al.* (2013), and a parallel with a major slumped interval in the Vocontian Basin (Joseph *et al.*, 1988; Bulot *et al.*, 1994; Bulot, 1995) is suggested.

An important transgressive phase, which started in the latest Berriasian and ended in the earliest Valanginian, is documented with the uppermost part of the UOL in Dräckloch, and more generally with the Vitznau Fm in the Helvetic domain. This transgressive phase is also well recorded in the Jura with the Guiers Mb, but the amplitude of sea-level rise appears less important (Morales et al., 2013). Here again, the transgression effects have probably been amplified by a phase of subsidence. The Jura area may have been less strongly subjected to subsidence, and as such, platform carbonate production was able to catch up, and a photozoan carbonate platform was able to subsist (sequence f), which is not documented in the Helvetic.

The overlaying heterozoan deposits of sequences g and h, materialised by the Betlis Limestone in the Helvetic domain and corresponding to the Bourget and Calcaires Roux Fms in the Jura were deposed, again in an enhanced subsiding context in the Helvetic domain.

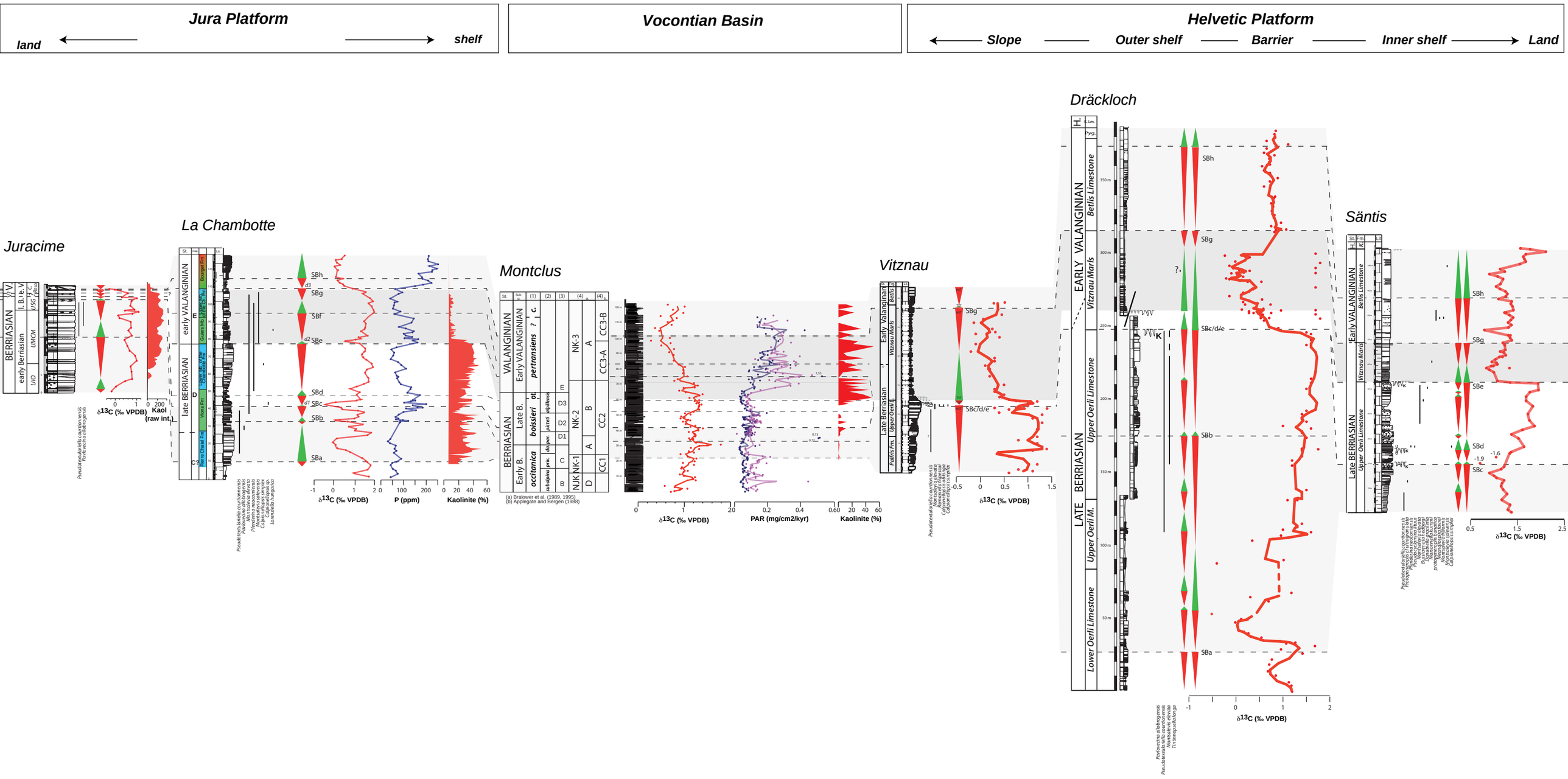

(a) Bralower et al. (1989, 1995)
(b) Applegate and Bergen (1988)

Fig. 3.16: Correlation of the Jura and the Helvetic Platforms with the Vocontian Basin

3.6.2. Palaeoenvironmental and palaeoclimatic changes

In the late early and early late Berriasian, the increase in phosphorus and detrital input observed in sequence a (upper part of LOL and UOM) are linked in the Helvetic platform to a period of transgression. The following sequences do not show major changes in these parameters, which is different from the Jura areas, where an increase in quartz and phosphorus is observed in the sequences b and c of the Vions Fm). These changes appear therefore not correlated in the Jura-Helvetic realm and are probably of local origin, such as local river input.

An increase in phosphorus and detrital minerals is also recorded in the Vitznau Fm, which again corresponds to a sea-level rise of probably wider importance (Haq et al., 1987). The carbonate production changes from photozoan to heterozoan assemblages in the Helvetic realm. The correlation with the Jura and the Vocontian Trough indicates that this interval also corresponds to a maximum in humidity. Thus, with an important transgression and a highly hydrolysing climate, the platform encompassed a first stressful period leading to the disappearance of oligotrophic organisms.

The presence of phosphates and internal or reworked pelagic sediments on top of the UOL at Dräckloch, associated with a series of superimposed hardgrounds in all three sections indicate a platform drowning phase associated with this important transgressive phase. Following the drowning phase, a mesotrophic fauna including bryozoans, crinoids and prolifering oysters, brachiopods, ostracods and serpulids installed itself in the distal part of the platform. With the Betlis Limestone Fm (sequences g and f), the carbonate production catches up with regards to the accommodation space in a heterozoan mode. The excess in nutrients is also indicated by the presence of chert nodules, which are related to a higher proportion of siliceous sponges (which are filter feeders). The correlation with the Jura shows a decrease in humidity during this period. At the top of sequence f, strong detrital input is recorded.

The top of the sequence is poorly documented in the Jura (Hennig, 2003) and clay mineral analyses were not performed. Nevertheless, the abundance of mm-sized quartz grains (Fig. 3.8B and C) containing sometimes a ferruginous boarder, indicate an important phase of erosion on the continent. This is correlated with an increase in phosphorus contents, which suggest increased nutrient input to the ocean. This phase of weathering is responsible for the drowning of the carbonate platform during the Weissert episode – a platform which was already weakened by previous phases of rapid sea-level change and high nutrient levels.

3.7. CONCLUSIONS

With this transect across the Helvetic Alps, the installation, growth and demise of the Berriasian-Valanginian carbonate platform is documented. A more accurate age control is proposed for the studied sections of the Säntis, Dräckloch and Vitznau, based on benthic foraminifera, calpionellid and ammonite biostratigraphy, chemosratigraphy, and sequence stratigraphy. This allows for a correlation and a comparison with the Jura platform are established. The Helvetic sedimentological record is relatively different from the Jura archive, which is interpreted as reflecting a differentiation through enhanced tectonics, with the Helvetic domain more strongly subsiding. Additionally, block tilting is the more likely hypothesis to explain a major hiatus present in the upper part of the UOL, and encompassing an important part of the late Berriasian in the Dräckloch section. A major sea-level rise starting in the latest Berriasian, and progressively flooding the inner parts of the platform is documented in the Helvetics and correlated with the Jura. This sea-level rise, combined with a strongly subsiding setting and an enhanced humidity lead to the disappearance of photozoan faunas and a first major drowning phase in the Helvetic domain, whereas in the less subsiding settings of the Jura they were able to persist until a little later in the early Valanginian. During the late early and early late Valanginian, phases of enhanced detrital input linked with strong continental weathering was responsible for a second, smaller, and a third, widespread demise of the carbonate platform (near the boundary of the *pertransiens – campylotoxus* zone and during the *verrucosum* zone). This latter shallow-water carbonate crisis is materialised by a quartz-rich phosphatic and glauconitic crust on top of a hardground (Gemsmättli Bed) or a quartz and phosphate-rich, highly bioturbated interval (Pygurus Mb). These are condensed horizons, which document the almost complete disappearance of shallow-water calcifying organisms disappear for more than 3 my. The renewed installation of a carbonate platform in the Helvetic region is only recorded from the middle early Hauterivian onwards.

References

Adatte, T., Stinnesbeck, W. and Keller, G. (1996) Lithostratigraphic and mineralogic correlations of near K/T boundary sediments in northeastern Mexico: Implications for origin and nature of deposition. In: *The Cretaceous-Tertiary Event and Other Catastrophes in Earth History*. (Ed G. Ryder, Fastovsky, D. and Gartner, S.,), **307**, pp. 211-226. Geological Society of America Special Paper, Boulder, Colorado.

Arnaud-Vanneau, A. and Arnaud, H. (2005) Carbonate facies and microfacies of the Lower Cretaceous carbonate platforms. In: *The Hauterivian-Lower Aptian sequence stratigraphy from Jura Platform to Vocontian Basin: A multidisciplinary approach* (Ed T. Adatte, Arnaud-Vanneau, A., Arnaud, H., Blanc-Aletru, M.-C.,

Bodin, S., Carrio-Schaffhauser, E., Föllmi, K. B., Godet, A., Raddadi, M. C. and Vermeulen, J.), **7**, pp. 39-68. Géologie Alpine, Série Spéciale «Colloques et Excursions» Grenoble.

Beaudoin, B., Joseph, P. and Cojan, I. (1987) Resédimentation au Jurassique terminal - Berriasien: Mécanismes et paléomorpologies. *Géologie Alpine, mém. h.s.*, **13,** 187-196.

Bodin, S. (2006) *Palaeoceanographic and palaeoclimatic changes during the Late Hauterivian - Barremian and their impact on the northern Tethyan margin: A combined sedimentological and geochemical approach*, Université de Neuchâtel, Neuchâtel, 269 pp.

Bodin, S., Godet, A., Föllmi, K.B., Vermeulen, J., Arnaud, H., Strasser, A., Fiet, N. and Adatte, T. (2006) The late Hauterivian Faraoni oceanic anoxic event in the western Tethys: Evidence from phosphorus burial rates. *Palaeogeography, Palaeoclimatology, Palaeoecology*, **235,** 245-264.

Bonin, A., Vennin, E., Pucéat, E., Guiraud, M., Arnaud-Vanneau, A., Adatte, T., Pittet, B. and Mattioli, E. (2012) Community replacement of neritic carbonate organisms during the late Valanginian platform demise: A new record from the Provence Platform. *Palaeogeography, Palaeoclimatology, Palaeoecology*, **365-366,** 57-80.

Burger, H. (1985) *Palfris-Formation, Öhrli-Formation und Vitznau-Mergel (Basale kreide des helvetikums zwischen reuss und rhein). Stratigraphische, fazielle, mineralogische und paläogeographische Untersuchungen.*, Zürich, Zürich, 237 pp.

Burger, H. (1986) Fazielle Entwicklung und paläogeographische Rekonstruktion des helvetischen Schelfs während der untersten Kreide in der Zentral- und Ostschweiz. *Eclogae Geologicae Helveticae*, **79,** 561-615.

Detraz, H., Charollais, J. and Remane, J. (1987) Le Jurassique supérieur - Valanginian des chaînes subalpines septentrionales (massif des bornes et de Platé, Haute-Savoie; Alpes occidentales): Analyse des resédimentations, architecture du bassin et influences des bordures. *Eclogae Geologicae Helveticae*, **80,** 69-108.

Detraz, H. and Steinhauser, N. (1988) Le bassin delphino-helvétique savoyard et sa marge jurassienne sous contrôle tectonique entre le Kimméridgien et le Valanginien. *Eclogae Geologicae Helveticae*, **81,** 125-154.

Duchamp-Alphonse, S., Gardin, S., Fiet, N., Bartolini, A., Blamart, D. and Pagel, M. (2007) Fertilization of the northwestern Tethys (Vocontian basin, SE France) during the Valanginian carbon isotope perturbation: Evidence from calcareous nannofossils and trace element data. *Palaeogeography, Palaeoclimatology, Palaeoecology*, **243,** 132-151.

Föllmi, K.B. (1995) 160 m.y. record of marine sedimentary phosphorus burial: Coupling of climate and continental weathering under greenhouse and icehouse conditions. *Geology*, **23,** 859-862.

Föllmi, K.B. (2012) Early Cretaceous life, climate and anoxia. *Cretaceous Research*, **35,** 230-257.

Föllmi, K.B., Weissert, H., Bisping, M. and Funk, H. (1994) Phosphogenesis, carbon-isotope stratigraphy, and carbonate-platform evolution along the Lower Cretaceous northern Tethyan margin *Geological Society of America Bulletin*, **106,** 729-746.

Föllmi, K.B., Bodin, S., Godet, A., Linder, P. and van de Schootbrugge, B. (2007) Unlocking paleo-environmental information from Early Cretaceous shelf sediments in the Helvetic Alps: stratigraphy is the key! *Swiss journal of geosciences*, **100,** 349-369.

Funk, H. (1985) Mesozoische Subsidenzgeschichte im Helvetischen Schelf der Ostschweiz. *Eclogae Geologicae Helveticae*, **78,** 249-272.

Gréselle, B. and Pittet, B. (2010) Sea-level reconstructions from the Peri-Vocontian Zone (South-east France) point to Valanginian glacio-eustasy. *sedimentology*, **57,** 1640-1684.

Haldimann, P.A. (1977) *Sedimentologische Entwicklung der Schichten an einer Zyklengrenze der helvetischen Unterkreide*. Unpublished Ph.D. thesis, ETH Zürich, 182 pp.

Hallam, A., Grose, J.A. and Ruffell, A.H. (1991) Palaeoclimatic significance of changes in clay mineralogy across the Jurassic-Cretaceous boundary in England and France. *Palaeogeography, Palaeoclimatology, Palaeoecology*, **81,** 173-187.

Haq, B.U., Hardenbol, J. and Vail, P.R. (1987) Chronology of Fluctuating Sea Levels Since the Triassic. *Science*, **235,** 1156-1167.

Hardenbol, J., Thierry, J., Farley, M.B., Jacquin, T., De Graciansky, P.-C. and Vail, P.R. (1998) Mesozoic and cenozoic sequence statigraphy of european basins. Mesozoic and Cenozoic sequence chronostratigraphic framework of european basins. . *SEPM (Society for Sedimentary Geology)*, **Special Publication 60**.

Hennig, S. (2003) *Geochemical and sedimentological evidence for environmental changes in the Valanginian (early Cretaceous) ofthe Tethys region*, ETH Zurich, 189 pp.

Ischi, H. (1978) *Das Berriasien-Valanginien in der Wildhorn-Drusberg-Decke zwischen Thuner- und Vierwaldstättersee*, University of Bern, Bern, 142 pp.

Jacquin, T., Rusciadelli, G., Amédro, F., De Graciansky, P.-C. and Magniez-Jannin, F. (1998) The North Atlantic cycle: an overview of 2nd-order transgressive/regressive facies cycle in the Lower Cretaceous of Western Europe. *SEPM (Society for Sedimentary Geology) Special Publication*, **60,** 397-409.

Joseph, P., Beaudoin, B., Sempéré, T. and Maillart, J. (1988) Vallées sous-marines et systèmes d'épandages carbonatés du Berriasien vocontien (Alpes méridionales françaises). *Bulletin de la société géologique de France*, **8,** 363-374.

Joseph, P., Beaudoin, B., Fries, G. and Parize, O. (1989) Les vallées sous-marines enregistrent au Crétacé inférieur le fonctionnement en blocs basculés du domaine vocontien. *Comptes Rendus de l'Académie des Sciences - Series II*, **309,** 1031-1038.

Kübler, B. (1983) Dosage quantitatif des minéraux majeurs des roches sédimentaires par diffraction X. *Cahiers de l'Institut de Géologie, Université de Neuchâtel, Suisse*, **AX1.1 and 1.2** 1-13.

Kübler, B. (1987) Cristallinité de l'illite: méthodes normalisées de préparation, méthode normalisée de mesure, méthode automatique normalisée de mesure. *Cahiers de l'Institut de Géologie, Université de Neuchâtel, Suisse*, **ADX 2.**

Kübler, B. and Jaboyedoff, M. (2000) Illite crystallinity *Comptes Rendus de l'Académie des Sciences - Series IIA - Earth and Planetary Science*, **331,** 75-89.

Kuhn, O. (1996) *Der Einfluss von Verwitterung auf die Paläozeanographie zu Beginn des Kreide-Treibhausklimas (Valanginian und Hauterivian) in der West-Tethys*, Eidgenössische Technische Hochschule Zürich, 380 pp.

Mohr, H.M. (1992) *Der helvetische Schelf der Ostschweiz am Übergang vom späten Jura zur frühen Kreide*, Zurich, Zurich, 221 pp.

Morales, C., Gardin, S., Schnyder, J., Spangenberg, J., Arnaud-Vanneau, A., Arnaud, H., Adatte, T., Föllmi, K.B. (2013) Berriasian and early Valanginian environmental change along a transect from the Jura Platform to the Vocontian Basin. *Sedimentology*, **60**(1), 36-63.

Pantic, N.K. and Burger, H. (1981) Palynologische Untersuchungen in der untersten Kreide des östlichen Helvetikums. *Eclogae Geologicae Helveticae*, **74,** 661-672.

Pasquier, J.-B. (1995) *Sédimentologie, stratigraphe séquentielle et cyclostratigraphie de la marge Nord-Téthysienne au Berriasien en Suisse occidentale*, Université de Fribourg, Fribourg, 274 pp.

Remane, J. (1985) Calpionellids. In: *Plankton Stratigraphy* (Eds H.M. Bolli, J.B. Saunders and K. Perch-Nielsen), **1**, pp. 555-572. Cambridge University Press, Cambridge.

Remane, J., Bilal, U.H. and Anne, B. (1998) Calpionellids. In: *Introduction to Marine Micropaleontology (Second Edition)*, pp. 161-170. Elsevier Science B.V., Amsterdam.

Schlager, W. (1981) The paradox of drowned reefs and carbonate platforms. *Geological Society of America Bulletin*, 92, 197-211.

Schnyder, J., Gorin, G., Soussi, M., Baudin, F. and Deconinck, J.-F. (2005) Enregistrement de la variation climatique au passage Jurassique/Crétacé sur la marge sud de la Téthys : minéralogie des argiles et palynofaciès de la coupe du Jebel Meloussi (Tunisie centrale, formation Sidi Kralif). *Bulletin de la société géologique de France*, **176,** 171-182.

Spangenberg, J.E. and Herlec, U. (2006) Hydrocarbon biomarkers in the Topla-Mezica zinc–lead deposits, Northern Karavanke/Drau range, Slovenia: paleoenvironment at the site of ore formation. *Economic Geology*, **101,** 997-1021.

Spangenberg, J.E., Fontboté, L. and Macko, S.A. (1999) An evaluation of the inorganic and organic geochemistry of the San Vicente Mississippi Valley-type zinc-lead district, central Peru: implications for ore fluid composition, mixing processes and sulfate reduction. *Economic Geology*, **94,** 1067-1092

Spangenberg, J.E. and Macko, S.A. (1998) Organic geochemistry of the San Vicente zinc-lead district, eastern Pucarà Basin, Peru. *Chemical Geology*, **146,** 1-23.

Stampfli, G., Borel, G.D., Marchant, R. and Mosar, J. (2002) Western Alps geological constraints on western Tethyan reconstructions. In: *Reconstruction of the*

evolution of the Alpine-Himalayan Orogen (Eds G. Rosenbaum and G.S. Lister), **7**, pp. 75-104. Journal of the Virtual Explorer,.

Wyssling, G.W. (1986) Der frühkretazische helvetische Schelf im Vorarlberg und Allgäu. *Jahrbuch der Geologischen Bundesanstalt*, **129,** 161-265.

CHAPTER 4:

PALAEOENVIRONMENTAL CHANGE THROUGH THE ONSET OF THE VALANGINIAN CARBON-ISOTOPE EXCURSION: EVIDENCE FROM THE MID-POLISH TROUGH.

PALAEOENVIRONMENTAL CHANGE THROUGH THE ONSET OF THE VALANGINIAN CARBON-ISOTOPE EXCURSION: EVIDENCE FROM THE MID-POLISH TROUGH.

CHLOE MORALES*, ARIANE KUJAU**, ULRICH HEIMHOFER***, JOERG MUTTERLOSE**, JORGE E. SPANGENBERG*, THIERRY ADATTE, IZABELA PLOCH****, AND KARL B. FÖLLMI

* *Institute of Earth Sciences, Université de Lausanne, Géopolis, 1015 Lausanne, Switzerland*
** *Institute for Geology, Mineralogy and Geophysics, Ruhr-University, Universitätsstraße 150, D-44801 Bochum, Germany*
*** *Institute of Geology, Leibniz University Hannover, Callinstraße 30, D-30167 Hannover, Germany*
**** *Polish Geological Institute, National Research Institute, 4 Rakowiecka PL-00-975 Warsaw, Poland*

Submitted to Palaeogeography, Palaeoclimatology, Palaeoecology the 4/10/2012.

ABSTRACT

The Valanginian Weissert episode is associated with a positive excursion (CIE) in $\delta^{13}C_{carb}$ and $\delta^{13}C_{org}$ values, and the occurrence of a crisis in pelagic and neritic carbonate production. It has been interpreted to include the first oceanic anoxic event (OAE) of the Cretaceous associated with the formation of the Paraña-Etendeka large igneous province (LIP). Recently it was demonstrated that the extent of anoxia was limited to high-latitude epicontinental seas and the Pacific, and that the Paraña-Etendeka LIP postdates the Valanginian CIE, and with these observations, the question is open with regards to which type of palaeoenvironmental changes has lead to the perturbation of the carbon cycle during the Valanginian. Here we present the results of an analysis of the Wąwał drilling core, central Poland, which is situated in the Mid-Polish Trough. The Wąwał core is of particular interest because of its near-coastal setting and its exceptional preservation, demonstrated by the presence of up to 17 wt.% aragonite. It consists of lower to upper Valanginian silty to sandy clays deposited under fully marine conditions on top of an lower Berriasian karstified limestone filled in with an upper Berriasian lag deposit. The onset of the $\delta^{13}C$ shift is recorded both in the whole-rock as well as in a selection of handpicked faunas (ostracods, bivalves and Lenticulinid benthic foraminifera). A temporal lag is recorded between the $\delta^{13}C_{carb}$ and the $\delta^{13}C_{org}$ record, which is interpreted as a change in atmospheric pCO_2. This is accompanied by a change in the weathering

mode from very humid and highly hydrolysing toward less humid and seasonally contrasted conditions, indicated by the abrupt change from a kaolinite to a smectite-dominated clay-mineral association near the boundary between the early and late Valanginian. Moreover, two phosphate-rich horizons have been identified, which appear correlated in time to northern Tethyan occurrences in the Helvetic Alps. The lower level is associated with the early Valanginian transgression on top of the Berriasian lag deposit and corresponds to maximal humidity recorded in the Wąwał core section. The upper layer cannot be related to any palaeoclimatic or palaeoenvironmental change in the Carpathian seaway, but corresponds to the maximum of the Valanginian crisis in carbonate production. In the Wąwał core section, preserved organic matter is predominantly of terrestrial origin and evidence for anoxic conditions during the Valanginian CIE is lacking.

Keywords Valanginian, Climate change, Weissert Event, Polish Basin.

4.1. INTRODUCTION

The Valanginian stage witnessed the first major positive excursion in the inorganic and organic carbon ($\delta^{13}C_{carb}$ and $\delta^{13}C_{org}$) isotope records of the Cretaceous period. A positive shift of about 1.7‰ is observed in $\delta^{13}C_{carb}$ values near the end of the early and at the onset of the late Valanginian in sediments of the Atlantic, the Boreal and the Tethys oceans (Cotillon & Rio, 1984; Lini *et al.*, 1992; Föllmi *et al.,* 1994; Kuhn, 1996; Wortmann & Weissert, 2000; Erba *et al.,* 2004; Duchamp-Alphonse *et al.,* 2007). The carbon-isotope excursion (CIE) has been established from $\delta^{13}C_{carb}$ records in both deep- and shallow-marine domains (Weissert *et al.,* 1998; Hennig *et al.,* 1999), as well as from terrestrial environments ($\delta^{13}C_{org}$ shift of 4-5‰; Gröcke *et al.,* 2005). Associated with the CIE, the Valanginian encompasses a crisis in carbonate production observed in pelagic and neritic realms with a decline in calcareous nannofossils (Erba, 2004) and the demise of carbonate platforms (Föllmi *et al.,* 1994, 2007; Weissert *et al.,* 1998; Wortmann *et al.* 2000), respectively.

The Valanginian CIE has been associated with the first Oceanic Anoxic Event (OAE) of the Cretaceous - the "Weissert Event" (Erba *et al.,* 2004). As the main trigger of this event, a major phase of volcanic activity has generally been invoked, which led to the formation of the Paraña-Etendeka Large Igneous Province (LIP). Paraña-Etendeka volcanic activity is supposed to have increased the pCO_2 in the atmosphere leading to an intensification in continental biogeochemical weathering, and subsequently to an increase in marine primary productivity and organic-matter preservation (Föllmi *et al.,* 1994).

There are several recent observations, which diverge with these interpretations: (1) Paraña-Etendeka volcanic activity took place in a continental setting, which is in contrast to other Cretaceous OAEs, which are associated with oceanic provinces (Courtillot & Renne, 2003). Furthermore, recent age dates of the Paraña-Etendeka LIP indicate a main extrusive phase at 134.7 ± 1 Ma (Thiede & Vasconcelos, 2010), which would correspond to an early Hauterivian age according to the timetable by Ogg *et al.* (2008); (2) Valanginian sediments lack thicker and widespread marine organic carbon-rich levels such as those associated with the early Aptian OAE 1a and the end-Cenomanian OAE 2 (Schlanger & Jenkyns, 1976) and (3) centimetric organic-rich sediments deposited near the onset of the $\delta^{13}C$ excursion in the western Tethys do not document the presence of significant and long-term anoxic conditions (Westermann *et al.,* 2010; Kujau *et al.,* 2012). The Vocontian basin underwent local anoxic conditions documented by the Barrandes layers but their deposition occurred well before the $\delta^{13}C$ shift. Sediments deposited during the carbon-isotope perturbation, which exhibit oxygen-depleted conditions, are found only in a few localities such as the Weddell Sea and Shatsky Rise in the Pacific (O'Connell, 1990; Bralower *et al.,* 2002; Westermann *et al.,* 2010).

As such it appears that there is no evidence for a full-fledged OAE during the Valanginian and that increases in marine C_{org} burial rates may not have been sufficient to have provoked the CIE. An alternative trigger has therefore been proposed by Westermann *et al.* (2010). They suggested that the combination of the decrease in shallow-marine carbonate production and the enhanced burial of organic matter on the continent modified the carbon-isotope composition of sediments and organic matter. Indeed, enhanced continental fluxes into the ocean (in detrital and dissolved form) have probably boosted marine primary productivity (Föllmi, 1995; Duchamp-Alphonse *et al.,* 2007). However, associated eutrophication of the oceans was not sufficient, or paleoceanographic conditions did not allow for a corresponding increase in preservation rates of marine organic matter, at least not in the western Tethys.

The palaeoenvironmental conditions leading to the Valanginian CIE are still in need of a detailed investigation and sediments deposited in the Mid-Polish Trough may add valuable information. A drill core was obtained in Wąwał, where the Valanginian sandy and silty clay deposits document the initiation of the positive $\delta^{13}C$ shift in an exceptionally well-preserved sedimentary record. Moreover, the depositional environments of the cored sediments, which were strongly influenced by detrital input, and its palaeolocation in a strait connecting the Tethyan and Boreal realms are of particular interest, since information on the evolution of the climate on the adjacent continent is obtained, which divided the Tethyan and Boreal oceans (Fig. 4.1).

4.2. GEOLOGICAL SETTING

The village of Wąwał is located 90 km southwest of Warsaw, close to Tomaszów (Poland, Fig. 4.1). The Lower Cretaceous strata exposed in this region belong to the north-eastern flank of the Tomaszów Syncline, a structure of the Mid-Polish Anticlinorium (Fig. 4.1; Kutek *et al.*, 1989) linked to the uplift, which occurred during the Laramide episode of the Alpine-Carpathian intraplate compressional phase (latest Cretaceous – Cenozoic, Kutek, 2001). The sediments were deposited in the Mid-Polish Trough, an asymmetric, NW/SE oriented basin, which was shaped by extensional tectonic activity of the Teisseyre-Tornquist zone from the Permian to the Late Cretaceous (Kutek, 2001; Lamarche and Scheck-Wenderoth, 2005). The basin underwent multiple rifting phases, in particular during the Neocomian (Berriasian-Hauterivian) interval, which is documented by syndepositional faulting (Kutek, 2001). During the Valanginian, the Mid-Polish Trough was a narrow strait connecting the Tethyan and Boreal Oceans (Fig. 4.1) and fringed by the Bohemian massif to the SW and the Fenno-Scandian shield to the NE. The area of Wąwał was situated on the western margin of the southern part of the Mid-Polish Trough.

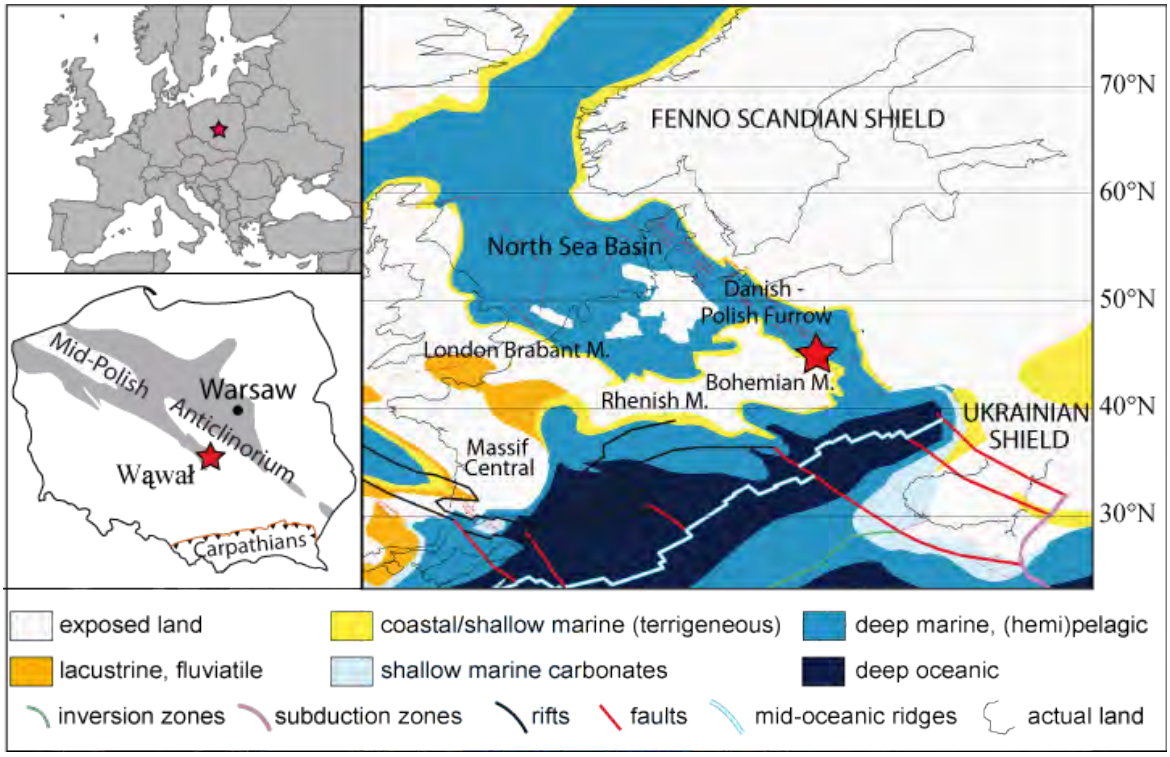

Fig. 4.1: Location of the drill core of Wąwał. Structural scheme after Kutek *et al.*, 1989; Palaeogeographic map compiled after Dercourt *et al.* (1993), Blakey (2005 ; http://jan.ucc.nau.edu/~rcb7/), and Stampfli and Hochard (2009).

A section of Valanginian age outcrops in a clay pit, which is now abandoned and filled in by a small lake, rendering its lower part inaccessible. Several studies have been carried out on the taxonomy of different faunal groups and a synthesis has been established by Kutek *et al.* (1989). These authors also established an ammonite stratigraphic frame based on the NW German zonation.

In spring 2009 an approximately 20 m-long core was drilled, which allowed to obtain a complete and unweathered section through the top of karstified Wealden limestone and 17 m of overlaying Valanginian sandy to silty clays.

4.3. MATERIAL AND METHODS

The core has been sampled in 10-cm intervals resulting in 188 samples. Analyses were performed at the University of Lausanne, except for the palynofacies analysis, which were carried out at the Ruhr-University Bochum. A documentation of the sample intervals is given in Fig. 4.2.

4.3.1. Preparation of microfauna and palynofacies

The samples were washed under water and the fraction ≥45µ was sieved. Bivalve fragments, valves of ostracods and benthic foraminifera were separated under a binocular. Selected specimens of each taxon were examined by scanning electron microscopy (SEM; Tescan Mira/LMU) to assess the degree of diagenetic overprint (Fig. 4.5). Additionally, only single valves of ostracods were used for isotope analyses in order to avoid contamination.

The foraminifera and ostracods belong to a large part to *Lenticulina* cf. *muensteri* and *Schuleridea* cf. *praethoerenensis,* respectively. We can not exclude that some *Lenticulina* specimen belong to other species and that all ostracods belong to the genera *Schuleridea*. The bivalve fragments were not determined.

To separate the sedimentary organic particles, cleaned and crushed samples were treated with HCl and HF following the standard palynological preparation techniques of Traverse (2007). The residue was sieved over an 11-µm-mesh sieve, and a short oxidation with HNO_3 was performed on all residues. A total of 300 sporomorphes were counted for each sample from strew mounts.

4.3.2. Stable-isotope analyses

Carbon and oxygen-isotope compositions were measured on bulk rock and on a selection of hand-picked benthic foraminifera *(Lenticulina)*, ostracods and bivalve fragments.

Carbon and oxygen-isotope analyses were performed on aliquots of whole rock samples and on the selection of hand-picked monogeneric benthic foraminifera (*Lenticulina* sp.), ostracods and bivalve fragments. The isotope analyses were performed on a Thermo Fisher Scientific (Bremen, Germany) GasBench II carbonate preparation device connected to a Thermo Fisher Scientific Delta Plus XL continuous flow isotope ratio mass spectrometer (IRMS). CO_2 was extracted at 70°C. Isotopic ratios of carbon and oxygen are reported in the delta (δ) notation as the per mil (‰) deviation relative to the Vienna Pee Dee belemnite standard (VPDB). The analytical reproducibility estimated from replicate analyses of the international calcite standard NBS-19 and the laboratory standards Carrara Marble was better than ±0.05‰ for $\delta^{13}C_{carb}$ and ±0.1‰ for $\delta^{18}O_{carb}$.

The samples for organic-carbon isotope analyses were treated with 10% HCl acid until the carbonate had entirely reacted. The carbon-isotope composition was determined by flash combustion on a Carlo Erba 1108 elemental analyser (EA) connected to a Thermo Fisher Scientific Delta V IRMS, which was operated in the continuous helium flow mode via a Conflo III split interface (EA–IRMS). The $\delta^{13}C_{org}$ values are reported relative to VPDB. The calibration and assessment of the reproducibility and accuracy of the isotope analysis are based on replicate analyses of laboratory standard materials (glycine, –26.1‰ $\delta^{13}C$; urea, –43.1‰; pyridine, –29.3‰). The reproducibility was better than 0.1‰.

4.3.3. Whole-rock and clay mineralogy

Whole-rock and clay-mineral compositions were analysed by a Thermo scientific ARL X'TRA IP2500 diffractometer. The samples were prepared following the procedures documented by Kübler (1983, 1987) and Adatte *et al.* (1996). The whole-rock composition is determined by a semi-quantification method using external standards with an error of 5%. A detrital index (DI) has been calculated using the ratio of detrital minerals (sum of % quartz, feldspar, plagioclase and phyllosilicates) to carbonates (sum of % calcite and aragonite).

Clay mineral analyses were performed on the <2 μm fraction. The peak intensities of identified minerals are measured in cps and an estimation of the proportion of clay minerals is given in relative per cent. A weathering index (WI) has been obtained by calculating the ratio of kaolinite and the sum of illite and chlorite (Duchamp-Alphonse *et al.,* 2011).

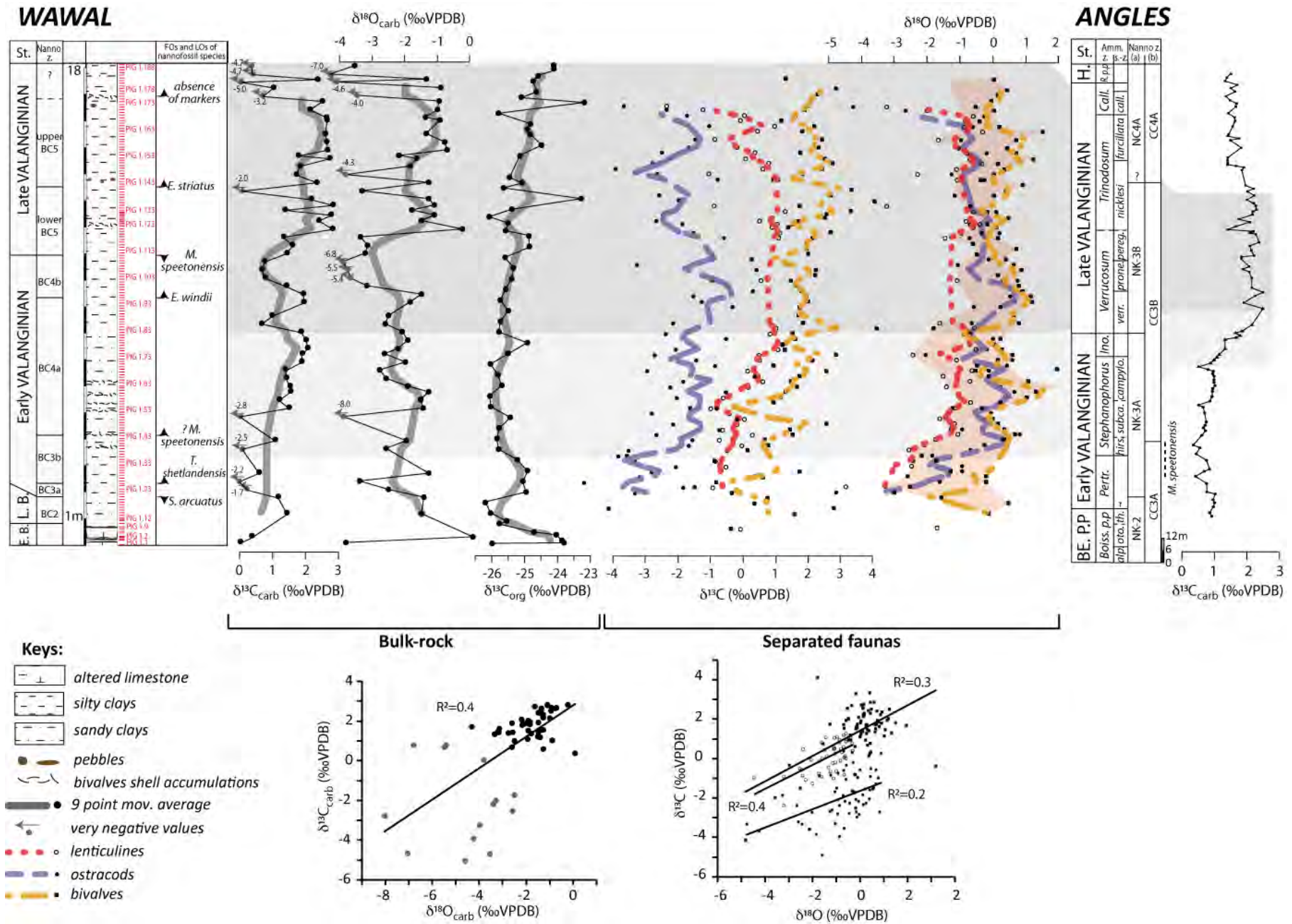
WAWAL
ANGLES
St.
Nanno z.
FOs and LOs of nannofossil species
Late VALANGINIAN
Early VALANGINIAN
upper BC5
lower BC5
BC4b
BC4a
BC3b
BC3a
BC2
L. B.
E. B.
absence of markers
E. striatus
M. speetonensis
E. windii
?M. speetonensis
T. shetlandensis
S. arcuatus
δ18Ocarb (‰VPDB)
δ13Ccarb (‰VPDB)
δ13Corg (‰VPDB)
δ18O (‰VPDB)
δ13C (‰VPDB)
H.
BE. P.P
Amm. z.
Nanno z.
Call.
Trinodosum
Verrucosum
Stephanophorus
Pertr.
Boiss. p.p
furcillata
nicklesi
verr.
hirs. subca.
alp
ota. fih.
NC4A
CC4A
NK-3B
CC3B
NK-3A
CC3A
NK-2
M. speetonensis
12m
6
0
Keys:
altered limestone
silty clays
sandy clays
pebbles
bivalves shell accumulations
9 point mov. average
very negative values
lenticulines
ostracods
bivalves
Bulk-rock
Separated faunas
R²=0.4
R²=0.3
R²=0.2
δ13Ccarb (‰VPDB)
δ18Ocarb (‰VPDB)
δ13C (‰VPDB)
δ18O (‰VPDB)

Fig. 4.2: Evolution of the $\delta^{13}C$ and $\delta^{18}O$ records in Wąwał and correlation with the $\delta^{13}C_{carb}$ record of the hypostratotypic section of Angles (Vocontian basin). Stable isotope values have been obtained from bulk rock, organic matter, and a selection of benthic fauna (ostracods, lenticulinid foraminifera, and bivalve fragments). A nine-point moving average has been calculated for the bulk-rock and organic-matter data, and a four-point moving average for the separated faunas. $\delta^{13}C$ vs. $\delta^{18}O$ crossplots highlight the absence of correlation between these proxies.

4.3.4. Major and trace elements

95 samples were analysed for major and trace elements using a FRX Philips PW2400 X-ray fluorescence spectrometer. Major elements (ME; P, K, Si, Ti, Cr and Al) were analysed after fusion of the samples with tetraborate, and trace elements (TE; U, V, Co, Ni, Cu, Ba, and Zr) on pressed pellets prepared from a mix between powder samples and Mowiol II polyvinyl alcohol. The detection limit for major elements is better than approximately 0.01 wt.%, and for trace elements is generally between 1 and 4 ppm, depending on the TE. Analytical accuracies were assessed by analyses of standard reference materials (NIM-G, SDC, BHVO, QLO). The chemical index of alteration (CIA*) corrected for carbonate contents was calculated following Nesbitt and Young (1982) and Nesbitt and Young (1989): $CIA^*=(100)[Al_2O_3/(Al_2O_3+CaO^*+Na_2O+K_2O)]$ with $CAO^*= Na_2O$. Enrichment factors (EF; Tribovillard *et al.*, 2006; Wedepohl, 1971, 1991) were calculated using the formula: $EF_{element\ X}=X/Al_{sample}/X/Al_{average\ shale}$.

The measured TEs have been used as proxies of (1) the detrital fraction, indicated by Ti, Zr, K, and Si ; (2) the biogenic fraction, composed of carbonate, silica and/or organic matter, with Ba, Ni, Cu and P; and (3) the authigenic fraction, mainly composed of sulphides and insoluble oxyhydroxides, with U, V, Cr and Co. The association of certain elements to the quoted fractions is discussed in section 4.3. Indeed, the source of silica and phosphorus can be associated to both productivity and detritism; and nickel and copper, are dependent both on productivity as well as redox conditions (Brumsack, 1989; Werne *et al.*, 2002; Sageman *et al.*, 2003; Algeo and Maynard, 2004; Tribovillard *et al.*, 2006; Riquier *et al.*, 2006). Crossplots of redox indices (V/Cr, U/Th, Ni/Co, V/(V+Ni) after Jones and Manning, 1994; Hatch and Leventhal, 1992 and Riquier *et al.*, 2006) have been used to assess the degree of oxygenation of the water column.

4.3.5. Rock-Eval analyses

Total organic carbon (TOC), T_{max}, and hydrogen and oxygen indices (HI and OI) were measured with a–Rock-Eval 6 with an instrumental precision of <2%. The T_{max} values (°C) indicates thermal maturity of the organic matter and allows the assessment of the diagenetic overprint (Espitalié *et al.*, 1985). The peaks S2 and S3 (corresponding to the amount of kerogen and CO_2 released during cracking of organic-matter between 300 and 600 °C) are used to calculate the amount of total organic carbon (TOC) and the

amount of mineral carbon (MINC). In addition, the so-called hydrogen index (HI =S2/TOC) and oxygen index (OI = S3/TOC) are calculated. The HI and OI indices are proportional to the H/C and O/C ratios of the organic matter, respectively, and are used for OM classification in Van-Krevelen-like diagrams (Espitalié *et al.,* 1985, 1986). The analyses were calibrated by analysing the standard reference material IFP-55000 (Institut Français du Pétrole; IFP 2001).

4.4. RESULTS

4.4.1. Sedimentology and stratigraphy

Kutek *et al.* (1989) established an ammonite zonation for the section of Wąwał, which, unfortunately shows some problems with regards to its correlation with the Tethyan ammonite zonation and the CIE. A stratigraphy based on boreal calcareous nannofossils was, therefore, established, which is used here to constrain the chronostratigraphic framework, and which is coherent with the carbon-isotope record (Kujau *et al.*, in prep.; Fig. 4.2).

The base of the core (first 0.8 m) consists of grey to brownish limestone, which is partly laminated and recrystallized, and which is typical of the Wealden sequences of Poland (Kutek *et al.,* 1989). It is dated as early Berriasian age by correlation with other sections in Poland on the base of ostracods and benthic foraminifera (Dziadzio *et al.*, 2004). The immediately overlying sediments (0.20 cm) represent a lag deposit containing calcareous pebbles and siderite nodules.
The second metre of the core shows the installation of dark brown sandy to silty clay containing sparse aragonitic shells. Calcareous nannofossils preserved in this interval point to a late Berriasian age.

At 2 m, the first bivalves and *Lenticulina* were found and a progressive change to darker and finer clays occurs, which continue until 3.8 m. Calcareous nannofossils place this interval in the BC3a and BC3b zones (basal Valanginian).

On top of this interval, until 8m, the sediments start to become more sandy. They are punctuated by levels containing aligned aragonitic bivalve shells. which may be related to storm deposits and attest an upper offshore depositional environment. This interval is dated as uppermost BC3b to lowermost BC5 (early to early late Valanginian).
From 8 to 11.2 m, a progressive change to more clayey deposits is observed. A sandy interval of 0.2 m follows, which precedes a generally more sandy sediment until 17.4 m. Layers with concentrations of bivalve and gastropod shells are present but less abundant.

Layers containing phosphate nodules are observed between 13.7 and 14 m and from 16.6 m to the top. An ammonite has been found at 16m (*Dichotomites* sp.). Glauconite appears at 17.2 m. This interval has been dated as BC5 zone (early late Valanginian).

Finally, the last interval is comprised between 17.5 and 18.2 m and shows a fining-upward trend from sandy to silty and then to very fine clay. Shells were not observed during sampling and the absence of micro or nannofauna prevents its age dating. As a whole, a sparse fauna of small bivalves, gastropods, benthic foraminifera, ostracods, and a few crinoidal remains and bryozoans is observed. The several discrete layers with bivalve and gastropod shell accumulations indicate an upper-offshore depositional environment.

4.4.2. Stable isotopes

4.1.1. Whole-rock carbonate and selected fossil groups

The $\delta^{13}C_{carb}$ records of whole rock, hand-picked ostracods, benthic foraminifera (*Lenticulina* sp.), and bivalve shell fragments show comparable long-term trends: an increase in $\delta^{13}C_{carb}$ values is observed from 3 to 7.5 m (of early Valanginian age) which is followed by relatively stable values in the upper part of the core section (of late-early and late Valanginian age).

In detail, the whole-rock $\delta^{13}C_{carb}$ values are close to 0‰ in the early Berriasian basal limestone, and fluctuate between 0.5 and about –2.5‰ in the following 4.5 m. Between 5 and 7.5 m, the values are less dispersed and progressively increase from 1.3 to 2‰, and in the following 3 m they decrease and reach values of 0.8‰. From 10.5 to 17.5 m, the $\delta^{13}C_{carb}$ values rise again up to 2.7‰ and they finally drop in the last 1.5 m, oscillating between –5 and 2‰.

The $\delta^{13}C_{carb}$ values of the picked ostracods, foraminifera (*Lenticulina*) and bivalve shells are less noisy. A relatively important offset (about 3‰) is observed between them, the ostracods having the lightest and the bivalves the heaviest values. The ostracods $\delta^{13}C_{carb}$ values increase around 5‰ from 2 to 9.6 m, then decrease around 4‰ until 14.2 m, increase again around 3‰ until 15.8 m, and decrease again around 2‰ until 16.6 m. Ostracods were not found in the last 1.5 m of the core. *Lenticulina* exhibit an increase in $\delta^{13}C_{carb}$ values of 2‰ from 2 to 8 m, subsequently the values remain stable until 12.8 m, and finally they drop around 3.5‰ until 17.5 m. *Lenticulina* was not found in the last 1.5 m of the core. The bivalve record increases approximately 3.5‰ from 1.8 to 8.5 m followed by relatively stable values until 17.5 m. Bivalve shells are not present in the remainder of the core.

The oxygen-isotope record of the whole-rock samples is significantly different from those of picked microfossils and bivalve fragments. The $\delta^{18}O_{carb}$ record is strongly fluctuating (within a 4‰ range) in the first metre of the core. A long-term decreasing trend of 1.7‰ (from –1.5 to –3.2‰) is identified from the base to 11.7 m, and superimposed on this trend slightly higher values (of about –1.5‰) are identified in the 6-m interval. Then, from 11.7 to 17.5 m an interval with relatively higher $\delta^{18}O_{carb}$ values between –2 and –0.3‰ is observed. The top of the core is characterised by very negative values (up to –8‰).

The trends in $\delta^{18}O_{carb}$ values of the picked microfossils are very similar from one group to another and a small systematic difference is observed between them: *Lenticulina* (which presents the highest fractionation) and bivalve shells (which have the lowest fractionation) exhibit a difference of about 1.3‰. The $\delta^{18}O_{carb}$ records of *Lenticulina*, ostracods, and bivalves start with relatively negative values (up to –5‰), followed by a progressive increase of 3‰ in the overlaying 2 metres. Between 4 and 16.2 m, the values remain stable. Then, the two last points of the ostracods and *Lenticulina* records exhibit a strong shift toward negative values (up to –4.2‰) at 17m, not observed in the bivalve record, which still documents stables values up to 17.5 m, which corresponds to the highest level containing shells in the core.

Whole-rock stable-isotope data exhibiting a strong deviation toward negative values ($\delta^{13}C_{carb}$ values <0‰ and $\delta^{18}O_{carb}$ values <–4‰) are signalled by grey points and were omitted from further discussion (Fig. 4.2). The related samples are mostly found between 2 and 5 m, in the 11 m interval and in the last 1.5 m of the core section. Consequently a 9-point moving average was applied to the $\delta^{13}C_{carb}$ and $\delta^{18}O_{carb}$ bulk-rock data, in order to visualise longer-term trends (Fig. 4.2). As $\delta^{13}C_{carb}$ values of ostracods valves, *Lenticulina* tests and bivalve fragments are less dispersed, a 4-points moving average was applied.

4.1.2. $\delta^{13}C_{org}$ values of total organic carbon

A 9-point moving average was obtained for the data of the organic-carbon isotope analyses. When disregarding the first data point obtained from the early Berriasian karstified limestone, the highest $\delta^{13}C_{org}$ values (–23.8‰) correspond to sediments infilling the karst depressions at the base of the core section (Fig. 4.2). The overlying late Berriasian sediments (from 0.7 to 1.8 m) show $\delta^{13}C_{org}$ values of about –26‰. Then, the earliest Valanginian deposits corresponding to the interval comprised between 1.8 and 3.2 m, are enriched in $^{13}C_{org}$ by up to 1‰. From 3.2 to 8 m (early Valanginian), the values are relatively stable around –26‰. Finally, in the upper lower and the upper Valanginian sediments (e.g. from 8 m to the top of the measured core), a long and progressive increase in $\delta^{13}C_{org}$ values of 1.5‰ is observed (Fig. 4.2).

4.4.3. Mineralogy

4.4.3.1. Whole-rock mineralogy

The sediments are generally composed by quartz, phyllosilicates and carbonates (including calcite and aragonite). High contents in calcium apatite have been detected in some layers.

A sharp increase in quartz contents (up to 68%; Fig. 4.3) is observed in the first 1.5 m. Then, between 1.5 and 3.5 m, the amount of quartz decreases and a level rich in Ca-apatite is observed. In parallel, the first 4 metres show an increase in phyllosilicates from 10 to 50% of the bulk-rock composition. At about 8 m, a decrease in aragonite content is observed, which correlates well with the decrease in bivalve shells and the maximum in $\delta^{13}C_{carb}$ values. The aragonite content increases again at around 12m. From 12 to 17.5 m, a decrease in phyllosilicates from 50 to 10% is observed. In the uppermost metre of the core, aragonite and calcite nearly disappear whereas the phyllosilicate content rises up again and a second level rich in Ca-apatite is observed (Fig. 4.3).

4.4.3.2. Clay mineralogy

The composition of clays shows generally high contents in kaolinite and/or smectite, and low amount of micas and chlorite. Traces of goethite have been measured. In the first 1.5 m, the clay assemblage is dominated by kaolinite and illite, and the WI increases (Fig. 4.3). Between 1.5 and 3.5 m, the kaolinite content represents 90% of the total clay composition, and the WI reaches a value of 14. In the 3.5 – 9 m interval, kaolinite contents are stable at around 80% and the WI decreases and remains stable at more moderate values (of 2.8). Between 9 and 12 m, the kaolinite content progressively decreases and finally disappears to the benefit of smectite. The WI decreases to nearly 0. From 12 to 16.5 m, smectite dominates the clay assemblage. A further change occurs in the last 1.5 m where an increase in mica contents is observed (Fig. 4.3).

4.4.4. Major and trace elements

Basal sediments (up to 0.8 m) corresponding to the karstified level and karst infillings are enriched in U and Cu. Above, their contents are decreasing up to 3.6 m, and remain roughly constant in the rest of the core. The contents in major and trace elements have been converted into enrichment factors (EF) and a chemical index of weathering has been calculated (CIA*).

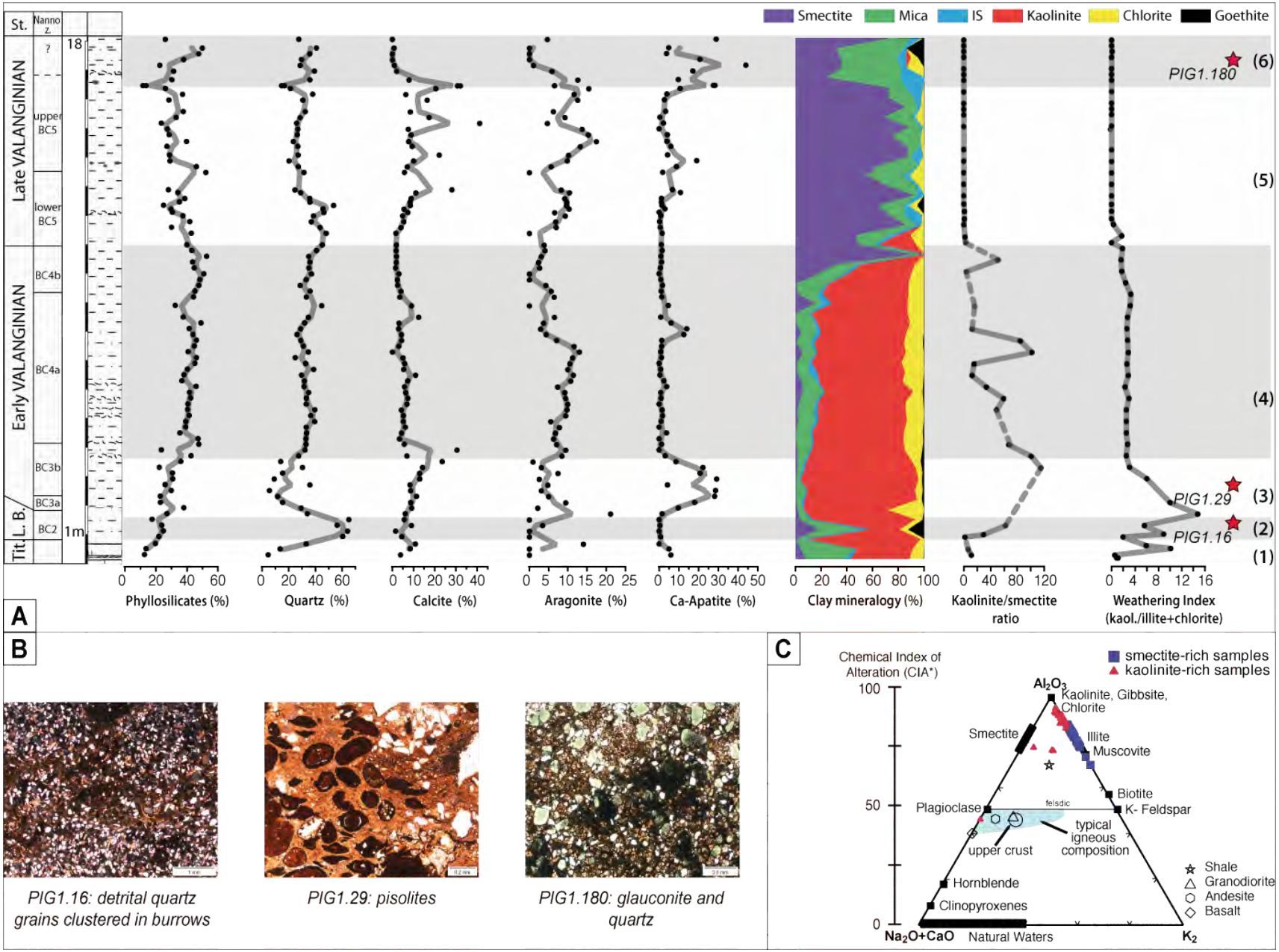

PIG1.16: detrital quartz grains clustered in burrows

PIG1.29: pisolites

PIG1.180: glauconite and quartz

Fig. 4.3: A) Changes in mineralogical composition of the bulk rock (expressed in relative %) and of the clay fraction (in relative % of the <2µ fraction). Grey and white alternating bands delimit the six intervals described in the text. B) Thin sections of selected intervals. C) Ternary Diagram after Nesbitt and Young (1984, 1989) showing the composition of a selection of major elements and the chemical index of weathering (CIA*) of smectite- and kaolinite-rich samples.

Almost all analysed elements (U, V, Cr, Co, Ni, Cu, Ba, P, Zr, Ti, K, and Si; Fig. 4.4) show important enrichments (relative to average shale) in sediments infilling the karst structures near the base of the core section. This is correlated with an increase in CIA* values in the infillings. In the overlying sediments (from 0.65 to 1.7 m), the concentrations of these elements remain relatively high and this is correlated with very high CIA* values (up to 95). Then (from 1.7 to 3.6 m), Si, Ti, K, Zr, Ni, Cu, Ba, and P decrease. However, the P_{tot} concentrations are very high, and correlate well with the XRD-derived Ca-apatite contents. The remainder of the core (from 3.6 m to the top) shows relatively monotonous trends. A decrease in CIA* from 87 to 82 is observed at about 11.5 m.
No further significant variation is observed, although discrete levels of slight enrichment in Cu, Ni, Ba, and Pq. The elemental ratios (Fig. 4.4) V/Cr, U/Th, and Ni/Co are relatively low, but the ratio V(V+Ni) is very high (close to 0.8 in average).

4.4.5. Total organic carbon contents, Rock-Eval data, and palynofacies results

Total organic carbon (TOC) contents in the lower core section (up to 7.5 m) correspond to 0.5 wt.% in average (Fig. 4.6). Between 7.5-13.5 m, the TOC content decreases to 0.08 wt.% in average. Finally, the top interval of the core shows a rise in TOC values to 1 wt.% in average, and locally reaches a value of 1.4 wt.%. The hydrogen indices (HI) are all comprised between 0 and 70 mg HC/g TOC and only two samples exhibit T_{max} values higher than 430°C (Fig. 4.6 and 7). Oxygen indices (OI) have values of 210 mg HC/g TOC in average, and only three samples have values higher than 300 mg HC/g TOC (Fig. 4.6 and 4.7).

Translucent phytoclasts represent on average 45% of the total organic debris in the interval from 0.5 to 3.5 m, they decrease to 35% in the interval from 3.5 to 9 m, and finally drop to 20% in the interval from 9 to 18 m. In contrast, marine dinocysts correspond to 10% of the total organic debris in average in the interval from 0.5 to 9 m, and increases to 20% in the interval from 9 to 18 m. A marine/terrestrial ratio have been calculated from plant-derived material (true charcoals, translucent and opaque phytoclasts, cuticles, spores and pollen) compared to the marine (foram linings, dinoflagellate cysts, acritarchs) palynofacies fraction.

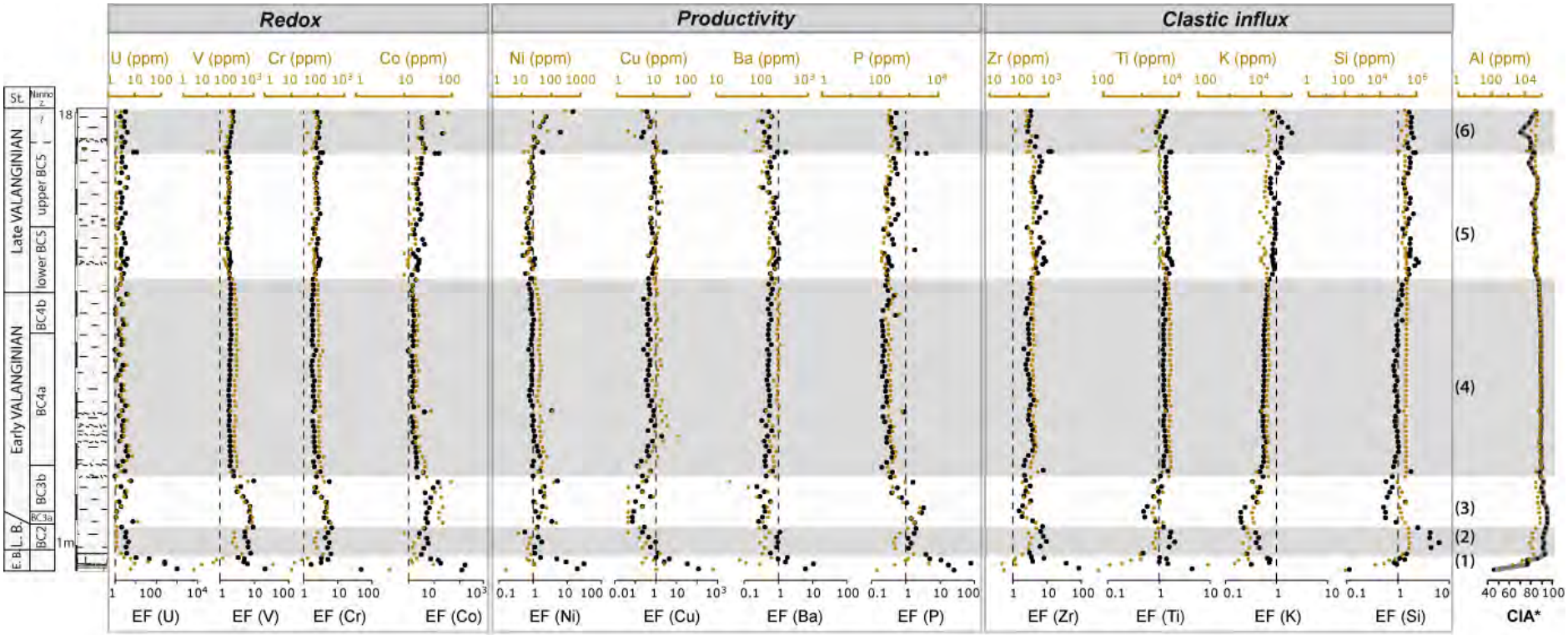
Redox
Productivity
Clastic influx
U (ppm)
V (ppm)
Cr (ppm)
Co (ppm)
Ni (ppm)
Cu (ppm)
Ba (ppm)
P (ppm)
Zr (ppm)
Ti (ppm)
K (ppm)
Si (ppm)
Al (ppm)
St.
Nanno
Late VALANGINIAN
upper BC5
lower BC5
BC4b
Early VALANGINIAN
BC4a
BC3b
BC3a
BC2
L. B.
E. B.
18
1m
(6)
(5)
(4)
(3)
(2)
(1)
EF (U)
EF (V)
EF (Cr)
EF (Co)
EF (Ni)
EF (Cu)
EF (Ba)
EF (P)
EF (Zr)
EF (Ti)
EF (K)
EF (Si)
CIA*

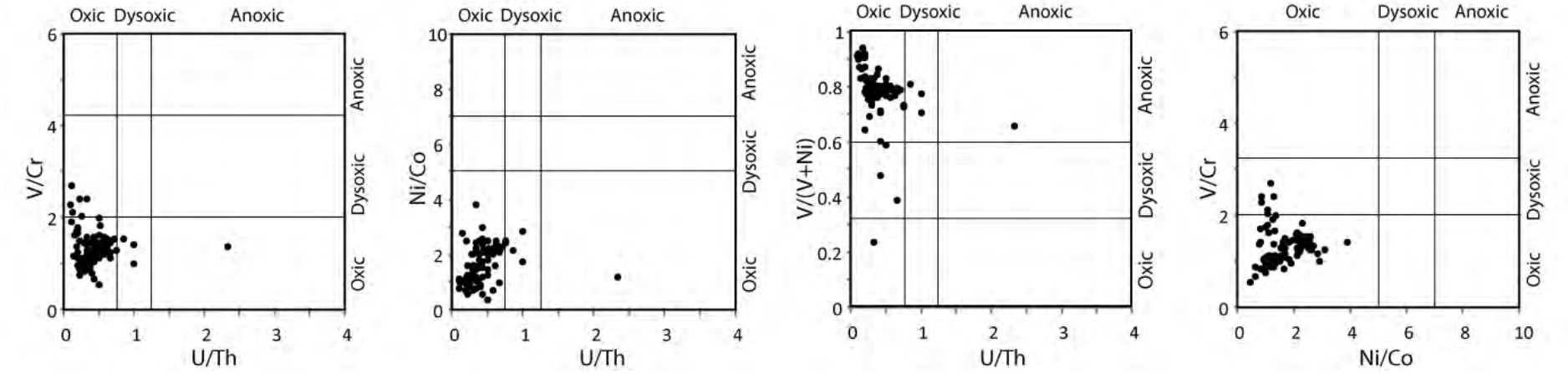
Oxic
Dysoxic
Anoxic
V/Cr
U/Th
Ni/Co
V/(V+Ni)

Fig. 4.4: Evolution of major and trace elements clustered as a function of their palaeoenvironmental significance. The data are shown in absolute contents (ppm; brown colour) and in enrichment factors (EF) relative to the average shale values calculated by Wedepohl (1971, 1991). The CIA* has been calculated and plotted against the aluminium absolute content to underline their rapport. Redox crossplots highlight the absence of anoxia (Jones and Manning, 1994; Hatch and Leventhal, 1992; Riquier *et al.*, 2006).

4.5. DISCUSSION

4.5.1. Evaluation of the diagenetic overprint

4.5.1.1. Whole rock isotopic data

The low $\delta^{13}C_{carb}$-$\delta^{18}O_{carb}$ correlation coefficient of 0.4 (Fig. 4.2) indicates that overprint of the original geochemical signature by burial diagenesis is overall relatively weak (Choquette and James, 1987). A low degree of diagenetic recrystallization is supported by the exceptional preservation of aragonite in ammonite and bivalve shells, observed during sampling and confirmed by XRD whole-rock analyses (up to 17% aragonite). Some samples, however, show very negative $\delta^{18}O_{carb}$ values coupled with $^{13}C_{carb}$ depletion (Fig. 4.2). They correspond to three sedimentary layers: the first is comprised between 2 and 5 m, the second between 10 and 11 m, and the third between 17 and 18.2 m. In the 2-5 m interval and the uppermost 1.2 m, both $\delta^{13}C_{carb}$ and $\delta^{18}O_{carb}$ values are depleted. These three intervals are characterised by the nearly disappearance of calcite and aragonite contents (Fig. 4.3), indicating that the measured isotope values are not reflecting a primary signal. In the lower interval, some samples (between 2 and 2.5 m) show a strong negative $\delta^{13}C_{carb}$ deviation and low $^{18}O_{carb}$ depletion.

These two intervals are also characterised by a higher amount of organic matter (up to 1.4 wt.% TOC). This suggests that diagenetic organic-matter oxidation and incorporation of ^{13}C-depleted CO_2 in carbonate cements changed the primary isotope signature. This is particularly visible in the uppermost 1.5 m, where very negative values both in $\delta^{13}C_{carb}$ and $\delta^{18}O_{carb}$ are associated with the disappearance of biogenic carbonates, illustrated by the absence of calcareous nannofossils, benthic foraminifera, ostracods and bivalves (Fig. 4.2), and by the very low amount of calcite and aragonite (0 to 1% and 0 to 4.5% respectively, Fig. 4.3). Consequently, the whole-rock isotope composition is controlled by the occurrence of diagenetic cements in this layer. The 11-m level is also a particular case because very negative (from -5.4 to -6.8‰) $\delta^{18}O_{carb}$ values are coupled to slight $^{13}C_{carb}$ depletion (between 0.7 and 0.8‰, compared to the 1.4‰ of the whole rock). This level contains a very low amount of organic matter (0.1 to 0.2 %wt), which may explain why the $\delta^{13}C_{carb}$ values have not been strongly modified, but almost no calcite and aragonite (Fig. 4.3), indicating that the $\delta^{18}O$ values do not represent primary carbonate, but rather diagenetic and/or other mineral phases.

4.5.1.2. Ostracods, foraminifera and bivalve fragments

The SEM images of the ostracod, foraminifer and bivalve shell structures show only minor recrystallization (Fig. 4.5). Pyrite infills the shells, which are otherwise well preserved. The ostracods display a dense monolayer calcite shell, in which the pore canals are preserved (Fig. 4.4, sample PIG 1.127; e.g., Benson, 1981); the lenticulinid foraminifera expose walls composed of one or more layers, composed of subvertical, elongated calcite crystals (Fig. 4.4, sample PIG 1.77; e.g., Hansen and Reiss, 1971); and the bivalve fragments show a randomly and partly zig-zag oriented meshwork of calcite crystals (Fig. 4.4, sample PIG 1.127; e.g., Dauphin and Denis, 2000). Crossplots of oxygen versus carbon isotope values show low correlation coefficients (0.2 for ostracods, 0.4 for *Lenticulina* and 0.3 for bivalves, Fig. 4.2), which indicate low diagenetic overprint. The three intervals identified with the anomalous bulk-rock isotope values mentioned above are not replicated by the isotope data on separated fauna. Moreover, the different faunas exhibit more stable and less scattered values, with comparable variations, which slightly differ from the trends observed in the whole-rock records (specially for the $\delta^{18}O$ record). This corroborates our interpretation that whole-rock $\delta^{13}C$ and $\delta^{18}O$ values of the aforementioned layers are not reflecting the original ocean chemistry but rather the absence of primary carbonates.

4.5.1.3. Mineralogical and Rock-Eval data

The preservation of aragonite, the low amount of illite/smectite mixed layers and the presence of abundant smectite and kaolinite (Fig. 4.3) all witness that the sediments cored at Wąwał have not been subjected to strong diagenetic overprint. This is equally confirmed by the T_{max} values which rarely exceed 430°C (Fig. 4.6) and indicated in the HI versus T_{max} diagram (Fig. 4.7; Espitalié *et al.*, 1985).

4.5.2. Chemostratigraphic significance

The Weissert episode is characterised by a global $\delta^{13}C_{carb}$ positive shift of about 1.7‰ (Cotillon & Rio, 1984; Lini *et al.*, 1992), which starts in the late *campylotoxus* ammonite zone. Maximum and moderately stable $\delta^{13}C_{carb}$ values are reached during the *verrucosum* ammonite zone, forming a “plateau” before they decrease in the latest *verrucosum* ammonite zone (Duchamp-Alphonse *et al.*, 2007; Föllmi *et al.*, 2007). Given the scatter of the whole-rock $\delta^{13}C_{carb}$ values, the measurements on ostracods, *Lenticulina* and bivalves were used to determine as accurately as possible the onset and the “plateau” of the CIE of the Valanginian. Indeed, the measurement of the isotope composition on separated fauna allows both for the discrimination of the diagenetic influence on trends in $\delta^{13}C_{carb}$ and $\delta^{18}O_{carb,}$ as well as for the overcoming of cumulative vital effects of various organisms that may influence the bulk-rock isotope composition.

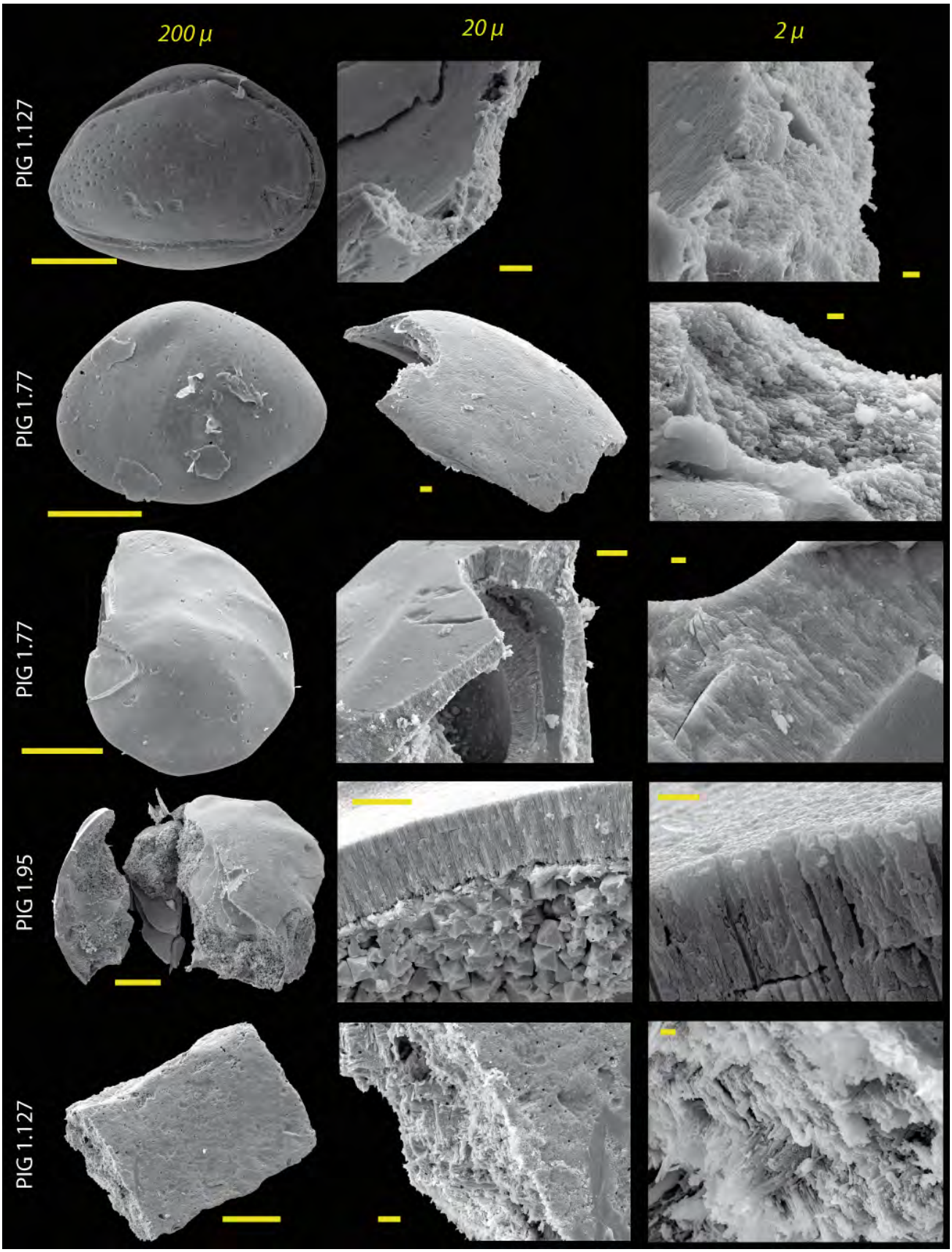

Fig. 4.5: SEM illustrations of the handpicked fauna. Ostracods (*Schuleridea* cf. *praethoerenensis*) belonging to samples PIG 1.77 and PIG 1.127, benthic foraminifera of samples PIG 1.77 and PIG 1.95 (*Lenticulina* cf. *muensteri*), and bivalve fragments of sample PIG1.127 are used as examples. Both the ostracod and *Lenticulina* tests as well as the bivalve shell fragements show no evidence of recrystallization, which may have affected the initial isotope composition of the shells. Note the presence of diagenetic pyrite inside the *Lenticulina* shell (PIG 1.95).

Surprisingly, the trends in $\delta^{13}C$ seem to be more affected by vital effects than those in $\delta^{18}O$: a 2-3‰ overall difference in $\delta^{13}C$ values is observed between ostracods and *Lenticulina* and the difference rises to around 4‰ between ostracods and bivalves (Fig. 4.2). These differences are mainly related to the $\delta^{13}C$ signal of ostracods, which absolute values are lighter. Bornemann *et al.* (2012) recently highlighted these deviations and attributed them to metabolic controls or to their diet, rather to their microhabitat. Additionally, strong differences in $\delta^{13}C$ fractionation exist between ostracods species living in a similar environment (Didié and Bauch, 2002; Bornemann *et al.*, 2012) and this may explain the slight discrepancies in the $\delta^{13}C$ trends, since a minority of the ostracod samples does not belong to *Schuleridea* cf. *praethoerenensis*, but to other species. The measurements performed on *Lenticulina* sp. show lower background discrepancies because a monogeneric assemblage was picked and measured throughout the core.

The isotope tendencies show similar trends between *Lenticulina*, bivalves and ostracods and express well the onset of the positive CIE of about 1.7 to 2‰ for *Lenticulina* and bivalves, and nearly 3‰ for the ostracods. With that, the ostracods appear most sensitive to the changes in the carbon cycle associated with the CIE. As such, the inception of the CIE is placed in the boreal calcareous nannofossil zone BC3b (in light grey, Fig. 4.2), and the plateau is reached in BC4a (in darker grey, Fig. 4.2). BC3b corresponds to the Boreal *Platylenticeras robustum* ammonite zone and BC4a starts with the Boreal *Platylenticeras heteropleurum* ammonite zone (Pauly *et al.*, 2012). These zones correlate with the Tethyan *pertransiens* ammonite zone and highlights the relatively poor correspondence between Boreal and Tethyan biostratigraphies, since the onset of the CIE is dated as late *campylotoxus* ammonite zone in the Tethyan Realm. The CIE also allows for a precise correlation of the Boreal Realm with the Tethyan basins (Fig. 4.2, by assuming its global synchronicity) where the stratigraphic framework of the Weissert episode is well established by ammonites and calcareous nannofossils (Erba, 2004; Duchamp-Alphonse *et al.*, 2007). Consequently, the Valanginian portion of the Wąwał core comprises the interval between the *otopeta* and *nicklesi* ammonite zones (Fig. 4.2, Föllmi *et al.*, 2007; Duchamp-Alphonse *et al.*, 2007).

5.3. Palaeoclimatic and palaeoenvironmental changes

5.3.1. Temperature *vs* salinity changes

A difference of about 1.3‰ is observed between the $\delta^{18}O$ record of *Lenticulina* and bivalves (which are the groups having the highest difference in $\delta^{18}O$ values) but all groups show a similar trend. This implies that the evolution of the $\delta^{18}O$ values is coherent and that the discrepancy between species is likely linked to vital effects, since they are all benthic. Very negative values are observed at the top and at the base of the core, which

may be characteristic of fresh-water influences. Converting the evolution of the $\delta^{18}O$ values into temperature change following the equation of Anderson & Arthur (1983) assuming that the organisms have built their shell in equilibrium with seawater, implies a cooling of 10°C of bottom waters during the onset of the Valanginian CIE in the Carpathian Seaway. A cooling of this amplitude is difficult to consider, even in shallow-water settings. The enhanced $\delta^{18}O$ values are rather attributed to variations in salinity due to increased fresh-water influence (Föllmi, 2012). It is not surprising to observe a stronger influence of continental waters at the beginning of the transgressive phase of the early Valanginian, given the proximity of the continent.

5.3.2. Chronology and implication of changes in mineralogy and major and trace element composition

Given the excellent overall preservation, the bulk-rock and clay mineralogies are used here as palaeoenvironmental and palaeoclimatic indicators. According to the position of the Wąwał core within the rather narrow Mid-Polish Seaway, nearby the Rhenobohemia continent, the clay-mineral assemblages are interpreted here to reflect the climate conditions on the nearby continent. The high proportion of kaolinite or smectite (which reach 90 and 70% of the clay assemblages, respectively) suggests a weak influence of secondary sources (e.g. reworking of kaolinite) and supports the hypothesis of a major continental influence.

Accordingly, the kaolinite/smectite ratio and the weathering index (WI) are taken here to trace changes in humidity and weathering intensity.

The evolution of major and trace-element contents is also used here to reconstruct palaeoclimatic and palaeoenvironmental changes. Focusing first on absolute contents (in ppm), similar trends are observed between most major and trace elements (e.g., V, Cr, Co, Ni, Cu, Ba, P, Zr, Ti, K, Si, and Al). This implies that their distributions have probably been driven by variations in detrital input and underscores the importance of EF calculations. Variations in CIA* values equally follow the trends in Al. This shows that the CIA* is mostly driven by the Al content and confirms the role of weathering in the distribution of major and trace elements. Absolute contents in U and Cu do not exactly follow these trends: they are enriched in the karst infillings but their contents are very low in the remainder of the core, meaning that their distribution is not controlled by changes in detrital input but rather by the organic-matter content (which is relatively low: the TOC content does not exceed 1.5%wt in Wąwał). To eliminate the detrital signal, enrichment factors (EF) have been calculated. As such the U, V, Cr and Co can be used as redox proxies, and Ni, Cu, Ba and P to trace productivity (Tribovillard *et al.*, 2006; Riquier *et al.*, 2006).

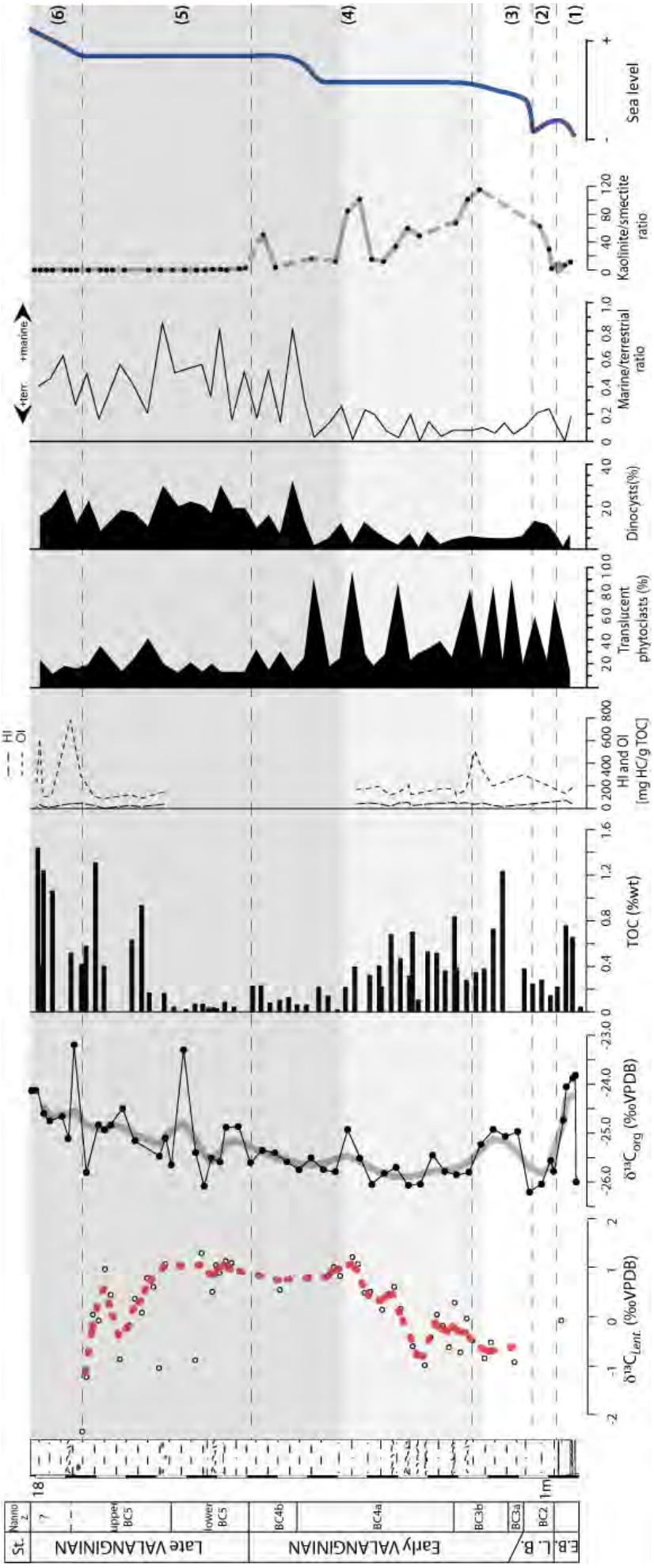

Fig. 4.6: The Valanginian perturbation of the carbon cycle: comparison of total organic carbon with the $\delta^{13}C_{lent}$ and $\delta^{13}C_{org}$ values, RockEval and palynofacies data and weathering changes (kaolinite/smectite ratio).

The Wawal core is subdivided into six units defined from their mineralogical and chemical composition. The first unit corresponds to the first meter of the core and comprises the lower Berriasian carbonate limestone and the overlaying upper Berriasian karst infills. Almost all analysed elements show important increases at the base of the core (observed both in absolute contents and EF), e.g., in sediments infilling the karsts and the lag deposit, which reflects the clastic influence of the continental setting.

The second unit (1.5-3.5 m) exhibits a significant enrichment in quartz contents. Thin sections reveal that the quartz grains are of detrital origin and generally clustered in burrows. High major and trace-element contents are observed, which may indicate an increase in detrital fluxes from the continent and thus enhanced weathering but also the relatively low sea level and the proximity of the continent. This level contains up to 60% quartz, very low calcite and aragonite contents (almost no shells), and possess very light $\delta^{18}O$ values recorded by the few handpicked shells (Fig. 4.2). The loss in carbonate and the negative $\delta^{18}O$ values may have been caused by the circulation of meteoric waters during late diagenesis given the significant change in sediment porosity linked to the strong increase in quartz content. Given this higher porosity, it is not excluded that a part of the kaolinite content is authigenic and formed during early diagenesis (Bjorkum and Gjelsvik, 1988; Baker and Golding, 1992).

In the third unit (3.5-9 m), the quartz content drops and a phosphatized level is observed. The presence of a marine benthic fauna and enhanced clay contents result from a transgressive phase. Kaolinite reaches 90% of the total clay composition and the related K/S ratio and WI exhibit very high values, indicating the presence of a strongly hydrolysing climate on the continent (Chamley, 1989). This is correlated with very high CIA* values and high absolute contents in nearly all elements and emphasises the intensification of the hydrological cycle at that time. A thin section reveals a large amount of reworked pisolites, which are typical for paleosoil structures.

The phosphate-rich interval is probably the consequence of sea-level rise combined with high continental geochemical weathering rates leading to enhanced nutrient fluxes to the ocean. Depletions in clastic proxies (EF of Zr, Ti, K and Si) and in some productivity proxies (EF of Cu and Ba) are thus observed. However, the concentration in elements used here as redox (EF of U, V, Cr, and Co) and productivity proxies (notably Ni and P) remains relatively high.

Four cross plots of redox indices have been carried out in order to determine changes in the oxygen level of the depositional environment (Fig. 4.4; Hatch and Leventhal, 1992; Jones and Manning, 1994; Riquier *et al.*, 2006). The V/Cr, U/Th, and Ni/Co ratios are all relatively low and indicate oxic conditions. The ratio V(V+Ni) is relatively elevated and show that the vanadium contents are very high compared to the nickel contents. Nevertheless, the trends in V contents (both in ppm and EF) are very similar to those in aluminium and the V contents are higher than for average shale all

along the core: so the high V content is probably of detrital origin and can as such not be used as an indicator of dys- or anoxic conditions. The relative increase in EF of elements used as redox proxies, which is observed in this first phosphate-rich layer, is rather due to a slow down in sedimentation rates with the occurrence of a phosphatic interval, which may concentrate redox-sensitive trace elements (e.g., Jarvis *et al.*, 1994).

In the fourth unit (9-12 m), coinciding with a progressive increase in $\delta^{13}C_{carb}$ values, kaolinite still dominates the clay assemblages but the WI decreases to more moderate stable values. Stable values for all elements are observed and correlated with relatively high absolute contents both in major and trace elements as well as in CIA*. These observations suggest less humid but still hydrolysing conditions on the continent.

In the fifth part (12-16.5 m), the kaolinite content decreases to the benefit of smectite and the absolute contents in Ti, Al, Cr, and V and the CIA* decrease. The highly hydrolysing climate conditions appear to have been replaced by less humid and seasonally more strongly contrasted conditions (Singer 1984, Chamley, 1989). The climatic signal was likely amplified by further sea-level rise, inducing a distance from sources as indicated by the increase in dinocyst abundance (Fig. 4.6). The EF of Co, Cr and K increase in this unit. The EF of P and Ca-apatite are also punctually increasing. This is interpreted as the result of enhanced condensation, which would be coherent with the timing of the drowning of Tethyan carbonate platforms (Hennig, 2003; Kuhn, 1996; Föllmi *et al.*, 2007). This interval corresponds to the plateau in $\delta^{13}C_{carb}$ values.

Finally, the upper part of the core (17.5-18.2 m) includes a second phosphate-rich bed, characterised by a high amount of glauconite, which is expressed by higher mica contents (about 50%), which is also observed in thin section, and the near disappearance of carbonate. The latter prevents a precise stratigraphy of this interval. This phosphatic interval probably constitutes the paroxysmal phase of the Valanginian Weissert episode and underscores the fact that the carbonate production crisis affected both benthic and pelagic calcareous faunas. This second phosphate-rich layer is not well expressed by the major and trace-element records, and only the EF of Co, Ni, K and P increase.

Discrete levels show a slight enrichment in redox and productivity proxies, but these enrichments do not appear significant and do not show evidence of dysoxic or anoxic conditions (see crossplot of redox indices in Fig. 4.4). Consequently, the Carpathian seaway does not appear to have undergone anoxic conditions during the Valanginian Weissert episode, at least not in the near-shore environment of the Wąwał core. The precipitation of octahedral and framboidal pyrite crystals of close to 4μm inside the benthic microfaunal shells (Fig. 4.5) testify rather to anoxic conditions inside the sediments, as is also indicated by the preservation of organic matter (up to 1.5 wt% TOC, Fig. 4.6). Additionally, no indices of climate change can be reliably related to this interval in the Wąwał core.

Consequently, the two phosphate-rich layers seem to occur in different palaeoenvironmental settings. The first documents the initiation of the transgression during the earliest Valanginian and is characterised by the strong reworking of continental series as well as enhanced continental weathering, and the presence of carbonates. It includes the entire BC3a and a part of the BC3b calcareous zones and precedes the onset of the $\delta^{13}C_{carb}$ shift. Using recent correlations between the boreal calcareous nannofossil zonation with the Russian and Tethyan ammonite zonations (Bown, 1998; Ogg *et al.*, 2008; Pauly *et al.*, 2012) and considering the evolution of the $\delta^{13}C_{carb}$ shift, this first phase of phosphogenesis would have occurred during the *pertransiens* and the beginning of the *campylotoxus* ammonite zones. The second phosphate-rich phase starts in the upper BC5 nannofossil zone and its duration is not known for the Wąwał core. A similar succession of two phosphate-rich layers has been observed in the Helvetic Alps (Kuhn, 1996; Föllmi *et al.*, 2007; Föllmi, 2012) where the first phosphate-rich layer - the Büls Bed - was deposited during the early Valanginian (*pertransiens* ammonite zone; Kuhn, 1996). The second phosphate-rich layer - the Gemsmättli Bed - is of longer extent and was deposited between the *verrucosum* and the *loryi* ammonite zones (e.g., five ammonite zones from the late Valanginian to the early Hauterivian; Föllmi *et al.*, 2007), and corresponds to the general phase of platform drowning occurring in the late Valanginian during the plateau of the $\delta^{13}C_{carb}$ shift (Masse and Phillip, 1981; Weissert *et al.*, 1998). The two phosphatic levels in the Carpathian seaway may correlate in time to those of the Helvetic platform.

5.3.4. Organic-matter preservation and characterisation

The HI and OI parameters (Fig. 4.7) are characteristic of a type-III organic matter, which is interpreted to be of continental origin in all samples as is already indicated by their $\delta^{13}C_{org}$ signature (Dean *et al.*, 1986; Gröcke, 2002; Hasegawa *et al.*, 2003) and the high proportion of phytoclasts (Fig. 4.6). The terrestrial origin of organic matter is not surprising in the palaeogeographical context of the Wąwał core.

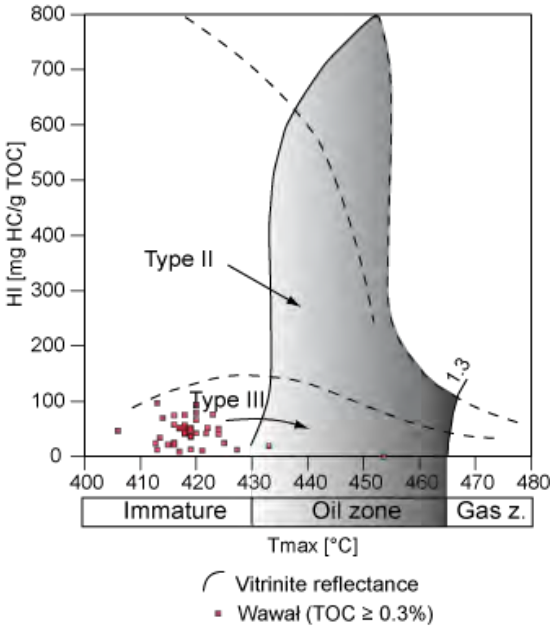

Fig. 4.7: HI/T_{max} diagram: the organic matter is poorly altered and a terrestrial provenance is indicated.

The TOC values and palynological quantifications (Fig. 4.6) allow for the identification of three main phases, disregarding the first sample, which belongs to the lower Berriasian karstified limestone. Relatively high TOC values (0.8wt%) and high phytoclast contents are observed in the interval corresponding to the increase in $\delta^{13}C_{carb}$ values and to high kaolinite relative contents. The humid climate prevailing in the region may have stimulated the development of terrestrial vegetation. In parallel, important weathering and runoff implies important detrital and dissolved fluxes to the ocean and favoured the accumulation of terrestrial organic matter in ocean basins (Westermann *et al.*, 2010).

The interval corresponding to the plateau in $\delta^{13}C_{carb}$ and to a mineralogical change toward smectite-dominant assemblages shows both very low TOC values as well as lower phytoclast contents. The relative proportion of dinocyts increases in the same interval. With a change toward less humid conditions combined with a transgression, the development of terrestrial vegetation and the continental fluxes to the ocean probably slowed down.

The last 3.5 metres of the core show enrichments in TOC values (with values reaching 1.4 wt). Major changes in mineralogy or palynology indicative of climate change are, however, not observed in this interval. The high contents in glauconite (Fig. 4.3) are the only indicator of palaeoenvironmental change and are viewed here as having resulted from lower sediment-accumulation rates in combination with sea-level rise.

In order to estimate if the increase in dinocysts relative content has significantly influenced the organic-matter composition and its isotope signal, correlations coefficients have been calculated between TOC values and the U and Cu absolute contents. Indeed, U and Cu are often linked to palaeoproductivity, amongst other factors (Tribovillard *et al.*, 2006). Their values of 0 and 0.1, respectively, suggest that U and Cu are not associated with organic matter. This tends to support the interpretation that the preserved organic matter is predominantly of terrestrial origin.

4.5.4. Changes in atmospheric CO_2 and the carbon cycle

The $\delta^{13}C_{org}$ long-term trend is relatively different from that of $\delta^{13}C_{carb}$. During the onset of the $\delta^{13}C_{carb}$ shift, $\delta^{13}C_{org}$ values are rather stable at around -25.8‰. They start to increase only when the $\delta^{13}C_{carb}$ values reach the plateau. The preserved organic matter is predominantly of terrestrial origin, and the 10% increase in dinocycsts at 9 m is probably too small to drive the observed increase in the $\delta^{13}C_{org}$. This is also shown by the continuing increase in the $\delta^{13}C_{org}$ record in the remainder of the core, whereas the number of dinocysts remains stable.

The time lag between the $\delta^{13}C_{carb}$ and $\delta^{13}C_{org}$ records has already been observed in the western Atlantic (DSDP Site 535, Cotillon and Rio, 1986; and Patton *et al.,* 1986) and in the western Tethys (Lombardian Basin, Lini *et al.,* 1992). This implies that it may be of global importance. The difference between the $\delta^{13}C_{carb}$ and the $\delta^{13}C_{org}$ trends (expressed by $\Delta\ \delta$) is habitually used to reconstruct temporal changes in atmospheric pCO_2 (Kump and Arthur, 1999; Jarvis *et al.,* 2011). During OAE2, for example, an increase in $\Delta\ \delta$ combined with biomarker $\delta^{13}C$ and leaf stomata data has been interpreted as the result of a phase of increased atmospheric pCO_2 preceding the $\delta^{13}C_{carb}$ excursion (Jarvis *et al.,* 2011). This proxy can, however, only be applied under certain circumstances, such as insignificant diagenetic overprint, limited productivity effects and the lack of temporal changes in the type of organic matter. In the Lombardian basin and the western Atlantic, the organic matter is of mixed marine and terrestrial origin. More particularly, at DSDP Site 535, HI and OI reveal a change toward a dominance in marine organic matter during the $\delta^{13}C_{carb}$ excursion, which may have resulted in an increase in $\delta^{13}C_{org}$ values. Moreover, we are not aware of any demonstration linking variations in $\Delta\ \delta$ with pCO_2 changes in the case of a terrestrial $\delta^{13}C_{org}$ record.

Interestingly, a terrestrial $\delta^{13}C_{org}$ positive shift has been reported in arctic Russia (Nunn *et al.,* 2010) and Crimea (Gröcke *et al.,* 2005) where the analyses were performed on selected coals and charcoals. Even if no precise comparison with the carbonate record was established, the terrestrial $\delta^{13}C_{org}$ signal appears to be global and coherent. Besides other factors, atmospheric pCO_2 directly affects the terrestrial $\delta^{13}C_{org}$ composition (Arens *et al.,* 2000; Jarvis *et al.,* 2009), where enhanced pCO_2 generates a decrease in terrestrial $\delta^{13}C_{org}$. The increase in terrestrial $\delta^{13}C_{org}$ observed near the early-late Valanginian boundary could therefore likely reflect a decrease in atmospheric pCO_2 following a relatively long period of higher pCO_2 during the early Valanginian (Fig. 4.8). The section of Polaveno, which is the only section which records the entire negative $\delta^{13}C_{org}$ shift, is not precisely dated but points to a change towards higher atmospheric pCO_2 during the earliest Valanginian. At Wawal, the interpretation of a decrease in pCO_2 near the early-late Valanginian based on a coeval $\delta^{13}C_{org}$ shift is coherent with a climate change toward less humid conditions recorded by the clay minerals and the CIA*.

From this it appears that the late Valanginian carbonate crisis was associated with a decrease in atmospheric pCO_2. Enhanced fertilisation and increased productivity recorded by various proxies (Sr/Ca, phosphorus, nannofossils; Lini et al, 1992; Föllmi, 1995; Föllmi *et al.,* 1994, 2007; Erba, 2004; Duchamp-Alphonse *et al.,* 2007) may have acted as a carbon pump at that time. However this increase in marine productivity did not result in black shale accumulation (Westermann *et al.,* 2010; Kujau *et al.* 2012). This raises the question of organic-matter preservation, which depends (among others) of the level of oxygenation and the quantity of marine productivity. The drowning of carbonate platforms is viewed as the consequence of these high nutrient supplies in a context of sea-level rise.

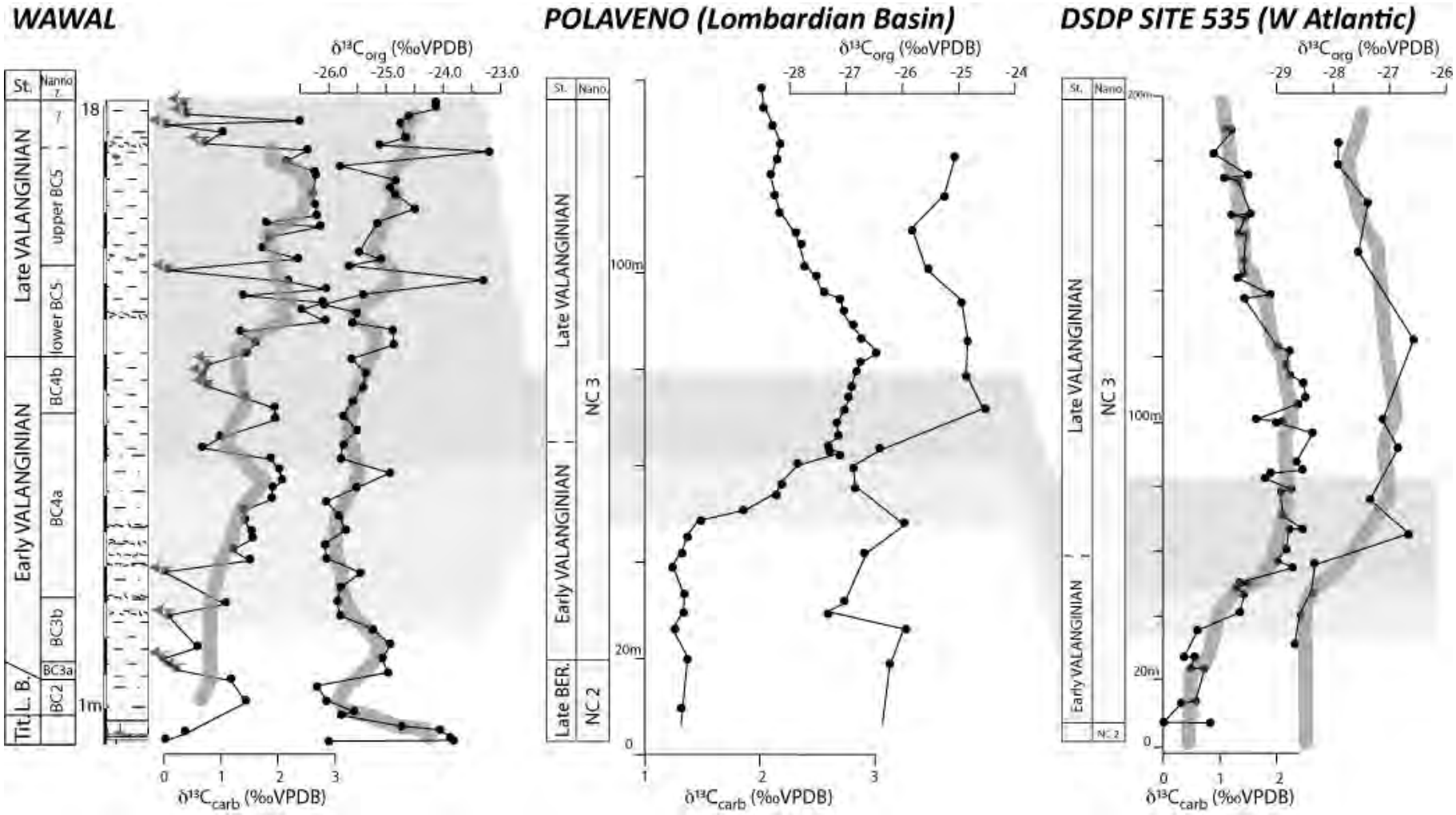

Fig. 4.8: Correlation of the stable carbon isotope record in Wąwał ($\delta^{13}C_{carb}$ and $\delta^{13}C_{org}$) with already published sections in the Lombardian Basin (Polaveno, Lini *et al.*, 1992) and the western part of the Atlantic (DSDP Site 535, Cotillon and Rio, 1984; Patton *et al.*, 1984).

This also suggests that the positive $\delta^{13}C_{org}$ excursion is a consequence of early Valanginian environmental change and that the controlling factor(s) should be searched ahead of the CIE. A phase of intense volcanic activity is a likely candidate; the latest age dates of the Paraña-Etendeka LIP point, however, to the early Hauterivian (Thiede and Vasconcelos, 2010) and an alternative LIP of sufficient importance has not been identified so far. It is therefore not clear, which events led to higher pCO_2 levels and a more humid climate during the early Valanginian. These conditions may have induced enhanced preservation of organic matter on the continents and to their export into the oceans. This is well expressed in Wąwał where an increase in TOC values is observed before and at the initiation of the $\delta^{13}C_{carb}$ shift.

The enhanced preservation of organic matter of terrestrial and mixed origin has already been reported in the eastern, central and western part of the Atlantic (Cotillon and Rio, 1986; Meyers, 1983; Herbin *et al.*, 1987; Stein and Rullkötter, 1988; Bornemann and Mutterlose, 2008), and the western Tethys (Lombardian and Vocontian basins: Bersezio *et al.*, 2002; Reboulet *et al.*, 2003; Westermann *et al.*, 2010). This supports the hypothesis that enhanced organic-matter preservation occurred on the continent (Budyko *et al.*, 1987; Westermann *et al.*, 2010).

On a larger scale, an increase in humidity during the late Berriasian/early Valanginian is observed in England, the Netherlands (Hallam *et al.*, 1991; Schnyder *et al.*, 2009), and NE and SE France (Adatte, 1988, Deconinck *et al.*, 1985). Moreover, the Early Cretaceous is recognised as one of the three major periods of coal deposition in Earth's history (together with the Carboniferous–Permian and the Paleocene–Eocene, Budyko *et al.*, 1987; Haszeldine, 1989). This was in particular favoured by the palaeogeographic configuration of the continents, with the presence of numerous extensional basins related to the ongoing disintegration of the Pangea supercontinent (Stämpfli and Borel, 2002; Föllmi, 2012).

For the Berriasian–Hauterivian period, coal depositions are known from USA, Russia, China, India, Indonesia, Australia and Canada (Ziegler *et al.*, 1987; McCabe and Totman Parrish, 1992). It remains ambiguous, however, if an increase in atmospheric pCO_2 has led to the enhanced storage of organic matter or if enhanced remobilisation and oxidation of previously stored organic-matter released CO_2 in the atmosphere. Without precise age models for the coals deposits, it remains difficult to establish causal links between atmospheric pCO_2 and organic-rich deposits.

4.6. CONCLUSIONS

The Wąwał core records the sea-level highstand of the early Valanginian. Two phosphate-rich horizons have been identified. The first documents the early Valanginian transgression on lower Berriasian emersive deposits; the second corresponds to a crisis in carbonate production. A similar succession of two Ca-apatite enriched levels is observed in the Northern Tethys (Helvetic platform), where the second level corresponds to the major drowning phase of the Valanginian platform. In the Polish basin, the youngest part of the early Valanginian is characterised by very humid and strongly hydrolysing conditions, which have lead to the deposition of kaolinite-dominated clay assemblages (around 80%), the development of a dense vegetation on land, and the exportation of terrestrial organic-matter into the nearby Polish basin and elsewhere. A major climate change toward less humid and seasonally contrasted conditions combined with a sea-level rise was identified near the early-late Valanginian boundary. This also corresponds to an increase in terrestrial $\delta^{13}C_{org}$, which may be interpreted as the result of a decrease in atmospheric pCO_2 and which may indicate the containment of the Valanginian disturbance. The carbonate crisis appears to be disconnected from other climate proxies and results from an external perturbation, which has not been highlighted in this study, but which may be related to an excess in nutrients in seawater (Föllmi *et al.*, 2007, Duchamp-Alphonse *et al.*, 2007). There is no evidence of anoxia in the Polish basin during the Valanginian time interval covered by the sediments cored in Wąwał.

Acknowledgments

The authors would like to thank Tiffany Monier and André Villars for assistance in laboratory work. We are also grateful to H. Weissert (ETH Zürich) and J.-F. Deconinck (University of Dijon) for stimulating discussions, and to F.W. Luppold (University of Hannover) for his help with the ostracod taxonomy. Financial support from the Swiss National Science Foundation (project 200020_126455) is appreciatively acknowledged.

References

Adatte, T., 1988. Etude sédimentologique, minéralogique, micropaléontologique et stratigraphique du Beriasien - Valanginien du Jura central. Unpublished Ph.D. thesis, University of Neuchâtel, Neuchâtel, p. 481.

Adatte, T., Stinnesbeck, W. and **Keller, G.,** 1996. Lithostratigraphic and mineralogic correlations of near K/T boundary sediments in northeastern Mexico: Implications for origin and nature of deposition, in: Ryder, G., Fastovsky, D. And Gartner, S., (Ed.), The Cretaceous-Tertiary Event and Other Catastrophes in Earth History.

Geological Society of America Special Paper, Boulder, Colorado, pp. 211-226.

Algeo, T. J. and **Maynard, J. B.,** 2004. Trace-element behavior and redox facies in core shales of Upper Pennsylvanian Kansas-type cyclothems. Chemical Geology. 206, 289-318.

Anderson, T. F. and **Arthur, M. A.,** 1983. Stable isotopes of oxygen and carbon and their applications to sedimentological and paleoenvironmental problems, in: Arthur, M. A., Anderson, T.F., Kaplan, I.R., Veizer, J., Land, L.S. (Ed.), Stable Isotopes in Sedimentary Geology. Society of Economic Paleontologists and Mineralogists, Short course, pp. 1-151.

Arens, J. C., Jahren, A. H. and **Amundson, R.,** 2000. Can C3 Plants Faithfully Record the Carbon Isotopic Composition of Atmospheric Carbon Dioxide? Paleontological Society. 26, 137-164.

Baker, J.C. and Golding, S.D. (1992) Occurence and palaeohdrological significance of authigenic kaolinite in the Aldebaran Sandstone, Denison Tough, Queensland, Australia. *Clays and Clay Minerals*, **40,** 273-279.

Benson, R.H., 1981. Form, function, and architecture of ostracod shells. Annual Reviews in Earth and Planetary Sciences, 9, 59-80.

Bersezio, R., Erba, E., Gorza, M. and **Riva, A.,** 2002. Berriasian-Aptian black shales of the Maiolica formation (Lombardian Basin, Southern Alps, Northern Italy): local to global events. Palaeogeography, Palaeoclimatology, Palaeoecology. 180, 253-275.

Bjorkum, A. and Gjelsvik, N. (1988) An Isochemical Model for Formation of Authigenic Kaolinite, K-Feldspar and Illite in Sediments. *Journal of Sedimentary Petrology*, **58,** 506-511.

Bornemann, A. and **Mutterlose, J.,** 2008. Calcareous nannofossil and d13C records from the Early Cretaceous of the Western Atlantic ocean: evidence of enhanced fertilization accross the Berriasian-Valanginian transition. Palaios. 23, 821-832.

Bornemann, A., Pirkenseer, C. M., De Deckker, P. and **Speijer, R. P., 2012.** Oxygen and carbon isotope fractionation of marine ostracod calcite from the eastern Mediterranean Sea. Chemical Geology. 310-311, 114-125.

Bown, P. R., Rutledge, D. C., Crux, J. A. and **Gallagher, L. T.,** 1998. Lower Cretaceous, in: Bown, P. R. (Ed.), Calcareous Nannofossil Biostratigraphy. Chapman and Hall, Cambridge, pp. 86-102.

Bralower, T. J., Premoli-Silva, I. and **Malone, M. J.,** 2002. New evidence for abrupt climate change in the Cretaceous and Paleogene: an ocean drilling program expedition to Shatsky Rise, northwest Pacific. GSA today. 12, 4.

Brumsack, H. J., 1989. Geochemistry of recent TOC-rich sediments from the Gulf of California and the Black Sea. Geologische Rundschau. 78, 851-882.

Budyko, M. I., Ronov, A. B. and **Yanshin, A. L.,** 1987. History of the Earth's Atmosphere. Springer-Verlag.

Chamley, H., 1989. Clay Sedimentology. Springer- Verlag, Berlin.

Choquette, P. W. and **James, N. P.,** 1987. Diagenesis in Limestones - 3. The Deep Burial Environment. Geoscience Canada. 14, 3-35.

Cotillon, P. and **Rio, M.,** 1984. Cyclic sedimentation in the Cretaceous of deep sea drilling project sites 535 and 540 (Gulf of Mexico), 534 (Central Atlantic), and in

the Vocontian basin (France), in: Buffler, R. T., Schlager, W., Bowdler, J. L., Cotillon, P., Halley, R. B., Kinoshita, H., Magoon, L. B. I., Mcnulty, C. L., Patton, J. W., Premoli-Silva, I., Suarez-Otmara, A., Testarmata, M. M., Tyson, R. V., Watkins, D. K. and Pisciotto, K. A. (Eds.), Initial Reports of the Deep Sea Drilling Project. Initial Reports of the Deep Sea Drilling Project, Washington, pp. 339-376.

Courtillot, V. E. and **Renne, P. R.,** 2003. On the ages of flood basalt events. Comptes Rendus Geosciences. 335, 113-140.

Dean, W. E., Arthur, M. A. and Claypool, G. E., 1986. Depletion of 13C in Cretaceous marine organic matter: Source, diagenetic, or environmental sigal? Marine Geology. 70, 119-157.

Dauphin, Y. and **Denis, A.,** 2000. Structure and composition of the aragonitic crossed lamellar layers in sic species of bivalvia and gastropoda. Comparative Biochemistry and Physiology – Part A : Molecular & Integrative Physiology, 128, 367-377.

Deconinck, J.-F., Beaudoin, B., Chamley, H., Joseph, P. and **Raoult, J. F.,** 1985. Contrôles tectonique, eustatique et climatique de la sédimentation argileuse du domaine subalpin français au Malm-Crétacé. Revue de géographie physique et de géologie dynamique 26, 311-320.

Dercourt, J., Gaetani, M., Vrielynck, B., Barrier, E., Biju-Duval, B., Brunet, M. F., Cadet, J. P., Crasquin, S. and **Sandulescu, M.,** 2000. Atlas Peri-Tethys, Palaeogeographical maps, 24 maps and explanatory notes. CCGM/CGMW, Paris.

Didie, C. and **Bauch, H., A.,** 2002. Implications of upper Quaternary stable isotope records of marine ostracodes and benthic foraminifers for paleoecological and paleoceanographical investigations. American Geophysical Union, Washington, DC, USA.

Duchamp-Alphonse, S., Fiet, N., Adatte, T. and **Pagel, M., 2011**. Climate and sea-level variations along the northwestern Tethyan margin during the Valanginian C-isotope excursion: Mineralogical evidence from the Vocontian Basin (SE France). Palaeogeography, Palaeoclimatology, Palaeoecology. 302, 243-254.

Duchamp-Alphonse, S., Gardin, S., Fiet, N., Bartolini, A., Blamart, D. and **Pagel, M.,** 2007. Fertilization of the northwestern Tethys (Vocontian basin, SE France) during the Valanginian carbon isotope perturbation: Evidence from calcareous nannofossils and trace element data. Palaeogeography, Palaeoclimatology, Palaeoecology. 243, 132-151.

Dziadzio, P. S., Gazdzicka, E., Ploch, I. and **Smolen, J.,** 2004. Biostratigraphy and sequence stratigraphy of the Lower cretaceous in central and SE Poland. Annales Societatis Geologorum Poloniae. 74, 125-196.

Erba, E., Bartolini, A. and **Larson, L. R.,** 2004. Valanginian Weissert oceanic anoxic event. Geology. 32, 149-152.

Espitalié, J., Deroo, G. and **Marquis, F.,** 1985. La pyrolyse Rock-Eval et ses applications. Revue de l'Institut Français du Pétrole. 40, 563–579.

Föllmi, K. B., 1995. 160 m.y. record of marine sedimentary phosphorus burial: Coupling of climate and continental weathering under greenhouse and icehouse conditions. Geology. 23, 859-862.

Föllmi, K. B., 2012. Early Cretaceous life, climate and anoxia. Cretaceous Research. 35,

230-257.

Föllmi, K. B., Bodin, S., Godet, A., Linder, P. and **Van De Schootbrugge, B.,** 2007. Unlocking paleo-environmental information from Early Cretaceous shelf sediments in the Helvetic Alps: stratigraphy is the key! Swiss journal of geosciences. 100, 349-369.

Föllmi, K. B., Weissert, H., Bisping, M. and **Funk, H.,** 1994. Phosphogenesis, carbon-isotope stratigraphy, and carbonate-platform evolution along the Lower Cretaceous northern Tethyan margin Geological Society of America Bulletin. 106, 729-746.

Gröcke, D. R., 2002. The carbon isotope composition of ancient CO2 based on higher-plant organic matter. Philosophical transactions of the Royal Society of London A. 360, 633-658.

Gröcke, D. R., Price, G. D., Robinson, S. A., Baraboshkin, E. Y., Mutterlose, J. and **Ruffell, A. H.,** 2005. The Upper Valanginian (Early Cretaceous) positive carbon-isotope event recorded in terrestrial plants. Earth and Planetary Science Letters. 240, 495-509.

Hallam, A., Grose, J. A. and **Ruffell, A. H.,** 1991. Palaeoclimatic significance of changes in clay mineralogy across the Jurassic-Cretaceous boundary in England and France. Palaeogeography, Palaeoclimatology, Palaeoecology. 81, 173-187.

Hansen, H.J. and **Reiss, Z.,** 1971. Electron microscopy of Rotaliacean wall structures. Bulletin of the geological Society of Denmark, 20, 329-346.

Hasegawa, T., 2003. Cretaceous terrestrial paleoenvironments of northeastern Asia suggested from carbon isotope stratigraphy: Increased atmospheric pCO_2-induced climate. Journal of Asian Earth Sciences. 21, 849-859.

Haszeldine, R. S., 1989. Coal reviewed: depositional controls, modern analogues and ancient climates, in: Whaetely, M. K. G. and Pickering, K. T. (Eds.), Deltas: Sites and Traps for Fossil Fuels. Geological Society, London, Special Publications. 41, 289-308.

Hatch, J. R. and **Leventhal, J. S.,** 1992. Relationship between inferred redox potential of the depositional environment and geochemistry of the Upper Pennsylvanian (Missourian) Stark Shale Member of the Dennis Limestone, Wabaunsee County, Kansas, U.S.A. Chemical Geology. 99, 65-82.

Hennig, S., 2003. Geochemical and sedimentological evidence for environmental changes in the Valanginian (early Cretaceous) ofthe Tethys region. ETH Zurich, p. 189.

Herbin, J. P., Deroo, G. and **Roucaché, J.,** 1983. Organic geochemistry of lower Cretaceous sediments from Site 535, leg 77, Florida Straits. Init. Rep. Deep Sea Drill. Proj. 77, 459-474.

Jarvis, I., Burnett, W.C., Nathan, Y., Almbaydin, F., Attia, K.M., Castro, L.N., Flicoteaux, R., Hilmy, M.E., Husain, V., Qutawna, A.A., Serjani, A. and **Zanin, Y.N.,** 1994. Phosphorite geochemistry: state-of-the-art and environmental concerns. In: Föllmi, K.B. (Editor), Concepts and controversies in phosphogenesis. Eclogae geologicae Helvetiae, 87, 643-700.

Jarvis, I., Lignum, J. S., Gröcke, D. R., Jenkyns, H. C. and **Pearce, M. A.,** 2011. Black shale deposition, atmospheric CO2 drawdown, and cooling during the

Cenomanian‐Turonian Oceanic Anoxic Event. *Paleoceanography*. 26, 1-17.

Jones, B. and **Manning, D. A. C.,** 1994. Comparison of geochemical indices used for the interpretation of palaeoredox conditions in ancient mudstones. Chemical Geology. 111, 111-129.

Kübler, B., 1983. Dosage quantitatif des minéraux majeurs des roches sédimentaires par diffraction X. Cahiers de l'Institut de Géologie, Université de Neuchâtel, Suisse. AX1.1 and 1.2 1-13.

Kübler, B., 1987. Cristallinité de l'illite: méthodes normalisées de préparation, méthode normalisée de mesure, méthode automatique normalisée de mesure. Cahiers de l'Institut de Géologie, Université de Neuchâtel, Suisse. ADX 2.

Kuhn, O., 1996. Der Einfluss von Verwitterung auf die Paläozeanographie zu Beginn des Kreide-Treibhausklimas (Valanginian und Hauterivian) in der West-Tethys. Unpublished Ph.D. thesis, ETH Zürich, Zürich, pp. 380.

Kujau, A., Heimhofer, U., Ostertag-Henning, C., Gréselle, B. and **Mutterlose, J.,** 2012. No evidence for anoxia during the Valanginian carbon isotope event - an organic-geochemical study from the Vocontian Basin, SE France. Global and Planetary Change. doi: 10.1016/j.gloplacha.2012.04.007.

Kump, L. R. and **Arthur, M. A.,** 1999. Interpreting carbon-isotope excursions: carbonates and organic matter. Chemical Geology. 161, 181-198.

Kutek, J., Marcinowski, R. and **Wiedmann, J.,** 1989. The Wąwał Section, Central Poland - An important Link betwen Boreal and Tethyan Valanginian in: Wiedmann, J. (Ed.), Cretaceous of the Western Tethys. Proceedings of the 3rd International Cretaceous Symposium, Tübingen, pp. 717-754.

Kutek, J. (2001) The Polish Permo-Mesozoic Rift Basin. In: *Peri-Tethys Memoir 6: Peri-Tethyan Rift/Wrench Basins and Passive Margins* (Eds A.M. Ziegler, W. Cavazza, A.H.F. Robertson and S. Crasquin-Soleau), **186,** pp. 213-236. Mémoires du Musée d'Histoire Naturelles, Paris.

Lamarche, J. and Scheck-Wenderoth, M. (2005) 3D structural model of the Polish Basin. *Tectonophysics*, **397,** 73-91.

Lini, A., Weissert, H. and **Erba, E.,** 1992. The Valanginian carbon isotope event: a first episode of greenhouse conditions during the Cretaceous. Terra Nova. 4, 374-384.

Masse, J. P. and **Philip, J.,** 1981. Cretaceous coral-rudistid buildups of France. SEPM Special Publication. 30, 399-426.

Mccabe, P. J. and **Totman Parrish, J.,** 1992. Tectonic and climatic controls on the distribution and quality of Cretaceous coals, in: Mccabe, P. J. and Totman Parrish, J. (Eds.), Controls on the Distribution and Quality of Cretaceous Coals. The Geological Society of America, Special Publication. 267, pp. 1-16.

Meyers, P. A., 1987. Organic-carbon content of sediments and rocks from Deep Sea Drilling Project Sites 603, 604 and 605, Western margin of the North Atlantic, in: Van Hinte, J. E., Wise, S. W., Jr., Biart, B. N. M., Covington, J. M., Dunn, D. A., Haggerty, J. A., Johns, M. W., Meyers, P. A., Moullade, M. R., Muza, J. P., Ogg, J. G., Okamura, M., Sarti, M., Von Rad, U., Blakeslee, J. H. and Whalen, E. (Eds.), Initial reports of the Deep Sea Drilling Project covering Leg 93 of the cruises of the

drilling vessel Glomar Challenger, Norfolk, Virginia, to Norfolk, Virginia, May-June, 1983. Initial Reports of the Deep Sea Drilling Project, pp. 1187-1194.

Nesbitt, H. W. and **Young, G. M.,** 1982. Early Proterozoic climates and plate motions inferred from major element chemistry of lutites. Nature. 299, 715-717.

Nesbitt, H. W. and **Young, G. M.,** 1989. Formation and diagenesis of weathering profiles. The Journal of Geology. 97, 129-147.

Nunn, E. V., Price, G. D., Gröcke, D. R., Baraboshkin, E. Y., Leng, M. J. and **Hart, M. B.,** 2010. The Valanginian positive carbon isotope event in Arctic Russia: Evidence from terrestrial and marine isotope records and implications for global carbon cycling. Cretaceous Research. 31, 577-592.

O'connell, S. B., 1990. Sedimentary facies and depositionnal environment of the Lower Cretaceous East Antartic margin: sites 692 and 693, in: Barker, P. F. and Kennet, J. P. (Eds.), Proceeding of the Ocean Drilling Program, Scientific results pp. 71-88.

Ogg, J. G., Ogg, G. and **Gradstein F.M.,** 2008. The Concise Geologic Time scale. Cambridge University press, pp. 177.

Patton, J. W., Choquette, P. W., Guennel, G. K., Kaltenback, A. J. and **Moore, A.,** 1984. Organic Geochemistry and Sedimentology of Lower to Mid-Cretaceous deep-sea carbonates, sites 535 and 540, leg 77, in: Buffler, R. T., Schlager, W., Bowdler, J. L., Cotillon, P. H., Halley, R. B., Kinoshita, H., Magoon, L. B., Iii, Mcnulty, C. L., Patton, J. W., Premoli Silva, I., Suarez, O. A., Testarmata, M. M., Tyson, R. V., Watkins, D. K. and Pisciotto, K. A. (Eds.), Initial reports of the Deep Sea Drilling Project, covering Leg 77 of the cruises of the drilling vessel Glomar Challenger; Ft. Lauderdale, Florida to San Juan, Puerto Rico, December 1980-February 1981. Initial Reports of the Deep Sea Drilling Project, pp. 417-443.

Pauly, S., Mutterlose, J. and **Alsen, P.,** 2012. Lower Cretaceous (upper Ryazanian-Hauterivian) chronostratigraphy of high latitudes (North-East Greenland). Cretaceous Research. 34, 308-326.

Reboulet, S., Mattioli, E., Pittet, B., Baudin, F., Olivero, D. and **Proux, O.,** 2003. Ammonoid and nannoplankton abundance in Valanginian (Early Cretaceous) limestone-marl successions from the southeast France basin: carbonate dilution or productivity? Palaeogeography, Palaeoclimatology, Palaeoecology 201, 113-139.

Riquier, L., Tribovillard, N., Averbuch, O., Devleeschouwer, X. and **Riboulleau, A.,** 2006. The Late Frasnian Kellwasser horizons of the Harz Mountains (Germany): Two oxygen-deficient periods resulting from different mechanisms. Chemical Geology. 233, 137-155.

Sageman, B. B., Murphy, A. E., Werne, J. P., Ver Straeten, C. A., Hollander, D. J. and **Lyons, T. W.,** 2003. A tale of shales: the relative roles of production, decomposition, and dilution in the accumulation of organic-rich strata, Middle-Upper Devonian, Appalachian basin. Chemical Geology. 195, 229-273.

Schlanger, S. O. and **Jenkyns, H. C.,** 1976. Cretaceous oceanic anoxic events: causes and consequences. Geologie en Mijnbouw. 55, 179-184.

Schnyder, J., Baudin, F. and **Deconinck, J.-F.,** 2009. Occurrence of organic-matter-rich beds in Early Cretaceous coastal evaporitic setting (Dorset, UK): a link to long-term palaeoclimate changes? Cretaceous Research. 30, 356-366.

Spangenberg, J. E., Fontboté, L. and **Macko, S. A.,** 1999. An evaluation of the inorganic and organic geochemistry of the San Vicente Mississippi Valley-type zinc-lead district, central Peru: implications for ore fluid composition, mixing processes and sulfate reduction. Economic Geology. 94, 1067-1092

Spangenberg, J. E. and **Herlec, U.,** 2006. Hydrocarbon biomarkers in the Topla-Mezica zinc–lead deposits, Northern Karavanke/Drau range, Slovenia: paleoenvironment at the site of ore formation. Economic Geology. 101, 997-1021.

Spangenberg, J. E. and **Macko, S. A.,** 1998. Organic geochemistry of the San Vicente zinc-lead district, eastern Pucarà Basin, Peru. Chemical Geology. 146, 1-23.

Stampfli, G. M. and **Borel, G. D.,** 2002. A plate tectonic model for the Paleozoic and Mesozoic constrained by dynamic plate boundaries and restored synthetic oceanic isochrons. Earth and Planetary Science Letters. 196, 17-33.

Stampfli, G. and **Hochard, C.,** 2009. Plate tectonics of the Alpine realm, in: Murphy, J. B., Keppie, J. D. and Hynes, A. J. (Eds.), Ancient Orogens and Modern Analogues. Geological Society, London, Special Publications, London, pp. 89-111.

Stein, R. and **Rullkötter, J.,** 1988. Organofacies reconstruction and lipid geochemistry of sediments from the Galicia Margin, Northeast Atlantic (ODP LEG 103), in: Boillot, G., Winterer, E. L., Meyer, A. W., Applegate, J., Baltuck, M., Bergen, J. A., Comas, M. C., Davies, T. A., Dunham, K. W., Evans, C. A., Girardeau, J., Goldberg, D., Haggerty, J. A., Jansa, L. F., Johnson, J. A., Kasahara, J., Loreau, J.-P., Luna, E., Moullade, M., Ogg, J. G., Sarti, M., Thurow, J., Williamson, M. A. and Mazzullo, E. K. (Eds.), Proceedings of the Ocean Drilling Program, Scientific results, Galicia margin; covering Leg 103 of the cruises of the drilling vessel JOIDES Resolution, Ponta Delgada, Azores, to Bremerhaven, Germany, 25 April 1985-19 June 1985. Proceeding of the Ocean Drilling Program, Scientific results, pp. 567-585.

Singer, A., 1984. The palaeoclimatic interpretation of clay minerals in sediments – a review. Earth Science Reviews. 21, 251-293.

Thiede, D. S. and **Vasconcelos, P. M.,** 2010. Paraná flood basalts: Rapid extrusion hypothesis confirmed by new $^{40}Ar/^{39}Ar$ results. Geology. 38, 747-750.

Tribovillard, N., Algeo, T. J., Lyons, T. and **Riboulleau, A.,** 2006. Trace metals as paleoredox and paleoproductivity proxies: An update. Chemical Geology. 232, 12-32.

Wedepohl, K. H., 1971. Environmental influences on the chemical composition of shales and clays, in: Ahrens, L. H., Press, F., Runcorn, S.K., Urey, H.C. (Ed.), Physics and Chemistry of the Earth. Pergamon, Oxford, pp. 307–331.

Wedepohl, K. H., 1991. Chemical composition and fractionation of the continental crust. Geologische Rundschau. 80, 207-223.

Weissert, H., Lini, A., Föllmi, K. B. and **Kuhn, O.,** 1998. Correlation of Early Cretaceous carbon isotope stratigraphy and platform drowning events: a possible link? Palaeogeography, Palaeoclimatology, Palaeoecology. 137, 189-203.

Werne, J. P., Sageman, B. B., Lyons, T. W. and **Hollander, D. J.,** 2002. An integrated assessment of a ‘‘type euxinic’’ deposit: evidence for multiple controls on black

shale deposition in the middle Devonian Oatka Creek Formation. American Journal of Science. 302, 110-143.

Westermann, S., Föllmi, K. B., Adatte, T., Matera, V., Schnyder, J., Fleitmann, D., Fiet, N., Ploch, I. and **Duchamp-Alphonse, S.,** 2010. The Valanginian $\delta^{13}C$ excursion may not be an expression of a global oceanic anoxic event. Earth and Planetary Science Letters. 290, 118-131.

Wortmann, U. G. and **Weissert, H.,** 2000. Tying platform drowning to perturbations of the global carbon cycle with a d13COrg-curve from the Valanginian of DSDP Site 416. Terra Nova. 12, 289-294.

Ziegler, P. A., Raymond, A. L., Gierlowski, T. C., Horell, M. A., Rowley, D. B. and **Lottes, A. L.,** 1987. Coal, climate and terrestrial productivity: the present and early Cretaceous compared, in: Scott, A. C. (Ed.), Coal and coal-bearing strata: Recent advances. Geological Society, London, Special Publications, London, pp. 25-49.

CHAPTER 5:

TWO PULSES IN ATMOSPHERIC CO_2 LEADING TO THE VALANGINIAN PERTURBATION IN THE GLOBAL CARBON CYCLE

5. TWO PULSES IN ATMOSPHERIC CO_2 LEADING TO THE VALANGINIAN PERTURBATION IN THE GLOBAL CARBON CYCLE

5.1. INTRODUCTION

The Cretaceous period has undergone a succession of major perturbations of the carbon cycle, which are marked in the geological record by intervals of exceptionally heavy $\delta^{13}C_{carb}$ signature. These intervals are associated with a crisis in carbonate production and, most of the time, with the spread of laminated organic-rich sediments deposited under anoxic conditions (e.g. black shale). Thus they are called oceanic anoxic events (OAEs; Schlanger and Jenkyns, 1976; Arthur and Schlanger, 1979; Jenkyns, 1980). The formation of large igneous provinces (LIPs) is generally evoked as a trigger (Courtillot and Renne, 2003; Jenkyns, 2003). The related excess of volcanogenic CO_2 in the ocean and the atmosphere leading to the acceleration of the hydrological cycle and the fertilisation of ocean waters is the mechanism commonly used to explain the enhanced OM burial, the carbonate crisis, and the subsequent carbon isotope excursion (CIE) (Jenkyns, 2003). A model of the carbon cycle developed by Kump and Arthur (1999) demonstrates that the offset between the $\delta^{13}C_{carb}$ and the marine $\delta^{13}C_{org}$ trends, expressed as $\Delta^{13}C$, reflect changes in pCO_2. The applicability of $\Delta^{13}C$ as a proxy for pCO_2 has then been demonstrated for the late Cretaceous OAE2, by comparing the results with those of others pCO_2 proxies, the counting of stomata in fossil leaves and marine biomarker data (Jarvis *et al.*, 2011). As such, these authors confirmed the key role of volcanism as a trigger.

The oldest Cretaceous episode of major change in the global carbon cycle started in the early Valanginian (late *B. campylotoxus* ammonite zone). It is expressed by a positive $\delta^{13}C_{carb}$ shift of approximately 1.7‰ in marine environments. The so-called Weissert episode has first been considered as an OAE, because of the following similarities: a prominent $\delta^{13}C_{carb}$ shift, a biocalcification crisis of calcareous nannofossils, the drowning of carbonate platforms, and the supposed synchronism with an important volcanism phase (Erba *et al.*, 2004). This has recently been questioned because the occurrence of black-shale deposits is rather restricted (e.g., central Pacific and the epicontinental Weddell Sea; O'Connel, 1990; Westermann *et al.*, 2010; Kujau *et al.*, 2012). Moreover, the implication of the Parana-Etendekà continental flood basalt as a potential trigger is uncertain given the most recent $^{40}Ar/^{39}Ar$ analyses, which attribute an age of 134.7 ma to the main volcanic phase (Thiede and Vasconcelos, 2010), which

corresponds to the early Hauterivian (Ogg *et al.*, 2008). Consequently, the Valanginian episode remains an enigmatic period for which the palaeoenvironmental and palaeoclimatic changes leading to the CIE are still under debate. The understanding of the changes in the carbon cycle is a central point to elucidate since carbon is the common point between volcanism, organic matter (OM) preservation, and carbonates.

The inorganic carbon isotope record is well documented; the organic record has, however, received less attention. For the continental record, a positive $\delta^{13}C_{org}$ shift has been detected in coals and charcoals of Crimea and Russia (Gröcke *et al.*, 2005; Nunn *et al.*, 2010) and in terrestrial OM of the Polish Basin (Morales et al., submitted). Concerning the marine OM record, the $\delta^{13}C_{org}$ shift is documented in the Western Atlantic (Wortmann and Weissert, 2000), the Lombardian Basin (Lini *et al.*, 1992; Weissert, pers. com.), and the Vocontian Trough (Kujau, 2012). However, these studies are either of very low resolution or document not the entire $\delta^{13}C_{org}$ shift. Moreover, the interpretation of the marine record may be problematic because the preserved OM may represent a mix of terrestrial and marine OM (Westermann et al., 2010), and the relative proportion of each is not always well assessed.

Consequently, the aim of this study is to provide a detailed and well-dated $\delta^{13}C_{org}$ curve for the Valanginian, which document the entire excursion and to compare it with the inorganic $\delta^{13}C$ record. The section of Angles (Vocontian Basin), which is the hypostratotype for the Valanginian stage (Busnardo *et al.*, 1979), has been chosen because it is well dated by ammonites, calcareous nannofossils and calpionellids (Duchamp-Alphonse *et al.*, 2007 and references therein), and because a series of palaeoenvironmental proxies has already been analysed (clay mineralogy, nutrient indexes, Sr/Ca ratio, phosphorus; in Duchamp-Alphonse, 2006; Duchamp-Alphonse *et al.*, 2007, 2011). In addition, a characterisation and quantification of preserved OM is provided here for the analysed section. The results are compared to those of others basins where similar palaeoenvironmental proxies are available (e.g. the sections of Capriolo in the Lombardian Basin and Wąwał in the Polish Basin; Lini *et al.*, 1992; Westermann *et al.*, 2010; Morales et al., submitted).

5.2. GEOLOGICAL SETTING

The section of Angles is located in SE France, 120km NE of Marseilles, close to the lake of Castillon (43° 56' 25.7676" N, 6° 32' 19.971" E). During the Valanginian, the area belonged to the southern part of the Vocontian Trough. The latter was a basin of about 150km wide and several hundred metres depth (Donze, 1979; Wilpshaar *et al.*, 1997; Duchamp-Alponse *et al.*, 2011), which was fringed by the Jura Platform to the northwest and the Provence Platform to the south (Fig. 5.1).

The section consists of hemipelagic marlstone and limestone; a more detailed lithology is given Fig. 5.2 and by Duchamp-Alphonse (2006) and Duchamp-Alphonse *et al.* (2007). Detailed and precise age control was obtained by calpionellids (Allemann and Remane, 1979), calcareous nannofossils (Manivit, 1979; Bergen, 1994 and Duchamp-Alphonse *et al.*, 2007 who used nannofossils zones of Bralower *et al.*, 1995 and Applegate and Bergen, 1986), and ammonoids (Bulot and Thieuloy, 1994; Reboulet, 1995; Reboulet and Atrops, 1999) following the standard zonation (Hoedemaeker and Rawson, 2000; Hoedemaeker *et al.*, 2003).

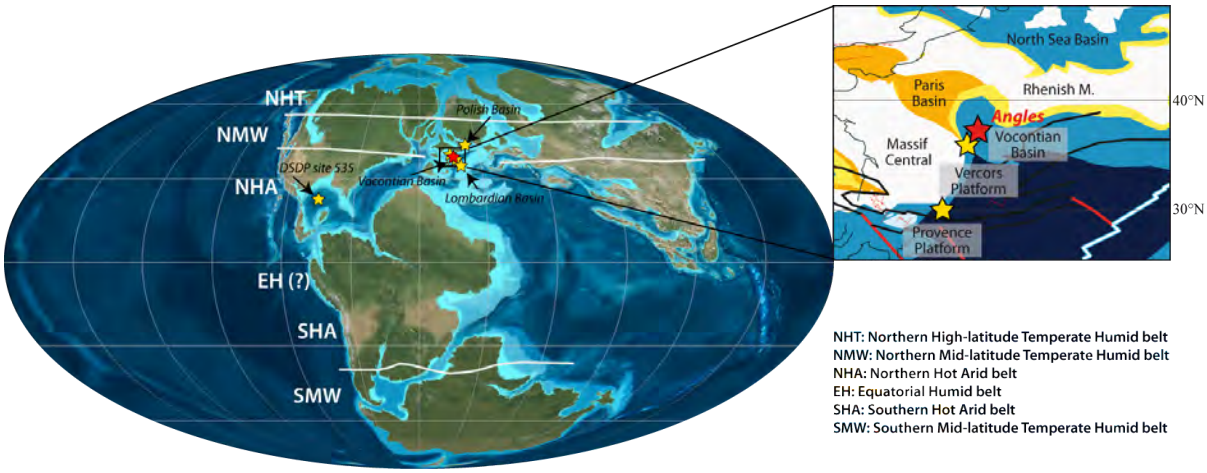

Fig. 5.1 : Palaeogeographic map. Red star : Angles section ; Yellow stars, key localities discussed in this study.

The section has already been the subject of many investigations which highlighted (among others) the $\delta^{13}C_{carb}$ positive shift and the associated palaeoenvironmental changes by studying the distribution and abundance of calcareous nannofossils, the evolution of major and trace-elements concentrations, and of clay minerals (Duchamp-Alphonse, 2006; Duchamp-Alphonse *et al.*, 2007 and Duchamp-Alphonse *et al.*, 2011) or the composition and migration of ammonite faunas (Reboulet and Atrops, 1995). For instance, an enhanced fertilization of the Tethyan waters from the earliest to the late Valanginian has been underlined with different proxies e.g. the Sr/Ca ratio and nutrient indexes based on nannofossils data (Duchamp-Alphonse, 2006, Duchamp Alphonse *et al.*, 2007).

5.3. MATERIEL AND METHOD

Being enriched in OM relative to the carbonates, only marly samples were run for $\delta^{13}C_{org}$ and Rock-Eval analyses.

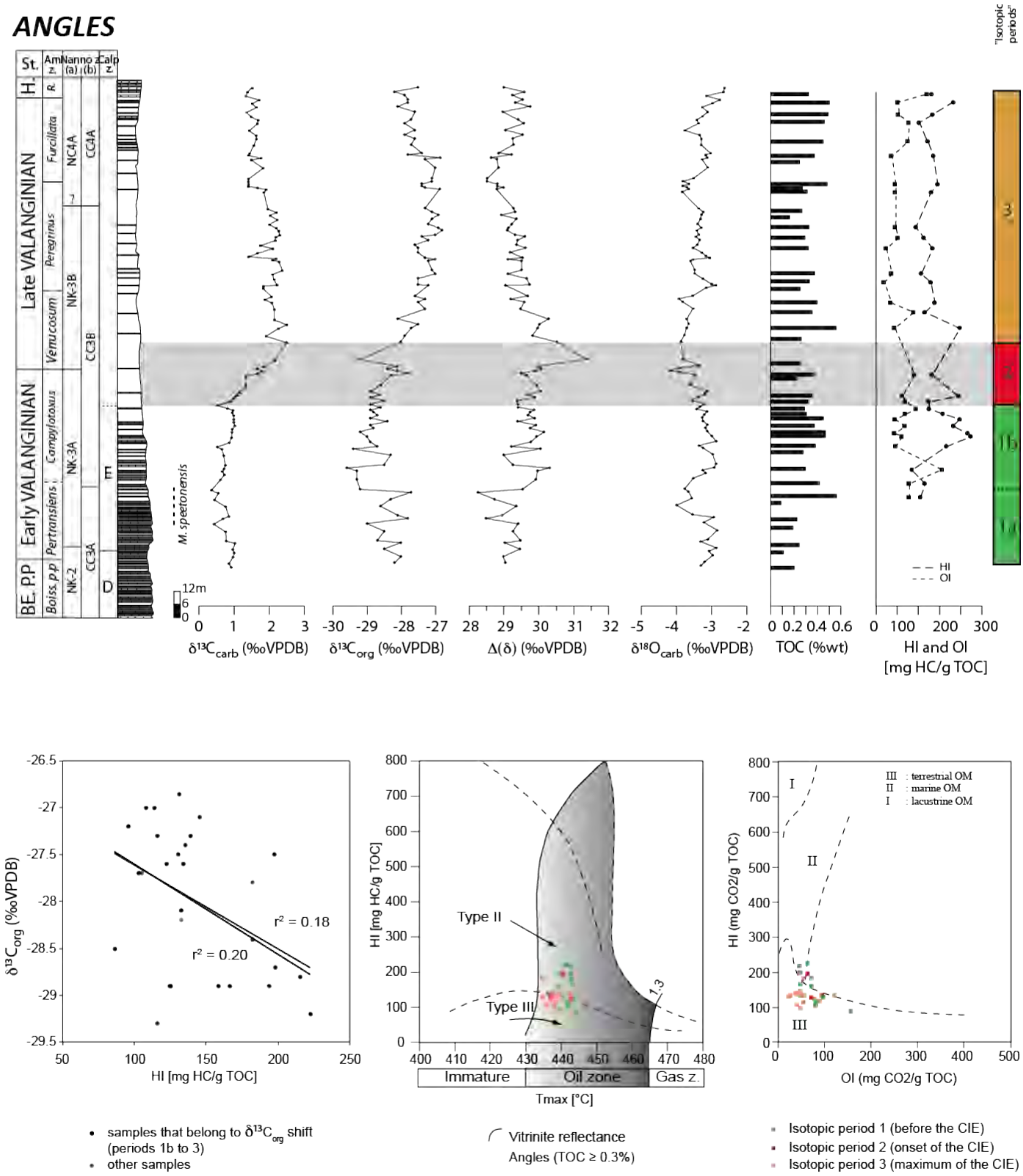

Fig. 5.2 : Stable isotope record and rock-eval data of the Angles section.
$\delta^{18}O$ and $\delta^{13}C_{carb}$ values are from Duchamp-Alphonse *et al.*, 2007.

5.3.1. Organic carbon isotope analyses

97 samples were treated with 10% HCl until the carbonate had entirely reacted. The carbon-isotope composition was determined by flash combustion on a Carlo Erba 1108 elemental analyzer (EA) connected to a Thermo Fisher Scientific Delta V IRMS, which was operated in the continuous helium flow mode via a Conflo III split interface (EA–IRMS). The $\delta^{13}C_{org}$ values are reported relative to VPDB. The calibration and assessment of the reproducibility and accuracy of the isotope analysis are based on replicate analyses of laboratory standard materials (glycine, –26.1‰ $\delta^{13}C$; urea, –43.1‰; pyridine, –29.3‰). The reproducibility was better than 0.1‰. The $\Delta^{13}C$ record represents the difference between $\delta^{13}C_{carb}$ (of Duchamp-Alphonse *et al.*, 2007) and $\delta^{13}C_{org}$ values, measured on the same samples.

5.3.2. Rock-Eval Analyses

46 samples were run for Rock-Eval analyses. Total organic carbon (TOC), T_{max}, and hydrogen and oxygen indices (HI and OI) were measured with a Rock-Eval 6 with an instrumental precision of <2%. The T_{max} values (°C) indicate thermal maturity of the organic matter and allow the assessment of the diagenetic overprint (Espitalié et al., 1985). The peaks S2 and S3 (corresponding to the amount of kerogen and CO_2 released during cracking of organic-matter between 300 and 600 °C) are used to calculate the amount of total organic carbon (TOC) and the amount of mineral carbon (MINC). In addition, the so-called hydrogen index (HI =S2/TOC) and oxygen index (OI = S3/TOC) are calculated. The HI and OI indices are proportional to the H/C and O/C ratios of the organic matter, respectively, and are used for OM classification in Van-Krevelen-like diagrams (Espitalié et al., 1985). The analyses were calibrated by analysing the standard reference material IFP-55000 (Institut Français du Pétrole; IFP 2001)

5.4. RESULTS

The $\delta^{13}C_{org}$ curve starts with relatively noisy values of about -28 ‰ in the uppermost Berriasian - lowest Valanginian interval (*Subthurmannia boissieri* p.p and *Tirnovella pertransiens* ammonite zones). This interval shows also a slight decrease in $\delta^{13}C_{carb}$ values from 1 to 0.4 ‰, low TOC values (0.2%wt in average, which is too low to characterise OM by their HI and OI indices), an increase in kaolinite content from 20 to 45% of the total clay composition, and a low nutrient index (Duchamp-Alphonse *et al.*, 2007, 2001).

Then an abrupt shift in the $\delta^{13}C_{org}$ record toward lighter values (-29.2‰) is observed within the lower Valanginian interval, in the *Olcostephanus stephanophorus* ammonite zone, *Stephanophorus hirsutus* ammonite sub-zone, which is not accompanied by a shift in $\delta^{13}C_{carb}$ values. The $\Delta^{13}C$ values abruptly increase by 1‰, the TOC values increase to 0.5 %wt and the HI and OI show values of 105 and 80 mg CO_2/g TOC, respectively.

The overlaying sediments show a progressive increase in $\delta^{13}C_{org}$ values of 2.4 ‰ and higher TOC content (0.35 %wt in average) until the lower upper Valanginian interval (*Himantoceras trinodosum* ammonite zone). Within this interval (*S. hirsutus* to *Criosarasinella furcillata* ammonite sub-zones), a first unit (from *S. hirsutus* to *Saynoceras verrucosum* ammonite sub-zones) is characterised by relatively light $\delta^{13}C_{org}$ values (comprised between -29.2 and -28‰), high $\Delta^{13}C$ values (of 29.8‰ in average), higher HI values (of 170 mg HC/g TOC in average) and a high nutrient index. A decrease in kaolinite content (from 45 to 12%) is observed when $\delta^{13}C_{carb}$ values are still relatively light (from *S. hirsutus* to *Busnardoites campylotoxus* ammonite sub-zones), which is followed by an increase in kaolinite (reaching 40% of the clay assemblages) during the onset of the $\delta^{13}C_{carb}$ shift (Duchamp-Alphonse *et al.*, 2011). The second unit (from *S. verrucosum* to *C. furcillata* ammonite sub-zones) has relatively heavy $\delta^{13}C_{org}$ values (of -27.3‰ in average), $\Delta^{13}C$ values decrease by 1.7‰, and both relatively low HI values (120mg HC/g TOC in average) as well as a decrease in kaolinite content from 40 to 10%, and in the nutrient index are observed.

Finally, the top of the section corresponding to the uppermost Valanginian/lowermost Hauterivian (*C. furcillata* to *Acanthodiscus radiatus* ammonite sub-zone and zone) shows a decrease in $\delta^{13}C_{org}$ values (from -27.2 to -28.2‰), relatively stable $\Delta^{13}C$ values, and a relatively low nutrient index (Duchamp-Alphonse *et al.*, 2007).

5.5. DISCUSSION

5.5.1. Evaluation of the diagenetic impact

The section of Angles witnessed relatively significant diagenetic overprint as is indicated by the Rock-Eval analyses, which show temperatures of OM cracking of more than 430° (T_{max} between 435 and 445°), suggesting that OM passed through the onset of the oil window (Fig. 5.2).

Bodin *et al.* (2009) demonstrated, however, that the trends in bulk-rock $\delta^{18}O$ values (Valanginian data from Angles after Duchamp-Alphonse *et al.*, 2007) are conserved, by comparison with the trends in $\delta^{18}O$ of belemnites (Mc Arthur *et al.*, 2007). Carbon isotopes are less sensitive to diagenesis (Choquette and James, 1987) and the trends in $\delta^{13}C_{carb}$ are well preserved (Duchamp-Alphonse *et al.*, 2007). Duchamp-Alphonse *et al.* (2007) also calculated a coefficient of correlation between $\delta^{13}C_{carb}$ and $\delta^{18}O$ of 0.09 and noted that calcareous nannofossil assemblages have not significantly been affected by etching or secondary calcite overgrowth. This underlines the weak overprint of diagenesis on carbonate carbon and oxygen isotopes. OM is more sensitive to heath, consequently to burial diagenesis. The potential impact of diagenesis on OM can be evaluated by comparing $\delta^{13}C_{org}$ values of Angles with records obtained from other localities. In Fig. 5.3, a correlation of $\delta^{13}C_{carb}$ and $\delta^{13}C_{org}$ trends with the western Atlantic, the Lombardian Basin, and a further section located in the Vocontian Basin (Vergol-Morenas) is proposed. Absolute values are shifted by 1‰ compared to the section of Vergol-Morenas (Vocontian Basin) and 2‰ compared to the sections of Capriolo and Polaveno (Lombardian basin). The Lombardian basin is more distal than the Vocontian Basin, thus this lag may reflect changes in proportion of marine versus terrestrial OM. Conversely, the lag with the Vergol-Morenas section, which is located in the same basin and at similar depth, probably testifies to enhanced diagenesis in Angles. Indeed, isotopically enriched components of marine OM (such as carbohydrate carbon) may be more sensitive to diagenesis (Sinninghe Damsté and Köster, 1998; Forster *et al.*, 2008) However, since a relatively precise correlation can be established between the sections (Fig. 5.3), the trends in $\delta^{13}C_{org}$ appear to be conserved in Angles and are therefore used here to trace changes in the carbon cycle.

The degree of diagenesis in the marly lithologies of the Angles section and of the Vocontian Trough in general probably led to the partial disappearance of smectite and to an enhanced proportion of illite layers relative to smectite layers in illite-smectite interstratified clay minerals (Kübler and Jaboyedoff, 2000). In limestone lithologies, smectite tends to disappear to the benefit of chlorite (Deconinck and Debrabant, 1985), due to lower K contents in limestone compared to marl (which contains more detrital mica and feldspar). In Angles, the proportion of illite-smectite interstratified clay is relatively low (less than 5%), except for the base of the section (up to 40%), which is more calcareous (Fig. 5.4). This shows that the formation of new, authigenic clay minerals during diagenesis was not too important and that the composition of the clay mineralogy and stratigraphic variations therein can be used in Angles as a palaeoenvironmental proxy (Godet *et al.*, 2006). Moreover, burial diagenesis may not have affected the kaolinite content (Kübler and Jaboyedoff, 2000), as is suggested by the relatively high proportion of kaolinite in the clay assemblages (up to 45%, Fig. 5.4).

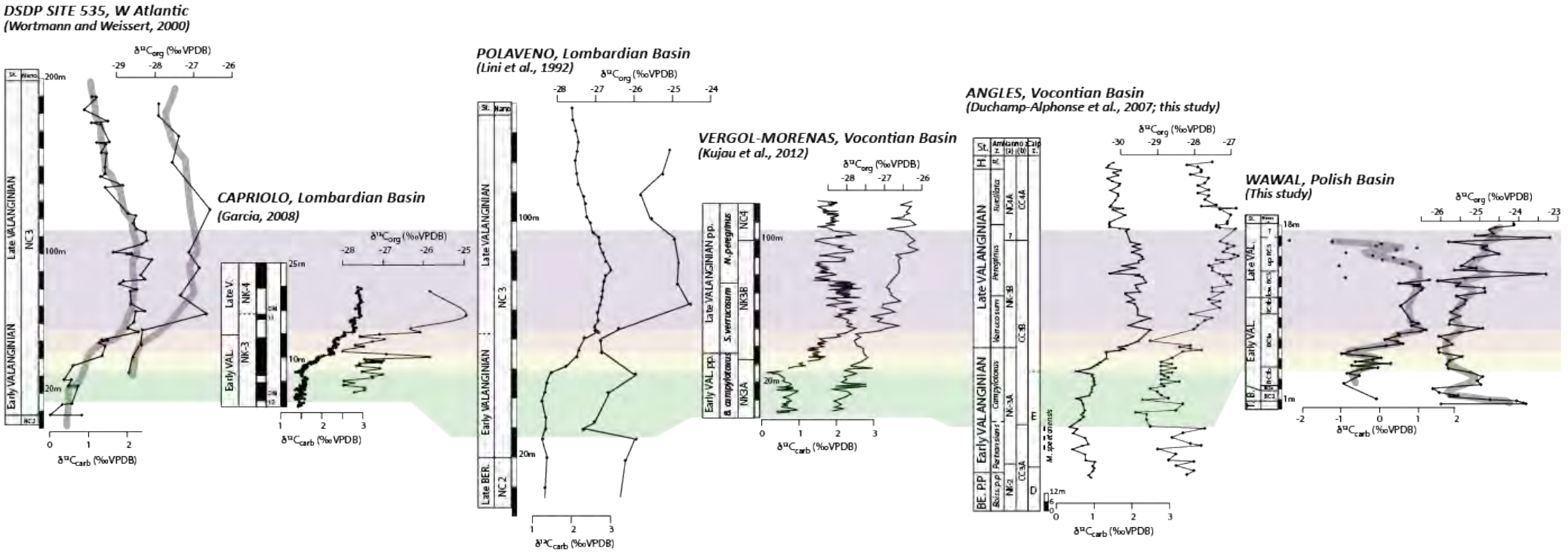

Correlation of the inorganic and organic stable-isotope record of the West Atlantic, Lombardian, Vocontian and Mid-Polish Basins.

5.5.2. The perturbation of the carbon cycle: a link with atmospheric pCO_2 changes?

The entire excursion in $\delta^{13}C_{org}$ values is recorded in Angles. The perturbation starts with a negative shift of approximately 1.3 ‰ in the latest *T. pertransiens* ammonite zone (early Valanginian), which then progressively increase of 2.4 ‰ until the *Neocomites peregrinus* ammonite zone (late Valanginian). Superimposed on this longer-term trend, an interval with more negative values is observed in the early *S. verrucosum* ammonite zone (early-late Valanginian boundary interval). The interval with lighter $\delta^{13}C_{org}$ values shows globally higher TOC and HI values, which may indicate that the proportion of marine organic matter increased, which again may have had an influence on the organic carbon isotope record.

Since the Cretaceous was a period of high pCO_2 (Berner and Kothavala, 2001), and marine phytoplankton increase their C^{12}/C^{13} fractionation under high pCO_2 (Dean *et al.*, 1986), the marine $\delta^{13}C_{org}$ signature was probably 5 to 7‰ lighter than today (Arthur *et al.*, 1985; Popp *et al.*, 1989). This is confirmed by comparing the signatures of typically terrestrial OM obtained in the Polish Basin, which range from -26 to -22 ‰, with those of mixed terrestrial and marine OM preserved in the deep-marine environments of the Vocontian and Lombardian basins and of the west Atlantic, which range from -29 to -25 ‰ (Fig. 5.3). Consequently, for the period considered, marine OM had $\delta^{13}C_{org}$ values, which were approximately 2 ‰ lighter than terrestrial OM. This is consistent with similar data obtained for the OAE2 (Kuypers *et al.*, 2004; Jarvis *et al.*, 2011).

To examine to which extent the variations in $\delta^{13}C_{org}$ values are linked with the type of OM stored in the sediments, a $\delta^{13}C_{org}$ versus HI plot is realised (Fig. 5.2). The coefficient of determination is 0.2, when considering the whole data, and also 0.2, when considering only the interval of isotope change in the carbon cycle (e.g. from the negative shift in $\delta^{13}C_{org}$ to the end of the high $\delta^{13}C_{org}$ values). This signifies that the type of OM has probably not significantly driven the $\delta^{13}C_{org}$ variations. The fact that HI values increase slightly after the onset of the $\delta^{13}C_{org}$ negative shift highlights the weak direct link between these two proxies.

Another factor, which may have influenced the $\delta^{13}C_{org}$ trends, is marine productivity and changes therein. With an increase in nutrients, marine phytoplankton increases their fractionation leading to a decrease in marine $\delta^{13}C_{org}$ values. This may induce the enrichment in ^{13}C of sea-surface waters, which then lead to a following increase in marine $\delta^{13}C_{org}$. With this mechanism, the $\delta^{13}C$ signal of the carbonate carbon reservoir is supposed to be initially buffered following changes in nutrient stocks.

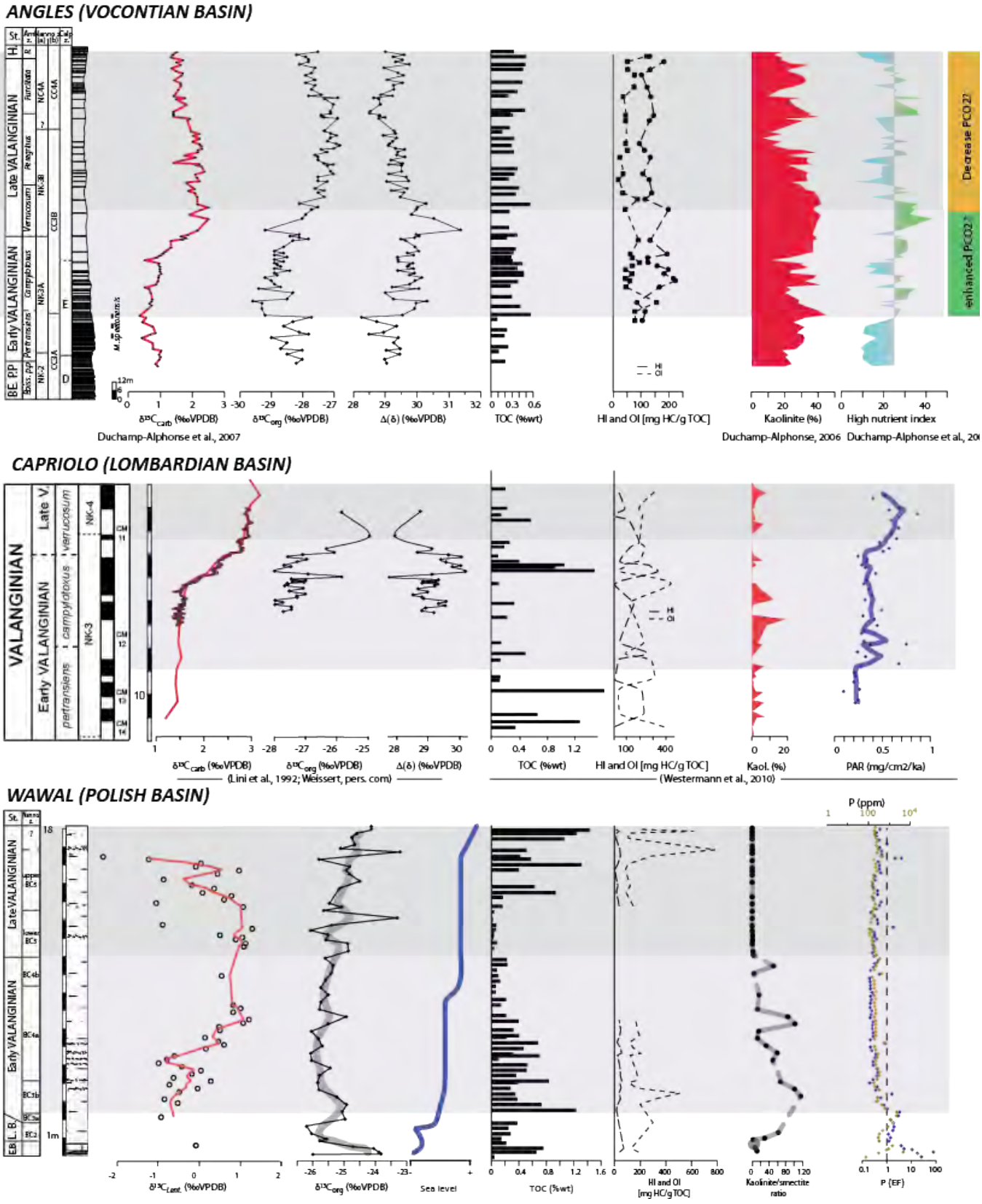

Fig. 5.4: Compilation of $\delta^{13}C_{carb}$ and $\delta^{13}C_{org}$ records, rock-eval data, kaolinite and phosphorus contents of the Vocontian, Lombardian, and Mid-Polish Basins for the Valanginian period

The data show that the increase in the nutrient index is coeval with the base of the $\delta^{13}C_{org}$ negative shift and that a progressive increase in $\delta^{13}C_{org}$ values followed the negative shift, which argues in favour of this hypothesis. This is also supported by the fact that the isotopic signature of carbonates is not initially affected by the rise in nutrients and that the onset of the $\delta^{13}C_{org}$ shift is coeval with the decline in nannoconids (Erba *et al.*, 2004; Duchamp-Alphonse *et al.*, 2007; Barbarin *et al.*, 2012).

The $\delta^{13}C_{org}$ trend detected in Angles can be correlated with other basinal sections in the Vocontian Trough, in the Lombardian Basin and the West Atlantic (DSDP site 535; preserved OM mainly of marine origin; Patton *et al.*, 1984) but also with the shallow-water record (terrestrial OM) of the section of Wąwał in the Polish Basin (Fig. 5.3). Thus the global perturbation of the carbon cycle, which characterises the Valanginian probably started during the late *T. pertransiens* zone as is suggested by the organic record.

Of interest in this context is the observation that also the terrestrial OM archives record a shift in $\delta^{13}C_{org}$ values, and the question arises in how far the terrestrial vegetation was influenced by changes in nutrient stocks. This may have been the case, as changes in the mobilisation and flux rates of important biophile elements such as P, K and Fe are directly related to changes in biogeochemical weathering on the continent. A further, probably equally or even more important factor to be considered in interpreting the comparable changes in the terrestrial and marine $\delta^{13}C_{org}$ records is an increase in atmospheric pCO_2. Rising atmospheric pCO_2 values may have led to the decrease both in marine and terrestrial $\delta^{13}C_{org}$ records, since marine and terrestrial vegetation increase their fractionation under high pCO_2.

The $\Delta^{13}C$ record, which traces the difference between the $\delta^{13}C_{carb}$ and the $\delta^{13}C_{org}$ records, has indeed been employed as a tool for the reconstruction of changes in atmospheric pCO_2 (Kump and Arthur, 1999; Jarvis *et al.*, 2011). Its quality as a proxy of atmospheric pCO_2 is dependent of certain conditions including a weak diagenetic overprint, no significant change in productivity, and no change in the type of OM. In the case of the Angles section, these conditions are not always fulfilled, since the section has undergone a certain diagenetic overprint, and changes in nutrient stocks and the proportion between preserved marine and terrestrial OM occurred. The advantage of the approach chosen here, however, is that the proxies used here (nutrient index based on calcareous nannofossils; Duchamp-Alphonse et al., 2007; HI and OI of preserved OM) allows to have an independent control on those parameters.

To this comes that the $\Delta^{13}C$ trends appear to be correlated between the Vocontian and Lombardian basins, and the West Atlantic (Fig. 5.5), which may emphasize the impact of changes in atmospheric pCO_2 on the $\Delta^{13}C$ trends. As such the $\Delta^{13}C$ trends would indicate higher pCO_2 from the late *T. pertransiens* to the middle *S. verrucosum* ammonite zones and a decrease in pCO_2 later in the late Valanginian.

Moreover, the high $\Delta^{13}C$ values are very well correlated with high nutrient index values (Fig. 5.4). More particurlarly, the two peaks in $\Delta^{13}C$ values in the early *B. campylotoxus* and early *S. verrucosum* ammonite zones correspond to two peaks in the high nutrient index values of Duchamp-Alphonse *et al.* (2007). As a consequence, it is likely that pCO_2 and nutrient levels are strongly linked. The increase in pCO_2 led to enhanced nutrient fluxes to the ocean and to the fertilization of ocean waters from the late *T. pertransiens* to the mid *S. verrucosum* ammonite zones interval, and to the decline of nannoconids, which inhabited warm and oligotrophic surface waters (Noël and Busson, 1990; Busson and Noël, 1991; Coccioni et al., 1992; Bornemann et al., 2003). HI values start to increase only after the onset of the increase in nutrient index and in $\Delta\delta$ values, which indicates that enhanced marine OM preservation is the consequence of the fertilization of ocean waters and higher pCO_2 levels.

Two peaks can be individualised within the general high $\Delta^{13}C$ values: the first characterise the initiation of the excursion in the latest *T. pertransiens* - earliest *B. campylotoxus* ammonite zones and the second the maximum of the excursion at the early-late Valanginian boundary. These two peaks can be identified in the Lombardian and the Vocontian basins (the other $\Delta^{13}C$ records being not complete enough to observe the first peak) and may indicate the occurrence of two important pulses in atmospheric pCO_2.

In shallow-water environments (Fig. 5.6), the first peak in $\Delta\delta$ values would correspond to the onset in the deposition of the heterozoan Calcaires Roux Fm in the Jura and a first platform drowning phase of the carbonate platform preserved in the Helvetic Alps (Büls Bed; Kuhn, 1996; Föllmi et al., 2007), and the second one to a widespread drowning phase of carbonate platforms. With the proposed model for the Valanginian episode (Fig. 5.7), the $\delta^{13}C_{carb}$ positive shift is driven by the drowning of carbonate platforms and likely also by the increased OM preservation on the continent (Westermann *et al.*, 2010). Finally, the late Valanginian corresponds to a decrease in $\Delta^{13}C$ values and nutrient index. This may indicate that a decrease in pCO_2 followed, leading to a decrease in nutrient mobilisation and transfer rates.

5.5.3. Which effect on palaeoenvironments?

In the NW Tethyan area, the Berriasian and the earliest Valanginian climate is characterised by progressively enhanced humidity, which is recorded, among others, by the clay minerals on a platform-basin transect from the Jura to the Vocontian Trough (Morales et al., 2013). A change in platform morphology marked by the disappearance of barriers and protected lagoons is noted through the Berriasian-Valanginian boundary, which allows for a better transport of detrital fluxes from the continent to the basins. Consequently during the Valanginian, segregation effects linked with the occurrence of a rimmed platform did not affect clay mineral contents of the Vocontian sediments, as it was observed with the kaolinite record for the Berriasian stage (Morales et al., 2013).

SW NE

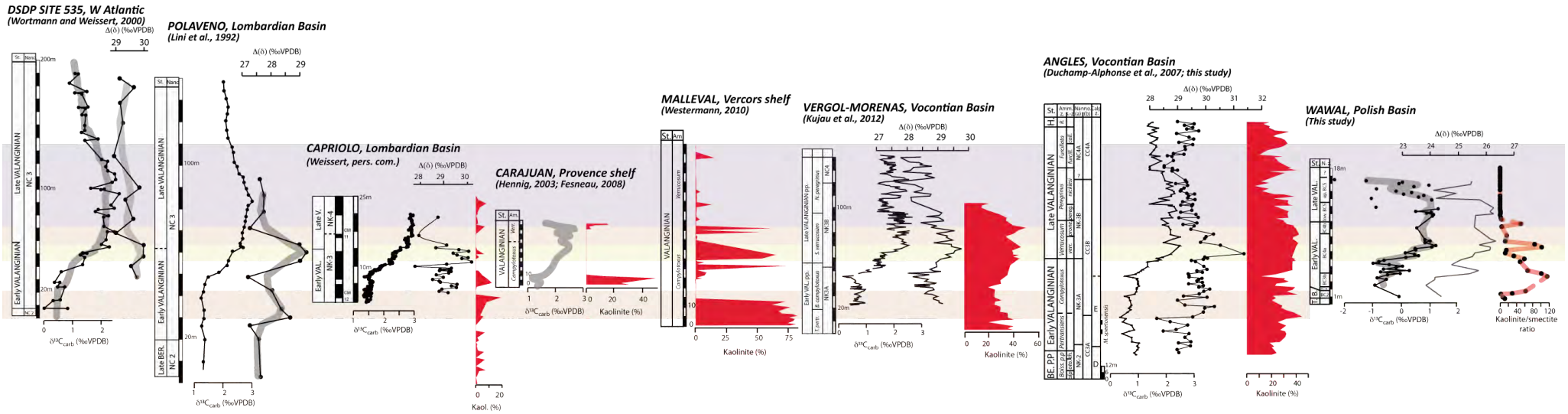

Fig. 5.5 : Correlation of the $\delta^{13}C_{carb}$ and $\Delta^{13}C$ records with kaolinite trends in the West-Atlantic, Lombardian, Vocontian and Mid-Polish Basins, and the Provence platform.

Another factor that may play an important role in the distribution of clay minerals are sea-level variations. Generally, during a sea-level rise the detrital sources become more distant and heavier clay minerals such as kaolinite become segregated across the shelf (Adatte *et al.*, 1984; Deconinck *et al.*, 1985; Adatte, 1988; Chamley, 1989; Godet et al., 2008). This explains the difference in kaolinite content in the pelagic sections of the Lombardian basin, which contain a very low amount of kaolinite, compared to the hemipelagic sections of the Vocontian Trough and the outer shelf sections of Carajuan (Provence platform, SE France), Malleval (Vercors patform E France) or Wawal (Mid-Polish Basin, central Poland).

In Angles, a decrease in kaolinite content is observed during the late *T. pertransiens* - early *B. campylotoxus* ammonite zones, followed by an increase through the late *B. campylotoxus* - early *S. verrucosum* ammonite zones, which correspond to the Valanginian CIE. These trends can be correlated with other sections of the Vocontian Basin: Vergol-Morenas and Montclus (except for La Charce, which is slumped in this interval; Fesneau, 2008); and Spain (Galicia Margin, ODP leg 1031; after Meyers *et al.*, 1988; and Betic Cordillera; Fesneau, 2008). The decrease in kaolinite in the early Valanginian can be correlated with the Vercors platform (outer shelf section of Malleval, Westermann, 2010); and with the inner Jura platform (La Chambotte), where kaolinite disappears from the clay assemblages in time-equivalent sediments. Consequently, the decrease in kaolinite occurring during the late *T. pertransiens* - early *B. campylotoxus* ammonite zones is related to a decrease in humidity on the continent in this region.

The increase in kaolinite during the late early Valanginian is also recorded in the Polish Basin (Wawal section; Morales et al., submitted), and probably reflects a peak in humidity in western and central Europe. This time period is also marked by the disappearance or the strong depletion of kaolinite in the Lombardian Basin (Capriolo; Westermann, 2010), in the outer Provence platform (Carajuan; Fesneau, 2008), and in another section of the Vocontian Basin, La Charce, where the related sediments are slumped (Fesneau, 2008). Mineralogical studies have been carried out in England and Germany but a precise correlation with the Tethyan domain remains difficult given the different age dates and the lack of chemostratigraphic data and correlation. In Yorkshire, the trends appear, however, to be consistent with the northern Tethyan area (Fesneau, 2008, and references therein).

To resume, sections representing the European continent (e.g. located in the Vocontian Trough and further to the north) show a decrease in humidity in the late *T. pertransiens* - early *B. campylotoxus* ammonite zones, followed by enhanced humidity during the onset of the CIE (late *B. campylotoxus* - early *S. verrucosum* ammonite zones). These trends in kaolinite are in phase with the results of palynological analyses performed in the Vocontian Basin (with a slight time lag, Kujau, 2012; Kujau *et al.*, 2012) and emphasise the climatic dimension of palaeoenvironmental changes during the early Valanginian.

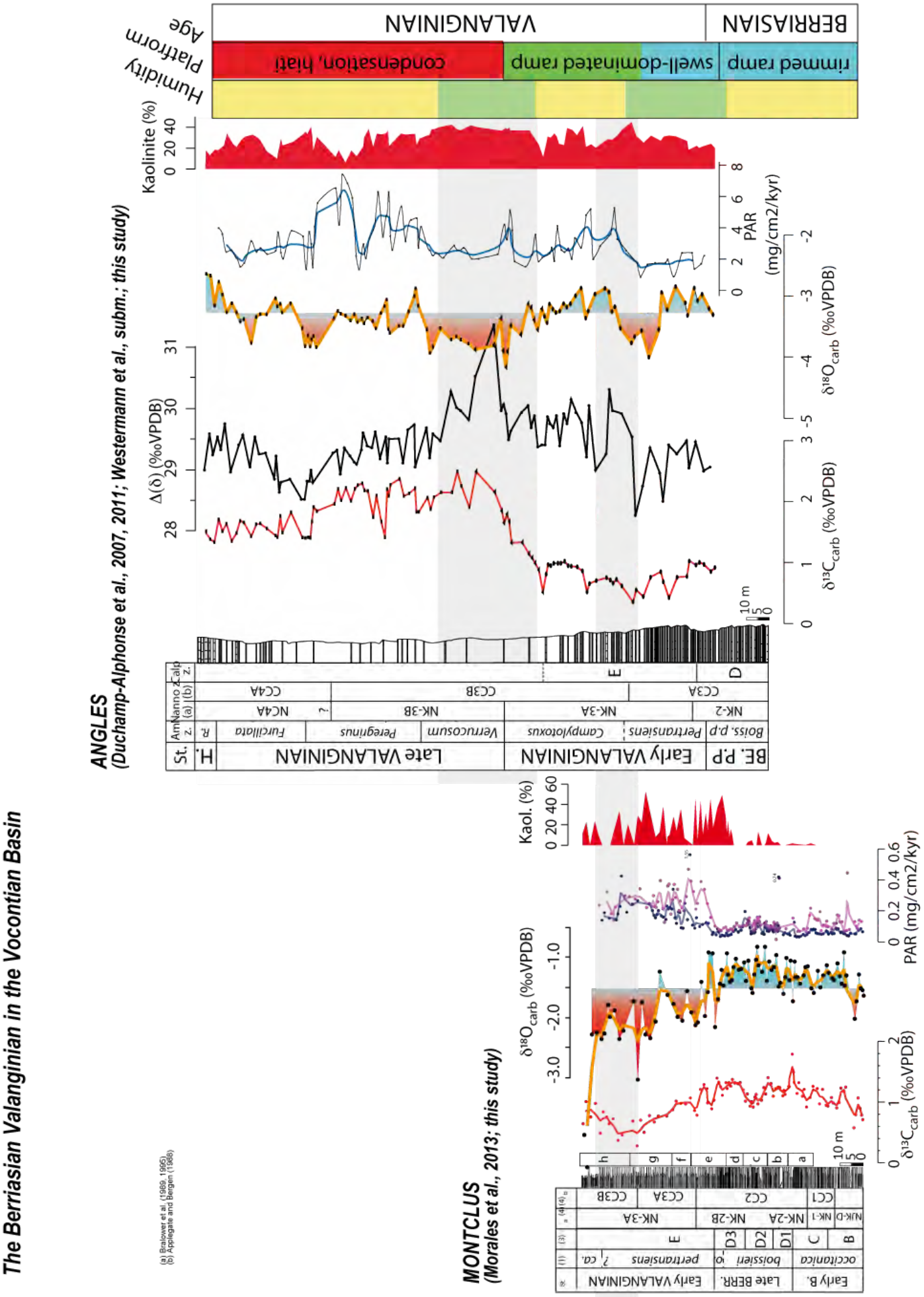

Fig. 5.6 : Synthesis of the $\delta^{13}C_{carb}$, $\delta^{18}O$ and $\delta^{13}C$ records, and phosphorus and kaolinite contents for the Berriasian Valanginian interval in the Vocontian Basin.

This appear to be opposite in the central Tethys and the isolated Provence platform, which encompassed more humid conditions followed by arid conditions during the CIE. Kujau (2012) relates the incoming of the more arid phase in the Vocontian Basin to the northward migration of climate belts with the expansion of Hadley cells, linked with the first peak in pCO_2 (as it is the case with the actual climate change). This is in agreement with this study, which shows that the onset of the $\delta^{13}C_{org}$ perturbation (and of $\Delta^{13}C$ changes) and the beginning of the arid phase in NW Europe are synchronous. This might also explain why the Lombardian Basin, which is located in the central Tethys, record higher kaolinite contents: with the migration northward of climate belts, the central part of the Tethys might record the enhanced influence of the equatorial humid zone.

During the late *B. campylotoxus* - early *S. verrucosum* ammonite zones, corresponding to the onset of the $\delta^{13}C_{carb}$ positive excursion, enhanced kaolinite contents are recorded in NW Tethyan area, which are correlated with an increase in $\Delta^{13}C$ values. This is particularly well documented in Vergol-Morenas, where the trends are very similar. This is also expressed in Angles but less clearly, possibly because of a stronger diagenetic overprint. As a matter of fact, a second increase in pCO_2 probably lead to the reinstallation of high moisture levels on the European continent. Kujau (2012) interpreted this as the shrinking of the Hadley cells (following the model proposed for the mid-Cretaceous interval by Hasegawa *et al.*, 2011), which may have occurred when a threshold of pCO_2 in the atmosphere was reached. Hasegawa *et al.* (2011), however, did not mention this mechanism for the Valanginian, while they studied the whole Cretaceous.

Anyway, this second phase of humidity and high pCO_2 levels corresponds to the demise of carbonate platforms in the North Tethyan margin (Föllmi *et al.*, 1994, 2007; Weissert *et al.*, 1998), which were already weakened by the increase in nutrients linked to the previous increase in pCO_2. The occurrence of a sea-level rise during this time interval probably contributed to the crisis in shallow-water calcifying organisms, which could not keep up under stressful conditions (with high moisture and nutrient levels, and more acidic waters under high pCO_2 levels). From this it follows that important climate change related to two pulses in atmospheric pCO_2 has lead to the Valanginian perturbation in the global carbon cycle (Fig. 5.7).

5.6. CONCLUSION

With this study, we document the entire $\delta^{13}C_{org}$ perturbation associated with the Valanginian Weissert Event. The perturbation of the carbon cycle starts with a negative shift in $\delta^{13}C_{org}$ values in the late *T. pertransiens* ammonite zone, and continues with an increase until the *N. peregrinus* ammonite zone (late Valanginian).

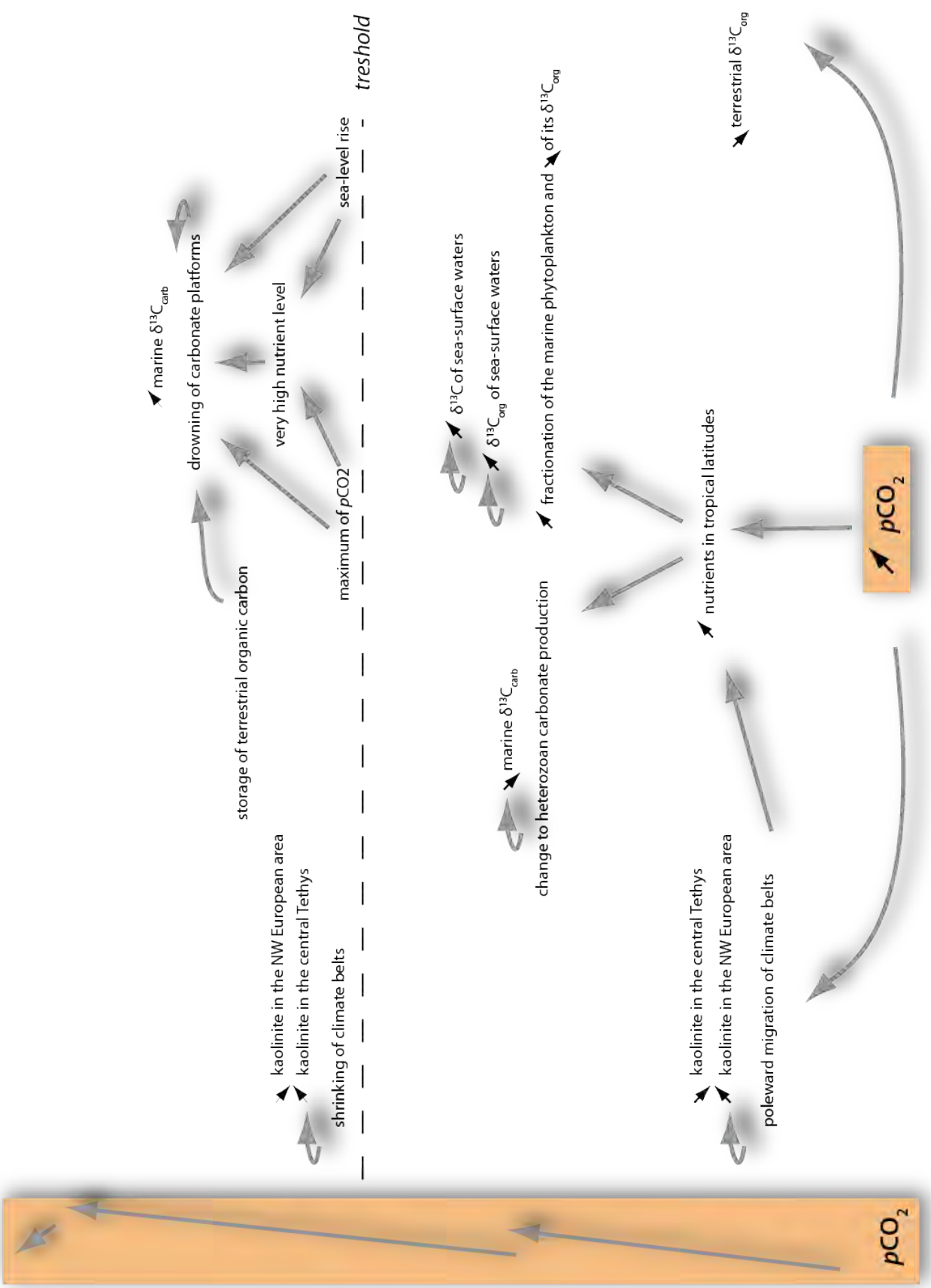

Fig. 5.7: Impact of a stepwise increase in *p*CO2 on environment, climate, and the organic and inorganic carbon isotopic record.

The $\delta^{13}C_{org}$ record appears to be global and synchronous. Changes in OM composition did not significantly affect the signal, with the possible exception of the earliest late Valanginian. More important were changes in marine productivity and their impact on the isotopic composition of OM. With the nutrient-induced increase in productivity, marine plankton increased its fractionation (the $\delta^{13}C_{org}$ values diminish), leaving surface waters enriched in ^{13}C. Subsequently, surface waters being enriched in heavy isotopes, the $\delta^{13}C_{org}$ values increase again. In addition, a two-step increase in pCO_2 is viewed as a major trigger of change within the carbon cycle. The following schedule of palaeoenvironmental perturbations linked with the Valanginian Weissert episode is proposed. The first peak in pCO_2 lead to the expansion of the Hadley cells and to a fertilization of sea-surface waters. As a consequence, more arid conditions settle in the European continent, whereas a first platform-drowning phase is registered on the northern Tethyan carbonate platform. The second peak in pCO_2 marks the return of hydrolysing conditions on the continent. The associated enhanced detrital fluxes and the sea-level rise induced a further, more important phase of demise of carbonate platforms, which were already weakened by the precedent excess in nutrients. With this model, the $\delta^{13}C_{carb}$ positive shift is principally viewed as the result of the demise of shallow-water carbonates (of the northern margin of the Tethys and in the central Atlantic) which have a $\delta^{13}C$ signature slightly enriched compared to the seawater. A further mechanism included the enhanced storage of organic matter on the continent during this phase of increased humidity.

References

Adatte, T. and Rumley, G. (1984) Microfaciès, minéralogie, stratigraphie et évolution des milieux de dépôts de la plateforme Berriaso-Valanginienne des régions de Sainte-Croix (VD), Cressier et du Landeron (NE). *Bulletin de la société Neuchâteloise des sciences naturelles***,** 221-239.

Adatte, T. (1988) *Etude sedimentologique, minéralogique, micropaléontologique et stratigraphique du Beriasien - Valanginien du Jura central.*, Neuchatel, Neuchatel, 481 pp.

Allemann, F. and Remane, J. (1979) Les faunes de calpionelles du Berriasien supérieur/Valanginien. In: *Hypostratotype Mésogeen de l'Etage Valanginian (Sud-Est de la France)* (Eds R. Busnardo, J.-P. Thieuloy and M. Moullade), **6**, pp. 99-109. Les Stratotypes Français, C.N.R.S. Paris.

Applegate, J.L. and Bergen, J.A. (1986) Cretaceous calcareous nannofossil biostratigraphy of sediments recovered from the Galicia Margin of Leg 103. *Proceeding of the Ocean Drilling Program, Scientific results,* **103,** 293-319.

Arthur, M.A. and Schlanger, S.O. (1979) Cretaceous "Oceanic Anoxic Events" as Causal Factors in Development of Reef-Reservoired Giant Oil Fields. *The American Association of Petroleum Geologists Bulletin*, **63,** 870-885.

Arthur, M.A., Dean, W.E. and Schlanger, S.O. (1985) Variations in the global carbon cycle during the Cretaceous related to climate, volcanism and changes in atmospheric CO2. In: *The Carbon Cycle and Atmospheric CO2: Natural Variations Archean to Present* (Eds E.T. Sundquist and W.S. Broecker), **32**, pp. 504-529. Geophysical Monograph Series, AGU, Washington D. C.

Barbarin, N., Bonin, A., Mattioli, E., Pucéat, E., Cappetta, H., Gréselle, B., Pittet, B., Vennin, E. and Joachimski, M. (2012) Evidence for a complex Valanginian nannoconid decline in the Vocontian basin (South East France). *Marine Micropaleontology*, **84,** 37-53.

Bergen, J.A. (1994) Berriasian to early Aptian calcareous nannofossils from the Vocontian trough (SE France) and deep-sea drilling site 534: new nannofossil taxa and summary of low-latitude biostratigraphic events. *Journal of Nannoplankton Research*, **16,** 56-69.

Berner, R.A. and Kothavala, Z. (2001) Geocarb III: A Revised Model of Atmospheric CO2 over Phanerozoic Time. *American Journal of Science*, **301,** 182-204.

Bodin, S., Fiet, N., Godet, A., Matera, V., Westermann, S., ClÈment, A., Janssen, N.M.M., Stille, P. and Föllmi, K.B. (2009) Early Cretaceous (late Berriasian to early Aptian) palaeoceanographic change along the northwestern Tethyan margin (Vocontian Trough, southeastern France): [delta]13C, [delta]18O and Sr-isotope belemnite and whole-rock records. *Cretaceous Research*, **30,** 1247-1262.

Bornemann, A., Aschwer, U. and Mutterlose, J. (2003) The impact of calcareous nannofossils on the pelagic carbonate accumulation across the Jurassic-Cretaceous boundary. *Palaeogeography, Palaeoclimatology, Palaeoecology*, **199,** 187-228.

Bralower, T.J., Leckie, R.M., Sliter, W.V. and Thierstein, H.R. (1995) An integrated Cretaceous microfossil biostratigraphy. *SEPM (Society for Sedimentary Geology) Special publication*, **54,** 65-79.

Bulot, L.G. and Thieuloy, J.-P. (1994) Les biohorizons du Valanginien du Sud-Est de la France : un outil fondamental pour les corrélations au sein de la Téthys occidentale. *Geologie Alpine, Mémoire H.S.*, **20,** 15-42.

Busnardo, R., Thieuloy, J.-P., Moullade, M., Allemann, F., Combemorel, R., Cotillon, R., Donze, P., Ferry, S., Manivit, H., Remane, J. and Rio, M. (1979) Hypostratotype Mésogéen de l'étage Valanginien (Sud-Est de la France). *Les stratotypes français*, **6,** 1-143.

Busson, G. and Noël, D. (1991) Les nannoconidés indicateurs environnementaux des océans et mers épicontinentales du Jurassique terminal et du Crétacé inférieur. *Oceanologica Acta*, **14,** 333-356.

Chamley, H. (1989) *Clay Sedimentology*. Springer- Verlag, Berlin.

Choquette, P.W. and James, N.P. (1987) Diagenesis in Limestones - 3. The Deep Burial Environment. *Geoscience Canada*, **14,** 3-35.

Coccioni, R., Erba, E. and Premoli Silva, I. (1992) Barremian-Aptian calcareous plankton biostratigraphy from the Gorgo Cerbara section (Marche, central Italy)

and implications for plankton evolution. *Cretaceous Research*, **13,** 517-537.

Courtillot, V.E. and Renne, P.R. (2003) On the ages of flood basalt events. *Comptes Rendus Geosciences*, **335,** 113-140.

Donze, P. (1979) Les ostracodes. In: *Hypostratotype Mesogeen de l'Etage Valanginien (Sud-Est de la France)*. (Eds R. Busnardo, J.-P. Thieuloy and M. Moullade), **Les Stratotypes Français 6**, pp. 77-86. C.N.R.S, Paris.

Dean, W.E., Arthur, M.A. and Claypool, G.E. (1986) Depletion of 13C in Cretaceous marine organic matter: Source, diagenetic, or environmental sigal? *Marine Geology*, **70,** 119-157.

Deconinck, J.-F., Beaudoin, B., Chamley, H., Joseph, P. and Raoult, J.F. (1985) Contrôles tectonique, eustatique et climatique de la sédimentation argileuse du domaine subalpin français au Malm-Crétacé. *Rev. Géol. Dyn. Géogr. Phys*, **26,** 311-320.

Duchamp-Alphonse, S. (2006) *Changements paléoenvironnementaux et production carbonatée hémipélagique de la marge Nord-Ouest Téthysienne durant le Valanginien. Approches minéralogique, micropaléontologique et géochimique.*, Paris, 303 pp.

Duchamp-Alphonse, S., Gardin, S., Fiet, N., Bartolini, A., Blamart, D. and Pagel, M. (2007) Fertilization of the northwestern Tethys (Vocontian basin, SE France) during the Valanginian carbon isotope perturbation: Evidence from calcareous nannofossils and trace element data. *Palaeogeography, Palaeoclimatology, Palaeoecology*, **243,** 132-151.

Duchamp-Alphonse, S., Fiet, N., Adatte, T. and Pagel, M. (2011) Climate and sea-level variations along the northwestern Tethyan margin during the Valanginian C-isotope excursion: Mineralogical evidence from the Vocontian Basin (SE France). *Palaeogeography, Palaeoclimatology, Palaeoecology*, **302,** 243-254.

Espitalié, J., Deroo, G. and Marquis, F. (1985) La pyrolyse Rock-Eval et ses applications. *Revue de l'Institut Français du Pétrole*, **40,** 563–579.

Erba, E., Bartolini, A. and Larson, L.R. (2004) Valanginian Weissert oceanic anoxic event. *Geology*, **32,** 149-152.

Fesneau, C. (2008) *Enregistrement des changements climatiques dans le domaine Tethysien au Valanginien*, Université de Bourgogne, Dijon, 340 pp.

Föllmi, K.B., Weissert, H., Bisping, M. and Funk, H. (1994) Phosphogenesis, carbon-isotope stratigraphy, and carbonate-platform evolution along the Lower Cretaceous northern Tethyan margin *Geological Society of America Bulletin*, **106,** 729-746.

Föllmi, K.B., Bodin, S., Godet, A., Linder, P. and van de Schootbrugge, B. (2007) Unlocking paleo-environmental information from Early Cretaceous shelf sediments in the Helvetic Alps: stratigraphy is the key! *Swiss journal of geosciences*, **100,** 349-369.

Forster, A., Schouten, S., Moriya, K., Wilson, P.A. and Sinninghe Damsté, J.S. (2007) Tropical warming and intermittent cooling during the Cenomanian/Turonian oceanic anoxic event 2: Sea surface temperature records from the equatorial Atlantic. *Paleoceanography*, **22**.

Godet, A., Bodin, S.p., Föllmi, K.B., Vermeulen, J., Gardin, S., Fiet, N., Adatte, T., Berner, Z., Stüben, D. and van de Schootbrugge, B. (2006) Evolution of the marine stable carbon-isotope record during the early Cretaceous: A focus on the late Hauterivian and Barremian in the Tethyan realm. *Earth and Planetary Science Letters*, **242,** 254-271.

Godet, A., Bodin, S., Adatte, T. and Föllmi, K.B. (2008) Platform-induced clay-mineral fractionation along a northern Tethyan basin-platform transect: implications for the interpretation of Early Cretaceous climate change (Late Hauterivian-Early Aptian). *Cretaceous Research*, **29,** 830-847.

Gröcke, D.R., Price, G.D., Robinson, S.A., Baraboshkin, E.Y., Mutterlose, J. and Ruffell, A.H. (2005) The Upper Valanginian (Early Cretaceous) positive carbon-isotope event recorded in terrestrial plants. *Earth and Planetary Science Letters*, **240,** 495-509.

Hasegawa, H., Tada, R., Jiang, X., Suganuma, Y., Imsamut, S., Charusiri, P., Ichinnorov, N. and Khand, Y. (2011) Drastic shrinking of the Hadley circulation during the mid-Cretaceous supergreenhouse. *Climate of the Past Discussions*, **7,** 119-151.

Hoedemaeker, P.J. and Rawson, P.F. (2000) Report on the 5th International Workshop of the Lower Cretaceous Cephalopod Team (Vienna, 5 September 2000). *Cretaceous Research*, **21,** 857-860.

Hoedemaeker, P.J. and Waldemar Herngreen, G.F. (2003) Correlation of Tethyan and Boreal Berriasian - Barremian strata with emphasis on strata in the subsurface of the Netherlands. *Cretaceous Research*, **24,** 253-275.

Jarvis, I., Lignum, J.S., Gröcke, D.R., Jenkyns, H.C. and Pearce, M.A. (2011) Black shale deposition, atmospheric CO2 drawdown, and cooling during the Cenomanian-Turonian Oceanic Anoxic Event. *Paleoceanography*, **26,** 1-17.

Jenkyns, H.C. (1980) Cretaceous anoxic events: from continents to oceans. *Journal of the Geological Society*, **137,** 171-188.

Jenkyns, H.C. (2003) Evidence for rapid climate change in the Mesozoic–Palaeogene greenhouse world. *Philosophical transactions of the Royal Society of London A*, **361,** 1885-1916.

Kübler, B. and Jaboyedoff, M. (2000) Illite crystallinity *Comptes Rendus de l'Académie des Sciences - Series IIA - Earth and Planetary Science*, **331,** 75-89.

Kuhn, O. (1996) *Der Einfluss von Verwitterung auf die Paläozeanographie zu Beginn des Kreide-Treibhausklimas (Valanginian und Hauterivian) in der West-Tethys*, Eidgenössische Technische Hochschule Zürich, 380 pp.

Kujau, A. (2012) *Climatic and environmental dynamics during the Valanginian carbon isotope event - Evidence from geochemistry and palynology*, Ruhr Universität, Bochum, 175 pp.

Kujau, A., Heimhofer, U., Ostertag-Henning, C., Gréselle, B. and Mutterlose, J. (2012) No evidence for anoxia during the Valanginian carbon isotope event - an organic-geochemical study from the Vocontian Basin, SE France. *Global and Planetary Change*, **doi: 10.1016/j.gloplacha.2012.04.007**.

Kump, L.R. and Arthur, M.A. (1999) Interpreting carbon-isotope excursions: carbonates and organic matter. *Chemical Geology,* **161,** 181-198.

Kuypers, M.M.M., Lourens, L.J., Rijpstra, W.I.C., Pancost, R.D., Nijenhuis, I.A. and Sinninghe Damst√©, J.S. (2004) Orbital forcing of organic carbon burial in the proto-North Atlantic during oceanic anoxic event 2. *Earth and Planetary Science Letters,* **228,** 465-482.

Lini, A., Weissert, H. and Erba, E. (1992) The Valanginian carbon isotope event: a first episode of greenhouse conditions during the Cretaceous. *Terra Nova,* **4,** 374-384.

Manivit, H. (1979) Les nannofossiles. In: *Hypostratotype Mésogeen de l'Etage Valanginian (Sud-Est de la France)*

(Eds R. Busnardo, J.-P. Thieuloy and M. Moullade), **6**, pp. 87-98. Les Stratotypes Français, C.N.R.S. Paris.

Mc Arthur J.M., Janssen N.M.M., Reboulet S., Leng, M.J., M.F., T. and B, V.D.S. (2007) Palaeotemperatures, polar ice-volume, and isotope stratigraphy (Mg/Ca, δ18O, δ13C, 87Sr/86Sr): The Early Cretaceous (Berriasian, Valanginian, Hauterivian). *Palaeogeography, Palaeoclimatology,Palaeoecology*, **248,** 341-430.

Morales, C., Gardin, S., Schnyder, J., Spangenberg, J., Arnaud-Vanneau, A., Arnaud, H., Adatte, T., Föllmi, K.B. (2013) Berriasian and early Valanginian environmental change along a transect from the Jura Platform to the Vocontian Basin. *Sedimentology,* **60**(1), 36-63.

Nunn, E.V., Price, G.D., Gröcke, D.R., Baraboshkin, E.Y., Leng, M.J. and Hart, M.B. (2010) The Valanginian positive carbon isotope event in Arctic Russia: Evidence from terrestrial and marine isotope records and implications for global carbon cycling. *Cretaceous Research,* **31,** 577-592.

Noël, D. and Busson, G. (1991) L'importance des schizosphères, stomiosphères, Conusphaera et Nannoconus dans la genèse des calcaires fins pélagiques du Jurassique et du Crétacé inférieur. *Sci. Géol. Bull*, **43,** 63-93.

O'Connell, S.B. (1990) Sedimentary facies and depositionnal environment of the Lower Cretaceous East Antartic margin: sites 692 and 693. In: *Proceeding of the Ocean Drilling Program, Scientific results* (Eds P.F. Barker and J.P. Kennet), **113**, pp. 71-88.

Ogg, J.G., Ogg, G. and Gradstein F.M. (2008) The Concise Geologic Time scale, pp. 177. Cambridge University press.

Patton, J.W., Choquette, P.W., Guennel, G.K., Kaltenback, A.J. and Moore, A. (1984) Organic Geochemistry and Sedimentology of Lower to Mid-Cretaceous deep-sea carbonates, sites 535 and 540, leg 77. In: *Initial reports of the Deep Sea Drilling Project, covering Leg 77 of the cruises of the drilling vessel Glomar Challenger; Ft. Lauderdale, Florida to San Juan, Puerto Rico, December 1980-February 1981* (Eds R.T. Buffler, W. Schlager, J.L. Bowdler, P.H. Cotillon, R.B. Halley, H. Kinoshita, L.B. Magoon, III, C.L. McNulty, J.W. Patton, I. Premoli Silva, O.A. Suarez, M.M. Testarmata, R.V. Tyson, D.K. Watkins and K.A. Pisciotto), **77**, pp. 417-443. Initial Reports of the Deep Sea Drilling Project.

Reboulet, S. (1995) *L'évolution des ammonites du Valanginien-Hautérivien inférieur du bassin Vocontien et de la plate-forme provençale (Sud-Est de la France):*

Relations avec la stratigraphie séquentielle et implications biostratigraphiques, Lyon, 371 pp.

Reboulet, S. and Atrops, F. (1995) Rôle du climat sur les migrationset la composition des peuplements d'ammonites du Valanginien supérieur du bassin vocontien (S-E de la France). *Geobios*, **28,** 357-365.

Reboulet, S. and Atrops, F. (1999) Comments and proposals about the Valanginian-Lower Hauterivian ammonite zonation of south-eastern France. *Eclogae Geologicae Helveticae*, **92**, 183-197.

Popp, B.N., Takigiku, R., Hayes, J.M., Louda, J.W. and Baker, E.W. (1989) The post-Paleozoic chronology and mechanism of 13C depletion in primary marine organic matter. *American Journal of Science*, **289,** 436-454.

Sinninghe Damsté, J.S. and Köster, J. (1998) A euxinic southern North Atlantic Ocean during the Cenomanian/Turonian oceanic anoxic event. *Earth and Planetary Science Letters*, **158,** 165-173.

Schlanger, S.O. and Jenkyns, H.C. (1976) Cretaceous oceanic anoxic events: causes and consequences. . *Geologie en Mijnbouw*, **55,** 179-184.

Thiede, D.S. and Vasconcelos, P.M. (2010) Paraná flood basalts: Rapid extrusion hypothesis confirmed by new 40Ar/39Ar results. *Geology*, **38,** 747-750.

Weissert, H., Lini, A., Föllmi, K.B. and Kuhn, O. (1998) Correlation of Early Cretaceous carbon isotope stratigraphy and platform drowning events: a possible link? *Palaeogeography, Palaeoclimatology, Palaeoecology*, **137,** 189-203.

Westermann, S. (2010) *Trace-element and phosphorus contents in sediments associated with Cretaceous anoxic events*, Université de Lausanne, 223 pp.

Westermann, S., Föllmi, K.B., Adatte, T., Matera, V., Schnyder, J., Fleitmann, D., Fiet, N., Ploch, I. and Duchamp-Alphonse, S. (2010) The Valanginian $\delta^{13}C$ excursion may not be an expression of a global oceanic anoxic event. *Earth and Planetary Science Letters*, **290,** 118-131.

Westermann, S., Duchamp-Alphonse, S., Fiet, N., Fleitmann, D., Matera, V., Adatte, T., and Föllmi, K.B. Paleoenvironmental changes during the Valanginian: new insights from variations in phosphorus contents and bulk- and clay mineralogies in the western Tethys. *Palaeogeography, Palaeoclimatology,Palaeoecology*, accepted.

Wilpshaar, M., Leereveld, H. and Visscher, H. (1997) Early Cretaceous sedimentary and tectonic development of the Dauphinois Basin (SE France). *Cretaceous Research*, **18,** 457-468.

Wortmann, U.G. and Weissert, H. (2000) Tying platform drowning to perturbations of the global carbon cycle with a d13COrg-curve from the Valanginian of DSDP Site 416. *Terra Nova*, **12,** 289-294.

CHAPTER 6:

CONCLUSIONS

6. CONCLUSIONS

6.1. SYNTHESIS

6.1.1 An improved stratigraphic scheme

With this project, the age control has been improved for all studied sections (except for Angles). This was possible by multiplying the biostratigraphical approaches (benthic foraminifera, calpionellids, nannofossils) and combining them with chemostratigraphy ($\delta^{13}C_{carb}$ essentially) and sequence stratigraphy. In the Jura (La Chambotte and Juracime sections), the Bourget and Calcaires Roux formations were previously dated as late Valanginian. The $\delta^{13}C$ positive shift of the Weissert episode is, however, not recorded, and therefore an early Valanginian age (*T. pertransiens*, early *B. campylotoxus*) is proposed. This highlights the diachronism of the "calcaires roux" lithology in which the $\delta^{13}C$ shift is recorded in the Lamoura and Maréchet sections (Hennig, 2003). The sequence stratigraphic scheme was correspondingly revised and a correlation with the hemipelagic section of Montclus was performed.

In the Helvetic Alps, the ages were principally assessed by ammonites found at the base of the Öhrli formation, or at the base of the Betlis Limestone and in the condensed layers of Büls and Gemsmättli (calpionellids and pollen and spores also contributed to the age control). A more detailed stratigraphic age model is proposed here, based on benthic foraminifera, calpionellids, an ammonite, $\delta^{13}C$ trends and sequence stratigraphy. This equally allows for a good correlation with the Jura area and the Vocontian basin. This also shows that benthic foraminiferal stratigraphy is a powerful tool at the scale of the NW Tethyan area.
Moreover, the hemipelagic section of Montclus has been dated by nannofossils, which allow for a good correlation with pelagic sections of the Lombardian Basin or with Atlantic DSDP and ODP sites.

Finally, the section of Wąwał was dated by boreal nannofossils and trends in the $\delta^{13}C$ record.

6.1.2. Evidence for tectonic instability and activity

The transect across the Helvetic platform permits to highlight the occurrence of block tectonic activity during the late Berriasian, leading to an emersion at the range of the tilted block, a deepening back of the range, and the deposit of a falling stage systems tract in the platform slope area. This is coherent with the generally enhanced subsidence rate known in the Helvetic area in a general context of extension of the Alpine Tethys (Stampfli and Borel, 2002; Stampfli *et al.*, 2002).

Berriasian
Valanginian
Early
Late
jacobi
occitanica
boissieri
pertransiens
campylotoxus
verrucosum
peregrinus
furcillata
145
140
(my)
Vocontian Basin
Mid-Polish Basin
Jura Platform
Helvetic Platform
PAR
kaolinite
decline in coccoliths abundance
slumps turbidites
slumps
slumps and turbidites
Wawal drill core
P(ppm)
Asteria Marls
Bourget
U. Chambotte
Guiers
L. Chambotte
Vions
P. Chatel
Purbeck Beds
fault activation?
Block tilting enhanced subsidence
Gemsmättli-Pygurus
Betlis Ls
Bulls
Vitznau Ms
Oehrli Ls
Graspass
Tros Mb
shelf
ramp
drowning
humidity
major transgressions
Climate
arid / humid / very humid
Benthic communitites and deposits:
photozoan, mesotrophic
photozoan, oligotrophic
condensation, phosphatogenesis
heterozoan

Fig. 6.1 : Sumary of the sedimentological, geochemical and mineralogical records through the Berriasian and the Valanginian for the North Tethyan margin. PAR (Phosphorus Accumulation Rates) in the Vocontian Basin after Föllmi *et al.* (2007), decline in coccoliths after Duchamp-Alphonse *et al.* (2007), sedimentary destabilisations in the Vocontian basin after Joseph *et al.* (1988) and Bulot (1995), subsidence rates in the Helvetic platform after Funk (1985) and Stampfli *et al.* (2002).

In the Jura, enhanced subsidence was probably recorded for the same time interval (sequences c and d, dated as calpionellid zones D2-D3 in the late Berriasian), and its likely expression is the presence of enhanced accommodation space in the southern Jura compared to the northern Jura.

An abrupt and important transgression is recorded in both the Helvetic and Jura platform in the latest Berriasian, close to the Berriasian-Valanginian boundary. The amplitude of the transgression is more important in the Helvetic domain, which may be related to a phase of rapid subsidence in this area, relative to the Jura realm.

6.1.3. Sea-level variations

Long-term sea-level change is reconstructed with the help of sequence stratigraphy. Sequence a (late early-early late Berriasian) is deposited in a globally transgressive context. Sequences b, c, and d (late Berriasian) document an overall regressive trend; and sequences e, f g and h (latest Berriasian – early Valanginian) show an alternation of transgressive and regressive intervals. The main condensation phase of the Weissert episode started during the TST of sequence h both in the Jura and Helvetic areas. This is mainly based on the microfacies trends analysed in the Säntis section, which is the only shallow-water carbonate section studied in this project, which records the $\delta^{13}C$ positive shift. In the Polish Basin, both the terrestrial/marine ratio of pollen and spores as well as microfacies observations support the beginning of a condensation phase in a transgressive context.

6.1.4. Climate change

Various authors already documented a progressive increase in humidity since the early Berriasian. This study highlights that a first maximum in humidity is reached in the latest Berriasian - earliest Valanginian in NW Europe, followed by more arid conditions recorded in the middle part of the early Valanginian (late *T. pertransiens*, early *B. campylotoxus* ammonite zone), and a renewed increase during the latest early - early late Valanginian (late *B. campylotoxus*, *S. verrucosum* ammonite zones). This is in line with previous studies and can be generalised for NW Europe (Hallam *et al.*, 1991; Fesneau, 2008) and in particular for the Polish Basin. The southern margin of the Tethys and the Provence, however, record reversal trends with enhanced humidity during the late *T. pertransiens* and early *B. campylotoxus* ammonite zones, and more arid conditions during the late *B. campylotoxus* and *S. verrucosum* ammonite zones. This may be explained by latitudinal migrations of climatic belts.

6.1.5. Changes in nutrient availability and ecological changes

Changes to more mesotrophic conditions are observed in the Jura during the late Berriasian (Vions Formation and Unité Supérieure Gréseuse) but they are not observed the Helvetic platform. They correspond to enhanced quartz and phosphorus content and microfacies show the proliferation of agglutinated foraminifers but remains relatively local since it could not be evidenced in the Helvetic platform and it is poorly recorded in the Vocontian Basin. This can be viewed as reflecting a stepwise increase humidity (instead of progressive) since the early Berriasian, with enhanced detrital fluxes delivered by local riverine input, and/or as reworking during transgressive intervals of sequences or parasequences.

However, through the Berriasian Valanginian boundary, an increase in nutrient is documented in the Jura and the Helvetic platforms, and in the Vocontian Basin. This corresponds to an important transgressive phase inducing reworking of continental deposits on the shelf, and to a maximum in humidity. As a result, a change in platform morphologies is observed in both the Jura and the Helvetic provinces. In the Helvetic area, this also corresponds to a subsidence phase that might be recorded in the southern Jura with less amplitude. Correspondingly, a long-term change to heterozoan carbonate production is observed in the Helvetic, and a shorter-term change is observed in the Jura.

In the Jura, photozoan carbonates persist in the early Valanginian with the Upper Member of the Chambotte Formation. Clearly and definitive heterozoan associations are observed in the Jura only with the “calcaires roux” lithologies and date of late *T. pertransiens*, early *B. campylotoxus* ammonite zones in the studied sections.

This is not the case in the Helvetic area where the platform has not been able to recover in the early Valanginian. This is explained by a less subsiding context than in the Helvetic area.

Later in the early Valanginian, the heterozoan facies spread to Western Europe with echinoderm and bryozoan-rich associations of the Betlis Limestone, and Calcaire Roux and Bourget Formations. This is interpreted as the recovery of carbonate production under relatively high nutrient levels and still rising sea-level.

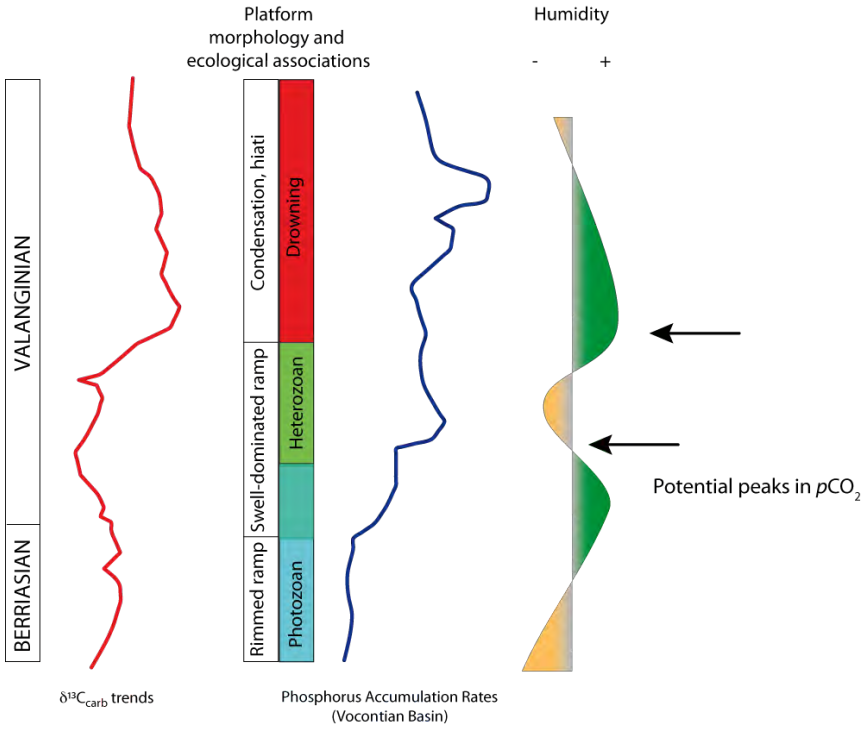

Fig. 6.2 : The Weissert episode with regards to climatic and environmental changes

The origin of nutrients in this interval remains problematic. The lighter $\delta^{18}O$ values during this interval (Mc Arthur *et al.,* 2007, this study) tends to indicate higher water temperature and thus enhanced upwellings appear unlikely. The reworking of lateritic soils during the (relative) sea-level rise has probably significantly contributed to the fertilization of the ocean waters. In parallel, the NW Tethyan margin undergoes less humid conditions during this period, which may in part explain the recovery of carbonates in this particular stressful interval.

6.1.6. Platform morphology

The platform morphology is controlled by the topography of the margin, sea level, climate, nutrient input and the ecological associations, which depend on the three preceding factors. Through the Berriasian-Valanginian the hydrolysing climate combined with an abrupt large-amplitude transgression lead to the disappearance of the barrier typical for the Berriasian photozoan platform and therefore to a change from a distally steepened ramp to a swell-dominated ramp in the Jura; and probably from a rimmed-shelf to a distally steepened ramp in the Helvetic. The disappearance of lagoonal environments involved profound changes in the distribution of continental fluxes to the ocean and influenced the sedimentary archives, in particular in terms of mineralogy, pollen and spores, and DIC and DOC fluxes.

6.1.7. Atmospheric pCO_2 as a possible trigger

With the combined record of $\delta^{13}C$ values in carbonates, predominantly terrestrial organic-matter (in the Wawal section) and mixed marine and terrestrial organic-matter (in the Angles section), the perturbation of the carbon cycle was investigated in more detail. The data show that the perturbation was already initiated during the late *T. pertransiens* ammonite zone in the organic record, with a negative shift of 1.5‰, followed by a progressive increase of 2.2‰ until the *H. trinodosum* zone. Both terrestrial and marine organic records appear to be affected. The carbon perturbation recorded in marine organic matter is interpreted as the effect of enhanced productivity in a context of enhanced nutrient input. However, these productivity effects combined with the perturbation of the carbon cycle in terrestrial organic-matter and changes in hydrolysing conditions argue for a common trigger: an increase in pCO_2. This implies that the marine $\delta^{13}C_{org}$ record probably results from enhanced productivity linked with changes in pCO_2. The difference between the $\delta^{13}C_{carb}$ and the $\delta^{13}C_{org}$ records (e.g. the $\Delta^{13}C$) indicates a two-step increase in pCO_2. The first corresponds to the general change toward heterozoan carbonate factories, and the second to the drowning of carbonate platforms.

6.2. GENERAL CONCLUSIONS AND OUTLOOK

The Valanginian Weissert episode resulted from the long-term addition of unfavourable conditions for platform growth. Enhanced humidity, nutrient availability and relative sea-level rise were responsible for the weakening of photozoan carbonate production, the loss of a barrier and the associated change in platform morphology. An increase in pCO_2 during the *T. pertransiens* ammonite zone and associated fertilization of ocean waters is viewed as the supplementary environmental change, which led to the long-term change toward heterozoan carbonate production. A second peak in pCO_2 combined with a sea-level rise in the latest early Valanginian is probably responsible for the widespread drowning of carbonate platforms.

The global carbon cycle perturbation of the Valanginian already started in the *T. pertransiens* ammonite zone as is indicated by a negative shift in $\delta^{13}C_{org}$ values.

Many interpretations given here still need further confirmation: the increase in pCO_2 during the early Valanginian has to be confirmed, for example. Stomata counting in well-preserved leafs and $\delta^{13}C_{org}$ analyses on fully marine organic-matter archives, or stable isotope analyses on well-dated pedogenic carbonates could deliver additional arguments. A complete and well-dated record of the terrestrial $\delta^{13}C_{org}$ perturbation would also be helpful.

The development of the Valanginian heterozoan platform should be better understood, and in particular the sequence stratigraphic framework of the Büls Beds in the Helvetic, and of the main condensation phase (Asteria Marls, Gemsmättli Bed) and of the upper Betlis Limestone Mb and upper Calcaires Roux Formation can also be improved, in order to better correlated these particular deposits.

The origin of the pCO_2 increase in the early Valanginian is still problematic, since the most recent analyses of the Paraña-Etendeka continental flood basalt indicate a Hauterivian age. The metamorphism of carbonaceous sediments during the onset of the inversion phase of the Alpine Tethys during the Balkan orogeny might be a possible trigger (Stämpfli and Hochard, 2009). A further point, which was not discussed here is the impact of pCO_2 changes on ocean acidification and biogenic calcification, which may eventually be traced by boron isotopes.

The generally controversial interpretation of climate dynamics in the Early Cretaceous (which type and extension of climate belts? Humid climates near the equator? Presence of polar ice caps?) constitutes a brake for our understanding of palaeoclimatic and palaeoenvironmental changes during this period. As such transects on a N/S axis by studying sections in Tunisia or Morocco together with Greenland, Russia or Sweden should be performed with an evaluation of their clay mineralogical content and a precise age control (bio and chemostratigraphy). The evolution of sea surface and deep-sea temperatures both in the Tethyan and Boreal Realms needs also a better comprehension.

References

Bulot, L.G., Thieuloy, J.-P., Arnaud, H. and Delanoy, G. (1994) The Lower Cretaceous of the South Vocontian basin and margins. *Géologie Alpine, Mémoire H:S:*, **20,** 383-400**.**

Duchamp-Alphonse, S., Gardin, S., Fiet, N., Bartolini, A., Blamart, D. and Pagel, M. (2007) Fertilization of the northwestern Tethys (Vocontian basin, SE France) during the Valanginian carbon isotope perturbation: Evidence from calcareous nannofossils and trace element data. *Palaeogeography, Palaeoclimatology, Palaeoecology*, **243,** 132-151.

Fesneau, C. (2008) *Enregistrement des changements climatiques dans le domaine Tethysien au Valanginien*, Université de Bourgogne, Dijon, 340 pp.

Föllmi, K.B., Bodin, S., Godet, A., Linder, P. and van de Schootbrugge, B. (2007) Unlocking paleo-environmental information from Early Cretaceous shelf sediments in the Helvetic Alps: stratigraphy is the key! *Swiss journal of geosciences*, **100,** 349-369.

Funk, H. (1985) Mesozoische Subsidenzgeschichte im Helvetischen Schelf der Ostschweiz. *Eclogae Geologicae Helveticae*, **78**, 249-272.

Hallam, A., Grose, J.A. and Ruffell, A.H. (1991) Palaeoclimatic significance of changes in clay mineralogy across the Jurassic-Cretaceous boundary in England and France. *Palaeogeography, Palaeoclimatology, Palaeoecology*, **81,** 173-187.

Hennig, S. (2003) *Geochemical and sedimentological evidence for environmental changes in the Valanginian (early Cretaceous) ofthe Tethys region*, ETH Zurich, 189 pp.

Joseph, P., Beaudoin, B., Sempéré, T. and Maillart, J. (1988) Vallées sous-marines et systèmes d'épandages carbonatés du Berriasien vocontien (Alpes méridionales françaises). *Bulletin de la société géologique de France*, **8,** 363-374.

Mc Arthur J.M., Janssen N.M.M., Reboulet S., Leng, M.J., M.F., T. and B, V.D.S. (2007) Palaeotemperatures, polar ice-volume, and isotope stratigraphy (Mg/Ca, δ18O, δ13C, 87Sr/86Sr): The Early Cretaceous (Berriasian, Valanginian, Hauterivian). *Palaeogeography, Palaeoclimatology,Palaeoecology*, **248,** 341-430.

Stampfli, G.M. and Borel, G.D. (2002) A plate tectonic model for the Paleozoic and Mesozoic constrained by dynamic plate boundaries and restored synthetic oceanic isochrons. *Earth and Planetary Science Letters*, **196,** 17-33.

Stampfli, G., Borel, G.D., Marchant, R. and Mosar, J. (2002) Western Alps geological constraints on western Tethyan reconstructions. In: *Reconstruction of the evolution of the Alpine-Himalayan Orogen* (Eds G. Rosenbaum and G.S. Lister), **7**, pp. 75-104. Journal of the Virtual Explorer.

Stampfli, G. and Hochard, C. (2009) Plate tectonics of the Alpine realm. In: *Ancient Orogens and Modern Analogues* (Eds J.B. Murphy, J.D. Keppie and A.J. Hynes), **327**, pp. 89-111. Geological Society, London, Special Publications, London.

ANNEXES

APPENDIX 1. ADDITIONAL DATA: THE SECTION OF CAPRIOLO

Data from the Berriasian part of the section (this work and Westermann, 2010) are compiled with data from the Valanginian part (Lini, 1992 ; Westermann, 2010)

A.1.1. Stable isotopes and phosphorus content.

PAR calculations are based on sedimentation rates provided by calpionelid zones combined with the report of ammonite zones (as explained in Westermann et al., 2010).

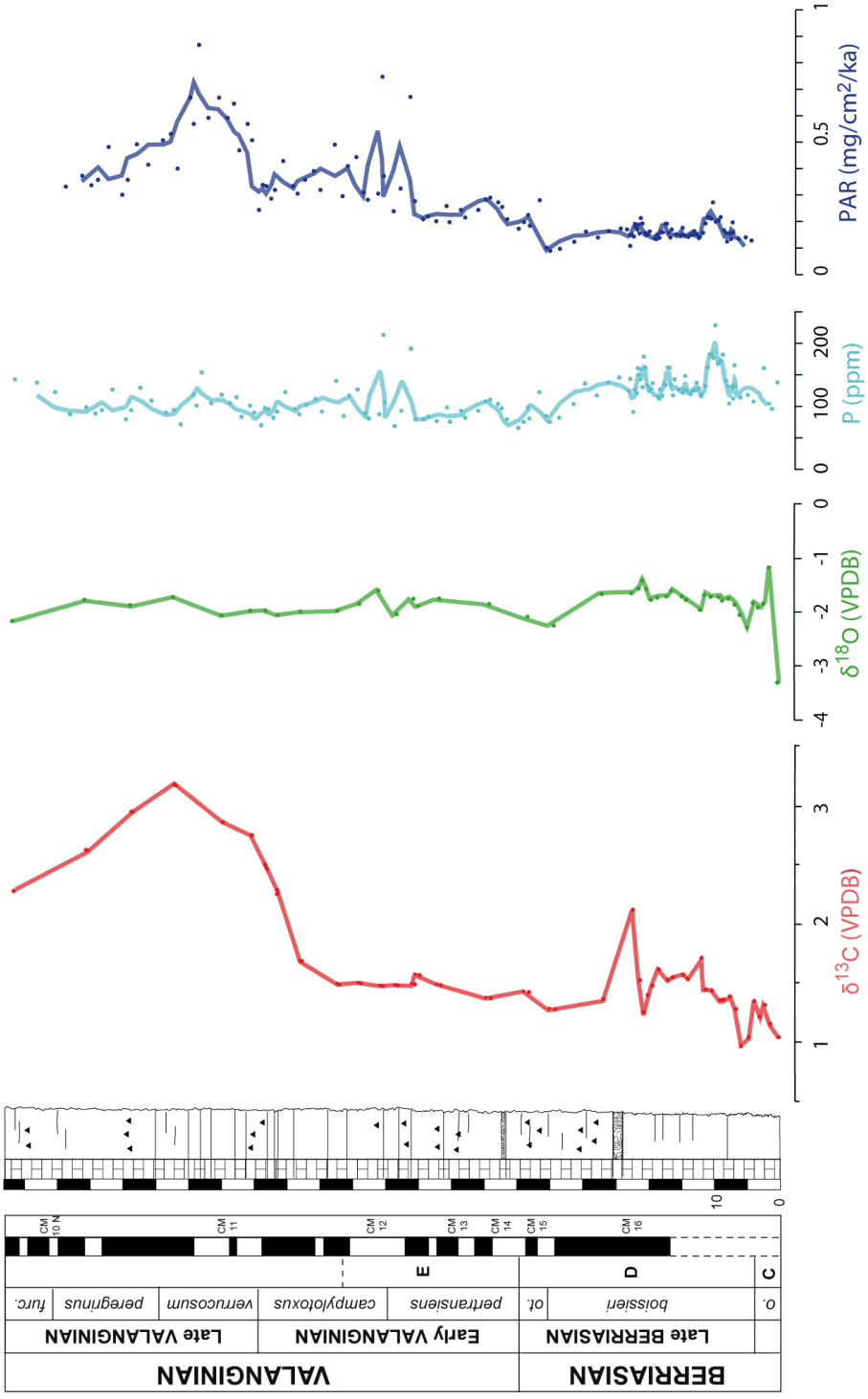

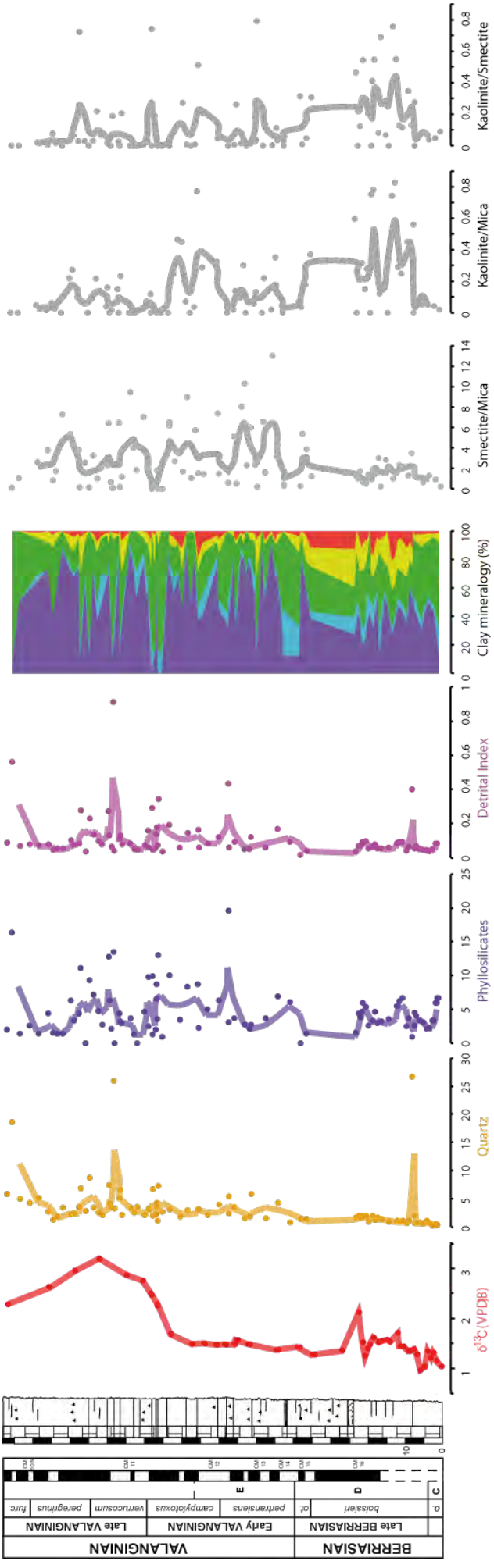
BERRIASIAN
VALANGINIAN
Late BERRIASIAN
Early VALANGINIAN
Late VALANGINIAN
C
D
E
boissieri
otopeta
pertransiens
campylotoxus
verrucosum
peregrinus
furc.
δ13C (VPDB)
Quartz
Phyllosilicates
Detrital Index
Clay mineralogy (%)
Smectite/Mica
Kaolinite/Mica
Kaolinite/Smectite

APPENDIX 2. RAW DATA

A.2.1. Inorganic stable isotope results

- Juracime and Capriolo sections

Depth (m)	Sample	d13C VPDB	d18O VPDB	Depth (m)	Sample	d13C VPDB	d18O VPDB
0.6	CBC17	1.1	-3.3	22.75	JuC1	-0.2	-3.1
1.9	CBC13	1.2	-1.2	24	JuC7	0.0	-3.0
2.7	CBC11	1.3	-1.8	25.4	JuC9	0.5	-2.1
3.55	CBC9	1.2	-1.9	26	JuC10a	0.8	-1.9
4.3	CBC7	1.4	-1.8	28	JuC13	0.8	-3.0
5.18	CBC5	1.1	-2.3	29.35	JuC14c	0.7	-4.0
6.3	CBC3	1.0	-2.1	30.9	JuC18	1.0	-3.8
7.10	CB60	1.3	-1.9	32.2	JuC19c	0.9	-4.5
8.05	CB55	1.4	-1.8	33.55	JuC20	0.7	-4.5
9.00	CB51	1.4	-1.8	34.85	JuC23b	0.6	-5.8
9.48	CB49	1.4	-1.7	36.5	JuC25c	0.4	-6.3
10.74	CB45	1.4	-1.7	37.6	JuC28	0.8	-3.4
11.68	CB42	1.5	-1.7	39	JuC30a	0.6	-6.0
12.36	CB39	1.7	-2.0	39.7	JuC31	0.7	-5.7
14.49	CB33	1.5	-1.8	41.3	JuC33	0.7	-4.0
15.13	CB30	1.6	-1.7	42.3	JuC34b	0.2	-5.5
16.70	CB26	1.6	-1.6	43	JuC34c	0.1	-4.5
17.47	CB23	1.5	-1.7	43.45	JE02	0.8	-3.9
18.83	CB18	1.6	-1.7	43.95	JE03	1.1	-3.5
19.80	CB14	1.5	-1.8	44.3	JuC37	0.5	-4.9
20.50	CB11	1.4	-1.6	44.6	JE06	0.9	-4.2
21.15	CB8	1.3	-1.4	45.6	JE10	0.7	-4.5
21.70	CB4	1.5	-1.6	46.8	JE14	0.8	-3.8
22.80	CB1	2.1	-1.7	46.95	JE15	0.8	-3.7
27.31	CA 7	1.4	-1.7	47.6	JE18	1.0	-3.7
34.6	CA 15	1.3	-2.3	47.8	JE19	0.3	-4.7
38.59	CA 25	1.4	-2.1	48.95	JE25	0.6	-4.4
				49.9	JE29	0.0	-4.0
				50.05	JE30	-0.3	-5.1

- La Chambotte section

Depth (m)	Sample	d13C VPDB	d18O VPDB	Depth (m)	Sample	d13C VPDB	d18O VPDB
1	chb1	1.8	-2.9	64.08	CH66	2.0	-2.7
2.98	chb3	1.0	-2.7	66.1	CH68	1.9	-3.4
4.85	chb5	1.7	-2.0	68.21	CH70	1.7	-3.1
7.38	chb9	1.9	-2.9	69.82	CH72	1.5	-3.2
9.21	chb11	1.7	-3.6	71.48	CH74	1.4	-5.3
9.88	chb13	1.6	-3.5	73	CH76	1.6	-3.8
11.6	chb15bis	1.4	-2.8	74.92	CH78	1.6	-3.8
15.01	chb18	0.9	-5.1	77.65	CH80	1.3	-3.8
16.19	chb20	0.6	-2.8	79.1	CH82	0.6	-2.5
17.3	chb22	0.2	-5.6	79.95	CH84	1.1	-2.9
19.15	ch1	0.1	-6.0	80.68	CH86	1.3	-3.4
20.45	ch2bis	0.0	-5.4	81.33	CH88	1.3	-3.2
22.92	CH4	0.2	-5.1	82.2	CH90	1.7	-8.6
24.9	CH6	1.7	-3.1	84.7	CH96	1.4	-3.1
26.29	CH8	1.9	-3.6	85.95	CH98	1.6	-2.8
27.45	CH10	1.1	-3.2	86.96	CH100	1.6	-2.9
28.33	CH12	1.1	-2.7	89.13	CH102	1.6	-2.5
29.8	CH14	0.8	-3.6	90.42	CH104	1.5	-3.0
30.98	CH16	1.5	-4.1	93.05	CH106	-2.4	-4.3
32.77	CH19	0.7	-2.9	95.75	CH108	2.0	-4.9
33.42	CH21	0.1	-4.4	96.95	CH110	2.0	-3.5
33.72	CH22	0.3	-3.4	99.12	CH112	1.9	-4.9
34.39	CH24	1.1	-3.1	100.7	CH114	1.8	-4.5
35.46	CH26	1.3	-2.1	101.92	CH116	2.0	-3.7
36.52	CH28	1.2	-3.7	103.8	CH118	1.8	-4.0
37.93	CH30	1.5	-4.3	106.43	CH120	1.5	-4.8
38.9	CH32	1.2	-3.4	107.3	CH122	1.6	-3.6
39.77	CH34	0.5	-3.1	109.22	CH124	1.0	-6.0
40.75	CH36	0.4	-2.8	110.94	CH126	0.6	-3.6
42.45	CH40	-0.3	-4.0	111.75	CH128	0.5	-4.1
43.79	CH42	0.1	-2.9	112.69	CH130	0.3	-3.8
44.84	CH44	1.2	-3.0	114.04	CH132	0.2	-4.2
45.32	CH46	1.3	-2.6	115.11	CH134	0.5	-3.8
48.19	CH48	1.2	-3.1	116.06	CH136	0.1	-3.7
49.62	CH50	1.3	-2.8	120.02	CH140	0.3	-4.4
51.65	CH52	0.9	-2.9	122.09	CH142	0.1	-6.5
52.75	CH54	1.2	-3.0	122.9	CH144	0.3	-4.7
54.4	CH56	1.5	-2.5	124.2	CH146	0.2	-5.5
55.62	CH58	1.8	-3.1	125.8	CH147	0.1	-6.1
57.98	CH60	1.8	-2.9	126.3	CH148	0.4	-6.2
60.82	CH62	1.6	-4.2	128.35	CH150	0.6	-5.9
62.57	CH64	1.7	-4.3				

- Montclus section

Depth (m)	Sample	d13C VPDB	d18O VPDB	Depth (m)	Sample	d13C VPDB	d18O VPDB
0.05	MA55	0.7	-1.6	48.83	MC70	0.9	-1.5
0.52	MG59	0.8	-1.5	50.05	MC75	1.1	-1.1
1.30	MG58	0.9	-1.5	51.03	MC 739	1.0	-1.4
2.27	MG57	1.1	-1.3	52.00	MC 733	1.2	-1.1
3.21	MA50	0.8	-1.7	53.14	MC 727	1.3	-1.2
3.95	MA49	0.6	-2.0	54.33	MC 721	1.3	-1.2
7.50	MA46	1.3	-1.3	55.53	MC 715	1.3	-1.0
8.25	MG51	1.2	-1.5	56.48	MC 709	1.4	-1.2
8.52	MA45	1.2	-0.9	57.43	MC 703	1.3	-1.4
9.65	MG49	1.2	-1.4	58.19	MC 697	1.3	-1.4
10.36	MA43	1.0	-1.3	58.81	MC 691	1.2	-1.3
11.46	MA41	0.9	-1.1	59.43	MC 685	1.3	-0.9
12.92	MG44	1.0	-1.4	61.03	MC 673	1.1	-1.5
13.65	MG43	1.1	-1.4	61.78	MC 667	1.3	-1.2
15.29	MA36	0.9	-1.2	62.53	MC 661	1.3	-1.4
16.05	MG41	0.9	-1.1	63.33	MC 655	1.4	-1.7
17.63	MG38	1.2	-1.3	64.43	MC 649	1.0	-2.1
18.94	MA32	1.0	-1.5	65.63	MC 643	0.9	-0.9
19.88	MA31	1.2	-1.2	67.23	MC 637	1.0	-0.9
21.80	MG32	1.3	-1.6	67.73	MC 634	1.2	-1.6
22.85	MG30	1.1	-1.5	69.01	MC 628	1.3	-2.0
24.41	MA25	0.9	-1.1	70.48	MC 622	1.2	-1.4
25.42	MG27	1.2	-1.2	71.96	MC 616	0.8	-2.1
26.20	MG26	1.1	-1.3	72.95	MC 610	0.9	-2.1
27.78	MA22	1.3	-1.4	74.85	MC604	1.1	-1.9
28.66	MA21	1.1	-1.3	76.75	MC598	1.0	-1.6
29.81	MG21	1.3	-1.3	78.80	MC592	1.0	-2.0
30.11	M20	1.5	-1.1	80.85	MC586	1.0	-2.0
30.69	M17	1.8	-1.7	82.50	MC580	0.9	-1.8
31.85	M14	1.3	-1.1	85.15	MC570	0.8	-1.6
32.32	M12	1.3	-1.4	88.55	MC560	0.8	-1.2
33.69	M6	1.1	-1.0	90.35	MC555	0.7	-2.1
34.24	M3	1.2	-1.3	92.50	MC550	0.8	-2.3
34.83	M1	1.1	-1.6	94.70	MC545	0.5	-2.3
36.15	MC1	1.2	-1.4	96.30	MC540	0.7	-1.7
36.87	MC5	1.2	-1.5	98.00	MC535	0.3	-3.0
37.97	MC10	1.2	-1.0	99.80	MC530	0.7	-1.7
38.92	MC15	1.1	-1.2	104.25	MC520	0.5	-2.2
39.95	NC20	1.3	-1.2	106.05	MC515	0.4	-2.4
41.07	NC25	1.4	-1.1	108.10	MC510	0.7	-1.9
42.10	MC30	1.1	-1.4	110.00	MC505	0.6	-2.0
42.87	NC35	1.2	-0.8	111.00	MC501	0.8	-1.8
44.10	MC40	1.0	-1.2	112.56	MVS 5	0.8	-2.3
45.60	MC45	1.0	-1.1	113.84	MVS 11	0.5	-2.4
46.34	MC50	1.1	-0.8	115.72	MVS 17	1.0	-2.2
46.86	MC55	1.1	-1.0	117.84	MVS 23	0.8	-2.3
47.65	MC60	0.9	-1.3	120.02	MVS 28	1.0	-4.5
48.34	MC65	1.0	-1.6	121.14	MVS 32	0.6	-3.9

- Säntis section

Depth (m)	Sample	d13C VPDB	d18O VPDB	Depth (m)	Sample	d13C VPDB	d18O VPDB
0.75	SA102	1.4	-3.6	63.97	SA46	1.2	-3.8
1.77	SA101	1.3	-3.7	65.02	SA45	1.2	-3.9
3.8	SA99BIS	1.3	-3.2	65.47	SA44	1.1	-4.1
5.8	SA98	1.2	-3.8	66.02	SA43	1.2	-4.1
8.1	SA96	1.3	-3.4	67.92	SA41 bis	1.2	-4.3
10	SA94	1.2	-3.8	68.02	SA41	1.2	-4.1
11.25	SA92	1.1	-3.4	68.97	SA40	1.2	-3.5
12.5	SA90	1.2	-3.4	69.97	SA39	1.4	-3.0
13.65	SA88	1.2	-3.4	70.92	SA38	1.3	-3.3
14.7	SA87	1.0	-3.7	71.92	SA37	1.3	-4.1
15.53	SA85	1.0	-3.8	71.92	SA37bis	1.3	-3.5
16.7	SA83	0.9	-4.5	74.07	SA35	1.2	-3.8
18.09	SA80	1.1	-3.4	75.07	SA34	1.3	-3.5
19.2	SA78	1.1	-3.3	76.12	SA33 tecto	1.4	-3.4
20.55	SA76	0.6	-3.7	77.07	SA32	1.3	-3.2
22.92	SA74	-1.9	-3.9	78.07	SA31	1.4	-3.7
24.4	SA72	1.3	-3.6	79.12	SA30	1.4	-3.8
25.02	SA70	1.4	-3.3	80.07	SA29	1.3	-3.9
27.06	SA62	1.6	-3.2	81.07	SA28	1.3	-4.4
30.47	I2	1.5	-3.1	81.07	SA28bis	1.2	-3.9
32.17	I3	1.4	-3.3	82.07	SA27	1.4	-4.2
33.87	I6	1.6	-3.3	83.57	SA26	1.4	-4.0
35.47	I7	1.9	-2.5	84.57	SA25	1.3	-3.8
37.77	I10	1.7	-3.2	85.57	SA24	1.4	-3.5
40.27	I12	1.7	-3.0	86.47	SA23	1.1	-3.6
43.52	I14	1.8	-3.5	87.57	SA21	1.2	-2.9
45.67	I16	1.7	-3.3	88.57	SA20	1.3	-3.6
47.32	I18	1.7	-4.0	89.57	SA19	1.2	-3.3
49.12	I21	1.8	-2.8	90.57	SA18	1.1	-3.9
49.97	I23	1.9	-3.6	91.57	SA17	1.0	-4.1
52.57	I26	1.9	-3.0	92.57	SA16	1.1	-3.5
52.97	SA60	1.3	-3.7	94.57	SA14	1.2	-3.3
53.57	SA59	1.1	-3.8	95.57	SA13	1.1	-2.9
57.12	SA56	1.0	-3.5	96.57	SA12	0.9	-4.0
58.02	SA55	0.9	-3.5	97.57	SA11	1.2	-3.0
58.67	SA54	0.8	-4.0	98.57	SA10	1.1	-3.2
58.82	SA53	1.2	-2.5	100.57	SA8	1.5	-3.4
59.62	SA52	0.9	-3.7	101.57	SA7	1.7	-3.8
59.62	SA52bis	1.0	-3.9	102.57	SA6	1.6	-3.1
60.27	SA51bis	1.1	-3.6	103.57	SA5	1.6	-3.3
60.97	SA50	1.0	-2.7	104.57	SA4	1.7	-3.1
61.27	SA49	0.9	-3.2	105.57	SA3	2.1	-3.2
62.27	SA48	1.0	-3.9	106.57	SA2	1.8	-3.7
63.17	SA47bis	1.1	-3.7	106.77	SA1	1.6	-3.1
63.27	SA47	1.2	-3.8				

- Dräckloch section

Depth (m)	Sample	d13C VPDB	d18O VPDB	Depth (m)	Sample	d13C VPDB	d18O VPDB
0.12	GAS 1	1.2	-5.5	179.72	GAS123	1.4	-2.7
6.77	GAS7	1.1	-4.5	182.56	GAS125	1.6	-2.2
11.18	GAS11	0.9	-4.5	184.10	GAS127	1.0	-2.5
14.00	GAS13	0.7	-4.3	187.00	GAS129	1.5	-2.5
19.10	GAS15	0.7	-4.7	188.82	GAS131	1.4	-2.3
22.20	GAS17	0.8	-4.3	190.15	GAS133	1.4	-2.5
26.40	GAS19	1.4	-4.2	192.25	GAS135	1.4	-2.4
29.40	GAS21	1.0	-3.7	194.90	GAS137	1.5	-2.2
31.80	GAS23	1.7	-3.3	199.20	GAS139	1.8	-2.3
33.40	GAS25	1.1	-3.5	202.35	GAS141	1.7	-2.2
34.20	GAS27	1.3	-2.9	204.90	GAS143	1.7	-2.1
34.70	GAS29	1.0	-3.4	209.60	GAS145	1.5	-2.4
37.70	GAS31	0.5	-3.9	213.80	GAS147	1.6	-2.5
40.20	GAS33	0.3	-4.5	216.60	GAS149	1.6	-2.5
41.70	GAS35	0.2	-4.5	220.48	GAS151	1.7	-2.6
45.20	GAS37	0.0	-4.4	230.48	GAS153	1.7	-3.0
47.60	GAS39	0.0	-4.3	234.20	GAS155	1.7	-2.5
48.80	GAS41	0.1	-3.8	237.60	GAS157	1.8	-3.1
50.40	GAS43	0.1	-3.5	239.80	GAS158	1.5	-3.1
53.80	GAS45	-0.5	-3.9	243.20	GAS159	1.6	-3.6
62.20	GAS48	0.7	-3.8	243.60	GAS160	1.7	-2.7
64.90	GAS50	0.3	-4.0	247.35	GAS161	1.6	-2.4
67.90	GAS52	1.2	-4.1	248.60	GAS162	1.5	-2.6
86.82	GAS58	-0.7	-5.9	251.40	GAS163	0.9	-4.0
88.56	GAS60	-0.9	-5.7	256.28	GAS166	0.6	-3.9
90.56	GAS62	1.0	-4.5	256.30	DU 1	0.7	-3.2
103.82	GAS64	0.3	-5.2	256.78	DU 3	0.5	-3.3
105.40	GAS66	0.8	-3.1	258.73	DU 5	0.5	-3.6
107.42	GAS68	1.0	-2.3	259.08	DU 7	0.6	-3.5
108.08	GAS70	1.7	-4.1	259.83	DU 8 bis	0.3	-3.6
109.70	GAS72	1.6	-3.6	259.88	DU 9	0.8	-3.0
111.65	GAS74	1.0	-3.0	260.26	DU 11	0.4	-3.5
113.45	GAS76	1.3	-3.9	261.08	DU 14	0.3	-4.1
115.45	GAS78	1.4	-3.9	262.03	DU 17	1.0	-3.4
131.65	GAS80	1.1	-3.6	262.56	DU 20	0.1	-3.8
132.60	GAS82	1.3	-3.9	263.08	DV23	0.6	-3.8
133.20	GAS101	1.3	-3.8	265.60	DV26	0.2	-3.7
137.92	GAS105	1.4	-3.4	266.08	DV29	0.7	-3.6
140.20	GAS107	1.5	-3.6	267.46	DV32	0.1	-3.8
157.00	GAS109	1.2	-2.4	269.36	DV35	0.6	-4.2
160.20	GAS111	1.2	-3.0	271.58	DV38	-0.1	-3.8
163.35	GAS113	1.4	-2.7	274.13	DV41	0.1	-4.0
167.42	GAS115	1.4	-2.9	275.83	DV44	0.3	-3.8
168.70	GAS118	1.4	-3.1	276.49	DV47	0.4	-3.5
176.01	GAS121	1.5	-2.6	276.98	DV50	0.4	-3.9
287.10	DV53	-0.1	-3.9	307.05	BE 10	1.0	-4.0
281.36	GASV1	0.5	-4.1	310.15	BE 12	0.8	-4.5
281.72	GASV2	0.2	-4.3	311.93	BE 14	0.8	-3.5
282.68	GASV3	0.1	-4.0	315.13	BE 16	0.8	-3.7
283.25	GASV4	-0.1	-4.1	316.56	BE 18	0.8	-3.8
283.75	GASV5	-0.2	-4.2	318.20	BE 20	0.8	-4.0
284.84	GASV6	0.2	-4.2	320.13	BE 22	0.8	-4.0
285.75	GASV7	0.1	-4.2	323.76	Be24	0.8	-3.7
286.85	GASV8	0.1	-4.3	325.06	BE 26	0.8	-3.7
288.08	GASV9	0.2	-4.0	331.98	BE 31	0.6	-4.0
288.72	GASV10	0.3	-3.9	335.06	BE 34	0.7	-3.8
289.80	GASV11	0.1	-4.2	337.43	BE 36	0.9	-3.6

290.33	GASV12	0.1	-4.5	339.86	BE 38	0.7	-3.6
290.98	GASV13	-0.1	-4.5	341.05	BE 40	0.7	-3.7
292.58	GASV15	-0.1	-4.6	342.85	BE 42	0.6	-3.8
295.18	GASV16	-1.1	-4.3	345.45	BE 44	0.6	-4.1
295.61	GASV17	0.0	-5.1	346.93	BE 46	0.7	-3.9
297.68	GASV18	0.3	-4.2	348.86	BE 48	0.7	-4.2
298.38	GASV19	0.3	-4.3	351.06	BE 50	0.7	-4.0
298.88	GASV20	0.2	-3.9	353.06	BE 52	0.8	-4.0
299.18	GASV21	0.3	-4.6	355.06	BE 54	0.6	-4.2
299.68	GASV22	-0.2	-5.5	358.06	BE 56	0.6	-4.6
300.53	BE 2	0.8	-4.4	360.68	Be58	1.1	-3.5
301.95	BE 4	0.9	-3.8	362.93	BE 60	0.7	-4.0
302.40	BE 5	1.1	-5.2	365.13	Be62	0.8	-3.9
302.95	BE 6	0.9	-3.9	367.93	Be 64	0.8	-4.7
304.85	BE 8	0.7	-3.7	370.23	Be 66	0.8	-4.7

- Vitznau section

Depth (m)	Sample	d13C VPDB	d18O VPDB	Depth (m)	Sample	d13C VPDB	d18O VPDB
0.05	Vz1	0.6	-4.9	25.2	Vz49	0.6	-3.9
0.64	Vz3	1.1	-4.1	25.88	Vz52	0.5	-4.4
1.18	Vz5	0.8	-4.9	26.12	Vz54	0.4	-4.1
3	Vz7	1.2	-3.4	26.9	Vz56	0.5	-4.0
4.91	Vz9	0.9	-4.0	27.42	Vz58	0.4	-3.9
5.8	Vz11	0.6	-3.5	28	Vz60	0.3	-3.7
6.6	Vz13	0.4	-3.8	28.8	Vz62	0.3	-3.6
7.1	VZ14	-0.4	-4.7	30.3	Vz64	0.5	-3.1
7.71	Vz15	1.1	-3.6	33.25	Vz68	0.2	-2.8
8.3	Vz17	1.4	-2.5	35.12	Vz70	0.2	-3.7
9	Vz19	1.3	-3.0	35.72	Vz72	0.2	-3.6
10.2	Vz21	1.2	-3.2	36.9	Vz74	0.1	-3.9
11.3	Vz23	0.8	-5.7	38.38	Vz77	0.3	-3.9
12.5	Vz25	1.2	-3.3	39.5	Vz79	0.3	-3.8
15.05	Vz27	1.2	-3.1	41.75	Vz82	-0.2	-2.7
17.25	Vz29	1.3	-2.8	44.3	Vz84	-0.1	-3.0
18.78	Vz31	1.1	-3.3	46.6	Vz86	0.4	-2.5
20	Vz33	1.3	-3.2	47.82	Vz88	-0.1	-3.3
20.72	VZ34	0.4	-4.6	48.4	Vz90	0.3	-2.6
21.8	Vz40	0.6	-3.4	49.5	Vz92	0.3	-2.5
22.15	Vz40BIS	1.4	-3.1	51.62	Vz94	-0.1	-2.7
22.4	Vz41	0.3	-3.5	52.9	Vz96	0.1	-3.2
23.04	Vz43	1.0	-3.7	54.4	Vz98	0.4	-2.7
23.75	Vz45	1.0	-3.3	56.25	Vz101	0.4	-3.4
24	VZ46	1.1	-3.2	58.35	Vb16	0.3	-3.3
24.6	Vz47	1.2	-2.9	58.6	Vb17	0.5	-3.4
24.8	VZ48	0.7	-3.7	scree	ammonite	0.2	-2.7

- Wawal section

Bulk rock

Depth (m)	Sample	d13C VPDB	d18O VPDB	Depth (m)	Sample	d13C VPDB	d18O VPDB
0.05	PIG1.1	0.0	-3.8	10.7	PIG1.110	1.4	-3.2
0.26	PIG1.4	0.4	0.1	11	PIG1.113	1.6	-3.1
1.11	PIG1.14	1.4	-1.5	11.3	PIG1.116	1.3	-3.4
1.71	PIG1.20	1.2	-1.4	11.6	PIG1.119	2.8	-0.2
2	PIG1.23	-1.7	-2.5	11.9	PIG1.122	2.4	-1.5
2.31	PIG1.26	-2.2	-3.4	12.12	PIG1.125	2.8	-1.1
2.61	PIG1.29	0.6	-1.3	12.3	PIG1.128	1.4	-1.8
3.51	PIG1.38	-2.5	-2.6	12.48	PIG1.131	2.8	-1.1
3.81	PIG1.41	1.1	-1.9	12.7	PIG1.134	2.2	-1.3
4.7	PIG1.50	-2.8	-8.0	13	PIG1.137	-2.0	-3.3
5	PIG1.53	1.5	-1.5	13.3	PIG1.140	2.3	-1.3
5.3	PIG1.56	1.2	-1.5	13.6	PIG1.143	1.7	-4.3
5.6	PIG1.59	1.5	-1.3	13.9	PIG1.146	1.8	-1.8
5.8	PIG1.61	1.5	-1.9	14.2	PIG1.149	2.7	-1.6
6.1	PIG1.64	1.4	-2.6	14.3	PIG1.150	1.8	-2.2
6.4	PIG1.67	1.4	-2.8	14.5	PIG1.152	2.7	-0.7
6.7	PIG1.70	1.9	-2.0	14.8	PIG1.155	2.6	-0.8
7	PIG1.73	1.9	-2.6	15.1	PIG1.158	2.6	-1.3
7.2	PIG1.75	2.1	-2.2	15.6	PIG1.163	2.7	-0.9
7.5	PIG1.78	2.0	-1.9	15.7	PIG1.164	2.6	-1.4
7.8	PIG1.81	1.9	-2.1	16	PIG1.167	2.1	-1.0
8.1	PIG1.84	0.7	-2.6	16.3	PIG1.170	2.5	-0.9
8.4	PIG1.87	1.0	-2.5	16.5	PIG1.172	-3.2	-4.0
8.9	PIG1.92	1.9	-1.8	16.5	PIG1.172bis	-3.9	-4.2
9.2	PIG1.95	1.9	-1.5	16.8	PIG1.175	1.0	-0.9
9.5	PIG1.98	1.4	-3.2	17	PIG1.177	-5.0	-4.6
9.8	PIG1.101	0.8	-5.4	17.1	PIG1.178	2.4	-1.3
10.1	PIG1.104	0.7	-5.5	17.3	PIG1.180	-4.7	-7.0
10.4	PIG1.107	0.8	-6.8	17.6	PIG1.183	-4.7	-3.5

Lenticulines

Depth (m)	Sample	d13C VPDB	d18O VPDB	Depth (m)	Sample	d13C VPDB	d18O VPDB
PIG1.10f	0.67	-0.1	-1.7	PIG1.85f	8.20	1.0	-0.6
PIG1.25f	2.23	-1.0	-4.5	PIG1.87f	8.40	0.8	-1.6
PIG1.33f	3.00	-0.6	-2.5	PIG1.103f	10.00	0.5	-1.1
PIG1.35f	3.21	-0.9	-2.4	PIG1.119f	11.60	1.1	-1.5
PIG1.39f	3.61	-0.5	-2.5	PIG1.121f	11.80	1.1	-1.0
PIG1.41f	3.81	-0.1	-2.1	PIG1.123f	12.00	0.9	-0.6
PIG1.43f	4.01	-0.8	-1.7	PIG1.125f	12.12	1.0	-0.4
PIG1.45f	4.20	0.3	-1.1	PIG1.127f	12.24	0.5	-0.8
PIG1.47f	4.40	-0.7	-1.3	PIG1.133f	12.60	1.3	-0.6
PIG1.49f	4.60	-0.2	-1.2	PIG1.135f	12.80	-0.9	-3.2
PIG1.51f	4.80	0.0	-1.6	PIG1.145f	13.80	1.1	-1.1
PIG1.53f	5.00	-0.4	-1.3	PIG1.147f	14.00	-1.1	-2.3
PIG1.55f	5.20	-1.0	-1.1	PIG1.149f	14.20	0.6	-1.1
PIG1.57f	5.40	-0.8	-0.7	PIG1.151f	14.40	0.8	-0.3
PIG1.59f	5.60	-0.6	-1.0	PIG1.153f	14.57	0.1	-0.7
PIG1.63f	6.00	0.1	-1.4	PIG1.155f	14.80	0.3	-0.8
PIG1.65f	6.20	0.6	-0.7	PIG1.157f	15.00	-0.2	-1.0
PIG1.67f	6.40	0.4	-1.5	PIG1.160f	15.30	-0.9	-1.6
PIG1.69f	6.60	0.1	-0.6	PIG1.163f	15.60	0.4	-0.3
PIG1.73f	7.00	0.5	-1.1	PIG1.165f	15.80	1.0	-0.9
PIG1.75f	7.20	0.5	-2.4	PIG1.167f	16.00	-0.1	-0.8
PIG1.77f	7.40	1.1	-0.5	PIG1.169f	16.20	0.0	-0.6
PIG1.79f	7.60	1.2	-0.7	PIG1.171f	16.40	-1.3	-2.0
PIG1.83f	8.00	0.8	-0.9	PIG1.173f	16.56	-2.4	-3.2

Bivalves

Depth (m)	Sample	d13C VPDB	d18O VPDB	Depth (m)	Sample	d13C VPDB	d18O VPDB
PIG 1.10b	0.67	-0.4	3.2	PIG1.101b	9.80	1.7	0.8
PIG 1.15b	1.21	1.6	-0.1	PIG1.103b	10.00	1.5	0.3
PIG 1.17b	1.41	-4.1	-4.8	PIG1.105b	10.20	2.2	0.1
PIG 1.19b	1.61	0.3	0.5	PIG1.107b	10.40	2.3	0.9
PIG 1.21b	1.81	0.8	-1.6	PIG1.109b	10.60	1.4	0.6
PIG1.23b	2.00	-0.3	-3.0	PIG1.111b	10.80	0.3	0.4
PIG 1.25b	2.23	-1.5	-2.5	PIG1.113b	11.00	2.0	-0.5
PIG 1.27b	2.41	-0.8	-0.2	PIG1.115b	11.20	1.9	0.7
PIG 1.29b	2.61	0.6	-0.2	PIG1.117b	11.40	2.0	-0.6
PIG 1.31b	2.81	1.8	-1.3	PIG1.119b	11.60	2.1	0.1
PIG 1.35b	3.21	-0.9	-1.7	PIG1.121b	11.80	2.7	-0.3
PIG 1.37b	3.41	-3.6	-2.1	PIG1.123b	12.00	1.4	0.1
PIG 1.39b	3.61	0.1	0.4	PIG1.125b	12.12	1.5	-0.2
PIG 1.41b	3.81	0.8	0.4	PIG1.127b	12.24	1.7	0.3
PIG 1.43b	4.01	0.7	0.3	PIG1.129b	12.36	2.5	0.5
PIG 1.45b	4.20	1.5	0.7	PIG1.131b	12.48	2.6	0.1
PIG 1.47b	4.40	1.4	0.4	PIG1.133b	12.60	3.3	-0.2
PIG 1.49b	4.60	2.6	0.1	PIG1.135b	12.80	1.7	-0.7
PIG 1.51b	4.80	1.1	0.0	PIG1.137b	13.00	-2.0	-3.6
PIG 1.55b	5.20	-1.6	-0.3	PIG1.139b	13.20	2.7	0.0
PIG 1.57b	5.40	0.9	0.2	PIG1.141b	13.40	3.4	0.4
PIG 1.59b	5.60	1.2	1.0	PIG1.143b	13.60	2.4	0.9
PIG 1.61b	5.80	1.3	1.3	PIG1.145b	13.80	0.9	-0.4
PIG 1.63b	6.00	1.7	1.9	PIG1.147b	14.00	1.8	0.0
PIG 1.65b	6.20	1.5	1.1	PIG1.149b	14.20	2.4	0.3
PIG 1.67b	6.40	1.8	-0.1	PIG1.151b	14.40	2.8	0.1
PIG 1.69b	6.60	2.6	-0.5	PIG1.153b	14.57	2.5	1.2
PIG 1.71b	6.80	0.9	-0.5	PIG1.155b	14.80	1.8	0.7
PIG 1.73b	7.00	2.1	0.1	PIG1.157b	15.00	2.3	0.4
PIG 1.75b	7.20	2.9	0.6	PIG1.160b	15.30	2.4	0.7
PIG 1.77b	7.40	1.3	0.3	PIG1.163b	15.60	1.8	1.5
PIG 1.79b	7.60	1.2	0.0	PIG1.165b	15.80	2.2	0.2
PIG 1.81b	7.80	1.6	0.2	PIG1.167b	16.00	1.2	-0.4
PIG 1.83b	8.00	1.5	-0.7	PIG1.169b	16.20	1.6	-0.2
PIG 1.85b	8.20	4.1	-1.8	PIG1.171b	16.40	1.9	0.0
PIG 1.87b	8.40	1.9	0.8	PIG1.173b	16.56	2.0	-0.5
PIG 1.90b	8.70	1.7	0.6	PIG1.175b	16.80	2.1	-0.1
PIG 1.93b	9.00	1.7	0.2	PIG1.177b	17.00	2.3	0.2
PIG 1.95b	9.20	2.0	1.2	PIG1.179b	17.20	2.9	0.4
PIG 1.97b	9.40	2.0	1.1	PIG1.183b	17.60	1.3	0.0
PIG 1.99b	9.60	1.8	0.9				

Ostracods

Depth (m)	Sample	d13C VPDB	d18O VPDB	Depth (m)	Sample	d13C VPDB	d18O VPDB
2.00	PIG1.23o	-3.3	-4.8	PIG1.87o	8.40	-2.2	-0.6
2.23	PIG1.25o	-1.9	-3.3	PIG1.93o	9.00	-0.3	-0.6
2.41	PIG1.27o	-4.9	-1.6	PIG1.183b	9.20	-1.3	0.7
2.61	PIG1.29o	-3.2	-2.6	PIG1.97o	9.40	-1.5	0.5
2.81	PIG1.31o	-2.8	-0.9	PIG1.99o	9.60	0.3	0.9
3.00	PIG1.33o	-2.1	-0.9	PIG1.101o	9.80	-0.5	0.5
3.21	PIG1.35o	-3.3	-2.4	PIG1.103o	10.00	-1.0	0.8
3.41	PIG1.37o	-3.8	-1.9	PIG1.107o	10.40	0.4	-0.7
3.61	PIG1.39o	-3.5	-0.7	PIG1.109o	10.60	-3.3	-1.1
3.81	PIG1.41o	-1.7	-0.2	PIG1.111o	10.80	-1.0	-0.1
4.01	PIG1.43o	-1.6	0.4	PIG1.119o	11.60	-0.6	-0.7
4.20	PIG1.45o	-2.7	0.8	PIG1.121o	11.80	-1.5	0.2
4.40	PIG1.47o	-0.7	-0.9	PIG1.125o	12.12	-1.9	-0.7
4.60	PIG1.49o	-2.2	-0.1	PIG1.127o	12.24	-2.7	-0.2
4.80	PIG1.51o	-0.2	-0.3	PIG1.131o	12.48	-2.5	-0.2
5.00	PIG1.53o	-2.8	0.0	PIG1.133o	12.60	-2.3	0.1
5.20	PIG1.55o	-0.8	-1.2	PIG1.139o	13.20	-2.6	-1.2
5.60	PIG1.59o	-2.1	0.4	PIG1.145o	13.80	-0.8	-0.2
5.80	PIG1.61o	-0.6	0.7	PIG1.147o	14.00	-2.7	-1.3
6.00	PIG1.63o	-2.2	0.2	PIG1.149o	14.20	-3.9	-0.9
6.20	PIG1.65o	-1.8	0.1	PIG1.151o	14.40	-2.8	-0.5
6.40	PIG1.67o	0.3	-0.3	PIG1.153o	14.57	-2.3	-0.4
6.60	PIG1.69o	-3.0	-0.1	PIG1.155o	14.80	-2.5	-0.2
6.80	PIG1.71o	-0.9	0.4	PIG1.157o	15.00	-1.7	-1.1
7.00	PIG1.73o	-1.5	0.6	PIG1.160o	15.30	-1.5	-1.0
7.20	PIG1.75o	-2.7	-2.0	PIG1.165o	15.80	-1.1	-0.6
7.40	PIG1.77o	-2.1	-0.2	PIG1.169o	16.20	-1.7	-0.2
7.80	PIG1.81o	-0.6	0.0	PIG1.171o	16.40	-2.4	-2.7
8.00	PIG1.83o	-2.4	-0.9	PIG1.173o	16.56	-3.7	-4.2

A.2.2. Organic stable isotope results

- Wawal section

Depth (m)	Sample	d13Corg	Depth (m)	Sample	d13Corg
0.18	PIG 1.2	-25.99	9.7	PIG 1.100	-25.57
0.2	PIG 1.3	-23.80	10.1	PIG 1.104	-25.39
0.29	PIG 1.5	-23.87	10.5	PIG 1.108	-25.34
0.5	PIG 1.8	-24.04	10.9	PIG 1.112	-25.59
0.6	PIG 1.9	-24.71	11.3	PIG 1.116	-24.85
0.92	PIG 1.12	-25.77	11.7	PIG 1.120	-24.87
1.02	PIG 1.13	-25.54	11.9	PIG 1.122	-25.58
1.31	PIG 1.16	-26.03	12.18	PIG 1.126	-25.50
1.71	PIG 1.20	-26.20	12.42	PIG 1.130	-26.07
2.1	PIG 1.24	-24.95	12.7	PIG 1.134	-25.39
2.51	PIG 1.28	-25.05	13.1	PIG 1.138	-23.28
2.91	PIG 1.32	-24.91	13.5	PIG 1.142	-25.64
3.31	PIG 1.36	-25.22	13.7	PIG 1.144	-25.08
3.71	PIG 1.40	-25.79	13.9	PIG 1.146	-25.46
4.11	PIG 1.44	-25.84	14.7	PIG 1.154	-25.14
4.5	PIG 1.48	-25.77	15.1	PIG 1.158	-24.48
4.9	PIG 1.52	-25.44	15.5	PIG 1.162	-24.83
5.3	PIG 1.56	-26.03	15.7	PIG 1.164	-24.92
5.7	PIG 1.60	-26.06	15.9	PIG 1.166	-24.82
6.1	PIG 1.64	-25.69	16.3	PIG 1.170	-25.79
6.5	PIG 1.68	-25.81	16.7	PIG 1.174	-23.18
6.9	PIG 1.72	-26.04	16.9	PIG 1.176	-25.10
7.3	PIG 1.76	-25.50	17.1	PIG 1.178	-24.64
7.7	PIG 1.80	-24.91	17.5	PIG 1.182	-24.74
8.1	PIG 1.84	-25.78	17.7	PIG 1.184	-24.59
8.5	PIG 1.88	-25.73	17.9	PIG 1.186	-24.11
8.9	PIG 1.92	-25.49	18.1	PIG 1.188	-24.12
9.3	PIG 1.96	-25.74			

- Angles section

Depth (dm)	Sample	d13Corg	Depth (dm)	Sample	d13Corg
155	96	-28.2	1436	03F51	-27.5
187	104	-28	1451	03F53	-27.3
224	123	-28.5	1465	03F56	-27.6
255	135	-28	1517	03F60	-27.2
266	139	-28.7	1523	03F61	-27.5
311	162	-28.5	1551	03F62	-27.5
349	172	-29	1575	03F63	-27
375	185	-27.8	1594	03F65	-27.1
387	188	-28.1	1637	03F66a	-27.2
434	214	-28.6	1644	03F67	-27
468	218	-28.3	1652	03F68	-27.3
501	228	-27.7	1679	03F71	-27.5
515	235	-29.2	1702	03F72	-27.5
567	251	-29.3	1717	03F73	-27.6
607	274	-29.3	1741	03F74	-27.2
620	279	-29.6	1757	03F75	-27.4
637	284	-28.5	1767	03F76	-27
685	291	-28.3	1788	03F77	-26.8
717	297	-29.4	1801	03F78	-26.9
728	304	-28.7	1820	03F79	-27.2
749	310	-28.9	1843	03F81	-27.1
776	323	-29	1865	03F82	-26.9
799	328	-29.2	1879	03F83	-27.1
815	03F31	-28.8	1896	03F84	-27.3
831	03F30	-28.9	1992	03F86	-26.86
849	03F29	-28.4	2000	03F87	-27.3
866	03F28	-28.9	2007	03F88	-27.4
881	03F27	-28.7	2017	04N26	-27.4
896	03F25	-28.8	2030	04N25	-27.1
908	03F24	-28.9	2044	04N24	-27.1
917	03F23	-28.6	2097	04N22	-27
932	03F22	-28.9	2137	04N20	-27.3
951	03F21	-28.5	2146	04N19	-26.85
967	03F20	-28.9	2159	04N18	-27.8
982	03F19	-28.6	2168	04N17	-27.4
995	03F18	-28.9	2209	04N14	-27.7
1028	03F14	-28.6	2239	03F102	-27.6
1077	03F05	-28.3	2257	03F101	-27.9
1088	03F04	-27.8	2280	03F100	-27.6
1098	03F03	-28.1	2315	03F99	-27.9
1111	03F02	-28.4	2332	03F98	-27.7
1122	03F32	-28.1	2371	03F96	-27.6
1154	03F36	-29.2	2395	03F95	-28.1
1241	03F39	-28	2414	03F94	-27.8
1272	03F40	-27.9	2431	03F93	-27.8
1308	03F42	-27.7	2451	03F92	-27.9
1328	03F45	-27.5	2469	03F91	-28.2
1352	03F47	-28.1	2489	03F90	-27.5
1403	03F50	-27.3			

A.2.3. Phosphorus content

- La Chambotte section

depth (m)	Sample	P (mg/g)	P (ppm)	depth (m)	Sample	P (mg/g)	P (ppm)
19.15	CH1	0.05	48.73	65.45	CH67	0.07	72.49
20.45	CH2	0.02	23.39	67.20	CH69	0.06	58.16
21.67	CH3	0.01	13.11	68.86	CH71	0.03	26.58
22.92	CH4	0.02	24.16	70.96	CH73	0.04	36.93
1.00	CHb1	0.03	28.19	72.65	CH75	0.04	41.94
2.98	CHb3	0.06	57.20	74.55	CH77	0.03	29.48
4.85	cHb5	0.05	48.18	75.62	CH79	0.05	50.94
5.70	CHb6	0.04	35.80	78.45	CH81	0.14	143.71
7.98	CHb9	0.03	26.17	79.60	CH83	0.12	124.46
9.21	CHb11	0.03	33.58	80.37	CH85	0.15	147.04
9.88	CHb13	0.05	51.40	80.91	CH87	0.09	86.47
11.60	CHb15bis	0.07	72.35	81.71	CH89	0.12	120.60
15.01	CHb18	0.04	40.19	82.50	CH91	0.09	92.91
16.19	CHb20	0.05	51.46	83.50	CH93	0.08	84.23
17.30	CHb22	0.04	43.58	84.35	CH95	0.12	122.21
32.39	CH18	0.07	65.18	84.95	CH97	0.13	127.61
32.77	CH19	0.07	67.90	86.51	CH99	0.09	92.82
33.25	CH20	0.07	68.28	87.40	CH101	0.06	63.53
33.42	CH21	0.10	103.01	89.92	CH103	0.12	117.64
33.72	CH21bis	0.08	79.74	92.20	CH105	0.13	127.82
34.30	CH23	0.05	49.43	94.76	CH107	0.04	44.62
34.71	CH25	0.06	60.11	96.35	CH109	0.07	67.99
35.64	CH27	0.05	47.16	98.00	CH111	0.04	36.39
37.03	CH29	0.06	61.17	99.80	CH113	0.04	40.31
38.42	CH31	0.08	82.26	101.50	CH115	0.04	43.33
39.52	CH33	0.14	137.21	101.92	CH116	0.05	54.10
40.56	CH35	0.09	93.11	103.80	CH118	0.03	25.02
40.90	CH37	0.17	167.18	106.43	CH120	0.06	61.72
41.29	CH39?	0.14	144.90	107.30	CH122	0.08	76.29
42.45	CH40?	0.12	123.88	109.22	CH124	0.05	45.96
43.09	CH41	0.18	182.74	110.94	CH126	0.13	133.63
43.79	CH42	0.09	85.36	111.75	CH128	0.17	167.71
44.60	CH43	0.11	114.48	112.69	CH130	0.20	204.34
45.08	CH45	0.13	134.40	114.04	CH132	0.19	190.40
45.32	CH46	0.12	123.42	115.11	CH134	0.17	166.11
48.19	CH48	0.15	154.73	116.06	CH136	0.16	164.25
49.62	CH50	0.10	98.82	118.10	CH137	0.15	148.83
51.65	CH52	0.11	113.61	119.21	CH139	0.21	207.74
52.75	CH54	0.12	116.49	120.02	CH140	0.21	209.85
54.40	CH56	0.07	71.39	120.92	CH141	0.23	228.98
55.62	CH58	0.06	63.93	122.40	CH143	0.20	196.12
57.98	CH60	0.05	54.31	123.50	CH145	0.23	234.47
58.75	CH60BIS	0.06	60.69	125.10	CH146BIS	0.19	192.36
59.40	CH61	0.05	53.33	126.30	CH148	0.19	189.67
61.20	CH63	0.05	46.27	128.35	CH150	0.19	193.77
63.43	CH65	0.09	93.98				

- Montclus section

Limestones

depth (m)	Sample	P (mg/g)	P (ppm)	PAR (mg/cm2/kyr)	thickness (cm) excentricity cycles	Sed. Rate (cm/kyr)
0.15	MG60	0.13	131.70	0.00		
0.52	MG59	0.11	114.19	0.63	220.00	2.20
1.30	MG58	0.15	150.45	0.83	220.00	2.20
2.27	MG57	0.13	131.83	0.73	220.00	2.20
3.52	MG56	0.14	141.00	0.49	140.00	1.40
3.77	MG55	0.14	139.82	0.49	140.00	1.40
5.80	MG54	0.18	180.33	0.54	120.00	1.20
6.60	MG53	0.12	119.42	0.36	120.00	1.20
7.26	MG52	0.14	140.31	0.38	109.00	1.09
8.25	MG51	0.15	153.19	0.50	130.00	1.30
8.76	MG50	0.16	157.85	0.51	130.00	1.30
9.65	MG49	0.15	154.54	0.61	157.00	1.57
10.02	MG48	0.15	145.77	0.57	157.00	1.57
11.11	MG47	0.18	183.56	0.83	180.00	1.80
11.70	MG46	0.17	173.87	0.78	180.00	1.80
12.00	MG45	0.26	262.36	1.18	180.00	1.80
12.92	MG44	0.16	159.95	0.52	129.00	1.29
13.65	MG43	0.16	155.31	0.50	129.00	1.29
14.20	MG42	0.17	170.16	0.60	140.00	1.40
15.29	MG41	0.13	129.68	0.48	149.00	1.49
15.80	MG40	0.17	170.54	0.64	149.00	1.49
16.25	MG39	0.18	183.22	0.68	149.00	1.49
17.63	MG38	0.15	153.20	0.49	129.00	1.29
18.38	MG37	0.19	187.39	0.47	100.00	1.00
19.22	MG36	0.13	129.48	0.50	153.00	1.53
20.11	MG35	0.13	133.03	0.51	153.00	1.53
20.70	MG34	0.13	125.95	0.55	175.00	1.75
21.06	MG33	0.18	178.10	0.78	175.00	1.75
21.80	MG32	0.18	182.30	0.80	175.00	1.75
22.28	MG31	0.17	173.69	0.74	171.00	1.71
22.85	MG30	0.18	182.67	0.78	171.00	1.71
23.71	MG29	0.14	135.88	0.58	171.00	1.71
24.60	MG28	0.17	174.56	0.45	103.00	1.03
25.42	MG27	0.15	150.60	0.38	100.00	1.00
26.20	MG26	0.14	139.41	0.45	130.00	1.30
27.31	MG25	0.14	143.10	0.34	95.00	0.95
28.02	MG24	0.12	122.74	0.29	95.00	0.95
28.55	MG23	0.15	154.84	0.31	80.00	0.80
29.10	MG22	0.12	122.29	0.29	95.00	0.95
29.81	MG21	0.14	140.70	0.33	95.00	0.95
30.11	M20	0.19	189.73	1.25	249.00	2.49
31.85	M14	0.15	149.66	0.40	249.00	2.49
32.32	M12	0.19	190.03	0.50	249.00	2.49
32.98	M9	0.19	186.18	0.49	140.00	1.40
34.24	M3	0.21	212.52	0.56	142.00	1.42
34.83	M1	0.16	164.27	0.44	142.00	1.42
36.60	MC4	1.80	1800.60	7.20	160.00	1.60
36.87	MC5	1.82	1820.02	7.28	160.00	1.60
37.02	MC6	0.26	256.50	1.03	160.00	1.60
37.35	MC7	0.16	163.40	0.65	160.00	1.60

37.75	MC9	0.18	180.40	0.72	160.00	1.60
38.10	MC11	0.20	201.20	0.80	160.00	1.60
38.37	MC12	0.25	254.72	1.08	170.00	1.70
38.77	MC14	0.19	194.86	0.83	170.00	1.70
39.12	MC16	0.15	146.57	0.62	170.00	1.70
39.45	MC18	0.17	165.37	0.70	170.00	1.70
39.80	MC19	0.21	205.14	0.87	170.00	1.70
39.95	MC20	0.21	214.31	0.86	160.00	1.60
40.40	MC22	0.25	251.24	1.00	160.00	1.60
40.90	MC24	0.18	177.56	0.71	160.00	1.60
41.17	MC26	0.17	165.20	0.66	160.00	1.60
41.34	MC27	0.20	199.42	0.80	160.00	1.60
41.80	MC29	0.16	156.72	0.68	173.00	1.73
42.10	MC30	0.20	195.12	0.84	173.00	1.73
42.50	MC32	0.26	257.13	1.11	173.00	1.73
42.67	MC34	0.21	213.95	0.93	173.00	1.73
42.87	MC35	0.28	276.43	1.20	173.00	1.73
43.15	MC36	0.18	178.06	0.47	105.00	1.05
43.35	MC37	0.18	181.29	0.48	105.00	1.05
43.50	MC38	0.19	194.45	0.51	105.00	1.05
43.75	MC39	0.22	220.50	0.58	105.00	1.05
44.10	MC40	0.20	197.88	0.52	105.00	1.05
45.25	MC43	0.22	219.44	1.26	230.00	2.30
45.60	MC45	0.21	212.90	1.22	230.00	2.30
46.00	MC47	0.16	163.88	0.94	230.00	2.30
46.20	MC49	0.23	231.71	1.33	230.00	2.30
46.42	MC51	0.22	218.28	1.26	230.00	2.30
46.86	MC55	0.27	272.79	0.82	120.00	1.20
47.10	MC57	0.21	205.28	0.62	120.00	1.20
47.45	MC59	0.18	184.69	0.55	120.00	1.20
47.78	MC61	0.19	194.47	0.58	120.00	1.20
48.05	MC63	0.22	216.98	0.57	105.00	1.05
48.34	MC65	0.20	202.97	0.53	105.00	1.05
48.45	MC67	0.25	245.88	0.65	105.00	1.05
48.55	MC68	0.21	214.69	0.56	105.00	1.05
48.65	MC69	0.24	237.73	0.62	105.00	1.05
48.83	MC70	0.19	190.12	0.50	105.00	1.05
49.25	MC71	0.16	162.04	0.89	220.00	2.20
49.80	MC73	0.24	240.83	1.32	220.00	2.20
50.05	MC75	0.26	260.96	1.44	220.00	2.20
50.30	MC76	0.20	203.01	1.12	220.00	2.20
51.43	MC736	0.43	428.33	1.95	182.00	1.82
52.48	MC730	0.21	211.29	0.96	182.00	1.82
53.14	MC727	0.16	160.33	0.73	182.00	1.82
54.33	MC721	0.15	150.55	0.60	160.00	1.60
55.53	MC715	0.19	192.01	0.79	165.00	1.65
56.48	MC709	0.16	157.04	0.65	165.00	1.65
57.43	MC703	0.13	134.62	0.45	135.00	1.35
58.19	MC697	0.15	146.27	0.41	112.00	1.12
58.81	MC691	0.13	134.23	0.38	112.00	1.12
59.43	MC685	0.19	189.68	0.55	115.00	1.15
60.24	MC679	0.13	126.37	0.35	112.00	1.12
61.03	MC673	0.14	135.10	0.38	112.00	1.12
61.38	MC670	0.16	164.30	0.41	100.00	1.00
62.13	MC664	0.13	128.02	0.32	100.00	1.00
62.81	MC658	0.25	248.14	0.62	100.00	1.00
63.33	MC655	0.32	324.86	0.81	100.00	1.00

63.93	MC652	0.16	155.08	0.43	110.00	1.10
65.16	MC646	0.18	180.30	0.59	130.00	1.30
65.63	MC643	0.14	135.33	0.44	130.00	1.30
67.23	MC637	0.26	255.54	1.18	185.00	1.85
68.28	MC631	0.22	218.54	1.22	224.00	2.24
69.82	MC625	0.20	197.08	1.10	224.00	2.24
71.09	MC619	0.16	158.00	0.97	245.00	2.45
72.45	MC613	0.27	267.54	1.54	230.00	2.30
73.90	MC607	0.15	149.80	0.86	230.00	2.30
75.80	MC601	0.17	166.06	1.06	255.00	2.55
77.85	MC595	1.88	1876.72	15.48	330.00	3.30
79.75	MC589	0.17	171.70	1.42	330.00	3.30
81.75	MC583	0.32	320.58	2.48	310.00	3.10
83.25	MC577	0.18	179.76	0.86	191.00	1.91
84.45	MC572	0.19	185.14	0.88	191.00	1.91
85.15	MC570	0.31	312.83	1.88	241.00	2.41
85.50	MC568	0.32	318.75	1.92	241.00	2.41
86.50	MC566	0.20	195.35	1.18	241.00	2.41
87.20	MC564	0.25	254.28	1.53	241.00	2.41
88.00	MC562	0.38	382.59	3.39	354.00	3.54
88.55	MC560	0.24	238.13	2.11	354.00	3.54
89.40	MC558	0.25	250.71	2.22	354.00	3.54
90.10	MC556	0.24	239.14	2.12	354.00	3.54
90.80	MC554	0.26	260.19	2.30	354.00	3.54
91.20	MC553	0.26	256.92	1.43	222.00	2.22
92.15	MC551	0.28	284.89	1.58	222.00	2.22
93.10	MC549	0.30	298.92	1.66	222.00	2.22
94.40	MC546	0.30	297.08	2.01	270.00	2.70
95.00	MC544	0.26	258.48	1.74	270.00	2.70
95.70	MC542	0.23	228.52	1.54	270.00	2.70
96.30	MC540	0.20	196.28	1.69	345.00	3.45
97.00	MC538	0.23	233.58	2.01	345.00	3.45
98.30	MC534	0.29	285.39	2.46	345.00	3.45
103.40	MC522	0.29	287.45	2.65	369.00	3.69
105.60	MC516	0.26	263.31	2.43	369.00	3.69
108.10	MC510	0.25	254.74	1.90	298.00	2.98
110.38	MC504	0.50	501.92	4.25	339.00	3.39
111.00	MC501	0.27	268.79	2.28	339.00	3.39
111.94	Mvs3	0.21	211.63	1.79	339.00	3.39
112.56	Mvs5	0.26	256.45	1.40	218.00	2.18
115.72	Mvs17	0.20	199.43	1.51	302.00	3.02
117.84	Mvs23	0.23	233.95	1.86	318.00	3.18
118.84	Mvs25	0.17	173.52	1.38	318.00	3.18

Marls

depth (m)	Sample	P (mg/g)	P (ppm)	PAR (mg/cm2/kyr)	thickness (cm) excentricity cycles	Sed. Rate (cm/kyr)
0.05	MA55	0.24	242.06			
0.32	MA54	0.22	216.69			
1.05	MA53	0.26	256.15	1.30	220.00	2.20
1.98	MA52	0.27	272.26	1.38	220.00	2.20
2.80	MA51	0.26	261.54	0.84	140.00	1.40
3.21	MA50	0.30	304.42	0.98	140.00	1.40
3.95	MA49	0.33	328.51	1.28	169.00	1.69
6.30	MA48	0.28	280.41	0.77	120.00	1.20
7.14	Ma47	1.78	1781.05	4.47	109.00	1.09

7.50	MA46	0.28	282.36	0.71	109.00	1.09
8.52	MA45	0.23	230.99	0.69	130.00	1.30
9.45	MA44	0.35	352.44	1.27	157.00	1.57
10.36	MA43	0.35	353.59	1.28	157.00	1.57
10.79	MA42	0.40	403.58	1.67	180.00	1.80
11.46	MA41	0.41	414.11	1.71	180.00	1.80
12.11	MA40	0.20	204.76	0.85	180.00	1.80
13.02	MA39	0.39	392.94	1.17	129.00	1.29
13.90	MA38	0.25	249.50	0.80	140.00	1.40
15.52	MA37	0.28	279.08	0.96	149.00	1.49
16.05	MA36	0.38	383.09	1.31	149.00	1.49
16.35	MA35	0.29	286.84	0.98	149.00	1.49
17.60	MA34	0.36	358.84	1.06	129.00	1.29
18.51	MA33	0.31	305.45	0.70	100.00	1.00
18.94	MA32	0.55	549.60	1.93	153.00	1.53
19.88	MA31	0.39	389.88	1.37	153.00	1.53
20.47	MA30	0.35	347.85	1.40	175.00	1.75
21.29	MA29	0.37	367.56	1.48	175.00	1.75
23.07	MA28	0.55	549.20	2.16	171.00	1.71
23.48	MA26	0.43	432.73	1.70	171.00	1.71
24.41	MA25	0.36	360.08	0.85	103.00	1.03
25.00	MA24	0.27	273.04	0.63	100.00	1.00
26.00	MA23	0.27	273.98	0.82	130.00	1.30
27.78	MA22	0.30	299.60	0.65	95.00	0.95
28.66	MA21	0.35	352.44	0.65	80.00	0.80
30.69	M17	0.23	229.75	1.51	249.00	2.49
33.69	M6	0.31	310.69	0.83	140.00	1.40
36.45	MC3	0.23	231.25	0.85	160.00	1.60
37.50	MC8	0.32	324.50	1.19	160.00	1.60
37.97	MC10	0.04	35.12	0.13	160.00	1.60
38.50	MC13	0.25	253.49	0.99	170.00	1.70
38.92	MC15	0.32	317.14	1.24	170.00	1.70
39.22	MC17	0.24	238.68	0.93	170.00	1.70
40.20	MC21	0.23	228.81	0.84	160.00	1.60
40.70	MC23	0.27	266.94	0.98	160.00	1.60
41.07	MC25	0.23	234.26	0.86	160.00	1.60
41.55	MC28	0.25	253.95	1.01	173.00	1.73
42.23	MC31	0.32	324.14	1.29	173.00	1.73
42.59	MC33	0.26	263.92	1.05	173.00	1.73
44.70	MC41	0.20	200.02	1.06	230.00	2.30
45.10	MC42	0.30	302.02	1.60	230.00	2.30
45.37	MC44	0.25	248.30	1.31	230.00	2.30
45.80	MC46	0.29	289.72	1.53	230.00	2.30
46.11	MC48	0.30	297.36	1.57	230.00	2.30
46.34	MC50	0.26	255.73	1.35	230.00	2.30
46.55	MC52	0.33	329.14	0.91	120.00	1.20
46.76	MC54	0.30	296.59	0.82	120.00	1.20
46.98	MC56	0.40	397.27	1.10	120.00	1.20
47.25	MC58	0.49	489.13	1.35	120.00	1.20
47.65	MC60	0.42	424.52	1.17	120.00	1.20
47.90	MC62	0.30	303.30	0.73	105.00	1.05
48.40	MC66	0.42	417.55	1.01	105.00	1.05
49.55	MC72	0.30	303.00	1.53	220.00	2.20
49.95	MC74	0.29	293.33	1.48	220.00	2.20
50.45	MC77	0.23	234.39	1.19	220.00	2.20
50.75	MC79	0.21	208.40	1.05	220.00	2.20
51.03	MC739	0.24	244.44	1.02	182.00	1.82

52.00	MC733	0.25	250.30	1.05	182.00	1.82
53.83	MC724	0.23	227.26	0.95	182.00	1.82
55.08	MC718	0.32	316.31	1.20	165.00	1.65
56.05	MC712	0.26	257.03	0.98	165.00	1.65
56.96	MC706	0.24	240.46	0.75	135.00	1.35
57.73	MC700	0.27	266.19	0.83	135.00	1.35
58.51	MC694	0.27	271.69	0.70	112.00	1.12
59.13	MC688	0.28	283.53	0.75	115.00	1.15
59.81	MC682	0.36	355.18	0.94	115.00	1.15
60.73	MC676	0.35	345.28	0.89	112.00	1.12
61.78	MC667	0.30	298.81	0.69	100.00	1.00
62.53	MC661	0.33	332.78	0.77	100.00	1.00
64.43	MC649	0.33	332.13	0.99	130.00	1.30
66.33	MC640	0.37	367.50	1.56	185.00	1.85
67.73	MC634	0.48	477.29	2.46	224.00	2.24
69.01	MC628	0.66	658.25	3.39	224.00	2.24
70.48	MC622	0.69	690.79	3.89	245.00	2.45
71.96	MC616	0.44	438.06	2.47	245.00	2.45
72.95	MC610	0.40	397.75	2.10	230.00	2.30
74.85	MC604	0.55	553.04	3.24	255.00	2.55
76.75	MC598	0.52	515.71	3.91	330.00	3.30
78.80	MC592	0.62	618.58	4.70	330.00	3.30
80.85	MC586	0.41	410.28	2.93	310.00	3.10
82.50	MC580	0.28	279.54	1.99	310.00	3.10
83.90	MC574	0.50	497.69	2.19	191.00	1.91
84.95	MC571	0.47	470.52	2.61	241.00	2.41
85.40	MC569	0.36	363.10	2.01	241.00	2.41
86.00	MC567	0.61	611.49	3.39	241.00	2.41
86.95	MC565	0.51	514.99	2.85	241.00	2.41
87.55	MC563	0.46	455.50	3.71	354.00	3.54
88.25	MC561	0.33	334.37	2.72	354.00	3.54
89.00	MC559	0.22	219.63	1.79	354.00	3.54
89.77	MC557	0.46	457.47	3.72	354.00	3.54
90.35	MC555	0.44	442.72	3.60	354.00	3.54
91.80	MC552	0.24	243.83	1.25	222.00	2.22
92.50	MC550	0.42	418.49	2.14	222.00	2.22
93.55	MC548	0.64	637.36	3.96	270.00	2.70
94.70	MC545	0.42	415.62	2.58	270.00	2.70
95.40	MC543	0.36	356.68	2.21	270.00	2.70
96.10	MC541	0.29	285.41	2.26	345.00	3.45
96.55	MC539	0.37	374.67	2.97	345.00	3.45
97.20	MC537	0.29	287.44	2.28	345.00	3.45
99.45	MC531	0.35	353.25	2.21	272.00	2.72
102.40	MC525	0.40	403.20	3.42	369.00	3.69
104.50	MC519	0.33	325.16	2.76	369.00	3.69
107.00	MC513	0.43	426.92	2.93	298.00	2.98
108.80	MC507	0.38	381.09	2.97	339.00	3.39
113.10	Mvs8	0.45	445.16	2.23	218.00	2.18
113.84	Mvs11	0.27	273.86	1.37	218.00	2.18
114.91	Mvs14	0.26	260.75	1.81	302.00	3.02
116.69	Mvs20	0.46	462.25	3.21	302.00	3.02
120.02	Mvs28	0.32	322.13	2.36	318.00	3.18
120.54	Mvs30	0.32	319.58			
121.14	Mvs32	0.27	270.62			

-

- Säntis section

depth (m)	Sample	P (mg/g)	P (ppm)	depth (m)	Sample	P (mg/g)	P (ppm)
3.80	SA99BIS	0.06	59.40	36.12	I8	0.03	33.42
4.80	SA99	0.06	61.13	36.77	I9	0.06	60.95
5.80	SA98	0.06	56.52	37.77	I10	0.04	37.35
6.80	SA97	0.06	57.70	38.97	I11	0.06	55.05
8.10	SA96	0.06	64.51	40.27	I12	0.07	66.84
8.80	SA95	0.06	55.49	41.52	I13	0.07	74.71
10.00	SA94	0.06	62.30	43.52	I14	0.06	57.01
10.70	SA93	0.06	61.72	44.27	I15	0.06	60.95
11.25	SA92	0.05	50.80	45.67	I16	0.05	49.15
11.60	SA91	0.07	69.16	46.67	I17	0.05	47.18
12.50	SA90	0.05	54.15	47.32	I18	0.04	37.35
13.20	SA89	0.06	59.22	47.97	I19	0.08	84.54
13.65	SA88	0.06	59.66	48.57	I20	0.08	80.60
14.30	SA87BIS	0.04	37.84	49.12	I21	0.05	45.22
14.70	SA87	0.05	47.12	49.47	I22	0.04	35.39
14.95	SA86	0.05	51.94	49.97	I23	0.02	21.63
15.53	SA85	0.05	52.46	50.57	I24	0.04	37.35
16.37	SA84	0.05	51.52	51.82	I25	0.04	39.32
16.70	SA83	0.05	49.50	52.57	I26	0.06	55.05
17.62	SA81	0.06	55.28	52.97	SA60	0.58	583.16
18.09	SA80	0.06	62.17	53.57	SA59	0.27	269.97
18.75	SA79	0.05	46.22	56.57	SA57	0.22	223.14
19.20	SA78	0.07	68.96	57.12	SA56	0.24	238.53
20.25	SA77	0.88	875.58	58.02	SA55	0.15	153.71
20.55	SA76	0.06	61.44	58.67	SA54	0.17	174.17
21.53	SA75	0.05	51.47	58.82	SA53	0.26	262.35
22.92	SA74	0.04	42.75	59.62	SA52	0.14	143.87
24.00	SA73	0.04	38.57	59.62	SA52	0.32	315.96
24.40	SA72	0.05	48.58	60.27	SA51	0.18	176.54
24.72	SA71	0.06	60.54	60.27	SA51	0.23	233.99
25.02	SA70	0.04	42.34	60.97	SA50	0.16	155.59
25.33	SA69	0.04	42.20	61.27	SA49	0.15	151.34
25.61	SA68	0.03	34.13	62.27	SA48	0.06	59.16
25.86	SA66	0.05	47.66	63.17	SA47bis	0.05	53.59
26.10	SA65	0.06	56.03	63.27	SA47	0.04	38.39
26.58	SA64	0.04	36.28	63.97	SA46	0.04	38.06
27.06	SA62	0.06	61.35	65.02	SA45	0.04	35.78
28.05	SA61bis	0.07	74.28	66.02	SA43	0.09	88.53
28.32	SA61	0.05	53.38	66.97	SA42	0.11	109.52
30.47	I2	0.06	60.95	67.92	SA41bis	0.04	35.03
32.17	I3	0.05	47.18	68.02	SA41	0.11	108.33
33.07	I4	0.07	72.74	68.97	SA40	0.11	109.62
33.27	I5	0.98	981.02	69.97	SA39	0.10	100.27
33.87	I6	0.02	21.63	70.92	SA38	0.12	116.74
35.47	I7	0.07	66.84	72.82	SA36bis	0.09	88.70
72.92	SA36	0.09	86.53	90.57	SA18	0.14	144.66
74.07	SA35	0.06	64.41	91.57	SA17	0.10	98.76
75.07	SA34	0.07	69.53	92.57	SA16	0.15	148.04
76.12	SA33 tecto	0.08	78.55	93.57	SA15	0.10	102.03
77.07	SA32	0.07	70.34	94.57	SA14	0.16	157.86
78.07	SA31	0.07	70.26	95.57	SA13	0.15	151.21
79.12	SA30	0.08	79.23	96.57	SA12	0.23	230.43
80.07	SA29	0.06	64.14	97.57	SA11	0.21	213.32
81.07	SA28	0.06	56.97	98.57	SA10	0.22	224.58
81.07	SA28	0.03	30.36	99.57	SA9	0.36	364.99
82.07	SA27	0.08	76.27	100.57	SA8	0.17	168.30
83.57	SA26	0.07	74.79	101.57	SA7	0.12	115.61
84.57	SA25	0.07	73.15	102.57	SA6	0.23	233.07
85.57	SA24	0.08	83.84	103.57	SA5	1.91	1908.90

86.47	SA23	0.07	74.09	104.57	SA4	0.38	383.03
86.67	SA22	0.16	162.98	105.57	SA3	0.34	338.00
88.57	SA20	0.10	100.33	106.57	SA2	3.70	3703.37
89.57	SA19	0.09	91.78	106.77	SA1	0.02	20.69

- Dräckloch section

depth (m)	Sample	P (mg/g)	P (ppm)	depth (m)	Sample	P (mg/g)	P (ppm)
0.12	GAS1	0.16	159.17	165.87	GAS118	0.10	95.38
2	GAS3	0.19	187.81	167.15	GAS121	0.07	68.25
4.42	GAS5	0.22	217.60	174.46	GAS123	0.08	75.32
6.77	GAS7	0.18	178.54	178.17	GAS125	0.18	183.55
11.18	GAS11	0.07	67.65	181.01	GAS127	0.08	75.32
14	GAS13	0.09	93.17	182.55	GAS129	0.09	92.98
19.1	GAS15	0.14	144.32	185.45	GAS131	0.08	78.54
22.2	GAS17	0.05	47.05	187.27	GAS133	0.03	32.64
26.4	GAS19	0.11	108.90	188.60	GAS135	0.04	43.05
29.4	GAS21	0.10	101.14	190.70	GAS137	0.04	38.95
31.8	GAS23	0.15	151.23	193.35	GAS139	0.04	42.88
33.4	GAS25	0.17	170.15	197.65	GAS141	0.07	67.57
34.2	GAS27	0.13	130.13	200.80	GAS143	0.08	76.48
34.7	GAS29	0.13	134.47	203.35	GAS145	0.10	100.46
37.7	GAS31	0.11	110.25	208.05	GAS147	0.06	64.88
40.2	GAS33	0.04	41.00	212.25	GAS149	0.08	80.86
41.7	GAS35	0.06	62.90	215.05	GAS151	0.10	96.06
45.2	GAS37	0.04	42.71	218.93	GAS153	0.04	36.20
47.6	GAS39	0.08	78.43	228.93	GAS155	0.05	54.36
48.8	GAS41	0.08	83.71	232.65	GAS157	0.04	39.21
50.4	GAS43	0.22	221.64	236.05	GAS158	0.06	59.52
53.8	GAS45	0.07	65.55	238.25	GAS159	0.04	39.67
62.2	GAS48	0.15	147.15	241.65	GAS160	0.07	74.02
64.9	GAS50	0.14	139.29	242.05	GAS161	0.07	68.64
67.9	GAS52	0.10	102.00	245.80	GAS162	0.06	57.46
86.82	GAS58	0.35	345.11	247.05	GAS163	0.03	27.29
88.56	GAS60	0.50	504.81	249.85	GAS165	0.02	23.05
90.56	GAS62	0.19	188.68	254.73	GAS166	0.03	25.97
103.82	GAS64	0.26	257.59	256.45	DV1	0.15	154.68
105.4	GAS66	0.37	370.82	256.93	DV3	0.08	80.95
107.42	GAS68	0.46	462.67	258.88	DV5	0.06	62.50
108.08	GAS70	0.10	104.53	259.23	DV7	0.06	55.18
109.7	GAS72	0.31	305.74	260.03	DV9	0.22	221.87
111.65	GAS74	0.27	269.85	260.41	DV11	0.16	158.83
113.45	GAS76	0.21	213.56	262.18	DV17	0.19	193.05
115.45	GAS78	0.34	341.73	262.71	DV20	0.12	117.68
131.65	GAS80	0.13	127.73	263.23	DV23	0.55	548.47
131.65	GAS101	0.08	75.74	265.75	DV26	0.16	164.09
132.6	GAS82	0.17	169.75	266.23	DV29	0.11	114.33
134.62	GAS105	0.10	99.45	267.61	DV32	0.19	191.39
136.37	GAS107	0.07	69.49	269.51	DV35	0.37	371.07
138.65	GAS109	0.07	71.34	271.73	DV38	0.00	3.74
155.45	GAS111	0.10	96.89	274.28	DV14	0.21	212.03
158.65	GAS113	0.06	62.29	275.98	DV44	0.16	157.14
161.8	GAS115	0.09	93.40	276.64	DV47	0.45	451.69
277.13	DV50	0.13	126.19	320.00	Be8	0.09	92.58
281.51	GASV1	0.25	253.07	322.20	Be10	0.09	87.71
281.87	GASV2	0.22	216.41	325.30	Be12	0.05	45.79
282.83	GASV3	0.23	228.82	327.08	Be14	0.19	193.10
283.4	GASV4	0.28	284.96	330.28	Be16	0.08	82.95
283.9	GASV5	0.19	191.39	331.71	Be18	0.10	103.38

284.99	GASV6	0.52	522.34	335.28	Be22	0.10	98.40
285.9	GASV7	0.18	183.81	338.91	Be24	0.08	84.61
287	GASV8	0.15	151.23	340.21	Be26	0.07	68.36
287.25	DV53	0.35	352.29	347.13	Be31	0.10	104.99
288.23	GASV9	0.12	116.85	350.21	Be34	0.07	70.58
288.87	GASV10	0.55	553.36	352.58	Be36	0.07	66.53
289.95	GASV11	0.19	186.94	355.01	Be38	0.08	84.10
290.48	GASV12	0.26	257.86	356.20	Be40	0.07	66.67
291.13	GASV13	0.14	135.38	358.00	Be42	0.09	85.22
292.13	GASV14	0.20	199.85	360.60	Be44	0.12	124.26
292.73	GASV15	0.01	14.58	362.08	Be46	0.07	68.15
295.33	GASV16	0.36	356.50	364.01	Be48	0.16	163.27
295.76	GASV17	0.34	339.90	366.21	Be50	0.18	177.88
297.83	GASV18	0.28	278.16	370.21	Be54	0.21	210.94
298.53	GASV19	0.32	318.61	373.21	Be56	0.15	146.41
299.03	GASV20	0.18	178.08	375.83	Be58	0.16	157.85
299.33	GASV21	0.21	209.42	378.08	Be60	0.17	167.41
299.83	GASV22	0.23	234.38	380.28	Be62	0.38	383.55
315.68	Be2	0.10	103.16	383.08	Be64	0.22	224.34
317.1	Be4	0.09	92.74	385.38	Be66	2.25	2249.31
318.1	Be6	0.08	82.59				

- Vitznau section

depth (m)	Sample	P (mg/g)	P (ppm)	depth (m)	Sample	P (mg/g)	P (ppm)
0.05	Vz1	0.25	254.30	26.12	Vz54	0.14	141.03
0.64	Vz3	0.22	218.03	26.9	Vz56	1.15	1152.21
1.18	Vz5	0.21	213.67	27.42	Vz58	0.12	116.73
3	Vz7	0.22	222.95	28	Vz60	0.16	163.23
4.91	Vz9	0.17	171.51	28.8	Vz62	0.13	134.02
5.8	Vz11	0.31	305.74	30.3	Vz64	0.37	365.53
6.6	Vz13	0.29	290.82	32.3	Vz66	0.17	165.86
7.71	Vz15	0.10	101.26	33.25	Vz68	0.32	321.78
8.3	Vz17	0.31	310.55	35.12	Vz70	0.13	128.28
9	Vz19	0.46	456.53	35.72	Vz72	0.13	126.87
10.2	Vz21	0.16	160.83	36.9	Vz74	0.17	170.03
11.3	Vz23	0.05	54.56	38.38	Vz77	0.42	416.71
12.5	Vz25	0.28	278.85	39.5	Vz79	0.34	335.74
15.05	Vz27	0.15	152.64	41.75	Vz82	0.36	355.96
17.25	Vz29	0.09	89.32	45.3	Vz85	0.25	248.04
18.78	Vz31	0.06	63.50	47.82	Vz88	0.27	265.11
20	Vz33	0.10	103.49	49.12	Vz91	0.27	265.51
21.8	Vz40	0.07	71.65	51.12	Vz93	0.25	248.53
22.4	Vz41	0.10	99.71	52.5	Vz95	0.63	625.10
23.04	Vz43	0.07	68.63	53.9	Vz97	0.18	183.32
23.75	Vz45	0.09	86.27	54.95	Vz99	0.16	155.24
24.6	Vz47	0.12	124.14	56.25	Vz101	0.25	249.52
25.2	Vz49	0.37	370.43	58.35	Vb16	0.16	161.36
25.88	Vz52	0.37	365.48	58.6	Vb17	0.23	225.63

- Wawal section

depth (m)	Sample	P (mg/g)	P (ppm)	depth (m)	Sample	P (mg/g)	P (ppm)
0.05	PIG 1.1	0.13	134.57	8.70	PIG 1.90	0.15	147.49
0.26	PIG 1.4	0.91	908.09	8.90	PIG 1.92	0.13	134.91
0.32	PIG 1.6	4.58	4578.75	9.10	PIG 1.94	0.17	169.26
0.44	PIG 1.7	0.78	784.36	9.3	PIG 1.96	0.14	141.32
0.5	PIG 1.8	0.92	920.26	9.5	PIG 1.98	0.14	138.70
0.67	PIG 1.10	1.47	1466.33	9.7	PIG 1.100	0.13	129.32
0.92	PIG 1.12	0.32	323.45	9.9	PIG 1.102	0.12	123.77
1.11	PIG 1.14	0.24	243.32	10.1	PIG 1.104	0.37	373.37
1.31	PIG 1.16	0.30	300.53	10.3	PIG 1.106	0.14	135.32
1.51	PIG 1.18	0.47	467.55	10.5	PIG 1.108	0.16	159.06
1.71	PIG 1.20	0.81	810.38	10.7	PIG 1.110	0.18	182.82
1.91	PIG 1.22	1.52	1517.46	10.9	PIG 1.112	0.27	266.62
2.11	PIG 1.24	0.75	747.87	11.1	PIG 1.114	0.16	160.68
2.31	PIG 1.26	1.52	1517.15	11.3	PIG 1.116	0.14	143.34
2.51	PIG 1.28	1.91	1908.37	11.5	PIG 1.118	0.14	141.60
2.71	PIG 1.30	0.68	682.33	11.7	PIG 1.120	0.10	101.07
2.91	PIG 1.32	0.52	523.67	11.9	PIG 1.122	0.12	124.39
3.11	PIG 1.34	0.34	344.86	12.06	PIG 1.124	0.10	97.48
3.31	PIG 1.36	0.36	363.24	12.18	PIG 1.126	0.11	111.00
3.51	PIG 1.38	0.74	742.72	12.3	PIG 1.128	0.11	105.43
3.71	PIG 1.40	0.29	286.19	12.42	PIG 1.130	0.10	95.47
3.91	PIG 1.42	0.17	167.69	12.54	PIG 1.132	0.09	90.15
4.11	PIG 1.44	0.16	155.35	12.70	PIG 1.134	0.73	725.35
4.30	PIG 1.46	0.20	204.38	12.90	PIG 1.136	0.11	108.52
4.50	PIG 1.48	0.28	283.98	13.10	PIG 1.138	0.11	109.93
4.70	PIG 1.50	0.26	263.62	13.30	PIG 1.140	0.13	126.33
4.90	PIG 1.52	0.24	237.80	13.50	PIG 1.142	0.11	109.49
5.10	PIG 1.54	0.18	180.66	13.70	PIG 1.144	0.16	159.26
5.30	PIG 1.56	0.19	187.87	13.90	PIG 1.146	0.12	118.73
5.50	PIG 1.58	0.21	205.20	14.10	PIG 1.148	0.16	157.59
5.70	PIG 1.60	0.22	224.38	14.30	PIG 1.150	0.12	122.68
5.90	PIG 1.62	0.18	180.66	14.50	PIG 1.152	0.12	118.67
6.10	PIG 1.64	0.17	167.97	14.70	PIG 1.154	0.13	128.79
6.30	PIG 1.66	0.60	603.04	14.90	PIG 1.156	0.12	124.64
6.50	PIG 1.68	0.16	155.03	15.10	PIG 1.158	0.12	116.42
6.70	PIG 1.70	0.16	159.71	15.30	PIG 1.160	0.15	147.78
6.90	PIG 1.72	0.18	175.38	15.50	PIG 1.162	0.15	145.05
7.10	PIG 1.74	0.17	170.75	15.70	PIG 1.164	0.18	181.70
7.30	PIG 1.76	0.18	175.52	15.90	PIG 1.166	0.14	142.55
7.50	PIG 1.78	0.19	186.49	16.10	PIG 1.168	0.14	141.32
7.70	PIG 1.80	0.15	147.93	16.30	PIG 1.170	0.15	152.21
7.90	PIG 1.82	0.17	165.31	16.50	PIG 1.172 bis	0.56	559.68
8.10	PIG 1.84	0.15	152.40	16.50	PIG 1.172	0.35	354.27
8.30	PIG 1.86	0.14	139.31	16.70	PIG 1.174	0.21	213.32
8.50	PIG 1.88	0.14	140.97	16.90	PIG 1.176	0.21	210.65
17.10	PIG 1.178	0.23	234.16	17.70	PIG 1.184	0.20	202.07
17.30	PIG 1.180	0.14	139.65	17.90	PIG 1.186	0.21	207.60
17.50	PIG 1.182	0.21	206.40	18.10	PIG 1.188	0.18	177.57

- Capriolo section

depth (m)	Sample	P (mg/g)	P (ppm)	PAR	Ammonite z.
0.6	CBc17	0.14	137.85		
1.45	CBc15	0.10	95.82		
1.9	CBc13	0.10	103.91		
2.7	CBc11	0.16	160.42		
4.3	CBc7	0.11	107.52	0.13	
5.18	CBc5	0.12	117.77	0.14	
6.3	CBc3	0.11	113.83	0.14	
7.10	CB60	0.13	132.67	0.16	
7.20	CB59	0.17	165.37	0.20	
7.42	CB58	0.11	112.18	0.13	
7.5	CBc1	0.13	132.34	0.16	
7.55	CB57	0.13	129.42	0.15	
8.05	CB55	0.10	104.14	0.12	
8.15	CB54	0.13	131.65	0.16	
8.50	CB53	0.14	140.22	0.17	
9.00	CB51	0.18	182.17	0.22	
9.35	CB50	0.17	172.14	0.20	
9.48	CB49	0.17	169.17	0.20	
9.75	CB48	0.17	167.48	0.20	
10.17	CB47	0.23	228.90	0.27	
10.45	CB46	0.18	177.22	0.21	
10.74	CB45	0.18	182.14	0.22	
10.99	CB44	0.18	182.68	0.22	
11.34	CB43	0.16	161.60	0.19	
11.68	CB42	0.13	132.17	0.16	
12.23	CB40	0.12	119.20	0.14	
12.36	CB39	0.12	115.67	0.14	
12.68	CB38	0.13	128.40	0.15	
13.04	CB37	0.14	137.44	0.16	
13.33	CB36	0.13	125.13	0.15	
13.63	CB35	0.13	125.13	0.15	Boissieri
13.95	CB34	0.12	119.15	0.14	Sed. Rate
14.49	CB33	0.12	124.52	0.15	0.475460123
14.81	CB32	0.15	148.30	0.18	
14.97	CB31	0.13	126.20	0.15	
15.13	CB30	0.12	121.38	0.14	
15.77	CB28	0.13	126.96	0.15	
16.46	CB27	0.14	142.59	0.17	
16.70	CB26	0.12	117.27	0.14	
16.94	CB25	0.13	133.48	0.16	
17.22	CB24	0.16	161.19	0.19	
17.47	CB23	0.16	161.17	0.19	
17.85	CB22	0.13	133.35	0.16	
18.10	CB21	0.13	134.97	0.16	
18.33	CB20	0.12	116.22	0.14	
18.68	CB19	0.13	126.71	0.15	
18.83	CB18	0.11	111.73	0.13	
19.02	CB17	0.11	114.68	0.14	
19.84	CB15	0.14	136.71	0.16	
20.13	CB14	0.13	127.55	0.15	
20.33	CB13	0.12	123.72	0.15	
20.55	CB12	0.13	132.88	0.16	
20.95	CB11	0.16	161.65	0.19	

21.18	CB10	0.18	178.96	0.21	
21.40	CB9	0.13	130.35	0.15	
21.59	CB8	0.16	158.43	0.19	
21.70	CB7	0.14	142.47	0.17	
22.00	CB6	0.15	149.97	0.18	
22.08	CB5	0.16	160.54	0.19	
22.25	CB4	0.12	120.53	0.14	
22.60	CB3	0.13	126.33	0.15	
22.80	CB2	0.09	90.98	0.11	
23.30	CB1	0.14	143.54	0.17	
22.8	CA 1	0.12	123.90	0.15	
24.25	CA 3	0.15	145.61	0.17	
26.04	CA 5	0.14	137.47	0.16	
27.71	CA 7	0.12	117.11	0.14	
29.54	CA 9	0.14	136.11	0.16	
31.32	CA 11	0.10	103.53	0.12	
33.52	CA 13	0.08	81.82	0.10	
35	CA 15	0.08	75.03	0.09	
35.55	CA 16	0.08	84.53	0.10	
36.6	CA 18	0.12	122.54	0.28	Otopeta
38.12	CA 20	0.08	80.46	0.18	Sed. Rate
38.34	CA 22	0.10	98.11	0.22	0.914893617

A.2.4. Rock-Eval data

- Angles section

Depth (dm)	Sample	TOC [%]	HI [mg HC/g TOC]	OI [mg CO2/g TOC]	Tmax [°C]
501	228	0.57	105	80	440
567	251	0.42	116	80	440
637	284	0.30	86	156	442
749	310	0.38	167	48	442
799	328	0.47	222	62	439
815	03F31	0.47	215	44	441
849	03F29	0.38	182	70	441
881	03F27	0.45	198	46	441
908	03F24	0.31	159	70	437
932	03F22	0.29	126	96	442
967	03F20	0.32	125	70	441
995	03F18	0.36	194	63	439
1098	03F03	0.38	133	91	437
1328	03F45	0.56	198	45	439
1403	03F50	0.36	116	89	442
1451	03F53	0.40	139	36	442
1551	03F62	0.33	130	20	438
1594	03F65	0.38	108	38	435
1717	03F73	0.32	134	25	437
1767	03F76	0.30	114	53	438
1820	03F79	0.33	96	47	440
1992	03F86	0.31	131	47	437
2030	04N25	0.49	146	47	437
2168	04N17	0.38	136	38	439
2239	03F102	0.45	123	76	437
2332	03F98	0.46	103	78	438
2371	03F96	0.49	134	54	437
2431	03F93	0.50	182	53	434
2469	03F91	0.33	132	121	435

- Wawal section

Depth (dm)	Sample	TOC [%]	HI [mg HC/g TOC]	OI [mg CO2/g TOC]	Tmax [°C]
0.05	PIG 1.1	0.05	688	556	420
0.29	PIG 1.5	0.66	46	185	406
0.5	PIG 1.8	0.76	70	129	414
0.8	PIG 1.11	0.21	66	354	420
1.02	PIG 1.13	0.15	76	451	423
1.31	PIG 1.16	0.28	51	294	422
1.61	PIG 1.19	0.24	50	397	424
1.91	PIG 1.22	0.38	25	299	416
2.61	PIG 1.29	1.24	19	225	433
2.91	PIG 1.32	0.73	25	201	425
3.21	PIG 1.35	0.38	40	320	424
3.51	PIG 1.38	0.35	35	505	427
3.81	PIG 1.57	0.28	75	239	418
4.11	PIG 1.41	0.39	46	166	418
4.2	PIG 1.44	0.84	36	108	419
4.5	PIG 1.45	0.36	52	168	418
4.8	PIG 1.48	0.52	42	175	418
5.1	PIG 1.51	0.53	41	164	418
5.4	PIG 1.54	0.10	117	622	417
5.6	PIG 1.59	0.70	21	119	416
5.7	PIG 1.60	0.31	51	204	417
6	PIG 1.63	0.47	44	145	418
6.3	PIG 1.66	0.68	13	118	413
6.6	PIG 1.69	0.22	51	250	417
6.7	PIG 1.70	0.40	38	192	419
7	PIG1.73	0.32	44	177	418
7.5	PIG1.78	0.40	36	164	419
7.8	PIG1.81	0.22	52	262	419
8.1	PIG1.84	0.02	390	2332	421
8.4	PIG1.87	0.14	79	345	420
8.7	PIG1.90	0.21	57	230	418
9.1	PIG1.94	0.06	136	619	417
9.4	PIG1.97	0.06	163	781	417
9.7	PIG1.100	0.13	74	354	416
10	PIG1.103	0.10	92	378	420
10.3	PIG1.106	0.08	96	492	421
10.6	PIG1.109	0.23	48	197	419
10.9	PIG1.112	0.22	42	201	420
11.5	PIG1.118	0.04	168	756	421
11.8	PIG1.121	0.09	96	538	413
12.06	PIG1.124	0.03	229	1639	416
12.18	PIG1.126	0.04	236	1471	419
12.36	PIG1.129	0.04	225	1340	414
12.54	PIG1.132	0.07	127	755	416
12.8	PIG1.135	0.07	138	689	419
13.1	PIG1.138	0.02	406	2157	414
13.5	PIG1.142	0.04	142	969	407
13.8	PIG1.171	0.16	94	418	420
14.3	PIG1.150	0.16	57	327	416
14.57	PIG1.153	0.94	13	84	419
14.9	PIG1.156	0.63	21	122	415
15.8	PIG1.145	0.40	34	145	414
16.1	PIG1.165	1.31	0	82	454
16.4	PIG1.168	0.57	23	103	413
16.56	PIG1.173	0.42	42	289	422
16.9	PIG1.176	0.51	38	784	422
17.5	PIG1.182	1.06	10	110	417
17.8	PIG1.185	1.24	11	103	421
17.9	PIG1.179	0.41	29	615	426
18	PIG1.188	1.44	12	213	427

A.2.5. Clay mineralogical content

- Montclus section

Depth (m)	Sample	Smectite *001*	Mica *001*	IS	Quartz	kaolinite *001*	Chlorite *002*
0.05	MA55	827	432	288	0	0	0
1.3	MG58	1691	142	56	363	0	26
3.95	MA49	936	485	172	0	0	0
6.6	MG53	543	224	41	498	0	113
9.45	MA44	77	0	0	0	0	0
11.7	MG46	2846	263	221	279	0	0
14.2	MG42	1732	203	113	193	0	0
16.05	MA36	640	557	44	0	0	0
18.38	MG37	1188	139	139	260	0	0
20.47	MA30	296	393	57	149	0	0
22.85	MG30	823	69	61	446	18	25
25	MA24	1028	269	154	173	0	0
29.81	MG21	518	219	0	380	11	16
34.83	M1	341	52	23	258	2	20
33.69	M6	1239	223	145	90	6	29
32.32	M12	472	138	19	127	5	18
30.69	M17	1077	176	71	49	24	98
42.87	MC35A	838	465	158	168	0	123
44.1	MC40	631	112	112	366	0	270
45.6	MC45	524	125	88	214	128	131
46.34	MC50	328	113	82	147	0	0
46.86	MC55	363	184	57	230	0	173
47.65	MC60	506	506	311		0	0
48.34	MC65	833	161	92	237	62	133
50.05	MC75	903	228	78	104	44	288
50.93	MC80	719	230	115	315	0	505
51.59	MC735	418	303	232	123	0	0
52.48	MC730	367	148	119	48	0	0
53.71	MC725	225	208	127	134	0	408
54.71	MC720	668	372	218	114	0	0
55.53	MC715	794	254	84	172	0	0
56.33	MC710	938	492	205	113	0	0
57.11	MC705	304	239	114	145	113	279
57.73	MC700	531	337	107	112	199	121
58.41	MC695	474	175	120	66	77	288
58.93	MC690	466	371	168	93	361	132
59.43	MC685	244	161	29	118	105	433
60.11	MC680	0	391	168	65	342	241
61.38	MC670	0	141	57	755	335	137
63.33	MC655	0	423	155	109	499	258
65.35	MC645	0	222	36	129	129	399
66.33	MC640	0	422	84	140	715	324
67.56	MC635A	288	363	103	155	384	812
67.56	MC635	310	413	68	182	233	1004
68.51	MC630	0	453	79	157	451	423
69.82	MC625	285	469	68	156	159	696
70.8	MC620	0	454	370	76	1026	463
72.08	MC615	351	477	159	166	37	260
72.75	MC610	0	316	166	169	739	377
73.58	MC605	0	338	44	148	0	0
75.28	MC595	0	312	72	131	76	623
76.13	MC590	318	358	161	114	633	302
77.13	MC585	0	106	61	92	63	230

77.91	MC580	638	390	223	118	624	358
78.58	MC575	221	230	114	146	107	346
79.66	MC570	0	335	138	85	98	623
80.15	MC568bis	74	86	47	93	0	77
81.5	MC565	0	514	113	152	617	389
83.12	MC560	0	394	64	125	134	462
84.89	MC555	314	211	32	218	48	29
89.24	MC545	552	502	188	128	1410	0
90.84	MC540	245	262	71	186	178	62
92.56	MC535	427	395	110	0	524	317
94.34	MC530	258	227	157	233	0	0
96.96	MC525	533	426	323	154	378	166
98.82	MC520	972	340	199	167	0	0
100.59	MC515A	217	295	55	139	475	0
100.59	MC515	0	493	130	119	379	113
104.04	MC506	306	383	209	105	306	227
104.52	MC505	69	506	0	223	0	0
107.06	MVS5	130	236	31	193	0	0
108.09	MVS10	477	337	82	181	0	0
109.71	MVS15	178	227	115	170	74	125
111.19	MVS20	581	182	118	148	318	137
113.34	MVS25	0	94	209	199	0	0
115.04	MVS30	373	200	57	114	186	0
116.42	MVS35	356	335	67	201	138	307

- Capriolo section

Depth (m)	**Sample**	**Smectite *001***	**Mica *001***	**IS**	**kaolinite *001***	**Chlorite *002***	**Rectorite**
0.6	CBC17	57	297	95	5	34	99
1.9	CBC13	207	234	17	10	10	231
3.55	CBC9	211	162	16	8	24	317
5.18	CBC5	124	212	28	10	35	105
7.10	CB60	172	145	33	8	18	229
7.5	CBC1	305	187	13	0	24	336
7.55	CB57	342	169	36	95	97	209
8.15	CB54	567	163	20	73	119	72
9.00	CB51	172	132	30	60	104	147
10.74	CB45	302	140	33	35	152	131
11.68	CB42	349	154	38	45	152	297
12.36	CB39	186	123	25	102	112	0
13.33	CB36	102	104	16	77	75	142
14.49	CB33	261	134	21	0	143	214
15.13	CB30	477	169	48	31	172	341
16.46	CB27	42	240	97	29	38	102
17.22	CB24	460	155	51	37	162	456
18.10	CB21	150	105	70	82	75	183
18.83	CB18	251	137	76	103	96	275
19.02	CB17	123	141	28	0	0	145
19.84	CB15	311	227	184	63	116	310
20.55	CB12	167	330	105	49	168	196
21.4	CB9	157	272	82	85	117	162
22	CB6	282	165	18	35	142	250
22.6	CB3	238	238	95	0	103	285
23.3	CB1	112	87	52	52	111	225

- Wawal section

Depth (m)	Sample	Smectite *001*	Mica *001*	IS	Quartz	kaolinite *001*	Chlorite *002*
0.18	PIG 1.2	41	159	25	147	245	62
0.2	PIG 1.3	51	578	24	163	593	125
0.29	PIG 1.5	92	171	38	48	115	35
0.5	PIG 1.8	0	147	54	157	2291	80
0.6	PIG 1.9	63	172	62	86	1857	139
0.92	PIG 1.12	70	318	23	214	4350	1892
1.02	PIG 1.13	0	301	88	111	5282	289
1.31	PIG 1.16	0	492	18	165	4763	357
1.71	PIG 1.20	0	123	43	42	4502	182
2.11	PIG 1.24	27	140	46	47	3114	172
2.91	PIG 1.32	18	146	19	83	1818	155
3.31	PIG 1.36	32	294	28	122	2158	409
3.71	PIG 1.40	0	745	67	192	4155	933
4.11	PIG 1.44	0	311	56	116	2048	429
4.50	PIG 1.48	52	508	74	90	2533	500
4.90	PIG 1.52	55	617	141	139	3282	694
5.30	PIG 1.56	82	516	90	137	2718	559
5.70	PIG 1.60	150	401	33	135	1809	206
6.10	PIG 1.64	228	604	102	161	3387	850
6.50	PIG 1.68	19	257	192	179	1930	430
6.90	PIG 1.72	28	302	70	190	2360	593
7.30	PIG 1.76	262	448	50	135	3193	668
7.70	PIG 1.80	0	438	123	133	2788	597
8.10	PIG 1.84	164	446	155	221	2629	553
8.50	PIG 1.88	0	637	82	294	3068	474
8.90	PIG 1.92	0	250	24	268	1771	309
9.3	PIG 1.96	674	225	364	239	2666	582
9.7	PIG 1.100	51	611	134	395	2608	484
10.1	PIG 1.104	0	597	24	708	1542	299
10.5	PIG 1.108	411	477	69	365	1191	256
10.9	PIG 1.112	887	432	96	325	1152	203
11.1	PIG 1.114	2874	227	70	130	0	0
11.3	PIG 1.116	1322	300	96	370	789	172
11.7	PIG 1.120	492	297	56	243	108	118
11.9	PIG 1.122	3571	336	183	238	0	98
12.18	PIG 1.126	3347	520	606	230	0	75
12.42	PIG 1.130	307	98	17	89	0	32
12.70	PIG 1.134	4014	84	260	255	0	0
13.10	PIG 1.138	1880	612	42	282	0	117
13.50	PIG 1.142	557	277	53	558	0	119
13.90	PIG 1.146	1087	540	0	247	0	85
14.30	PIG 1.150	4672	150	480	253	0	55
15.10	PIG 1.158	1791	188	33	107	0	58
15.50	PIG 1.162	1542	447	18	86	0	60
15.70	PIG 1.164	3886	424	78	141	0	51
15.90	PIG 1.166	483	162	14	101	0	53
16.30	PIG 1.170	1336	154	38	83	0	42
16.70	PIG 1.174	695	191	54	107	4	23
16.90	PIG 1.176	1832	328	346	94	0	23
17.10	PIG 1.178	98	235	77	92	0	0
17.50	PIG 1.182	57	74	7	55	0	22
17.70	PIG 1.184	75	93	16	53	8	11
17.90	PIG 1.186	81	138	7	77	0	0
18.10	PIG 1.188	934	207	111	64	0	15

A.2.6. Bulk rock mineralogical content

- La Chambotte section

Depth (m)	Samples	Phyllosil.	Quartz	Feldspath-K	Plagio-Na	Calcite	Dolomite	Pyrite	Ankerite	Indicies
1	CHB1	4.34	2.09	0.31	0.22	79.33	0.00	0.00	8.73	4.98
2.50	CHB2BIS	3.82	0.23	0.00	0.00	90.34	0.00	0.30	0.09	5.22
2.98	CHB3	4.34	0.82	0.35	0.19	91.11	0.14	0.00	0.22	2.83
4.85	CHB5	5.44	1.56	0.20	0.29	76.22	11.33	0.00	0.00	4.96
7.38	CHB9	8.10	0.24	0.26	0.29	50.23	37.99	0.00	0.00	2.89
9.21	CHB11	5.21	0.23	0.26	0.25	58.22	33.64	0.17	0.00	2.02
9.88	CHB13	3.56	0.22	0.38	0.23	90.22	0.09	0.00	0.00	5.29
11.6	CHB15BIS	4.27	0.21	0.00	0.26	93.22	0.11	0.00	0.11	1.80
15.01	CH18	3.57	0.43	0.28	0.34	91.23	0.22	0.00	0.00	3.93
16.19	CHB20	4.80	0.18	0.00	0.00	90.44	0.17	0.00	0.00	4.41
19.15	CH1	2.49	0.22	0.23	0.41	95.00	0.25	0.00	0.00	1.41
22.92	CH4	2.35	0.21	0.14	0.35	94.34	0.21	0.00	0.00	2.40
24.9	CH6	2.90	0.22	0.37	0.16	91.76	0.22	0.00	0.00	4.37
26.29	CH8	4.87	0.16	0.30	0.17	92.30	0.00	0.00	0.00	2.20
27.45	CH10	6.89	0.15	0.00	0.00	91.23	0.25	0.19	0.00	1.28
28.33	CH12	4.45	1.16	0.00	0.29	89.23	0.11	0.00	0.00	4.77
29.8	CH14	4.78	0.16	0.25	0.25	88.56	0.23	0.00	0.00	5.77
30.98	CH16	4.85	0.61	0.42	0.44	90.34	0.19	0.48	0.00	2.67
32.77	CH19	5.78	1.69	0.24	0.31	86.98	0.20	0.00	0.16	4.65
33.42	CH21paleosol	32.10	30.89	2.12	0.76	32.12	0.00	0.00	0.19	1.82
33.72	CH22	6.89	4.78	0.30	0.07	79.94	0.00	0.00	0.02	7.99
34.39	CH24	3.05	0.45	0.41	0.27	92.98	0.22	0.00	0.07	2.55
35.46	CH26	4.52	0.73	0.00	0.00	76.09	0.00	0.29	16.98	1.40
36.52	CH28	2.19	1.86	0.20	0.09	89.45	0.00	0.00	4.73	1.48
37.93	CH30	5.18	0.98	0.06	0.30	90.12	0.00	0.46	0.68	2.23
38.9	CH32	4.75	0.81	0.40	0.39	92.74	0.26	0.00	0.00	0.65
39.77	CH34	5.09	1.90	0.20	0.22	89.12	0.00	0.00	0.07	3.40
40.75	CH36	5.44	2.18	0.08	0.14	90.31	0.13	0.00	0.08	1.65
41.02	CH38	5.09	19.65	0.37	0.23	72.15	0.11	0.00	0.00	2.40
42.45	CH40	3.04	7.06	0.46	0.29	87.12	0.00	0.00	0.08	1.94
43.79	CH42	3.23	1.89	0.22	0.23	85.21	0.00	0.21	0.02	8.99
44.84	CH44	3.63	1.85	0.30	0.00	91.34	0.20	0.00	0.00	2.67
45.32	CH46	6.56	3.30	0.81	0.26	85.90	0.24	0.27	0.00	2.66
48.19	CH48	2.83	1.47	0.33	0.19	92.54	0.00	0.23	0.16	2.25
49.62	CH50	4.88	6.34	0.10	0.00	85.03	0.00	0.40	0.80	2.45

64.08	CH66	5.99	1.67	0.27	0.23	83.20	0.00	0.00	6.62	2.02
66.1	CH68	5.09	2.19	0.24	0.26	87.12	0.00	0.00	0.16	4.95
68.21	CH70	4.23	3.00	0.22	0.28	85.34	0.00	0.37	0.16	6.41
69.82	CH72	4.23	1.45	0.24	0.27	88.44	0.07	0.00	0.09	5.21
71.48	CH74	6.57	0.17	0.15	0.12	90.18	0.00	0.00	0.07	2.74
73	CH76	4.13	1.27	0.37	0.13	91.32	0.31	0.00	0.14	2.33
74.92	CH78	2.19	0.16	0.47	0.00	92.24	0.00	0.22	1.54	3.17
77.65	CH80	8.05	1.27	0.67	1.03	86.22	0.81	0.00	0.00	1.96
79.1	CH82	6.19	1.92	0.30	0.32	89.01	0.14	0.00	0.22	1.91
79.95	CH84	5.62	0.09	0.16	0.18	92.12	0.10	0.10	0.08	1.55
80.68	CH86	4.08	0.25	0.32	0.20	92.11	0.21	0.30	0.05	2.47
81.33	CH88	4.99	0.38	0.17	0.17	90.41	0.08	0.11	0.08	3.61
82.2	CH90	2.62	1.09	0.25	0.11	93.19	0.00	0.00	0.11	2.63
83.02	CH92	2.84	1.35	0.36	0.09	94.22	0.10	0.00	0.07	0.96
84.07	CH94	5.87	2.45	0.41	0.20	85.12	0.17	0.00	0.00	5.78
84.7	CH96	6.98	4.09	0.13	0.22	86.12	0.00	0.00	0.07	2.39
85.95	CH98	7.00	1.54	0.29	0.34	85.16	0.21	0.23	0.07	5.15
86.96	CH100	1.96	0.45	0.00	0.00	95.22	0.15	0.00	0.08	2.14
89.13	CH102	6.00	0.61	0.27	0.12	88.34	0.16	0.05	0.05	4.40
90.42	CH104	4.74	1.20	0.47	0.32	89.18	0.24	0.23	0.15	3.48
93.05	CH106	5.88	0.35	0.38	0.54	90.33	0.32	0.20	0.09	1.91
95.75	CH108	5.44	0.40	0.62	0.34	90.45	0.14	0.32	0.00	2.29
96.95	CH110	7.63	3.96	0.50	0.00	85.22	0.00	0.00	0.11	2.58
99.12	CH112	5.98	0.33	0.39	0.26	90.31	0.19	0.00	0.10	2.45
100.7	CH114	4.21	0.35	0.24	0.35	91.20	0.00	0.05	0.22	3.37
101.92	CH116	6.09	0.37	0.38	0.17	89.07	0.35	0.24	0.09	3.24
103.8	CH118	4.74	0.26	0.00	0.37	92.17	0.00	0.00	0.10	2.36
106.43	CH120	5.71	2.88	0.29	0.25	88.34	0.00	0.00	0.11	2.43
107.3	CH122	7.88	2.35	0.15	0.19	84.34	0.28	0.00	0.11	4.71
109.22	CH124	4.50	0.52	0.53	0.33	91.45	0.52	0.00	0.10	2.05
110.94	CH126	5.78	7.10	3.27	0.32	78.23	0.00	0.00	0.48	4.82
111.75	CH128	4.36	5.47	0.44	0.22	86.33	0.00	0.00	0.13	3.05
112.69	CH130	6.34	6.89	0.40	0.35	83.12	0.00	0.00	0.09	2.81
114.04	CH132	5.09	7.43	0.27	0.40	84.18	0.00	0.00	0.04	2.59
115.11	CH134	27.11	33.12	4.85	2.25	29.45	0.00	0.00	1.98	1.23
116.06	CH136	4.96	6.96	0.61	0.19	83.15	0.00	0.00	0.10	4.02
120.02	CH138	6.93	57.23	0.66	0.20	28.11	0.00	0.00	0.07	6.81
122.09	CH140	5.29	18.24	0.89	0.47	72.12	0.51	0.00	0.45	2.03
122.9	CH142	6.77	35.33	0.78	0.28	49.22	0.00	0.00	0.58	7.04
124.2	CH144	5.99	12.12	0.46	0.00	70.12	0.00	0.00	7.02	4.28
125.8	CH146	3.10	5.87	0.43	0.00	82.18	0.19	0.00	6.71	1.52
126.3	CH148	6.87	16.91	1.15	1.05	65.34	0.00	0.00	3.37	5.29
128.35	CH150	5.45	10.63	0.68	0.11	78.33	0.00	0.00	0.21	4.58

Depth (m)	Samples	Phyllosilicates	Quartz	Feldspath-K	Plagioclase-Na	Calcite	Dolomite	Pyrite	Ankerite
1.05	ma53	1.18	4.02	0.00	0.00	92.18	0.00	2.62	0.00
2.80	ma51	1.54	2.66	0.00	0.00	91.13	0.00	4.66	0.00
5.80	mg54	0.00	2.55	0.00	0.00	95.49	0.00	1.96	0.00
6.60	mg53	0.00	2.34	0.00	0.00	95.38	0.00	2.28	0.00
8.52	ma45	3.25	4.94	0.00	0.00	89.18	0.00	2.63	0.00
9.45	ma44	0.91	6.42	0.00	0.00	87.70	0.00	4.98	0.00
11.70	mg46	0.90	3.59	0.00	0.00	92.07	0.00	3.44	0.00
12.00	mg45	0.00	0.73	0.00	0.00	95.65	0.00	3.62	0.00
15.52	ma37	2.40	7.85	0.00	0.00	83.70	0.00	6.05	0.00
15.52	ma37b	0.31	2.74	0.00	0.00	90.57	0.00	4.36	2.02
16.05	ma36	1.93	5.50	0.00	0.00	89.22	0.00	3.34	0.00
17.63	mg38	0.00	2.04	0.00	0.00	92.70	0.00	5.26	0.00
18.38	mg37	0.00	3.22	0.00	0.00	93.86	0.00	2.92	0.00
21.29	ma29	4.02	8.91	0.00	0.00	84.25	0.00	2.82	0.00
22.85	mg30	0.00	3.07	0.00	0.00	92.88	0.00	4.05	0.00
23.07	ma28	2.48	5.96	0.00	0.00	88.78	0.00	2.78	0.00
23.71	mg29	0.00	6.09	0.00	0.00	91.46	0.00	2.46	0.00
28.66	ma21	0.00	4.13	0.00	0.00	89.84	0.00	3.38	2.65
28.66	ma21b	1.84	3.25	0.00	0.00	91.43	0.00	3.47	0.00
29.10	mg22	0.00	5.33	0.00	0.00	86.72	0.00	7.96	0.00
29.2	mg20	0.00	9.35	0.00	0.00	86.63	0.00	4.02	0.00
29.81	mg21	2.21	5.54	0.00	0.00	88.34	0.00	3.92	0.00
36.15	mc1	0.93	5.64	0.00	0.00	88.70	0.00	4.51	0.22
36.6	mc4	0.00	3.32	0.00	0.00	92.40	0.00	5.02	0.00
37.35	mc7	0.00	3.98	0.00	0.00	92.17	0.00	4.55	0.00
37.97	mc10	1.32	5.82	0.00	0.00	83.93	0.00	5.08	3.85
38.5	mc13	0.45	2.80	0.00	0.00	92.82	0.00	3.94	0.00
39.12	mc16	0.00	2.01	0.00	0.00	94.20	0.00	3.79	0.00
40.4	mc22	0.00	4.54	0.00	0.00	91.12	0.00	4.14	0.20
41.07	mc25	0.26	3.25	0.00	0.00	91.43	0.00	4.91	0.15
42.23	mc31	0.81	3.24	0.00	0.00	91.69	0.00	4.27	0.00
42.67	mc34	0.35	3.60	0.00	0.00	92.18	0.00	3.86	0.00
43.35	mc37	0.84	6.57	0.00	0.00	88.41	0.00	4.18	0.00
44.1	mc40	0.95	5.71	0.00	0.00	88.60	0.00	4.73	0.00
45.25	mc43	1.04	6.18	0.00	0.00	89.17	0.00	3.61	0.00
45.8	mc46	0.62	4.22	0.00	0.00	92.27	0.00	2.88	0.00
46.2	mc49	0.35	5.36	0.00	0.00	90.42	0.00	3.86	0.00
46.55	mc52	1.20	5.25	0.00	0.00	89.74	0.00	3.82	0.00
46.86	mc55	0.36	4.89	0.00	0.00	90.03	0.00	4.73	0.00

47.25	mc58	2.27	8.69	0.00	0.00	84.84	0.00	4.20	0.00
47.78	mc61	0.00	4.25	0.00	0.00	90.79	0.00	4.95	0.00
48.34	mc65	0.00	3.98	0.00	0.00	90.16	0.00	5.85	0.00
48.55	mc68	0.00	4.37	0.00	0.00	91.74	0.00	3.89	0.00
49.25	mc71	0.00	3.26	0.00	0.00	92.66	0.00	4.08	0.00
49.95	mc74	1.75	6.11	0.00	0.00	88.29	0.00	3.85	0.00
50.45	mc77	0.67	4.57	0.00	0.00	90.67	0.00	4.08	0.00
51.3	mc737	1.92	6.53	0.00	0.00	88.06	0.00	3.49	0.00
51.83	mc734	0.00	6.32	0.00	0.00	91.89	0.00	1.79	0.00
52.37	mc731	1.15	4.67	0.00	0.00	91.53	0.00	2.64	0.00
52.96	mc728	3.13	9.94	0.00	0.00	84.96	0.00	1.97	0.00
53.71	mc725	0.00	3.66	0.00	0.00	93.47	0.00	2.87	0.00
54.08	mc722	1.64	6.80	0.00	0.00	85.18	0.00	6.38	0.00
54.91	mc719	0.00	4.90	0.00	0.00	87.72	0.00	7.38	0.00
55.38	mc716	2.57	16.10	0.00	0.00	78.76	0.00	2.57	0.00
55.88	mc713	0.00	4.12	0.00	0.00	94.06	0.00	1.82	0.00
56.05	mc712	2.20	8.76	0.00	0.00	84.70	0.00	4.34	0.00
56.48	mc709	0.67	4.65	0.00	0.00	90.72	0.00	3.96	0.00
56.96	mc706	2.02	6.68	0.00	0.00	83.49	0.00	7.81	0.00
57.43	mc703	0.00	4.20	0.00	0.00	90.14	0.00	5.65	0.00
57.73	mc700	0.00	8.14	0.00	0.00	87.78	0.00	4.09	0.00
58.19	mc697	0.00	4.23	0.00	0.00	92.56	0.00	3.21	0.00
58.81	mc691	0.00	2.69	0.00	0.00	84.81	0.00	12.50	0.00
59.13	mc688	2.24	9.76	0.00	0.00	81.20	0.00	6.80	0.00
59.43	mc685	0.09	4.75	0.00	0.00	92.62	0.00	2.54	0.00
59.81	mc682	3.59	12.60	0.00	0.00	77.17	0.00	5.46	1.18
60.24	mc679	0.00	3.35	0.00	0.00	88.74	0.00	7.91	0.00
60.73	mc676	2.57	13.10	0.00	0.00	71.85	0.00	12.48	0.00
61.03	mc673	0.00	3.93	0.00	0.00	92.79	0.00	3.29	0.00
61.38	mc670	0.00	3.73	0.00	0.00	93.74	0.00	1.72	0.81
61.78	mc667	1.01	6.76	0.00	0.00	82.75	0.00	7.87	1.61
62.13	mc664	0.00	4.14	0.00	0.00	88.12	0.00	6.99	0.75
62.53	mc661	2.48	13.90	0.00	0.00	64.86	0.00	5.17	13.59
62.81	mc658	0.00	2.30	0.00	0.00	85.31	0.00	11.06	1.34
63.33	mc655	4.41	17.02	0.00	0.00	56.79	0.00	17.59	4.18
63.93	mc652	0.00	3.27	0.00	0.00	91.50	0.00	5.23	0.00
64.43	mc649	4.32	20.50	0.00	0.00	70.69	0.00	4.49	0.00
65.16	mc646	0.00	4.71	0.00	0.00	90.93	0.00	3.35	1.01
65.63	mc643	0.00	3.67	0.00	0.00	94.11	0.00	2.22	0.00

66.33	mc640	3.90	16.32	0.00	0.00	64.88	0.00	12.59	2.32
67.23	mc637	0.00	3.26	0.00	0.00	95.20	0.00	1.54	0.00
67.73	mc634	3.23	15.26	0.00	0.00	74.91	0.00	2.61	3.99
68.28	mc631	0.00	5.09	0.00	0.00	90.14	0.00	4.77	0.00
69.01	mc628	5.09	22.63	0.00	0.00	67.26	0.00	3.60	1.43
69.82	mc625	0.00	3.65	0.00	0.00	93.38	0.00	2.97	0.00
70.48	mc622	3.58	14.54	0.00	0.00	76.24	0.00	4.86	0.79
71.09	mc619	0.00	3.93	0.00	0.00	90.99	0.00	5.08	0.00
71.96	mc616	1.96	14.40	0.00	0.00	80.64	0.00	3.00	0.00
72.45	mc613	0.00	5.05	0.00	0.00	92.03	0.00	2.93	0.00
72.950	mc610	3.56	18.11	0.00	0.00	76.26	0.00	2.07	0.00
73.900	mc607	0.00	5.38	0.00	0.00	91.61	0.00	2.14	0.87
74.850	mc604	5.01	17.67	0.00	0.00	65.06	0.00	7.55	4.71
75.800	mc601	0.00	2.88	0.00	0.00	89.91	0.00	6.07	1.15
76.750	mc598	1.70	13.41	0.00	0.00	76.53	0.00	4.35	4.00
77.850	mc595	4.85	25.48	0.00	0.00	63.37	0.00	3.74	2.55
78.800	mc592	0.00	6.52	0.00	0.00	88.32	0.00	5.16	0.00
79.750	mc589	0.62	4.25	0.00	0.00	93.64	0.00	1.50	0.00
80.850	mc586	1.92	14.96	0.00	0.00	67.53	0.00	11.93	3.65
81.750	mc583	0.42	4.49	0.00	0.00	90.52	0.00	4.57	0.00
81.750	mc583b	0.24	4.29	0.00	0.00	87.52	0.00	7.96	0.00
82.500	mc580	2.30	16.27	0.00	0.00	71.77	0.00	4.82	4.84
83.250	mc577	0.00	5.48	0.00	0.00	91.07	0.00	3.45	0.00
83.900	mc574	4.76	16.31	0.00	0.00	69.31	0.00	5.47	4.15
84.950	mc571	1.90	10.41	0.00	0.00	82.36	0.00	5.33	0.00
85.500	mc568	0.00	7.12	0.00	0.00	90.97	0.00	1.91	0.00
86.950	mc565	3.90	16.12	0.00	0.00	76.69	0.00	3.28	0.00
88.000	mc562	0.00	8.59	0.00	0.00	85.36	0.00	6.06	0.00
89.000	mc559	0.00	0.00	0.00	0.00	100.00	0.00	0.00	0.00
90.100	mc556	0.00	4.49	0.00	0.00	92.15	0.00	3.37	0.00
91.200	mc553	0.00	5.72	0.00	0.00	88.66	0.00	5.62	0.00
92.500	mc550	2.66	18.08	0.00	0.00	74.90	0.00	4.36	0.00
93.9	mc547	0.06	5.22	0.00	0.00	88.26	0.00	6.47	0.00
95.000	mc544	0.56	6.38	0.00	0.00	87.58	0.00	5.48	0.00
96.100	mc541	2.19	16.26	0.00	0.00	75.74	0.00	5.82	0.00
97.000	mc538	2.44	15.52	0.00	0.00	76.43	0.00	5.60	0.00
98.300	mc534	0.82	6.01	0.00	0.00	88.02	0.00	5.15	0.00
99.450	mc531	3.22	15.96	0.00	0.00	75.95	0.00	4.87	0.00
101	mc528	0.21	6.11	0.00	0.00	88.91	0.00	4.77	0.00

102.400	mc525	2.50	12.87	0.00	0.00	79.63	0.00	5.00	0.00
103.400	mc522	0.17	6.16	0.00	0.00	89.45	0.00	4.22	0.00
104.500	mc519	1.81	11.55	0.00	0.00	82.32	0.00	4.31	0.00
105.600	mc516	0.31	6.16	0.00	0.00	89.35	0.00	4.18	0.00
107.000	mc513	1.75	11.09	0.00	0.00	82.88	0.00	4.28	0.00
108.100	mc510	0.56	8.36	0.00	0.00	86.95	0.00	4.13	0.00
108.800	mc507	1.84	13.28	0.00	0.00	80.35	0.00	4.52	0.00
110.380	mc504	1.71	9.45	0.00	0.00	85.01	0.00	3.83	0.00
111.94	mvs3	0.00	8.06	0.00	0.00	89.66	0.00	2.28	0.00
112.56	mvs5	0.00	7.38	0.00	0.00	90.68	0.00	1.93	0.00
113.1	mvs8	4.13	18.10	0.00	0.00	73.13	0.00	4.64	0.00
113.84	mvs11	1.81	8.45	0.00	0.00	86.10	0.00	3.64	0.00
114.91	mvs14	1.96	8.96	0.00	0.00	83.74	0.00	5.34	0.00
115.72	mvs17	1.08	7.95	0.00	0.00	85.84	0.00	5.14	0.00
116.69	mvs20	2.31	12.24	0.00	0.00	80.81	0.00	4.63	0.00
117.84	mvs23	1.20	10.51	0.00	0.00	82.75	0.00	5.54	0.00
118.84	mvs25	0.00	5.62	0.00	0.00	88.11	0.00	6.27	0.00
120.02	mvs28	1.73	12.17	0.00	0.00	80.71	0.00	5.39	0.00
120.54	mvs30	1.28	10.46	0.00	0.00	79.64	0.00	8.62	0.00
121.14	mvs32	0.00	6.98	0.00	0.00	91.60	0.00	1.42	0.00
121.65	mvs33	0.79	6.29	0.00	0.00	82.49	0.00	10.42	0.00

Depth (m)	Samples	Phyllosilicates	Quartz	Feldspath-K	Plagioclase-Na	Calcite	Dolomite	Goethite	Ankerite	Indicies
0.75	SA102	0.00	0.25	0.00	0.44	97.45	0.65	0.00	0.30	0.62
1.77	SA101	9.04	2.35	0.00	0.00	84.22	2.26	0.00	0.65	1.48
3.2	SA100	0.00	0.44	0.50	0.49	96.03	0.69	0.00	0.00	1.72
4.8	SA99	3.34	0.17	0.24	0.35	92.44	0.14	0.00	0.08	2.97
5.8	SA98	7.88	0.51	0.27	0.15	85.94	0.42	0.00	0.19	3.96
6.8	SA97	0.00	0.26	0.37	0.54	97.12	0.37	0.00	0.00	1.23
8.8	SA95	4.00	0.27	0.25	0.00	93.02	0.28	0.00	0.20	1.92
10.7	SA93	3.25	0.31	0.00	0.00	93.22	0.00	0.00	0.14	2.97
11.25	SA92	5.73	0.79	0.00	0.00	90.03	0.20	0.00	0.09	2.97
11.6	SA91	1.55	0.20	0.00	0.00	97.33	0.00	0.00	0.14	0.78
12.5	SA90	2.57	1.70	0.31	0.00	91.50	0.00	0.00	0.08	3.63
14.3	SA87	7.82	0.22	0.00	0.00	90.12	0.32	0.00	0.10	1.11
14.7	SA87BIS	0.00	0.18	0.00	0.00	97.44	0.00	0.00	0.13	2.25
14.95	SA86	3.43	0.24	0.32	0.00	92.11	0.31	0.00	0.26	3.33
15.53	SA85	5.54	0.66	0.00	0.00	90.78	0.00	0.00	0.17	2.85
16.37	SA84	1.80	0.57	0.00	0.00	93.23	0.00	0.00	1.00	3.14
17.62	SA81	3.74	0.20	0.31	0.48	91.45	0.30	0.00	0.78	2.74
18.09	SA80	3.87	0.10	0.51	0.22	88.33	0.00	0.00	0.13	6.83
18.75	SA79	2.79	0.19	0.46	0.31	91.33	0.00	0.00	0.07	4.85
19.2	SA78	3.70	0.20	0.00	0.00	90.12	0.00	0.00	0.19	5.78
20.25	SA77	4.03	0.17	0.00	0.00	90.32	0.00	0.00	4.40	0.94
20.55	SA76	3.23	0.28	0.00	0.00	92.44	0.41	0.00	0.27	3.37
21.53	SA75	2.23	0.59	0.00	0.00	95.44	0.41	0.00	0.00	1.34
22.92	SA74	0.00	1.36	0.00	0.00	96.89	0.00	0.00	0.71	1.04
24	SA73	2.34	0.29	0.00	0.00	95.03	0.23	0.00	0.32	1.64
24.4	SA72	0.00	0.24	0.00	0.00	97.70	0.12	0.38	0.10	1.45
24.72	SA71	2.04	0.47	0.00	0.00	94.32	0.16	0.00	0.48	2.53
25.02	SA70	3.18	0.24	0.00	0.00	91.45	0.00	0.00	0.14	4.99
25.33	SA69	3.03	0.89	0.00	0.00	94.34	0.00	0.00	0.71	1.03
25.61	SA68	5.63	0.14	0.00	0.00	91.23	0.00	0.00	0.04	2.96
25.86	SA66	3.17	0.15	0.41	0.29	90.89	0.19	0.00	0.00	4.83
26.1	SA65	1.72	0.28	0.00	1.59	92.56	0.00	0.00	0.14	3.71
26.58	SA64	3.44	0.96	0.00	0.00	87.43	0.00	0.00	0.13	8.03
27.06	SA62	5.09	0.28	0.00	0.00	90.31	0.00	0.00	0.39	3.93
28.05	SA61	4.23	0.92	0.00	0.00	91.23	0.00	0.00	0.62	3.00
28.32	SA61bis	5.78	0.72	0.00	0.26	88.45	0.00	0.00	2.95	1.83
30.47	I2	4.88	1.27	0.33	0.28	91.09	0.00	0.51	0.12	1.52
32.17	I3	4.06	0.32	0.32	0.25	93.12	0.44	0.25	0.08	1.16
33.07	I4	3.87	3.78	0.14	0.44	84.87	0.19	0.00	0.16	6.55

33.27	I5	2.07	12.31	0.20	0.43	73.99	0.46	0.62	1.41	8.50
33.87	I6	1.84	1.13	0.15	0.20	90.21	1.94	0.51	1.27	2.75
35.47	I7	6.45	2.89	0.25	0.29	82.31	0.40	0.00	1.00	6.40
36.12	I8	4.56	2.45	0.38	0.24	81.06	0.12	0.19	0.08	10.92
36.77	I9	3.00	0.37	0.42	0.15	94.65	0.18	0.13	0.07	1.03
37.77	I10	3.43	0.77	0.45	0.26	93.29	0.33	0.31	0.15	1.01
40.27	I12	4.34	2.45	0.18	0.28	86.12	0.16	0.20	0.71	5.55
43.52	I14	4.23	1.34	0.26	0.25	84.23	0.30	0.24	0.12	9.02
44.27	I15	4.28	4.45	0.43	0.43	79.32	0.45	0.38	0.35	9.91
45.67	I16	2.56	5.43	0.23	0.17	83.23	0.11	0.46	0.08	7.73
46.67	I17	4.54	7.45	0.34	0.55	85.21	0.01	0.64	0.04	1.22
47.32	I18	1.34	1.13	0.56	0.06	89.25	0.15	0.57	0.12	6.81
47.97	I19	4.33	6.34	0.12	0.35	74.17	0.20	0.43	0.00	14.06
48.57	I20	4.14	4.56	0.00	0.00	83.19	0.63	0.51	0.06	6.90
49.12	I21	1.45	1.45	0.00	0.00	83.22	0.00	0.23	0.10	13.54
49.47	I22	1.55	2.53	0.32	0.00	87.31	0.65	0.58	1.27	5.80
49.97	I23	1.10	0.53	0.66	0.17	93.83	0.09	0.00	0.11	3.51
50.57	I24	2.70	1.56	0.21	0.10	87.34	0.06	0.68	0.04	7.32
51.82	I25	2.31	0.60	0.00	0.00	95.45	0.34	0.20	0.15	0.95
52.57	I26	3.23	2.44	0.00	0.13	79.12	0.27	0.00	0.85	13.96
52.97	SA60	7.67	6.86	0.00	0.31	72.67	0.14	0.79	0.09	11.47
53.57	SA59	14.61	3.87	0.00	0.32	78.18	0.64	0.00	2.21	0.17
56.57	SA57	2.24	2.00	0.00	0.24	93.61	0.27	0.26	0.05	1.33
58.02	SA55	0.83	2.20	0.00	0.34	69.34	0.00	0.00	23.87	3.42
59.62	SA52	3.89	4.78	0.33	0.00	76.59	0.08	0.72	0.02	13.58
59.62	SA52bis	1.35	2.15	0.11	0.00	92.87	0.91	0.00	1.19	1.42
60.27	SA51	1.32	6.29	0.00	0.00	90.33	0.00	0.00	0.13	1.93
60.27	SA51bis	2.49	2.38	0.00	0.35	90.08	1.45	0.00	1.97	1.29
61.27	SA49	1.28	0.36	0.00	0.00	96.18	0.00	0.00	0.00	2.18
63.17	SA47bis	2.71	4.15	0.00	0.00	91.09	0.00	0.65	0.00	1.40
63.27	SA47	2.37	5.85	0.00	0.00	90.43	0.00	0.00	0.00	1.34
65.02	SA45	1.09	1.67	0.00	0.00	89.55	0.43	0.00	0.20	7.06
66.02	SA43	4.56	11.44	0.00	0.06	81.42	0.00	0.00	0.09	2.42
66.97	SA42	2.18	6.97	0.00	1.57	88.23	0.19	0.00	0.07	0.79
67.92	SA41bis	6.99	43.09	0.18	0.00	42.09	0.00	0.00	0.00	7.65
68.02	SA41	4.97	2.12	0.00	0.43	88.32	0.00	0.00	0.00	4.16
69.97	SA39	3.99	0.39	0.00	0.00	93.89	0.00	0.00	0.00	1.73
71.92	SA37	2.11	1.53	0.00	0.00	92.95	0.00	0.00	0.00	3.42
71.92	SA37bis	5.99	2.34	0.25	0.27	83.21	0.00	0.49	0.00	7.45

74.07	SA35	5.34	0.78	0.11	0.08	87.90	0.32	0.00	0.10	5.37
75.07	SA34	3.66	0.78	0.00	0.00	88.09	0.00	0.00	0.00	7.47
76.12	SA33	2.22	7.91	0.00	6.06	81.43	0.00	0.00	0.00	2.37
77.07	SA32	3.34	4.03	0.00	0.00	83.98	0.00	0.00	0.00	8.65
78.07	SA31	1.90	0.23	0.00	0.44	96.34	0.00	0.00	0.00	1.09
79.12	SA30	1.15	3.36	0.00	0.00	94.12	0.00	0.00	0.00	1.37
80.07	SA29	3.75	0.28	0.00	0.00	92.76	0.00	0.00	0.10	3.11
81.07	SA28	1.48	1.92	5.77	0.00	90.00	0.00	0.00	0.00	0.83
81.07	28bis	3.38	5.31	0.00	0.00	89.12	0.00	0.00	1.40	0.79
82.07	SA27	1.87	0.15	0.00	0.00	97.23	0.00	0.00	0.08	0.67
83.57	SA26	0.27	0.53	0.00	0.00	98.02	0.00	0.00	0.00	1.17
84.57	SA25	1.24	2.37	0.00	0.00	95.56	0.00	0.00	0.00	0.82
85.57	SA24	1.09	0.16	0.00	0.35	97.23	0.00	0.00	0.00	1.18
86.47	SA23	3.67	1.34	0.00	0.00	87.23	0.00	0.00	0.00	7.76
87.57	SA21	4.77	1.34	0.00	0.00	85.73	0.00	0.00	0.00	8.16
88.57	SA20	2.65	0.83	0.00	0.00	94.40	0.00	0.00	0.00	2.12
89.57	SA19	3.34	1.13	0.28	0.26	92.89	0.00	0.00	0.00	2.09
90.57	SA18	2.08	6.23	0.00	0.00	88.91	0.00	0.00	0.39	2.39
91.57	SA17	1.58	2.55	0.00	0.00	91.58	0.28	0.00	0.11	3.91
92.57	SA16	3.67	5.37	0.00	0.00	83.78	0.21	0.00	0.11	6.87
93.57	SA15	4.49	4.78	0.40	0.35	81.56	0.21	0.00	0.44	7.76
94.57	SA14	4.76	1.34	0.29	0.22	86.98	0.29	0.00	0.07	6.04
95.57	SA13	5.11	1.81	0.00	0.00	89.77	0.00	0.00	0.19	3.13
96.57	SA12	0.44	1.11	0.00	0.00	56.84	0.17	0.00	0.09	41.35
97.57	SA11	7.89	29.49	0.00	0.00	48.55	0.00	1.10	10.74	2.24
98.57	SA10	2.19	47.51	0.00	3.60	38.97	0.00	0.68	5.24	1.81
99.57	SA9	0.27	28.68	0.00	0.45	63.01	1.34	0.00	3.83	2.43
100.57	SA8	3.50	12.38	0.00	0.00	80.56	0.00	0.00	0.37	3.19
101.57	SA7	3.47	38.52	0.00	0.00	56.10	0.48	0.00	0.25	1.18
102.57	SA6	0.54	9.85	0.00	0.00	87.23	0.00	0.00	0.29	2.08
103.57	SA5	0.17	2.85	0.00	0.00	95.35	0.00	0.00	0.11	1.52
104.57	SA4	2.15	5.41	0.00	0.47	89.65	0.00	0.00	0.70	1.62
105.57	SA3	3.04	2.49	0.00	0.00	92.87	0.00	0.00	0.13	1.47
106.57	SA2	4.67	20.67	0.28	0.15	70.34	0.21	0.00	0.09	3.59
106.77	SA1	6.09	2.65	0.00	1.01	83.10	0.00	0.00	0.00	7.15

Depth (m)	Samples	Phyllosilicates	Quartz	Feldspath-K	Plagioclase-Na	Calcite	Dolomite	Pyrite	Ankerite	Indicies
0.12	GAS1	4.91	8.71	0.30	0.32	82.12	0.87	0.00	0.90	1.88
2	GAS3	11.56	14.67	0.66	0.35	68.23	0.20	0.00	0.05	4.27
4.42	GAS5	22.09	13.23	0.39	0.25	58.28	1.25	0.43	0.99	3.08
6.77	GAS7	8.52	7.10	0.63	0.32	78.56	0.26	0.45	0.34	3.82
11.18	GAS11	5.11	5.43	0.58	0.24	84.12	0.73	0.42	0.16	3.20
14.00	GAS13	7.65	4.26	0.60	0.30	82.43	0.83	0.50	0.43	3.01
19.10	GAS15	3.39	9.68	0.18	0.39	81.03	0.66	0.37	0.29	4.01
22.20	GAS17	4.67	1.24	0.40	0.27	87.23	0.78	0.00	0.13	5.28
26.40	GAS19	3.10	11.13	0.29	0.34	79.18	3.18	0.61	1.08	1.09
29.40	GAS21	6.92	6.09	0.42	0.22	75.34	2.58	0.16	3.13	5.14
31.80	GAS23	35.87	13.34	0.44	0.50	33.28	5.46	1.20	3.68	6.23
33.40	GAS25	20.78	8.66	0.76	0.21	53.05	7.68	0.40	6.17	2.27
34.20	GAS27	10.71	10.17	0.24	0.29	51.95	8.97	0.77	12.78	4.12
34.70	GAS29	9.25	7.47	0.14	0.41	66.89	4.79	1.17	5.82	4.06
37.70	GAS31	4.54	4.75	0.00	0.00	84.09	3.91	0.62	1.60	0.50
40.20	GAS33	4.94	1.32	0.53	0.48	90.45	0.40	0.28	0.09	1.51
41.70	GAS35	2.73	1.92	0.58	0.29	92.12	0.24	0.00	0.19	1.94
45.20	GAS37	3.36	0.35	0.36	0.22	93.00	0.63	0.00	1.05	1.02
47.60	GAS39	6.15	5.50	0.00	0.00	83.90	1.12	0.00	0.99	2.33
48.80	GAS41	7.56	6.45	0.56	0.23	78.17	1.24	2.53	1.19	2.07
50.40	GAS43	12.78	4.85	0.00	0.00	76.23	1.46	0.69	1.07	2.93
53.8	GAS45	4.75	1.39	0.00	0.43	90.29	0.58	0.41	0.02	2.14
62.20	GAS48	4.00	3.85	0.43	0.30	85.09	1.70	0.57	2.13	1.94
64.90	GAS50	5.14	3.87	0.00	0.00	88.45	0.34	0.52	0.08	1.60
67.90	GAS52	7.47	1.99	0.23	0.23	87.23	0.22	0.00	0.11	2.53
86.82	GAS58	23.19	16.20	0.55	0.34	47.78	0.00	0.00	0.00	11.95
88.56	GAS60	24.09	16.55	0.49	0.30	47.29	0.12	0.10	0.05	11.00
90.56	GAS62	23.99	19.22	0.85	0.55	50.34	0.45	0.00	0.21	4.39
103.82	GAS64	22.20	24.04	0.48	0.35	52.37	0.32	0.00	0.14	0.09
105.40	GAS66	23.79	16.44	0.29	0.52	48.98	0.00	0.00	0.00	9.98
107.42	GAS68	26.17	17.96	0.24	0.41	40.24	1.83	0.92	2.82	9.41
108.08	GAS70	7.89	5.55	0.24	0.18	78.23	0.91	0.33	0.15	6.52
109.70	GAS72	28.59	14.52	0.90	0.87	46.22	1.64	0.76	2.96	3.55
111.65	GAS74	34.89	19.22	0.14	0.50	33.19	5.19	0.97	2.82	3.08
113.45	GAS76	8.87	11.69	0.44	0.47	69.20	0.00	0.54	3.15	5.63
115.45	GAS78	6.18	8.74	0.26	0.13	77.32	0.41	1.54	1.25	4.16
131.65	GAS80	9.47	1.81	0.59	0.33	83.10	0.29	0.11	0.15	4.16
132.60	GAS82	5.13	6.91	0.00	0.00	82.37	0.15	0.37	0.64	4.44
133.20	GAS101	0.00	0.56	0.00	0.00	93.10	0.55	0.00	1.91	3.88

137.92	GAS105	0.00	2.22	1.12	0.52	91.23	2.60	0.62	1.04	0.64
140.20	GAS107	3.62	0.58	0.67	0.11	90.18	0.36	0.00	2.03	2.45
157.00	GAS109	5.36	0.67	0.00	0.00	89.10	0.64	0.26	0.09	3.89
160.20	GAS111	6.09	0.48	0.37	0.44	89.37	0.50	0.00	0.32	2.43
163.35	GAS113	4.03	0.27	0.39	0.27	92.10	0.20	0.14	0.12	2.49
167.42	GAS115	6.27	0.47	0.00	0.00	90.18	0.35	0.23	0.12	2.38
168.70	GAS118	4.31	3.61	0.59	1.02	85.12	0.63	0.00	2.98	1.75
176.01	GAS121	7.02	0.82	1.10	0.51	85.87	0.96	0.61	3.02	0.08
179.72	GAS123	5.19	0.56	0.61	0.43	89.09	0.79	0.42	0.18	2.73
182.56	GAS125	10.16	7.10	0.42	0.43	67.20	5.71	0.25	2.94	5.79
184.10	GAS127	2.58	0.26	0.32	0.32	95.03	0.10	0.00	0.13	1.25
187.00	GAS129	3.62	0.42	0.50	0.26	92.18	0.50	0.35	0.30	1.88
188.82	GAS131	4.02	1.81	0.93	0.72	89.24	0.89	0.00	0.18	2.20
190.15	GAS133	0.00	0.23	0.00	0.00	97.17	0.36	0.35	0.16	1.72
192.25	GAS135	8.89	1.04	0.00	0.00	86.67	0.68	0.00	0.00	2.71
194.90	GAS137	4.67	0.20	0.00	0.00	92.76	0.15	0.00	0.09	2.12
199.20	GAS139	4.52	0.33	0.00	0.00	92.09	0.38	0.00	0.23	2.45
202.35	GAS141	5.54	0.27	0.00	0.00	89.36	0.20	0.00	0.30	4.34
204.90	GAS143	6.62	1.72	0.00	0.28	88.62	0.49	0.00	0.30	1.98
209.60	GAS145	5.04	0.57	0.37	0.22	89.28	0.52	0.00	0.22	3.78
213.80	GAS147	8.02	0.30	0.00	0.37	89.00	0.30	0.00	0.28	1.73
216.60	GAS149	14.88	1.89	0.15	0.12	74.20	0.35	0.00	0.09	8.33
220.48	GAS151	4.21	1.69	0.00	0.00	88.25	1.47	0.10	0.85	3.43
230.48	GAS153	9.25	0.00	0.00	0.00	89.29	0.35	0.00	0.08	1.02
234.20	GAS155	3.52	0.58	0.25	0.23	93.92	0.19	0.29	0.15	0.87
237.60	GAS157	4.76	0.31	0.00	0.45	92.18	0.36	0.26	0.19	1.49
239.80	GAS158	7.53	0.68	0.57	0.35	87.12	1.66	0.29	0.31	1.48
243.20	GAS159	5.32	1.81	0.00	0.00	90.24	0.29	0.36	0.15	1.84
243.60	GAS160	6.12	1.05	0.28	0.72	90.38	0.51	0.00	0.31	0.63
247.35	GAS161	1.66	0.22	0.27	0.21	93.10	0.20	0.45	0.05	3.84
248.60	GAS162	1.25	0.25	0.22	0.17	96.12	0.20	0.34	0.05	1.40
251.40	GAS163	4.70	0.24	0.45	0.39	75.34	17.98	0.00	0.00	0.90
256.28	GAS166	2.28	0.33	0.39	0.38	94.03	0.25	0.28	0.07	2.00
256.30	DV1	11.39	2.13	0.00	0.31	79.98	0.52	0.56	0.71	4.40
256.78	DV3	2.96	1.03	0.00	0.00	91.32	0.22	0.00	0.22	4.25
258.73	DV5	4.35	1.06	0.25	0.36	91.23	0.26	0.00	0.15	2.35
259.08	DV7	1.64	0.42	0.17	0.18	96.12	0.17	0.00	0.13	1.17
259.83	DV8BIS	1.55	0.25	0.00	0.00	93.67	0.27	0.00	0.13	4.14
261.08	DV14	22.40	32.42	0.97	0.19	34.23	1.34	1.30	2.74	4.41

262.03	DV17	21.24	14.69	0.75	0.37	53.09	1.99	1.90	3.68	2.28
262.56	DV20	8.09	6.78	0.37	0.29	79.34	0.62	0.00	0.33	4.18
263.08	DV23	44.55	19.27	0.71	0.52	22.45	6.51	1.25	2.70	2.04
265.60	DV26	5.05	7.82	0.36	0.66	82.14	0.41	0.00	0.22	3.34
266.08	DV29	7.70	7.60	0.82	0.28	67.23	8.95	0.00	6.11	1.31
267.46	DV32	13.20	8.03	0.43	0.47	69.78	0.69	0.00	0.78	6.62
269.36	DV35	32.04	25.17	0.22	0.43	36.12	0.44	0.00	0.12	5.45
271.58	DV38	11.23	8.09	0.13	0.00	73.12	0.00	0.00	1.43	5.99
274.13	DV41	5.64	5.28	0.32	0.25	83.12	0.26	0.00	0.21	4.92
275.83	DV44	4.70	3.39	0.50	0.47	90.18	0.00	0.00	0.28	0.48
276.49	DV47	30.12	31.44	0.99	0.71	31.64	0.23	0.00	0.99	3.89
276.98	DV50	8.35	5.36	0.54	0.31	81.23	0.14	0.00	0.29	3.78
281.36	GASV1	15.19	23.44	1.34	1.34	52.34	0.19	0.00	0.06	6.10
281.72	GASV2	7.56	8.56	0.30	0.36	74.22	0.17	0.00	0.14	8.69
282.68	GASV3	8.03	44.34	0.00	0.22	33.56	6.34	0.00	5.34	2.17
283.25	GASV4	6.45	17.34	0.37	0.41	69.10	0.00	0.66	1.04	4.63
283.75	GASV5	7.67	8.60	0.48	0.56	80.23	0.60	0.00	0.52	1.34
284.84	GASV6	29.10	28.28	0.43	0.96	33.72	0.57	1.56	2.81	2.56
285.75	GASV7	8.69	6.08	0.39	0.41	82.10	0.22	0.00	0.06	2.05
286.85	GASV8	8.34	14.34	0.61	0.68	69.23	0.38	0.00	0.10	6.32
287.10	DV53	7.34	25.56	0.11	0.38	53.17	0.35	0.00	0.63	12.46
288.08	GASV9	5.78	13.93	0.76	0.37	75.89	0.11	0.00	0.17	3.00
288.72	GASV10	32.76	26.16	0.96	0.71	31.29	0.30	1.87	2.83	3.11
289.80	GASV11	8.19	10.38	0.41	0.43	76.53	0.10	0.00	0.17	3.78
290.33	GASV12	22.34	17.17	0.86	0.53	56.23	0.44	0.00	0.23	2.20
290.98	GASV13	3.56	8.60	0.76	0.59	84.05	0.16	0.00	0.19	2.10
292.13	GASV14	33.18	31.76	0.66	0.87	32.26	0.12	0.00	0.27	0.88
292.58	GASV15	7.48	6.00	0.47	0.36	80.94	0.21	0.00	0.07	4.47
295.33	GASV16	5.78	6.28	0.00	0.26	83.24	0.46	0.00	0.26	3.73
295.61	GASV17	30.47	22.83	0.58	0.42	38.95	0.46	0.67	0.16	5.45
297.68	GASV18	28.02	20.88	0.39	0.30	41.22	0.22	0.00	2.57	6.39
298.38	GASV19	28.67	16.15	0.58	0.61	47.79	0.68	0.82	2.35	2.35
298.88	GASV20	6.01	6.53	0.11	0.37	82.10	0.43	0.92	0.31	3.22
299.18	GASV21	35.50	21.19	0.67	0.64	36.61	0.43	2.11	0.51	2.35
299.68	GASV22	32.10	28.95	0.85	0.97	34.30	0.00	0.00	0.14	2.69
300.53	Be2	7.25	2.30	0.28	0.21	85.90	0.00	0.00	0.14	3.92
301.95	Be4	3.98	4.82	0.23	0.15	88.23	0.35	0.00	0.45	1.79
302.95	Be6	2.85	9.94	0.36	0.31	82.71	0.93	0.00	1.62	1.27
304.85	Be8	3.48	3.37	0.37	0.14	90.02	0.40	0.00	0.98	1.23

307.05	Be10	4.72	0.97	0.22	0.24	86.12	1.11	0.00	5.90	0.72
310.15	Be12	4.78	35.92	0.32	0.25	55.23	0.30	0.00	0.98	2.22
311.93	Be14	3.27	12.90	0.39	0.22	80.12	0.16	0.00	0.38	2.57
315.13	Be16	5.16	1.42	0.33	0.00	71.23	0.00	0.00	19.37	2.50
316.56	Be18	4.63	7.70	0.37	0.00	84.10	0.00	0.00	0.10	3.10
318.20	Be20	5.13	1.87	0.26	0.15	87.14	0.27	0.00	0.11	5.08
320.13	Be22	3.21	1.08	0.44	0.24	93.20	0.41	0.00	0.10	1.33
323.76	Be24	2.95	1.08	0.31	0.15	94.28	0.38	0.00	0.10	0.76
325.06	Be31	2.37	1.01	0.28	0.20	93.13	0.13	0.00	0.07	2.82
331.98	Be34	2.03	0.15	0.05	0.13	96.02	0.11	0.00	0.06	0.86
335.06	Be36	3.10	0.62	0.12	0.12	92.83	0.14	0.00	0.10	2.98
337.43	Be36	4.51	0.59	0.36	0.23	88.56	0.24	0.00	0.09	5.41
339.86	Be38	4.00	2.83	0.12	0.33	90.32	0.14	0.00	0.11	2.16
341.05	Be40	3.63	3.09	0.33	0.24	87.34	0.38	0.00	0.07	4.93
342.85	Be42	1.31	2.39	0.00	0.00	90.67	0.28	0.00	0.07	5.28
345.45	Be44	4.22	2.39	0.25	0.17	91.12	0.21	0.00	0.08	1.56
346.93	Be46	2.91	2.13	0.22	0.19	93.28	0.16	0.00	0.12	1.00
348.86	Be48	0.00	8.84	0.00	0.00	89.09	0.19	0.00	0.32	1.55
351.06	Be50	4.58	5.61	0.00	0.00	88.13	0.25	0.00	0.12	1.31
353.06	Be52	2.67	6.18	0.23	0.13	87.23	0.73	0.00	0.34	2.49
355.06	Be54	5.46	4.02	0.50	0.32	83.09	0.14	0.00	0.13	6.34
358.06	Be56	3.36	6.97	0.27	0.16	86.90	0.22	0.00	0.15	1.97
360.68	Be58	5.60	2.21	0.00	0.00	90.64	0.45	0.00	0.37	0.74
362.93	Be60	2.32	3.35	0.33	0.15	87.56	0.23	0.00	0.17	5.88
365.13	Be62	3.18	36.11	0.23	0.99	57.98	0.10	0.00	0.66	0.74
367.93	Be64	5.66	12.85	0.39	0.20	79.23	0.18	0.00	0.05	1.43
370.23	Be66	4.61	24.38	0.16	2.88	63.88	0.15	0.00	0.11	1.20

Depth (m)	Samples	Phyllosilicates	Quartz	Feldspath-K	Plagioclase-Na	Calcite	Dolomite	Pyrite	Ankerite	Indicies
0.05	VZ1	24.09	17.78	0.34	0.64	48.90	0.00	0.64	1.28	6.32
0.64	VZ3	22.67	19.76	0.69	0.90	46.00	0.00	1.10	3.48	5.40
1.18	VZ5	12.12	11.78	0.61	0.62	67.09	0.00	1.42	0.72	5.64
3	VZ7	7.48	7.44	0.43	0.69	80.23	0.00	0.49	0.88	2.37
4.91	VZ9	6.89	8.45	0.00	0.00	77.90	0.00	0.20	0.61	5.95
5.8	VZ11	6.00	17.09	0.00	2.25	65.44	0.00	0.42	1.31	7.49
6.6	VZ13	7.89	16.02	0.18	2.61	63.78	0.00	0.44	3.09	5.99
7.71	VZ15	6.33	11.16	0.00	0.63	79.09	0.00	0.34	0.00	2.45
9	VZ19	25.09	27.56	0.36	0.42	30.12	0.00	0.94	9.87	5.64
10.2	VZ21	19.37	21.32	0.29	0.58	48.23	0.00	0.55	6.00	3.66
11.3	VZ23	13.63	15.34	0.43	0.58	67.25	0.00	0.00	1.20	1.58
12.5	VZ25	22.69	20.56	0.59	0.54	39.10	0.00	0.73	13.20	2.59
15.05	VZ27	8.34	8.24	0.31	0.38	79.23	0.00	0.57	0.95	1.98
17.25	VZ29	4.34	4.13	0.25	0.31	87.10	0.00	0.33	2.17	1.36
18.78	VZ31	4.32	0.19	0.30	0.41	91.06	0.00	0.17	0.05	3.50
20	VZ33	3.61	2.10	0.22	0.12	90.39	0.00	0.43	0.37	2.75
21.8	VZ40	4.22	1.72	0.31	0.32	88.45	0.00	1.33	0.00	3.66
22.4	VZ41	7.41	1.47	0.46	0.18	86.03	0.00	0.27	0.15	4.02
23.04	VZ43	2.74	1.80	0.37	0.25	91.12	0.00	0.19	0.58	2.95
23.75	VZ45	4.30	1.96	0.52	0.33	90.33	0.14	0.12	0.17	2.14
24.6	VZ47	5.81	3.75	0.19	0.29	75.98	0.00	0.42	11.38	2.18
25.2	VZ49	4.33	2.61	0.40	0.40	89.12	0.47	0.12	0.20	2.36
25.88	VZ52	3.77	3.56	0.36	0.00	87.23	0.33	0.00	0.00	4.75
26.12	VZ54	3.63	2.44	0.39	0.25	88.00	0.00	0.44	0.60	4.26
26.9	VZ56	14.66	7.81	0.00	0.42	73.02	0.00	0.54	0.98	2.57
27.42	VZ58	3.22	13.78	0.29	0.84	76.34	0.00	0.53	0.25	4.75
28	VZ60	4.66	5.48	0.50	0.49	80.24	0.18	0.34	0.08	8.02
28.8	VZ62	15.34	8.23	0.58	0.37	68.19	0.00	0.35	0.88	6.06
30.3	VZ64	4.78	5.09	0.47	0.22	85.18	0.00	0.39	0.47	3.40
32.3	VZ66	5.34	6.56	0.43	0.20	80.32	0.00	0.36	0.44	6.35
33.25	VZ68	26.56	25.89	0.46	1.01	37.02	0.00	0.74	3.20	5.12
35.12	VZ70	7.77	11.74	0.54	0.39	74.38	0.00	0.32	0.37	4.48
35.72	VZ72	7.89	10.56	0.36	0.41	72.45	0.00	0.82	0.29	7.22
36.9	VZ74	9.36	8.01	0.59	0.69	79.23	0.00	0.57	0.17	1.37
38.38	VZ77	47.55	2.45	3.06	2.81	36.34	0.00	1.38	2.78	3.63
39.5	VZ79	34.21	25.00	1.12	0.80	30.34	0.00	1.27	4.77	2.50
41.75	VZ82	16.90	25.48	0.55	0.87	37.12	0.00	0.67	16.60	1.81
45.3	VZ85	12.34	20.45	0.43	1.03	57.33	0.00	0.63	5.61	2.18
47.82	VZ88	7.44	19.78	0.52	1.20	62.87	0.00	4.14	1.09	2.96
49.12	VZ91	7.61	24.99	0.47	0.94	59.34	0.00	0.78	3.50	2.37
51.12	VZ93	30.56	25.87	0.82	0.97	30.79	0.00	1.57	6.03	3.38
52.5	VZ95	34.40	32.45	0.58	0.69	21.45	0.00	1.70	5.46	3.27
53.9	VZ97	11.11	6.34	0.00	0.37	79.27	0.00	0.59	0.13	2.21
54.95	VZ99	7.89	6.34	0.38	0.39	81.34	0.00	0.44	0.00	3.22
56.25	VZ101	25.81	22.16	0.75	0.74	40.33	0.00	0.87	7.30	2.05
58.35	VB16	6.57	13.32	0.55	0.61	74.45	0.23	0.66	0.16	3.45
58.6	VB17	4.44	21.49	0.57	0.42	69.34	0.00	0.43	0.00	3.30

Depth (m)	Samples	Phyllosilic.	Quartz	Feldsp.-K	Plagio-Na	Calcite	Aragonite	Pyrite	Goethite	Gypsum	Ankerite	Ca-Apatite	Indicies
0.29	PIG1.5	12.56	4.67	0.40	0.41	3.89	0.00	0.00	0.00	0.00	40.78	5.98	31.31
0.5	PIG1.8	13.54	13.56	0.00	0.00	8.41	0.00	0.35	0.00	0.00	38.56	5.03	20.55
0.67	PIG1.10	19.66	33.09	0.00	0.00	10.89	14.04	0.08	3.78	0.00	14.90	0.00	3.56
0.92	PIG1.12	21.90	60.34	0.35	0.51	4.44	0.00	0.00	1.96	0.00	3.67	0.79	6.03
1.11	PIG1.14	24.78	64.09	0.00	0.00	1.56	0.00	0.00	1.58	0.00	3.23	0.00	4.76
1.31	PIG1.16	23.77	56.21	0.00	0.00	8.95	3.42	0.00	1.67	0.00	1.68	0.46	3.84
1.51	PIG1.18	17.45	65.03	0.42	0.49	5.64	0.00	0.00	1.86	0.00	3.54	0.00	5.57
1.71	PIG1.20	27.03	33.88	0.26	1.08	6.09	21.12	0.00	2.89	1.24	3.78	1.45	1.19
1.91	PIG1.22	37.90	29.34	0.42	0.45	9.14	2.18	1.10	5.08	2.96	0.77	9.67	0.99
2.1	PIG1.24	22.90	15.34	0.00	0.00	8.67	9.45	0.65	12.56	0.00	3.45	17.98	9.00
2.31	PIG1.26	22.74	11.67	0.09	0.07	11.41	5.00	0.38	13.09	0.25	5.09	28.12	2.10
2.51	PIG1.28	29.89	5.56	0.31	0.24	8.66	3.10	1.51	11.38	1.90	7.01	28.56	1.89
2.71	PIG1.30	25.89	35.87	0.00	0.27	8.34	4.78	3.13	3.82	5.07	8.43	4.23	0.17
2.91	PIG1.32	30.88	9.09	1.14	0.25	12.90	2.56	1.45	3.56	2.45	5.09	29.09	1.54
3.11	PIG1.34	30.67	15.34	1.44	0.13	12.89	7.45	2.67	3.09	2.02	3.09	20.76	0.45
3.31	PIG1.36	22.21	30.34	0.45	0.34	14.23	3.09	0.45	2.23	0.00	4.45	22.16	0.05
3.51	PIG1.38	36.05	13.96	0.00	0.56	23.54	0.91	1.18	7.09	2.21	4.51	8.56	1.43
3.71	PIG1.40	42.59	27.37	0.41	0.41	6.89	8.47	1.74	2.70	2.45	1.59	3.05	2.32
3.91	PIG1.42	23.45	32.14	0.68	0.00	30.51	9.45	1.22	0.00	0.00	0.80	0.00	1.76
4.11	PIG1.44	47.63	32.94	0.38	0.57	5.66	7.08	2.77	0.00	0.00	0.43	1.23	1.32
4.3	PIG1.46	47.23	32.85	1.67	1.52	3.39	6.28	3.45	0.00	0.00	0.00	0.00	3.60
4.5	PIG1.48	35.45	33.38	3.23	1.38	4.30	6.76	2.01	0.00	2.68	1.11	3.78	5.93
4.7	PIG1.50	39.28	33.12	2.02	1.49	6.12	7.79	1.72	2.24	1.46	1.94	0.00	2.82
4.9	PIG1.52	39.23	39.45	2.43	1.38	5.09	5.56	1.12	1.34	1.16	1.12	1.02	1.10
5.1	PIG1.54	41.45	36.48	1.00	0.48	5.27	9.45	1.12	0.45	0.92	0.68	1.80	0.91
5.3	PIG1.56	40.39	39.56	0.99	0.48	4.22	9.78	0.98	0.12	0.91	0.68	1.53	0.36
5.5	PIG1.58	40.66	33.12	2.69	1.16	6.83	9.99	1.48	0.00	0.91	0.43	0.00	2.73
5.7	PIG1.60	42.47	33.19	2.90	0.00	7.34	9.43	0.56	0.98	0.45	0.76	1.05	0.87
5.9	PIG1.62	41.67	34.89	2.18	1.16	6.36	9.23	1.48	0.00	0.00	0.07	0.75	2.20
6.1	44.98	45.91	31.43	0.62	0.57	5.66	7.34	2.19	1.37	0.55	0.16	3.82	0.38
6.3	PIG1.66	36.73	31.84	0.18	0.34	7.22	10.76	4.86	0.00	2.12	1.55	2.40	2.00
6.5	PIG1.68	38.00	29.67	0.36	0.42	10.99	11.45	1.10	0.00	0.00	0.00	0.43	7.58
6.7	PIG1.70	40.29	38.65	0.05	0.00	5.36	9.99	0.84	0.00	0.00	0.56	0.80	3.45
6.9	PIG1.72	45.11	32.77	2.29	0.26	5.79	10.56	0.97	0.00	1.16	0.45	0.00	0.65
7.1	PIG1.74	46.09	24.85	3.56	1.31	5.03	11.23	0.94	2.32	0.96	0.66	1.21	1.84
7.3	PIG1.76	40.76	34.67	0.71	0.41	0.00	12.99	1.34	0.00	0.00	1.84	0.75	6.54
7.5	PIG1.78	44.78	30.87	1.90	0.53	3.09	11.64	1.14	0.00	0.93	2.43	1.24	1.45
7.7	PIG1.80	46.12	29.09	5.08	1.47	4.35	7.05	1.02	1.56	1.12	0.76	1.32	1.06
7.9	PIG1.82	43.97	26.19	1.90	1.23	4.34	4.34	1.36	0.56	1.08	0.45	12.49	2.09
8.1	PIG1.84	41.42	28.93	2.55	0.76	2.90	2.89	1.21	2.04	1.33	0.70	14.03	1.24
8.3	PIG1.86	49.04	31.94	1.03	0.33	3.13	3.67	1.44	0.00	1.36	1.06	6.05	0.95
8.5	PIG1.88	37.56	34.67	2.22	1.09	12.45	6.54	1.18	0.74	0.00	0.34	0.78	2.43
8.9	PIG1.92	32.41	44.62	2.23	1.23	9.06	0.00	1.25	0.00	1.18	0.76	4.64	2.62
9.2	PIG1.95	44.21	33.19	2.38	2.90	3.54	6.45	0.00	0.79	1.19	0.29	1.34	3.72
9.4	PIG1.97	45.09	36.03	2.12	1.10	4.11	5.66	0.00	0.00	0.91	0.11	0.98	3.88

9.6	PIG1.99	47.73	28.52	2.58	0.40	2.47	4.27	1.11	2.48	0.00	0.20	1.75	8.49
9.8	PIG1.101	48.35	33.11	0.39	0.75	2.30	0.00	0.92	2.19	2.73	0.43	0.87	7.96
10	PIG1.103	50.90	36.98	1.67	1.24	3.08	0.00	1.30	0.00	0.00	0.00	0.00	4.83
10.2	PIG1.105	44.76	35.09	11.09	0.61	1.47	2.67	1.90	0.37	0.00	0.10	0.70	1.24
10.4	PIG1.107	43.67	35.83	10.96	1.11	1.85	2.37	0.97	0.00	0.19	0.00	1.29	1.75
10.6	PIG1.109	52.76	34.98	0.77	0.63	1.98	3.09	1.47	0.00	0.23	0.08	0.83	3.18
10.8	PIG1.111	43.12	40.87	2.66	1.16	1.77	4.05	1.29	0.00	0.15	0.33	1.60	3.01
11	pig1.113	39.89	45.18	4.67	0.62	1.88	3.83	0.92	0.41	0.34	0.00	1.16	1.10
11.4	PIG1.117	42.78	47.98	1.84	1.04	1.69	0.00	0.93	0.00	0.00	0.38	1.57	1.77
11.6	PIG1.119	30.03	43.54	12.12	1.15	4.09	6.97	0.74	0.00	0.00	0.30	0.55	0.50
11.8	PIG1.121	41.87	36.95	2.32	0.35	5.42	6.84	0.48	0.00	1.51	0.11	0.24	3.90
12	PIG1.123	37.40	38.56	1.60	1.55	4.89	9.36	0.68	0.00	0.00	0.16	0.91	4.90
12.12	PIG1.125	30.51	46.42	4.51	0.00	7.28	6.58	1.61	0.00	0.00	1.99	0.00	1.10
12.24	PIG1.127	29.78	45.67	2.94	0.00	5.45	10.34	0.88	0.00	0.00	0.41	2.97	1.56
12.36	PIG1.129	24.90	53.56	0.00	0.00	8.45	9.66	1.02	0.00	0.00	0.38	1.43	0.59
12.48	PIG1.131	35.10	35.85	1.87	0.29	8.32	9.76	0.97	0.00	0.00	1.68	1.08	5.08
12.6	PIG1.133	38.67	35.71	1.49	0.00	8.82	9.19	1.16	0.00	0.00	0.23	1.21	3.53
12.8	PIG1.135	34.12	28.98	0.00	0.18	11.09	10.43	0.84	0.00	0.00	0.65	10.77	2.94
12.9	PIG1.136	28.07	24.65	0.00	0.09	28.15	8.29	0.00	0.37	0.00	1.64	6.77	1.98
13.5	PIG1.142	52.23	31.50	0.79	0.34	5.67	0.00	1.03	1.09	0.37	0.13	1.78	5.07
13.7	PIG1.144	46.10	27.19	1.53	0.22	7.03	5.67	1.20	0.00	1.18	0.72	8.78	0.37
13.9	PIG1.146	29.03	20.22	5.07	0.00	9.98	9.87	0.17	0.00	0.00	0.68	18.98	6.00
14.1	PIG1.148	28.83	27.08	0.70	0.00	22.13	10.18	0.52	0.00	0.00	1.01	4.31	5.25
14.4	PIG1.151	27.04	26.88	9.35	0.00	9.33	13.25	0.83	0.00	0.95	0.67	5.92	5.78
14.57	PIG1.153	39.77	23.45	1.90	0.00	7.70	17.43	0.30	0.00	0.78	0.17	3.88	4.63
14.8	PIG1.155	28.56	26.45	0.00	0.55	8.87	15.34	0.84	0.00	0.76	2.16	4.17	12.29
15	PIG1.157	27.44	26.90	0.00	0.00	7.55	13.73	1.05	0.00	0.00	0.00	0.00	23.33
15.2	PIG1.159	23.44	25.89	0.00	0.39	41.27	4.67	0.34	0.00	0.00	0.21	2.16	1.62
15.4	PIG1.161	33.02	28.45	3.82	1.04	17.30	9.27	1.19	0.00	0.00	2.32	0.39	3.19
15.6	PIG1.163	37.60	32.44	7.36	0.28	8.44	6.23	0.92	0.00	0.35	1.83	3.29	1.24
16	PIG1.167	28.33	30.56	0.00	0.25	16.43	12.55	0.74	0.00	0.00	1.45	2.65	7.04
16.2	PIG1.169	37.13	37.96	0.00	0.50	6.33	11.64	0.90	0.00	0.00	0.14	3.89	1.52
16.4	PIG1.171	26.04	21.34	0.00	1.23	20.55	15.45	0.61	0.00	0.00	0.46	10.66	3.65
16.5	PIG1.172BIS	13.66	14.67	0.00	0.18	32.12	6.54	0.39	0.00	0.00	2.38	27.46	2.60
16.5	PIG1.172	11.56	16.78	0.00	0.00	30.77	6.57	0.39	0.00	0.00	0.54	28.23	5.16
16.7	PIG1.174	30.26	35.90	0.00	0.94	7.90	12.61	0.76	0.00	0.00	0.65	9.67	1.31
17	PIG1.177	31.45	39.21	0.00	0.54	2.03	5.88	1.12	0.00	0.00	0.98	17.09	1.70
17.2	PIG1.179	22.45	28.56	0.45	0.34	0.92	1.06	1.23	0.00	0.00	0.00	43.89	1.10
17.4	PIG1.181	37.90	29.67	0.98	0.00	0.00	0.00	1.16	1.45	0.00	0.10	20.67	8.07
17.6	PIG1.183	47.65	35.76	4.74	1.33	0.00	0.00	1.08	1.34	0.87	0.00	3.78	3.45
17.8	PIG1.185	49.88	40.78	0.61	0.14	0.82	0.00	1.23	0.23	0.00	0.00	4.88	1.44
18.1	PIG1.188	26.09	27.56	0.29	0.17	0.00	4.66	1.65	2.98	1.13	0.12	28.90	6.45

Depth (m)	Samples	Phyllosilicates	Quartz	Feldspath-K	Plagioclase-Na	Calcite	Dolomite	Goethite	Ankerite	Indicies
1.45	CBC15	6.66	0.37	0.51	0.15	90.55	0.00	0.00	0.13	1.63
1.9	CBC13	5.88	0.58	0.11	0.34	84.00	0.00	0.00	0.10	8.73
2.7	CBC11	3.32	0.23	0.35	0.46	89.33	0.00	0.00	0.08	6.08
3.55	CBC9	2.20	0.70	0.23	0.27	88.45	0.24	0.00	0.09	7.81
4.3	CBC7	2.14	1.09	0.34	0.32	86.34	0.28	0.00	0.10	9.05
5.18	CBC5	3.07	0.61	0.15	0.17	87.43	0.19	0.00	0.08	8.12
6.3	CBC3	3.34	0.78	0.28	0.28	91.27	0.00	0.00	0.09	2.98
7.10	CB60	3.98	0.61	0.57	0.66	82.45	0.00	0.00	0.10	11.46
7.5	CBC1	4.48	0.59	0.00	0.00	92.61	0.00	0.00	0.07	2.17
7.55	CB57	2.61	1.88	0.52	0.22	92.77	0.00	0.00	0.00	0.92
8.15	CB54	0.93	26.73	0.30	0.23	70.21	0.00	0.00	0.02	1.46
9.00	CB51	3.68	1.09	0.27	0.64	88.77	0.22	0.00	0.06	5.02
9.75	CB48	2.51	0.63	0.27	0.18	88.34	0.00	0.00	0.08	7.83
10.74	CB45	6.65	1.13	0.32	0.09	90.04	0.00	0.00	0.06	1.47
11.68	CB42	6.17	0.94	0.46	0.27	85.23	0.00	0.00	0.08	6.63
12.03	CB41	5.41	1.10	0.19	0.74	86.54	0.00	0.00	0.07	4.83
12.36	CB39	5.48	0.94	0.47	0.27	87.62	0.38	0.00	0.07	3.96
14.49	CB33	3.49	0.87	0.41	0.23	87.45	0.00	0.00	0.05	6.38
16.46	CB27	3.13	1.30	0.15	0.20	87.45	0.00	0.00	0.12	7.46
17.47	CB23	2.97	1.60	0.28	0.00	91.20	0.00	0.00	0.04	3.84
18.10	CB21	4.56	1.28	0.26	0.38	85.15	0.00	0.00	0.06	8.31
18.83	CB18	3.25	1.94	0.19	0.24	88.45	0.00	0.00	0.02	5.91
19.84	CB15	2.59	0.95	0.17	0.45	77.32	0.00	0.00	0.06	18.46
20.55	CB12	5.39	1.92	0.36	0.25	80.45	0.00	0.00	0.09	11.53
21.40	CB9	5.89	1.80	0.27	0.36	89.26	0.00	0.00	0.03	2.24
21.70	CB7	4.65	1.93	0.29	0.29	90.45	0.00	0.00	0.14	2.26
22.08	CB5	3.78	1.70	0.00	0.00	82.12	0.00	0.00	0.04	12.36
22.60	CB3	4.42	1.99	0.00	0.00	92.34	0.00	0.00	0.17	1.09
23.30	CB1	1.49	1.68	0.00	0.00	89.90	0.00	0.00	0.00	4.21
36.50	CA 19	1.40	1.43	0.00	1.04	94.45	0.00	0.23	0.00	1.45
38.20	CA 23	0.00	1.30	0.19	0.00	97.45	0.16	0.00	0.06	0.84
41.05	CA 27	6.02	0.86	0.43	0.07	79.41	0.12	0.45	0.03	12.53

Depth (m)	Samples	SiO2	TiO2	Al2O3	Fe2O3	MnO	MgO	CaO	Na2O	K2O	P2O5	LOI	Cr2O3	NiO
		wt-%	wt-%	wt-%	wt-%	wt-%	wt-%	wt-%	wt-%	wt-%	wt-%	wt-%	wt-%	wt-%
18.1	P188	46.95	0.51	8.12	22.90	0.17	1.17	1.39	0.00	1.49	0.05	16.78	0.02	0.03
17.9	P186	64.51	0.55	9.82	9.63	0.04	1.44	0.79	0.00	2.36	0.04	10.79	0.01	0.01
17.7	P184	62.09	0.51	9.76	11.22	0.03	1.53	0.82	0.00	2.65	0.04	11.40	0.02	0.01
17.5	P182	60.06	0.43	9.41	13.69	0.04	1.67	0.76	0.00	3.38	0.05	10.56	0.01	0.01
17.3	P180	30.25	0.18	4.60	39.27	0.33	1.11	2.20	0.00	1.97	0.06	19.84	0.01	0.01
17.1	P178	61.33	0.52	8.61	13.07	0.07	1.44	1.60	0.00	2.36	0.05	11.05	0.01	0.01
16.9	P176	49.19	0.49	9.11	15.17	0.11	1.57	6.47	0.00	2.36	0.07	14.53	0.02	0.01
16.7	P174	43.30	0.41	7.66	11.40	0.07	1.44	14.29	0.00	2.06	0.06	18.38	0.01	0.01
16.5	P172B	18.46	0.19	2.38	9.50	0.11	0.95	35.26	0.00	0.49	0.11	31.67	0.01	0.00
16.5	P172	23.52	0.25	3.31	9.97	0.10	1.09	31.08	0.00	0.72	0.09	28.98	0.01	0.00
16.3	P170	48.16	0.51	8.13	7.12	0.03	1.48	14.46	0.00	2.01	0.04	17.16	0.01	0.01
16.1	P168	51.08	0.52	8.30	7.12	0.01	1.55	12.40	0.00	2.36	0.05	15.59	0.01	0.01
15.9	P166	50.26	0.52	8.46	6.63	0.01	1.56	13.06	0.00	2.09	0.05	16.35	0.01	0.00
15.7	P164	46.49	0.53	8.40	5.39	0.02	1.61	16.24	0.00	1.82	0.06	18.58	0.01	0.01
15.5	P162	47.52	0.64	10.30	4.95	0.02	1.77	13.80	0.00	1.71	0.04	18.34	0.01	0.01
15.3	P160	47.60	0.64	10.56	5.13	0.01	1.75	13.47	0.00	1.74	0.04	18.22	0.01	0.01
15.1	P158	49.77	0.66	10.51	4.56	0.02	1.67	12.34	0.00	1.72	0.03	17.76	0.01	0.01
14.9	P156	49.26	0.61	9.83	4.33	0.02	1.63	13.88	0.00	1.67	0.03	17.86	0.01	0.01
14.7	P154	50.39	0.57	8.19	4.24	0.01	1.45	15.02	0.00	1.60	0.04	17.60	0.01	0.00
14.5	P152	50.28	0.52	8.32	5.59	0.01	1.44	14.01	0.00	1.99	0.04	16.85	0.01	0.01
14.3	P150	49.18	0.59	9.57	5.24	0.02	1.72	13.59	0.00	1.86	0.03	17.24	0.02	0.01
14.1	P148	39.73	0.42	5.58	5.33	0.05	1.34	22.88	0.00	1.18	0.04	22.56	0.01	0.00
13.9	P146	46.13	0.53	8.00	6.57	0.05	1.60	15.84	0.00	1.56	0.05	18.84	0.01	0.00
13.7	P144	52.03	0.63	9.46	6.59	0.03	1.65	11.28	0.00	1.90	0.04	15.42	0.01	0.00
13.5	P142	57.51	0.77	13.09	5.30	0.02	1.90	5.53	0.00	2.67	0.03	12.44	0.01	0.00
13.3	P140	53.02	0.66	11.23	4.98	0.02	1.81	10.56	0.00	2.36	0.04	14.74	0.01	0.00
13.1	P138	40.15	0.45	6.59	7.44	0.06	1.49	19.90	0.00	1.32	0.03	21.68	0.01	0.00
12.9	P136	33.54	0.38	5.65	6.33	0.07	1.40	25.45	0.00	1.06	0.03	25.16	0.01	0.00
12.7	P134	51.37	0.58	8.32	4.39	0.03	1.44	14.79	0.00	1.55	0.18	16.44	0.01	0.00
12.54	P132	55.31	0.63	9.23	3.52	0.01	1.37	12.28	0.00	1.76	0.03	14.94	0.01	0.00
12.42	P130	55.66	0.61	9.42	3.58	0.02	1.43	12.03	0.00	1.67	0.03	15.01	0.01	0.00
12.3	P128	52.65	0.49	6.62	3.47	0.03	1.17	16.94	0.00	1.24	0.03	16.52	0.01	0.00
12.18	P126	59.37	0.55	6.75	2.96	0.02	1.05	13.02	0.00	1.26	0.03	14.34	0.01	0.00
12.06	P124	58.56	0.65	7.86	6.56	0.02	1.24	10.97	0.00	1.51	0.04	11.69	0.01	0.01
11.9	P122	54.42	0.62	9.73	3.87	0.02	1.49	12.44	0.00	1.94	0.03	14.60	0.01	0.00
11.7	P120	61.34	0.75	10.44	3.45	0.01	1.39	7.98	0.00	1.87	0.04	12.19	0.01	0.00
11.5	P118	67.05	0.80	12.81	3.87	0.01	1.35	2.57	0.00	1.99	0.05	9.61	0.02	0.01
11.3	P116	62.93	0.87	14.64	4.23	0.01	1.45	2.63	0.00	2.13	0.04	11.25	0.02	0.01

11.1	P114	62.05	0.91	15.02	4.20	0.01	1.39	2.83	0.00	2.13	0.05	11.45	0.02	0.01
10.9	P112	62.32	0.88	14.54	3.91	0.01	1.29	3.16	0.00	2.08	0.08	10.76	0.02	0.01
10.7	P110	59.94	0.94	16.42	4.31	0.01	1.41	2.78	0.00	2.27	0.06	11.76	0.02	0.01
10.5	P108	63.04	0.95	15.66	4.09	0.01	1.28	2.31	0.00	2.12	0.05	10.54	0.02	0.01
10.3	P106	60.89	0.96	17.08	4.08	0.01	1.33	2.29	0.00	2.28	0.04	11.07	0.02	0.01
10.1	P104	59.28	0.96	17.60	4.09	0.02	1.37	2.80	0.00	2.37	0.11	11.35	0.02	0.01
9.9	P102	64.50	0.92	15.05	3.91	0.01	1.10	2.60	0.00	1.96	0.04	9.88	0.02	0.01
9.7	P100	58.02	0.99	17.63	3.92	0.01	1.27	3.80	0.00	2.19	0.04	12.10	0.02	0.01
9.5	P98	58.60	0.94	16.84	4.06	0.02	1.21	4.03	0.00	2.10	0.04	11.90	0.02	0.01
9.3	P96	58.41	0.96	17.07	3.87	0.02	1.21	4.10	0.00	2.10	0.04	11.67	0.02	0.01
9.1	P94	59.41	0.98	17.20	3.69	0.02	1.22	3.62	0.00	2.15	0.05	11.26	0.02	0.01
8.9	P92	58.81	0.98	16.90	3.77	0.01	1.20	3.86	0.00	2.10	0.04	11.65	0.02	0.01
8.7	P90	56.50	1.03	18.83	4.09	0.01	1.30	3.37	0.00	2.31	0.05	12.24	0.02	0.01
8.5	P88	58.48	0.96	16.88	4.10	0.01	1.17	4.13	0.00	2.11	0.04	11.64	0.02	0.01
8.3	P86	54.65	0.98	17.52	5.24	0.03	1.30	4.58	0.00	2.19	0.04	12.92	0.02	0.01
8.1	P84	52.68	0.99	18.00	6.42	0.03	1.34	4.46	0.00	2.24	0.05	13.44	0.02	0.01
7.9	P82	54.42	1.03	18.44	4.68	0.02	1.33	4.43	0.00	2.29	0.05	12.90	0.02	0.01
7.7	P80	54.23	0.98	17.52	4.05	0.01	1.23	5.38	0.00	2.11	0.04	13.69	0.02	0.01
7.5	P78	53.88	0.90	15.65	4.12	0.01	1.14	7.59	0.00	1.95	0.05	13.83	0.02	0.01
7.3	P76	52.20	0.93	16.64	4.00	0.02	1.20	7.79	0.00	2.03	0.05	14.25	0.02	0.01
7.1	P74	52.15	0.94	16.91	4.00	0.02	1.21	7.38	0.00	2.05	0.05	14.31	0.02	0.01
6.9	P72	53.82	0.93	15.58	3.61	0.02	1.15	8.13	0.00	1.92	0.05	13.93	0.02	0.01
6.7	P70	53.65	0.94	15.54	3.32	0.02	1.09	8.90	0.00	1.83	0.05	13.75	0.02	0.01
6.5	P68	55.06	1.04	17.12	3.66	0.02	1.19	5.89	0.00	2.04	0.04	13.22	0.02	0.01
6.3	P66	43.34	0.75	11.85	16.04	0.03	0.83	10.01	0.13	1.31	0.13	14.64	0.01	0.02
6.1	P64	53.04	0.96	16.64	4.03	0.02	1.17	7.35	0.00	1.98	0.04	13.86	0.02	0.01
5.9	P62	52.74	0.98	17.30	3.85	0.02	1.21	6.86	0.00	2.07	0.05	14.14	0.02	0.01
5.7	P60	50.08	0.91	16.00	3.59	0.02	1.21	10.16	0.00	1.91	0.07	15.05	0.02	0.01
5.5	P58	52.02	0.89	15.21	3.58	0.02	1.15	9.92	0.00	1.87	0.06	14.33	0.02	0.01
5.3	P56	52.13	0.91	15.34	3.70	0.02	1.16	10.06	0.00	1.95	0.05	13.67	0.02	0.01
5.1	P54	55.20	0.96	15.63	3.55	0.02	1.23	7.82	0.00	2.11	0.05	12.59	0.02	0.01
4.9	P52	53.19	0.91	14.67	4.21	0.01	1.11	8.70	0.00	1.79	0.07	14.35	0.02	0.01
4.7	P50	55.47	0.97	15.13	3.94	0.01	1.13	6.89	0.00	1.91	0.08	13.61	0.02	0.01
4.5	P48	53.33	0.97	16.93	4.54	0.01	1.19	6.04	0.00	2.05	0.08	14.05	0.02	0.01
4.3	P46	54.61	1.01	17.92	4.85	0.01	1.26	4.06	0.00	2.21	0.06	13.14	0.02	0.01
4.11	P44	51.93	1.01	18.16	5.08	0.01	1.19	5.24	0.00	2.07	0.04	14.53	0.02	0.01
3.91	P42	56.80	0.61	8.86	2.98	0.03	0.70	13.92	0.13	0.92	0.04	14.29	0.01	0.01
3.71	P40	49.67	0.90	18.31	5.48	0.03	1.40	7.10	0.05	2.19	0.08	14.61	0.02	0.01
3.51	P38	18.14	0.33	8.81	26.82	0.16	2.45	15.62	0.07	0.64	0.17	26.76	0.02	0.01
3.31	P36	24.39	0.45	8.86	28.73	0.17	3.29	8.40	0.06	0.90	0.06	24.64	0.02	0.00

3.11	P34	33.53	0.62	13.72	17.06	0.10	2.18	10.13	0.03	1.30	0.06	21.12	0.02	0.01
2.91	P32	24.16	0.39	10.97	24.27	0.14	2.55	12.28	0.08	0.84	0.10	24.23	0.02	0.01
2.71	P30	55.70	0.52	11.24	6.90	0.03	1.62	7.97	0.09	1.01	0.14	14.89	0.02	0.01
2.51	P28	25.64	0.37	13.71	26.00	0.13	2.10	9.16	0.07	0.73	0.54	21.54	0.02	0.01
2.31	P26	28.66	0.33	14.36	26.34	0.12	1.56	7.23	0.06	0.61	0.49	20.25	0.02	0.01
2.1	P24	32.45	0.39	15.92	25.51	0.10	1.31	4.69	0.07	0.70	0.27	18.60	0.02	0.01
1.91	P22	51.56	0.62	15.85	6.98	0.04	1.01	7.41	0.08	0.70	0.34	15.28	0.03	0.02
1.71	P20	73.32	0.49	8.55	3.86	0.03	0.53	3.98	0.10	0.42	0.20	8.38	0.02	0.00
1.51	P18	78.85	0.42	5.27	1.94	0.01	0.72	4.82	0.00	0.45	0.11	7.50	0.01	0.00
1.31	P16	79.88	0.41	5.46	1.87	0.01	0.76	3.92	0.00	0.54	0.07	7.01	0.01	0.00
1.11	P14	85.00	0.35	3.83	1.20	0.01	0.48	3.35	0.00	0.33	0.07	5.32	0.01	0.00
0.92	P12	81.67	0.38	5.29	1.83	0.01	0.64	3.09	0.00	0.53	0.07	6.45	0.01	0.00
0.67	P10	36.49	0.16	7.06	2.51	0.04	5.49	21.68	0.07	0.41	0.33	25.90	0.01	0.00
0.5	P8	13.14	0.16	3.47	2.52	0.09	15.68	26.70	0.03	0.50	0.21	37.60	0.00	0.01
0.44	P7	6.67	0.09	1.38	3.43	0.11	17.25	29.86	0.10	0.23	0.17	40.63	0.00	0.00
0.32	P6	3.40	0.05	1.14	3.75	0.08	17.60	31.53	0.08	0.18	1.06	40.87	0.00	0.01
0.26	P4	1.14	0.02	0.35	3.25	0.15	0.76	53.54	0.04	0.02	0.07	40.16	0.00	0.01
0.05	P1	0.02	0.01	0.06	0.87	0.09	0.55	57.10	0.04	0.00	0.02	41.07	0.00	0.00

A.2.7. Trace elements content

- Wawal section

Depth (m)	Samples	Nb (ppm)	Zr (ppm)	Y (ppm)	Sr (ppm)	U (ppm)	Rb (ppm)	Th (ppm)	Pb (ppm)
18.1	P188	18	170	28	56	3	62	9	15
17.9	P186	14	205	22	52	2	105	10	12
17.7	P184	16	179	19	53	3	108	11	15
17.5	P182	12	169	14	46	3	116	7	13
17.3	P180	14	77	6	32	2	40	3	8
17.1	P178	12	262	13	55	2	83	7	6
16.9	P176	15	179	18	306	3	105	7	6
16.7	P174	11	215	18	667	2	77	8	2
16.5	P172B	3	196	14	624	3	12	6	2
16.5	P172	5	234	16	667	3	21	7	2
16.3	P170	10	302	16	675	2	76	6	2
16.1	P168	9	368	16	569	2	80	5	2
15.9	P166	9	327	14	609	3	76	8	2
15.7	P164	13	304	19	749	2	74	10	2
15.5	P162	16	254	20	603	5	84	10	3
15.3	P160	11	240	16	513	2	73	7	2
15.1	P158	16	268	18	608	4	87	10	5
14.9	P156	15	274	18	687	2	81	9	2
14.7	P154	8	329	13	583	2	57	6	2
14.5	P152	11	299	15	626	2	77	8	2
14.3	P150	10	290	16	531	2	83	10	2
14.1	P148	7	323	19	712	2	43	9	2
13.9	P146	7	298	16	515	2	59	8	2
13.7	P144	9	298	15	411	2	75	7	2
13.5	P142	12	215	14	205	2	117	6	2
13.3	P140	12	243	20	471	3	112	8	2
13.1	P138	8	262	19	561	2	55	7	2
12.9	P136	6	266	19	571	2	38	9	2
12.7	P134	9	307	21	569	2	62	9	2
12.54	P132	10	294	17	510	2	76	7	2
12.42	P130	7	291	14	484	2	72	5	2
12.3	P128	8	334	18	630	3	51	10	4
12.18	P126	8	381	16	523	2	52	7	2
12.06	P124	10	356	18	469	3	62	8	13
11.9	P122	11	287	18	481	2	81	7	2
11.7	P120	12	345	19	331	3	82	8	8
11.5	P118	16	294	18	135	3	97	7	14
11.3	P116	13	287	19	132	3	102	6	18
11.1	P114	15	326	20	152	2	102	7	14
10.9	P112	16	301	23	178	6	103	7	25
10.7	P110	14	279	19	145	3	106	6	15
10.5	P108	20	312	24	148	4	116	7	21
10.3	P106	14	282	19	133	2	114	6	21
10.1	P104	20	267	31	168	2	134	6	24
9.9	P102	17	322	22	156	4	103	6	20
9.7	P100	19	308	25	231	5	116	7	23
9.5	P98	17	301	22	206	3	104	7	17
9.3	P96	18	319	22	223	3	107	7	17
9.1	P94	19	317	25	194	4	111	7	16
8.9	P92	20	329	26	222	4	112	6	18
8.7	P90	18	250	18	162	2	101	14	13
8.5	P88	15	295	24	233	3	105	7	17

Depth (m)	Samples	Ni (ppm)	Co (ppm)	Cr (ppm)	V (ppm)	Ce (ppm)	Nd (ppm)	Ba (ppm)	La (ppm)	Hf (ppm)	Sc (ppm)	As (ppm)
18.1	P188	312	80	69	101	3	4	103	20	3	26	16
17.9	P186	62	24	88	115	38	16	154	38	6	15	31
17.7	P184	51	24	102	121	31	17	83	35	7	20	34
17.5	P182	40	22	90	101	8	6	129	26	5	16	28
17.3	P180	76	69	42	50	3	4	45	5	1	19	13
17.1	P178	25	19	85	86	4	4	114	16	7	15	25
16.9	P176	33	25	71	85	3	11	110	25	7	14	18
16.7	P174	22	24	64	70	3	15	108	18	4	8	14
16.5	P172B	12	26	30	18	3	11	94	16	1	2	6
16.5	P172	17	26	36	27	3	17	76	16	4	2	6
16.3	P170	21	18	75	70	9	18	154	13	7	5	18
16.1	P168	18	19	92	78	15	19	116	20	11	3	19
15.9	P166	21	17	75	72	15	21	131	21	6	5	18
15.7	P164	22	19	69	83	14	25	102	22	9	2	15
15.5	P162	26	17	76	89	27	30	131	28	5	3	12
15.3	P160	21	15	88	96	25	22	141	29	8	6	13
15.1	P158	28	17	87	98	33	31	92	26	9	6	13
14.9	P156	22	18	83	88	24	27	131	30	8	2	16
14.7	P154	17	13	79	74	22	30	169	23	7	10	11
14.5	P152	18	18	78	72	17	26	150	26	8	6	12
14.3	P150	16	16	85	88	17	16	172	36	4	2	9
14.1	P148	13	13	60	49	3	21	128	25	4	2	10
13.9	P146	16	16	73	75	12	24	154	30	6	2	9
13.7	P144	17	14	75	86	18	18	146	26	6	6	13
13.5	P142	23	15	89	121	52	29	189	32	6	9	13
13.3	P140	23	14	82	95	30	28	200	29	6	5	9
13.1	P138	14	17	62	55	3	17	145	20	5	2	11
12.9	P136	11	17	50	46	3	24	141	19	1	2	7
12.7	P134	19	14	68	70	26	33	150	30	8	3	14
12.54	P132	17	10	75	87	27	25	177	27	6	4	15
12.42	P130	13	13	78	89	33	30	171	30	7	8	15
12.3	P128	20	12	71	63	14	22	164	28	6	2	20
12.18	P126	18	12	67	71	25	26	145	24	11	2	24
12.06	P124	23	12	76	76	26	24	140	22	8	6	24
11.9	P122	25	16	77	87	32	25	191	26	7	3	21
11.7	P120	17	10	81	99	42	24	156	27	7	7	16
11.5	P118	29	18	85	127	59	29	205	33	6	15	36
11.3	P116	29	15	99	150	73	33	189	32	7	15	18
11.1	P114	32	15	104	157	84	33	245	38	7	17	18
10.9	P112	34	15	94	150	83	39	223	32	7	14	17
10.7	P110	38	18	100	168	91	45	200	39	6	15	20
10.5	P108	39	17	105	156	86	35	235	41	7	13	20
10.3	P106	39	18	107	172	86	35	216	36	6	15	20
10.1	P104	44	20	108	176	85	41	246	40	6	17	18
9.9	P102	41	17	102	158	79	39	226	32	8	14	18
9.7	P100	45	19	111	176	93	43	227	40	7	16	22
9.5	P98	42	19	109	177	89	42	219	44	8	14	28
9.3	P96	44	17	113	181	98	48	214	38	9	13	25
9.1	P94	40	19	106	174	97	47	218	37	8	15	29
8.9	P92	40	18	110	167	96	52	255	37	7	14	21
8.7	P90	37	13	155	190	132	52	220	62	9	16	20
8.5	P88	42	17	118	171	106	53	230	39	6	15	23

8.3	P86	20	291	25	239	2	112	6	16	21	71
8.1	P84	21	267	26	215	5	117	8	17	22	72
7.9	P82	20	288	25	218	4	121	7	17	23	80
7.7	P80	20	311	25	300	3	108	8	16	21	76
7.5	P78	11	310	18	377	2	79	6	5	17	68
7.3	P76	19	313	25	447	4	101	8	14	20	74
7.1	P74	15	309	24	404	4	96	7	9	19	70
6.9	P72	12	321	19	397	3	79	8	8	17	62
6.7	P70	18	399	25	488	4	89	7	10	19	68
6.5	P68	22	357	30	318	6	110	9	21	24	81
6.3	P66	12	227	20	439	3	53	7	27	15	60
6.1	P64	19	311	26	402	3	101	7	19	21	78
5.9	P62	25	307	29	378	5	111	8	21	21	79
5.7	P60	21	338	28	534	4	99	9	15	20	74
5.5	P58	20	359	27	515	4	93	8	15	18	75
5.3	P56	17	327	24	487	4	90	7	10	18	174
5.1	P54	22	363	28	407	3	111	9	17	20	74
4.9	P52	21	386	27	477	6	93	8	18	17	75
4.7	P50	21	354	27	403	6	99	8	21	19	83
4.5	P48	23	303	26	350	8	110	8	24	21	90
4.3	P46	9	255	13	186	5	87	5	2	19	75
4.11	P44	5	241	10	195	3	71	5	2	17	57
3.91	P42	10	423	16	583	3	43	10	2	12	33
3.71	P40	9	252	14	255	2	89	9	2	19	45
3.51	P38	14	130	17	195	6	23	26	2	12	57
3.31	P36	14	174	13	172	2	34	6	5	13	70
3.11	P34	15	208	18	350	5	58	10	4	16	56
2.91	P32	12	145	18	221	4	31	16	2	11	61
2.71	P30	1	231	7	94	2	23	11	2	9	21
2.51	P28	9	168	26	106	3	22	25	2	10	71
2.31	P26	2	136	16	64	2	14	20	2	10	60
2.1	P24	8	187	11	67	2	22	19	2	12	75
1.91	P22	4	371	33	88	13	28	25	13	10	34
1.71	P20	8	391	19	105	2	21	19	5	9	548
1.51	P18	1	211	6	44	2	8	11	6	7	70
1.31	P16	3	262	9	75	2	19	10	3	8	130
1.11	P14	7	231	10	86	2	16	13	6	7	109
0.92	P12	4	209	9	66	2	19	10	3	9	83
0.67	P10	2	134	18	435	3	16	15	2	6	209
0.5	P8	1	74	10	113	4	15	7	2	6	58
0.44	P7	1	68	15	181	7	13	3	2	5	485
0.32	P6	1	27	58	222	32	12	2	5	6	98
0.26	P4	1	77	7	659	10	1	8	2	5	98
0.05	P1	1	31	7	419	7	1	4	2	3	200

8.3	P86	42	18	112	172	85	48	225	38	9	14	17
8.1	P84	45	18	108	173	75	41	223	37	9	15	21
7.9	P82	46	20	115	182	81	44	229	41	7	15	25
7.7	P80	41	16	115	174	100	54	223	45	9	11	23
7.5	P78	39	18	115	147	86	45	179	42	7	10	21
7.3	P76	40	18	111	156	81	42	210	42	5	9	36
7.1	P74	37	17	115	157	83	47	217	41	7	10	26
6.9	P72	32	15	105	140	72	43	216	46	8	9	35
6.7	P70	35	16	116	149	81	54	212	41	9	8	26
6.5	P68	44	20	123	163	91	48	239	53	11	12	27
6.3	P66	112	36	82	107	19	26	125	32	8	12	242
6.1	P64	43	16	115	160	79	49	225	43	8	10	20
5.9	P62	47	18	113	164	87	53	141	41	7	11	21
5.7	P60	40	18	110	145	73	53	173	44	10	6	18
5.5	P58	42	16	111	144	71	50	238	37	7	7	22
5.3	P56	46	20	109	151	78	51	186	41	8	7	26
5.1	P54	43	17	111	152	73	42	148	37	9	8	20
4.9	P52	51	20	111	148	69	46	159	38	8	9	26
4.7	P50	55	21	114	153	78	44	202	43	8	11	32
4.5	P48	70	24	163	176	90	49	174	38	9	13	26
4.3	P46	50	27	123	183	97	51	182	44	4	17	45
4.11	P44	46	27	132	180	84	42	188	50	6	14	49
3.91	P42	37	24	95	107	27	32	148	29	9	3	48
3.71	P40	49	29	153	237	71	44	197	47	3	13	46
3.51	P38	120	92	176	432	3	5	20	14	1	15	42
3.31	P36	50	58	71	176	3	4	52	5	3	28	26
3.11	P34	60	44	102	211	3	19	134	20	1	16	57
2.91	P32	63	59	128	266	3	11	78	16	1	21	80
2.71	P30	31	38	185	329	52	42	163	49	7	13	115
2.51	P28	68	64	233	512	3	9	132	19	1	44	77
2.31	P26	45	53	218	515	3	4	147	21	1	47	48
2.1	P24	62	53	225	617	3	4	133	13	1	55	61
1.91	P22	147	64	314	592	55	71	107	43	7	18	62
1.71	P20	31	25	200	395	50	34	87	31	12	15	87
1.51	P18	8	10	97	141	39	18	147	20	7	10	44
1.31	P16	20	20	82	147	42	19	119	20	8	10	46
1.11	P14	18	16	75	127	37	16	92	22	8	8	43
0.92	P12	16	15	94	173	36	17	117	22	7	10	59
0.67	P10	21	16	158	275	14	41	103	46	1	2	48
0.5	P8	15	18	40	59	26	37	159	20	1	2	40
0.44	P7	18	14	25	36	25	32	34	6	1	2	29
0.32	P6	28	15	13	28	35	35	45	62	1	10	28
0.26	P4	28	40	2	11	3	15	91	5	1	2	204
0.05	P1	3	5	10	6	3	11	9	4	1	2	6

APPENDIX 3. AFFILIATED PAPER

Review of Palaeobotany and Palynology 197 (2013) 50–69

Contents lists available at SciVerse ScienceDirect

Review of Palaeobotany and Palynology

journal homepage: www.elsevier.com/locate/revpalbo

Research paper

Reconstructing Valanginian (Early Cretaceous) mid-latitude vegetation and climate dynamics based on spore–pollen assemblages

Ariane Kujau [a], Ulrich Heimhofer [b], Peter A. Hochuli [c], Sebastian Pauly [a], Chloé Morales [d], Thierry Adatte [d], Karl Föllmi [d], Izabella Ploch [e], Jörg Mutterlose [a]

[a] Ruhr-University Bochum, Germany
[b] Leibniz University Hannover, Germany
[c] University of Zurich, Switzerland
[d] University of Lausanne, Switzerland
[e] Polish Institute of Geology, Warsaw, Poland

article info

Article history:
Received 2 September 2012
Received in revised form 4 May 2013
Accepted 9 May 2013
Available online 21 May 2013

Keywords:
Early Cretaceous
Valanginian palynology
vegetation
$\delta^{13}C_{org}$ chemostratigraphy
nannofossil biostratigraphy
paleoclimate

abstract

Changes in terrestrial vegetation patterns during the Valanginian (Early Cretaceous) and their link to major climatic and environmental alterations are poorly studied. In this study, the spatial and temporal changes in plant community structure are reconstructed based on spore–pollen records from two mid-latitude sites located in the Mid-Polish Trough (MPT, central Poland), and the Vocontian Basin (VB, southeast France). Stratigraphic control is provided by $\delta^{13}C_{carb}$ chemostratigraphy and calcareous nannofossil biostratigraphy. Reconstruction of hinterland vegetation is based on palynological investigations of 83 samples from hemipelagic (VB) and marginal marine (MPT) sediments rich in terrestrial palynomorphs. A total of 45 palynomorph taxa were identified at generic level (30 spores, 15 pollen). Vegetation around the MPT was dominated by araucarian/cupressacean conifers while that surrounding the VB was dominated by drought-resistant cheirolepidiacean conifers. At both sites the understorey and/or vegetation of open areas was dominated by pteridophytes. An early Valanginian gradual trend towards humid conditions at the MPT, well expressed by a distinct increase in the spore–pollen ratio, culminates in a short-lived spore-maximum stratigraphically located at the lower/upper Valanginian boundary. It is characterized by low conifer abundances and high abundances of the fern spore taxa Cyathidites, Leiotriletes and Gleicheniidites accompanied by enhanced abundances of the pteridosperm pollen Vitreisporites pallidus, whose parent plants are assumed to be indicative of swamp habitats. The spore-maximum is coeval to a similar peak observed in the VB, characterized by essentially the same taxa. Here, the spore-maximum is preceded by a protracted phase of arid conditions, characterized by low spore abundances and exceptionally high numbers of the cheirolepidiacean conifer pollen Classopollis. Changes in moisture, identified as the key climatic factor determining trends and turnovers in vegetation, were probably controlled by a monsoonal circulation. The supra-regional humid phase expressed by the coeval spore maxima was probably induced by an intensified monsoonal climate. The temporal influence of a northern hemisphere arid belt at the VB, under the influence of the subtropical high-pressure belt, may have caused the temporal drying not affecting the MPT site, located further north.

1. Introduction

The Valanginian (Early Cretaceous) was characterized by several alterations of the ocean–atmosphere system. These primarily include prominent perturbations of the carbon cycle that were globally recorded by a positive carbon isotope excursion (CIE; e.g. Cotillon and Rio, 1984; Lini et al., 1992; Hennig et al., 1999; Wortmann and Weissert, 2000; Weissert and Erba, 2004; Gröcke et al., 2005; Föllmi et al., 2006; Nunn et al., 2010). This CIE was accompanied by fluctuations in atmospheric pCO_2 concentration, probably connected to volcanic activity (e.g. Lini et al., 1992; Price and Mutterlose, 2004; Weissert and Erba, 2004). Furthermore, changes in terrigenous input to ocean margins (Weissert, 1989; Föllmi et al., 1994; Weissert et al., 1998; Weissert and Erba, 2004; Föllmi et al., 2006) and a pronounced phase of climatic cooling were proposed based on geochemical analyses (Weissert and Lini, 1991; Podlaha et al., 1998; Pucéat et al., 2003; McArthur et al., 2007; Brassell, 2009; Price and Nunn, 2010) as well as on changes in calcareous nannofossil assemblages (Mutterlose and Kessels, 2000; Melinte and Mutterlose, 2001; Mutterlose et al., 2003). Indirect evidence for the establishment of high-latitude ice caps in the form of ice-rafted debris and glendonites has been discussed (Kemper, 1987; Frakes and Francis, 1988; Price, 1999; Gréselle and Pittet, 2010, and references therein). So far, most studies have concentrated on changes in the marine biosphere and on turnovers in numerous marine organisms (e.g. Mutterlose and Kessels,

Corresponding author at: Universitätsstraße 150, 44801 Bochum, Germany. Tel.: +49 234 32 23255; fax: +49 234 32 14571.
E-mail address: ariane.kujau@rub.de (A. Kujau).

0034-6667/$ – see front matter © 2013 Elsevier B.V. All rights reserved.
http://dx.doi.org/10.1016/j.revpalbo.2013.05.003

2000; Melinte and Mutterlose, 2001; Mutterlose et al., 2003), including a "biocalcification crisis" in pelagic settings associated with a widespread river-influenced carbonate platform demise (e.g. Weissert and Erba, 2004) and a nannoconid decline (e.g. Barbarin et al., 2012). In contrast, continental environments have received less attention. Little is known about the interdependence of terrestrial plant communities and the extreme environmental and climatic perturbations associated with the Valanginian CIE. Other than for stratigraphic purposes information on Valanginian vegetation changes is scarce.

Here, we present two palynological records covering Valanginian strata. The first section consists of sediments deposited in a marginal setting within the Mid-Polish Trough (MPT) of central Poland. It was located within the Carpathian Seaway that connected the Boreal Realm and the Tethys. The second record is derived from hemipelagic deposits cropping out in the Vocontian Basin (VB) of southeast France, which was located further south and part of the northwestern Tethys. From a paleophytogeographic perspective, both sites were situated within the humid, warm-temperate European region, rich in ferns (Ziegler et al., 1987). In order to assess changes in vegetation structure and in associated paleoenvironmental parameters, encountered palynomorphs were determined taxonomically and their stratigraphic distribution is presented for both sites. To compare the palynological records from the two localities, stratigraphic correlation has been carried out based on calcarous nannofossil biostratigraphy and trends in carbon isotopes ($\delta^{13}C_{carb}$ chemostratigraphy). Variations in the abundances of the spore–pollen allowed the definition of local palynological assemblages for both sites. Based on botanical affinities to modern plants, ecological preferences of the fossil palynomorph taxa are deduced, providing information on changes in physical environmental parameters (e.g. moisture). Due to their paleogeographic position under the influence of the subtropical high-pressure belt, the vegetation from both sites serves as a sensitive recorder of changes in climatic patterns. The absence of large polar ice-caps in combination with the plate-tectonic configuration during the Valanginian and a large ocean, the Tethys, in the south of paleo-Europe, is favorable for the establishment of a monsoonal climate on the southern margin of paleo-Europe. This potential monsoonal influence expressed in vegetation changes has been investigated.

2. Geological setting and stratigraphy of studied sections

2.1. The Mid-Polish Trough (MPT) record

Material from a core (PIG1) which was drilled close to the village of Wąwał (E 19°15 0 , N 52°25 0) by the Polish Institute of Geology, Warsaw, was studied (Figs. 1A and 2). Wąwał is located about 4 km southeast of the city of Tomaszów Mazowiecki, and about 115 km southwest of Warsaw. The highly condensed succession has a thickness of 18 m. Its lithology is composed of clay and claystone with layers of more sandy intervals, shells and sideritic, calcareous and phosphatic nodules. The basal part (80 cm) consists of limestone, presumably of Berriasian age (Kutek et al., 1989). The core material lacks ammonites of biostratigraphic significance; the age model is based on calcareous nannofossil biostratigraphy and $\delta^{13}C_{org}$–$\delta^{13}C_{carb}$ chemostratigraphy. Additional stratigraphic control is supplied by lithostratigraphic correlation of the core with a near-by clay pit well dated by ammonites (Kutek et al., 1989; Kaim, 2001). Accordingly, the PIG1 core from Wąwał covers deposits of Berriasian/early Valanginian to late Valanginian age (Fig. 2). During the Cretaceous, the Carpathian Seaway connected the Tethys and the Boreal Realm via the Lower Saxony Basin and the North Sea Basin (Kutek et al., 1989; Mutterlose, 1992; Kaim, 2001). The study site is located in the MPT in the center of the Carpathian Seaway at a paleolatitude of ~35–40°N (e.g. Blakey, 2010).

2.2. The Vocontian Basin (VB) record

The material studied in the VB is derived from three outcrops (La Charce, Vergol, Morenas) located in the Drome department (Figs. 1B and 2). The Vergol section (E 5°25 9 , N 44°12 12) is located between the villages Montbrun-les-Bains and Vergol. Logged and sampled strata (thickness of ~57 m) cover sedimentary rocks from the lower Valanginian (Busnardoites campylotoxus Zone) to the upper Valanginian (Saynoceras verrucosum Subzone). To compensate for a hiatus of slumping, the interval between 25 and 30 m of the Vergol section was covered by samples collected nearby at the lithostratigraphically well correlated Morenas section (E 5°25 23 , N 44°13 52). The La Charce section (E 5°26 23 , N 44°28 13) is easily accessible on the hill slopes west of the village of La Charce. Logged and sampled strata (thickness of ~113 m) cover the stratigraphic interval from the lower part of the Upper Valanginian (Karakaschiceras pronecostatum Subzone) to the Lower Hauterivian (Acanthodiscus radiatus Zone; Gréselle and Pittet, 2010, and references therein). During the Early Cretaceous the VB was located at a paleolatitude of ~30°N in a marginal marine position of the Western Ligurian Tethys Ocean, open to the east. To the north the VB was separated from the Boreal Realm by the archipelago of mid-European continents (Ziegler, 1982; Masse, 1993; Hay et al., 1999; Blakey, 2010). The central part of the VB is characterized by hemipelagic deposits composed of autochthonous carbonates, allochthonous fine-grained carbonate exported from three surrounding platforms (Fig. 1A; Reboulet et al., 2003; Gréselle and Pittet, 2010), and terrigenous material, mostly eroded from the Massif Central area (Bréhéret, 1994; Fesneau et al., 2009). The studied deposits are rich in marine invertebrate fossils and consist of

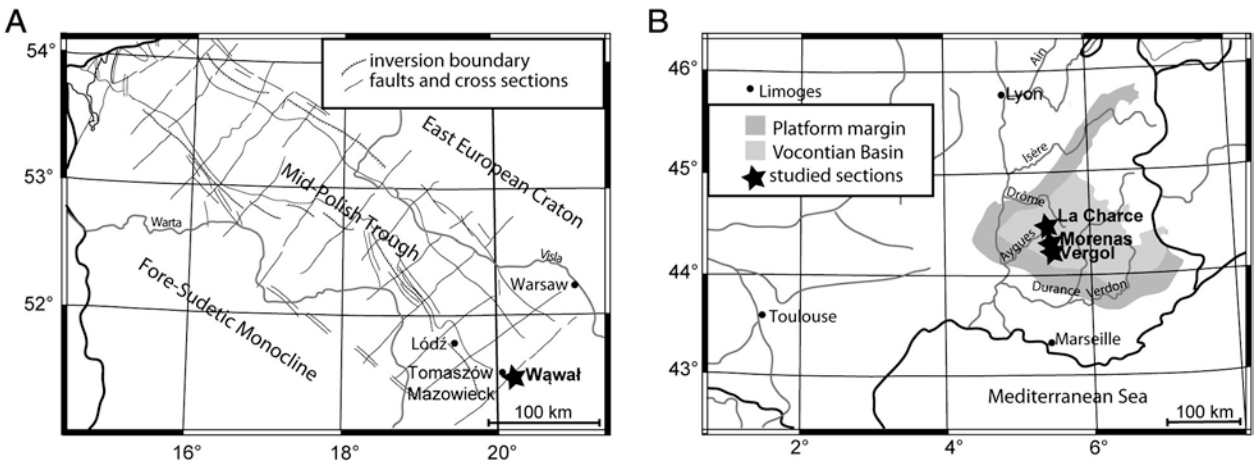

Fig. 1. Location of sites. A) Polish site (Wąwał) within the Mid-Polish Trough (MPT; modified after Daldez, 2003), B) French site (La Charce, Vergol, Morenas) within the Vocontian Basin (VB; modified after Gréselle, 2007).

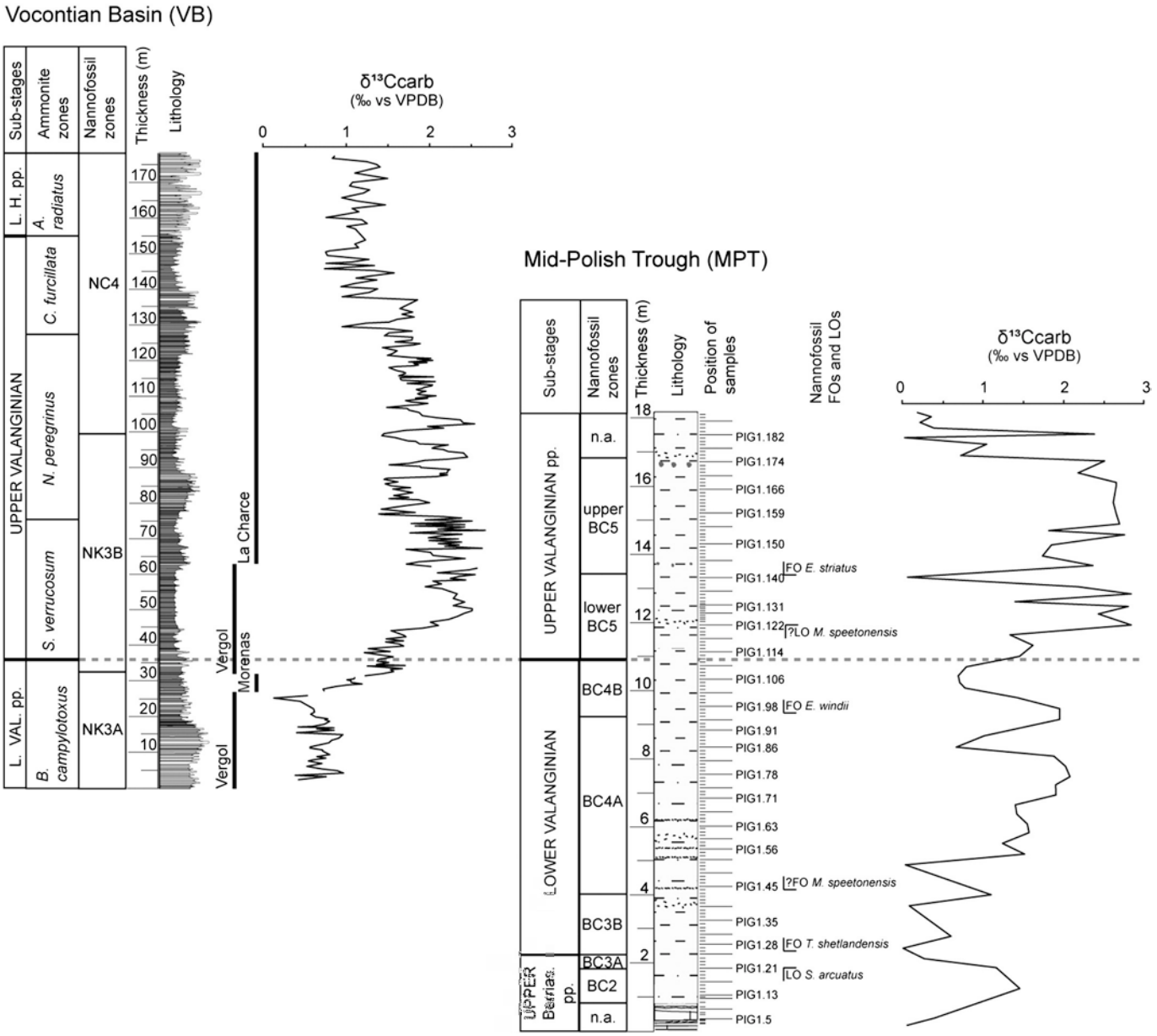

Fig. 2. Biostratigraphic (nannofossils) and chemostratigraphic (δ13Ccarb) correlation of VB (left) and MPT (right from Morales et al., in prep.). Furthermore, thickness, lithology (for legend see Fig. 3 and 4), composition of VB composite succession (Vergol, Morenas, La Charce), and position of samples (MPT; for VB see Fig. 4) are shown. Nannofossil correlation is based on Tethyan (NK, NC after Gréselle et al., 2011) and Boreal (BC, this study) nannofossil zones, following Bown (1998). FO = first occurrence, LO = last occurrence. Position of palynologic samples is marked as elongated horizontal lines (only MPT), short lines mark additional samples for δ13C. Orientation is following the Lower to Upper Valanginian boundary (light dashed line).

well exposed orbitally-controlled marl-limestone alternations, stacked in bundles (Gréselle and Pittet, 2010). The composite section has a well-established age model based on ammonites, calcareous nannofossils, and cyclostratigraphy; it covers sediments from the lower Valanginian to lower Hauterivian (Gréselle et al., 2011 and references therein). Age control is also provided by $\delta^{13}C_{carb}$ chemostratigraphy that was compared to existing, well dated Tethyan records (Kujau et al., 2012). The composite succession has a total thickness of ~175 m and covers the interval of the lower Valanginian B. campylotoxus to lower Hauterivian A. radiatus ammonite zones (Gréselle and Pittet, 2010, Fig. 2).

3. Material and methods

3.1. Terrestrial palynology

A total of 83 palynological samples (46 from MPT and 37 from the VB) was studied quantitatively and qualitatively using transmitted light microscopy on an OLYMPUS BX-51. For samples from the MPT locality contamination by modern plant material can be excluded due to sampling of fresh drill core material. In order to minimize contamination of the VB based samples, the uppermost 15–20 cm of sediment was removed before sampling. Preparation of strew slides was done at the Geological Survey NRW, Germany, following standard procedures (Traverse, 2007). For plotting the results the software Tilia® was used. For each sample a total of 300 palynomorphs (+/−5) were counted. This was done on one to two slides depending on the richness of palynomorphs in the samples.

3.2. Nannofossil biostratigraphy

For the investigation of calcareous nannofossils from the MPT a total of 135 of samples were studied, the preparation of standard smear slides follows Bown (1998). Nannofossil information for the VB, using the Tethyan (NC) zonation scheme, was adopted from Gréselle et al. (2011).

Identification of calcareous nannofossils for the MPT was carried out using an OLYMPUS BH-2 light microscope with cross-polarized light at a magnification of ×1250. At least two traverses of each smear slide were studied. Identification of taxa follows the taxonomic concepts of Perch-Nielsen (1985) and Bown et al. (1998). For this section we used the BC (Boreal calcareous nannofossil) zonation scheme of Bown et al. (1998).

3.3. Stable carbon isotopes

The stable carbon isotope record ($\delta^{13}C_{carb}$) for the MPT is adopted from Morales et al. (pers. comm.), performed on the same core (PIG 1). Measurements of $\delta^{13}C_{carb}$ for the VB sections were carried out on powdered bulk sample material (~0.6 mg) on 295 samples (the first 97 are already presented in Kujau et al., 2012). A Thermo Fisher Scientific Gasbench II carbonate device connected to a Thermo Fisher Scientific Delta S isotope ratio mass spectrometer, available at the Ruhr-University Bochum, Germany, was used for stable isotope analyses. The gas bench uses 100% phosphoric acid at 70 °C to release CO_2 of the calcite from the sample material 1 h prior to the start of the measurement. Repeated analyses of certified carbonate standards (CO-1, CO-8, NBS-19) show an external reproducibility ±0.1‰ for $\delta^{18}O$ and ±0.06‰ for $\delta^{13}C_{carb}$. Values are expressed in conventional delta notation relative to the VPDB international standard, in per (‰). Duplicate measurements (31) show that the measured values are representative and indicate that the samples are homogenous (max. dev. $\delta^{18}O \pm 0.17$ and $\delta^{13}C \pm 0.12$).

4. Results

4.1. Terrestrial palynology

A total of 45 palynomorph taxa, were identified on the generic level (30 spores and 15 pollen) throughout the investigated samples. Botanical affinities and ecologic preferences of the parent plant are provided in Tables 1 and 2. Palynological results from the two areas show strong similarities regarding diversity of taxa. Only four spores found in the MPT

Table 1
Recorded sporomorph taxa from the composite section of the Vocontian Basin and the Wawal core and their probable botanical affinities. For describing author see Table 2.

	Taxa	Botanical affinity
Pollen	Araucariacites[1]	Araucariaceae[1]
	Callialasporites[2]	Araucariaceae[1,2]
	Inaperturopollenites[3]	Cupressaceae (formerly Taxodiaceae, e.g. Birkenmajer et al., 2010)/Araucarian[1/3]
	Perinopollenites[4]	Cupressaceae (formerly Taxodiaceae)/Araucarian[1/3]
	Cerebropollenites[5]	Cupressaceae (formerly Taxodiaceae)[4]
	Cycadopites[6]	Cycadales, Bennettitales, Ginkgoales[3]
	Eucommiidites[7]	Cycadales[1,5]
	Ephedripites[8]	Ephedrales/Ephedraceae[6]
	Classopollis[9] (=Corollina, Circulina)	Cheirolepidiaceae[7,5]
	Exesipollenites[10]	Bennettitales[8,9]
	Alisporites group[11] (bisaccate)	Conifers and Pteridospermae/Corystospermales (Pteridosperms)[2,10/1,5]
	Vitreisporites pallidus[15] (bisaccate)	Caytoniales (Pteridosperms)[1]
	Parvisaccites[12] (bisaccate)	Podocarpaceae[11]
	Podocarpidites[14] (bisaccate)	Podocarpaceae[12]
	Pinuspollenites[13] (bisaccate)	Coniferopsida[13]
Spores	Cyathidites[16] (Deltoidospora)	Dicksoniaceae, Cyatheaceae, Dipteridaceae, Filicopsida, Matoniaceae[3,4,5,14]
	Trilobosporites[19]	Dicksoniaceae[15,3]
	Gleicheniidites[20]	Gleicheniaceae[16]
	Neoraistrickia[21]	Lycopodiales[3]
	Clavatisporites[22]	Filicopsida[17]
	Biretisporites[23]	Filicopsida[17]
	Leiotriletes[24] (Deltoidospora)	Filicopsida[17]
	Osmundacidites[25]	Filicopsida or Osmundaceae (Osmunda-type)[7,3]
	Gemmatriletes[26]	Filicopsida[17]
	Verrucosisporites	Filicopsida[17]
	Klukisporites[27]	(Filicopsida or) Schizaeaceae[18]
	Todisporites[28]	Osmundaceae (Todites-type)[7,3]
	Retriletes[29]	Lycopodiaceae (Lycopodium type)[16,3]
	Camarozonosporites[30]	Lycopodiaceae[19]
	Lycopodiumsporites[31]	Lycopsida: Lycopodiaceae (Lycopodium)[17]
	Leptolepidites[32]	Lycopodiales[19,3]
	Lycopodiacidites[33]	Lycopodiales[19]
	Staplinisporites[34]	Bryophyta and Lycopodiaceae[16,2,3]
	Aratrisporites[35]	Lycopsida[17]
	Densoisporites[36]	Lycopodiaceae or Pleuromeiaceae (Selaginella)/Pleuromeiaceae[20,21,/22,3]
	Cicatricosisporites[37]	Schizaeaceae, Anemia/Mohria type[23,24,3]
	Ischyosporites[38]	Schizaeaceae, Lygodium-type[23,24,3]
	Stereisporites[39]	Bryophyta[19]
	Aequitriradites[40]	Bryophyta[17]
	Foraminisporis[41]	Bryophyta, namely hepatics/Anthocerotaceae[25/19]
	Concavissimisporites[42] (Deltoidospora)	Dickinsoniaceae, Cyatheaceae[26,3]
	Concavisporites[43]	Matoniaceae[14]
	Foveosporites[44]	Lycopodiales/Selaginellales[27/28]
	Echinatisporis[45]	Lycopods/Selaginella[19]
	Microreticulatisporites	?
Zygnemataceae	Ovoidites (Scafati et al., 2009; freshwater algae)	
Prasinophyceae	Leiosphaeridia (Scafati et al., 2009; marine to freshwater algae)	
Acritarch	Leiofusa (van de Schootbrugge et al., 2007; "disaster species")	

Selected references for botanical affinities: [1]Van Konijnenburg-Van Cittert (1971), [2]Boulter and Windle (1993), [3]Abbink et al. (2004), [4]van der Burgh and Van Konijnenburg-Van Cittert (1989), [5]Balme (1995), [6]Azéma and Boltenhagen (1974), [7]Van Konijnenburg-Van Cittert (1987), [8]Harris (1969, [9]1974), [10]Traverse (2007), [11]Schrank (2010), [12]Raine et al. (2006), [13]Larsson (2009), [14]Van Konijnenburg-Van Cittert (1993), [15]Venkatachala et al. (1969), [16]Potonié (1967), [17]Raine et al. (2008), [18]Couper (1958), [19]Filatoff (1975), [20]Knox (1950), [21]Lundblad (1950), [22]Raine et al. (1988), [23]Van Konijnenburg-Van Cittert (1981, [24]1991), [25]Dettmann (1963), [26]Potonié (1970), [27]Döring (1965), and [28]Courtinat (1989).

Table 2
Spores and pollen grouped according to family/genera level with exemplary reference and author of first description, plate and figure, and affiliation to classis with short description of ecological preference of parent plant for important taxa, if known.

Genera	Author and reference	Plate and figure	Botanical affinity	Ecological preference of parent plants
Bisaccate pollen:				
Vitreisporites	(Reissinger) Nilsson (1958), in Baltes (1967)	Plate I, 11	Pteridosperms/Ginkgos (Balme, 1995)	Deltaic environments, flood plain to backswamps, indicative of humid environments (Abbink et al., 2004 and references therein).
Alisporites	Couper (1958), in Hochuli and Kelts (1980)	Plate I, 1, 2	Pteridosperms/Ginkgos (or conifers) (Batten, 1975; Balme, 1995; Schrank, 2010)	
Parvisaccites	Couper (1958), in Balme (1995)	Plate I, 3, 4	Conifers (Balme, 1995)	Mountain habitats, cooler conditions, sometimes ascribed as typical floral elements of boreal regions with broad temperature range but preference for relatively humid conditions (Hochuli and Kelts, 1980; Schrank, 2010).
Podocarpidites	(Cookson) Couper (1953), in Balme (1995)	Plate I, 5	Conifers (Balme, 1995)	Preferences like Parvisaccites.
Pinuspollenites	Potonié (1958) in Balme (1995)	Plate I, 6	Conifers	Typical floral element of boreal regions, growing under relatively humid conditions with a broad range of temperature tolerance (Hochuli and Kelts, 1980).
Non-saccate pollen:				
Araucariacites	(Cookson) Couper (1953), in Balme (1995)	Plate I, 7, 8	Conifers (Balme, 1995)	Wide ranging, rainforests to cool temperate forests, recent Araucaria mostly occurring in moist temperate environments on tropical mountain flanks. High abundances of Araucaria indicative of relatively arid conditions, low abundances connected with high diversity indicative of humid conditions (Schrank, 2010).
Callialasporites	Sukh Dev (1961), in Balme (1995)	Plate I, 9, 10	Conifers/(Balme, 1995)	Preferences like Araucariacites.
Inaperturopollenites	Balme (1957), in Conway (1996)	Plate I, 12, 13	Conifers (Balme, 1995)	Metasequoia type, indicative of more humid conditions (Birkenmajer et al., 2010).
Perinopollenites	Couper (1958), in Balme (1995)	Plate I, 14	Conifers (Balme, 1995; Vajda, 2001)	Probably warm and arid coastal environments (Balme, 1995; Vajda, 2001).
Cerebropollenites	(Couper) Nilsson (1958), in Herngreen (1971)	Plate I, 15,16	Conifers (Vajda, 2001)	Supposed to be related to recent tree Tsuga (Vajda, 2001 and references therein), therewith may have grown in humid and cool habitats.
Classopollis (=Corrollina, Circulina; Yi et al., 1993)	Maljavkina (1949), in Balme (1995)	Plate I, 17, 18	Conifers (Balme, 1995)	Cosmopolitan, highly diverse family, adapted to wide range of habitats. Most commonly assigned to semi-arid to arid lowland shoreline habitats, arid to seasonally arid conditions, and probably assigned to high temperatures. Some may have been adapted to coastal saline soil conditions, probably assigned to high temperatures (Vakhrameev, 1981; Doyle et al., 1982; Batten, 1984; Schrank, 2010).
Exesipollenites	Balme (1957), in Balme (1995)	Plate I, 22	Conifers (or cycads) (Balme, 1995)	Arid conditions (Schrank, 2010).
Cycadopites	Wilson and Webster (1946), in Balme (1995)	Plate I, 19, 20	Cycads (Balme, 1995; Abbink et al., 2004)	Arid, warm conditions, modern flora mainly tropical to subtropical, probably not in wetlands (Yi et al., 1993; Balme, 1995; Abbink et al., 2004; Coiffard et al., 2007; Vakhrameev, 2010).
Eucommiidites	(Erdtman) Potonié (1958), in Balme (1995)	Plate I, 23	Cycads (or gnetales) (Balme, 1995; Batten and Dutta, 1997)	–
Ephedripites	Bolkhovitina ex Potonié (1958), in Balme (1995)	Plate I, 21	Gnetales (Schrank, 2010)	May indicate warm semi-arid to arid conditions, also wider range. Low percentages also due to parent plants being weak pollen producers, pollen is not easily transported. High percentages point to occurrence of parent plants close to site of deposition (Schrank, 2010). Modern plants adapted to extreme temperature conditions (hot and cold; Yi et al., 1993).
Spores:				
Cyathidites (= Deltoidospora?)	Couper (1953), in Balme (1995)	Plate I, 31	Ferns (Schrank, 2010)	Modern relatives preferentially grow under tropical to subtropical conditions (Yi et al., 1993).
Leiotriletes (= Deltoidospora?)	(Loose) Potonié and Kremp (1954), in Balme (1995)	Plate I, 24, 25	Ferns (Balme, 1995; Schrank, 2010)	Vegetation close to shoreline, herbaceous swamps (Wilde, 1989).
Concavisporites (= Deltoidospora?)	(Couper, 1953) Krutzsch (1959) in Raine et al. (2008)	Plate I, 35, 36	Ferns (Raine et al., 2008)	–

Table 2 (continued)

Genera	Author and reference	Plate and figure	Botanical affinity	Ecological preference of parent plants
Concavissimisporites	(Delcourt and Sprumont) Delcourt, Dettmann and Hughes (1963), in Herngreen (1971)	Plate I, 38	Ferns (Schrank, 2010)	–
Spores:				
Trilobosporites	Couper (1958), in Herngreen (1971)	Plate I, 29	Ferns (Schrank, 2010)	–
Cicatricosisporites	Potonié and Gelletich (1933), in Balme (1995)	Plate I, 26, 27	Ferns (Balme, 1995)	May point to humid conditions, grown in marshes, river ecosystems or understorey in forests. May also be adapted to more arid conditions of heathlands like recent schizaeaceous fern Anemia (Schrank and Mahmoud, 1998; Schrank, 2010).
Klukisporites	Couper (1958), in Herngreen (1971)	Plate II, 41	Ferns (Schrank, 2010)	–
Ischyosporites	Balme (1957), in Balme (1995)	Plate II, 33, 34	Ferns (Schrank, 2010)	–
Osmundacidites	Couper (1953), in Balme (1995)	Plate II, 47	Ferns (Schrank, 2010)	–
Clavatisporites	Kedves and Simoncsics (1965), in Schrank and Mahmoud (1998)	Plate II, 44	Ferns (Raine et al., 2008)	–
Gleicheniidites (including Clavifera)	Ross (1949), in Balme (1995), Bolkhovitina (1966), in Waksmundzka (1981)	Plate II, 39	Ferns (Balme, 1995)	Opportunistic, pioneering plants, also growing in unstable environments, ruderal strategists (Coiffard et al, 2007).
Todisporites	Couper (1958) in Schrank, 2010	Plate II, 42	Ferns (Schrank, 2010)	May point to humid conditions grown in marshes, river ecosystems or as understorey in forests. May also be adapted to more arid conditions (Schrank, 2010).
Gemmatriletes	(Brenner) Singh (1971), in Zobaa (2006)	Plate II, 30	Ferns (Raine et al., 2008)	–
Biretisporites	Delcourt and Sprumont (1955), in Taugourdeau-Lantz (1988)	Plate II, 43	Ferns (Raine et al., 2008)	–
Verrucosisporites	Volkheimer (1972), in Raine et al. (2008)	Plate II, 40	Ferns (Raine et al., 2008)	–
Neoraistrickia	(Cookson) Potonié (1956), in Zobaa (2006)	Plate II, 32	Lycopods (Abbink et al., 2004)	–
Retriletes	(Cookson) Döring et al. (1963), in Conway (1996)	Plate II, 45, 46	Lycopods (Abbink et al., 2004)	–
Camarozonosporites	Hedlund (1966), Norris (1967), in Granzow (2000)	Plate II, 48	Lycopods (Abbink et al., 2004)	–
Aratrisporites	Leschik (1956), in Balme (1995)	Plate II, 28	Lycopods (Balme, 1995)	–
Densoisporites	Weyland and Krieger (1953), in Balme (1995)	Plate II, 50	Lycopods (Balme, 1995)	Tidally-influenced ecosystem (Schrank, 2010), does not tolerate aridity (Hedlund, 1966).
Foveosporites	Balme (1957), in Balme (1995)	Plate II, 51	Lycopods (Abbink et al., 2004)	–
Lycopodiacidites	Couper (1953), in Raine et al. (2008)	Plate II, 52	Lycopods (Raine et al., 2008)	–
Echinatisporis	Krutzsch (1963, in Schrank et al. (2010)	Plate II, 53	Lycopods (Abbink et al., 2004)	–
Leptolepidites	Norris (1969), in Zobaa (2006)	Plate II, 58	Lycopods (or ferns) (Abbink et al., 2004; Schrank, 2010)	–
Lycopodiumsporites	Singh (1964), in Taugourdeau-Lantz (1988)	Plate II, 54	Lycopods (Waksmundzka, 1981)	Favor humid conditions but can tolerate long periods of drought (Schrank, 2010)
Staplinisporites	(Balme) Pocock (1962), in Taugourdeau-Lantz (1988)	Plate II, 56	Bryophytes (or lycopods) (Abbink et al., 2004)	–
Foraminisporis	Döring (1973), in Schrank (2010)	Plate II, 55	Bryophytes (Schrank, 2010)	–
Stereisporites	(Wilson and Webster) Dettmann (1963), in Vajda (2001)	Plate II, 57	(Sphagnum) bryophytes (Waksmundzka, 1981)	Habitats like peat bogs and mires.
Aequitriradites	(Cookson and Dettman) Dettman (1961), in Herngreen (1971)	Plate II, 59	Lycopods (marchantiophyta, liverworts) (Schrank and Mahmoud, 1998)	Near river sites or arid places, probably xerophytic (Schrank and Mahmoud, 1998).
Microreticulatisporites	Knox (1950) in Pérez Loinaze and César (2004)	Plate II, 60	?	–

section (Aratrisporites, Staplinisporites, Clavatisporites, Todisporites) are absent from the VB. Cyathidites represents the most abundant spore at both localities. All identified pollen grains occur at both sites. The most abundant pollen for the VB sections is Classopollis, for the MPT it is Callialasporites. Angiosperm pollen are absent from all samples.

Colors of thin walled palynomorphs for both sites range from light yellowish to orange (low thermal alteration index = 2+; e.g. Zobaa, 2006), with lighter colors for the MPT. The degree of preservation is consistent throughout the samples of each site, no sign of carbonization is observed. Reworking and contamination with palynomorphs of younger or older strata can thereby probably be largely excluded. Due to pre- or post-depositional stress preservation of the spore and pollen grains varies from excellently preserved to highly fragmented specimens. A high degree of fragmentation hampers the determination especially between inaperturate palynomorphs like Araucariacites, Inaperturopollenites and simple thin-walled leiospheres (e.g. Filatoff, 1975; Vajda, 2001; Schrank, 2010). Furthermore, pollen of Araucariacites and Callialasporites are known to show high polymorphism, and between the two genera transitional forms seem to exist (Balme, 1995; Schrank, 2010). In some cases identification of bisaccate pollen and spores (mainly deltoid ones) was impossible due to poor preservation, fragmentation, or a cover of amorphous organic matter or pyrite, or due to their orientation in the slide. Consequently, these forms were labeled and grouped as undifferentiated bisaccates and undifferentiated spores. A total of four samples (MOR5, VER24, VER26, VER29) were excluded from spore–pollen analysis due to high amounts of amorphous organic matter, which did not allow for palynomorph identification. The stratigraphic occurrence, range, and diversity of spore–pollen taxa are given in Figs. 3 and 4.

The abundances in percentage of palynomorphs and variations therein are shown for the MPT (Fig. 5) and the VB (Fig. 6) sites. The arrangement of assemblages is based on changes in these abundances. Stratigraphic ranges are shown in Figs. 3 and 4, the main features of

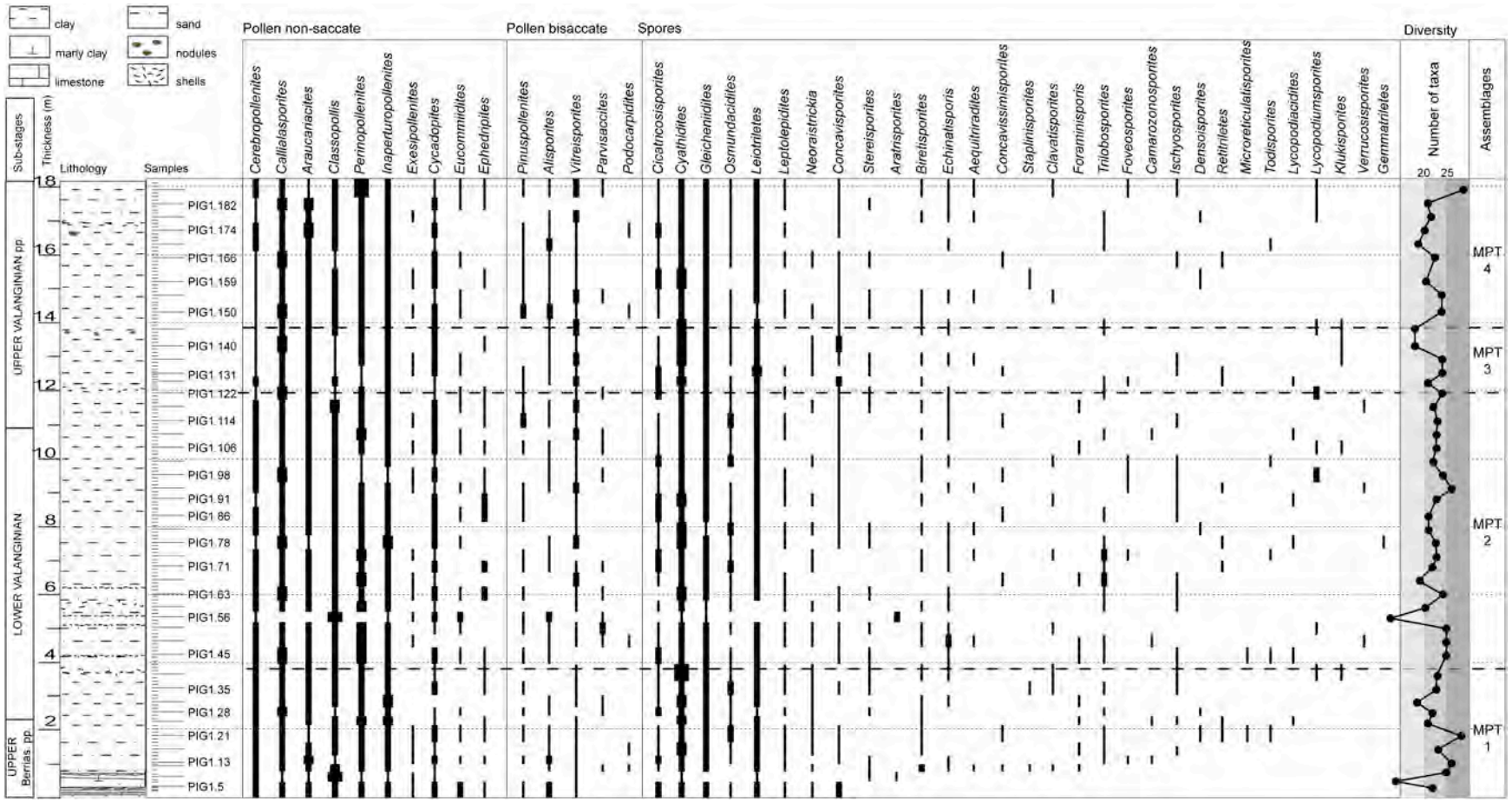

Fig. 3. Abundances (for legend see Fig. 4) and stratigraphic occurrences of spore-pollen taxa of the MPT, arranged by stratigraphic first occurrences. Sub-stages, thickness, lithology (see legend for details), position of samples (long lines palynologic samples, short lines δ13C), diversity based on number of taxa, and spore-pollen assemblages.

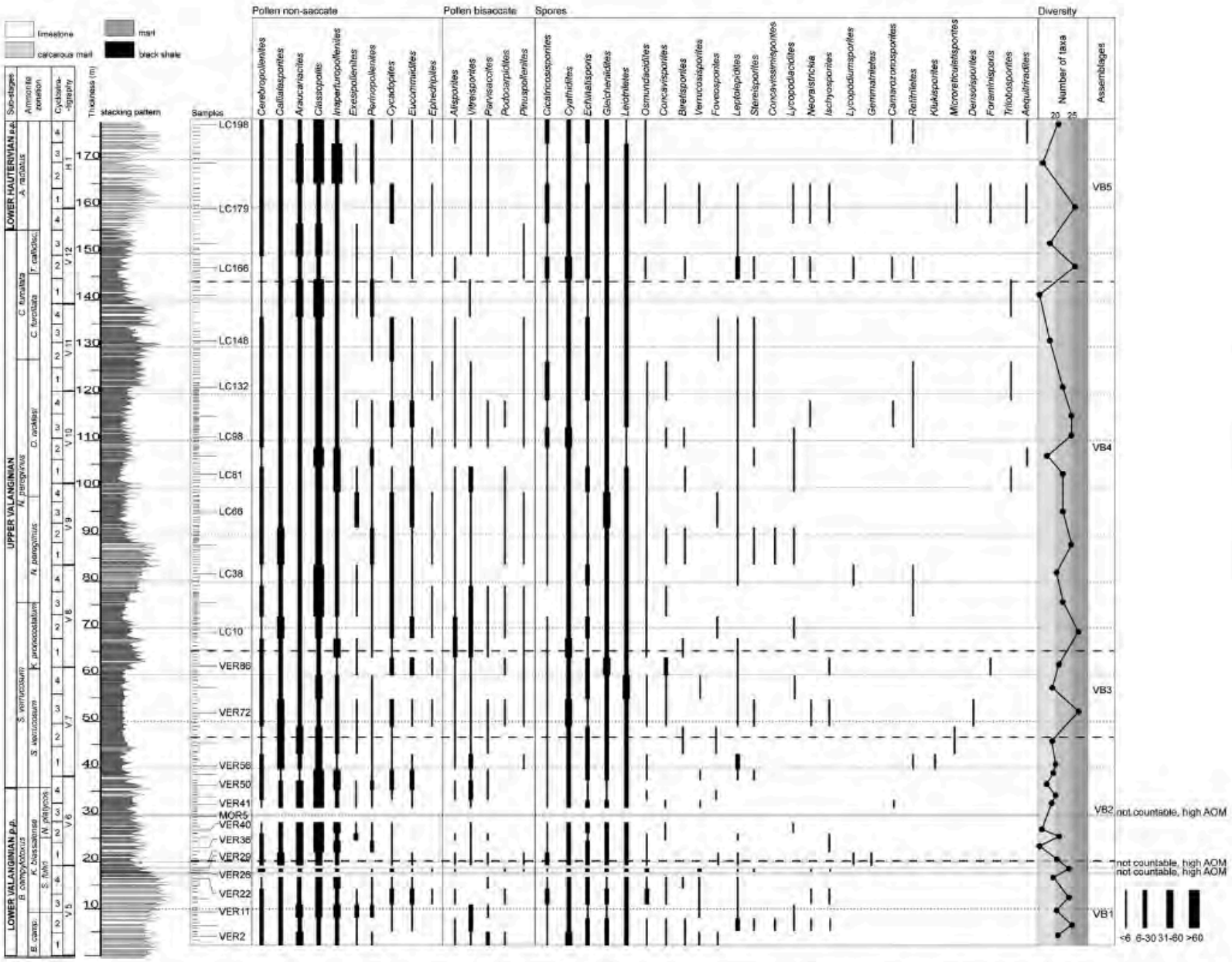

Fig. 4. Abundances (legend on the right) and stratigraphic occurrences of spore-pollen taxa of the VB, arranged by stratigraphic first occurrences. Sub-stages, thickness, lithology (see legend for details), position of samples (long lines palynologic samples, short lines δ13C), diversity based on number of taxa, and spore-pollen assemblages.

each assemblage are given below. For the MPT site four assemblages are proposed (MPT 1–4), for the VB site five assemblages can be distinguished (VB 1–5).

4.1.1. Palynological assemblages and abundances for the Mid-Polish Trough (MPT) record

The spore–pollen assemblage identified for the MPT is predominantly composed of gymnosperm pollen (average (ø) 52.1%) with Cerebropollenites (Plate I, 15, 16), Callialasporites (Plate I, 9, 10), Araucariacites (Plate I, 7, 8), Perinopollis (Plate I, 14) and Inaperturopollenites (Plate I, 12, 13) being the most important non-saccate forms. On average Classopollis (Plate I, 17, 18) accounts for only 6.3% with the exception of two samples where these pollen reach up to more than 73%. Exesipollenites is of minor importance and ranges between 0.0 and 1.6%. Less common non-conifer forms include Eucommiidites (Plate I, 23), Cycadopites (Plate I, 19, 20) and Ephedripites (Plate I, 21), which account for less than ø ~2.2%. Most common bisaccates are Vitreisporites pallidus and Alisporites with ø 1.5 and 0.8%, respectively.

Spores represent an important component of the spore–pollen assemblages and account for ø 45.4%. Dominant taxa include the fern spores Cyathidites (Plate I, 31), Gleicheniidites (Plate I, 39), and Leiotriletes (Plate I, 24, 25). Abundant non-fern spores are the lycopod-derived Echinatisporis (Plate II, Fig. 13), Neoraistrickia (Plate I, 32), and Leptolepidites (Plate II, 18), with none of them exceeding 0.5%. Aratrisporites (Plate I, 28) is restricted to two samples only, where it shows relatively high abundances up to 7.0%. Spores of bryophyte origin are rare components of the assemblage, including Stereisporites (Plate II, 17) amongst other forms.

Assemblage MPT1 — Upper Berriasian to lower Valanginian (0 to 3.9 m).

This assemblage shows an increase in spore abundances up to 54.8%, with Cyathidites being prominent (ø 10.6%) and showing its peak occurrence (max. 21.5%), decreasing values for bisaccates (avg. 17.4%), and relatively stable conditions for non-saccate pollen (ø 40.5%). Araucariacites shows a spike (max. 13.3%) in a generally increasing trend (ø 4.5%). Cycadopites shows peak values (max. 7.0%). Following a peak in the middle of the assemblage diversity is decreasing.

Assemblage MPT 2 — Lower Valanginian to upper Valanginian (3.9 to 11.9 m).

This assemblage is characterized by relatively stable abundances of non-saccate pollen (ø 38.0%). Perinopollenites is decreasing (~15.0 to 7.0%) whereas Callialasporites shows a steady increase (~10.0 to 15.9%). Ephedripites is comparatively abundant in this assemblage (ø 0.8%). Bisaccates show a decreasing trend (ø 13.6%). Spores are gradually increasing (ø 45.8%) with only Cyathidites showing a decreasing trend (ø 8.3%). Monolete spores show slightly increased abundances (ø 0.4%). Diversity is medium (20–25 taxa).

Assemblage MPT 3 — Upper Valanginian (11.9 to 13.9 m).

The assemblage is characterized by peak of spore abundances (max. 61.3%), mainly due to high abundances of Cyathidites (max. 13.7%), Gleicheniitides (7.4%) and Leiotriletes (14.1%). In contrast non-saccate (max. 32.1%) and bisaccate pollen (max. 14.7%) show low abundances. Classopollis is very rare (ø 1.4%). Vitreisporites pallidus shows an exception from this pattern and reaches peak values (max. 6.3%). Diversity is decreasing.

Assemblage MPT 4 — Upper Valanginian (13.9 to 17.8 m).

This uppermost assemblage of the Wąwał section is characterized by two pronounced peaks in bisaccates pollen (max. 31.1%). Vitreisporites pallidus shows maximum values around 4.3%. Araucariacites shows an increasing trend (ø 7.4%) while percentages of non-saccate pollen remain relatively stable (ø 36.9%). Perinopollenites peaks towards the end of the assemblage (max. 18.7%). Spore abundances are quite stable (ø 44.0%) after a minimum at the beginning of the assemblage (23.8%), with the exception of declining numbers of Cyathidites (ø 7.0%) and Leiotriletes (avg. 3.6%). Diversity is medium with the uppermost sample being of especially high (>25 taxa) diversity.

4.1.2. Palynological assemblages and abundances for the Vocontian Basin (VB) record

In the VB, the identified spore–pollen assemblages are mainly composed of gymnosperm pollen (ø 60.2%) with Classopollis (Plate I, 17, 18), Araucariacites (Plate I, 7, 8), Inaperturopollenites (Plate I, 12, 13), and Callialasporites (Plate I, 9, 10) being the most important non-saccate forms. Cerebropollenites (Plate I, 15, 16) is of minor importance with ø 3.8%, but reaches maxima of up to 11.7%. Less abundant non-conifer forms include Eucommiidites (Plate I, 23), Cycadopites (Plate I, 19, 20) and Ephedripites (Plate I, 21), which account for less than ø ~1.6%. Most common bisaccates are Vitreisporites pallidus and Alisporites with ø 1.3 and 0.6%, respectively. Spores occur with ø 38.6%. The fern spores Cyathidites (Plate I, 31), followed by Gleicheniidites (Plate I, 39) and Leiotriletes (Plate I, 24, 25) are dominant spores. Abundant non-fern spores are the lycopods Echinatisporis (Plate II, 13), and Leptolepidites (Plate II, 18), with numbers up to ø 2.8%. A regularly recorded bryophyte is Stereisporites (Plate II, 17; ø 0.2%).

Assemblage VB1 — Lower Valanginian (0 to 19 m).

This assemblage is characterized by relatively high abundances of spores, exhibiting a decreasing trend (ø 43.5%), with the dominant taxa being Cyathidites (max. 14.7%), Gleicheniidites (max. 9.3%) and Leiotriletes (max. 7.0%). Bisaccates as well show a decreasing trend (ø 9.7%). Classopollis (ø 12.3%), Inaperturopollenites (ø 8.6%), and Araucariacites (ø 9.4%) are dominant non-saccate pollen. Diversity is medium (20–25 taxa).

Assemblage VB2 — Lower Valanginian to upper Valanginian (19 to 47 m).

Non-saccate pollen peak in the middle part of this assemblage (max. 74.3%), whereas spores (ø 26.8%) and bisaccates (ø 9.4%) are sharply decreasing in abundances. Classopollis (max. 45.0%) and Araucariacites (max. 19.0%) represent the dominant non-saccate pollen. Callialasporites shows high abundances in the uppermost part of the assemblage (max. 15.0%). Spores are dominated by Leiotriletes (max. 6.7%) and Cyathidites (max. 10.0%). Diversity is low (b20 taxa).

Assemblage VB3 — Upper Valanginian (47 to 65 m).

This assemblage is characterized by a pronounced increase in spore abundances (max. 56.0%). Leiotriletes (max. 11.7%), Gleicheniidites (max. 15.3%), and Concavisporites (max. 2.7%) show maximum abundances. Non-saccate pollen (ø 35.0%) and bisaccates (ø 13.4%) show only low abundances. Classopollis (max. 11.0%) and Inaperturopollenites (max. 12.7%) show their lowest abundances. Diversity is fluctuating from high to low.

Assemblage VB4 — Upper Valanginian (65 to 145 m).

This assemblage is characterized by an increasing trend in the abundance of spores (ø 40.1%) following low values at the very base of this assemblage (min. 31.3%). Cyathidites is dominating (max. 15.3%) and Echinatisporis (max. 7.7%) reaches maximum values in the upper part of the assemblage. Bisaccates show an opposing trend, after peak values at the beginning of the assemblage (max. 27.3%) abundances are decreasing (min. 3.7%). The pteridosperms/ginkgos Vitreisporites pallidus and Alisporites show maximum abundances (max. 4.7%, and max. 4.7%, respectively). Non-saccate pollen are relatively stable (ø 44.0%), with Classopollis being the dominant taxon (max. 28.0%). Diversity is declining towards the uppermost part of the assemblage.

Assemblage VB5 — Upper Valanginian to Lower Hauterivian (145 to 176 m).

This assemblage is characterized by a second maximum in spore abundances (max. 63.6%) at the very base, followed by a decreasing trend,

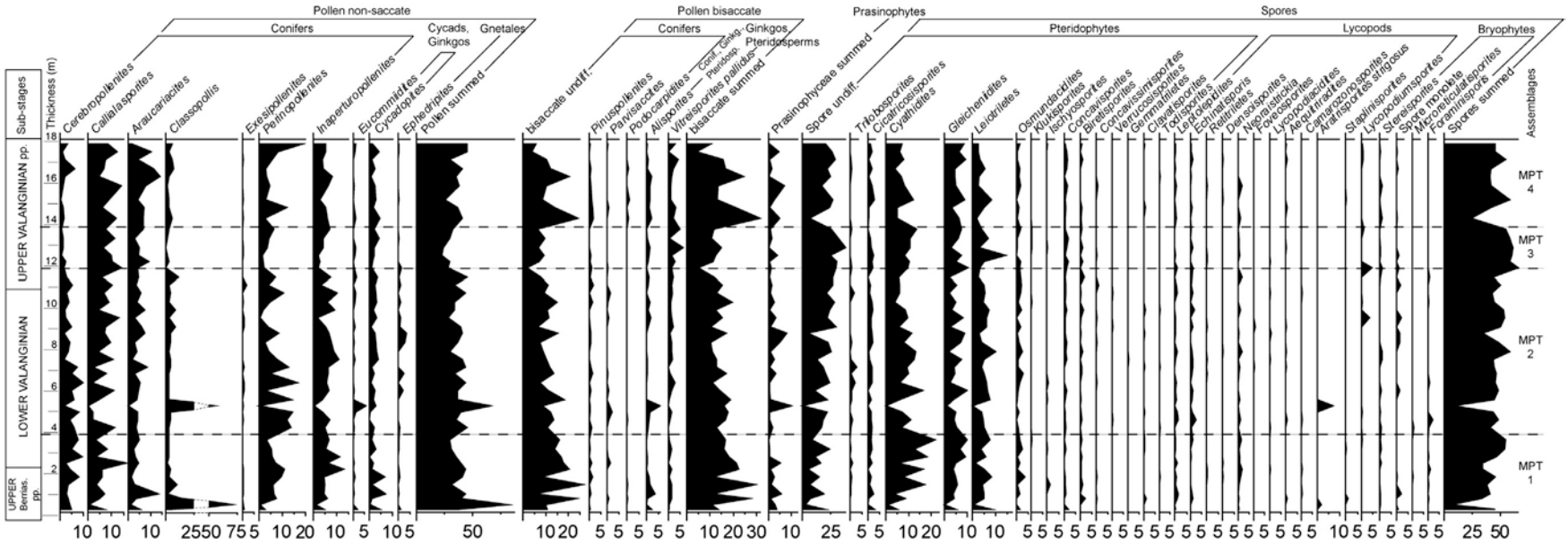

Fig. 5. Spore-pollen-assemblages MPT. Sub-stages, thickness, abundances of spore-pollen in %, and spore-pollen assemblages.

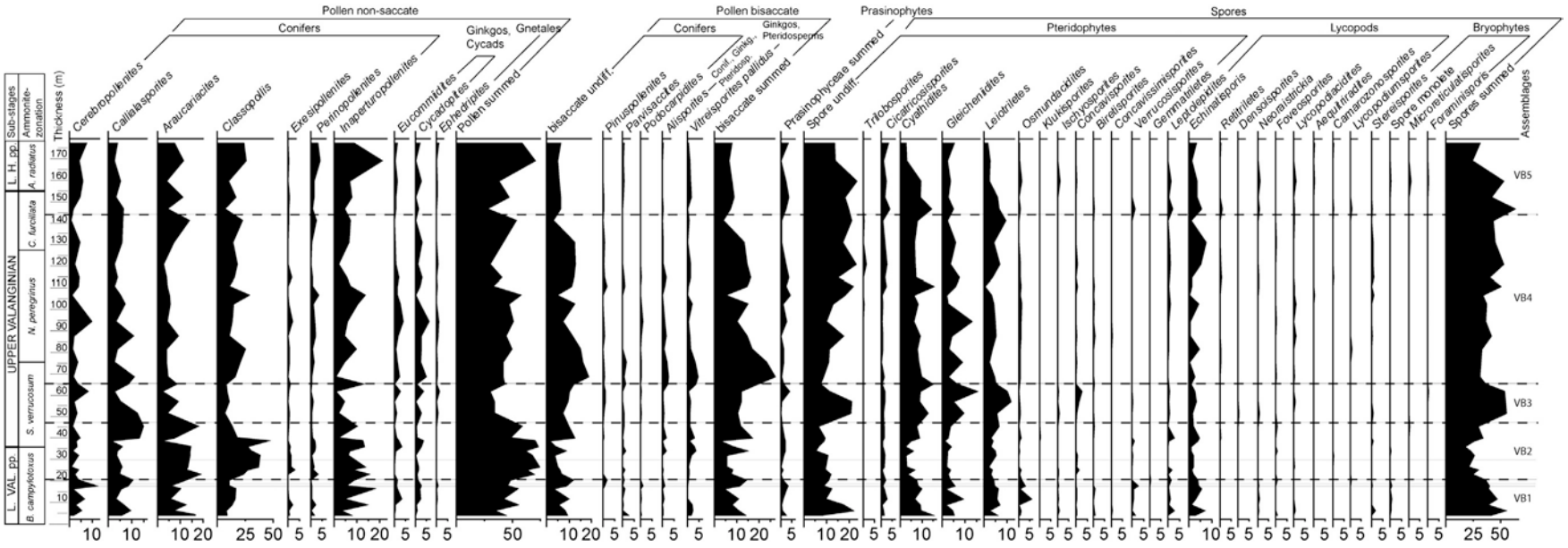

Fig. 6. Spore-pollen assemblages VB. Sub-stages, ammonite zones, thickness, abundances of spore-pollen in %, and spore-pollen assemblages.

while non-saccate pollen (ø 47.7%) show an opposing pattern. Bisaccates remain relatively stable (ø 7.5%). Classopollis and Inaperturopollenites are the dominant non-saccate pollen taxa (max. 25.8%, and max. 20.9%, respectively) with the latter showing maximum values for the whole section. Diversity is fluctuating.

4.2. Nannofossil biostratigraphy

The preservation of the calcareous nannofossil assemblages of the MPT varies throughout the studied section. Samples PIG 1.1 to 1.9 are barren of calcareous nannofossils, samples PIG 1.10 and 1.11 yield only a few preserved specimens. The calcareous nannofossils of interval PIG 1.12 to 1.175 are well preserved, except for nine samples, PIG 1.12, PIG 1.16, PIG 1.19, PIG 1.25, PIG 1.114, PIG 1.116, PIG 1.118, PIG 1.174, and PIG 1.175, which show a moderate preservation. Samples PIG 1.178 to 1.188 are barren.

Seven nannofossil events including first occurrences (FOs) and last occurrences (LOs) were observed throughout the upper Berriasian to Valanginian interval. These allowed the recognition of four Boreal calcareous nannofossil zones (BC2–BC5). The occurrence of Sollasites arcuatus in samples PIG 1.012 to 1.021 implies a late Berriasian age (BC2) for this interval. Based on the absence of both S. arcuatus and Triquerhabdulus shetlandensis in samples PIG 1.22 to 1.25 this interval was assigned to nannofossil subzone BC3a (Berriasian/Valanginian boundary). The base of the following BC3b subzone (lowermost Valanginian) is marked by the FO of T. shetlandensis (sample PIG 1.26). The top of this zone is defined by the FO of Micrantholithus speetonensis (sample PIG 1.44). The total range of M. speetonensis, a taxon which is rare throughout the studied section, spans the lower Valanginian (BC4 Zone; samples PIG 1.44 to 1.112). This zone can further be subdivided into the subzones BC4a and BC4b by using the FO of Eiffellithus windii (sample PIG 1.96). The BC5 Zone (samples PIG 1.113 to 1.175) spans the entire upper Valanginian and can be subdivided by the FO of Eiffellithus striatus (sample PIG 1.142). The base of this zone is defined by the LO of M. speetonensis, the top by the LO of T. shetlandensis. The upper boundary of this zone, however, is arbitrary since the overlying interval is barren of calcareous nannofossils.

4.3. Stable carbon isotopes

The $\delta^{13}C_{carb}$ signals for the VB vary between 0.1 and 2.6‰ and show a positive CIE of about 2‰ (Fig. 2). The record shows no offset of $\delta^{13}C_{carb}$ values between the different sections, enabling the establishment of a composite curve. In the NK3A nannofossil zone values are comparatively stable at the beginning (0 to 26 m, ~0.7‰), with a sharp decrease to lowest values (~0.1‰ at 26 m). After that a first increase to more positive values up to ~1.7‰ (26 to 32 m) can be observed. In the lowest NK3B zone (32 to 45 m) values are stable around 1.5‰, followed by a rapid shift to more positive values (to ~2.5‰ at 45 to 50 m). Values remain high with two phases of maximum values of up to ~2.7‰ in the middle of NK3B and around the transition between zone NK3B and NC4. In zone NC4 a decreasing trend establishes up to the upper part of zone NC4, where stable values (around 1.1‰) are observed. The lower part of the Vergol and Morenas sections shows comparable patterns to other Tethyan $\delta^{13}C_{carb}$ records (Kujau et al., 2012), which affirms the applicability of the $\delta^{13}C_{carb}$ record of the here presented sections as a stratigraphic tool.

5. Discussion

5.1. Correlation of sites

The two studied sites are correlated following Bown (1998; Fig. 2) by using the calcareous nannofossil zonation schemes of the Tethys (NC) and of the Boreal Realm (BC). The NC zonation for the well dated VB was adopted from Gréselle et al. (2011; see also Reboulet et al., 2003), accomplished independently for the same sampling sites. The Polish site covers sediments from the Berriasian/lower Valanginian to upper Valanginian, evidenced by the Boreal nannofossil zones BC2 to BC5. For the VB a range between the lower Valanginian to Lower Hauterivian is documented by the Tethyan nannofossil zones NK3A to NC4. Additional time constraint is provided by chemostratigraphic correlation of the two sites; both $\delta^{13}C_{carb}$ records reveal comparable trends. The comparatively low $\delta^{13}C$ values established prior to the lower/upper Valanginian boundary (MPT ~1‰, VB ~0.5‰), are followed by a sharp increase across the lower/upper Valanginian boundary (MPT up to ~3‰, VB up to ~2.5‰). Subsequently, values remain high (interrupted by one sample of especially low values at the MPT at 13.3 m) before they start to decrease (MPT at 17.0 m, VB at ~120 m). However, the MPT record (Morales et al., pers. comm.) is characterized by high fluctuations hampering a high-resolution chemostratigraphic correlation. Following the Boreal–Tethys correlation of Bown (1998), the overlapping interval for the MPT and the VB spans sediments from the lower Valanginian to upper Valanginian (upper NK3A to NK3B and upper BC4a to BC5, respectively).

Plate I. Names of taxa with sample and coordinates of the photo. Latin numbers according to pictures on plates, indicating one (two) example(s) of taxa. For references see Table 2.

Pollen:

1 Alisporites PIG1.56, 133.3/13.1
2 Alisporites PIG1.56, 146.9/19.9
3 Parvisaccites PIG1.56, 146.1/11.3
4 Parvisaccites PIG1.56, 134.0/16.5
5 Podocarpidites PIG1.56, 140.1/13.4
6 Pinuspollenites PIG1.122, 140.7/18.1
7 Araucariacites PIG1.21, 130.8/10.4
8 Araucariacites PIG1.122, 141.9/6.7
9 Callialasporites PIG1.98, 142.9/19.5
10 Callialasporites PIG1.13, 131.4/7.5
11 Vitreisporites PIG1.35, 135.1/16.3
12 Inaperturopollenites PIG1.98, 134.9/13.3
13 Inaperturopollenites PIG1.28, 141.7/18.7
14 Perinopollenites PIG1.45, 134.2/7.9
15 Cerebropollenites PIG1.56, 129.4/7.3
16 Cerebropollenites PIG1.56, 149.1/14.2
17 Classopollis PIG1.56, 146.2/14.2
18 Classopollis PIG1.122, 146.7/16.7
19 Cycadopites PIG1.56, 132.9/17.8
20 Cycadopites PIG1.35, 144.2/4.2
21 Ephedripites PIG1.71, 134.5/12.0
22 Exesipollenites PIG1.71, 135.3/18.7
23 Eucommiidites PIG1.13, 126.7/12.7.

Spores:

24 Leiotriletes PIG1.71, 126.4/8.7
25 Leiotriletes PIG1.21, 144.3/10.4
26 Cicatricosisporites PIG1.5, 142.1/11.9
27 Cicatricosisporites PIG1.13, 136.3/13.8
28 Aratrisporites PIG1.56, 137.8/10.0
29 Trilobosporites PIG1.63, 132.8/7.3
30 Gemmatriletes PIG1.166, 152.8/6.2
31 Cyathidites VER78, 144.5/17.4
32 Neoraistrickia PIG1.174, 144.6/19.1
33 Ischyosporites PIG1.45, 138.5/7.9
34 Ischyosporites PIG1.45, 132.4/7.7
35 Concavisporites PIG1.91, 134.9/4.5
36 Concavisporites PIG1.45, 143.9/19.9
37 Trilobosporites PIG1.35, 140.9/11.5
38 Concavissimisporites PIG1.114, 138.5/13.3
39 Gleicheniidites PIG1.91, 128.9/15.5
40 Verrucosisporites PIG1.49, 149.1/9.6.

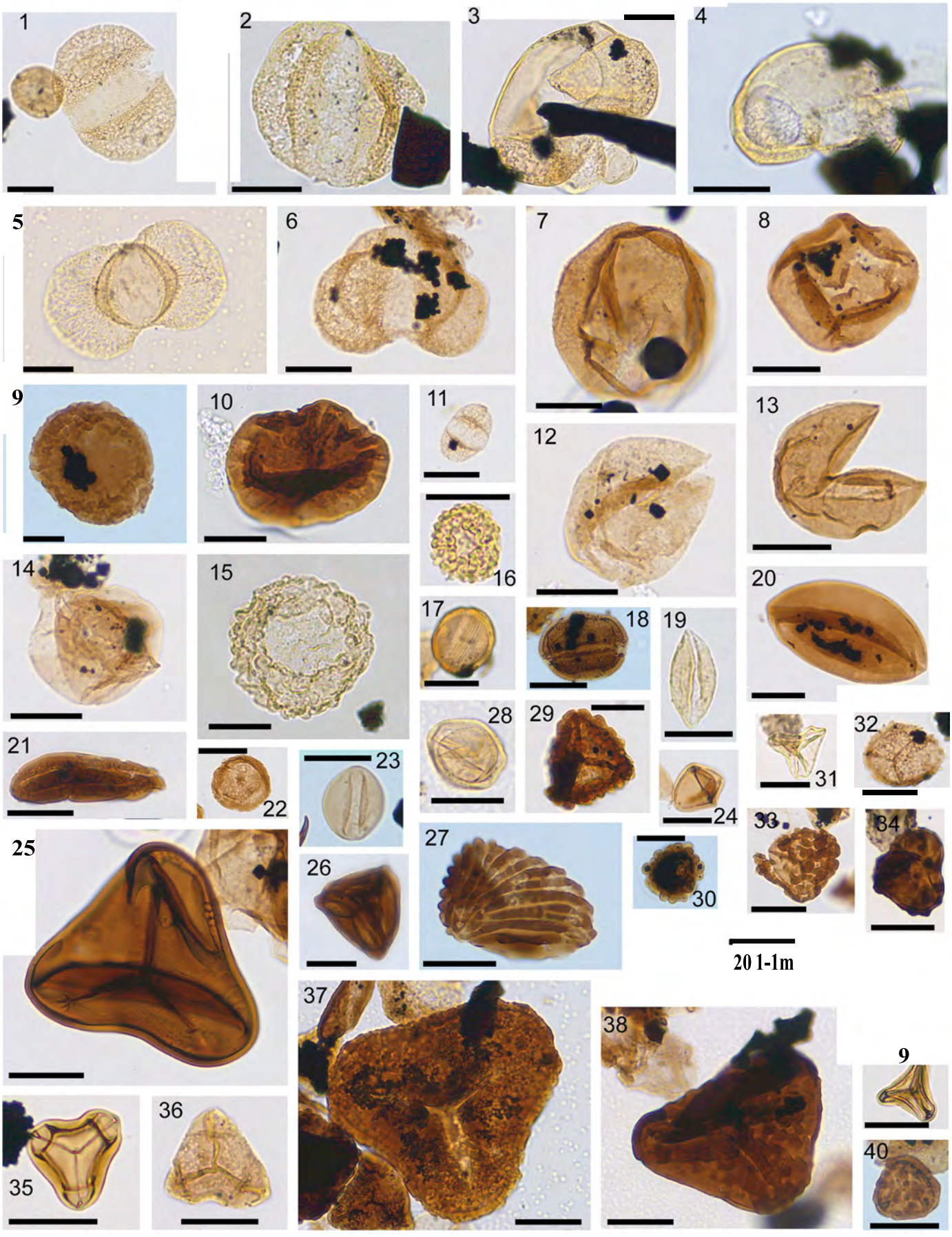
1
2
3
4
5
6
7
8
9
10
11
12
13
14
15
16
17
18
19
20
21
22
23
24
25
26
27
28
29
30
31
32
33
34
20 1-1m
35
36
37
38
9
40

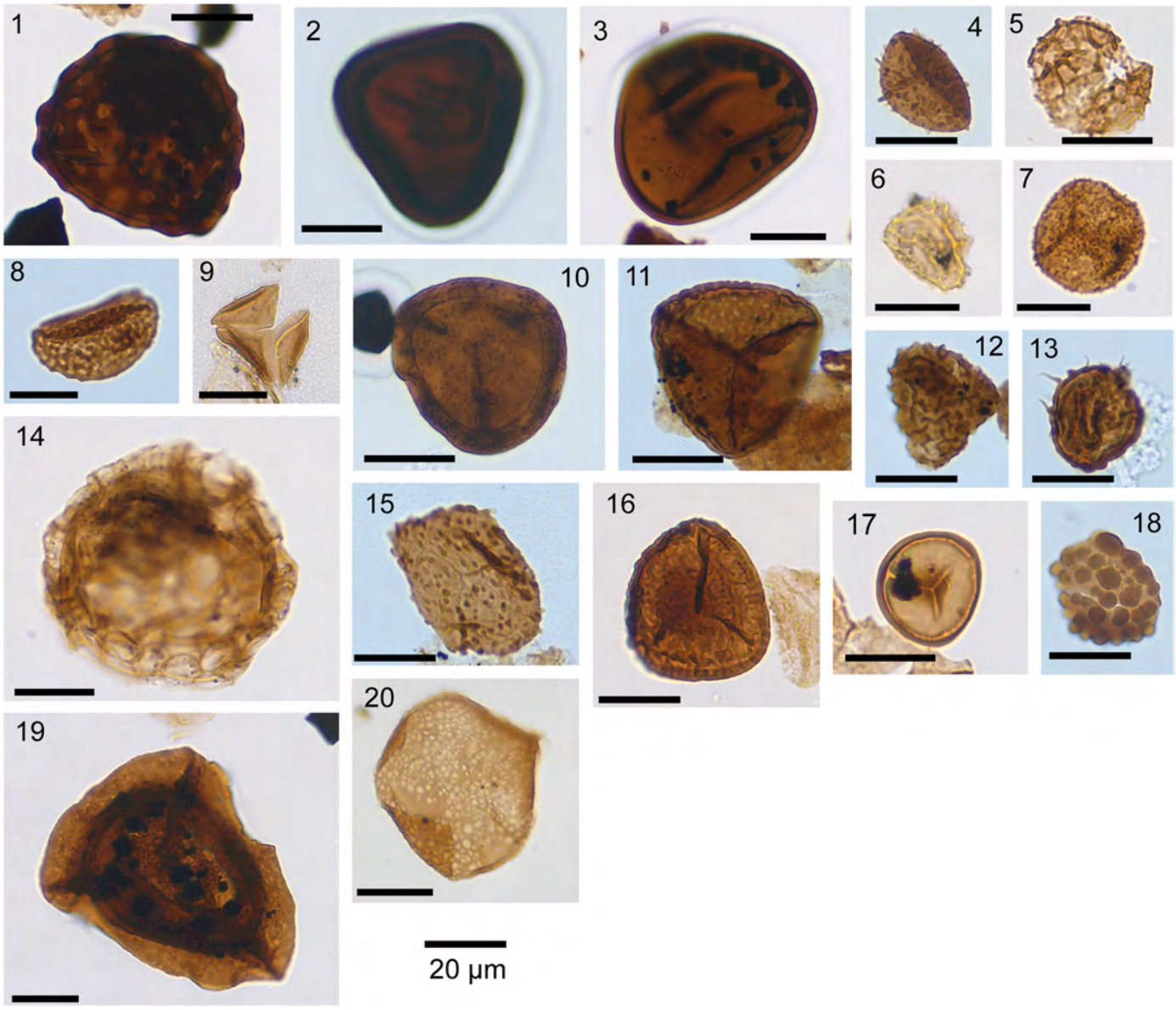

Plate II.

Spores:

1 Klukisporites PIG1.35, 145.2/6.0
2 Todisporites PIG1.150, 129.3/9.7
3 Biretisporites PIG1.91, 150.7/15.6
4 Clavatisporites PIG1.35, 148.6/7.6
5 Retitriletes PIG1.166, 148.9/7.1
6 Retitriletes PIG1.56, 128.5/5.7
7 Osmundacidites PIG1.166, 150.0/14.7
8 Camarozonosporites PIG1.13, 130.0/14.5
9 Gleicheniidites PIG1.45, 139.5/11.6
10 Densoisporites PIG1.21, 146.8/8.7
11 Foveosporites PIG1.159, 140.0/15.4
12 Lycopodiacidites PIG1.91, 143.5/4.3
13 Echinatisporis PIG1.13, 148.2/12.6
14 Lycopodiumsporites PIG1.106, 136.3/8.6
15 Foraminisporis PIG1.45, 139.2/9.7
16 Staplinisporites PIG1.159, 140.0/15.4
17 Stereisporites PIG1.71, 150.1/10.5
18 Leptolepidites PIG1.59, 14.1/133.4
19 Aequitriradites PIG1.45, 138.4/16.5
20 Microreticulatisporites PIG1.45, 147.5/17.4.

5.2. Paleoenvironmental significance

Early Cretaceous spore–pollen taxa are known to be long-ranging and therefore they are not a suitable biostratigraphic tool on time scales shorter than a few million years (Taugourdeau-Lantz, 1988). They can, however, be used for reconstructing paleoenvironments. Most spore–pollen can be assigned to parent plants or major plant groups (botanical affinity). Spore–pollen assemblages therefore reflect changes in the vegetation of the hinterland (e.g. Traverse, 2007). By comparing the spore–pollen assemblages of two different sites, supra-regional trends in environments and climate can be differentiated from those of only local expression. However, the composition and abundances of spores and pollen in the sedimentary record reflects not only the vegetation of a particular area. It is also influenced by a number of factors that affect the transport of palynomorphs, such as wind direction and strength, as well as by sedimentation processes in connection with changes in sea-level, marine currents, and river drainage (Hochuli and Kelts, 1980; Schrank, 2010 and references therein). Due to the specific morphology of some taxa, like bisaccates and Classopollis, that favors long-distance atmospheric and hydrologic transport (Tyson, 1995; Birkenmajer et al., 2010; Schrank, 2010), these taxa may be of selectively enhanced abundance in marine environments. Another factor influencing abundances of spore–pollen is the number of palynomorphs produced by the assigned parent plant. Pinus trees for example produce high pollen numbers per plant (Tyson, 1995; Birkenmajer et al., 2010 and references therein). Despite these limitations overall environmental and climatic trends as well as comparisons between different sites can be inferred from palynological records.

5.3. Paleophytogeographic framework

For the middle to Late Cretaceous a wealth of studies dealing with continental palynology exist (e.g. Brenner, 1976; Hochuli, 1981; Batten, 1984; Chumakov et al., 1995; Zhichen and Fei, 1997), whereas publications focusing on the earliest Cretaceous are comparatively rare. Two major floral provinces have been proposed for the northern hemisphere of the Early Cretaceous by Ziegler et al. (1987) with a boundary around 50°N, namely a cool temperate northern Siberian–Canadian province, dominated by gingkos and gingko-like Czekanowskiales, and a more southern, warm temperate (Indo-)European province, rich in pteridophytes, including Weichselia, and pteridosperms like Tempskya. During the Early Cretaceous, unlike today, maximum plant productivity and diversity was concentrated at mid- and high latitudes (cf. Ziegler et al., 1987; Rees Mc Allister et al., 2004; Vakhrameev, 2010). The continental areas around the VB and the MPT were part of the warm temperate European province, without seasonal freezing.

The composition of the vegetation of the northern hemisphere changed markedly close to the Jurassic–Cretaceous boundary, with the rapid appearance of many new groups of pteridophytes in the mid-latitudes (Batten, 1984; Herngreen et al., 1996). This change can probably be assigned to the ongoing separation of land masses and fluctuations in sea-level that caused the formation of epicontinental seas and archipelagic coastal habitats, accelerating endemic evolution (e.g. Diéguez et al., 2010). A general increase in pteridophyte abundances compared to the Jurassic was interpreted as an increase in humidity (Vajda, 2001). Pteridophytes are a dominant and diverse floral element at both investigated sites. Observed pteridophytes are of dickinsoniacean, cyatheacean, dipteridacean, filicopsidan or matoniacean as well as gleicheniacean origin. Most abundant forms are Cyathidites, Gleicheniidites and Leiotriletes. Gleicheniaceae and Schizeaceae were reported to have spread during the Early Cretaceous, being typical floral elements of Europe, with Gleicheniaceae being the dominant ferns (Herngreen et al., 1996; Vakhrameev, 2010). High abundances of Deltoidospora (e.g. Vajda, 2001, probably synonymous with Cyathidites and Leiotriletes), Clavifera (in this study assigned to Gleicheniidites), and Gleicheniidites, were also reported from Sweden (Vajda, 2001). Also in accordance to the Swedish study are low abundances of Schizeaceae like Cicatricosisporites and Klukisporites. Reported common Jurassic forms that were still abundant in the Early Cretaceous and were found in this study are Gleicheniidites, Ischyosporites, Klukisporites, Concavissimisporites, and Trilobosporites.

Apart from similarities in the composition of pteridophyte assemblages, the MPT and VB sites reveal distinct differences. The paleoflora surrounding the MPT is dominated by conifers of araucarian and cupressaceaen origin, whereas cheirolepidiacean conifers are of minor importance. The paleoflora in the hinterland of the VB is as well characterized by conifers like Araucarians and Cupressaceans, but also by drought-resistant Cheirolepidiaceans. Herngreen et al. (1996) reported the abundance of gymnosperm pollen like Araucariacites (Araucariaceae)/Inaperturopollenites and Calliallasporites for the European realm. The contribution of Cheirolepidiaceae like Brachyophyllum, Pagiophyllum, Frenelopsis and Pseudofrenelopsis, reflected in high numbers of Classopollis (up to 70% during arid intervals) was reported in addition to be significant for European assemblages (Herngreen et al., 1996; Vakhrameev, 2010). Their rarity at the MPT may be related to the more northern paleoposition of this site.

In contrast to observations by Ziegler et al. (1987), but in accordance with Herngreen et al. (1996) ephedroid and monosulcate pollen are scarce at the MPT and VB. Ginkgoaceae were reported to be of low diversity, only reflected by the genus Ginkgo (Vakhrameev, 2010). In this study Cycadopites of potential cycadalean, bennettitalean or ginkgoalean origin shows only temporarily moderate abundance. The discrepancies may be due to specific local characters of the analyzed vegetation. Ginkgoales, Czekanowskiales, and cycadophytes are supposed to have dramatically declined from the Jurassic to the Early Cretaceous (MacLeod and Hills, 1991).

Moderate abundance was observed for Pinaceae and Podocarpaceae (Batten, 1984; Vakhrameev, 2010). Herngreen et al. (1996), however, mentioned considerable numbers of bisaccates like Podocarpidites, Vitreisporites, and Alisporites. The latter two taxa can probably both be assigned to the pteridosperms, which were reported as important and diverse floral elements of the European realm (Ziegler et al., 1987; Herngreen et al., 1996). This is in accordance with the present study, where at both sites Vitreisporites and Alisporites show high abundances. A more detailed analysis of the bisaccates is, however, hampered by the high amount of non-identifiable pollen at both sites.

5.4. Temporal evolution of habitats and environmental moisture levels

A spore–pollen ratio for each site was calculated (Fig. 7), with high values indicating high spore abundances. Spore-producing plants (pteridophytes, lycopods, bryophytes) are generally considered to be abundant under relatively humid conditions, optimal for their growth and reproduction. High spore abundances are thereby interpreted to reflect increased humidity available to plants (Visscher and van der Zwan, 1981; Fowell et al., 1994; Abbink, 1998; Vajda, 2001; Bornemann et al., 2005; Hochuli and Vigran, 2010; Schrank, 2010). On the other hand, gymnosperms are assumed to dominate over spore-producers under comparatively dry conditions (Fowell et al., 1994). Therewith, the spore–pollen ratio is used here to infer trends in environmental moisture levels. Further indication of moisture trends stems from variations in the abundance of the drought-resistant conifer pollen Classopollis of cheirolepidiacean origin, with high values pointing to arid conditions (Fig. 7). Besides changes in the spore–pollen ratio and Classopollis abundances, successive changes in plant community structure, habitat, and moisture availability are described based on botanical affinities of significant taxa (Table 2, cf. Figs. 5 and 6).

5.4.1. The MPT site

Abundances of Classopollis are overall low (max. 13.3%), with temporarily slightly higher values pointing to drier conditions. Two samples of the lower MPT1 (PIG1.8) and lower MPT2 (PIG1.56) assemblages are

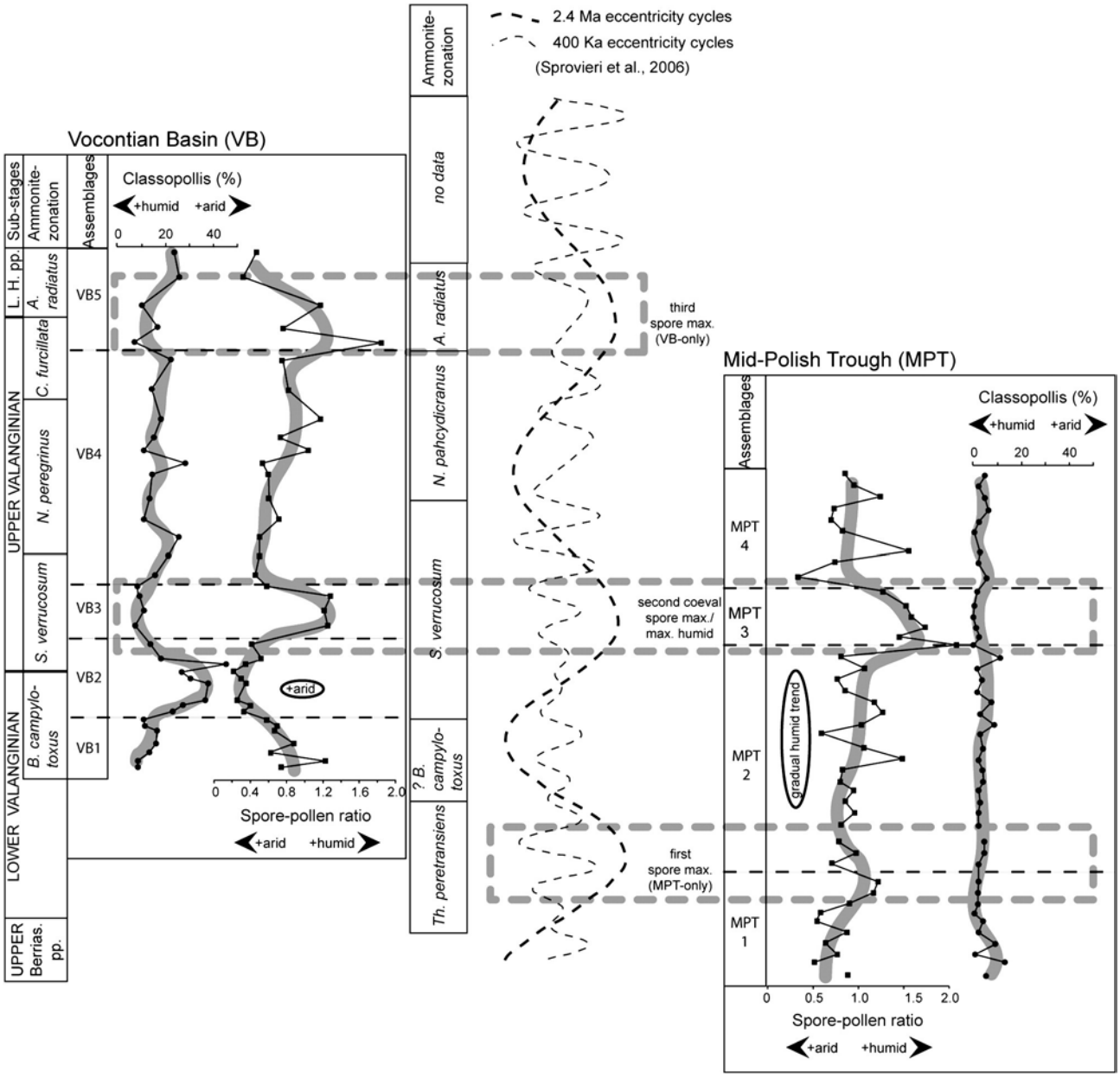

Fig. 7. Comparison of moisture trends between the VB (left) and the MPT (right), plotted against eccentricity cycles (middle; Sprovieri et al., 2006). Sub-stages, ammonite zones, spore-pollen assemblages, Classopollis %, spore-pollen ratio, main trends in humidity changes as bold grey lines, spore maxima coeval with eccentricity maxima in dashed lined boxes. Orientation is following the Lower to Upper Valanginian boundary.

excluded from interpretation due to their extremely high numbers of Classopollis (73.0 and 55%, respectively, see Fig. 5). They may represent short-lived extremely dry conditions but more probably do not reflect changes in the vegetation structure but changes in sedimentological processes, e.g. in connection with changes in sea-level and marine currents, artificially enhancing the Classopollis abundances in these samples (see also Section 5.2). This interpretation is supported by the fact that these samples represent intervals rich in carbonate and shells deviating from the rest of the section (Fig. 3).

Spore abundance increases in the MPT1 assemblage, and culminates in a first spore maximum at the MPT1 to MPT2 assemblage boundary. This peak is characterized by high abundances of the fern spores Cyathidites and Gleicheniidites and a reduction in the gymnosperm pollen of conifer origin, namely of Perinopollenites, pointing to a reduction in Cupressaceae/Taxodiaceae. High numbers of the conifer pollen of probably araucarian and taxodiacean type (Inaperturopollentites, Callialasporites, Cerebropollenites) in assemblages MPT1 and MPT2 point to a swampy shoreline environment (Markevich et al., 2009).

In assemblage MPT2 times, a gradual trend towards more humid conditions is suggested by an increase in the number of spores. In late assemblage MPT2 times, the spore–pollen ratio strongly fluctuates. Lycopods are slightly more common up to the end of assemblage MPT2 times, as reflected in high numbers of Neoraistrickia, pointing towards humid lowland, river or tidally-influenced habitats (Abbink et al., 2004). The gymnosperm pollen Callialasporites and Inaperturopollenites become the dominant tree pollen. Persistently higher numbers of the fern spore Osmundacidites is a further indication for a humid environment of floodplains and swamps (Coiffard et al., 2007). Towards the end of MPT2 Cyathidites is declining while non-identifiable spores are increasing. The gradual change in plant communities might partly be due to a reduction of coastal plains by increasing sea-level. This is confirmed by a decrease in the conifer pollen Perinopollenites, of probably

cupressacean or taxodiacean origin, whose parent plants were probably adapted to coastal environments, which would be expected to be reduced under rising sea-level.

Maximum humidity is established relatively abruptly in assemblage MPT3 times, evidenced by a pronounced spore maximum characterized by high numbers of the fern spores Cyathidites, Gleicheniidites and Leiotriletes, e.g. of dickinsoniaceaen, gleicheniaceaen, and osmundaceaen origin as well as by undifferentiated spores. The generally abundant gymnosperm pollen of cupressacean/taxodiacean origin, Cerebropollenites and Perinopollenites, are decreasing. Classopollis abundances consequently show their lowest values. Bryophytes are increasing towards assemblage MPT3 times, confirming a trend towards higher humidity (Schrank, 2010). High abundances of the bisaccate pteridosperm pollen Vitreisporites pallidus peaking in assemblage MPT3 times accompanying the spore-maximum provide evidence for the establishment of swamps and a dominance of deltaic environments and backswamps. The peak in the fern spore Leiotriletes points to abundant herbaceous swamps. Trees represent rare floral elements in assemblage MPT3 times identified by low numbers of e.g. araucarian and bisaccate pollen. Assemblage MPT4 is characterized by high bisaccate numbers as well as by high amounts of the araucarian pollen Calliallasporites and Araucariacites, indicating relatively moist, temperate conditions. The spore–pollen ratio is decreasing to pre-maximum abundances.

5.4.2. The VB site

For the VB Classopollis shows overall high abundances, temporarily up to 45%. Assemblage VB1 time is characterized by a trend towards arid conditions, indicated by a decreasing spore–pollen ratio and increasing Classopollis abundances (cf. Fig. 6). Abundances of other conifer pollen like Callialasporites, Cerebropollenites, and Inaperturopollenites are decreasing. A loss in diversity (Fig. 4) may also be caused by this aridification event culminating in assemblage VB2 times.

This comparatively dry interval is followed by an abrupt shift in the spore–pollen ratio to maximum values in assemblage VB3 times, indicating relatively humid conditions. This maximum in the spore–pollen ratio is characterized by high abundances of the fern spores Cyathidites, Gleicheniidites, and Leiotriletes of e.g. dickinsoniaceaen, gleicheniaceaen, and osmundaceaen origin as well as by spores of unclear taxonomy. At the same time, the coniferous gymnosperm pollen Classopollis shows low abundances, indicating a reduction in xerophytic vegetation. A peak in Leiotriletes in assemblage VB3 times points to abundant herbaceous swamps, with a rare arborescent vegetation.

High abundances of the pteridosperm pollen Vitreisporites points to the establishment of deltaic environments and backswamps at the VB3/VB4 assemblage boundary. Climatic conditions in assemblage VB4 times are interpreted as relatively cool and rather dry, based on a combination of high numbers of bisaccates and a low diversity in fern spores (Herngreen et al., 1996). Increased abundances of Exesipollenites and Cycadopites as well point to drier conditions. A re-establishment of forested areas may be inferred from an increase in Araucariacites pollen towards the end of the assemblage.

A gradual shift towards humid conditions culminates in another spore maximum at the assemblage boundary between VB4 and VB5. This second spore maximum shows again high numbers of the fern spores Cyathidites, Gleicheniidites, and Leiotriletes as well as of undefined spores. Bisaccate pollen show low abundances. In assemblage VB5 times, a trend towards more arid conditions follows the second maximum in the spore–pollen ratio, accompanied by the establishment of a tree-dominated vegetation, with abundant Araucariacites, Perinopollenites, and Cerebropollenites. Unlike the first spore maximum in assemblage VB3, this second spore-maximum is not preceded by elevated numbers of Classopollis.

In the VB, abundances in Classopollis are significantly higher (max. 45.0%) compared to the MPT (max. 13.3%). Furthermore, in this area, the abundances of Classopollis show strong fluctuations, while at the MPT abundances are comparatively stable. This may be due to an in general higher level of humidity around the MPT, in accordance with abundant swamp habitats, whereas around the VB swamp habitats were only temporarily abundant. The most characteristic feature observed at both sites is a coeval maximum in the spore–pollen ratio (assemblages VB3/MPT3), interpreted to reflect supra-regionally exceptionally humid conditions in the early late Valanginian. The composition of spore taxa during this spore maximum is shown to be similar at both sites. Subsequently, climatic conditions became drier again at both localities. At the MPT site, the phase of increased humidity is preceded by a gradual trend towards humid conditions. In contrast, at the VB a protracted phase of relatively arid conditions preceded the humidity peak. At both sites comparable vegetation structures reflect especially humid conditions after the early/late Valanginian boundary. Preceding conditions are, however, dissimilar, indicating different environmental evolutions.

5.5. Paleoclimatic implications

During the Valanginian the coastlines of Paleo-Europe showed an archipelagic arrangement (Diéguez et al., 2010); Paleo-Europe was located 10° closer to the equator than today, adjoining the Tethys Ocean to the south, while the North Atlantic was not yet well established (e.g. Ziegler et al., 1987). Accordingly, the major moisture source for the southern part of Paleo-Europe was the Tethys, probably controlled by a monsoonal climate. During northern hemisphere summer, southern monsoonal trade winds were likely to be established over the northwestern Tethys (Fig. 8; cf. Herrle et al., 2003; Wang, 2009; Giorgioni et al., 2012). On geologic time scales variations in the monsoonal circulation are significantly controlled by changes in orbital parameters, known as Milankovitch cycles, which control the geographic distribution of insolation (cf. Mayer and Appel, 1999; Crowley, 2002; Wang, 2009).

The gradual increase in humidity in assemblage MPT2 times (Fig. 7), culminating in extremely humid conditions expressed at both sites in assemblages MPT3/VB3, may represent an increase in the intensity of a monsoonal precipitation, and/or an extension of the annual humid period. This may explain for the observed restructuring of the vegetation towards a pteridophyte dominance. Eccentricity cycles are known to be responsible for longer-term variations in monsoonal intensity, with phases of high intensity occurring during maxima in eccentricity

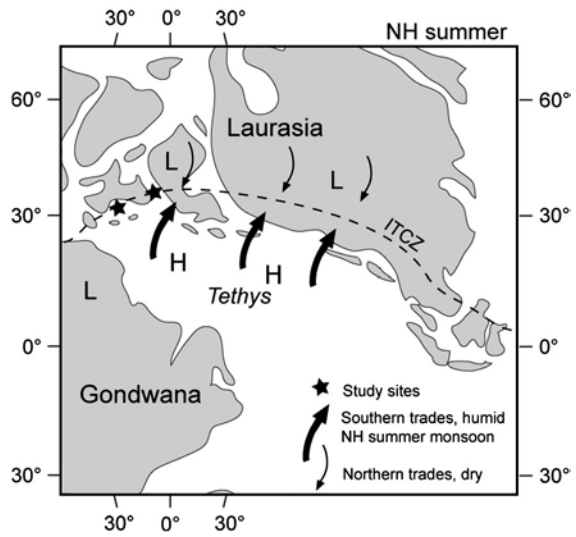

Fig. 8. Paleogeographic map of Valanginian, with supposed land in grey (based on Ziegler et al., 1987; Smith et al., 1994; Rees McAllister et al., 2004; Hay, 2002; Mutterlose et al., 2003; Blakey, 2010; Vakhrameev, 2010). Asterisks mark study sites (upper one MPT, lower one VB), arrows mark trade winds. Potential northernmost ITCZ trajectory of Valanginian northern hemisphere summer (broken line) defining the area of influence of a northern hemisphere paleo-summer monsoon. H = high pressure, L = low pressure.

(e.g. Wang, 2009). The 2.4 Ma eccentricity cycle was shown to be in a maximum during the initial phase of the positive carbon isotope excursion of the Valanginian (Sprovieri et al., 2006). This phase coincides with the interval of the coeval spore maxima (Fig. 7). Consequently monsoonal precipitation can be expected to have been in a maximum. This scenario of enhanced precipitation may have been intensified by a general northward shift of the Intertropical Convergence Zone (ITCZ), defining the center of northern and southern trade winds (e.g. Roedel and Wagner, 2011). This may have prolonged the annual humid period for both sites. This shift in the ITCZ can be caused by specific configurations of the orbital parameters obliquity and precision, controlling the orientation of the ITCZ track towards the northern or southern hemisphere, explaining for short-term variations and insolation differences between hemispheres (Häckel, 1999; Wang et al., 2003; Lauer and Bendix, 2006). Furthermore, factors like solar maxima or positive precipitation–vegetation-feedbacks may have additionally influenced humidity (e.g. Ganopolski et al., 1998). The preceding and subsequent phases of less pronounced maxima in the spore–pollen ratios (assemblage boundaries MPT1/2 and VB4/5, respectively) coincide with a preceding and a subsequent eccentricity maximum (Sprovieri et al., 2006, Fig. 7). The fact that these spore maxima are less pronounced compared to that of assemblages MPT3/VB3 may be explained by the lack of further intensifying factors.

The abrupt drying indicated for the VB in assemblage VB2, preceding the supra-regional pronounced humid phase of the coeval spore-maximum, is characterized by high abundances of Classopollis and low spore abundances. It may reflect a northward shift or expansion of the northern hemisphere arid belt, probably due to a northward shift/expansion of the subtropical high-pressure belt (cf. Hasegawa et al., 2010). This extension of the arid belt may have reduced moisture availability in the hinterland of the VB. The fact that this dry phase is not reflected in the continental areas surrounding the Carpathian seaway may be due to its paleogeographic position at a higher latitude. Further evidence for a meandering Valanginian arid belt is provided by aeolian deposits found on the Asian continent up to ~44°N (Hasegawa et al., 2011). Based on abundances of Classopollis, Herngreen et al. (1996) also described an arid belt affecting the northern Tethys coastline throughout the Berriasian to Hauterivian. The subsequent phase of supra-regional humid conditions probably reflects a retreat of the arid belt.

6. Conclusions

Based on spore–pollen abundances of two mid-latitudinal sites of Paleo-Europe in the MPT and the VB, changes in Valanginian vegetation patterns were analyzed and used to deduce varying moisture levels. Both sites are similarly characterized by high pteridophyte abundances represented by Cyathidites, Leiotriletes and Gleicheniidites. Dominant pollen are different at both sites, at the MPT araucarians/cupressaceans dominate, while at the VB cheirolepediaceans are most abundant, which are extremely rare at the MPT. Bisaccates are of moderate abundance at both sites. Moisture availability was probably the determining factor for changes in vegetation patterns, controlled by a monsoonal circulation. A supra-regional interval of pronounced humid conditions indicated by a coeval spore-maximum is established for the interval following the early/late Valanginian boundary, probably under strong monsoonal influence. Prior to the early/late Valanginian boundary a temporary northward shift or expansion of an arid belt is expressed by local differences between the sites causing a temporary drying at the VB, characterized by increased abundances of the drought-resistant conifer pollen Classopollis and reduced spore-abundances. This dry phase is not reflected by the vegetation around the MPT.

Acknowledgments

Special thanks are due to Benjamin Gréselle (Neftex Petroleum Consultants Ltd., Oxfordshire, UK) for his assistance during field work in France. Financial support from the DFG project HE4467/2-1 and the Swiss National Science Foundation (project 200020_126455) are gratefully acknowledged.

References

Abbink, O.A., 1998. Palynological Investigations in the Jurassic of the North Sea region. Universiteit Utrecht, The Netherlands (thesis, 192 pp.).
Abbink, O.A., Van Konijnenburg-Van Cittert, J.H.A., Visscher, H., 2004. A sporomorph ecogroup model for the Northwest European Jurassic–Lower Cretaceous: concepts and framework. Netherlands Journal of Geosciences/Geologie en Mijnbouw 83, 17–38.
Azéma, C., Boltenhagen, E., 1974. Pollen du Crétacé moyen du Gabon attribué aux Ephedrales. Paléobiologie Continental 5 (1), 1–37.
Balme, B.E., 1995. Fossil in situ spores and pollen grains: an annotated catalogue. Review of Palaeobotany and Palynology 87, 81–323.
Baltes, N., 1967. The microflora of the Albian "Green Sands" in the moesic platform (Rumania). Review of Palaeobotany and Palynology 5, 183–197.
Barbarin, N., Bonin, A., Mattioli, E., Pucéat, E., Cappetta, H., Gréselle, B., Pittet, B., Vennin, E., Joachimski, M., 2012. Evidence for a complex Valanginian nannoconid decline in the Vocontian basin (South East France). Marine Micropaleontology 84–85, 37–53.
Batten, D.J., 1975. Wealden paleoecology from the distribution of plant fossils. Proceedings of the Geologists Association 85 (4), 433–458.
Batten, D.J., 1984. Palynology, climate and the development of Late Cretaceous floral provinces in the Northern Hemisphere; a review. In: Brenchley, P.J. (Ed.), Fossils and Climate. Wiley, Chichester, pp. 127–164.
Batten, D.J., Dutta, R.J., 1997. Ultrastructure of exine of gymnospermous pollen grains from Jurassic and basal Cretaceous deposits in Northwest Europe and implications for botanical relationships. Review of Palaeobotany and Palynology 99, 25–54.
Birkenmajer, K., Gedl, P., Worobiec, E., 2010. Dinoflagellate cyst and spore–pollen spectra from the Lower Oligocene Krabbedalen Formation at Kap Brewster, East Greenland. Polish Polar Research 31 (2), 103–140.
Blakey, R., 2010. Early Cretaceous European Paleogeographic Map. available online: http://cpgeosystems.com/125_Cret_EurMap_sm.jpg (21.10.2010).
Bornemann, A., Pross, J., Reichelt, K., Herrle, J.O., Hemleben, C., Mutterlose, J., 2005. Reconstruction of short-term palaeoceanographic changes during the formation of the Late Albian, Niveau Breistroffer' black shales (Oceanic Anoxic Event 1d, SE France). Journal of the Geological Society of London 162, 623–639.
Boulter, M.C., Windle, T., 1993. A reconstruction of some Middle Jurassic vegetation in Northern Europe. Special papers in Palaeontology 49, 125–154.
Bown, P.R., 1998. Calcarous nannofossil biostratigraphy, 1st edition. British Micropalaeontological Society Publication SeriesChapman and Hall, London (199 pp.).
Bown, P.R., Rutledge, D.C., Crux, J.A., Gallagher, L.T., 1998. Lower Cretaceous. In: Bown, P.R. (Ed.), Calcarous Nannofossil Biostratigraphy. Chapman and Hall, Cambridge, pp. 86–102.
Brassell, S.C., 2009. Steryl ethers in a Valanginian claystone: molecular evidence for cooler waters in the central Pacific during the Early Cretaceous? Palaeogeography, Palaeoclimatology, Palaeoecology 282, 45–57.
Bréhéret, J.-G., 1994. The Mid-Cretaceous organic-rich sediments from the Vocontian Zone of the French southeast basin. In: Mascle, A. (Ed.), Hydrocarbons and petroleum geology of France. : The European Association of Petroleum Geoscientists Special Publications. Springer-Verlag, Berlin/Heidelberg, pp. 295–320.
Brenner, J.C., 1976. Middle Cretaceous floral provinces and early migration of Angiosperms. In: Beck, C.B. (Ed.), Origin and Early Evolution of Angiosperms. Columbia University Press, New York, N.Y., USA, pp. 23–44.
Chumakov, N.M., Zharkov, M.A., Herman, A.B., Doludenko, M.P., Kalandadze, N.N., Lebedev, E.L., Ponomarenko, A.G., Rautian, A.S., 1995. Climatic belts of the mid-Cretaceous time. Stratigraphy and Geological Correlation 3 (3), 241–260.
Coiffard, C., Gomez, B., Thevenard, F., 2007. Early Cretaceous angiosperm invasion of Western Europe and major environmental changes. Annals of Botany 100, 545–553.
Conway, B., 1996. A palynological investigation across the Jurassic–Cretaceous boundary on the south-east flanks of Mount Hermon, Israel. Cretaceous Research 17, 197–214.
Cotillon, P., Rio, M., 1984. Cyclic sedimentation in the Cretaceous of the Deep Sea Drilling Project sites 535 and 540 (Gulf of Mexico), 534 (Central Atlantic), and in the Vocontian Basin (France). Initial Reports of the Deep Sea Drilling Project 77, 339–376.
Couper, R.A., 1958. British Mesozoic microspores and pollen grains. Palaeontographica Abteilung B 103, 75–179.
Courtinat, B., 1989. Les organoclastes des formations lithologiques du Malm dans le Jura méridional. Systématique, biostratigraphie et éléments d'interprétation paléoécologique. Documents des Laboratoires de Géologie Lyon 105, 1–361.
Crowley, T., 2002. Cycles, cycles everywhere. Science 295, 1473–1474.
Daldez, R., 2003. Mesozoic thickness pattern in the Mid-Polish Trough. Geological Quarterly 47 (3), 223–240.
Dettmann, M.E., 1963. Upper Mesozoic microfloras from south-eastern Australia. Proceedings of the Royal Society of Victoria 77 (1), 1–148.
Diéguez, C., Peyrot, D., Barrón, E., 2010. Floristic vegetational changes in the Iberian Peninsula during Jurassic and Cretaceous. Review of Palaeobotany and Palynology 162, 325–340.
Döring, H., 1965. Die sporenpaläontologische Gliederung des Wealden in Westmecklenburg (Struktur Werle). Geologie (Beiheft 47), 1–118 (Jahrgang 14).
Doyle, J.A., Jardiné, S., Doerenkamp, A., 1982. Afropollis, a new genus of early angiosperm pollen, with notes on the Cretaceous palynostratigraphy and paleoenvironemts of northern Gondwana. Bulletin des Centres de Recherches Exploration–Production Elf-Aquitaine 6, 39–117.
Fesneau, C., Deconinck, J.-F., Pellenard, P., Reboulet, S., 2009. Evidence of aerial volcanic activity during the Valanginian along the northern Tethys margin. Cretaceous Research 30, 533–539.

Filatoff, J., 1975. Jurassic palynology of the Perth Basin, Western Australia. Palaeontographica Abteilung B 154, 1–113.
Föllmi, K., Weissert, H., Bisping, M., Funk, H., 1994. Phosphogenesis, carbon-isotope stratigraphy, and carbonate-platform evolution along the Lower Cretaceous northern Tethyan margin. Geological Society of America Bulletin 106, 729–746.
Föllmi, K., Godet, A., Bodin, S., Linder, P., 2006. Interactions between environmental change and shallow water carbonate buildup along the northern Tethyan margin and their impact on the Early Cretaceous carbon isotope record. Paleoceanography 21, 1–6.
Fowell, S.J., Cornet, B., Olsen, P.E., 1994. Geologically rapid Late Triassic extinctions: palynological evidence from the Newark Supergroup. In: Klein, G.D. (Ed.), Pangea: paleoclimate, tectonics, and sedimentation during accretion, zenith, and breakup of a supercontinent. Boulder, Colorado, USA: Geological Society of America Special Paper, 288, pp. 197–206.
Frakes, L.A., Francis, J.E., 1988. A guide to Phanerozoic cold polar climates from high-latitude ice-rafting in the Cretaceous. Nature 333, 547–549.
Ganopolski, A., Kubatzki, C., Claussen, M., Brovkin, V., Petoukhov, V., 1998. The Influence of vegetation–atmosphere–ocean interaction on climate during the Mid-Holocene. Science 280, 1960-1919.
Giorgioni, M., Weissert, H., Bernasconi, S.M., Hochuli, P.A., Coccioni, R., Keller, C.E., 2012. Orbital control on carbon cycle and oceanography in the mid-Cretaceous greenhouse. Paleoceanography 27, PAI204. http://dx.doi.org/10.1029/2011PA002163.
Granzow, W., 2000. Abkürzungen und Symbole in der biologischen Nomenklatur. Senckenbergiana Lethaea 80, 355–370.
Gréselle, B., 2007. Impact des variations paléoclimatiques sur la sédimentation carbonatée au Valanginien. Université Lyon1 — Claude Bernard, France (PhD thesis, 182 pp.).
Gréselle, B., Pittet, B., 2010. Sea-level reconstructions from the Peri-Vocontian Zone (SE France) point to Valanginian glacio-eustasy. Sedimentology 57 (7), 1640–1684.
Gréselle, B., Pittet, B., Mattioli, E., Joachimski, M., Barbarin, N., Riquier, L., Reboulet, S., Pucéat, E., 2011. The Valanginian isotope event: a complex suite of palaeoenvironmental perturbations. Palaeogeography, Palaeoclimatology, Palaeoecology 306, 41–57.
Gröcke, D.R., Price, G.D., Robinson, S.A., Baraboshkin, E.Y., Mutterlose, J., Ruffell, A.H., 2005. The Upper Valanginian (Early Cretaceous) positive carbon-isotope event recorded in terrestrial plants. Earth and Planetary Science Letters 240, 495–509.
Häckel, H., 1999. Meteorologie, 4th edition. UTB, Stuttgart.
Harris, T.M., 1969. The Yorkshire Jurassic flora, III. Bennettitales.British Museum (Natural History), London (186 pp.).
Harris, T.M., 1974. Williamsoniella lignieri; its pollen and the compression of spherical pollen grains. Palaeontology 17, 125–148.
Hasegawa, H., Insamut, S., Charusiri, P., Tada, R., Horiuchi, Y., Hisada, K.-I., 2010. 'Thailand was a desert' during the mid-Cretaceous: equatorward shift of the subtropical high-pressure belt indicated by eolian deposits (Phu Thok Formation) in the Khorat Basin, northeastern Thailand. Island Arc 19, 605–621.
Hasegawa, H., Tada, R., Jiang, X., Suganuma, Y., Imsamut, S., Charusiri, P., Ichinnorov, N., Khand, Y., 2011. Drastic shrinking of the Hadley circulation during the mid-Cretaceous supergreenhouse. Climate of the Past Discussions 7, 119–151.
Hay, W.W., 2002. A new view of Cretaceous paleoceanography. In: Michalik, J. (Ed.), Tethyan/Boreal Cretaceous Correlation. VEDA Publishing House of the Slovak Academy of Sciences, Bratislava, Slovak Republic, pp. 11–37.
Hay, W.W., DeConto, R., Wold, C.N., Wislon, K.M., Voigt, S., Schulz, M., Wold-Rossby, A., Dullo, W.C., Ronov, A.B., Balukhovsky, A.N., Soeding, E., 1999. Alternative global Cretaceous paleogeography. In: Barera, E., Johnson, C.C. (Eds.), Evolution of the Cretaceous ocean–climate system: Special Paper, Geological Society of America, 332, pp. 1–47.
Hedlund, R.W., 1966. Palynology of the Red Branch Member (Woodbine Formation). Oklahoma Geological Survey, Bulletin, 112 (96 pp.).
Hennig, S., Weissert, H., Bulot, L., 1999. C-isotope stratigraphy, a calibration tool between ammonite- and magnetostratigraphy: the Valanginian–Hauterivian transition. Geologica Carpathica 50, 91–96.
Herngreen, G.F.W., 1971. Palynology of a Wealden Section (Lower Cretaceous) in the "Carrière de Longueville", the Boulonnais (France). Review of Palaeobotany and Palynology 12, 271–302.
Herngreen, G.F.W., Kedves, M., Rovnina, L.V., Smirnova, S.B., 1996. Chapter 29, Vegetational History, 29C. Cretaceous palynofloral provinces: a review. In: Jansonius, J., McGregor, D.C. (Eds.), Palynology: principles and applications: American Association of Stratigraphic Palynologists Foundation, 3, pp. 1157–1188.
Herrle, J.O., Pross, J., Friedrich, O., Kößler, P., Hemleben, C., 2003. Forcing mechanisms for mid-Cretaceous black shale formation: evidence from the Upper Aptian and Lower Albian of the Vocontian Basin (SE France). Palaeogeography, Palaeoclimatology, Palaeoecology 190, 399–426.
Hochuli, P.A., 1981. North Gondwana floral elements in Lower to middle Cretaceous sediments of the Southern Alps (Southern Switzerland, Northern Italy). Review of Palaeobotany and Palynology 35 (2–4), 337–358.
Hochuli, P.A., Kelts, K., 1980. Palynology of Middle Cretaceous black clay facies from DSDP sites 417 and 418 of the western North Atlantic. Initial Reports of the Deep Sea Drilling Project 51–53, 897–935.
Hochuli, P.A., Vigran, J.O., 2010. Climate variations in the Boreal Triassic — inferred from palynological records from the Barents Sea. Palaeogeography, Palaeoclimatology, Palaeoecology 290, 20–40.
Kaim, A., 2001. Faunal dynamics of juvenile gastropods and associated organisms across the Valanginian transgression–regression cycle in central Poland. Cretaceous Research 22, 333–351.
Kemper, 1987. Das Klima der Kreide-Zeit. Geologisches Jahrbuch, Reihe A 96, 5–185.
Knox, E.M., 1950. The spores of Lycopodium, Phylloglossum, Selaginella and Isoetes and their values in the study of microfossils of Palaeozoic origin. Transactions and Proceedings of the Botanical Society of Edinburgh 35, 209–357.
Kujau, A., Heimhofer, U., Ostertag-Henning, C., Gréselle, B., Mutterlose, J., 2012. No evidence for anoxia during the Valanginian carbon isotope event — an organic-geochemical study from the Vocontian Basin, SE France. Global and Planetary Change 92–93, 93–104.
Kutek, J., Marcinowski, R., Wiedmann, J., 1989. The Wąwał Section, central Poland — an important link between Boreal and Tethyan Valanginian. Cretaceous of the Western Tethys. In: Wiedmann, J. (Ed.), Proceedings of the 3rd International Cretaceous Symposium, Tübingen 1987. Schweizbart, Stuttgart, pp. 717–754.
Larsson, L., 2009. Palynostratigraphy of the Triassic–Jurassic transition in southern Sweden. GFF 131 (1), 147–163.
Lauer, W., Bendix, J., 2006. Klimatologie, 2nd edition. Westermann, Braunschweig.
Lini, A., Weissert, H., Erba, E., 1992. The Valanginian carbon isotope event: a first episode of greenhouse climate conditions during the Cretaceous. Terra Nova 4, 374–384.
Lundblad, B., 1950. Studies in the Rhaeto-Liassic floras of Sweden. Kungliga Svenska Vetenskaps-Akademiens Handlingar 4 (1, 8), 1–82.
MacLeod, S.E., Hills, L.V., 1991. Conformable Late Jurassic (Oxfordian) to Early Cretaceous strata, northern Bowser Basin, British Columbia: a sedimentological and paleontological model: reply. Canadian Journal of Earth Sciences 28, 1497–1502.
Markevich, V.S., Bugdaeva, E.V., Ge, S., 2009. Palynoflora of Wulaga dinosaur site in Jiayin (Zeya-Bureya Basin, China). Global Geology 12 (3), 117–121.
Masse, J.P., 1993. Systématique, stratigraphie et paléobiogéographie du genre Lovetchnia (Requieniidae) du Crétacé inférieur méditerranéen. (Taxonomy, stratigraphy and paleobiogeography of the Lovetchnia genus (Requieniidae) from the Mediterranean Early Cretaceous). Geobios 26 (6), 699–708.
Mayer, H., Appel, E., 1999. Milankovitch cyclicity and rock-magnetic signatures of palaeoclimatic change in the Early Cretaceous Biancone Formation of the Southern Alps, Italy. Cretaceous Research 20, 189–214.
McArthur, J.M., Janssen, N.M.M., Reboulet, S., Leng, M.J., Thirlwall, M.F., van de Schootbrugge, B., 2007. Paleotemperatures, polar ice-volume, and isotope stratigraphy (Mg/Ca, δ18O, δ13C, 87Sr/86Sr): the Early Cretaceous (Berriasian, Valanginian, Hauterivian). Palaeogeography, Palaeoclimatology, Palaeoecology 248, 391–430.
Melinte, M., Mutterlose, J., 2001. A Valanginian (Early Cretaceous) 'boreal nannoplankton excursion' in sections from Romania. Marine Micropaleontology 43 (1–2), 1–25.
Mutterlose, J., 1992. Migration and evolution patterns of floras and faunas in marine Early Cretaceous sediments of NW Europe. Palaeogeography, Palaeoclimatology, Palaeoecology 94, 261–282.
Mutterlose, J., Kessels, K., 2000. Early Cretaceous calcarous nannofossils from high latitudes: implications for palaeobiogeography and palaeoclimate. Palaeogeography, Palaeoclimatology, Palaeoecology 160 (3–4), 347–372.
Mutterlose, J., Brumsack, H., Flögel, S., Hay, W., Klein, C., Langrock, U., Lipinski, M., Ricken, W., Söding, E., Stein, R., Swientek, O., 2003. The Greenland–Norwegian Seaway: a key area for understanding Late Jurassic to Early Cretaceous palaeoenvironments. Paleoceanography 18, PA 000625.
Nunn, E.V., Price, G.D., Gröcke, D.R., Baraboshkin, E.Y., Leng, M.J., Hart, M.B., 2010. The Valanginian positive carbon isotope event in Arctic Russia: evidence from terrestrial and marine isotope records and implications for global carbon cycling. Cretaceous Research 31, 577–592.
Perch-Nielsen, K., 1985. Mesozoic calcareous nannofossils. In: Bolli, H.M., Saunders, J.B., Perch-Nielsen, K. (Eds.), Plankton Stratigraphy. Cambridge University Press, Cambridge, pp. 329–426.
Pérez Loinaze, V.S., Césari, S.N., 2004. Palynology of the Estratos de Mascasín, Upper Carboniferous, Paganzo Basin, Argentina: systematic descriptions and stratigraphic considerations. Revista Española de Micropaleontología 36 (3), 407–438.
Podlaha, O.G., Mutterlose, J., Veizer, J., 1998. Preservation of $\delta^{18}O$ and $\delta^{13}C$ in belemnite rostra from the Jurassic/Early Cretaceous successions. American Journal of Science 298, 324–347.
Potonié, R., 1967. Versuch der Einordnung der fossilen Sporae dispersae in das phylogenetische System der Pflanzenfamilien. Forschungsberichte des Landes Nordrhein-Westfalen 1761, 11–310.
Potonié, R., 1970. Synopsis der Gattung der Sporae dispersae V. Teil: Nachträge zu allen Gruppen (Turmae). Beiheft zum Geologischen Jahrbuch, 87 (222 pp.).
Price, G.D., 1999. The evidence and implications of polar ice during the Mesozoic. Earth-Science Reviews 48, 183–210.
Price, G.D., Mutterlose, J., 2004. Isotopic signals from Late Jurassic–Early Cretaceous (Volgian–Valanginian) sub-Arctic belemnites, Yatria River, Western Siberia. Journal of the Geological Society of London 161, 959–968.
Price, G.D., Nunn, E.V., 2010. Valanginian isotope variation in glendonites and belemnites from Arctic Svalbard: transient glacial temperatures during the Cretaceous greenhouse. Geology 38 (3), 251–254.
Pucéat, E., Lécuyer, C., Sheppard, S.M.F., Dromart, G., Reboulet, S., Grandjean, P., 2003. Thermal evolution of Cretaceous Tethyan marine waters inferred from oxygen isotope composition of fish tooth enamels. Paleoceanography 18 (2), 1029. http://dx.doi.org/10.1029/2002PA000823.
Raine, J.I., de Jersey, N.J., Ryan, K.G., 1988. Ultrastructure and lycopsid affinity of Densoisporites psilatus (de Jersey) com. nov. from the Triassic of New Zealand and Queensland. Memoirs of the Association of Australasian Palaeontologists 5, 79–88.
Raine, J.I., Mildenhall, D.C., Kennedy, E.M., 2006. New Zealand Fossil Spores and Pollen: An Illustrated Catalogue, 2nd edition. GNS Science miscellaneous series, 4.
Raine, J.I., Mildenhall, D.C., Kennedy, E.M., 2008. New Zealand Fossil Spores and Pollen: An Illustrated Catalogue, 3rd edition. GNS Science miscellaneous series, 4.
Reboulet, S., Mattioli, E., Pittet, B., Baudin, F., Olivero, D., Proux, O., 2003. Ammonoid and nannoplankton abundance in the Valanginian (Early Cretaceous) limestone-marl successions from the southeast France Basin. Palaeogeography, Palaeoclimatology, Palaeoecology 201, 113–139.
Rees McAllister, P., Noto, C.R., Parrish, J.M., Parrish, J.T., 2004. Late Jurassic climates, vegetation, and dinosaur distributions. Journal of Geology 112, 643–653.

Roedel, W., Wagner, T., 2011. Physik unserer Umwelt - Die Atmosphäre, 4th edition. Springer, Berlin, Heidelberg (589 pp.).
Scafati, L., Melendi, D.L., Volkheimer, W., 2009. A Danian subtropical lacustrine palynobiota from South America (Bororó Formation, San Jorge Basin, Patagonia — Argentina). Geologica Acta 7 (1–2), 35–61.
Schrank, E., 2010. Pollen and spores from the Tendaguru Beds, Upper Jurassic and Lower Cretaceous of southeast Tanzania: palynostratigraphical and paleoecological implications. Palynology 34 (1), 3–42.
Schrank, E., Mahmoud, M.S., 1998. Palynology (pollen, spores and dinoflagellates) and Cretaceous stratigraphy of the Dakhla Oasis, central Egypt. Journal of African Earth Sciences 26 (2), 167–193.
Smith, A.C., Smith, D.G., Funnell, B.M., 1994. Atlas of Mesozoic and Cenozoic Coastlines. Cambridge University Press, Cambridge (109 pp.).
Sprovieri, M., Coccioni, R., Lirer, F., Pelosi, N., Lozar, F., 2006. Orbital tuning of a Lower Cretaceous composite record (Maiolica Formation, central Italy). Paleoceanography 21 (19 pp.).
Taugourdeau-Lantz, J., 1988. Stratigraphic implications of Early Cretaceous spores and pollen grains at Holes 638B, 638C, and 641C, LEG 103, off the Iberian Margin, eastern North Atlantic. In: Boilot, G., Winterer, E.L., et al. (Eds.), Proceedings of the Ocean Drilling Program: Scientific Results, 103, pp. 419–428.
Traverse, A., 2007. Paleopalynology, 2nd edition. Springer, Dordrecht, The Netherlands (813 pp.).
Tyson, R.V., 1995. Sedimentary Organic Matter — Organic Facies and Palynofacies. Chapman & Hall, London (615 pp.).
Vajda, V., 2001. Aalenian to Cenomanian terrestrial palynofloras of SW Scania, Sweden. Acta Palaeontologica Polonica 46 (3), 403–426.
Vakhrameev, V.A., 1981. Pollen Classopollis: indicator of Jurassic and Cretaceous climates. Palaeobotanist 28–29, 301–307.
Vakhrameev, V.A., 2010. Jurassic and Cretaceous Floras and Climates of the Earth, 1st paperback edition. Cambridge University Press, Cambridge (318 pp.).
Van de Schootbrugge, B., Tremolada, F., Rosenthal, Y., Bailey, T.R., Feist-Burkhardt, S., Brinkhuis, H., Pross, J., Kent, D.V., Falkowski, P.G., 2007. End-Triassic calcification crisis and blooms of organic-walled 'disaster species'. Palaeogeography, Palaeoclimatology, Palaeoecology 244, 126–141.
Van der Burgh, J., Van Konijnenburg-Van Cittert, J.H.A., 1989. A drifted flora from the Kimmeridgian (Upper Jurassic) of Lothberg Point, Sutherland, Scotland. Review of Paleobotany and Palynology 43, 359–396.
Van Konijnenburg-Van Cittert, J.H.A., 1971. In situ gymnosperm pollen from the Middle Jurassic of Yorkshire. Acta Botanica Neerlandica 20 (1), 1–97.
Van Konijnenburg-Van Cittert, J.H.A., 1981. Schizaeaceous spores in situ from the Jurassic of Yorkshire, England. Review of Palaeobotany and Palynology 33, 169–181.
Van Konijnenburg-Van Cittert, J.H.A., 1987. New data on Pagiophyllum maculosum Kendall and its male cone from the Jurassic of North Yorkshire. Review of Paleobotany and Palynology 51, 95–105.
Van Konijnenburg-Van Cittert, J.H.A., 1991. Diversification of spores in fossil and extant Schizaeaceae. In: Blackmore, S., Barnes, S.H. (Eds.), Pollen and spores, patterns of diversification: Systematics Association Special, vol. 44, pp. 103–118.
Van Konijnenburg-Van Cittert, J.H.A., 1993. A review of the Matoniaceae based on in situ spores. Review of Palaeobotany and Palynology 78, 235–267.
Venkatachala, B.S., Kar, R.H., Raza, S., 1969. Palynology of the Mesozoic sediments of Kutch, W. India 5. Spores and pollen from Katrol exposures near Bhuj, Kutch District, Gujarat Atate. Palaeobotanist 17, 184–207.
Visscher, H., Van der Zwan, C.J., 1981. Palynology of the Circum-Mediterranean Triassic: phytogeographical and palaeoclimatological Implications. Geologische Rundschau 70 (2), 625–634.
Waksmundzka, M., 1981. Palynological analysis of Lower Cretaceous sediments from Kujawy (Poland). Acta Palaeontologica Polonica 26 (3/4), 257–280.
Wang, P.X., 2009. Global monsoon in a geological perspective. Chinese Science Bulletin 54 (7), 1113–1136.
Wang, B., Clemens, S.C., Liu, P., 2003. Contrasting the Indian and East Asian monsoons: implications on geologic time scales. Marine Geology 201, 5–21.
Weissert, H., 1989. C-isotope stratigraphy, a monitor of paleoenvironmental change: a case study from the Early Cretaceous. Surveys in Geophysics 10, 1–61.
Weissert, H., Erba, E., 2004. Volcanism, CO_2 and paleoclimate: a Late Jurassic–Early Cretaceous carbon and oxygen isotope record. Journal of the Geological Society of London 161, 695–702.
Weissert, H., Lini, A., 1991. Ice age interludes during the time of Cretaceous greenhouse climate? In: Müller, D.W., McKenzie, J.A., Weissert, H. (Eds.), Controversies in Modern Geology: Evolution of Geological Theories in Sedimentology, Earth History and Tectonics. Academic Press, London, pp. 173–191.
Weissert, H., Lini, A., Föllmi, K.B., Kuhn, O., 1998. Correlation of Early Cretaceous carbon isotope stratigraphy and platform drowning events: a possible link? Palaeogeography, Palaeoclimatology, Palaeoecology 137, 189–203.
Wilde, V., 1989. Untersuchungen zur Systematik der Blattreste aus dem Mitteleozän der Grube Messel bei Darmstadt (Hessen, Deutschland). Courier Forschungsinstitut Senckenberg 115, 1–123.
Wortmann, U., Weissert, H., 2000. Tying platform drowning to perturbations of the global carbon cycle with a δ13Corg-curve from the Valanginian of DSDP Site 416. Terra Nova 12, 289–294.
Yi, M.-S., Choi, S.-J., Yun, H., 1993. Cretaceous palynomorphs from the Iljik Formation in the Euiseong Area, Korea. Journal of the Paleontologic Society Korea 9 (2), 166–179.
Zhichen, S., Fei, H., 1997. The boundaries between the Southern Laurasian and Northern Gondwana Provinces and the Aquilapollenites and Normapolles palynofloras in East Asia. Cretaceous Research 18, 1–15.
Ziegler, P.A., 1982. Geological Atlas of Western and Central Europe. Shell International Petroleum Maatschappij B.V., The Hague, The Netherlands (133 pp.).
Ziegler, A.M., Raymond, A.L., Gierlowski, T.C., Horrell, M.A., Rowley, D.B., Lottes, A.L., 1987. Coal, climate and terrestrial productivity: the present and Early Cretaceous compared. In: Scott, A.C. (Ed.), Coal and coal-bearing strata: recent advances: Geological Society Special Publications, 32, pp. 25–49.
Zobaa, M.K., 2006. Subsurface Jurassic–Cretaceous Applied Palynology of the Sharib-IX and Ghoroud-IX Wells, North Western Desert, Egypt. Benha University, Egypt (PhD thesis, 196 pp.).